

Lincoln University Digital Thesis

Copyright Statement

The digital copy of this thesis is protected by the Copyright Act 1994 (New Zealand).

This thesis may be consulted by you, provided you comply with the provisions of the Act and the following conditions of use:

- you will use the copy only for the purposes of research or private study
- you will recognise the author's right to be identified as the author of the thesis and due acknowledgement will be made to the author where appropriate
- you will obtain the author's permission before publishing any material from the thesis.

DETERMINATION OF GENES INVOLVED IN BACTERIAL PHOSPHATE SOLUBILISATION

A thesis submitted in fulfilment of the requirements for the
Degree of Doctor of Philosophy

at

Lincoln University

by

Pei-Chun (Lisa) Hsu

Lincoln University

New Zealand

2014

Abstract of a thesis submitted in fulfilment of the requirements for the

Degree of Doctor of Philosophy in Molecular Microbiology

Determination of Genes Involved in Bacterial Phosphate Solubilisation

Pei-Chun (Lisa) Hsu

Agricultural systems depend on continued inputs of phosphate fertiliser to maintain productivity. However, due to ever increasing global demand, the finite reserves of phosphate rock are being rapidly depleted. This is compounded by the fact that half of the soluble phosphate in fertiliser applied to soil is converted to sparingly-soluble minerals such as calcium phosphate which are unavailable for plant uptake. It is therefore important to investigate strategies that will improve the utilisation of phosphate in soil-plant systems. While it has been demonstrated that phosphate-solubilising bacteria can utilise sparingly-soluble phosphate minerals in soil, the mechanisms by which this occur remain unclear.

In this project, 105 rhizobacteria were assessed for a number of plant growth-promoting traits, such as production of 1-aminocyclopropane-1-carboxylate deaminase, phytase, and inorganic phosphate solubilisation using plate screening assays. Ten of the most effective phosphate-solubilising isolates were further assessed using an *in vitro* hydroxyapatite liquid culture assay. Analysis of culture filtrates revealed that the effective phosphate-solubilising isolates, *Pseudomonas* spp. and *Burkholderia* sp., were predominantly secreting 2-keto-gluconic acid rather than the expected gluconic acid. In addition, a yet to be characterised organic acid was secreted by several *Pseudomonas* spp. strains which may also be involved in phosphate solubilisation.

In an attempt to identify novel genes involved in phosphate solubilisation, three isolates of different bacterial genera, *Enterobacter* sp. Wi28, *Pseudomonas* sp. Ha200 and *Burkholderia* sp. Ha185, derived from diverse geographic locations were subjected to random transposon mutagenesis. This enabled the identification of two unique uncharacterised genes from *Burkholderia* sp. Ha185. One mutant, *hemX*::Tn5(F18), with a mutation in *hemX* gene involved in haem biosynthesis, exhibited an almost complete abolition in hydroxyapatite solubilisation. The second mutant *bxpC*::Tn5(F13)

exhibited partial and delayed solubilisation. The translated product of the *bxpC* gene encodes a novel hypothetical protein with unknown function. However, based on a combination of organic acid, qRT-PCR and bioinformatics analysis, it is hypothesised that BxpC is a potential cargo protein involved in protection and transport of the calcium bound 2-ketogluconic acid compound.

Through the use of a *Burkholderia* sp. Ha185 GFP-tagged strain in conjunction with a gnotobiotic *in vivo* plant assay developed in this study, the colonisation pattern of *Burkholderia* sp. Ha185 and its derivatives on ryegrass roots over three week duration was defined. The preliminary characterisation of the *bxpC* and *hemX* identified in the study and defining the interaction of *Burkholderia* sp. Ha185 on the plant root provides a greater understanding of phosphate cycling by bacteria and its relationship to the plant. The novel pathways and findings of this study have provided further insights into the underlying mechanisms of inorganic phosphate solubilisation in soil-plant systems.

Keywords: *Burkholderia*, *Pseudomonas*, phosphate solubilisation, perennial ryegrass, plant-growth promotion, hydroxyapatite, gene regulation, rhizosphere, rhizoplane.

Acknowledgements

First and foremost, I would like to express my sincere appreciation to Dr. Mark Hurst, for the inspiration he has been to me and who has shown the elements of a genius. His valuable and constructive suggestions have guided me through many difficulties and challenges faced during this research. His willingness to give precious time and effort in this project highlighted his generosity and benevolent personality, which has been very much appreciated. Without Dr. Mark Hurst's daily supervision and constant help, this PhD research would not have been possible.

I would like to extend my heartfelt gratitude to Dr. Maureen O'Callaghan and Dr. Carolyn Mander for giving me the opportunity to undertake this challenging project and fulfil the Degree of Doctor of Philosophy. I am extremely grateful to both of them for constant support and advice throughout this project, for professional guidance and for patiently reading and proofreading my thesis even during the stressful periods and afterhours.

I would also like to express my sincere gratitude to my supervisor Professor Leo Condon for the enormous support throughout the study and research. I am particularly grateful for his motivation, enthusiasm, optimism, and positive spirit! His guidance and endless encouragement helped me all the way through. The success and final outcome of this research project would simply not have been possible without Professor Leo Condon, and I could not have imagined having a better supervisor for my PhD study. Advice and supervision given by Professor Tim Clough and Dr. Steven Wakelin has been a great help, especially by sharing the most current journal articles related to this field of research from time to time and by providing useful critiques of this research work.

In addition, I wish to thank my office mates Daria Rybakova, and Molly and Polly who constantly supported me throughout these years. Thanks for putting up with me unconditionally through the ups and downs and for understanding the stresses encountered during the PhD study. I could not possibly go through the PhD without all of your company and support.

I wish to acknowledge the help provided by the following colleagues from AgResearch; thanks to Emily Gerard for technical support and assistance in the lab, Sandra Young for thoughtful discussion and sharing her professional knowledge in microbiology, Lincoln Harper for his help and patient explanations of molecular techniques, Amy Beattie for her company in the lab and whose presence created a comfortable workspace, thanks to Sandra Jones who taught me and guided me through protein purification, and shared valuable personal experiences, Dr. Jana Monk for sharing her methodology in various microbiology experiments, Dr. Sean Marshall for insightful guidance and

encouragement, Dr. Chikako van Koten for mathematical calculation and statistical assessments, Paul Maclean and Aurelie Laugraud for their bioinformatics support, Pauline Hunt for preparing posters for conferences and amazing artistic drawing in this thesis, Brent Conlan and Russel McAuliffe for IT support.

I would also like to extend my many thanks to the Lincoln University analytical group, especially Joy Jiao for developing and optimising the HPLC method, and Lynne Clucas for the ICP assessment and analysis. Special thanks to Manfred Ingerfeld from Canterbury University at the Confocal Microscope Facility for assisting with plant sample preparation and taking images using the confocal microscope. I would also like to thank Dr. Sam Yu from Izon Science Ltd. who offered the quantitative size measurement of particles by qNano. Furthermore, I wish to thank Dr. Courtney Giles, Dr. Alan Richardson and Dr. Jane Hill for their support and kind collaborations. Special thanks to Dr. Courtney Giles for hosting me while I visited her at the University of Vermont and her new research group, Research on Adaptation to Climate Change, USA in 2012.

I also thank the Ministry of Business, Innovation and Employment (MBIE) for funding this project and granting my scholarship over three years. Many thanks to both MBIE and AgResearch for granting my attendance and travel to the New Zealand Microbiological Society conference, Rhizosphere 3 conference, and to the International Society for Microbial Ecology 14 conference.

Last but not least, I would like to express my deepest gratitude and appreciation to my beloved parents Tony Hsu and Mei Wang, my brother David Hsu, and my partner Mark Mai for their tremendous support both morally and financially. Thank you all for always being there for me, believing in me, understanding me, and for your unconditional love throughout these years. Without all of your constant encouragement and support I would have never made it this far.

The *Pseudomonas* sp. Ha200 strain characterised from this study has been published in:

Giles, C. D., Hsu, P.-C., Richardson, A. E., Hurst, M. R. H., & Hill, J. E. (2014). Plant assimilation of phosphorus from an insoluble organic form is improved by addition of an organic anion producing *Pseudomonas* sp. *Soil Biology and Biochemistry*, 68(0), 263-269. doi: <http://dx.doi.org/10.1016/j.soilbio.2013.09.026>

Table of Contents

Abstract.....	
Acknowledgements.....	iii
Table of Contents	v
List of Table	x
List of Figures	xii
Acronyms and Abbreviations	xvii

Chapter 1 Introduction and Literature Review

1.1	Introduction	1
1.1.1.	An overview of phosphate rock and phosphate fertilisers.....	2
1.1.2.	Environmental impacts of overuse of phosphate fertilisers	3
1.2	Plant growth-promoting rhizobacteria	5
1.2.1.	Traits of growth-promoting rhizobacteria.....	5
1.2.1.1	1-aminocyclopropane-1-carboxylate deaminase	6
1.2.1.2	Plant hormone indole-3-acetic acid.....	7
1.2.1.3	Siderophore production.....	7
1.2.1.4	Organic phosphate mineralisation by phytase	8
1.3	Phosphate solubilisation by phosphate solubilising bacteria	9
1.3.1.	Organic acid production and plant growth promotion by phosphate solubilising bacteria.....	10
1.3.2.	Underlying mechanism of phosphate solubilisation and increased plant biomass	11
1.3.3.	Genes involved in phosphate solubilisation	11
1.3.4.	Genes involved in glucose dehydrogenase and pyrroloquinoline quinone production as a cofactor	12
1.3.5.	Other proteins that may also be involved in mineral phosphate solubilisation.....	16
1.4	Conclusions.....	19
1.5	Research hypothesis, objectives, and work flow.....	19
1.5.1.	Hypothesis	19
1.5.2.	Objectives and work flow	20

Chapter 2 Selection and Characterisation of Phosphate-Solubilising Bacteria

2.1	Selection of phosphate-solubilising bacteria.....	21
2.2	Methods	25
2.2.1.	Effective phosphate solubiliser strain selection	25
2.2.1.1	In vitro phosphate solubilisation	25
2.2.1.2	Tricalcium phosphate solubilisation by PSB.....	26
2.2.1.3	Detection of bacterial acidification of medium during tricalcium phosphate solubilisation.....	27
2.2.1.4	Hydroxyapatite solubilisation by PSB using glucose or sucrose as the sole carbon source	27
2.2.1.5	Iron phosphate solubilisation by PSB.....	28
2.2.1.6	ACC deaminase production by PSB.....	28
2.2.1.7	Phytase mineralisation by PSB.....	28
2.2.2.	Identification by 16S rRNA gene sequencing.....	29
2.2.3.	Further characterisation of isolates	29
2.2.3.1	Production of indole-3-acetic acid.....	29
2.2.3.2	Siderophore production.....	30
2.2.3.3	Hydroxyapatite solubilisation	31
2.2.4.	Organic acid profiling by High Performance Liquid Chromatography	32
2.2.5.	Effect of selected phosphate-solubilising bacteria on growth of ryegrass.....	35
2.2.6.	Statistical analysis.....	36

2.3	Results.....	38
2.3.1.	Screening for plant growth-promoting traits.....	38
2.3.2.	Identification of bacterial genera using 16S rRNA gene sequencing.....	39
2.3.3.	Statistical analysis of plant growth-promoting traits.....	42
2.3.4.	Selection of potential phosphate-solubilising bacteria - plant growth promoting bacteria.....	45
2.3.4.1	Phosphate solubilisation and organic acid production.....	45
2.3.4.2	Effect of EPS isolates on growth of ryegrass.....	47
2.4	Discussion.....	51
2.4.1.	Relationship between phosphate solubilisation bacteria, plant growth-promoting traits and ryegrass growth promotion.....	51
2.4.2.	Organic acid profile of the ten EPS strains.....	53
2.4.3.	Selection of three EPS strains for mutagenesis.....	54

Chapter 3 Identificaiton of Genes Implicated in Phosphate Solubilisaiton

3.1	Introduction.....	58
3.2	Methods.....	59
3.2.1.	Bacterial strains and culture conditions.....	59
3.2.2.	Construction of Mini-Tn5Km1 transposon mutant library.....	59
3.2.3.	Storage of the mini-Tn5Km1 transposon mutant library.....	60
3.2.4.	Mutant selection.....	62
3.2.5.	Solubilisation index of wildtype strains and mutants.....	64
3.2.6.	Identification of transposon insertion sites by touchdown PCR.....	64
3.2.7.	Transposon insertion site identification by cloning strategy.....	68
3.2.8.	Tricalcium phosphate liquid culture assay and colourimetric analysis.....	69
3.2.9.	The HSU HydroxP liquid culture assay.....	70
3.2.10.	Organic acid analysis.....	70
3.3	Results.....	71
3.3.1	Mini-Tn5Km1 mutant libraries - <i>Pseudomonas</i> sp. Ha200, <i>Enterobacter</i> sp. Wi28, and <i>Burkholderia</i> sp. Ha185.....	71
3.3.2.	Identification of mini-Tn5Km1 transposon insertion site.....	72
3.3.3.	Phosphate solubilisation by wildtype and mutants on tricalcium phosphate agar plates.....	73
3.3.4.	Phosphate solubilisation by wildtype and mutants in tricalcium phosphate liquid culture medium.....	77
3.3.5.	Genes involved in phosphate solubilisation in <i>Pseudomonas</i> sp. Ha200.....	79
3.3.6.	Phosphate solubilisation of <i>Pseudomonas</i> sp. Ha200 and mutant strain B8 involved in organic acid production.....	85
3.4	Discussion.....	87

Chapter 4 Genes Involved in Phosphate Solubilisation by *Burkholderia* sp. Ha185

4.1	Introduction.....	92
4.1.1.	Genome sequencing of <i>Burkholderia</i> sp. Ha185.....	93
4.1.1.1	Introduction to <i>Burkholderia xenovorans</i> LB400.....	93
4.1.1.2	Introduction to <i>Burkholderia phytofirmans</i> PsJN.....	94
4.2	Methods.....	97
4.2.1.	Genome sequencing of <i>Burkholderia</i> sp. Ha185.....	97
4.2.2.	Identify proteins of interest within the <i>Burkholderia</i> sp. Ha185 genome.....	97
4.2.3.	Inorganic phosphate solubilisation.....	98
4.2.3.1	Hydroxyapatite solubilisation by <i>Burkholderia</i> sp. Ha185 and the derivative mutants in HSU liquid culture assay.....	98
4.2.3.2	Hydroxyapatite solubilisation by organic acids.....	99
4.2.4.	Optimisation of PCR for amplification of the GC-rich <i>hem</i> operon.....	100
4.2.5.	Quantifying gene expression using Reverse Transcriptase-qPCR.....	100

4.2.5.1	Isolation of RNA from <i>Burkholderia</i> sp. Ha185 and synthesis of complementary DNA	100
4.2.5.2	PCR using cDNA template	102
4.2.5.3	Reverse Transcriptase-qPCR from cDNA template	102
4.2.6.	Protein expression	104
4.2.6.1	pARA- and pGEX-based expression of <i>bxpC</i>	104
4.2.6.2	Protein purification using a GST tag.....	105
4.2.6.3	Acrylamide gel electrophoresis.....	105
4.2.7.	Statistical analysis.....	106
4.3	Results.....	109
4.3.1.	Physiology of <i>Burkholderia</i> sp. Ha185	109
4.3.2.	The <i>bxp</i> operon.....	110
4.3.2.1	<i>bxp</i> genes arrangement, annotation and transcription.....	110
4.3.2.2	Confirming the <i>bxp</i> operon by PCR.....	114
4.3.2.3	Trans-complementation of the <i>bxpC</i> ::Tn5(F13) mutant.....	116
4.3.3.	The <i>hem</i> operon	118
4.3.3.1	<i>hem</i> gene arrangement, annotation and transcription.....	118
4.3.3.2	Defining functional protein association networks of HemX through STRING analysis	123
4.3.3.3	Trans-complementation of the <i>hemX</i> ::Tn5(F18) mutant	127
4.3.4.	Defining the mechanism of phosphate solubilisation by <i>Burkholderia</i> sp. Ha185 and the <i>bxpC</i> ::Tn5(F13) and <i>hemX</i> ::Tn5(F18) mutants	130
4.3.4.1	Mannitol utilisation by <i>Burkholderia</i> sp. Ha185	130
4.3.4.2	Phosphate released by <i>Burkholderia</i> sp. Ha185 wildtype and the derivative mutant strains	131
4.3.4.3	Culture acidification, phosphate solubilisation and organic acid production.....	134
4.3.4.4	Soluble phosphate and 2-keto-D-gluconic acid in the bacterial cytosol.....	140
4.3.4.5	Concentration of soluble phosphate and 2-keto-D-gluconic acid released over time	143
4.3.4.6	Hydroxyapatite solubilisation by organic acids in vitro	146
4.3.4.7	Relative expression levels of <i>hemC</i> , <i>hemX</i> , <i>bxpC</i> and <i>ppc</i> as determined by qRT-PCR	148
4.3.5.	Defining the role and expression of <i>BxpC</i>	152
4.3.5.1	Cloning <i>bxpC</i> into the pAY2-4 and pGEX expression vectors.....	152
4.3.5.2	Expression of <i>BxpC</i> using expression vectors pAY2-4 and pGEX.....	154
4.3.5.3	In silico analysis of <i>BxpC</i>	157
4.3.5.4	<i>BxpC</i> sequence alignment.....	160
4.3.6.	<i>hemX</i> encodes a bifunctional uroporphyrinogen-III synthetase/ uroporphyrin-III C-methyltransferase	163
4.3.6.1	Relationship between HemX and haem-dependent gluconate 2-dehydrogenase (acceptor).....	165
4.4	Discussion.....	170
4.4.1.	Direct oxidation pathway in <i>Burkholderia</i> spp.	170
4.4.2.	2-ketogluconic acid is the predominant organic acid released by <i>Burkholderia</i> sp. Ha185	171
4.4.3.	Mannitol metabolism of <i>Burkholderia</i> sp. Ha185.....	175
4.4.4.	pH-dependent hydroxyapatite solubilisation	176
4.4.5.	Genes of the <i>hem</i> operon.....	178
4.4.6.	Haem-dependent gluconate 2-dehydrogenase.....	180
4.4.7.	Gene redundancy in <i>Burkholderia</i> sp. Ha185	182
4.4.8.	Genes of the <i>bxp</i> operon and their resultant protein function.....	183
4.4.8.1	<i>bxpA</i> is related to <i>vgrG</i> from T6SS loci.....	183
4.4.8.2	<i>BxpB</i> contains a classical EF-hand calcium binding domain.....	187
4.4.8.3	<i>BxpC</i> contains a conserved <i>duf1311</i> domain with unknown function	188
4.4.8.4	<i>BxpD</i> contains a newly-described PAAR-repeat protein interects with <i>VgrG</i>	190
4.4.8.5	Unknown function of <i>BxpE</i>	191
4.4.9.	Putative transport model of the <i>Bxp</i> complex	191
4.4.10.	Alternative model of the <i>Bxp</i> complex	193

Chapter 5 *In situ* Localisation of *Burkholderia* sp. Ha185 in the Rhizosphere of Ryegrass

5.1	Root colonisation by <i>Burkholderia phytofirmans</i> strain PsJN	194
5.2	Methods	195
5.2.1.	Construction of GFP-tagged <i>Burkholderia</i> sp. Ha185	195
5.2.2.	Construction of in-frame <i>bxpC::gfp</i> and <i>hemX::gfp</i> fusions	196
5.2.2.1	Construction of <i>bxpC::gfp</i> (Ha185).....	196
5.2.2.2	Construction of <i>hemX::gfp</i> (Ha185)	199
5.2.3.	<i>In vivo</i> ryegrass plant bioassay.....	202
5.2.3.1	Perlite tube preparation.....	202
5.2.3.2	Ryegrass seed preparation and germination	203
5.2.3.3	Plant inoculation with GFP-tagged <i>Burkholderia</i> sp. Ha185	203
5.2.3.4	Ryegrass and bacterial cell harvesting	205
5.2.3.5	Hydroxyapatite solubilisation by <i>Burkholderia</i> sp. Ha185 in a plant-based plate assay.....	205
5.3	Results	205
5.3.1.	Phosphate solubilisation by <i>Burkholderia</i> sp. Ha185 in the rhizosphere	205
5.3.2.	<i>In situ</i> colonisation of GFP-tagged Ha185(pWM1007) on ryegrass roots.....	207
5.3.3.	Visualisation of <i>bxpC::gfp</i> (Ha185) and <i>hemX::gfp</i> (Ha185) fusion strains using fluorescence and confocal microscopy	213
5.4	Discussion	215
5.4.1.	Root colonisation by <i>Burkholderia</i> sp. Ha185	215
5.4.2.	Colonisation pattern of <i>Burkholderia</i> sp. Ha185 on ryegrass roots.....	216
5.4.3.	Expression of in-frame <i>hemX::gfp</i> (Ha185) and <i>bxpC::gfp</i> (Ha185) gene fusions	219

Chapter 6 General Discussion

6.1	Effective phosphate solubilisers	221
6.2	Hydroxyapatite solubilisation by 2-ketogluconate released by <i>Burkholderia</i> sp. Ha185	221
6.3	Novel genes associated with phosphate solubilisation	222
6.3.1.	<i>hemX</i> involved in 2-keto-gluconic acid production.....	222
6.3.2.	Putative 2-keto-gluconate transporter model of the Bxp complex.....	224
6.4	Plant root associated <i>Burkholderia</i> sp. Ha185	225
6.5	Future research	227
6.5.1.	Identify the unknown organic acid	227
6.5.2.	Identify the full complement of components involved in the HEM-GADH complex	227
6.5.3.	Identify the key function of BxpC protein.....	228
6.5.4.	Defining the interrelationship between the expression of <i>hemX::Tn5</i> (F18) and <i>bxpC::Tn5</i> (F13)	228
References	229

Appendix

Appendix A Chemicals and Reagents

A.1	Buffers and Solutions	263
A.1.1	Solutions for alkaline lysis plasmid mini-preps	263
A.1.2	SpecM solution	263
A.1.3	5X M9 salt solution	264
A.1.4	10x Trace elements solution.....	264
A.1.5	Molybdenum Blue reagent.....	264
A.1.6	Phosphate buffered saline (PBS)	264

A.1.7	Hoagland's solution	265
A.1.8	FeEDTA solution	265
A.2	Media	265
A.2.1	National Botanical Research Institute's Phosphate (NBRIP) growth media plates	265
A.2.2	Tricalcium or hydroxyapatite agar plate (TCaP/HydroxP)	265
A.2.3	Tricalcium Phosphate (TCaP) Liquid culture medium.....	266
A.2.4	HSU HydroxP Liquid culture medium	266
A.2.5	10x HSU buffer (pH 5.5).....	267
A.2.6	M9 minimal medium	267
A.2.7	SDS-PAGE solution Composition	267

Appendix B Microbiology Techniques

B.1	Optical density reading.....	268
B.2	Growth Curve determination and serial dilution plate counts	268

Appendix C Molecular Techniques and Manipulation

C.2	DNA techniques and manipulations.....	270
C.2.1	Isolation of genomic DNA from bacteria	270
C.2.2	Isolation of plasmid DNA from bacteria (mini-preps).....	270
C.2.3	DNA restriction enzyme digestions	270
C.2.4	DNA precipitation	271
C.2.5	Preparation of chemical-competent cells	271
C.2.6	Preparation of electrocompetent cells.....	271
C.2.7	Transformation of chemical-competent cells.....	271
C.2.8	Transformation of electrocompetent cells.....	272
C.2.9	Polymerase chain reaction (PCR).....	272
C.2.10	Agarose gel electrophoresis	273
C.2.11	DNA ligation.....	273
C.2.12	DNA sequencing preparation	273
C.2.13	Colony validation by BOX-PCR genomic fingerprinting	273
C.2.14	Visualising <i>Burkholderia</i> sp. Ha185 using a transmission electron microscope	275

Appendix D High-Throughput Screening of Plant Growth Promoting Traits of Each Phosphate-Solubilising Bacterial Isolates..... 275

Appendix E Quantitative Size Measurement of Hydroxyapatite and *Burkholderia* sp. Ha185 Particles..... 278

List of Tables

Table 1.3.1	Cloning of genes involved in mineral phosphate solubilisation.	15
Table 2.2.1	Organic acid standard profile analysed by HPLC.	34
Table 2.3.1	Screening for plant growth-promoting traits and identification of phosphate solubilising bacteria.	40
Table 2.3.2	Cluster grouping of PSB isolates screened for PGP traits by R statistical software.	43
Table 2.3.3	Two-way ANOSIM statistical analysis for differences between sites and bacteria genera.	44
Table 2.3.4	One-way SIMPER analysis between bacterial groups.	44
Table 2.3.5	Soluble phosphate detected and organic acids released by the ten EPS strains after 3 and 7 days incubated in HSU HydroxP medium.	48
Table 2.3.6	Combined data - PGP traits and pot-trial results for the EPS strains.	49
Table 2.4.1	Environmental habitat and organic acid produced by <i>Pseudomonas</i> spp., <i>Enterobacter</i> spp., and <i>Burkholderia</i> spp.	56
Table 3.2.1	Bacterial strains and plasmids used in this study.	61
Table 3.2.2	A list of oligonucleotide primers used in this study.	62
Table 3.3.1	Mutant library of <i>Pseudomonas</i> sp. Ha200 (B), <i>Enterobacter</i> sp. Wi28 (D) and <i>Burkholderia</i> sp. Ha185 (F).	74
Table 3.3.2	Solubilisation Index of wildtype <i>Pseudomonas</i> sp. Ha200, <i>Enterobacter</i> sp. Wi28, <i>Burkholderia</i> sp. Ha185 and their derivative mutants on TCaP and NBRIP plates.	76
Table 3.3.3	Colony forming units of wildtype <i>Burkholderia</i> sp. Ha185, <i>Pseudomonas</i> sp. Ha200, <i>Enterobacter</i> sp. Wi28, and their derivative mutants in TCaP liquid culture assay before incubation and at 72 h.	79
Table 3.3.4	Predicted homology for <i>Pseudomonas</i> sp. Ha200 ORFs identified from DNA sequencing.	82
Table 3.3.5	Soluble phosphate and organic acids released from HSU HydroxP liquid culture assay by wildtype <i>Pseudomonas</i> sp. Ha200 and <i>gcd::Tn5(B8)</i> over 72 h.	86
Table 4.1.1	Description of <i>B. xenovorans</i> LB400, <i>B. phytofirmans</i> PsJN and <i>Burkholderia</i> sp. Ha185.	96
Table 4.2.1	Bacterial strains and plasmid used in this study.	107
Table 4.2.2	Oligonucleotide primers used in this study.	108
Table 4.3.1	Predicted <i>bxp</i> operon homology for <i>Burkholderia</i> sp. Ha185 ORFs identified from DNA sequencing and protein sequence analysis.	112
Table 4.3.2	Predicted domains and ligand-binding motifs for the <i>Burkholderia</i> sp. Ha185 <i>bxp</i> operon.	113

Table 4.3.3	Predicted <i>hem</i> operon homology of <i>Burkholderia</i> sp. Ha185 ORFs identified from DNA sequencing and protein sequence analysis.....	125
Table 4.3.4	Predicted domains and ligand-binding motifs for the <i>Burkholderia</i> sp. Ha185 <i>hem</i> operon.....	126
Table 4.3.5	Soluble phosphate released by <i>Burkholderia</i> sp. Ha185 and its derivatives grown in HSU hydroxyapatite liquid culture medium with either glucose or mannitol.....	133
Table 4.3.6	Organic acid concentrations in culture supernatants of wildtype <i>Burkholderia</i> sp. Ha185 and its derivatives at 24, 48 and 72 h post-inoculation in HSU HydroxP culture with glucose or mannitol.....	138
Table 4.3.7	Organic acids present in sonicated cultures of wildtype <i>Burkholderia</i> sp. Ha185 and derivative mutant cells collected 72 h post-inoculation in HSU HydroxP medium with glucose or mannitol.....	143
Table 4.3.8	Organic acids produced by wildtype <i>Burkholderia</i> sp. Ha185 collected at various time points following incubation in HSU HydroxP medium containing glucose.	144
Table 4.3.9	PCR efficiencies and R ² values for primer pairs used in this study.....	150
Table 5.2.1	Bacteria strains and plasmids used in this study.....	201
Table 5.2.2	A list of oligonucleotide primers used in this study	202

List of Figures

Figure 1.1.1	The P cycle in soil.	3
Figure 1.2.1	Schematic diagram of plant growth-promoting rhizobacteria implicated in siderophore production, release of phytases, increased concentrations of indole-3-acetic acid (IAA), secretion of 1-aminocyclopropane-1-carboxylate (ACC) deaminase, and phosphate (P) solubilisation.	6
Figure 1.3.1	Schematic of Glucose dehydrogenase (Gcd) and gluconate dehydrogenase (Gad, or Gadh) involved in periplasmic glucose metabolism via direct oxidation pathway involved with pyrroloquinoline quinone (PQQ) in <i>Pseudomonas</i> spp.....	12
Figure 1.3.2	Schematic of of the <i>G. diazotrophicus</i> PA15 <i>pqq</i> cluster showing Tn5 transposon insertion (A) in <i>pqqB</i> (GDP12F6), <i>pqqC</i> (GDP29H1 and GDP9G4), and <i>pqqE</i> (GDP23A12) and in <i>gdhA</i> (GDP29H4) (B)	13
Figure 1.3.3	Acid production indicated by methyl red medium (A) and tricalcium phosphate solubilisation (B) on NBRIP plates by <i>P. fluorescens</i> CHA0 and the Δgcd , Δgad , and $\Delta gcd\Delta gad$ double mutants.	14
Figure 1.3.4	Glucose metabolism of <i>P. fluorescens</i> ATCC 13525 and the response of <i>S. elongatus</i> PCC 6301 <i>ppc</i> overexpression in <i>P. fluorescens</i>	18
Figure 1.5.1	An overview of experimental approach with four objectives.	20
Figure 2.1.1	Location of sampling sites where bacterial strains were isolated.....	22

Figure 2.1.2	Workflow of bacterial selection carried out in this study	23
Figure 2.2.1	Microtitre plate of soluble phosphate concentration measured by Murphy and Riley's colourimetric method.....	26
Figure 2.2.2	Photographs of the liquid culture assay	32
Figure 2.2.3	HPLC chromatogram of working standard organic acids.....	34
Figure 2.2.4	Pot trial 46 days after sowing (before 1 st cut)	36
Figure 2.3.1	Sample plates of screening phosphate solubilising isolates with plant growth-promoting traits.	38
Figure 2.3.2	Heatmap of two-way clustering generated by R statistical software version 2.12.2.....	42
Figure 2.3.3	Phosphate released from insoluble hydroxyapatite by the ten EPS strains and organic acid 2-keto-D-gluconic acid, pyruvic acid and an unknown acid detected from the HSU liquid culture filtrate at day 3 and day 7 analysed by HPLC.....	46
Figure 2.3.4	Glasshouse pot trial of the ten EPS inoculants. The mean dry weight of ryegrass is recorded as gram per pot ($n = 14$).....	47
Figure 2.3.5	Glasshouse pot trials of ten EPS isolates showed a significant correlation between dry shoot weight and total phosphorus.	50
Figure 3.2.1	An example of an initial screen of <i>Burkholderia</i> sp. mutants and their ability to solubilise tricalcium P on TCaP plate (A) and NBRIP (B1) after 3 days and 7 days respectively at 25°C. ..	63
Figure 3.2.2	The National Botanical Research Institute's Phosphate agar (NBRIP) seeded with approximately 10^6 cfu <i>Burkholderia</i> sp. Ha185 and incubated for 14 days at 25°C.	64
Figure 3.2.3	A schematic diagram of the genome walking strategy using touchdown PCR followed by cloning PCR amplicons into the pGEM [®] -T easy Vector.	67
Figure 3.2.4	Example of a 1% agarose gel showing PCR amplicons after touchdown PCR of mutants F66, F68, F69, F70, F72 and B37 using primer combinations of Sp2A + T7 and Sp2B + T7.	68
Figure 3.2.5	Cloning strategy for mutants F18 and F86 where the mini-Tn5 <i>Km1</i> transposon and unknown gDNA was cloned into the <i>Pst</i> I site of the pUC19 vector.	69
Figure 3.3.1	Image of mini-Tn5 <i>Km1</i> transposon mutants derived from <i>Burkholderia</i> sp. Ha185 patched on casamino (C, left) and glucose (G, right) M9 minimal medium.	72
Figure 3.3.2	Soluble phosphate measured by molybdenum blue reagent after incubating wildtype strains and their derivative non-auxotrophic mutants in TCaP liquid culture assay.....	78
Figure 3.3.3	Schematic of the <i>Pseudomonas</i> sp. Ha200 glucose dehydrogenase (<i>gcd</i>) encoding region.	81
Figure 3.3.4	Schematic representation of the membrane bound quinoprotein glucose dehydrogenase (<i>gcd</i>) arrangement in different gram-negative <i>Pseudomonas</i> spp. bacteria species and an <i>Enterobacter</i> sp. isolate.....	81
Figure 3.3.5	Schematic diagram of <i>pqq</i> gene ortholog neighbourhood analysis across several bacteria families by STRING 9.05.....	84

Figure 3.3.6	Schematic diagram of the <i>Pqq</i> open reading frame of <i>Pseudomonas fluorescens</i> Pf0-1 which consists of <i>pqqF</i> , <i>pqqA – E</i> , followed by a putative Peptidase S9.	85
Figure 3.3.7	Chromatogram of organic acids released by wildtype <i>Pseudomonas</i> sp. Ha200 in HSU HydroxP liquid culture medium at 24 h (black) and standard solution of 2-keto-D-gluconic acid (200 ppm) and 5-keto-D-gluconic acid (200 ppm) resuspend in HSU medium control (pink).	87
Figure 3.4.1	Glucose dehydrogenase (Gcd) and gluconate dehydrogenase (Gad) involved in periplasmic glucose metabolism via direct oxidation pathway involved with pyrroloquinoline quinone (PQQ) in <i>Pseudomonas</i> spp.	88
Figure 4.1.1	Phylogenetic tree based on 16S rRNA nucleotide sequences from <i>Burkholderia</i> species.	95
Figure 4.3.1	Electron microscope images of <i>Burkholderia</i> sp. Ha185. Red arrow indicates a single flagellum	109
Figure 4.3.2	Schematic representation of the <i>Burkholderia</i> sp. Ha185 <i>bxp</i> gene arrangement (A), domain annotations at the relative location of each open reading frame (B) and GC content of the <i>bxp</i> operon (C).	111
Figure 4.3.3	Schematic representation of the <i>Burkholderia</i> sp. Ha185 <i>bxp</i> gene arrangement and the location of the Tn5 transposon insertion (A), and agarose gel showing the corresponding amplification products (B).	115
Figure 4.3.4	Schematic diagram of the <i>bxp</i> operon. Green arrows denote the five ORFs, <i>bxpA</i> , <i>bxpB</i> , <i>bxpC</i> , <i>bxpD</i> and <i>bxpE</i> , predicted to compose the <i>bxp</i> operon.	116
Figure 4.3.5	Diagram of the p1311CMPB plasmid construct. The <i>bxpC</i> complementation plasmid was constructed by ligating the PCR amplicon (as shown in Figure 3.1.18) into the <i>Bgl</i> III site of the pME6010 plasmid.	117
Figure 4.3.6	Phosphate solubilisation assay. Bacterial strains <i>Burkholderia</i> sp. Ha185 wildtype, <i>hemX</i> ::Tn5(F18), <i>bxpC</i> ::Tn5(F13) and complementation strain 1311CMPB2 were incubated for 2 weeks at 25°C on a hydroxyapatite agar plate.	118
Figure 4.3.7	Schematic representation of <i>Burkholderia</i> sp. Ha185 <i>hem</i> gene arrangement (A) and domain annotations at the relative location of each open reading frame (B).	120
Figure 4.3.8	Schematic diagram of precorrin-2 biosynthesis.	122
Figure 4.3.9	Protein networks of HemX as determined by STRING analysis using <i>Burkholderia multivorans</i> 17616 as a model organism	124
Figure 4.3.10	Schematic diagram of the <i>hem</i> operon, consisting of three ORFs: <i>hemC</i> , <i>hemX</i> and <i>hemY</i>	128
Figure 4.3.11	DNA gel electrophoresis of PCR optimisation for the <i>hemC</i> + <i>hemX</i> and <i>hemX</i> DNA amplifications.	128
Figure 4.3.12	Phosphate solubilisation by <i>Burkholderia</i> sp. Ha185 wildtype, mutant <i>hemX</i> ::Tn5(F18) and its complementation strains.	129
Figure 4.3.13	<i>Burkholderia</i> sp. Ha185 (~10 ⁵ cfu) inoculated onto HydroxP agar containing either glucose (HydroxP - G) or mannitol (HydroxP - M)	130
Figure 4.3.14	Growth of <i>Burkholderia</i> sp. Ha185 and its derivatives in HSU hydroxyapatite liquid culture medium.	131

Figure 4.3.15	Phosphate released by <i>Burkholderia</i> sp. Ha185 and its derivatives in HSU hydroxyapatite liquid culture medium with glucose..	133
Figure 4.3.16	The pH of the medium (A) and amount of phosphate released (B) in the bacterial culture filtrates following 72 h incubation in HSU hydroxyapatite medium. Error bars denote SEM of three independent experiments ($n=3$).	135
Figure 4.3.17	Chromatograms of organic acids released by wildtype <i>Burkholderia</i> sp. Ha185 and derivative mutants..	137
Figure 4.3.18	Quantification of 2-keto-D-gluconic acid from HSU hydroxyapatite culture filtrate by HPLC analysis.	139
Figure 4.3.19	Chromatograms showing organic acids released by wildtype <i>Burkholderia</i> sp. Ha185 in HSU HydroxP liquid culture medium at 72 h with glucose (A) and in mannitol medium (HydroxP-M) (B).	140
Figure 4.3.20	Soluble phosphate and 2-keto-D-gluconic acid quantification from 1 mL of sonicated filtrate from cell pellet of bacteria grown in HSU hydroxyapatite liquid culture medium.	142
Figure 4.3.21	Liquid culture assay of <i>Burkholderia</i> sp. Ha185. Amounts of organic acids and soluble phosphate released by wildtype <i>Burkholderia</i> sp. Ha185 at 24, 36, 40, 44, 48 and 72 h post-inoculation (A).	144
Figure 4.3.22	Structure of calcium 2-keto-gluconate	145
Figure 4.3.23	Observed relationship between soluble phosphate concentration and 2-keto-D-gluconic acid released by wildtype <i>Burkholderia</i> sp. Ha185 in HSU HydroxP liquid culture medium based on a second order polynomial regression (blue solid line, solid triangle) ($R^2= 0.999$, $p < 0.001$).	146
Figure 4.3.24	Chemical structure of organic acids produced by <i>Burkholderia</i> sp. Ha185.	147
Figure 4.3.25	Hydroxyapatite solubilised by 2-keto-D-gluconic acid, DL-lactic acid, D-gluconic acid, pyruvic acid and D-malic acid in 1 mL of HSU HydroxP medium without glucose.	148
Figure 4.3.26	Expression ratios of the <i>Burkholderia</i> sp. Ha185 <i>hemC</i> , <i>hemX</i> , <i>bxpC</i> and <i>ppc</i> genes at 24, 36, 40, 48 and 72 h post-induction.	151
Figure 4.3.27	Analysis of the High resolution melting analysis (HRM) plot from <i>Burkholderia</i> sp. Ha185 (-dF/dT vs T).	151
Figure 4.3.28	Output from the SignalP 4.1 web-server for BxpC sequence analysis.	152
Figure 4.3.29	Diagram of the pGEXL3 plasmid construct. pGEXL3 was constructed by ligating the <i>bxpC</i> amplicon between the <i>Bam</i> HI and <i>Sal</i> I restriction sites in the pGEX-6P-1 expression vector.	154
Figure 4.3.30	Silver-stained polyacrylamide gel (15%) showing proteins expressed by pAY2-4 and pARAC3.	155
Figure 4.3.31	SDS-polyacrylamide slab gel (15%) showing expressed GST-BxpC. Sonicated cell pellet of <i>E. coli</i> DH10B pGEXL3 (L1) induced by IPTG at 20°C for 22 h, and its sonicated filtrate (L2).	156
Figure 4.3.32	Secondary structure and disorder prediction using the Phyre ² web-based server for BxpC aligned with the sequence of a protein of unknown function, duf1311 (PDB3gi7A).	158
Figure 4.3.33	Tertiary structure of BxpC predicted by I-TASSER using the crystal structures of a duf1311 family protein (PDB3gi7A) and cytochrome c nitrite reductase (PDB1qdbA) as templates.	159

Figure 4.3.34	Quaternary protein structure of the tetrameric duf1311 family protein (PDB3gi7).....	160
Figure 4.3.35	<i>Burkholderia</i> sp. Ha185 BxpC and homologous protein sequences obtained by BLASTp (rows 1–7) were aligned to a hypothetical protein with a duf1311 domain (highlighted in yellow) from <i>P. putida</i> kt2440 (row 8, NP_742474.1)..	162
Figure 4.3.36	Co-occurrence analysis of <i>Burkholderia</i> spp. PPC, HemC, HemX and HemY regions across different bacterial families using STRING 9.05.....	164
Figure 4.3.37	ClustalW alignment of FAD-dependent gluconate 2-dehydrogenase (subunit I) from <i>E. cypripedii</i> ATCC 29267, <i>B. phytofirmans</i> PsJN and protein sequences from <i>Burkholderia</i> sp. Ha185 (Contig00115).	166
Figure 4.3.38	ClustalW alignment of haem-dependent gluconate 2-dehydrogenase (acceptor) (subunit II) from <i>B. phytofirmans</i> strain PsJN and protein sequences from <i>Burkholderia</i> sp. Ha185.	167
Figure 4.3.39	ClustalW alignment of gluconate 2-dehydrogenase (acceptor) (subunit III) from <i>B. phytofirmans</i> strain PsJN, <i>E. cypripedii</i> and protein sequences from <i>Burkholderia</i> sp. Ha185.	168
Figure 4.3.40	ClustalW alignment of partial haem-dependent gluconate 2-dehydrogenase (acceptor) sequences from <i>B. phytofirmans</i> strain PsJN and <i>Burkholderia</i> sp. Ha185 (81–160 amino acid residues).	169
Figure 4.4.1	Direct oxidation pathway model for <i>Burkholderia</i> sp. Ha185. Hydroxyapatite solubilisation by 2-KGA derived from membrane-bound haem-dependent gluconate 2-dehydrogenase (HEM-GADH) using GA as a substrate and a haem molecule as the cofactor.	173
Figure 4.4.2	Schematic of the central carbon metabolism of acetic acid bacterium <i>Gluconobacter oxydans</i> using mannitol as a substrate.....	177
Figure 4.4.3	<i>Burkholderia</i> sp. Ha185 Contig00447 and Contig00115 (dark purple) are homologous to the <i>B. phytofirmans</i> PsJN <i>gadh</i> operon	181
Figure 4.4.4	Schematic representations showing bacteriophage T4 structure (A), T6SS assembly (B), the solid surface of the VgrG-PAAR complex crystal structure (C) and secondary protein structure of the VgrG-PAAR complex, represented in a ribbon diagram (D).	185
Figure 4.4.5	Rhs element Vgr protein alignment of <i>Burkholderia</i> sp. Ha185 and <i>Burkholderia</i> spp. using the BioCyc database collection.	186
Figure 4.4.6	Proposed model for Bxp complex-mediated transportation of 2-KGA from the extracellular space into the periplasmic space of <i>Burkholderia</i> sp. Ha185.....	192
Figure 5.2.1	GFP-tagged <i>Burkholderia</i> sp. Ha185(pWM1007) expressing GFP constitutively under fluorescent microscope (x60 magnification).....	196
Figure 5.2.2	Cloning strategy for in-frame <i>gfp</i> gene fusion for <i>bxpC::gfp</i> where <i>bxpC::gfp</i> was cloned into <i>KpnI</i> site of the pJP5608 vector resulting pBxpCGFP.	198
Figure 5.2.3	Schematic of in-frame gene fusion of the <i>bxpC::gfp</i> gene recombinant from pBxpCGFP transconjugated into <i>Burkholderia</i> sp. Ha185 genome.....	199
Figure 5.2.4	Schematic of the in-frame gene fusion of the <i>hemX::gfp</i> gene recombinant from pHemXGFP transconjugated into <i>Burkholderia</i> sp. Ha185 genome.....	200
Figure 5.2.5	A work-flow photograph of plant assay preparation.	204

Figure 5.3.1	Gyegrass growing on Hyp-G plate inoculated with (A) wildtype <i>Burkholderia</i> sp. Ha185 and <i>hemX::Tn5(F18)</i> (B) for 14 days.	207
Figure 5.3.2	Schematic of colonisation pattern of Ha185(pWM1007) on ryegrass root during plant growth.	208
Figure 5.3.3	Brightfield and fluorescent microscope images of GFP-tagged Ha185(pWM1007) colonising at various locations on ryegrass root.....	209
Figure 5.3.4	Brightfield and fluorescent microscope images of GFP-tagged Ha185(pWM1007) colonising both rhizodermis and epidermis of ryegrass root	211
Figure 5.3.5	Confocal microscope images of Ha185(pWM1007) colonisation.....	212
Figure 5.3.6	Fluorescent microscope images of <i>hemX::gfp</i> (Ha185) (A & B) and <i>bxpC::gfp</i> (Ha185) (C & D).	213
Figure 5.3.7	Confocal microscope images of <i>hemX::gfp</i> (Ha185) and <i>bxpC::gfp</i> (Ha185) colonisation.	214
Figure 5.3.8	Model of <i>Burkholderia</i> sp. Ha185(pWM1007) ryegrass root colonisation.....	218
Figure 6.4.1	Schematic diagram of <i>Burkholderia</i> sp. Ha185 in close proximity to a hydroxyapatite compound, plant root and root hair.....	226
Figure B.2	Growth of <i>Burkholderia</i> sp. Ha185 in LB broth medium (orange) and the MES HydroxP medium.....	271
Figure C.2	An example of DNA fingerprinting by BOX-PCR. Isolate Ha185 and its variants displayed similar band patterns.....	276
Figure E.1	Size distribution of control HydroxP particles and <i>Burkholderia</i> sp. Ha185 bacterial cell particles.....	281
Figure E.2	Size distribution of <i>Burkholderia</i> sp. Ha185 in MES HydroxP medium at 24 h, 48 h and 60 h incubation.....	283

Acronyms and Abbreviations

2, 5-KGA	2, 5-diketo-gluconic acid
2K-6P-GA	2-keto-6-phosphogluconate
2-KGA	2-keto-D-gluconic acid
5-KGA	5-keto-D-gluconic acid
6P-GA	6-phospho-D-gluconate
ACC	1-aminocyclopropane-1-carboxylate
Al	Aluminium
AlP	Aluminium phosphate
AMF	Mycorrhizal fungi
ANOSIM	Analysis of multivariate similarities
ANOVA	One-way analysis of variance
Ba	Ballantrae
BCC	<i>Burkholderia cepacia</i> complex
Ca	Calcium
Cd	Cadmium
cDNA	Complementary DNA
DCaP	Dicalcium phosphate
DMSO	Dimethyl sulfoxide
dsDNA	Double-stranded DNA
ED pathway	Entner-Doudoroff pathway
EE	Eyrewell exotic forest
EN	Eyrewell native forest
EPS	Effective P solubilisers
FeP	Iron phosphate
GA	Gluconic acid
GADH	Gluconate dehydrogenase
Gcd	Glucose dehydrogenase
gDNA	Genomic DNA
GFP	Green fluorescent protein
Ha	Haast
HEM-GADH	Haem-dependent gluconate 2-dehydrogenase
Hog	Hoagland's solution
HPLC	High Performance Liquid Chromatography

HRM	High Resolution Melting Analysis
HydroxP	Hydroxyapatite
IAA	Indole-3-acetic acid
ICP-MS	Inductively Coupled Plasma Mass Spectrometry
IMG	Integrated Microbial Genomes
IPTG	Isopropylthio- β -galactoside
KEGG	Kyoto Encyclopedia of Genes and Genomes
LA	Lactic acid
MA	L-Malic acid
MDH	Malate dehydrogenase
MDW	Mean dry weight
MFS	Major facilitator superfamily protein
MPS	Mineral phosphate solubilisation
Na-Phy	Sodium phytate
NBRIP	National Botanical Research Institute Phosphorus
NCBI	National Center for Biotechnology Information
NGS	Next Generation Sequencing
P	Phosphorous
PBE	Plant-associated beneficial and environmental group
PBG	Porphobilinogen
PDB	Protein Data Bank
PEP	Phosphoenolpyruvate
PEPC	Phosphoenolpyruvate carboxylase
PGP	Plant growth-promoting
PGPR	Plant growth-promoting rhizobacteria
PQQ	Pyrroloquinoline quinone
PR	Phosphate rock
PSB	Phosphate-solubilising bacteria
PSB-PGPB	Phosphate-solubilising bacteria – plant growth promoting bacteria
PyrA	Pyruvic acid
qRT-PCR	Quantitative real-time PCR
RE-PCR	Restriction site PCR
RSO	Restriction Site Oligomers
SDS-PAGE	Sodium dodecyl sulphate-polyacrylamide gel electrophoresis
SEM	Standard errors of mean
SI	Solubilisation index

SIMPER	Similarity percentages - species contributions
T3SS	Type III secretion system
T6SS	Type VI secretion system
TCA	Tricarboxylic acid cycle
TCaP	Tricalcium phosphate
TECP	Tris(2-carboxyethyl) phosphine
TRP	Tetratricopeptide repeat domain
TSB	Tryptic soy broth
Un2	Unknown2
VgrG	Valine-glycine repeats G
Wh	Whatawhata
Wi	Winchmore
ZnP	Zinc phosphite

Chapter 1

Introduction and Literature Review

1.1 Introduction

The main agricultural system in New Zealand is pastoral farming; the total area under pasture is 15 million hectares which is more than half of the total land area of New Zealand (27 million hectares). Farms in New Zealand carry a total of 32.4 million sheep, 9.7 million dairy and beef cattle, and 1.1 million deer (Agriculture Production Statistics, 2009). Continued inputs of phosphate (P) fertiliser are required to increase and maintain soil fertility and productivity of pastures in New Zealand. In 2007, 1.62 million tonnes of phosphorus (P) fertiliser was applied to New Zealand farmland (Fertiliser and Lime Applied 2007). These ongoing P inputs result in long term accumulation of P in soil, together with contaminants, such as cadmium and fluoride, which can be passed on in the food chain and are potentially toxic to animals and humans (Cronin et al., 2000; Loganathan et al., 2001, Järup and Åkesson, 2009). Excessive P inputs also accelerate eutrophication via leaching and run-off to waterways (Figure 1.1.1) (Caruso, 2000; Heath, 2007; Özkundakci et al., 2010).

Environmental and economic concerns associated with P fertiliser use have highlighted the need for effective strategies for P management. Microorganisms from the rhizosphere are known to contribute to plant growth promotion by several mechanisms, one of which is to solubilise adsorbed or precipitated P in the rhizosphere, releasing soluble P for plant uptake (Chen et al., 2006). Phosphate solubilising bacteria (PSB) are able to solubilise insoluble P that is already present in soil, primarily as a result of fertiliser applications (Chen et al., 2006; Naik et al., 2008; Elkoca et al., 2008).

This research was part of the MBIE-funded programme “Microbes for reduced P inputs” (C10X0904), and aimed to identify novel genes in PSB involved with P solubilisation. There is limited understanding of the mechanisms involved in microbial P solubilisation, therefore, this research endeavoured to identify and characterise the expression of genes involved in mineral P solubilisation (MPS). This work will contribute to the greater goal of increasing the efficiency of P utilisation in pastoral agriculture.

1.1.1. An overview of phosphate rock and phosphate fertilisers

Modern agricultural system depend on continued application of P fertiliser to increase and maintain production (Haygarth et al., 2013). This in turn relies on importation of phosphate rock to manufacture P fertilisers such as superphosphate. Phosphate rock is currently imported into New Zealand predominately from China, USA and Morocco. These countries hold the world's largest phosphate rock reserves, accounting for 66% of the world total (Jasinki, 2008). The chemical composition of phosphate rock varies depending on the geology of the source mine, but they contain mainly fluorapatite ($\text{Ca}_{10}\text{F}_2(\text{PO}_4)_6$) and hydroxyapatite ($\text{Ca}_{10}\text{OH}_2(\text{PO}_4)_6$), and can also contain other iron, aluminium and calcium minerals (Khasawneh and Doll, 1978; Bolan et al., 1990). Phosphate rock is a non-renewable resource and world consumption has been forecast to increase by 3-4% each year into the future (Maene, 2007). Moreover, worldwide phosphate rock supplies are projected to decline in the next 50-100 years as readily available reserves decline and the world population continues to grow and the demand for foods increases (Smil, 2000; Jasinski, 2008; Cordell et al., 2009). For these reasons, more effective use of soil and fertiliser P resources is required to increase plant P availability, maintain crop production and thereby reduce P fertiliser inputs.

Phosphate is an essential element and is second only to nitrogen for limiting plant growth. The P cycle in soil is a complex system which involves both organic P and inorganic P. The soil contains three main P "pools"; plant available soluble P, unavailable organic P and unavailable sparingly soluble mineral P. Organic P resides in plant residues, animal excreta and microbial detritus. Organic P is not directly available to plants and inorganic P must be released from organic P by biochemical mineralisation before it can be taken up by plants from the soil solution. Inorganic and organic P in soil are increased by inputs of P fertilisers, and the fertilisers mainly used in New Zealand are superphosphate and diammonium P ($(\text{NH}_4)_2\text{HPO}_4$). Single superphosphate contains approximately 30% calcium dihydrogen phosphate ($3\text{Ca}(\text{H}_2\text{PO}_4)_2 \cdot \text{H}_2\text{O}$), 45% gypsum, 10% dicalcium phosphate (CaHPO_4), 10% iron, silicon and aluminium oxides, and 5% water (Budavari et al., 1996). The P in superphosphate is mainly water soluble and is therefore immediately available to plants, although the availability reduces with time due to adsorption of P on soil mineral surfaces and the formation of sparingly soluble minerals (Condrón et al., 1995; Goldstein, 1987; Rodríguez and Fraga, 1999). As a result a large fraction of P becomes "fixed" in soil (Figure 1.1.1). Precipitation or adsorption occurs readily by chelating with aluminium (Al) and iron (Fe) in acidic soil and with calcium (Ca) in alkaline soil, forming insoluble mineral precipitates (Goldstein, 1987; Rodríguez and Fraga, 1999). Insoluble P derived from fertilisers must be solubilised before plant uptake, in the form of orthophosphate (HPO_4^{2-} , H_2PO_4^-) in soil solution. However, plant available P in soil solution is usually lower than 1% of the total amount of P present in soil (Pierzynski, 1991). Haynes and Williams (1992) analysed the

long-term effect of P fertiliser inputs on soil P under grazed pasture, and showed there was a 144% increase in Ca-bound P, and increases of 87% and 17% in Al- and Fe-bound P, respectively, in fertilised soils compared with unfertilised soil.

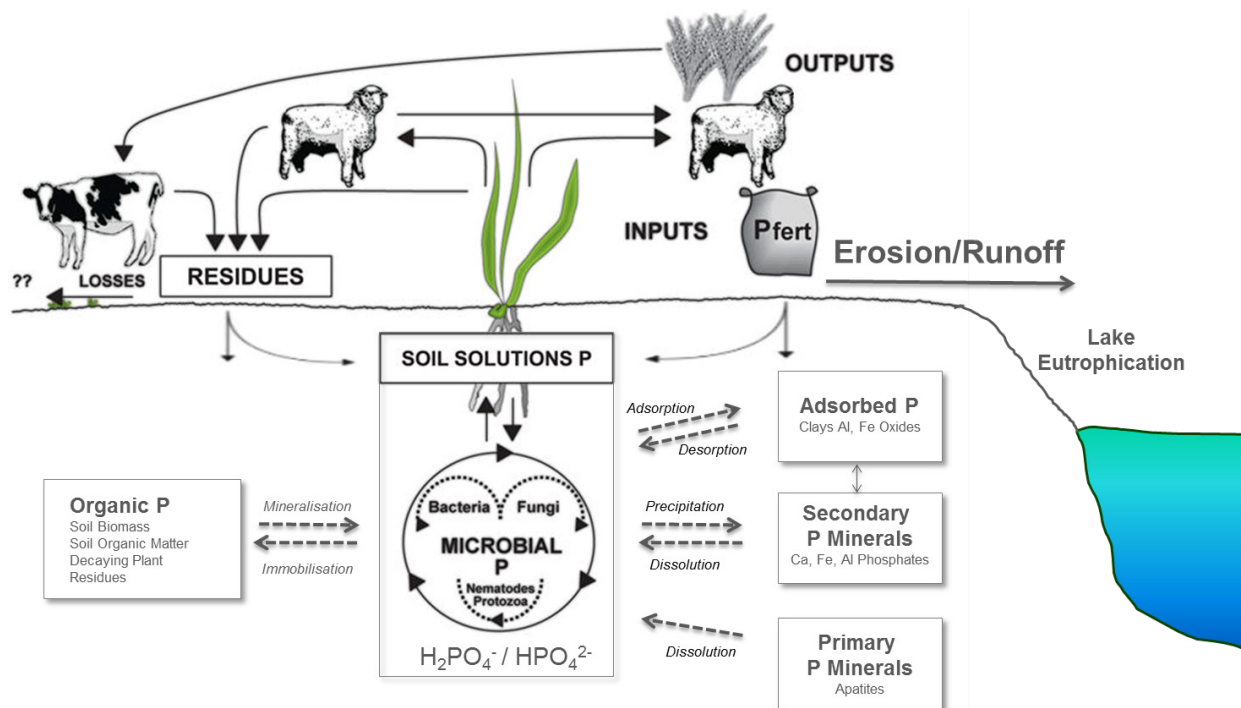


Figure 1.1.1 The P cycle in soil. An overview of soil chemistry, physical and microbiological processes influencing the direction of soil solution, inorganic and organic phosphate (modified from Richardson et al., 2009).

1.1.2. Environmental impacts of overuse of phosphate fertilisers

Significant amounts of P fertiliser are applied to soil each year to maintain agricultural production. However, the presence of large amounts of P in soil increases the risk of loss of P to waterways. The annual input of P fertiliser was estimated at 2.11 million tonnes throughout New Zealand in 2001, and P losses were approximately 34% (0.71 million tonnes) of the total input through erosion of soil, effluent ponds on farm, burial after erosion, and agricultural run-off (Parfitt et al., 2008). This has raised concerns about accelerated eutrophication of New Zealand rivers and lakes and associated declines in water quality, and consequent risks to human and livestock health (Heath, 2007; Bayer et al., 2008). Eutrophication occurs when excessive growth of phytoplankton, such as algae and aquatic plants results in imbalance of primary and secondary productivities and the lake ecosystem (Khan

and Ansari, 2005). Phosphorus is one of the limiting nutrients causing eutrophication of rivers and lakes, and most P lost to waterways is through a combination of leaching and surface run-off (Figure 1.1.1) (Parfitt et al., 2008). Lake water quality in New Zealand is negatively correlated with proximity to areas under intensive agriculture such as dairying, and is more likely to occur in shallow water bodies (Lake Water Quality in New Zealand, 2007). There are 3,756 lakes in New Zealand, and 43% of these are located in areas by pasture farming. The most eutrophic lakes (i.e. hypertrophic) are located in the Waikato region, due to the intensive farming systems, which support a third of New Zealand's dairy farms. Many New Zealand lakes are continuously declining in water quality (Hamill, 2006).

Ongoing P fertiliser applications can also result in accumulation of the toxic contaminants, such as fluoride (F) and cadmium (Cd). Fluoride and Cd are present in trace amounts in superphosphate, where F is primarily from fluorapatite ($\text{Ca}_{10}(\text{PO}_4)_6\text{F}_2$) (Kim, 2005). It was estimated that 48 tonnes of Cd entered soil from fertiliser applied throughout New Zealand in 2002 and 20% of grazing animals exceeded the maximum limit for Cd concentration in kidneys, as set by the New Zealand Food Authorities (Loganathan et al., 2003). Furthermore, it was estimated 7-30 tonne $\text{ha}^{-1} \text{yr}^{-1}$ of particulate-bound and colloiddally-bound Cd is lost by surface runoff and directly to waterways in horticultural cropping soils (Kim, 2005). Cadmium is considered a highly toxic heavy metal and farm workers may be at risk of chronic poisoning through exposure to low concentrations of Cd over an extended period of time (Kim, 2005). The most common effects of Cd chronic poisoning in humans are kidney damage, liver cirrhosis and lung disease (Hallenbeck, 1984; Pan et al., 2010).

There is a clear need to investigate means of improving the plant availability and utilisation of soil and fertiliser P, especially in intensive, high input agricultural systems such as dairying in New Zealand. One strategy is to employ microorganisms sourced from New Zealand soil as biofertilisers to improve P acquisition and plant growth. The rhizosphere is defined as the area of soil immediately adjacent to plant roots where biological activity is stimulated and mediated by energy-rich carbon from plants root exudates (Shi et al., 2011). Bacteria that colonise the rhizosphere are known as "rhizobacteria", and their activity and diversity is known to be influenced by organic carbon produced by the root in the form of soluble root exudates and lysed root cells, which differ between plant species (Berendsen et al., 2012; Peiffer et al., 2013; Bakker et al., 2013; Shi et al., 2013). Many rhizobacteria are known to promote plant growth by several mechanisms (Saharan and Nehra, 2011).

1.2 Plant growth-promoting rhizobacteria

1.2.1. Traits of growth-promoting rhizobacteria

Rhizosphere microorganisms are known to play a key role in plant growth promotion and can be categorised into three major groups; mycorrhizal fungi, nitrogen-fixing bacteria, and plant growth-promoting rhizobacteria (PGPR) (Souchie et al., 2006; Patel et al., 2008; Adesemoye et al., 2009). In particular, PGPR facilitate nutrient uptake, improve tolerance of plants to environmental stress and increase crop production (Vessey, 2003; Khalid et al., 2004). The phenomena of mutualism and symbiosis between PGPR and plants within the rhizosphere were proposed by Goldstein et al. (1999). Plants provide carbon sources for microorganisms via root exudates and PGPR provide nutrients, hormones, or antibiotics that promote plant growth. Several mechanisms underpin the close relationship between PGPR and plant roots and include indirect and direct mechanisms. Indirect mechanisms are those which promote plant growth by suppression of plant pathogens, such as the production of antibiotics, phenazines or siderophores (Waller and Cook, 1983). Bacterial production of plant growth-promoting substances such as cytokinins, 1-aminocyclopropane-1-carboxylate (ACC) deaminase and indole-3-acetic acid (IAA) are direct mechanisms (Berea et al., 1976; Naik et al., 2008). Phosphate solubilisation by organic acid production and/or other mechanisms by bacteria is also an important plant growth-promoting mechanism (Chen et al., 2006). There has been growing interest worldwide in the application of PGPR as biofertilisers, especially rhizobacteria capable of P solubilisation, to sustain agricultural production under reduced P fertiliser inputs (Lucy et al., 2004; Lugtenberg and Kamilova, 2009). Yazdani et al. (2009) were able to maintain corn production while reducing P fertiliser inputs by 50% using a mixture of PGPR consisting of *Azotobacter corooococum*, *Azospirillum brasilense*, *Pseudomonas putida*, and *Bacillus lentus*. Plant growth-promoting rhizobacteria have also been successfully applied in horticultural systems. For example, Esitken et al. (2010) showed a significant increase in total biomass and fruit production of strawberry by using PGPR *Pseudomonas* BA-8, *Bacillus* OSU-142 and *Bacillus* M-3. Total P concentration in strawberry leaves also significantly increased.

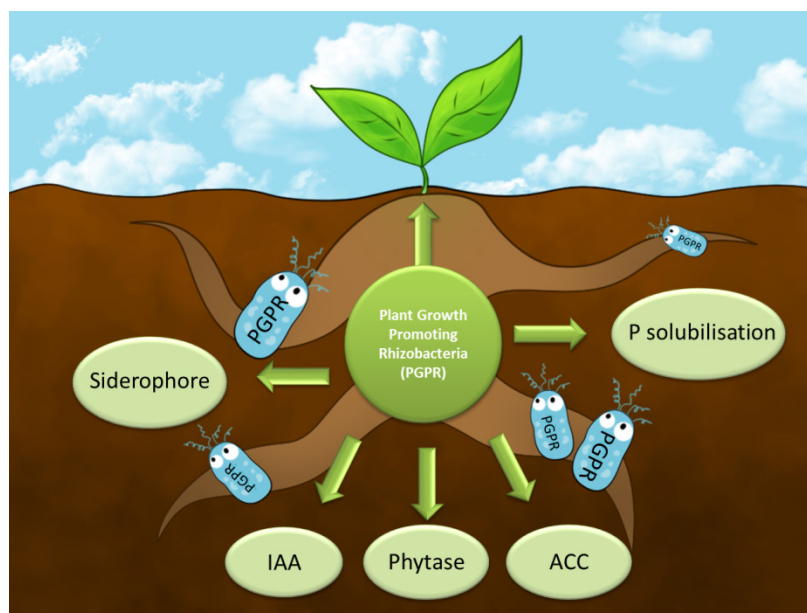


Figure 1.2.1 Schematic diagram of plant growth-promoting rhizobacteria implicated in siderophore production, release of phytases, increased concentrations of indole-3-acetic acid (IAA), secretion of 1-aminocyclopropane-1-carboxylate (ACC) deaminase, and phosphate (P) solubilisation.

1.2.1.1 1-aminocyclopropane-1-carboxylate deaminase

The bacterial enzyme ACC deaminase is found to promote plant growth by lowering plant ethylene levels (Bernard et al. 1998). The chemical compound ACC is an immediate precursor of ethylene, a hormone that inhibits root elongation and is synthesised and exuded from plant roots (Honma and Shimomura, 1978). Bacteria expressing ACC deaminase promote hydrolysis of ACC to ammonia and α -ketobutyrate. This decreases concentrations of ACC and ethylene that are produced by stressed plant roots during development and therefore stimulates root growth. Mutation of the ACC deaminase gene (*acdS*) of *Enterobacter cloacae* UW4 has been shown to significantly decrease root elongation in canola seedlings (Li et al., 2000). Moreover, ACC deaminase producing strains, such as *Pseudomonas* spp. isolated from maize rhizosphere, have been shown to increase total maize biomass (Shaharoon et al., 2006). Production of ACC diaminase by rhizobacteria is an important factor in reducing the effects of biotic and abiotic stressors on the plant root (Glick et al., 2007). For example, plant tolerance to heavy metals in soil may be increased by the application of PGPR. Madhaiyan et al. (2007) demonstrated increased tomato plant growth by using PGPR *Methylobacterium oryzae* strain CBMB20 and *Burkholderia* sp. strain CBMB40, concluding these PGPR reduced stress-induced ethylene production, caused by nickel and cadmium, via the secretion

of ACC deaminase. Furthermore, ACC deaminase-producing PGPR would be essential for effective phytoremediation of copper contaminated soils (Zhang et al., 2011), and are considered as excellent candidates for metal contaminated soil remediation (Khan et al., 2009).

1.2.1.2 Plant hormone indole-3-acetic acid

Indole-3-acetic acid (IAA) is a major plant hormone (also known as auxin). IAA is well known as an important plant growth-promoting factor due to its role in the initiation of cell division and differentiation and root elongation and proliferation (Idris et al., 2007; Peer et al., 2011). Plant growth-promoting rhizobacteria can synthesise IAA via three major tryptophan-dependent pathways; the indoleacetamide, the indoleacetonitrile, and the indolepyruvate pathways which are widespread among soil bacteria (Bartiel, 1997; Patten et al., 2012). Auxin has been detected in liquid culture supernatants of some rhizobacteria and has been suggested as a signalling molecule that activates several plant colonisation and adaptation genes (Van Puyvelde et al., 2011; Zúñiga et al., 2013). Zúñiga et al. (2013) showed that *Arabidopsis thaliana* plants increased in total fresh weight, primary root length, chlorophyll content, and the number of root hairs when inoculated with IAA producing *Burkholderia phytofirmans* PsJN strain, although the authors reported that both ACC deaminase activity and quorum sensing signalling by *N*-acyl-homoserine lactones (AHL) also played key roles in plant growth promotion by *B. phytofirmans* PsJN. It was found that AHL produced by *Sinorhizobium meliloti* enhanced accumulation of IAA in root and shoot tissues of the legume *Medicago truncatula* (Mathesius et al., 2003). Type VI secretion systems are extracellular protein secretion systems postulated to puncture the cell membranes of targeted cells and deliver effector proteins using an apparatus that is structurally similar to bacteriophage tail (Leiman et al., 2009; Cascales and Cambillau, 2012). Interestingly, genes encoding for type VI secretion system (T6SS) were found upregulated during IAA production in *Azospirillum brasilense* (Van Puyvelde et al., 2011). This indicates that the expression of T6SS may be altered by plant IAA and has direct interaction with plant signalling pathways by the production of surface and transporter proteins (Van Puyvelde et al., 2011).

1.2.1.3 Siderophore production

Iron is essential to metabolic function but is not readily bioavailable due to the low solubility of the iron-oxide forms in soil. Rhizobacteria scavenge iron from the environment by the secretion of siderophores which facilitate cellular absorption of iron and are considered beneficial to both the rhizobacteria and the plant (Andrews et al., 2003; Peralta et al., 2012). Siderophores are low molecular weight (<1000 Da), high affinity iron(III) chelating compounds and form ferri-siderophore complexes (Hider and Kong, 2010). These complexes are transported into the cytosol by cytosolic membrane ATP-binding cassette (ABC) transporters via the TonB transporters at the periplasmic

space, followed by redox reduction to iron(II) in the cytosol (Crosa et al., 2002; Hider and Kong, 2010). To date, more than 500 different siderophores have been documented but only 270 of them have been structurally characterised (Hider and Kong, 2009). Siderophores produced by rhizobacteria can inhibit pathogenic fungal growth in the rhizosphere as fungal siderophores exhibit lower affinity for iron(III) (O'Sullivan et al., 1992). In particular, the siderophore producing rhizobacteria *Pseudomonas fluorescens* strain MPF47 suppressed the proliferation of the fungal pathogen *Rhizoctonia solani*, and facilitated iron uptake by tomato (*Lycopersicon esculentum* Mill.) plants (Solanki et al., 2013). *P. fluorescens* strain MPF47 also enhanced plant height, total biomass, total fruit number, available iron and total chlorophyll content compared with the infected control. Therefore, siderophores produced by rhizobacteria are considered as a possible option for biocontrol against fungal pathogens and phytopathogenic microorganisms, and subsequently promote plant growth (Beneduzi et al., 2012). Moreover, siderophore producing rhizobacteria as bioinoculants have potential to replace conventional chemical fungicides and insecticides for suppressing root diseases and promoting plant growth (Ahemad et al., 2011; Beneduzi et al., 2012).

1.2.1.4 Organic phosphate mineralisation by phytase

A large proportion of P in soil exists as *myo*-inositol hexakisphosphate (commonly referred to as phytic acid or phytate) and is not available for plant uptake (Pierzynski, 1991). Phytate most commonly exists as metal ion precipitates such as calcium, sodium, aluminium or iron phytate, as well as phytate ions adsorbed to soil particles (Turner et al., 2002). Phytate is found to be the most abundant form of organic P in soil where organic P accounts for at least 20 - 80 % of total soil P (Dalal, 1977; Richardson, 1980; Giles et al., 2011). Release of inorganic P from phytate involves a combination of dissolution and enzyme hydrolysis (Condrón et al., 2005). Phytate can be hydrolysed by four distinct families of phytase enzymes; histidine acid phosphatases, β -propeller phytases, purple acid phosphatases, as well as cysteine phytase (Chu et al., 2004; Lei et al., 2007). However, it has been demonstrated by Tang et al. (2006) that low molecular weight organic acids are able to increase P released from insoluble phytate salts. Citric acid was found to be more effective than malic and oxalic acids in solubilising phytate salts before enzyme hydrolysis by metal mediated phytase activation or solubilisation via divalent metal chelation (Tang et al., 2006). Furthermore, the organic acid producing isolate *Pseudomonas* sp. CCAR59 improved shoot P accumulation of a wildtype *Nicotiana tabacum* (tobacco) plant-line and a citric acid over-producing tobacco line by approximately 7-fold and 9-fold respectively, using insoluble calcium phytate as sole P source (Giles et al., 2013). Phytate mineralisation by phytase-producing microorganisms is increasingly of interest as a potential mechanism to increase plant production (Singh et al., 2011, Kumar et al., 2013, Gujjar et al., 2013). In addition, acidification by microorganisms complements mobilisation of P in soil by

ligand mineral dissolution (chelation) or direct ligand exchange (sorption) which enhances phytate mineralisation and P acquisition at the rhizosphere. Therefore, more efficient nutrient P management systems using organic acid producing and phytate-mineralizing soil rhizobacteria have been proposed (Richardson et al., 2011; Giles et al., 2013)

1.3 Phosphate solubilisation by phosphate solubilising bacteria

The production of low molecular weight organic acids by microorganisms in proximity to the plant root is a widely accepted mechanism for solubilisation of soil P (Jones, 1998; Rodríguez and Fraga, 1999; Richardson, 2001). In particular, organic acids are known to reduce pH and acidify the rhizosphere which directly increases the solubility of various precipitated forms of P such as aluminium P, iron P and the most abundant form in pasture soil, calcium P (Awasthi et al., 2011). Some microorganisms have been found to solubilise P from phosphate rocks. Applying PSB as biofertilisers is one approach that could be taken to improve plant access to P reserves stored in pasture soil, thereby reducing the need for ongoing fertiliser inputs. However, the mechanisms by which PSB solubilise P are not fully understood. Phosphate-solubilising bacteria have been isolated from various environments, including agro-industrial wastes (Vassileva et al., 2010), subtropical soil (Chen et al., 2006), rice and banana fields (Naik et al., 2008), rhizosphere soil of sugarcane plant (*Saccharum* spp.) (Upadhyay et al., 2009), maize (*Zea mays*) (Vyas and Gulti, 2009; Oliveira et al., 2009) and from white clover (*Trifolium repens*) and pine trees (*Pinus radiata*) (Bolan et al., 1994). Phosphate solubilising bacteria have been shown to solubilise insoluble forms of P such as tricalcium P (TCaP), hydroxyapatite (HydroxP) and phosphate rocks under laboratory conditions. The P solubilisation phenotype is often identified by a zone of clearance around bacterial colonies on Pikovskaya's agar or National Botanical Research Institute Phosphorus (NBRIP) agar and/or colour change on agar with methyl red as a pH indicator (Pikovskaya, 1948; Nautiyal, 1999). Isolates from these studies belong to a range of bacterial and fungal genera including *Aspergillus*, *Arthrobacter*, *Bacillus*, *Burkholderia*, *Chryseobacterium*, *Penicillium*, *Pseudomonas*, *Rhodococcus*, and *Serratia*. Other commonly reported PSB include *Achromobacter*, *Agrobacterium*, *Burkholderia*, *Enterobacter*, *Erwinia*, *Flavobacterium*, *Micrococcus*, and *Rhizobium* spp. (Goldstein, 1987; Rodríguez and Fraga, 1999). While a range of bacterial genera have been reported to solubilise P, only a few studies have isolated PSB from pasture soil. Phosphate solubilising *Bacillus* spp. were isolated from pasture in Brazil (Souchie et al., 2006), pastures and wetlands in the Himalayas (Pal, 1998), and P-solubilising *Actinobacteria*, *Pseudomonadaceae* and *Moraxellaceae* were found to be abundant in New Zealand pasture soil (Mander et al., 2012).

1.3.1. Organic acid production and plant growth promotion by phosphate solubilising bacteria

It has been proposed that low molecular weight organic acids produced by PSB decrease the adsorption of P to metal ions, facilitating increased P solubilisation in soil through the formation of metal-organo compounds (i.e. the Fe, Ca or Al ions in soil are chelated by the organic anions) releasing soluble P into the soil solution (Illmer and Schinner, 1992; Rodríguez and Fraga, 1999). Bolan et al. (1994) showed that annual ryegrass (*Lolium rigidum*) dry matter could be increased by 73% and 88% with the addition of oxalic and citric acid to phosphate rock respectively. Organic acids produced by PSB are therefore considered the main mechanism responsible for P solubilisation. Chen et al. (2006) identified a highly effective *Arthrobacter* sp. strain from subtropical soil and showed that production of citric and lactic acids were key mechanisms in P solubilisation. Vyas and Gulti (2009) demonstrated that PSB fluorescent *Pseudomonas* sp. isolated from the rhizosphere of sea-buckthorn (*Hippophae rhamnoides*) produced gluconic acid, oxalic acid, 2-ketogluconic acid, lactic acid, succinic acid, formic acid, citric acid and malic acid in culture filtrates that contained TCaP as the primary P source. The isolates also caused extended root length and plant height as well as increased shoot and root dry weights in *Zea mays* var. Girija. Many studies have reported increased plant biomass resulting from treatment with PSB. Elkoca et al. (2008) demonstrated increased plant height and shoot and root dry weights in chickpea (*Cicer arietium*) inoculated with PSB *Bacillus megaterium* in a field trial. *Serratia marcescens* and *Pseudomonas* sp. also increased maize biomass by 50% and 18%, respectively, in a 96 day field trial (Hameeda et al., 2008). These two PSB strains were found to produce gluconic acid and survived for up to 96 days after sowing. Seed inoculation of finger millet (*Eloisine coracana*), maize (*Zea mays*), amaranth (*Amaranthus hypochondriacus*), buckwheat (*Fagopyrium esculentum*), and frenchbean (*Phaseolous vulgaris*) with *Bacillus* sp. isolates from pasture and wetland (acidic soil) were found to increase crop production (Pal, 1998). The author concluded seed inoculation with an efficient PSB strain was beneficial in boosting crop yield.

1.3.2. Underlying mechanism of phosphate solubilisation and increased plant biomass

Although the studies reported above have demonstrated that PSB promote plant growth and increase total biomass, they have not investigated other plant growth-promoting traits such as production of IAA and siderophores or organic P mineralisation enzymes (i.e. phosphatases and phytase). Increases in total plant biomass may have resulted from plant growth-promoting traits other than MPS. For example, De Freitas et al. (1997) demonstrated that a PSB *Bacillus thuringiensis* isolate was the most effective inoculant for increasing canola pod number and seed yield, but these increases were observed without the addition of phosphate rock to the soil. The author concluded that P solubilisation was not the main mechanism of plant growth promotion. Hariprasad and Niranjana (2009) showed increased tomato (*Lycopersicon esculentum* Mill.) biomass by a PSB *Bacillus subtilis* isolate without production of IAA, siderophore, chitinase, β -1,3 glucanase, nor any detectable organic acid. However, phytase activity was detected. It is possible that phytase production by *B. subtilis* resulted in enhanced mineralisation of P from organic phytate present in the soil, allowing increased tomato plant growth. Furthermore, other plant growth-promoting traits, such as production of ACC deaminase, may have enhanced plant growth. Gyaneshwar et al. (2002) suggested that many studies failed to demonstrate a direct role for P solubilisation by microorganisms because no increase in total biomass was found in about 70% of the experiments, the increases in crop yields were not compared with crop yields with additional superphosphates, and plant growth-promoting traits other than P solubilisation were not determined.

1.3.3. Genes involved in phosphate solubilisation

Given the poor understanding of the actual mechanisms involved in plant growth promotion via P solubilisation, it is important to identify the specific association between genes involved in P solubilisation and the host plant. However, to date little is known regarding the gene(s) involved in MPS. Organic acid production is the key mechanism proposed for MPS due to the chelation of calcium ions from mineral P precipitates to the anion provided in organic acids. Acid production elevates positive ions at the periplasmic space of PSB, reducing the surrounding pH in the associated rhizosphere. The production of gluconic acid via the direct oxidation pathway by PSB has been identified as an important mechanism for MPS (Goldstein and Liu, 1987; Liu et al., 1992). Glucose dehydrogenase (Gcd) is a member of the largest group of quinoproteins which are located in the periplasmic space of the cytoplasmic membrane in Gram-negative bacteria (de Werra et al., 2009, Figure 1.3.1). Protein Gcd requires the redox co-factor pyrroloquinoline quinone (PQQ), and the

biosynthesis of PQQ requires six genes (*pqqA-F*) encoded by an operon that varies among bacterial strains (Duine, 1991).

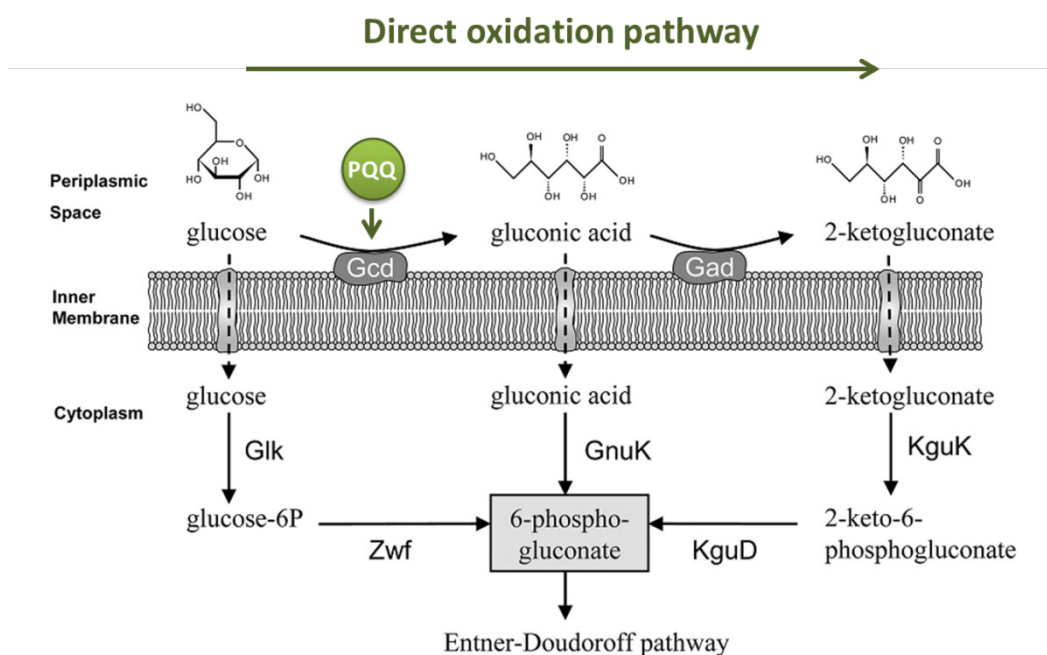


Figure 1.3.1 Schematic of Glucose dehydrogenase (Gcd) and gluconate dehydrogenase (Gad, or Gadh) involved in periplasmic glucose metabolism via direct oxidation pathway involved with pyrroloquinoline quinone (PQQ) in *Pseudomonas* spp. Glk, glucokinase; Zwf, glucose-6-phosphate 1-dehydrogenase; GnuK, gluconokinase; KguK, 2-ketogluconate kinase; and KguD, 2-ketogluconate 6-phosphate reductase. (Modified from de Werra et al. 2009).

1.3.4. Genes involved in glucose dehydrogenase and pyrroloquinoline quinone production as a cofactor

The co-factor PQQ is essential for the production of gluconic acid by Gcd in Gram-negative bacteria, and therefore indirectly promotes MPS. Goldstein and Liu (1987) were the first to clone the *mps* (mineral P solubilisation gene) from a PSB *Erwinia herbicola* isolate into *E. coli* HB101 (Table 1.3.1) and confirmed the ability of this *E. coli* recombinant to solubilise HydroxP with enhanced MPS phenotype via production of gluconic acid. Later sequencing of the *E. herbicola mps* gene revealed that it shares 60% DNA identity with the *Acinetobacter calcoaceticus pqq* III (which harbours *pqqE*) (Liu et al., 1992). How a single gene fragment has the ability to complete the production of gluconic acid remains to be answered, with the authors suggesting that different *E. coli* strains carry some but not all of the *pqq* genes.

Kim et al. (2003) isolated PSB *Enterobacter intermedium* (60-2G) from the rhizosphere of grass and the strain was found to have a strong MPS phenotype. They cloned a *pqq* cluster that comprised of six open reading frames (*pqqA-F*) into the *E. coli* strain DH5 α which encodes Gcd but not the PQQ cofactor. When in *E. coli* strain DH5 α containing either of the plasmids p7EH8 (*pqqA-E*) or p7HB5 (*pqqA-E*), the recombinant strain exhibited an increased production of gluconic acid or 2-ketogluconic acid two fold over the control. The plasmid p7HH2 which only encoded for *pqqF* was unable to solubilise P in an *E. coli* background. The authors concluded that the *E. intermedium pqq* cluster solubilised P by PQQ synthesis and completed the gluconic acid production by the *E. coli* DH5 α derived Gcd.

Research on *pqq* was also carried out by Intorne et al. (2009), who targeted mutations in components of the PSB *Gluconacetobacter diazotrophicus* PA15 *pqq* clusters *pqqB*, *pqqC*, and *pqqE* (Figure 1.3.2). On HydroxP medium, the mutants lost the ability to solubilise P. Interestingly, a mutation of *gdhA* that encodes for glucose dehydrogenase (referred to as Gcd) exhibited partial reduction in MPS. Based on this observation the authors suggested that a second *gdhA* may be present in *G. diazotrophicus* giving partial MPS activity in the *gdhA* mutant.

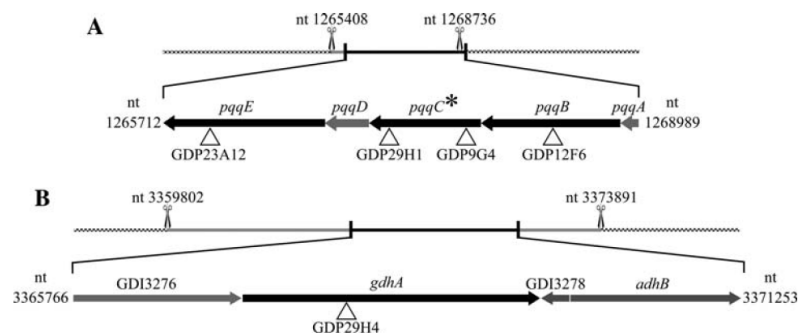


Figure 1.3.2 Schematic of of the *G. diazotrophicus* PA15 *pqq* cluster showing Tn5 transposon insertion (A) in *pqqB* (GDP12F6), *pqqC* (GDP29H1 and GDP9G4), and *pqqE* (GDP23A12) and in *gdhA* (GDP29H4) (B) (Intorne et al. 2009, Permission granted: order License ID 3187960120563).

Sashidhar and Podile (2009) cloned the *gcd* gene of *E. coli* DH5 α in plasmids pMMBEGS1 and pMMBEPs1 under the control of the *Azotobacter vinelandii* AvOP glutamine synthetase (*glnA*) or phosphate transport system (*pts*) promoters respectively. When expressed *in trans* in *A. vinelandii* AvOP, the strains showed significant increases in MPS, evidenced by colour change on MacConkey plates denoting acid production, and clear zones on NBRIP medium which indicated P solubilisation.

Genome sequence analysis of *A. vinelandii* AvOP revealed the presence of ORFs which had significant similarity to components of PQQ cofactor biosynthesis genes suggesting that the bacterium is able to produce PQQ. Increased production of gluconic acid was also detected by HPLC and through bioassay plant growth-promoting activity was also observed. The author concluded enhanced MPS phenotype was due to an additional copy of the *gcd* gene from *E. coli* DH5 α in the *A. vinelandii* AvOP mutant strains.

De Werra et al. (2009) performed in-frame deletions of PSB *Pseudomonas fluorescens* CHA0 genes that encoded for Gcd and gluconate dehydrogenase (Gad, referred to as GADH in this thesis) and constructed a double mutant of both genes. The Gad protein converts gluconic acid to 2-ketogluconate by the direct oxidation pathway (Figure 1.3.1). An in-frame deletion of *gcd* (Δgcd) reduced the production of gluconic acid and the mutant lost the ability to solubilise TCaP (Figure 1.3.1). However, deletion of *gad* (Δgad) decreased pH, as identified using methyl red medium. It was therefore postulated that increased gluconic acid production promoted that MPS phenotype. This resulted in significantly greater MPS on NBRIP plates which suggested MPS by *P. fluorescens* is largely dependent on the production of gluconic acid, a substrate of Gad which was not converted into 2-ketogluconate. The double deletion mutant of both genes ($\Delta gcd\Delta gad$) exhibited no MPS phenotype and the authors suggested this was due to the lack of gluconic acid production. However, the organic acid profiles of these mutants were not determined.

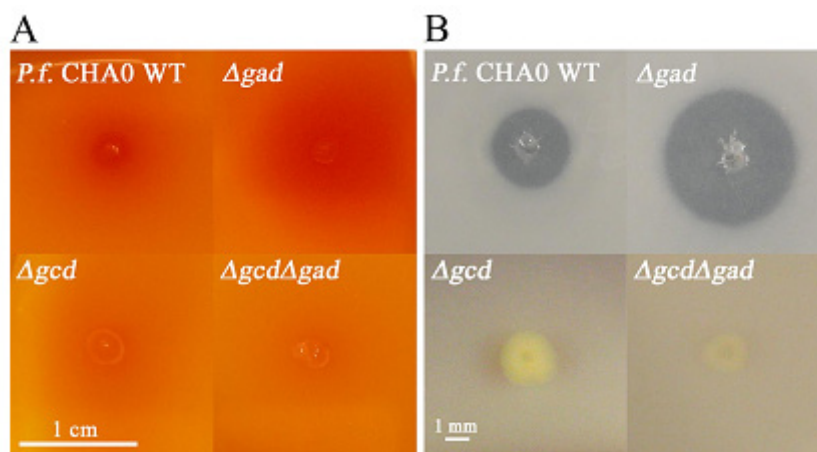


Figure 1.3.3 Acid production indicated by methyl red medium (A) and tricalcium phosphate solubilisation (B) on NBRIP plates by *P. fluorescens* CHA0 and the Δgcd , Δgad , and $\Delta gcd\Delta gad$ double mutants. Tricalcium phosphate solubilisation resulted zone of clearance by wildtype and Δgad mutant (B) and shown to produce acid (A). Impaired phosphate solubilisation by Δgcd and $\Delta gcd\Delta gad$ mutant as indicated by NBRIP plate with no halo formation (B) and no obvious colour changes on the methyl red medium (A) (De Werra et al., 2009).

Table 1.3.1 Cloning of genes involved in mineral phosphate solubilisation.

Microorganism	Plasmid	Features	Reference
<i>Erwinia herbicola</i>		Produced gluconic acid and solubilised P in <i>E. coli</i> HB101	Goldstein and Liu (1987)
	pMCG898	Production of PQQ as a <i>gcd</i> cofactor was important for MPS	Liu et al. (1992)
	pL230	Cloning PQQ synthase from <i>E. herbicola</i> into <i>E. coli</i> MC1061 showed MPS phenotype	Rodríguez et al. (2000)
<i>Rahnella aquatilis</i>	pKIM10	A 7 kb <i>EcoRI</i> fragment from <i>R. aquatilis</i> was cloned into <i>E. coli</i> HB101 and DH5 α confirmed the ability to solubilise HydroxP via production of gluconic acid with <i>pqqE</i> and <i>pqqD</i>	Kim et al. (1997)
<i>Enterobacter intermedium</i>	p7EH8	Gene cluster <i>pqqA-E</i> was cloned into <i>E. coli</i> DH5 α	Kim et al. (2003)
	p7HB5	Solubilise P by gluconic acid production and PQQ synthesis	
<i>Gluconacetobacter diazotrophicus</i>		Mutation on <i>pqq</i> clusters demonstrated loss of function (Mps-) Mutation on <i>gdhA</i> showed partial MPS phenotype	Intorne et al. (2009)
<i>Azotobacter vinelandii</i> AvOP	pGDEGS1 pGDEPS1	Expression of <i>E. coli gcd</i> , <i>glnA</i> and <i>pts</i> demonstrated MPS and plant growth-promoting ability with little nitrogen fixing activity	Sashidhar and Podile (2009)
<i>Pseudomonas fluorescens</i> CHA0	pUKF12	Three in-frame deletion mutants, Δgcd , Δgad , and $\Delta gcd \Delta gad$ were compared	De Werra et al. (2009)
	pUKF34	Δgcd exhibited Mps- whereas Δgad showed Mps++ phenotype MPS was strongly dependent on its ability to produce gluconic acid	
<i>Serratia marcescens</i> CTM 50650	pMBF2	<i>pqqABCDE</i> operon and the <i>gcd</i> from <i>S. marcescens</i> coexpressed in <i>E. coli</i> DH5 α showed	Farhat et al. (2013)
	pMBF3	overexpression of MPS	
<i>Pseudomonas cepacia</i> [‡]	pSLY4	<i>gabY</i> encodes 14.235 kDa protein which exhibited a Mps+ phenotype	Babu-Khan et al. (1995)
	pGAB1	GabY protein increased the production of gluconic acid PQQ is the key factor involved with P solubilisation	
	pYM359	<i>gabY</i> expressed in <i>E. coli</i> BL21(DE3)pLySs exhibited MPS phenotype and is postulated GabY protein involved in organic acid transportation	
<i>Synechococcus elongates</i>	pAB3	<i>ppc</i> showed a 14-fold increase in PPC activity under P-sufficiency	Buch et al. (2010)
<i>Enterobacter agglomerans</i>	pHC79	<i>mps</i> were cloned into <i>E. coli</i> JM109 demonstrated strong Mps+	Kim et al. (1997)
	pKKY	pH of the liquid culture did not drop indicating other MPS mechanisms plasmid encoded genes are unknown	
<i>Penicillium oxalicum</i> C2	pET32a- mMDH	mMDH from <i>P. oxalicum</i> C2 was cloned into <i>E. coli</i> BL21(DE3) and found enhanced MPS via over release of malate, acetate, citrate, oxalate and lactate	Lü et al. (2012)
<i>Pseudomonas putida</i> KT 2440	pCNK14	Plasmid containing <i>gadh</i> operon from <i>P. putida</i> KT 2440 expressed in <i>Enterobacter asburiae</i> PS13 demonstrated MPS phenotype by releasing gluconic acid and 2-ketogluconic acid	Kumar et al. (2013)

Abbreviations: Mineral phosphate solubilisation, MPS; pyrroloquinoline quinone, PQQ; phosphate transport system, *pts*; gluconate dehydrogenase, *gdh*; phosphoenol pyruvate carboxylase, *ppc*; glucose dehydrogenase, *gcd*; glutamine synthetase, *glnA*; mitochondrial malate dehydrogenase, mMDH.

[‡] *Pseudomonas cepacia* is also classified as *Burkholderia cepacia*

1.3.5. Other proteins that may also be involved in mineral phosphate solubilisation

The *gabY* gene from *Pseudomonas cepacia* (also known as *Burkholderia cepacia*) encoding for a 14.7 kDa protein designated GabY was found to be involved with P solubilisation. A disruption of *gabY* by mutagenesis of the wildtype strain revealed a loss of MPS and a reduction in gluconic acid production as determined by HPLC. Regions of the *gabY* were highly similar to a gene encoding for a membrane-bound protein HisQ involving in the histidine permease system (Babu-Khan et al., 1995). The authors also found that production of GabY increased the concentration of gluconic acid 10-fold when 1 μ M of exogenous PQQ was present. The authors proposed that GabY protein plays some role in the expression and/or regulation of the direct oxidation pathway during gluconic acid production in *P. cepacia*. However, the translated product of the *gabY* was found to share similarities with transmembrane amino acid ABC transporters. The *gabY* from *Burkholderia cepacia* SCAUK0330 was recently cloned and expressed *in trans* in *E. coli* BL21(DE3)pLySs by Zhao et al. (2013). The clone pYM359 was expressed and the recombinant was able to solubilise P on Pikovskaya's medium supplemented with TCaP. The authors also found the GabY protein contains a 28 amino acid residue signal peptide, indicating GabY could be secreted outside of bacterial cell and is possibly a membrane bound protein. The authors concluded that it was plausible the GabY protein was linked to release of organic acid.

Buch et al. (2010) overexpressed the *Synechococcus elongates* PPC 6301 phosphoenolpyruvate carboxylase (*Ppc*) in *Pseudomonas fluorescens* ATCC 13525 under a P limiting environment. As a result, *Ppc* production increased 12-fold, and carbon flow was decreased via the direct oxidative pathway (Figure 1.3.4). Overexpression of *ppc* was found reduce in *Gcd* activity and increased associated glucose-6-phosphate dehydrogenase activity. This correlated with increased release of pyruvate and acetate which are the final products of intracellular phosphorylative oxidation of glucose. Patching the bacteria on dicalcium phosphate Pikovskaya's agar increased the zone of clearance in the mutant that carried the *pcc* gene relative to wildtype. The authors suggested factors involved in 6-phosphogluconate pathway and the subsequent tricarboxylic acid cycle (TCA cycle, Figure 1.3.4) in *P. fluorescens* could provide an attractive new pathway for genetic engineering strategies to increase the efficiency of MPS by PSB rather than targeting PQQ biosynthesis.

The process of increasing organic acid production, reduction of the surrounding pH of PSB and subsequent solubilisation of mineral P does not always occur. The level of P solubilisation was not

always correlated to the reduction of pH (Asea et al., 1988; Kim et al., 1997). Phosphate solubilisation *mps* genes from *Enterobacter agglomerans* were cloned to form the plasmid pKKY in the *E. coli* strain JM109. The plasmid pKKY in an *E. coli* background caused a significant increase in P concentration in liquid culture medium, but there was no significant reduction in pH compared to the control (pHC79, a weak PSB). This further indicates chelation by organic anion may have occurred, which suggests a mechanism independent of pH. However, to date, the DNA sequence of the genes encoded on pKKY has yet to be determined, so the mechanism remains unknown.

The involvement of *mps* genes such as *pqq*, *gad*, and *ppc* in MPS, and the production of PQQ by PSB are widely accepted (Table 1.3.1). Many authors have drawn the correlation between the MPS phenotype by PSB isolated from different environments, and associated increases in plant biomass. However, *in situ* localisation of PSB at the rhizosphere of plant root of these bacteria has not been determined. To confirm the *mps* has a direct influence on plant growth, *in vivo* plant bioassays are needed to determine the localisation and the colonisation pattern of PSB. The influence of factors, such as plant root exudation, on *mps* regulation has yet to be investigated. Therefore, plant bioassays will be required to examine the the effects of loss of function and overexpression of *mps*.

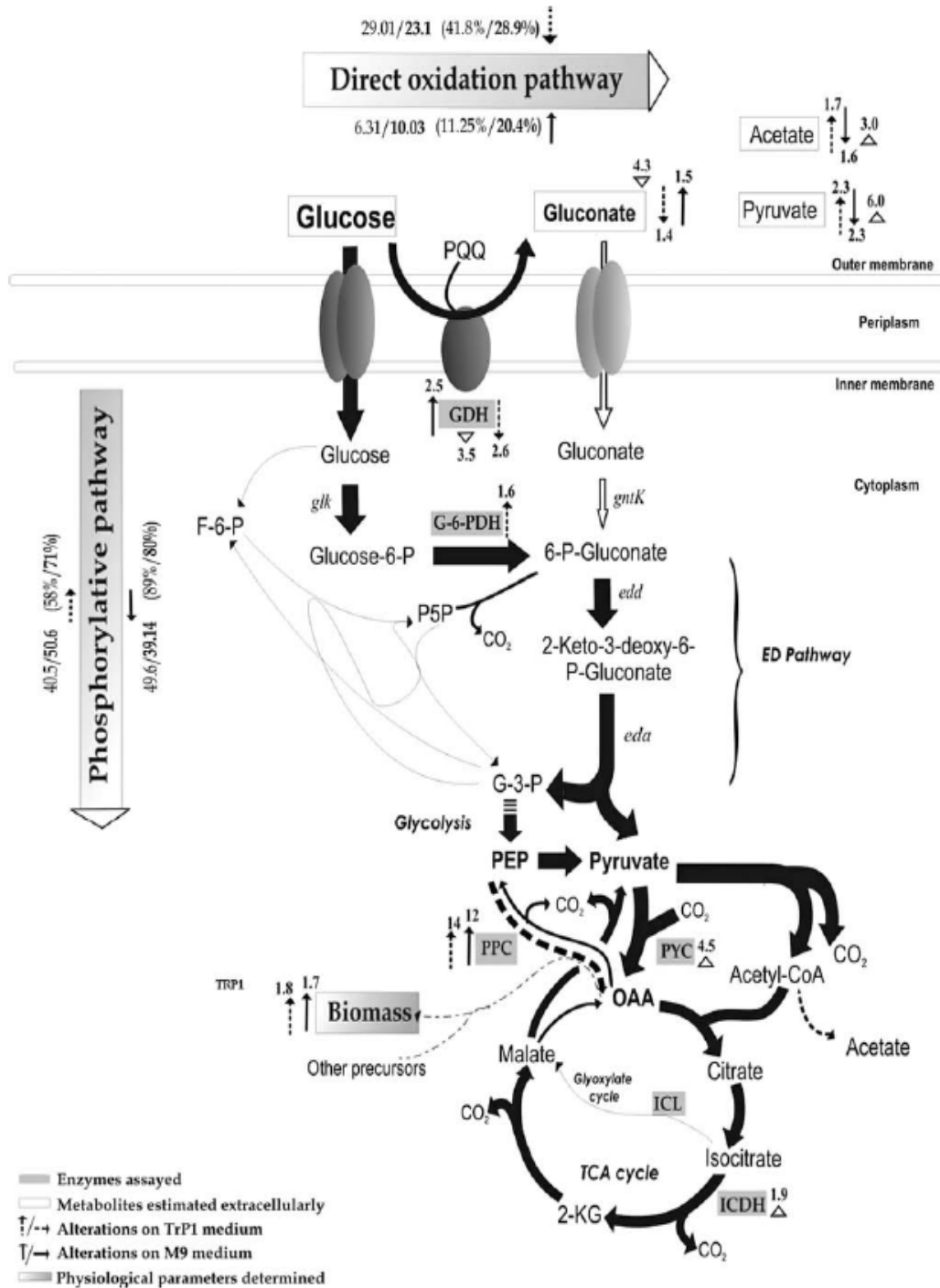


Figure 1.3.4 Glucose metabolism of *P. fluorescens* ATCC 13525 and the response of *S. elongatus* PCC 6301 *ppc* overexpression in *P. fluorescens*. Numbers on the arrows represent the fold change in response to *ppc* overexpression on M9 (P-limited) and TrP1 (P-sufficient) minimal media. Overexpressed *ppc* enhanced catabolism through intracellular phosphorylative pathway by increasing metabolic by-products such as pyruvate and acetate. (Buch et al. 2010). Permission granted: order License ID 3196231478972).

1.4 Conclusions

Conclusion from the literature to date:

- There is high demand for P fertilisers as the global population increases and global reserves of phosphate rocks will be steadily depleted;
- Up to 50 - 90% of P applied as fertiliser is converted to sparingly soluble forms in soil and approximately 34% of the total P input is lost through soil erosion and agricultural run-off to waterways;
- Phosphate solubilising bacteria can promote plant growth by solubilising P and making it available for uptake by plants;
- There is poor knowledge of the link between PSB and other plant growth promotion traits expressed by bacteria;
- Phosphate solubilising bacteria are able to solubilise P but little is known about the gene(s) involved in P solubilisation and their regulation under specific conditions;
- Production of gluconic acid via the direct oxidation pathway has been identified as the main mechanism for MPS by membrane-bound Gcd which requires PQQ redox co-factor;
- Although reduction of pH by the production of organic acid is generally accepted as the main mechanism for MPS, the level of P solubilisation is not always correlated to the reduction of pH. This may be due to other mechanisms such as mineral chelation by organic anions ;
- There have been no definitive *in vivo* plant bioassays to determine the expression of genes implicated in MPS at the rhizosphere.

1.5 Research hypothesis, objectives, and work flow

1.5.1. Hypothesis

Ryegrass growth can be increased in an environment limited for soluble P by the expression of *mps* genes in the rhizosphere.

1.5.2. Objectives and work flow

1. Characterise effective PSB isolated from New Zealand, and demonstrate their potential to promote perennial ryegrass (*Lolium perenne*) growth (Chapter 2).
2. To construct mutant libraries in PSB from three different bacteria genera and identify novel gene(s) involved in MPS (Chapter 3).
3. To compare activity/function of wildtype, and null mutants under controlled conditions, and assess key factors involved in MPS (Chapter 4).
4. To determine *in situ* localisation and expression of PSB in the rhizosphere of ryegrass (Chapter 5).

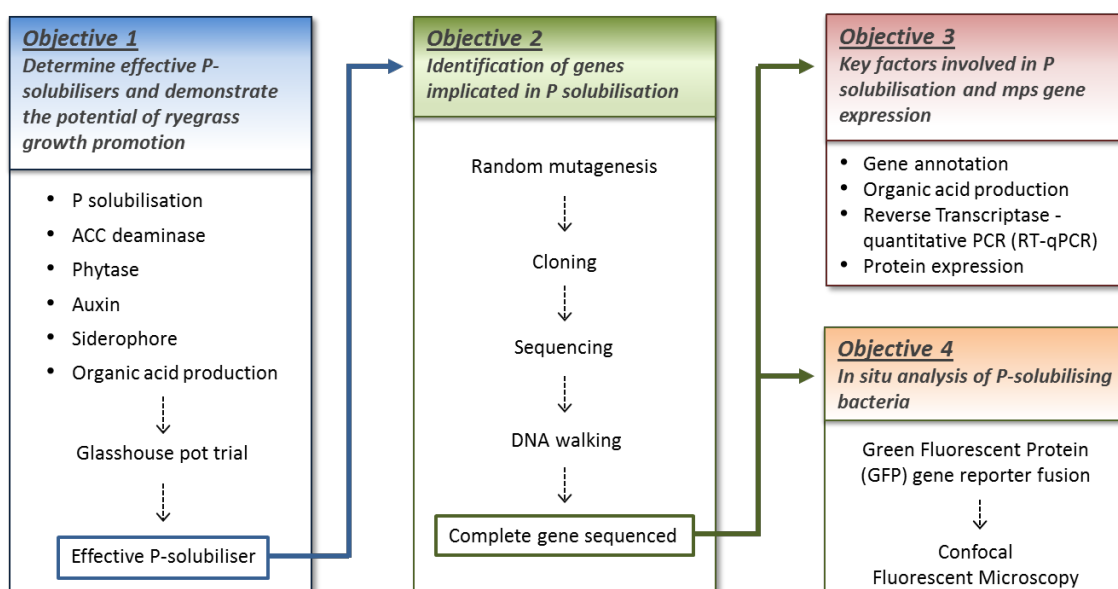


Figure 1.5.1 An overview of experimental approach with four objectives.

Chapter 2

Selection and Characterisation of Phosphate-Solubilising Bacteria

2.1 Selection of phosphate-solubilising bacteria

Initial selection of the phosphate-solubilising bacteria used in this study was carried out in conjunction with the MBIE programme “Microbes for reduced P inputs” led by Dr Carolyn Mander, AgResearch (C10X0904). In this programme, bacterial isolates (rhizobacteria and bacteria from bulk soil) were collected from a range of sites within New Zealand including the North Island sites Ballantrae (Ba) (Palmerston North, 40° 19' S 175° 50' E), and Whatawhata (Hamilton, 37° 48' S 175°09' E), and the South Island sites of Winchmore (Wi) (Canterbury 43° 47' S 171°48' E) (described in Mander et al., 2012), Eyrewell exotic/native forest (Canterbury, 43° 25' S 172°16' E), and native forest at Haast (Ha) (West Coast, 43° 43' S 169°04' E) (isolated from the Haast Chronosequence project; Jangid et al., 2013)(Figure 2.1.1). Isolates collected from the various locations were selected for their ability to solubilise sparingly-soluble mineral P ($\text{Ca}_2\text{OH}(\text{PO}_4)_3$ and CaHPO_4) on a double layered root exudate agar (REA), where carbon sources were collected from the root exudates of perennial ryegrass as described previously (Mander et al., 2012). Isolates that exhibited the mineral phosphate solubilisation (MPS) phenotype (i.e. where a visible halo was observed around the colony) were selected for further study and are referred to as “phosphate-solubilising bacteria” (PSB). A collection of 105 isolates from a range of geographical locations and covering a range of bacterial genera was established as the starting point for this study: ten bacterial isolates from pasture soil at Winchmore (Wi); 14 isolates from pasture soil at Ballantrae (Ba); 16 isolates from pasture soil at Whatawhata (Wh); 27 isolates from native forest soil at Haast (Ha); 19 isolates from Eyrewell exotic forest soil (EE); and 19 isolates from Eyrewell native forest soil (EN).



Figure 2.1.1 Location of sampling sites where bacterial strains were isolated.

The aim of this part of the study was to (1) select ten strains for further characterisation, (2) examine the relationship between plant growth-promoting (PGP) traits of these strains and ryegrass growth promotion, and (3) to select three PSB strains from different geological locations and from a range of genera to maximise the likelihood of identifying novel genes implicated in MPS (Chapter 3). Figure 2.1.2 is a schematic diagram of the bacterial selection workflow for this study.

Initially a liquid culture assay was used to quantify soluble phosphate (P) released from dicalcium phosphate (DCaP) by the 105 PSB. Secondly, isolates were tested in *in vitro* assays to determine if they possessed additional PGP traits including 1) ability to utilise 1-aminocyclopropane-1-carboxylate (ACC) indicating the production of ACC deaminase; 2) ability of isolates to mineralise sodium phytate (Na-Phy), potentially show phytase activity; and 3) ability to solubilise tricalcium P (TCaP), hydroxyapatite (HydroxP), and iron phosphate (FeP). Selection of which inorganic P for use in *in vitro* screening depends on the soil type of interest or where the PSB may be used as an inoculant in the future. The majority of insoluble P in pasture soil has been found to be calcium-bound P (Ozanne &

Shaw, 1967; Haynes & Williams, 1992), and these compounds occur as dicalcium P (CaHPO_4 , DCaP), tricalcium P ($\text{Ca}_3(\text{PO}_4)_2$, TCaP), and hydroxyapatite ($\text{Ca}_5(\text{PO}_4)_3\text{OH}$, HydroxP). Tricalcium phosphate has reduced solubility in comparison with DCaP, $-\log K_{\text{sp}}$ 28.9 vs $-\log K_{\text{sp}}$ 6.90, where the larger the $-\log K_{\text{sp}}$ value, the more difficult to solubilise (Dorozhkin & Epple, 2002). HydroxP is less soluble than TCaP ($-\log K_{\text{sp}}$ 116.8 and $-\log K_{\text{sp}}$ 28.9, respectively). It is known that free P can be adsorbed to iron in acidic soil (Sanyal and Datta, 1991; Rodriguez and Fraga, 1999) and exists in soil as strengite ($\text{FePO}_4 \cdot 2\text{H}_2\text{O}$) such that P ions are not available for plant uptake (Richardson, 2001).

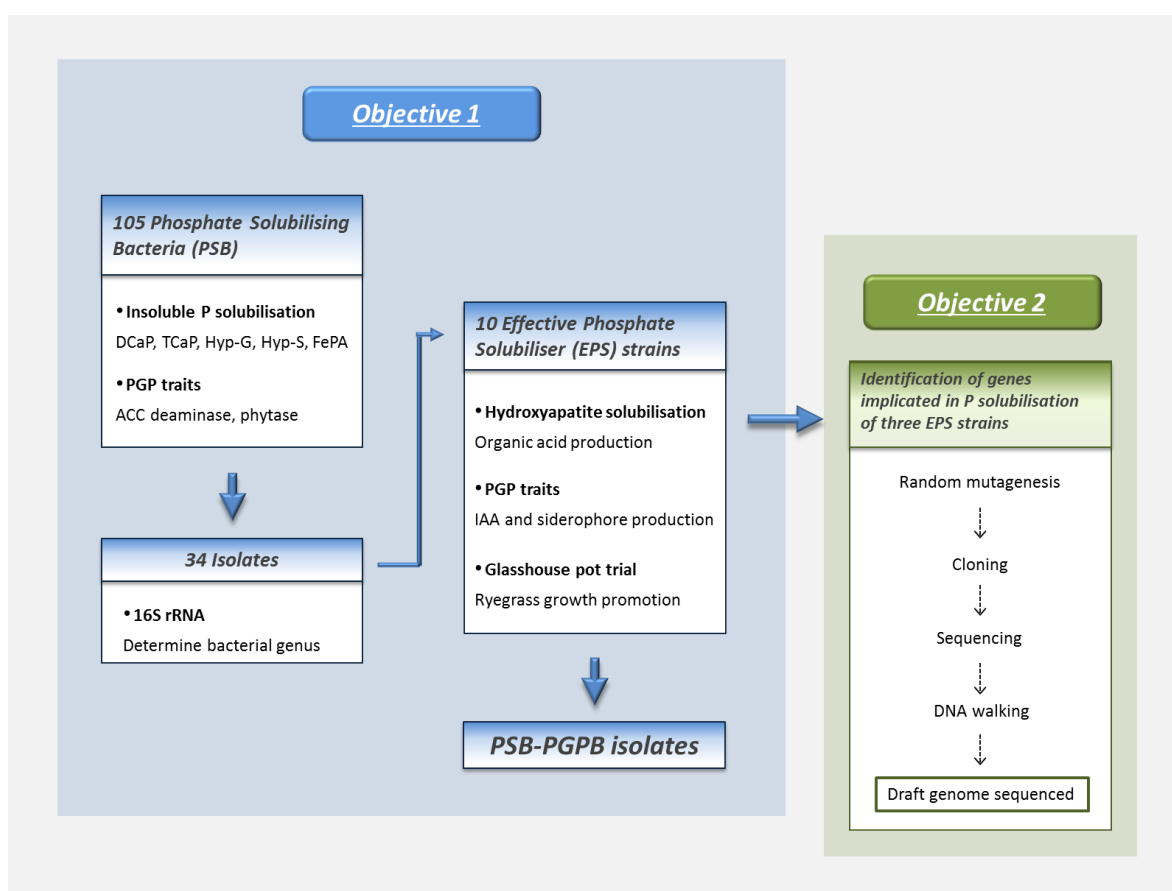


Figure 2.1.2 Workflow of bacterial selection carried out in this study

A subset of 34 isolates able to release more than 4 mM (an arbitrary concentration) of soluble P from the DCaP liquid culture assay were selected for 16S rRNA gene sequencing. These isolates were from a range of geographically distinct sites and ranged in colony morphology (suggestive of a range of genera), and also had at least three additional PGP traits. One to two isolates from each site that

released less than 4 mM of soluble P were also selected if they also had at least four PGP traits. Multivariate analysis and two-way clustering analysis were carried out to determine if the relationships of occurrence of PGP phenotypes of traits among the PSB to investigate links between PGP phenotypes and their origin (habitat). Ten strains were then selected based on the following criteria: different geographical location of isolation; different bacterial genera; ability to release > 4 mM of soluble P from the liquid culture assay; ability to solubilise both TCaP and HydroxP. Isolates selected were not listed in the “Unwanted Organisms Database” that is defined in the Biosecurity Act 1993, New Zealand (<http://www1.maf.govt.nz/uor/searchframe.htm>), as being absent from the “plant pathogenic bacteria” list (Bull et al., 2010; Bull et al., 2012). These ten strains selected are referred to hereafter as “Effective P Solubilising” (EPS) strains and were further tested for additional PGP traits such as production of indole-3-acetic acid (IAA) and siderophore production.

Phosphate solubilisation in soil by low molecular weight organic acid producing bacteria close to the plant rhizosphere is widely accepted (Jones, 1998; Rodríguez & Fraga, 1999; Richardson, 2001). It has been proposed that low molecular weight organic acids produced by PSB facilitate dissolution of P bound to metal ions such as Ca^{2+} (Illmer and Schinner, 1992; Rodríguez and Fraga, 1999). The various P-metal precipitates exhibit a broad range of ‘dissociation-strengths’, and these further vary with organic acids. It is empirically difficult to assess the P-solubilising activity of each PSB against all the different forms of precipitated phosphate present in soils, and this may vary for each isolate as the relative composition of organic acids produced in culture may also vary over time. Furthermore, in many cases, P-solubilising activity has been screened on ‘reasonably soluble’ precipitates of Ca-P, where the phenotype observed may be attributable simply to reduction in local pH and not exudation of significant quantities of organic acids. This has been noted by authors such as Bashan et al. (2013), who proposed that to define a potential PSB isolate, a liquid culture assay must be performed to validate P solubilising activity observed on agar, and preferably using a pH buffered solution. Further to this, the use of highly insoluble forms of calcium phosphate, such as hydroxyapatite, have become the *de facto* standard for characterisation of P-solubilising activity. HydroxP is the least soluble form of calcium P ($-\log K_{sp} = 116.8$) and is mainly found in phosphate rocks (PR) (Dorozhkin & Epple, 2002; Bolan et al., 1990). Therefore, HydroxP was used in the subsequent liquid culture assays as the only P source supplied to bacteria, and the amount of organic acid released was quantified by High Performance Liquid Chromatography (HPLC).

To select EPS that will contribute to the overall goal of increasing the efficiency of P utilisation in pasture soil, a model pasture plant, perennial ryegrass (*Lolium perenne* L.), was used in this study. Ten EPS isolates were tested in a glasshouse pot trial to determine their ability to increase ryegrass

growth under low soil P conditions. The correlation between P content of ryegrass root and shoot biomass was also investigated. Isolates that demonstrated effective HydroxP solubilisation and increased ryegrass shoot P in the glasshouse pot trial, as well as increasing total shoot biomass were considered as Phosphate Solubilising Bacteria – Plant Growth Promoting Bacteria (PSB-PGPB) isolates.

2.2 Methods

2.2.1. Effective phosphate solubiliser strain selection

Isolates were screened for PGP traits of ACC deaminase, and ability to solubilise phytate, TCaP, HydroxP, and FeP. The screening was carried out using agar plate assays using a 96 pronged colony replicator. At this stage of the screening, there was no attempt to quantify cell numbers and reactions on agar plates were scored visually, using the scoring systems described below. A strain PSB85 previously shown to solubilise inorganic P from the REA plate where a zone of clearance could be observed was used as a positive reference strain for every plate assay. This enabled both validation of media composition and a reference from which to define a relative increase or decrease in halo size of other patched bacteria. Raw data from the screening assays are in Appendix D.

2.2.1.1 *In vitro* phosphate solubilisation

Previously, the ability of the 105 isolates to solubilise P was assessed by Dr. Carolyn Mander in the MBIE programme “Microbes for reduced P inputs”. The culture medium consisted of various sugars (listed below) at concentrations that reflected the composition of ryegrass root exudates (Mander et al., 2012). Each litre of culture broth contained 5.0 g fructose, 2.5 g sucrose, 1.5 g glucose, 0.5 g inositol, 0.5 g mannitol and 10 mL of trace elements solution (0.4 g NH_4NO_3 , 0.4 g $\text{MgSO}_4 \cdot 7\text{H}_2\text{O}$, 0.3 g KCl, 0.2 g NaCl, and 0.04 g FeSO_4 in 1 L). The pH of the culture broth was adjusted to pH 7.0 prior to autoclaving for 15 min at 1.1 kg/cm², 121°C, and 20 mL of culture broth was placed in a 50 mL conical flask with 30 mg of dry-autoclaved insoluble DCaP (CaHPO_4). Bacteria were grown overnight at 25°C in LB broth, and 100 µL was used as a starter culture. Each conical flask was incubated for 7 days (25°C, 250 rpm) prior to a colourimetric assay developed by Murphy and Riley (1962) which measures the amount of soluble P present in the culture medium. This assay is based on the reaction of acid ammonium molybdate with orthophosphate to form phosphomolybdenum complexes. These complexes are then reduced to molybdenum blue by sulphuric acid with a resultant blue colour change as shown in Figure 2.2.1. The molybdenum blue reagent contained 51 mM ammonium molybdate, 259 mM ferrous sulphate, 6.4 mL of 10% sulphuric acid, and the total volume was

adjusted to 20 mL with dsH₂O (Appendix A.1.5). Each reaction was performed by incubating equal volumes of sample supernatant with the molybdenum blue reagent for 30 min at room temperature, and colour changes were measured at 850 nm using the FLUOstar Omega microplate reader (BGM Labtech, Ortenberg, Germany). The negative control (blank) comprised a flask of culture medium that had not been inoculated with bacteria which was incubated under the same conditions as the treatments. The standard curve was made by dipotassium hydrogen orthophosphate (K₂HPO₄) solutions at 200, 400, 600, 800 and 1000 µM concentrations (Figure 2.2.1). Each sample was diluted using dsH₂O to appropriate dilutions within the range of the standard curve and the value from the negative control (uninoculated culture medium, blank) was subtracted before calculations.

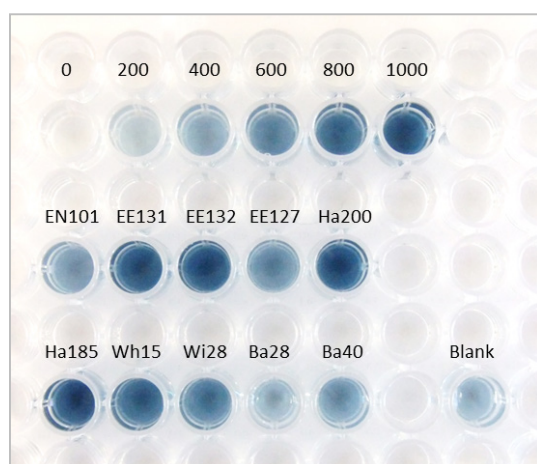


Figure 2.2.1 Microtitre plate of soluble phosphate concentration measured by Murphy and Riley's colourimetric method. Colourimetric change from colourless to blue corresponding to the concentration of soluble phosphate. The amount of phosphate released from the *in vitro* phosphate solubilising assay after 7 days incubation (25°C) by ten isolates, and was determined after 20-fold dilution. The positive standard controls were 0, 200, 400, 600, 800, 1000 µM of dipotassium hydrogen orthophosphate (K₂HPO₄) on the top row, and the absorbance was measured at 850 nm. The blank (uninoculated culture medium) was measured without dilution.

2.2.1.2 Tricalcium phosphate solubilisation by PSB

To increase the possibility of finding more effective PSBs, β-tricalcium phosphate (TCaP) was used in agar medium instead of DCaP. The TCaP plate assay was based on a method described by Richardson & Hadobas (1997) for a phytate plate with slight modifications using TCaP instead of sodium phytate. This minimal medium contained glucose for bacterial growth, various salts to provide essential elements, and TCaP as the only P source for bacterial growth. The medium contained 55.5 mM glucose, 62.5 mM NH₄NO₃, 6.7 mM KCl, 2.0 mM MgSO₄, 0.006 mM MnSO₄, 0.04 mM FeSO₄, 6 g of β-

tricalcium phosphate (β - $\text{Ca}_3(\text{PO}_4)_2$) (Sigma-Aldrich, USA, Cat. 21218), and 15 g of agarose gel per litre of medium. The mixture was adjusted to pH 7 and autoclaved. Prior to pouring the agar plates, 100 μL of 10 x trace element solution was added and mixed (original recipe from Hoagland's solution, Appendix A.1.7, Hoagland (1950)). Each isolate was then patched on the TCaP plate and the strain PSB85 used as a reference strain (Figure 2.3.1). The plates were incubated at 25°C for 3 days. The ability of each isolate to solubilise TCaP was then defined by the halo size. Isolates scored as "3" produced a large halo with diameter ≥ 8 mm, "2" produced a medium sized halo of 5 – 7 mm, "1" a small halo of ≤ 4 mm, and "0" where no halo was observed.

2.2.1.3 Detection of bacterial acidification of medium during tricalcium phosphate solubilisation

To detect organic acid production by PSBs, methyl red was used as an indicator dye in the agar-based screening system. This indicator dye changes from yellow to red as pH decreases from 6.2 to 4.4, indicating organic acid production by the bacterial isolate (Divya et al., 2008). The agar plates were made by adding 1% methyl red into the TCaP agar mixture after autoclaving and mixing well before being poured into petri dishes. The final TCaP plate containing methyl red was designated as Me-Red. Each isolate was patched onto Me-Red plates and strain PSB85 was included on plates as a reference strain. The plates were incubated at 25°C for 3 days. Isolates that produced large red circles around the colony after 7 days were scored as "3", pink circles were scored "2", faint pink colour changes were scored a "1" and colonies were scored as "0" when no colour change was detected in the agar.

2.2.1.4 Hydroxyapatite solubilisation by PSB using glucose or sucrose as the sole carbon source

Ability of isolates to solubilise hydroxyapatite (HydroxP) was also assessed. Many different carbon sources can be found in root exudates; in addition to glucose, sucrose is one of the sugars most commonly found (Jaeger et al., 1999, Paterson et al., 2007). For this reason the ability of isolates to solubilise P in the presence of glucose or sucrose was compared. Hydroxyapatite (HydroxP) medium was based on the TCaP plate medium described above, but contained HydroxP as the P substrate instead of TCaP. The medium contained 6 g of HydroxP ($\text{Ca}_5(\text{OH})(\text{PO}_4)_3$) (Sigma-Aldrich, USA, Cat. 04238), and 55.5 mM of either glucose or sucrose (referred to as Hyp-G or Hyp-S, respectively). The mixture was adjusted to pH 7 and autoclaved. Prior to pouring the plates, 100 μL of 10 x sterile trace element solution (Appendix A.1.4) was added and mixed. Isolates were then patched on either Hyp-G or Hyp-S plate and allowed to grow for 3 days (25°C). PSB85 was used as a reference strain. Isolates

were scored as “1” if there is a visible halo around the colony, and “0” if no halo was observed (Figure 2.3.1). This scoring system was used instead of comparing the halo size, as the majority of isolates screened in the assay exhibited no obvious HydroxP solubilisation using either glucose or sucrose as a carbon source.

2.2.1.5 Iron phosphate solubilisation by PSB

Isolates were patched onto iron phosphate plates (FePA, $\text{FePO}_4 \cdot 2\text{H}_2\text{O}$), prepared as for TCaP plates described in Section 2.2.1.2 but with a slight modification. It is known that Fe-P precipitates are found in acidic soil, so the agar plates were made to be acidic. The pH was adjusted to pH 4 before FePO_4 was added to the mixture, and the composition of other elements remained the same as for TCaP, as described above. Isolates were then patched onto FePA plates and allowed to grow for 3 days at 25°C. Using this medium, visually different halo sizes were produced around the colonies. A large halo size (≥ 8 mm) was scored as “3”, medium size halo (5 – 7 mm) as “2”, small halo size (≤ 4 mm) was scored as “1” and “0” where no halo was observed (Figure 2.3.1).

2.2.1.6 ACC deaminase production by PSB

Each isolate was patched onto ACC deaminase agar plates to screen for isolates capable of utilising ACC as the sole nitrogen source i.e. ability to produce ACC deaminase. The plates were prepared as described by Li et al. (2000) using a combination of Dworkin and Foster (DF) salt minimal medium (Dworkin and Foster, 1958) with addition of 3 mM of ACC. DF salt medium consisted of 29.4 mM KH_2PO_4 , 42.3 mM Na_2HPO_4 , 0.8 mM $\text{Mg}_2\text{SO}_4 \cdot 7\text{H}_2\text{O}$, 11 mM glucose, 10.2 mM gluconic acid, 10.4 mM citric acid, and 100 μL of 10 x trace element solution (Appendix A.1.4). The solution was adjusted to pH 7.2 prior to adding ACC to a final concentration of 3 mM. The mixture was autoclaved before being poured into sterile petri dishes. Isolates were then patched onto the ACC plates and allowed to grow for 3 days at 25°C. Given that ACC was the sole nitrogen source, isolates that had grown by this time were able to utilise ACC and were considered as ACC deaminase-producing bacteria. Bacteria that grew on these plates were scored as “1” while isolates that failed to grow were scored “0”

2.2.1.7 Phytase mineralisation by PSB

Ability of strains to solubilise phytate was measured on Sodium phytate plates (Na-Phy) using the method described in Richardson & Hadobas (1997) with slight modifications. The Na-Phy medium contained 62.5 mM NH_4NO_3 , 18 mM CaCl_2 , 6.7 mM KCl, 4.2 mM MgSO_4 , 0.006 mM MnSO_4 , 0.04 mM FeSO_4 , 4 g of sodium phytate (phytic acid sodium salt hydrate, $\text{C}_6\text{H}_{18}\text{O}_{24}\text{P}_6 \cdot x\text{Na}^+$ (Sigma-Aldrich, USA,

CAS 14306-25-3), and 15g of agarose gel per litre of medium. The mixture was adjusted to pH 7 and autoclaved. Prior to pouring the agar plates, 10 mL of 20% glucose, 100 μ L of 10 x trace element solution (Appendix A.1.4) and 200 μ L of thiamine (10 mg/mL) was added and mixed well using a magnetic stirrer. Isolates were then patched onto the Na-Phy plates. The plates were incubated at 25°C for 3 days and the ability of each isolate to utilise sodium phytate was defined by the halo size and scored as three sizes, “3” as large halo (≥ 8 mm), “2” as medium size halo (5 – 7 mm), “1” as small halo (≤ 4 mm), and “0” as no halo observed (Figure 2.3.1).

2.2.2. Identification by 16S rRNA gene sequencing

Thirty four isolates were sequenced. The 16S rRNA gene PCR amplification was carried out using the two primers, U16a (5'AGAGTTTGATCCTGGCTC3') and 1087R (5'CTCGTTGCGGGACTTAACCC3') (Wang & Wang 1996). PCR was carried out using 3 μ L of diluted bacteria cells as template (a single colony in 500 μ L of distilled water (dsH₂O)) in a total of 50 μ L PCR reaction. A full description of the PCR is given in Appendix C.2.9, except the initial denature step was set at 94°C for 15 min to ensure total disruption of bacterial cell walls and release of gDNA. Amplification of correct size amplicons (~ 1600 bp) was confirmed by agarose gel electrophoresis (Appendix C.2.10) and the amplicon was purified by Roche High-Pure PCR kit (Appendix C.2.12). Sequencing was performed using the Applied Biosystems 3730xl and 9 ABI 3700 through Macrogen sequencing services (<http://dna.macrogen.com/eng/>)

2.2.3. Further characterisation of isolates

2.2.3.1 Production of indole-3-acetic acid

A modified method for IAA detection from Sawar and Kermer (1995) was carried out. The IAA growth medium consisted of 5 g of glucose, 0.025 g yeast extract, and 0.204 g of L-tryptophan (Sigma-Aldrich, USA, CAS 73-22-3) in 1 L and the growth medium was autoclaved. The ten EPS isolates were propagated in 3 mL of tryptic soy broth (TSB) for 24 h followed by two washing steps with the IAA medium before inoculating 500 μ L aliquots of the washed culture into 10 mL of the IAA growth medium in McCartney bottles. After incubating for 72 h (20°C, 250 rpm) in the dark, 1 mL of cell culture was centrifuged for 10 min (15,7000 $\times g$). A 90 μ L aliquot of the supernatant was then incubated with 60 μ L of freshly prepared Salkowski reagent in 96 well plates (Costar®, flat bottom, Bio-Rad, California, U.S.) in the dark for 30 min. Salkowski reagent consisted of 1 part of 500 mM iron

chloride (FeCl_3) and 49 mL of 35 % perchloric acid (HClO_4). The concentration of IAA in each culture medium was determined by comparison with a standard curve. The standard curve was made from a stock 0.1 % IAA solution at 6, 15, 30, 45, 60, 90 and 120 $\mu\text{g IAA mL}^{-1}$ concentrations and incubated with Salkowski reagent as described for the treatment samples above. Colour changes from colourless to pink were measured at 530 nm using the FLUOstar Omega microplate reader (BGM Labtech, Ortenberg, Germany). The negative control (blank) comprised a culture filtrate that had not been inoculated with bacteria which was incubated under the same conditions as the treatments and the value from the negative control was subtracted before calculations. IAA produced by each isolate was measured in triplicate.

2.2.3.2 *Siderophore production*

The siderophore assay is based on competition for iron between the Fe(III) complex of an indicator dye, Chromazurol S (CAS, Merck KGaA, Darmstadt, Germany), where a strong chelator produced by siderophore-producing rhizobacteria removes the iron from the dye resulting a colour change from blue to orange. The colour change can be detected by a modified CAS plate assay (Schwyn & Neilands 1987) (Figure 2.3.1). To identify siderophore producing rhizobacteria, the CAS agar medium was prepared by mixing three solutions. Solution I consisted of 50 mL autoclaved distilled water, 60.5 mg Chromazurol S, 10 mL filter sterilised iron chloride (FeCl_3) solution (1 mM FeCl_3 in 10 mM HCl); solution II consisted of 40 mL autoclaved distilled water, 72.9 mg cetrimonium bromide (hexadecyltrimethyl-ammonium bromide); and Solution III consisted of 850 mL distilled water, 6.4 g Na_2PO_4 , 0.3 g KH_2PO_4 , 2.5 g NaCl, 2.5 g NH_4Cl , 30.24 g PIPES (2-[4-(2-sulfoethyl)piperazin-1-yl]ethanesulfonic acid), 12 g of 50% NaOH, 15 g agar and adjusted the pH to 6.8 with sterilised 50% NaOH and the mixture was autoclaved. Filter sterilised glucose with a pH of 6.8 (20 mL, 20 %), and filter sterilised casamino acid (30 mL, 10 %, pH 6.8) was also added to solution III and the pH was maintained at 6.8. Adjust Solution II to pH 6.8 using filter sterile 4 M NaOH before mixing with Solution I followed by adding the mixture to Solution III. The CAS agar was settled into sterile petri dishes before the green agar mixture turned into blue when setting. To standardise the assays, 1 μL of an overnight culture (with approximately $\sim 10^5$ cfu) of each isolate was aliquoted onto the CAS agar plates, which were incubated for 7 days at 25°C. The development of yellow halos indicated the production of siderophores (Figure 2.3.1).

2.2.3.3 *Hydroxyapatite solubilisation*

To quantify the amount of soluble P released during P solubilisation, as well as to obtain an organic acid profile released by each isolates using High Performance Liquid Chromatography (HPLC), liquid cultures were used. The HSU HydroxP liquid culture medium used in this study was modified from the HSU buffer as described in Giles et al., (2014), where additional iron (II) sulfate was included and calcium phytate precipitate was replaced with HydroxP that is known to be a less soluble form of calcium phosphate ($-\log K_{sp} = 116.8$) (Dorozhkin & Epple, 2002) (Appendix A.2.4). The reason for using the HSU medium is because this medium contains a low salt concentration, and is used for maintaining positive selection pressure on wildtype bacteria to produce essential amino acids and vitamins. Furthermore, to maintain a constant solute ion at the stationary phase for HPLC separation, low salt concentration as well as chloride ions was used as the major anion in the HSU solution to retain the ion effect on the HPLC column.

Quantification of soluble P released by ten EPS isolates were performed by growing each isolate in HSU liquid culture medium with the only P source from HydroxP ($\text{Ca}_5(\text{PO}_4)_3(\text{OH})$). This was carried out in 250 mL Erlenmeyer flasks containing 50 mL of HSU liquid culture medium (55.5 mM glucose, 1.38 mM K_2SO_4 , 2.63 mM MgCl_2 , 4.67 mM NH_4Cl , 0.27 mM CaCl_2 , 24.98 mM NaCl , and 0.3 g of HydroxP, Appendix A.2.4, Figure 2.2.2). The HSU HydroxP medium was adjusted to pH 6.5 and the flasks were covered with non-absorbent cotton before autoclaving. Before starting the HSU liquid culture assay, each isolate was grown in LB broth for 24 h at 25°C except isolate Ha185, which was grown for 48 h, and was shaking at 250 rpm until the OD_{600} reached ~ 4.0 . At this OD_{600} , each isolate was pelleted by centrifugation for 3 min at $5900 \times g$ at room temperature. The starter culture was prepared by resuspending each cell pellet independently to a final $\text{OD}_{600} \sim 2.0$ with filtered sterilised HSU liquid culture medium that contained no HydroxP. Each flask was inoculated with 100 μL of the starter culture to give a bacterial suspension of $\sim 10^6$ cfu mL^{-1} , which was confirmed by serial dilution plating (Appendix B.2). The HSU liquid culture medium was incubated at 25°C and shaking at 250 rpm in a Raytek orbital incubator. One millilitre of each sample was pelleted after day 3 and day 7 post inoculation and centrifuged at $15,700 \times g$ for 10 min. The supernatant was filtered by 0.22 μm PVDF syringe filter (13 mm, Thermofisher scientific, Massachusetts, USA) before the amount of soluble P was measured by Murphy and Riley's method (1962) as described in Section 2.2.1.1. Colony forming units (CFUs) was also enumerated for each HSU liquid culture at day 3 and day 7 by serial dilution plating (Appendix B.2). This experiment was performed at three independent times for statistical analysis.

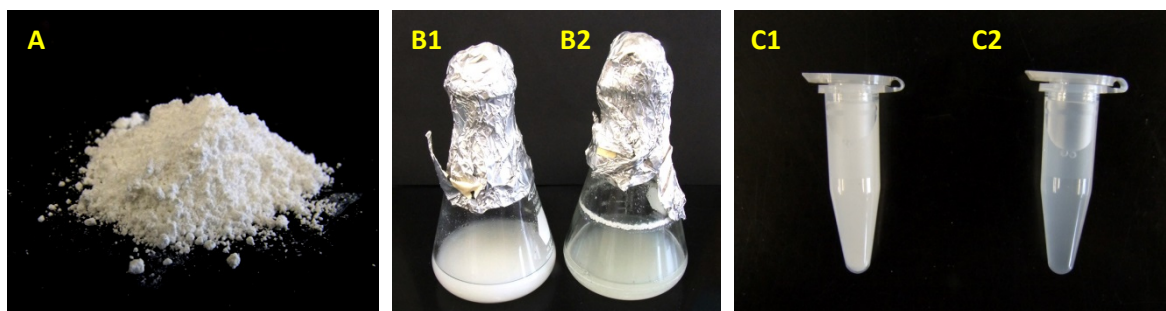


Figure 2.2.2 Photographs of the liquid culture assay. Insoluble hydroxyapatite (HydroxP) is a white powder (A), 50 mL uninoculant HSU HydroxP medium in Erlenmeyer flasks and 1.5 mL aliquot in Eppendorf tube (B1 and C1 respectively), HSU HydroxP medium with isolate Ha185 inoculation for 7 days at 25°C in Erlenmeyer flasks and 1.5 mL aliquot in Eppendorf tube (B2 and C2 respectively). Note the clearing in C2 indicating solubilisation of HydroxP insoluble particles by Ha185 isolate after 7 days incubation.

2.2.4. Organic acid profiling by High Performance Liquid Chromatography

Organic acid profiles produced by the ten EPS were analysed and quantified by HPLC conducted at Lincoln University by Mrs. Joy Jiao. The HPLC method is based on Giles et al. (2014) with modifications as described below. The HPLC was conducted using Shimadzu LC system (Shimadzu Corporation, Kyoto, Japan) consisting of a system controller (CMM-20A), a pump (LC-20 AD), a degas (DGU-20A5), an auto-sampler (SIL-10AF), a sample cooler, an UV detector (SPD-20A) and a column oven (CTO-10 ASvp). Standard stock solutions were prepared by dissolving organic acid in the HSU liquid culture medium without HydroxP.

D-gluconic acid sodium salt (GA, 99%, CAS 527-07-1), 2-keto-D-gluconic acid hemicalcium salt hydrate (2-KGA, 100%, CAS 1040352-40-6), 5-keto-D-gluconic acid potassium salt (5-KGA, 98.0 % CAS 91446-96-7), pyruvic acid (PyrA, 98%, CAS 127-17-3), malonic acid (MA, 99%, CAS 141-82-2), shikimic acid (SA, 99%, CAS 138-59-0), and L-malic acid (MA, >99%, CAS 97-67-6) were purchased from Sigma-Aldrich (Missouri, United States); DL-lactic acid (85%, CAS 50-21-5) from Acros Organics (Geel, Belgium); formic acid (FA, 98%, CAS 64-18-6) was purchased from Anala R, and acetic acid (100%, CAS 64-19-7) was from BDH (Doha, Qatar). Standard stock solutions were prepared as follows; shikimic acid (50 ppm), pyruvic acid (500 ppm) and the remaining organic acids were prepared to a final concentration of 2000 ppm. Working standard solutions were made by mixture of standard stock solutions with HSU medium, where 2-KGA varied from 0, 2, 5, 10, 50, 100, 200, 500, 800 ppm; SA varied from 0, 0.025, 0.05, 0.125, 0.25, 0.5, 1.25, 2.5, 5 ppm; PyrA varied from 0.25, 0.5, 1.25, 2.5, 5, 12.5, 25, 50 ppm; and the rest of organic acids concentration varied from 0, 1, 2, 5, 10, 20, 50, 100, 200 ppm. Standard stock solutions and working solutions were kept in 4°C.

Rezex ROA-Organic Acid H+ (8%) column (3000 x 7.8mm, Phenomenex) with a Guard column (Carbo-H 4x3.0; Phenomenex) was employed to separate and quantify organic acids. The column contained sulfonated styrene-divinylbenzene spheres in 8% cross-link resin with hydrogen ionic form. The HPLC mobile phase, sulphuric acid (5 mM) was prepared by filtering through a 0.45 µm cellulose acetate membrane (47 mm, Cat No C045A047A, Advantec MFS Inc, USA). Each biological sample was filtered through 0.2 µm Nylon membranes, and samples were diluted either 10 or 20 fold with HSU medium or without dilution and were stored at 4°C prior to analysis. Samples were injected (20 µL) at a flow rate of 0.5 ml/min, column temperature at 55°C and detection wavelength at 210 nm. Organic acids were detected by comparing the retention time of sample to standards. Sample quantification was determined by the peak height of chromatograms using the external calibration standard curve. All data were processed using LC solution software.

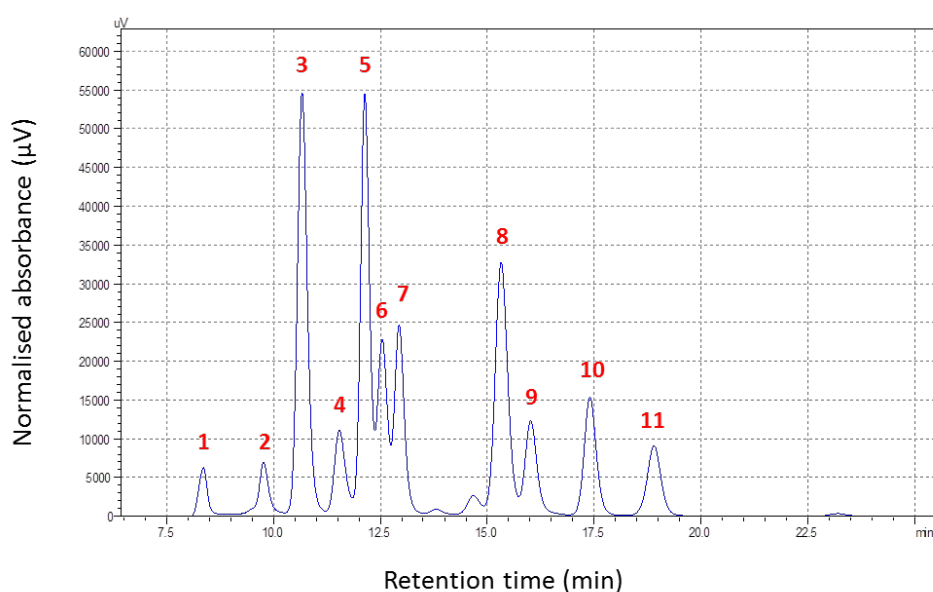


Figure 2.2.3 HPLC chromatogram of working standard organic acids. Individual peaks represents each organic acid listed below, (3) 2-keto-D-gluconic acid at 800 ppm, (4) D-gluconic acid at 200 ppm, (5) pyruvic acid at 50 ppm, (6) L-malic acid at 200 ppm, (7) malonic acid at 200 ppm, (8) shikimic acid at 5 ppm, (9) DL-lactic acid at 200 ppm, (10) formic acid at 200 ppm, and (11) acetic acid at 200 ppm. The chromatogram was normalised by filtered sterilised blank HSU HydroxP medium with glucose. Peak 1 and 2 are background (unknown) peaks from the medium.

Table 2.2.1 Organic acid standard profile analysed by HPLC.

Peak No.	Organic Acid	Abbreviation	Retention Time (min)	Concentration (ppm)
1	Medium	-		unknown
2	Unknown1	Un1	9.82	unknown
3	2-Keto-D-Gluconic acid	2-KGA	10.64	800
4	D-Gluconic acid	GA	11.55	200
5	Pyruvic acid	PyrA	12.11	50
6	L-Malic acid	MA	12.52	200
7	Malonic acid	MoA	12.92	200
8	Shikimic acid	SkA	15.32	5
9	DL-Lactic acid	LA	15.99	200
10	Formic acid	FA	17.38	200
11	Acetic acid	AA	18.90	200

A second HPLC method was developed to specifically analyse L-tartaric acid (TA), citric acid, (CA) and succinic acid (SA), as these organic acid could not be separated using the Rezex ROA-Organic Acid H+ (8%) column used previously. A Prevail™ organic acid column (250 x 4.6 mm, 5 µm particle size; Grace Darison Discovery Sciences) with a Guard column (7.5 x 4.6 mm, 5 µm particle size; Grace Darison Discovery Sciences) was used for this analysis. The mobile phase was prepared by 25 mM phosphoric acid, (KH₂PO₄, pH 2.5 adjusted by H₂PO₄) filtered through a 0.45 µm membrane of cellulose acetate. Sample was injected (20 µl) through the HPLC column with a flow rate of 0.6 ml/min at 50°C, and detection wavelength at 210 nm. However, this method was not able to separate GA and 2-KGA (data not shown).

2.2.5. Effect of selected phosphate-solubilising bacteria on growth of ryegrass

A glasshouse pot-trial supervised by Dr Steve Wakelin at the Lincoln University glasshouse was undertaken. A randomised block design was used with 14 replicate pots prepared for each bacterial treatment. Soil was collected near Hororata, mid Canterbury. The soil is from the Lismore series and characterised as a silt-loam with pH of 5.5 (1:2 soil/water) and an Olsen P of 6 mg kg⁻¹ soil (tested by Hill Laboratories, New Zealand). HydroxP (500 g) was mixed with 30 L of horticulture sand and then blended with sieved soil in 1:2 ratio (HydroxP mix + sand). The final mixture contained 4 g kg⁻¹ of HydroxP to give a total P concentration of 740 mg kg⁻¹.

Twenty perennial ryegrass (Nil endophyte) seeds were sown into each pot (80 mm diameter x 60 mm height) containing HydroxP sand-soil mixture on 28th October (2011). The pots were covered with plastic and were watered as required until seed germination. Prior to bacterial inoculation, the number of seedlings per pot was counted to obtain the germination rate. Bacterial treatments were applied to the ryegrass seedlings 10 d after germination. The ten EPS strains were prepared by culturing in 100 mL nutrient broth in 250 mL conical flasks for 18 h at 30°C (200 rpm) until cell density reached ~ 10⁹ cfu mL⁻¹, with the exception of one slow growing bacterium, isolate Ha185, that was grown for 48 h at 25°. Bacterial cells were harvested by centrifugation at 2300 × g (10 min) and were resuspended in 0.7% sterile saline solution. Ten mL of each bacterial culture were applied to the soil surface of the pots (~10¹⁰ cfu pot⁻¹). The Nil treatment pots were supplied with 10 mL of sterilised 0.7% saline solution.

Pots were watered regularly and 10 mL of Hoagland's solution (Hog-P, Appendix A.1.7) without soluble P was applied to each treatment pot including the Nil-bacteria (Nil) treatment pots at 13 days and 47 days to provide essential nutrients for plant growth. Ryegrass shoots were harvested twice, 47 days (Figure 2.2.4) and 76 days after sowing, by cutting to the tiller level, and were dried at 80° for two days. The combined mean dry weight (MDW) from the two cuts is presented in Table 2.3.6. Total shoot P and calcium was determined by inductively coupled plasma mass spectrometry (ICP-MS) analysis carried out by Lynne Clucas, Department of Soil and Physical Sciences, Lincoln University. The ICP-MS generates electrically conductive gas of ions and electrons by ionizing each sample with inductively coupled plasma after it evaporates solid into liquid vapours. Phosphate and calcium ions were quantified by mass spectrometer (Beauchemin, 2008) and the data are reported in Table 2.3.6 as mean weight matter, mg per each pot.



Figure 2.2.4 Pot trial 46 days after sowing (before 1st cut)

2.2.6. Statistical analysis

In an attempt to define a relationship in expression of PGP phenotypes isolated from different soil types, data on ACC deaminase and phytate mineralisation, and TCaP, HydroxP and FeP solubilisation, and bacterial acidification (Me-Red) from each isolate were recorded using either presence/absence data (1 and 0) or a rating system from 0 to 3 as described above (Sections 2.2.1.2 - 2.2.1.7). To visualise relationships in expression of PGP phenotypes among the samples, the data were first grouped using two-way hierarchical clustering and the organised data matrix visualised graphically as a heatmap. These analyses were conducted in the R statistics package (R Project, Version 2.12.2,

<http://www.r-project.org>). Each value from the raw data set listed in Appendix D of screening for PGP traits on plate assays was standardised to have a mean of zero and standard deviation of 1 using the standardisation formula: $(x - \text{mean}) / \text{standard deviation}$. The clustering method used was hierarchical clustering with complete linkage. The heatmap matrix generated using this method is indicated by the colour scheme from dark red to yellow. Isolates with similar colour coding represent similar characteristics with respect to the PGP traits tested. The darker the colour (i.e. dark red) shown in the matrix, the higher the recorded value.

Statistical analysis to determine whether there was phenotypic variation in bacterial isolates based on environmental habitat (sampling location) or bacterial genera was carried out using multivariate statistics. The raw data (Appendix D) based on the high-throughput screening of 105 isolates was standardised (as before) and similarity of phenotypes among samples measured using Euclidean distance. Similarity in phenotypic attributes of the bacteria was tested using sample location as a factor. In addition, to determine if phenotypic properties were linked to bacterial genotypes, testing was also conducted using bacteria genera as a factor. In both cases, testing was conducted using analysis of multivariate similarities (ANOSIM). To further determine the relationships between environment or genera and phenotype, the data were tested using similarity percentages - species contributions (SIMPER) analysis. In this test, the variables (phenotypes) that contribute to differences between genera can be identified. Multivariate analysis was conducted in PRIMER-E (Version 6.1.150) using methods described in Clarke et al. (2006) and Clarke et al. (2008).

All numerical data from the HPLC analysis are expressed as the mean of three replicates with associated standard errors of mean (mean \pm SEM). Data obtained from the glasshouse pot trial were expressed as MDW. Generalised linear modelling was used to generate pair-wise correlations between soluble P released, concentration of organic acid released by each isolate, and MDW of ryegrass from the pot trial. One-way analysis of variance (ANOVA) was used to calculate significant differences between treatments ($*p < 0.05$) and grouping information was achieved using the Tukey's Method at 95% confidence. Duncans system of lettering was used where mean values that do not significantly vary (at the 5% level) between treatments share the same letter. These analyses were carried out using Minitab version 15 (Minitab, Inc., www.minitab.com).

2.3 Results

2.3.1. Screening for plant growth-promoting traits

The raw data of the screening for PGP traits for the 105 PSB isolates are recorded in Appendix D and examples for plate screening is shown in Figure 2.3.1. The majority of isolates had some PGP traits, and this was most obvious for isolates that were able to release more than 4 mM of soluble P in the liquid culture assay. The high proportion of isolates from Haast and Eyrewell (exotic and native forest) had strong ability to solubilise DCaP, TCaP, and Hyp-G, but these isolates were not able to solubilise HydroxP using sucrose as the carbon source (Table 2.3.1). For example, isolate EE127 released 9.05 mM P from DCaP and solubilised HydroxP in glucose, but lacked the ability to utilise sucrose for HydroxP solubilisation (Hyp-S) (Table 2.3.1).

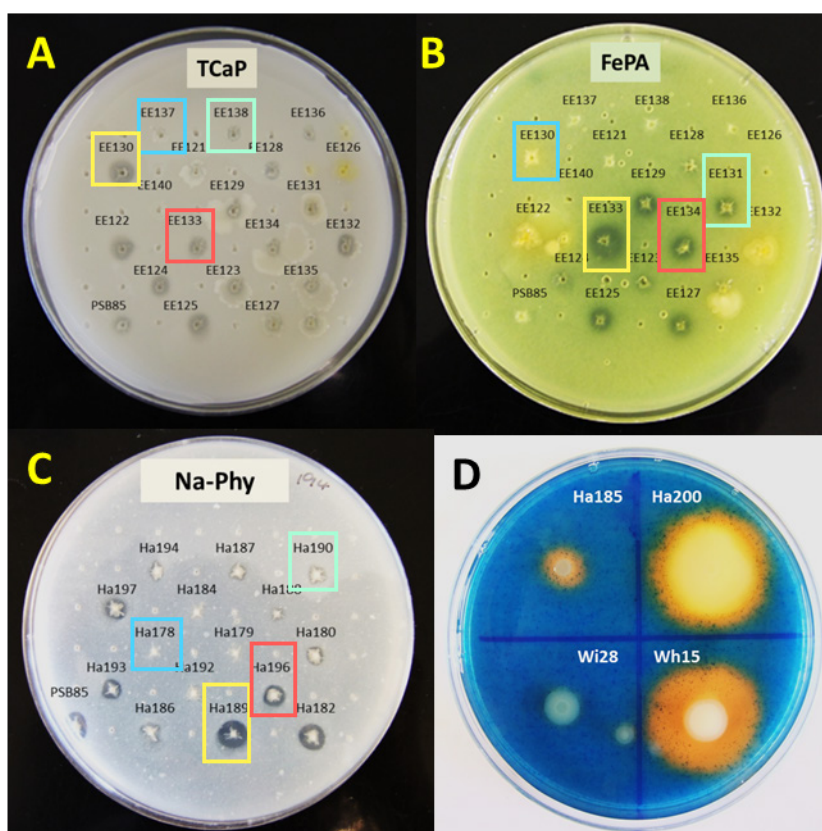


Figure 2.3.1 Sample plates of screening phosphate solubilising isolates with plant growth-promoting traits. Phosphate solubilising bacteria from Eyrewell (exotic forest soil origin) on a tricalcium phosphate plate (TCaP) (A), on Iron phosphate plate (FePA) (B) and isolates from Haast on sodium phytate plate (Na-Phy) (C). Visible halo formation indicates TCaP or iron phosphate has been solubilised by the isolate. Isolates scored as “3” produced a large halo (diameter ≥ 8 mm) indicated by yellow box, “2” produced a medium sized halo (5 – 7 mm) as indicated by red box, “1” a small halo (≤ 4 mm) indicated by green box, and “0” where no halo was observed as indicated by blue box. Siderophore producing rhizobacteria detected by CAS agar plate (D) by removing Fe(III) from the Chromazurol S indicated by colour changes from blue to orange. The CAS plate indicates isolate Wi28 did not produce siderophores, whereas Ha185, Ha200 and Wh15 are siderophore producing bacteria.

Results from methyl red agar plate (Me-Red) assay showed some correlation with the amount of P released from insoluble DCaP in liquid culture assay. Isolates that produced the most acid also released higher amounts of soluble P in culture filtrate (> 6 mM). Isolates from Haast and Eyrewell that were capable of solubilising DCaP were also able to solubilise insoluble iron phosphate on FePA agar plate at low pH (pH 4). For example, isolate Ha200 released 7.56 mM soluble P from DCaP, could solubilise TCaP, produced organic acids on Me-Red plate assay and could solubilise iron phosphate. The majority of isolates exhibited some PGP traits except for two isolates from Ballantrae pasture soil, Ba30 and Ba31 and two isolates from Winchmore pasture soil, Wi6 and Wi16, which did not exhibit any of the PGP traits tested in this study (Appendix D).

2.3.2. Identification of bacterial genera using 16S rRNA gene sequencing

The bacterial 16S rRNA gene sequences were compared against those on the NCBI database using the BlastN search tool. The closest matches to named species on the NCBI database were inferred as being correct and were used for bacteria identification. DNA sequences were subjected to BlastN searches against the reference 16S ribosomal RNA sequence from bacteria data collection to determine bacteria genera and species (Table 2.3.1). A universal cut-off for bacterial speciation is described by Stackebrandt and Goebel (1994), where a 97% of 16S rRNA similarity level was proposed. Drancourt et al. (2000) proposed a 99% and 97% sequence similarity as the cut-off for species and genus identification, respectively. While bacterial speciation using solely 16S rRNA sequencing remains debatable (Teng et al., 2011), it remains the most practical and therefore widely used approach today. In this study, isolates were identified to genus level with the best matching 16S rRNA gene sequencing result list in Table 2.3.1 with species ID name and accession numbers from NCBI database. Isolates that are potentially new bacterial species using <97% similarity cut-off are indicated with a € sign in Table 2.3.1. In soil collected from Haast and Eyrewell, regardless of local land-use, the strongest P-solubilising bacteria (> 4 mM of P from DCaP, able to solubilise both TCaP and HydroxP in plate assays), were all in the genera *Pseudomonas* spp. or *Burkholderia* spp., with the exception of a single *Serratia* strain. At Winchmore, the P solubilisation taxa were *Pseudomonas* and *Enterobacter*, and at Ballantrae *Pseudomonas* and *Serratia* were the dominant P-solubilising taxa (Table 2.3.1). Five PSB isolates belonging to the genus *Arthrobacter* (Ba6, Wh5, Wi30, Ha194, and Ha188, from Ballantrae, Whatawhata, Winchmore and Haast) released the lowest P concentration in the DCaP liquid culture assay (Table 2.3.1), suggesting isolates from this genus may be less effective P solubilisers. However, all isolates from this genus were able to solubilise HydroxP using both glucose and sucrose as a carbon source. This suggests *Arthrobacter* spp. may have multiple pathways for P solubilisation, at least in the plate assay.

Table 2.3.1 Screening for plant growth-promoting traits and identification of phosphate solubilising bacteria.

Location & Soil type	Isolate [‡]	Pcon (mM) [†]	ACC [§]	Na-Phy [¶]	TCaP [¶]	Me-Red [¶]	Hyp-G [§]	Hyp-S [§]	FePA [¶]	16S rRNA gene sequencing [†]		
										Species Identification#	Accession Number#	Max Index
Ballantrae (Pasture soil)	Ba6 [€]	0.50	1	2	1	1	1	1	0	<i>Arthrobacter globiformis</i> strain DSM 20124	NR_026187.1	96%
	Ba40	4.51	1	2	2	2	1	1	1	<i>Serratia grimesii</i> strain DSM 30063	NR_025340.1	97%
	Ba28	4.51	1	2	2	2	1	1	0	<i>S. grimesii</i> strain DSM 30063	NR_025340.1	99%
	Ba21	6.24	1	2	2	3	1	1	0	<i>Pseudomonas costantinii</i> strain CFBP 5705	NR_025164.1	99%
Whatawhata (Pasture soil)	Wh5 [€]	0.59	1	2	2	1	1	1	0	<i>Arthrobacter methylotrophus</i> strain TGA	NR_025083.1	96%
	Wh8 [€]	3.16	0	3	2	1	1	1	1	<i>Paenibacillus amylolyticus</i> strain NRRL NRS-290	NR_025882.1	94%
	Wh15 [€]	4.86	0	3	1	1	1	0	0	<i>Pseudomonas costantinii</i> strain CFBP 5705	NR_025164.1	95%
	Wh22 [€]	8.55	1	2	3	3	1	0	0	<i>Pseudomonas graminis</i> strain DSM 11363	NR_026395.1	94%
Winchmore (Pasture soil)	Wi30	1.35	1	2	1	1	1	1	0	<i>Arthrobacter nitroguajacolicus</i> strain G2-1	NR_027199.1	99%
	Wi11	5.95	1	1	1	2	1	0	1	<i>Enterobacter amnigenus</i> strain JCM1237	NR_024642.1	99%
	Wi18 [€]	6.36	1	2	1	3	1	1	0	<i>Pseudomonas jessenii</i> strain CIP 105274	NR_024918.1	95%
	Wi14	7.94	1	2	1	2	1	0	2	<i>Pseudomonas cedrina</i> strain CFML 96-198	NR_024912.1	98%
	Wi28 [€]	10.73	1	2	2	3	1	0	2	<i>E. amnigenus</i> strain JCM1237	NR_024642.1	94%
Haast (Native forest)	Ha194	0.61	1	1	2	1	1	1	0	<i>A. methylotrophus</i> strain TGA	NR_025083.1	98%
	Ha188	1.02	0	1	2	1	1	1	1	<i>A. methylotrophus</i> strain TGA	NR_025083.1	98%
	Ha197	1.25	1	2	1	0	1	1	1	<i>P. amylolyticus</i> strain NRRL NRS-290	NR_025882.1	97%
	Ha182 [€]	4.16	1	2	3	0	1	0	0	<i>Burkholderia xenovorans</i> LB400	NR_029199.1	96%
	Ha189 [€]	4.55	1	3	3	0	1	0	0	<i>Burkholderia fungorum</i> strain LMG 16225	NR_025058.1	95%
	Ha185 [€]	5.93	1	2	3	1	1	0	0	<i>B. xenovorans</i> LB400	NR_029199.1	95%
	Ha183	6.05	1	2	1	1	1	0	0	<i>B. xenovorans</i> LB400	NR_029199.1	97%
	Ha186	6.84	1	1	1	1	0	0	0	<i>B. xenovorans</i> LB400	NR_029199.1	97%
	Ha200 [€]	7.56	0	2	2	3	1	0	2	<i>Pseudomonas frederiksbergensis</i> strain JAJ28	NR_028906.1	96%
	Ha203	9.07	0	3	2	3	1	0	2	<i>P. frederiksbergensis</i> strain JAJ28	NR_028906.1	98%
Ha201 [€]	9.11	0	2	2	2	1	0	1	<i>P. frederiksbergensis</i> strain JAJ28	NR_028906.1	93%	

Eyrewell (Exotic forest)	EE128	3.57	1	3	2	1	1	0	1	<i>S. proteamaculans</i> strain DSM 4543	NR_025341.1	97%
	EE130	5.22	1	3	3	3	1	0	0	<i>Pseudomonas brenneri</i> strain CFML 97-391	NR_025103.1	98%
	EE131	7.36	1	3	1	3	1	0	1	<i>Pseudomonas umsongensis</i> strain Ps 3-10	NR_025227.1	97%
	EE132	7.66	1	3	2	3	1	0	0	<i>P. jessenii</i> strain CIP 105274	NR_024918.1	98%
	EE133	8.06	1	3	2	3	1	0	3	<i>P. jessenii</i> strain CIP 105274	NR_024918.1	98%
	EE127[€]	9.05	1	3	2	3	1	0	2	<i>P. brenneri</i> strain CFML 97-391	NR_025103.1	93%
Eyrewell (Native forest)	EN102	4.83	1	2	2	3	1	0	1	<i>P. brenneri</i> strain CFML 97-391	NR_025103.1	97%
	EN116[€]	5.09	0	1	2	2	1	1	0	<i>Serratia proteamaculans</i> strain 4364	NR_037112.1	96%
	EN101[€]	8.04	1	2	2	3	1	0	2	<i>P. brenneri</i> strain CFML 97-391	NR_025103.1	96%
	EN108	9.13	1	3	2	2	1	0	1	<i>P. brenneri</i> strain CFML 97-391	NR_025103.1	97%
Ballantrae (internal control)	PSB85	10.38	0	2	1	3	0	0	2	<i>Pseudomonas fluorescens</i> strain IAM 12022	NR_042199.1	99%

†Phosphate released by incubating 7 days with dicalcium phosphate (CaHPO₄) determined by Murphy and Riley's colourimetric assay.

§ Value presented as presence/absence data, 1 and 0.

£Rating system where scored as "3" produced a large halo (diameter ≥ 8 mm), "2" produced a medium sized halo (5 - 7 mm), "1" a small halo (≤ 4 mm) and "0" indicates no halo was observed.

¥Stains chosen for glass house pot-trial are highlighted in light green.

#Bacterial genera and species identification by 16S rRNA gene sequencing where top DNA BlastN searched accession number and ID name

€ Potential new species using a relaxed cut-off of <97% similarity.

†BlastN results based on NCBI search in August 2011

2.3.3. Statistical analysis of plant growth-promoting traits

Two-way hierarchical clustering based on the PGP traits tested revealed that the 105 isolates could be separated into two distinct functional clades. With reference to Figure 2.3.2 the clearest grouping, between the top and lower half of the heat map, show how traits are conserved across some phenotypes. Generally, strong Me-Red, TCaP, and Na-Phy activity are conserved among the bacteria, however these phenotypes are not associated with FePA, Hyp-S, or Hyp-G activity. For example, selection of isolates based on Me-Red phenotype or TCaP solubilising is a poor indicator of ability to solubilise hydroxyapatite. There was also clear horizontal grouping of isolates, and the main groups are denoted A and B (Table 2.3.2). Isolates from group A not only had ability to produce acid (Me-Red), solubilise TCaP, and mineralise Na-Phy, but also had other PGP traits such as solubilising HydroxP in both glucose and sucrose, as well as ACC deaminase production. Isolates from group B lacked the ability to solubilise hydroxyapatite, particularly when supplied with glucose, but some strains were able to solubilise FePA. Most importantly, group A isolates generally had ACC activity whereas this was absent in the group B isolates. Overall, this indicates PSB isolates from group A possess additional PGP traits that can possibly provide improved ryegrass growth.

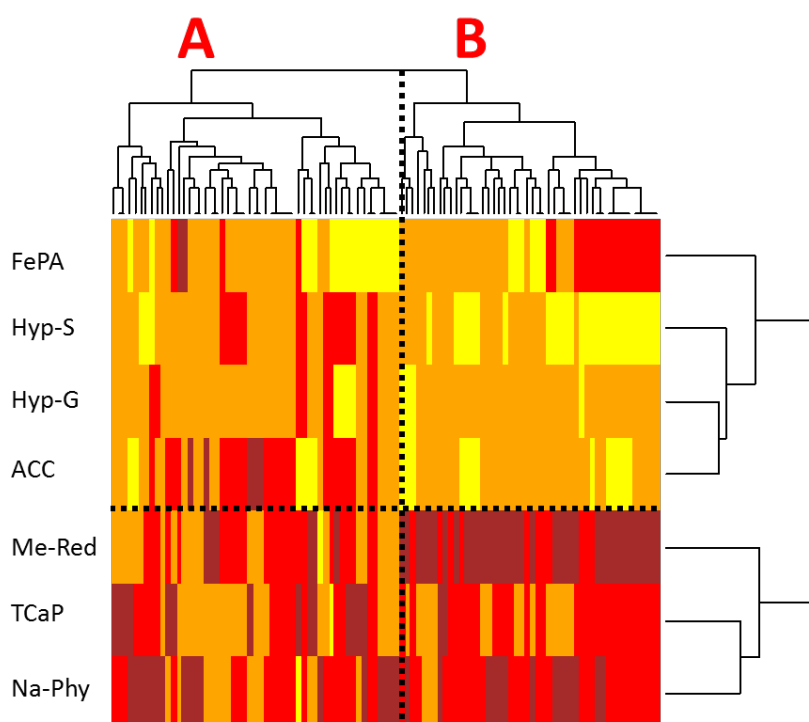


Figure 2.3.2 Heatmap of two-way clustering generated by R statistical software version 2.12.2. Hierarchical clustering with complete linkage method was performed and separated isolates into two groups, A and B.

Table 2.3.2 Cluster grouping of PSB isolates screened for PGP traits by R statistical software.

Site	Group A	Group B
Ballantrae (Pasture)	Ba6, Ba17, Ba3, Ba8, Ba12, Ba29, Ba11, Ba5	Ba40, Ba28, Ba21, Ba27,
Whatawhata (Pasture)	Wh5, Wh8, Wh15, Wh11, Wh6, Wh24, Wh23, Wh9, Wh12, Wh7, Wh10	Wh17, Wh16, Wh21, Wh18, Wh22
Winchmore (Pasture)	Wi30, Wi21, Wi3	Wi11, Wi18, Wi14, Wi28, Wi17,
Haast (Native forest)	Ha194, Ha188, Ha197, Ha182, Ha189, Ha185, Ha183, Ha186, Ha178, Ha179, Ha192, Ha181, Ha193, Ha190, Ha187, Ha196, Ha180, Ha184,	Ha200, Ha203, Ha201, Ha191, Ha204, Ha202, Ha199, Ha195, Ha198,
Eyrewell (Exotic forest)	EE128, EE126, EE138, EE136, EE140, EE121, EE137	EE130, EE131, EE132, EE133, EE127, EE122, EE135, EE134, EE123, EE129, EE125, EE124
Eyrewell (Native forest)	EN116, EN108, EN106, EN118, EN120, EN110	EN102, EN107, EN114, EN115, EN112, EN109, EN113, EN104, EN117, EN101, EN105, EN103, EN111

Note: The ten effective phosphate solubiliser (EPS) chosen for the following experiments are highlighted in red.

The majority of isolates from Ballantrae pasture soil, Whatawhata pasture soil and Haast native forest resided in group A, whereas the majority of isolates from Winchmore pasture soil, and both Eyrewell exotic/native forest resided in group B (Table 2.3.2). This observation was formally tested using two-way crossed ANOSIM analysis. Isolates from Ballantrae were significantly different from Haast, Eyrewell exotic and native forest ($p < 0.05$) (Table 2.3.3). Isolates from Haast native forest differed from those found in Whatawhata pasture soil ($p < 0.05$). Interestingly, there was no significant difference between Haast native forest and both Eyrewell (native/exotic) forest ($p > 0.05$). Thus, bacterial PGP phenotypes are under strong site-based influence, but the site-to-site relationships are complex and understanding the underlying drivers will require in depth investigation.

ANOSIM analysis for differences between known bacterial genera (34 isolates) was also performed. Results showed *Arthrobacter* spp. were significantly different from *Burkholderia* spp. in relation to the PGP traits tested on plate assays ($p < 0.05$) (Table 2.3.3). *Pseudomonas* spp. also differed significantly from *Burkholderia* spp. ($p < 0.05$) (Table 2.3.3). The numbers of isolates sequenced using 16S rRNA gene sequencing for bacterial genera *Enterobacter* spp., *Paenibacillus* spp., and *Serratia* spp. were too low to allow meaningful comparisons, so the pair-wise effects between these species groups are not given in Table 2.3.3.

Table 2.3.3 Two-way ANOSIM statistical analysis for differences between sites and bacteria genera.

Groups (Pairwise tests)	R Statistic	Significance Level %
Sites		
Winchmore, Eyrewell (Native)	0.351	0.7
Ballantrae, Haast	0.227	1.2
Ballantrae, Eyrewell (Exotic)	0.217	2.2
Ballantrae, Eyrewell (Native)	0.473	0.1
Haast, Whatawhata	0.127	3.5
Eyrewell (Native), Whatawhata	0.345	0.1
Bacteria genera		
<i>Arthrobacter</i> spp., <i>Burkholderia</i> spp.	0.691	4.8
<i>Pseudomonas</i> spp., <i>Burkholderia</i> spp.	0.897	1.8

To determine the variables that contributed to the differences between two bacterial genera, one-way similarity percentage - species contribution analysis (SIMPER) analysis was performed on groups that were shown to be significantly different in the ANOSIM analysis; *Arthrobacter* with *Burkholderia*, and *Pseudomonas* and *Burkholderia*. Results are summarised in Table 2.3.4. The main phenotypic difference separating *Arthrobacter* and *Burkholderia* was ability to solubilise Hyp-S. This was strong in *Arthrobacter* spp. but generally not present in *Burkholderia* and contributed most strongly to their separation (44.02 %). This was also the strongest factor separating *Pseudomonas* and *Burkholderia*. The next strongest separating variable was TCaP solubilisation with *Pseudomonas* > *Burkholderia* > *Arthrobacteria*. The other phenotypes each contributed to relatively minor proportions of the differences.

Table 2.3.4 One-way SIMPER analysis between bacterial groups.

Variable	Groups					
	<i>Arthrobacter</i> (n = 5) Av.Value	<i>Burkholderia</i> (n = 5) Av.Value	Contrib %	<i>Pseudomonas</i> (n = 17) Av.Value	<i>Burkholderia</i> (n = 5) Av.Value	Contrib %
Hyp-S	<u>1.33</u>	-0.744	44.02	<u>0.812</u>	-0.996	29.07
TCaP	0.348	<u>1.03</u>	20.43	<u>0.614</u>	-0.756	24.31
Me-Red	-0.242	<u>0.175</u>	10.66	<u>0.612</u>	1.03	14.14
ACC	0.202	0.64	9.78	-8.94E-02	<u>0.64</u>	12.1
Hyp-G	0.759	0.347	8.71	0.645	0.347	7.53
Na-Phy	0.905	0.175	7.41	0.905	0.175	7.41

Underline indicates higher average value that contributes to > 10% of the differences between two bacterial genera.

2.3.4. Selection of potential phosphate-solubilising bacteria - plant growth promoting bacteria

Based on the selection criteria mentioned in Section 2, a subset of ten isolates EN101, EE131, EE132, EE127, Ha200, Ha185, Wh15, Wi28, Ba28 and Ba40 were chosen for further study. These ten strains (hereafter referred to as EPS) were further tested for ability to produce IAA (auxin) and siderophores. In addition to this their organic acid profiles during HydroxP solubilisation were also determined. From here the ten isolates were tested for their ability to increase growth of ryegrass in a glasshouse pot trial in which HydroxP was supplied as the main P source in soil.

2.3.4.1 Phosphate solubilisation and organic acid production

All isolates were tested using HydroxP as the substrate and glucose as the sole carbon source. The strain Ha185 was found to be the best HydroxP solubiliser with 19.01 ± 0.80 mM soluble P detected in the HSU HydroxP liquid culture filtrate, followed by strain Ha200 where 18.75 ± 0.52 mM soluble P was detected at 3 days culture (Table 2.3.5). Half of the isolates (EN101, EE131, EE127, Ha185 and Wh15) showed significant reduction in the amount of soluble P in the culture filtrate at 7 days ($p < 0.05$) (Figure 2.3.3). From this assay the isolates EN101, EE131, EE127, Ha185 and Wh15 may have utilised P from culture filtrate. Day 3 was defined as the optimal time point to determine the amount of soluble P released by PSB instead of 7 days, where the ability of an isolate to solubilise P may be underestimated.

Through HPLC analysis of culture supernatants derived from each of the EPS isolates after either 3 or 7 days incubation, several organic acids were identified. The most abundant organic acid was 2-keto-D-gluconic acid (2-KGA) followed by pyruvic acid (PyrA) and potentially followed by an unknown organic acid named Unknown2 (Un2) (Table 2.3.5). The Un2 organic acid (retention time 10.95 min) is presented here as an arbitrary unit (AU) as it was not possible to construct a standard curve from which concentration data could be derived. Interestingly, no gluconic acid (GA) was detected, with the exception of isolate EE132 (*Pseudomonas* sp.) where 9.83 ± 1.92 mM of GA was found in culture filtrate at day 3 (Table 2.3.5), but was not detected at day 7. Furthermore, this isolate did not produce 2-KGA (Figure 2.3.3), but produced high amounts of Un2 organic acid (51.03 ± 1.83 AU). It is possible both GA and Un2 may have contributed in P solubilisation as well as a low concentration of PyrA (2.66 ± 0.28 mM) for isolate EE132.

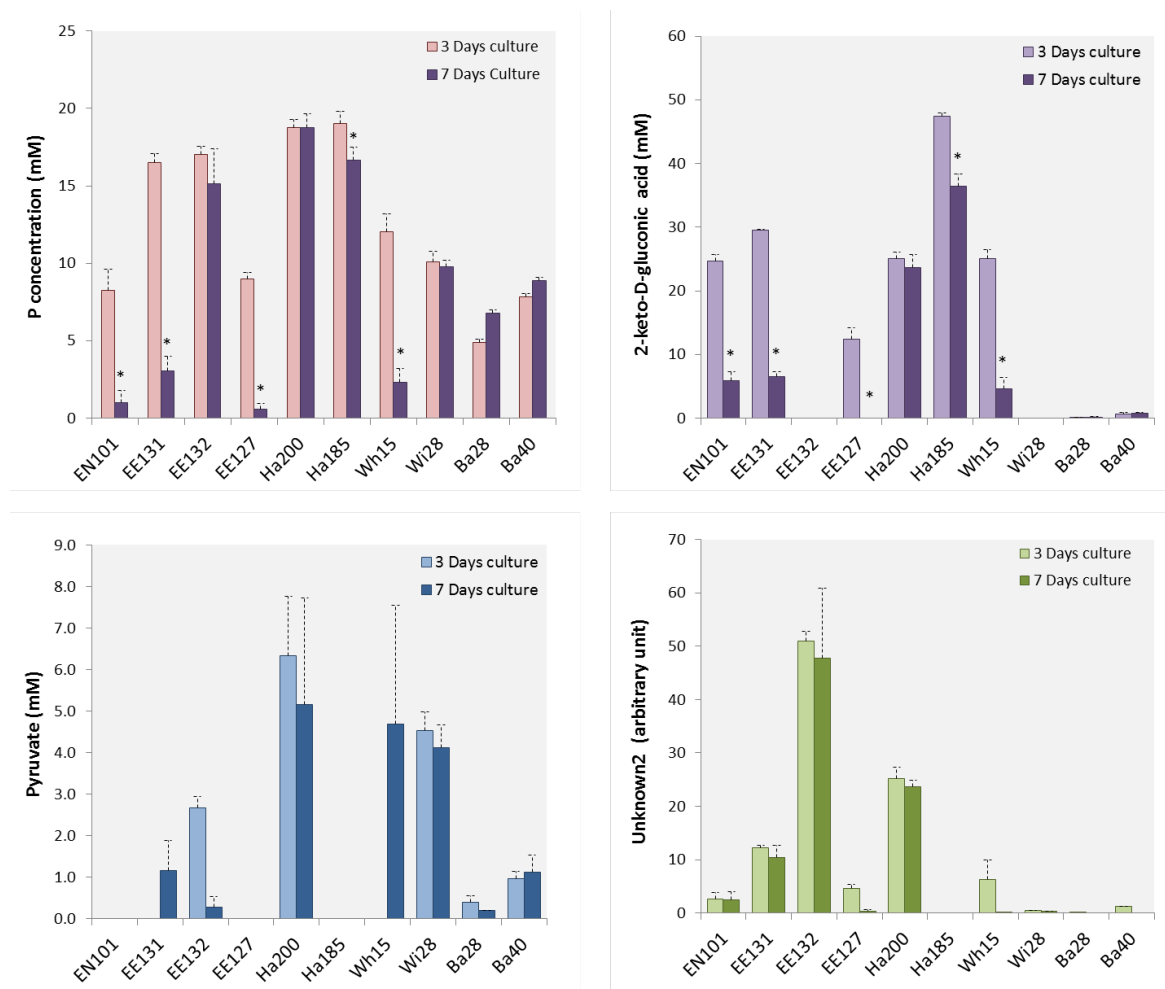


Figure 2.3.3 Phosphate released from insoluble hydroxyapatite by the ten EPS strains and organic acid 2-keto-D-gluconic acid, pyruvic acid and an unknown acid detected from the HSU liquid culture filtrate at day 3 and day 7 analysed by HPLC. * Indicates significantly different from the 3 days culture at 5 % level ($P < 0.05$). Error bars denote the standard error of the mean (SEM). Refer to Table 2.3.1 for strain designation.

The predominant organic acid produced by PSB isolates was 2-KGA as shown in Figure 2.3.3. Isolates N101, EE131, EE127, Ha200, Ha185 and Wh15 all released high concentration of 2-KGA at 3 days but the amount of 2-KGA found in culture filtrate decreased significantly at 7 days culture ($p < 0.05$, Figure 2.3.3) except for Ha200 isolate (*Pseudomonas* sp.) where the concentration of 2-KGA did not differ. It is possible that 2-KGA was taken up by bacterial cells at 7 days. Interestingly, this correlates with soluble P found in the culture filtrate where the concentration of soluble P was found to be significantly reduced from 3 days to 7 days for isolates EN101, EE131, EE132, Ha185 and Wh15. PyrA and lactic acid (LA) were low in concentration compared with 2-KGA (Table 2.3.5). Furthermore, amounts of both PyrA and Un2 were not significantly different between 3 days and 7 days cultures (Figure 2.3.3). Isolate Ha200 not only released 2-KGA (25.04 ± 1.05 mM, 3 days) and Un2, but also the

highest amount of PyrA (6.33 ± 1.42 mM, 3d) amongst all the isolates (Table 2.3.5). This suggests that 2-KGA, PyrA and Un2 may all have been involved in HydroxP solubilisation.

Strain Ha185 (*Burkholderia* sp.) released the highest concentration of 2-KGA (47.36 ± 0.54 mM) and a low concentration of LA (0.78 ± 0.11 mM) at 3 days, and of the isolates tested was the best HydroxP solubiliser (19.01 ± 0.80 mM of soluble P in the culture filtrate at 3 days) (Table 2.3.5). Isolates Ba28 and Ba40 (*Serratia* spp. from Ballantrae pasture soil), showed different organic acid profiles where all organic acids were detected in low concentrations or were not present (Table 2.3.5). Organic acids that may have contributed in P solubilisation for Ba40 are 2-KGA, Un2, PyrA, and L-Malic acid (MA). Both PyrA and MA are involved in the tricarboxylic acid cycle (TCA cycle) of the central metabolic pathway, therefore, it is likely Ba40 employs a wide range of organic acids involved in essential cellular metabolism for MPS. This is quite likely to be the case for isolate Wi28 (*Enterobacter* sp. from Winchmore pasture soil) from which GA and 2-KGA were not detected, but 0.41 ± 0.04 AU of Un2, 4.53 ± 0.45 mM of PyrA and 2.78 ± 0.51 mM of LA were detected, which may have contributed to release of 10.09 ± 0.67 mM of soluble P (3 days) (Table 2.3.5).

2.3.4.2 Effect of EPS isolates on growth of ryegrass

Four isolates resulted in significant increases in MDW in comparison with the Nil control; Ba28 (3.37 g pot⁻¹), Wi28 (3.40 g pot⁻¹), EE131 (3.42 g pot⁻¹) and Wh15 (3.44 g pot⁻¹) vs Nil control (3.04 g pot⁻¹) (Figure 2.3.4, Table 2.3.6). Isolates EE127, EE132, Ba40 and Ha185 also increased growth of ryegrass but at a level that was not statistically significant at the 5% level (Figure 2.3.4). Two isolates (EN101 and Ha200) reduced the overall MDW of ryegrass but this difference was not statistically significant (Table 2.3.6, Figure 2.3.4).

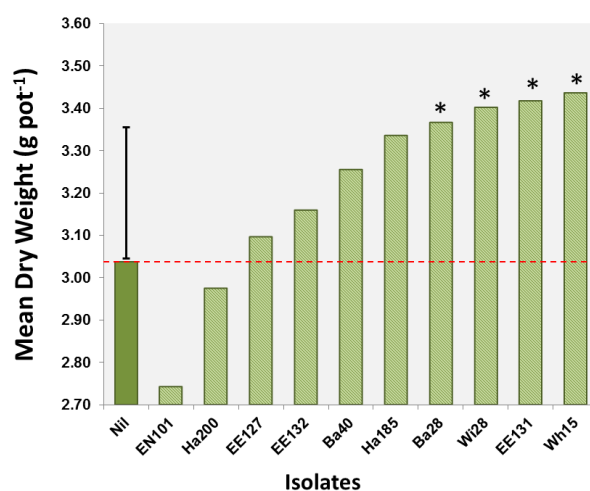


Figure 2.3.4 Glasshouse pot trial of the ten EPS inoculants. The mean dry weight of ryegrass is recorded as gram per pot ($n = 14$). The non-inoculated negative control is indicated as the Nil treatment. Error bar denotes LSD at 5% level (LSD = 0.30). Red line indicates MDW of the Nil treatment (3.04 g pot⁻¹).

Table 2.3.5 Soluble phosphate detected and organic acids released by the ten EPS strains after 3 and 7 days incubated in HSU HydroxP medium

3 Days	P Conc	Organic acid concentration (mM) [£]					
		2Keto-D-gluconic acid	Unknown [§]	D-gluconic acid	Pyruvic acid	L-Malic acid	DL-Lactic acid
EN101	8.28 ± 1.33	24.61 ± 1.08	2.55 ± 1.21	nd	nd	nd	nd
EE131	16.50 ± 0.57	29.51 ± 0.14	12.28 ± 0.36	nd	nd	nd	nd
EE132	17.04 ± 0.50	nd	51.03 ± 1.83	9.83 ± 1.92	2.66 ± 0.28	nd	nd
EE127	9.00 ± 0.38	12.46 ± 1.69	4.64 ± 0.65	nd	nd	nd	nd
Ha200	18.75 ± 0.52	25.04 ± 1.05	25.26 ± 2.06	nd	6.33 ± 1.42	nd	nd
Ha185	19.01 ± 0.80	47.36 ± 0.54	nd	nd	nd	nd	0.78 ± 0.11
Wh15	12.05 ± 1.13	25.12 ± 1.36	6.28 ± 3.60	nd	nd	nd	nd
Wi28	10.09 ± 0.67	nd	0.41 ± 0.04	nd	4.53 ± 0.45	nd	2.78 ± 0.51
Ba28	4.90 ± 0.19	nd	nd	nd	0.40 ± 0.15	nd	nd
Ba40	7.84 ± 0.22	0.60 ± 0.30	1.17 ± 0.08	nd	0.96 ± 0.18	1.16 ± 0.06	nd
7 Days							
EN101	0.99 ± 0.80*	5.92 ± 1.42*	2.47 ± 1.45	nd	nd	nd	nd
EE131	3.07 ± 0.90*	6.55 ± 0.79*	10.34 ± 2.41	nd	1.15 ± 0.74	nd	nd
EE132	15.12 ± 2.27	nd	47.69 ± 13.12	nd*	nd	nd	nd
EE127	0.59 ± 0.38*	nd*	nd	nd	nd	nd	nd
Ha200	18.77 ± 0.91	23.63 ± 2.05	23.71 ± 1.13	nd	5.15 ± 2.58	nd	nd
Ha185	16.64 ± 0.85*	36.40 ± 1.88*	nd	nd	nd	nd	nd*
Wh15	2.32 ± 0.91*	4.61 ± 1.83*	nd	nd	4.69 ± 2.86	nd	nd
Wi28	9.79 ± 0.41	nd	0.29 ± 0.02	nd	4.11 ± 0.55	nd	1.21 ± 0.37
Ba28	6.79 ± 0.22	nd	nd	nd	nd	nd	nd
Ba40	8.89 ± 0.17	0.83 ± 0.05	nd	nd	1.11 ± 0.42	nd*	nd

† Soluble P released from HSU HydroxP medium determined by Murphy and Riley's colourimetric assay.

£ Value represents mean ± standard error of mean (n=3); nd, not detected.

§ Unknown organic acid presented in arbitrary units (AU)

* Indicates significantly different from the three days culture within each column at $p < 0.05$.

Table 2.3.6 Combined data - PGP traits and pot-trial results for the EPS strains

EPS Unit	P released [‡] (mM)	IAA [€] (µg IAA/mL)	Hyp-S [#]	ACC [‡]	Na-Phy [‡]	Siderophore ^Ω	Glasshouse pot-trial					
							MDW [¥]	% Weight increased	% P increased	Mean Ca [§]	% Ca increased	
							g/pot	%	mg/Pot	%	mg/pot	%
Nil							3.04 ^{abc}	0	10.43	0	30.64	0
EN101	8.28 ± 1.33	0.69 ± 0.19	-	+	++	+++	2.74 ^a	-9.86	9.69	-7.05	33.32	8.74
Ha200	18.75 ± 0.52	3.51 ± 0.69	-	-	++	+++	2.98 ^{ab}	-2.04	10.37	-0.54	30.78	0.43
EE127	9.00 ± 0.38	0.83 ± 0.07	-	+	+++	+++	3.10 ^{bcd}	1.98	10.38	-0.40	29.83	-2.67
EE132	17.04 ± 0.50	3.72 ± 0.70	-	+	+++	++	3.16 ^{bcd}	4.08	11.27	8.11	33.25	8.49
Ba40	7.84 ± 0.22	8.20 ± 2.23	+	+	++	++	3.26 ^{bcd}	7.21	11.12	6.63	28.10	-8.31
Ha185	19.01 ± 0.80	1.23 ± 0.19	-	+	++	+	3.34 ^{cde}	9.85	10.84	3.97	32.80	7.03
Ba28	4.90 ± 0.19	5.21 ± 1.11	+	+	++	++	3.37 ^{de}	10.87	11.51	10.36	34.23	11.69
Wi28	10.09 ± 0.67	3.82 ± 0.67	-	+	++	-	3.40 ^{de}	12.05	11.78	12.98	34.59	12.86
EE131	16.50 ± 0.57	2.35 ± 0.74	-	+	+++	+++	3.42 ^e	12.55	11.69	12.16	32.63	6.49
Wh15	12.05 ± 1.13	3.58 ± 0.44	-	-	+++	+++	3.44 ^e	13.20	11.84	13.52	29.02	5.30*

[‡] Soluble P released from HSU HydroxP medium at 3 days determined by Murphy and Riley's colourimetric assay.

[‡], [€] Value represents mean ± standard error of mean (n = 3).

[#] Isolates able to solubilise HydroxP by utilising sucrose indicated as "+" or "-" which indicates no solubilisation.

[‡] Isolates produce ACC deaminase indicated as "+" or "-" which does not produce the enzyme.

[‡] Halo size ≥ 8 mm indicated as +++ and size between 5 – 7 mm, ++.

^Ω No colour changes indicated as -; orange halo size < 20 mm, +; 20 – 30 mm, ++; > 30 mm, +++.

- The symbol "-" in the % Weight increased, P and Ca increased column indicates a % decrease.

[¥] Rows sorted by ascending mean dry weight for isolate treatment from the glasshouse pot-trial (n = 14).

[§] Total P and calcium (Ca) analysed by ICP-MS.

Grouping information using Tukey's Method and groups which do not have a letter in common differ statistically significantly at the 5% level (LSD = 0.31).

Nil represents no inoculant for the pot-trial.

Treatment group that improved ryegrass growth significantly compared to Nil treatment are highlighted in purple.

Through generalised linear modelling, the correlation between P increases in ryegrass shoots and shoot biomass is depicted in Figure 2.3.5. In the pot trial, inoculation of ryegrass with isolate EE132 resulted in an 8.11 % of increase in P in the plant biomass, while making little contribution to plant growth (4.08 % increase). In contrast, inoculation with isolate Ha185 resulted in 9.85 % increase in MDW, but the mean P per pot (plant biomass) increased by only 3.97 %; a number outside the 95% confidence interval of expected outcomes derived across the rest of the dataset (Figure 2.3.5). In a strictly P limited system there would be a strong expectation for increased P to relate to plant growth increase and this was observed across the data. Isolate Ha185 was able to increase P uptake for ryegrass. Isolates Ha200 and EN101 did not significantly increase MDW, despite the fact that these isolates were shown to release P from HydroxP, phytate mineralisation and siderophore (Table 2.3.6). Both Ba28 and Wi28 increased shoot calcium by 11.69 and 12.86 % respectively, indicating that additional calcium was released from HydroxP ($\text{Ca}_5(\text{OH})(\text{PO}_4)_3$) by these isolates and was taken up by ryegrass. However, there was no correlation between calcium uptake and ryegrass growth (Table 2.3.6). Four isolates Wh15, EE131, Wi28, and Ba28 (circled in green, Figure 2.3.5), increased ryegrass growth significantly in comparison with the Nil treatment control (Table 2.3.6) and the % increase in plant growth was positively correlated with the % increase in mean P per pot within 95 % confidence (Figure 2.3.5). These isolates were considered as PSB-PGPB, highlighted in green circle in Figure 2.3.5.

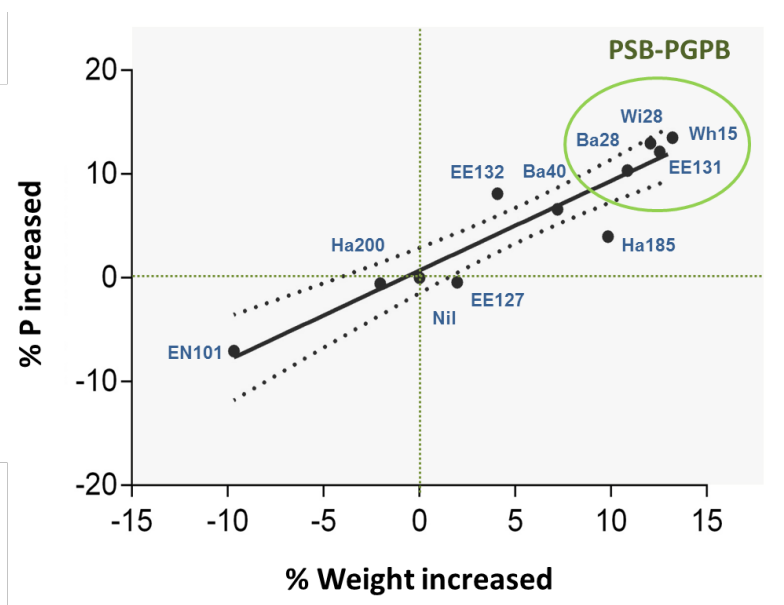


Figure 2.3.5 Glasshouse pot trials of ten EPS isolates showed a significant correlation between dry shoot weight and total phosphorus. Each full circle (●) denotes different bacterial treatment and the 95% confidence interval is indicated by black dotted lines (.....)($R^2 = 0.8742$). Isolates within green shade increased ryegrass growth and isolates within green circle are PSB-PGPB which MDW of ryegrass increased significantly compared to Nil treatment control.

Through 16S rRNA analysis the PSB-PGPB isolate Ba28 was identified to be *Serratia grimesii* with 99 % 16S rRNA similarity (Table 2.3.1). Based on this the isolate was designated *Serratia grimesii* Ba28. Although this isolate is the least effective HydroxP solubiliser out of the 10 EPS strains using glucose as substrate, it gave a 10.36 % of the total P in ryegrass shoot and an 11% increase in dry weight (Figure 2.3.5). The best performing PSB-PGPB isolate among all EPS strains was found to be Wh15, an isolate that shared 95 % similarity to the 16S rRNA of *Pseudomonas costantinii* (Table 2.3.1), hereafter named *Pseudomonas* sp. Wh15. This isolate was shown to increase ryegrass growth by 13.2 % compared to the Nil treatment. It was found that *Pseudomonas* sp. Wh15 was capable of releasing high amount of P from the HSU HydroxP medium, produced IAA, siderophores, and could also mineralise phytate (Table 2.4.1). However, this isolate was unable to release ACC deaminase. This indicated that plant growth promotion was not due to decreased concentration of ACC and ethylene of ryegrass roots alone.

2.4 Discussion

2.4.1. Relationship between phosphate solubilisation bacteria, plant growth-promoting traits and ryegrass growth promotion

Based on two-way hierarchical clustering, 105 PSB isolates tested in this study could be separated into two groups, with isolates in group B capable of organic acid production and TCaP solubilisation and Na-Phy mineralisation. PSB isolates from this group were better at acidification as well as TCaP solubilisation, possibly by reduction in overall pH by protonation as well as production of organic acids, which is known to reduce surrounding pH and solubilise TCap and Na-Phy plate. The link between Na-Phy mineralisation and acid production is in an agreement with Giles et al., (2014) who found acidification by microorganisms, such as *Pseudomonas* sp. CCAR59, is the first step to solubilise phytate by dissolution or sorption which facilitated phytate mineralisation and subsequently enhanced tobacco plant growth by 7 fold compared to the non-inoculant control. Phosphate-solubilising bacteria from Haast native forest or Eyrewell (exotic/native) were significantly different (with respect to their PGP traits) from PSB from Whatawhata and Ballantrae pasture soil, where high levels of P fertiliser had been previously applied. This suggests that the bacterial community structures may differ in relation to the presence of PGP traits of PSB from different environmental habitats and can be shaped by previous history of P application. This finding is similar to that Mander et al. (2012) who reported the incidence of PSB bacteria was significantly higher in low P soil and long

term P application affects the taxonomic composition of bacteria which indicated there is a selection pressure for the occurrence of MPS traits depending on the availability of soil P.

Synergistic effects of ACC deaminase and IAA production by rhizobacteria in directly stimulating plant growth have been reported in many studies in which IAA has been shown to stimulate the auxin signal transduction pathway (Gamalero et al., 2008; Glick, 2012). Moreover, the absence of ACC deaminase limited transcription of auxin response factors, and the synthesis of additional ethylene was increased, which reduced cellular growth (Glick et al., 2007). *Pseudomonas* sp. Wh15 synthesised IAA but did not produce ACC deaminase, and was found to be the most effective PSB-PGPB in this study. This indicates a possible synergistic effect between ACC deaminase and IAA is not always the case for plant growth promotion. In future studies, synergistic interactions between multiple PGP traits should be considered when identifying potential PGP isolate for improved plant growth promotion.

Interestingly, isolates capable of Hyp-S solubility were generally less effective at P solubilisation using glucose as carbon source. It is possible that increased ryegrass growth by Ba28 resulted from its ability to solubilise HydroxP using sucrose as a carbon source. After glucose, sucrose is found in highest concentrations of the carbon sugars produced by ryegrass roots (Mander et al., 2013). Therefore, *S. grimesii* Ba28 is possibly using another pathway for HydroxP solubilisation by utilising sucrose and releasing organic acids involved in the tricarboxylic acid cycle (TCA cycle) e.g. PyrA, MA or LA. Liquid culture assay with sucrose carbon could be done to determine organic acid profile of Ba28 while solubilising HydroxP. The total calcium in shoots of ryegrass plants treated with *S. grimesii* Ba28 was increased by 11.69 %, indicating additional calcium became available from the HydroxP sand mixture (Table 2.4.1). Interestingly, *S. grimesii* DSM 30063^T has previously been identified as PSB isolated from P-rich soil which exhibited strong TCaP solubilisation activity. This strain was also considered to have the potential for development as biophosphate fertiliser (Yang et al., 2012). However, HydroxP solubilisation was not the only PGP trait determined from *S. grimesii* Ba28; the strain had the second greatest rate of IAA production, had ACC activity, and produced siderophores (Table 2.3.6.). As such, the ryegrass growth promotion may have been due, in some part, to P solubilisation but other plant growth promoting mechanisms may have supported this. It is further likely that these mechanisms are additive in nature, where IAA stimulates 'growth potential' of the plant and the increase in P lets the plant fully realise this. *Serratia grimesii* Ba28 was also able to mineralise organic P from the phytate source. Phytate is one of the most common forms of soil organic P and, while not explicitly measured in the soil, the organic matter fraction will undoubtedly

have a strong phytate component (Condrón and Goh, 1989). As such, there may be a further contribution of P mineralisation by this strain in contributing towards the observed PGP.

The PSB-PGPB isolate Wi28 was most closely matched to *Enterobacter amnigenus* strain JCM1237 with 94 % 16s rRNA gene similarity and may potentially be a new species (<97% similarity cut-off) (Table 2.3.1). Therefore, it was named as *Enterobacter* sp. Wi28. *Enterobacter* sp. Wi28 was isolated from Winchmore pasture soil and was not only able to solubilise HydroxP, but it also produced IAA, ACC deaminase, and possibly phytase, and most importantly it promoted ryegrass growth by 12.05 % compared with the Nil control (Table 2.4.1). Interestingly, this isolate did not produce siderophore, indicating that plant growth promotion observed in this glasshouse pot trial, where soluble iron was given as iron sulphate as Hoagland's solution, was probably not playing a role in plant growth promotion. Some strains exhibited several PGP traits, however, in the pot trial ryegrass growth was not significantly improved. For instance, isolate EN101 were found able to solubilise HydroxP, produce siderophore, and ACC deaminase, as well as releasing P from Na-Phy plate, but shoot P was 7.05 % decreased compared to Nil control and the overall MDW was found not significantly different to the control.

2.4.2. Organic acid profile of the ten EPS strains

The *in vitro* HSU HydroxP solubilisation by the ten EPS strains showed that the predominant organic acids produced were 2-KGA and Un2 organic acid when glucose was supplied. Although the concentration of Un2 has yet to be determined, isolate EE132 produced the highest amount of Un2 among all of the isolates with no 2-KGA detected and released high concentration of P from HydroxP. This suggests that Un2 also plays a role in P solubilisation. This finding differs from most commonly accepted MPS mechanisms, reported to be mainly due to GA alone. Many studies have demonstrated MPS by various isolates from different bacterial genera, such as *Enterobacter* spp., *Pseudomonas* spp., and *Burkholderia* spp. (Table 2.4.1). However, most studies did not identify the key organic acids released by the PSB isolates and organic acid profiles remain unknown (Table 2.4.1). Despite this, MPS by GA remains the most widely accepted mechanism of MPS by bacteria (Goldstein and Liu, 1987; Liu et al., 1992). De Werra et al. (2009) performed in-frame deletions of *gcd* gene from *P. fluorescens* CHA0 and found loss of MPS phenotype, whereas mutation in the *gad* gene (Δ *gad*) encoding for gluconate dehydrogenase (Gad) enhanced MPS and the authors concluded it was possibly due to the accumulation of GA (detailed mechanism outlined in Chapter 1.3.4). This

suggested MPS by *P. fluorescens* CHA0 depended on production of GA via the direct oxidation pathway.

Possible reasons for the difference between the findings of this study with previous research include: (i) differences in methodologies used in different studies. Detection of 2-KGA organic acid was not carried out by HPLC and may have been missed from the analysis in other studies; (ii) Because of the similar molecular structure of GA and 2-KGA, these two organic acids could not be separated by the Prevail TM organic acid HPLC column used in this study but the separation was resolved using the Rezex ROA-Organic Acid H+ (8%) column. Therefore, it is likely 2-KGA was co-eluted with GA and the concentration of organic acid released by bacteria and the precise profiles have not been determined in other studies due to analytical difficulties; (iii) Historically, most studies employed TCaP as the sole phosphate (P) substrate instead of less soluble HydroxP (Bashan et al., 2013, Table 2.4.1). It is likely that GA produced by bacteria is not as efficient as 2-KGA at solubilising HydroxP. It is known that HydroxP possesses larger $-\log K_{sp}$ value than TCaP which is more difficult to solubilise, while 2-KGA has lower pK_a dissociation constant than GA ($pK_a = 2.66$ and $pK_a = 3.41$ respectively), where the smaller the pK_a value, the stronger the acid and better at solubilising CaP (Moghimi & Tate, 1978; Bashan et al., 2013). Therefore, it is possible that GA released by a bacterium is not as efficient as 2-KGA at solubilising the most insoluble form of CaP, HydroxP. Hwangbo et al. (2003) found 2-KGA was produced by *Enterobacter intermedium* when phosphate rock (PR) was being solubilised. Phosphate rock contains mainly fluorapatite and HydroxP and is known to include a high amount of P mineral. It is also plausible that 2-KGA produced by *E. intermedium* may only be produced in the presence of HydroxP, which is known to be the most insoluble form of CaP (Dorozhkin & Epple, 2002).

2.4.3. Selection of three EPS strains for mutagenesis

Three EPS were selected for random mutagenesis in the next part of the study, to address the overall aim of identifying novel gene(s) involving in MPS. Genetic modification of strains isolated from the North Island of New Zealand (ie. one of the PSB-PGPB strain Ba28) could not be undertaken as under the controls of the AgResearch's approval GMD09010, only isolates from Ngāi Tahu derestriction (The majority of the South Island New Zealand) are allowed to be manipulated under PC2 containment. For this reason and to increase the possibility of identifying novel genes involved in P solubilisation, three EPS from different genera collected from the South Island of New Zealand were chosen for further investigation in Chapter 3: *Enterobacter* sp. Wi28, isolate Ha200 and isolate Ha185.

Enterobacter sp. Wi28 does not produce GA nor 2-KGA but did produce PyrA, LA and Un2. This suggests it is possible that MPS does not occur via the direct oxidation pathway (detailed mechanism described in Chapter 1) which converts glucose to GA by membrane bound quinoprotein glucose dehydrogenase (Gcd) and its cofactor PQQ did not implicated in P solubilisation by *Enterobacter* sp. Wi28. This suggests there may be an unknown mechanism other than the traditionally accepted pathway present in this strain, and potentially involving a novel gene or pathway involving in MPS.

The 16S rRNA gene sequencing revealed Ha185 is closely related to *B. xenovorans* LB400 (95 % similarity) but below the <97 % similarity cut-off, it is hereafter named *Burkholderia* sp. Ha185. Isolate Ha200 was also found to be closely related to *Pseudomonas frederiksbergensis* but possessed low similarity of 96 %, therefore this isolate is named *Pseudomonas* sp. Ha200. *Burkholderia* sp. Ha185 resided in group A whereas *Pseudomonas* sp. Ha200 resided in group B (Figure 2.3.2).

Table 2.4.1 Environmental habitat and organic acid produced by *Pseudomonas* spp., *Enterobacter* spp., and *Burkholderia* spp.

Microorganisms	Environmental habitat	Substrate [‡]	MPS by organic acid	References
<i>Enterobacter</i> spp.				
<i>Enterobacter intermedium</i>	Grass rhizosphere	PR	2-keto-gluconic acid	Hwangbo et al., (2003)
<i>Enterobacter agglomerans</i>	Rhizosphere soil, Mexico silt loam	HydroxP	Acid production [#]	Kim et al., (1997)
<i>Enterobacter asburiae</i>	Rhizosphere agriculture soil	DCaP	Gluconic, succinic and acetic acids	Gyaneshwar et al., (1999)
<i>Enterobacter aerogenes</i>	Acid soil	TCaP	Undefined	Collavino et al., (2010)
<i>Enterobacter</i> sp. SM1-B1	Lead contaminated soil	TCaP	Organic acid [#]	Park et al., (2011)
<i>Enterobacter</i> sp. LCR1	Paddy fields	TCaP	Organic acid [#]	Kumar et al., (2010)
<i>Pseudomonas</i> spp.				
<i>Pseudomonas fluorescens</i>	Forest soil	ZnP	Gluconic acid	Di Simine et al., (1998)
<i>P. fluorescens</i> RAF15	Ginseng rhizosphere soils	TCaP	Gluconic acid, tartaric acid	Park et al., (2009)
<i>Pseudomonas corrugata</i>	Maize rhizosphere	TCaP	Gluconic acid and 2-keto-gluconic acid	Trivedi & Sa, (2008)
<i>Pseudomonas aeruginosa</i> ,	Rice rhizosphere soil	TCaP	Organic acid [#]	Jha et al., (2009)
<i>Pseudomonas fragi</i> CS11RH1	Garlic rhizosphere	TCaP	Organic acid [#]	Selvakumar et al., (2009)
<i>Pseudomonas putida</i> BIRD-1	Garden soil	DCaP, TCaP, RP	Organic acid [#]	Roca et al., (2013)
<i>Burkholderia</i> spp.				
<i>Burkholderia cepacia</i> 342	Unknown soil	CaP	Acid production [#]	Braz & Nahas, (2012)
<i>B. cepacia</i> DA23	High salt and phosphate soil	TCaP	Gluconic acid	Song et al., (2008)
<i>B. cepacia</i> SCAUK0330	Maize rhizosphere	TCaP	Acid production [#]	Zhao et al., (2013)
<i>B. cepacia</i> LMG 1222 ^T	Unknown	DCaP, AIP, FeP	Unknown	Marra et al., (2011)
<i>Burkholderia tuberum</i> STM678 ^T	Nodulated legume plant	DCaP	Organic acid [#]	Angus et al., (2013)
<i>Burkholderia gladioli</i>	Stevia plant rhizosphere	PR	Unknown	Gupta et al., (2011)

[‡] Insoluble phosphate substrate; Zinc phosphate, ZnP; tricalcium phosphate, TCaP; phosphate rock, PR; hydroxyapatite, HydroxP; di-calcium phosphate, DCaP; undefined calcium phosphate, CaP.

[#] Undefined acid or organic acid

These isolates were originally from chronosequence forest soil which is previously known to have minimal disturbance from human activities such as fertiliser input (Parfitt et al., 2005). Furthermore, Haast chronosequences forest soil was found to exhibit a decline in total P availability with exposition of old soil post glacial deposits over the last 6500 years (Parfitt et al., 2005; Turner al., 2012). This may possibly provide an excellent location for isolating bacteria that contain ancestor genes from ancient origins with limited P exposure. Furthermore, there was no GA detected in the culture supernatant for both selected strain *Pseudomonas* sp. Ha200 and *Burkholderia* sp. Ha185, yet these two isolates released the highest concentration of soluble P from the liquid culture assay among all the EPS strains tested. These two strains were shown to be the most effective HydroxP solubilisers *in vitro* (Table 2.3.5). However, the organic acid profiles of these two strains were found to be different. *Pseudomonas* sp. Ha200 released Un2 organic acid, whereas *Burkholderia* sp. Ha185 did not produce Un2. Most of the organic acid released by *Pseudomonas* sp. Ha200 was 2-KGA and Un2, but the predominant organic acid produced by *Burkholderia* sp. Ha185 was 2-KGA. This indicates the MPS pathways for these two isolates are different. As such there are likely to be as-yet unknown mechanisms present other than the production of GA which is thought to be the key organic acid responsible for MPS. Therefore, both *Pseudomonas* sp. Ha200 and *Burkholderia* sp. Ha185 have the potential for identifying novel gene(s) implicated in MPS and were also subjected to random mutagenesis in Chapter 3.

Chapter 3

Identification of Genes Implicated in Phosphate Solubilisation

3.1 Introduction

Many soil rhizobacteria of different bacterial genera have been documented to exhibit mineral phosphate solubilisation (MPS) and plant growth promoting activities (Collavino et al., 2010; Castagno et al., 2011). These phosphate solubilising bacteria (PSB) are very diverse and can be isolated from many different environments including agricultural and horticultural soils (Naik et al., 2008; Karagöz et al., 2012; Cordero et al., 2012; Hussain et al., 2013), agro-industrial wastes (Vassileva et al., 2010), as well as heavy metal contaminated soil (Park et al., 2011). The wide range of PSB of differing bacterial genera from diverse geographic habitats provided the potential to identify novel genes involved in MPS. On this basis, three isolates of different bacterial genera *Enterobacter* sp. Wi28, *Pseudomonas* sp. Ha200 and *Burkholderia* sp. Ha185 were chosen from a total of 105 screened for their ability to MPS (Chapter 2), and were further assessed for genes involved in P solubilisation.

Bacterial mediated MPS typically occurs through the direct oxidation pathway located at the periplasmic membrane (Chapter 1.3.3). Goldstein and Liu (1987) were the first to clone the *pqq* gene cluster from *Erwinia herbicola* into *E. coli* HB101 and demonstrate MPS by *E. coli* HB101, validating the production of gluconic acid (GA) as the key organic acid involved in MPS. The result confirmed the role of the cofactor PQQ and the relationship between PQQ and the membrane bound quinoprotein glucose dehydrogenase (Gcd), that converts glucose to GA. Since then, many studies have been carried out to investigate the role of *pqq* genes from different bacterial genera, including *Rahnella*, *Enterobacter*, *Gluconacetobacter* and *Serratia* (Rodríguez et al., 2000; Kim et al., 1997; Kim et al., 2003; Intorne et al., 2009; Farhat et al., 2013). To help define the presence of the direct oxidation pathway in various bacteria, degenerate primers PCR that amplify the most conserved regions of *gcd* or *pqq* genes cluster (*pqqE* or *pqqC*) have been developed (Perez et al., 2007; Meyer et al., 2011).

Previous results from Chapter 2 identified that the isolate *Enterobacter* sp. Wi28 does not produce GA nor 2-keto-D-gluconic acid (2-KGA) which are known to be involved in the direct oxidation pathway. Furthermore, no GA was detected in 3 days culture filtrates from both *Pseudomonas* sp.

Ha200 and *Burkholderia* sp. Ha185 grown on Hydroxyapatite (HydroxP). For these reasons, a mini-Tn5Km1 transposon mutant library was constructed for the three selected strains enabling the potential identification of novel genes in PBS. The aim of this chapter was to define the main pathways involved in MPS by *Enterobacter* sp. Wi28, *Pseudomonas* sp. Ha200 and *Burkholderia* sp. Ha185, and determine novel gene(s) implicated in MPS.

3.2 Methods

3.2.1. Bacterial strains and culture conditions

Bacterial strains and plasmids used in this study are listed in **Table 3.2.1**. Bacteria were grown in Luria–Bertani (LB) broth or on LB agar (Sambrook et al., 1989), at 37°C for *E. coli* and at 25°C for *Enterobacter* sp. Wi28, *Pseudomonas* sp. Ha200, and *Burkholderia* sp. Ha185. Cultures were incubated with shaking at 250 rpm in a Raytek orbital incubator. Standard DNA techniques were performed as described in Sambrook et al. (1989) and are outlined in Appendix C. To allow antibiotic selection in either *Enterobacter* sp. Wi28, *Pseudomonas* sp. Ha200, or *Burkholderia* sp. Ha185, the gentamicin resistant plasmid pBBR1MCS-5 was transformed into each of these parent strains (Table 3.1). Electrocompetent cells were prepared as described in Appendix C.2.6 and the cells were electroporated using a Biorad Gene Pulser (25 μF , 2.5 kV and 200 ohms) (Dower et al., 1988). The cells were incubated for 1 h at 25°C before being plated on LB agar plates containing gentamicin at a final concentration of 20 $\mu\text{g mL}^{-1}$.

3.2.2. Construction of Mini-Tn5Km1 transposon mutant library

Transposon mutagenesis was performed using the mini-Tn5 derivative Tn5Km1 as described by de Lorenzo et al. (1990). The three recipient bacterial strains, *Enterobacter* sp. Wi28, *Pseudomonas* sp. Ha200, and *Burkholderia* sp. Ha185, each containing pBBR1MCS-5, were grown overnight in LB broth containing 20 $\mu\text{g mL}^{-1}$ of gentamicin at 25°C. The *E. coli* donor cells, S17-1 λpir (pUTKm1), were grown in LB broth containing kanamycin (50 $\mu\text{g mL}^{-1}$) at 37°C. Two independent 1.5 mL aliquots of each recipient and donor overnight cultures were centrifuged for 3 min at 5900 $\times g$. The pellets were resuspended in 1 mL of sterile LB broth, and 100 μL of each donor and recipient cell suspension were pipetted onto the same LB agar plates that contained no antibiotics. The agar plates were gently moved in a circular motion to homogeneously distribute bacterial cells, before being incubated upright for 6 hours at 25°C to allow conjugation of pUTKm1 into the recipient strain. Two hundred

microliters of LB broth were then pipetted onto the plates and the putative transconjugants were resuspended by swirling with a glass hockey stick. The resuspended cells were then plated on LB agar containing both gentamicin and kanamycin to select for recipient strains containing the transferred plasmid while preventing growth of donor cells. Ten microlitre aliquots of the donor and recipient strains from the overnight cultures were independently applied to separate LB agar plates containing both gentamicin and kanamycin, as negative controls. The plates were then incubated at 25°C overnight for *Enterobacter* sp. Wi28 and *Pseudomonas* sp. Ha200, and 72 h for *Burkholderia* sp. Ha185.

3.2.3. Storage of the mini-Tn5Km1 transposon mutant library

To store the mini-Tn5Km1 mutant libraries, the colonies containing pUTKm1 were patched in a grid pattern corresponding to the prongs of a 96-well colony replicator onto LB agar plates containing kanamycin. A 96 pronged colony replicator was used to inoculate colonies into sterile 96-well plates containing 100 µL 10% glycerol LB broth and kanamycin in each well. Plates were covered with gas permeable adhesive seals (ABgene) and incubated overnight at 25°C with shaking at 250 rpm. The 96-well plates were then sealed with foil PCR seals (ABgene) and stored at -80°C.

Table 3.2.1 Bacterial strains and plasmids used in this study.

Bacterial strains and plasmids	Description	References
Strains		
<i>E. coli</i> DH10B	F- <i>mcrA</i> Δ <i>mrr-hsdRMS-mcrBC</i> Δ 80d <i>lacZ</i> Δ M15 Δ <i>lacX74</i> endA1 <i>recA1</i> <i>deoR</i> Δ <i>ara</i> , <i>leu7697</i> <i>araD139</i> <i>galUgalKnupGrpsL</i> Δ -	Lorow and Jessee, 1990
<i>Burkholderia</i> sp. Ha185	Gm ^R ; Field isolate from Haast, New Zealand, <i>Burkholderia</i> sp. parent strain containing pBBR1MCS-5 broad host range vector	This study
F13	Gm ^R , Kn ^R ; <i>bypC</i> ::Tn5 insertion at 44 bp 3' of the initiation codon, derivative of <i>Burkholderia</i> sp. Ha185	This study
F18	Gm ^R , Kn ^R ; <i>hemX</i> ::Tn5 insertion at 50 bp 3' of the initiation codon, derivative of <i>Burkholderia</i> sp. Ha185	This study
<i>Pseudomonas</i> sp. Ha200	Gm ^R ; Field isolate from Haast, New Zealand, <i>Pseudomonas</i> sp. parent strain containing pBBR1MCS-5 broad host range vector	This study
B8	Gm ^R , Kn ^R ; <i>gcd</i> ::Tn5 insertion at 1818 bp 3' of the initiation codon, derivative of <i>Pseudomonas</i> sp. Ha200	This study
B50	Gm ^R , Kn ^R ; Tn5 <i>Km1</i> insertion at 35 bp 5' of the <i>pqqA</i> initiation codon, derivative of <i>Pseudomonas</i> sp. Ha200	This study
<i>Enterobacter</i> sp. Wi28	Gm ^R ; Field isolate from Winchmore, New Zealand, <i>Enterobacter</i> sp. parent strain containing pBBR1MCS-5 broad host range vector	This study
D23	Gm ^R , Kn ^R ; <i>gltD</i> ::Tn5 insertion, derivative of <i>Enterobacter</i> sp. Wi28	This study
Plasmids		
pBBR1MCS-5	Gm ^R ; broad host range vector	Kovach et al. (1995)
pUTKm1	Kn ^R ; mini-Tn5 <i>Km1</i> transposon delivery vector	De Lorenzo et al. (1990)
pGEM [®] -T Easy	Am ^R ; <i>lacZ</i> multi-cloning site	Yanisch-Perron et al. (1985)
pUC19	Am ^R , <i>lacZ</i> multi-cloning site	

Table 3.2.2 A list of oligonucleotide primers used in this study.

Purpose	Oligonucleotides	Sequences (5'→ 3') ^a
Genome walking and cloning	Uni1 [†]	AAT <u>ACGACTCACTATAG</u> N10 GATC
	Uni 2 [†]	AAT <u>ACGACTCACTATAG</u> N10 GAATTC
	Uni 4 [†]	AAT <u>ACGACTCACTATAG</u> N10 GCGC
	Uni 5 [†]	GTAAT <u>ACGACTCACTATAG</u> GGC N10 GCAGC
	T7	TAAT <u>ACGACTCACTATAG</u> GG
	Sp1	CAGGCTGACCCTGCGCGCTGCGCA
	Sp2A	GGATCCTCTAGAGTCGACCTGCAG
	Sp2B	CCCCGGGTACCGAGCTCGAATTCGG
	Gene sequencing	M13F [‡]
M13R [‡]		GCGGATAACAATTCACACAGG
TnPst2		GGCCTAGGCGGCCAGATCTGATC
Primer walking	PAAR153F	AGAGTAAGGTCGCTGGTTGTCGC
	PAAR755R	ATGACAGCCACATGTCGCGAGATGGC
	B8B11-Gcd-RF	ATCTATCCGGGTAACGTCGG
	B8B11-Gcd-R1	TABTGCTTDCRCCCTTGC
	B8B11-Gcd-LR	ATGTTCCGGCGAGTTGCGG
	B8B11-Gcd-L2	ATNNTGCTNCTGCTRATGGGC
	gcd3R	TTGCCGCTAACGCTTATCCGGC
	2br3Fgsd	ACCTGCAATACATCCGCCATCC
	2bf1gsd	CGTACAGCCCCAGCGCGCACGCCGT
	2br2gsd	CAGGACACCGAATACAGCGCCGA
	gcd1	CCCGTTCCGACCTGAACCTGCTGGCC
	gcd2	CAGTTTGTACGCGATCACATAGTCGC
	B50B54-PQQA-RF	AACTGCAACTGCGTGAAGTGC
	B50B54-PQQA-R1	TTCRATGCCCGTCNTR
	B50B54-PQQA-R3	ATCCASGGGTAATGCTGCG

Oligonucleotide primers designed and used in this study

[†]Oligonucleotide primers from Sarkar et al., (1993)

[‡]Oligonucleotide primers from Macrogen primer list

^aUnderscore denotes specific oligonucleotide from the Restriction Site Oligomers (RSO) corresponding to the internal T7 sequence

3.2.4. Mutant selection

The mutants in the mutant library were screened for loss or gain of function, i.e. the ability to solubilise mineral P, by measuring reduced or increased zones of clearance on tricalcium P agar plates (TCaP) containing trace elements, glucose as a carbon source and tricalcium P (Ca₃O₈P₂) (Appendix A.2.2). This was undertaken by a high-throughput mutant screening system using a 96 pronged colony replicator. Each colony was transferred from the 96-well plate mutant library onto a TCaP plate. Mutants were then allowed to grow at 25°C for 7 days. Colonies with greater or reduced zones of clearance compared to the wildtype strain were identified and sub-cultured on to the National Botanical Research Institute's Phosphate agar NBRIP (see **Figure 3.2.1**). The NBRIP plate was

used here to confirm the loss of phenotype of these mutants. This agar plate was proposed by Nautiyal (1999) as an appropriate and effective medium screening for TCaP solubilising soil bacteria, however unlike the TCaP plate, NBRIP lacks some trace elements including iron, manganese, zinc and copper. The components for insoluble P agar plates are listed in Appendix A.2.2. Auxotrophic mutants were identified by transferring each mutant from LB agar plates onto two types of M9 minimal media that contained either 0.4% casamino acid or 0.4% glucose as the sole carbon source (Appendix A.2.6). Casamino acid is derived from acid hydrolysis of casein and contains a mixture of amino acids which provide a carbon source for bacterial growth (Miller and Johnson, 1940). However, when glucose was supplied as the sole carbon source, bacteria utilise glucose via the Entner–Doudoroff pathway first and synthesise amino acids. Failure of mutants to grow on glucose M9 minimal medium indicates a mutation may have occurred in a gene encoding for a protein involved in a major metabolic pathway that is essential for bacterial growth.

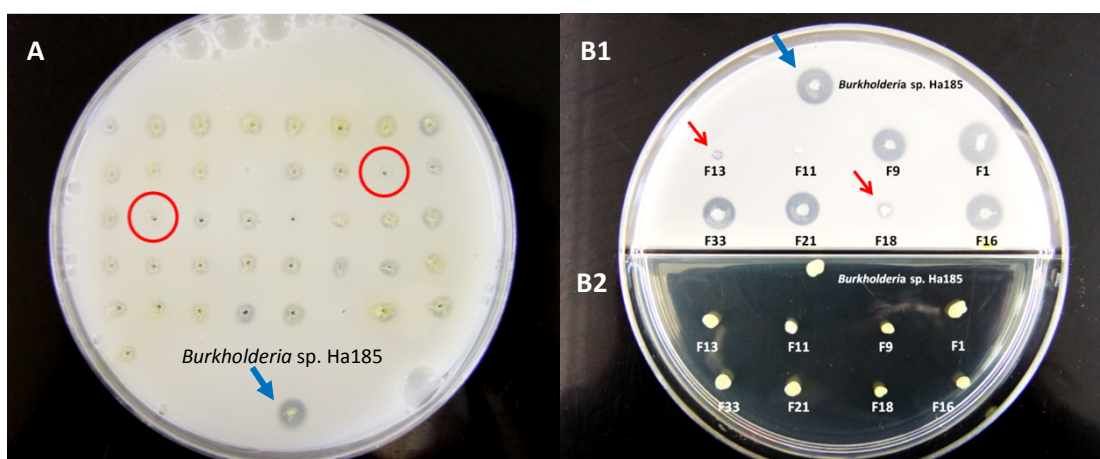


Figure 3.2.1 An example of an initial screen of *Burkholderia* sp. mutants and their ability to solubilise tricalcium P on TCaP plate (A) and NBRIP (B1) after 3 days and 7 days respectively at 25°C. Red circles denote mutants with no P solubilisation ability. Red arrows denote reduced zones of clearance on NBRIP agar (B1) indicating reduced utilisation of sparingly soluble TCaP. B2 shows the growth of corresponding mutants on LB agar. Blue arrows denote wildtype *Burkholderia* sp. Ha185. Screening was performed in triplicate.

3.2.5. Solubilisation index of wildtype strains and mutants

The P solubilisation index (SI) is defined as the ratio of zone of clearance (width of halo zone + colony) relative to the colony width (see **Figure 3.2.2**) on TCaP and NBRIP plates, calculated as described by Edi Premone et al. (1996). To standardise the assays, 1 μL of an overnight culture ($\sim 10^5$ cfu) of the wildtype and each of the mutants was aliquoted onto TCaP and NBRIP plates, and incubated for 14 days at 25°C. Three independent replicates of the experiment were performed. The SI was recorded as a ratio, and the data were analysed by ANOVA to calculate the standard error of the mean (SEM). The ANOVA was carried out using statistical software Minitab version 15. The standard error of the difference between two means (SEM) was calculated for each mutant compared to its wildtype. The P-value of the comparison was calculated by dividing the difference of the means by the SEM. The least significant difference (LSD) is the minimum difference required for the two means to be statistically significantly different at the 5% level ($P \leq 0.05$) and is denoted by * in **Table 3.2.2**.

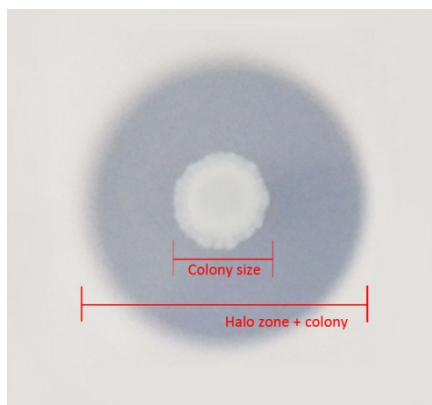


Figure 3.2.2 The National Botanical Research Institute's Phosphate agar (NBRIP) seeded with approximately 10^6 cfu *Burkholderia* sp. Ha185 and incubated for 14 days at 25°C. The solubilisation index (SI) is defined as the ratio of zone of clearance (halo zone + colony) relative to the colony width.

3.2.6. Identification of transposon insertion sites by touchdown PCR

To identify the insertion site of the mini-Tn5*Km1* transposon, genomic DNA (gDNA) was isolated from each mutant (Appendix C.2.1) and was subjected to genome walking using a combination of methods described by Sarkar et al. (1993) and Guo & Xiong, (2006). The insertion site of the mini-Tn5*Km1* transposon was identified by sequencing the product of a restriction site PCR (RE-PCR) using touchdown PCR. With reference to Figure 3.2.3, mini-Tn5*Km1* transposon specific primers were designed, where Sp1 bound to both the inner site of the IS elements of transposon, whereas two other specific primers, Sp2A and Sp2B, were designed from different but nearby regions at each end

of the transposon (Figure 3.2.3). These primers were used in four independent reactions with four universal primers, termed Restriction Site Oligomers (RSOs). Each RSO contained a T7 tail that, based on its degeneracy (**Table 3.2.2**) would bind in random locations to unknown sequences. Universal primer 1 (Uni1) is flanked by a *Sau3AI* restriction site, universal primer 2 (Uni2) is flanked by an *EcoRI* site, and universal primer 5 (Uni5) binds to the *BbvI* restriction site of the mini-Tn5*Km1* transposon (**Table 3.2.2**). The PCR amplification was carried out using Platinum® Taq DNA Polymerase High Fidelity (Life Technologies, California, USA) according to manufacturer's instructions (Appendix C.2.9).

The first round of PCR was performed using 0.2 µM of Sp1 primer and one of each of the universal primers in different reactions. Each reaction comprised 0.2 µM gDNA, 10X High Fidelity reaction buffer, 0.2 mM dNTPs, 2 mM MgCl₂, 1 U of Platinum Taq DNA polymerase and dH₂O to make up a total volume of 20 µL. Touchdown PCR cycles were set using a range of annealing temperature gradients as follows; 94°C for 2 min, followed by three initial cycles of 94°C for 20 s, 60°C for 20 s, and 68°C for 2 min; 3 cycles of the following steps, denaturing at 94°C for 20 s, annealing at 57°C, 55°C, and 45°C for 20 s, and extension at 68°C for 2 min; 35 cycles of 94°C for 20 s, 50°C for 20 s, and 68°C for 2 min. A final extension step of 68°C for 5 min was carried out then held at 4°C prior to the next round of PCR.

The PCR products obtained from the first round were used as DNA template for the second round of touchdown PCR. Either Sp2A or Sp2B was used as the forward primer and T7 as the reverse primer. The Sp2A primer bound to the 5' end outer site of the mini-Tn5*Km1* transposon and the Sp2B primer bound to 3' end of the transposon and both primers were located internal to the Sp1 primer (Figure 3.2.2). Both reactions were undertaken with the T7 universal primer that binds to the T7 tail sequence of the RSO primer incorporated during the first run (Figure 3.2.3). The second round of PCR was carried out as follows; 94°C for 20 s, 60°C for 20 s, 68°C for 2 min; with 3 cycles of each denaturing step, annealing at 57°C and 55°C, and extension at 68°C for 2 min; 35 cycles of 94°C for 20 s, 50°C for 20 s, 68°C for 2 min. A final extension step of 68°C for 5 min was carried out and the final PCR product was then held at 4°C.

The PCR products from each mutant were electrophoresed on a 1% agarose gel (Appendix C.2.10, Figure 3.1.4) and if bands of a greater than 300 bp size were observed, the remaining PCR product was purified using the commercial High Pure PCR Purification kit (Roche Applied Science, Cat No. 11732676001, Basel, Switzerland) according to manufacturer's instructions. Purified PCR products were cloned into the multi cloning site of the pGEM®-T Easy vector using the LigaFast™ Rapid DNA Ligation System (Promega #A1360, Madison, USA) according to manufacturer's instructions

(Appendix C.2.11). The single 3' terminal thymidine overhangs at the multi-cloning site of this vector facilitating ligation of PCR products with adenine overhangs into the plasmids by preventing recircularisation of the vector. The transformants were plated on LB agar plates containing ampicillin to select for the vector. The LB agar plates also contained X-gal (BCIG, 5-bromo-4-chloro-3-indolyl- β -D-galactopyranoside) enabling blue/white selection, where white colonies contain cloned inserts and blue colonies indicate the vector with no insert. The insertion of each amplicon was validated by restriction profile using *EcoRI* restriction enzyme, as *EcoRI* restriction sites flank the amplicon cloning site (Appendix C.2.3). To enable DNA sequencing of the cloned region, plasmid DNA of each clone was isolated using the high pure plasmid isolation kit (Roche Applied Science, Cat No. 11754785001, Basel, Switzerland) in accordance with the manufacturer's instructions. The DNA concentration was then measured using a Nanodrop spectrophotometer (Eppendorf, ND-1000 spectrophotometer, Hamburg, Germany) and plasmid DNA was sequenced using the pGEM[®]-T Easy M13F and M13R specific primers. The names of primers used in this study and their sequences are listed in **Table 3.2.2**. Sequencing was carried out using the Applied Biosystems 3730xl and 9 ABI 3700 from Macrogen (<http://dna.macrogen.com/eng/>). Databases at the National Center for Biotechnology Information (NCBI) were searched using BlastX under the Reference proteins database (Altschul et al., 1997; Schäffer et al., 2001). At least two cloned PCR amplicons were sequenced. Each sequence was aligned to confirm the presence of mini-Tn5*Km1* transposon using sequence analysis software Sequencher[®] version 5.1 (Gene Codes Corporation, Ann Arbor, MI USA <http://www.genecodes.com>).

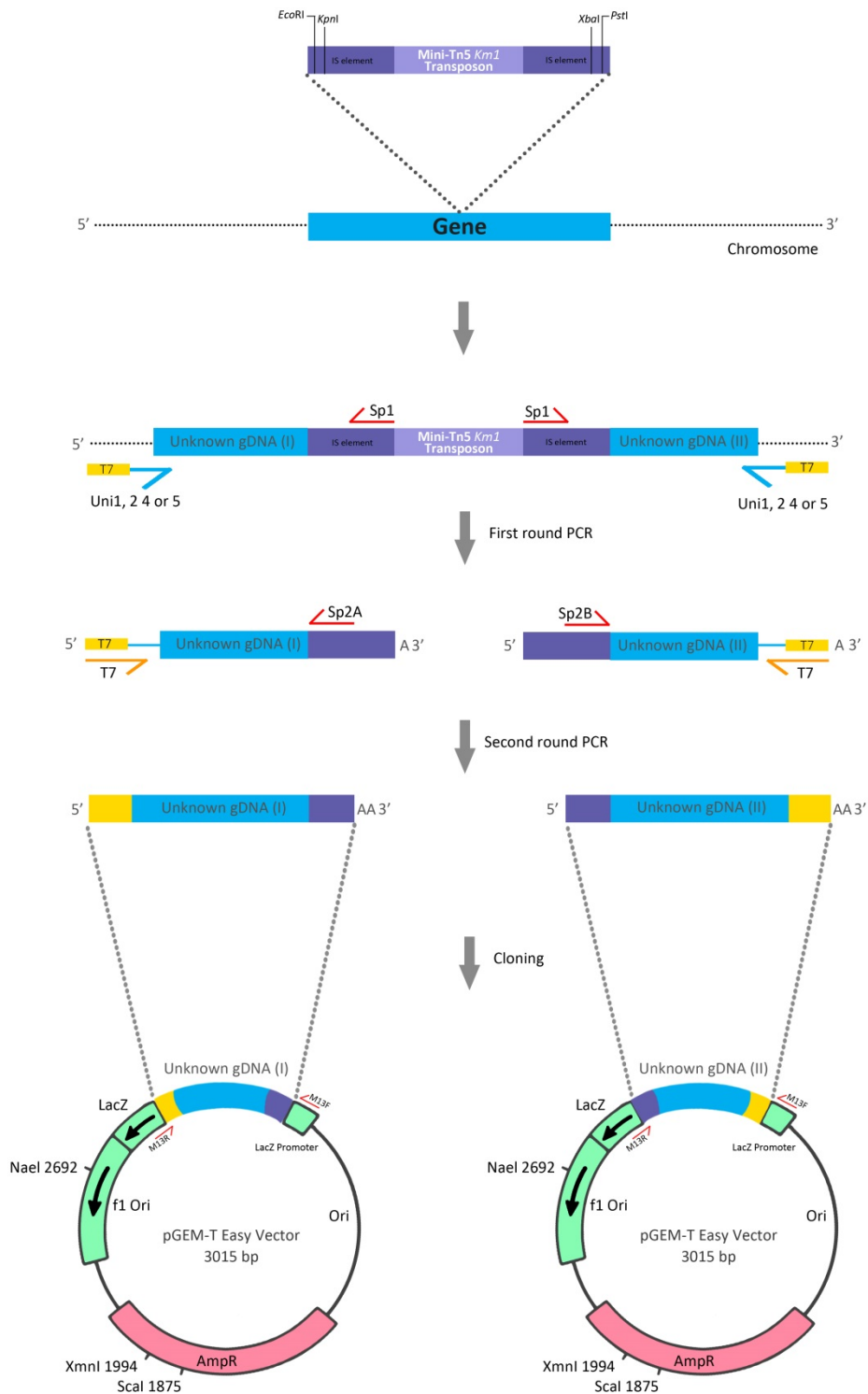


Figure 3.2.3 A schematic diagram of the genome walking strategy using touchdown PCR followed by cloning PCR amplicons into the pGEM[®]-T easy Vector.

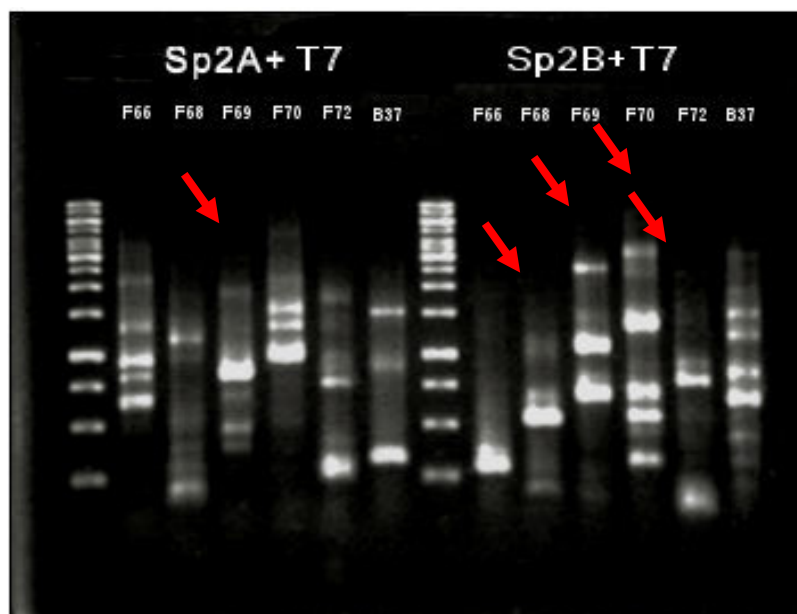


Figure 3.2.4 Example of a 1% agarose gel showing PCR amplicons after touchdown PCR of mutants F66, F68, F69, F70, F72 and B37 using primer combinations of Sp2A + T7 and Sp2B + T7. Red arrows denote PCR amplicons targeted for cloning into pGEM[®]-T easy.

3.2.7. Transposon insertion site identification by cloning strategy

For mutants that proved recalcitrant to genome walking, an alternate cloning approach to identify the mutation site was undertaken. With reference to Figure 3.2.5, 10 μ L of gDNA from each mutant was digested independently with restriction enzymes *EcoRI*, *PstI*, *KpnI* or *XbaI* that flanked the kanamycin resistance encoding gene (Figure 3.2.5) according to the manufacturer's specifications (Appendix C.2.3). The region of DNA encompassing the transposon with the kanamycin resistance gene and the flanking region of gDNA was ligated into the analogous sites of the *lacZ* multiple cloning site of plasmid pUC19 in a 3:1 ratio using T4 DNA ligase from Roche Diagnostics (GmbH, Mannheim, Germany) (Appendix C.2.11) (Figure 3.2.5). The high copy number pUC19 vector derived from pMB1 origin encodes an ampicillin resistance gene allowing its selection (Yanisch-Perron et al., 1985). A 2 μ L aliquot of the ligation was transformed into 100 μ L of chemically competent *E. coli* strain DH10B cells (Appendix C.2.5). The correct clones containing the vector, transposon and associated unknown gDNA were selected for by plating the transformants on agar containing ampicillin and kanamycin, the latter enabling the selection of the mini-Tn5*Km1* kanamycin resistance transposon. To confirm a single insertion, plasmid DNA of the transformants was purified (Appendix C.2.2) and subjected to restriction digest using enzymes targeting the restriction sites flanking the ligation site (Figure 3.2.5). The validated transformants were then sequenced using the Tn5*Km1* transposon specific primer

TnPst2 (Table 3.2.2) that was located 5' to the insertion point, allowing sequencing from the transposon into the flanking region of unknown gDNA, thereby sequencing the gene into which the transposon had inserted (Figure 3.2.5).

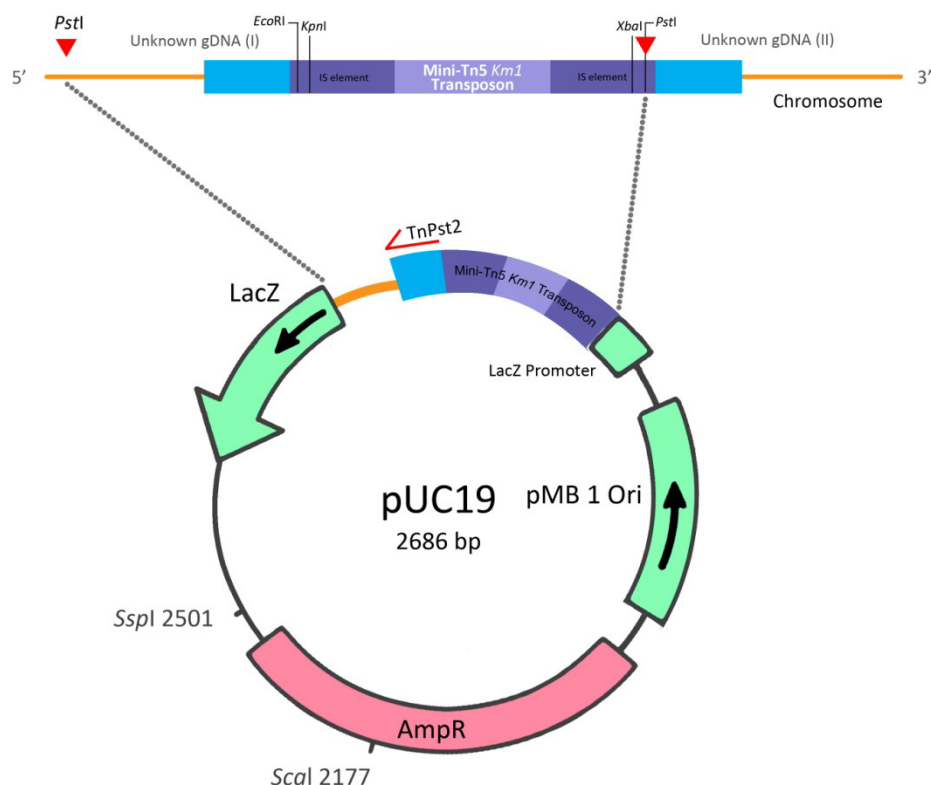


Figure 3.2.5 Cloning strategy for mutants F18 and F86 where the mini-Tn5Km1 transposon and unknown gDNA was cloned into the PstI site of the pUC19 vector. The vector confers ampicillin resistance to the host cell.

3.2.8. Tricalcium phosphate liquid culture assay and colourimetric analysis

Quantification of free P released by *Enterobacter* sp. Wi28, *Pseudomonas* sp. Ha200, *Burkholderia* sp. Ha185 and their mutants was performed by growing each isolate in liquid culture medium supplemented with tricalcium P ($\text{Ca}_3(\text{PO}_4)_2$, TCaP). This was undertaken in 250 mL Erlenmeyer flasks containing 50 mL of liquid culture medium (55.5 mM glucose, 62.5 mM ammonium nitrate, 6.7 mM potassium chloride, 2.0 mM magnesium sulphate, 5.9 nM manganese sulphate, 5.9 nM iron sulphate, and 0.3 g of TCaP, Appendix A.2.3). The medium was adjusted to pH 6.5 before autoclaving for 15 min at 1.1 kg/cm², 121°C. *Enterobacter* sp. Wi28, *Pseudomonas* sp. Ha200 and their corresponding

mutants were grown in LB broth overnight at 25°C with shaking at 250 rpm until the OD₆₀₀ reached ~4.0. Slow growing *Burkholderia* sp. Ha185 and its mutant were grown for 48h under the same conditions. A culture of *E. coli* DH10B was prepared under the same conditions as mentioned above but grown at 37°C. This bacterial strain served as a negative control because of its inability to solubilise P due to the absence of the *pqq* operon (Grigoriev et al., 2012). Prior to inoculation, 1 mL of each isolate was pelleted by centrifugation for 3 min at 5900 × *g* at room temperature. The supernatant was discarded and the pellet was suspended in 1 mL of the liquid culture medium without TCaP. Each flask was then inoculated with the bacterial suspension to a final concentration of 10⁴ cfu mL⁻¹, confirmed by serial dilution and plate counts (Appendix B.2). The 50 mL liquid culture medium was then incubated at 25°C with shaking at 250 rpm. After 72 hours, 1 mL of each culture sample was pelleted by centrifugation at 15,700 × *g* for 10 min. The supernatant was then used to assess the amount of P released from the liquid culture assay after 72 h. The amount of free P in liquid culture filtrate was measured using a colourimetric method of Murphy and Riley (1962) as described in Chapter 2.2.1.1.

3.2.9. The HSU HydroxP liquid culture assay

The HSU liquid culture assay was performed using the HSU buffer described in Chapter 2, and the amount of soluble phosphate (P) released by the wildtype strain and the derivative mutant isolates were measured by Murphy and Riley's colourimetric method (1962) as described in Chapter 2.

3.2.10. Organic acid analysis

The organic acid profile produced by wildtype *Pseudomonas* sp. Ha200 was analysed and quantified by high performance liquid chromatography (HPLC) as described in Chapter 2.

3.3 Results

3.3.1 Mini-Tn5Km1 mutant libraries - *Pseudomonas* sp. Ha200, *Enterobacter* sp. Wi28, and *Burkholderia* sp. Ha185

Transposon mutant libraries were constructed by random transposon mutagenesis using mini-Tn5Km1 (de Lorenzo et al., 1990) for each of the selected strain, *Enterobacter* sp. Wi28, *Pseudomonas* sp. Ha200 and *Burkholderia* sp. Ha185. Mutants were initially selected for kanamycin resistance on LB plate indicating the presence of mini-Tn5Km1 transposon which carries a kanamycin resistance gene. Mutants were later screened for reduced or enhanced ability to solubilise P on TCap or NBRIP plate (Table 3.3.2). The MPS phenotype on TCap plates is recorded in Table 3.3.2. The scoring system is based on the ratio of the halo size to the colony size, where + indicates reduced ratio meaning reduced solubility; ++ denotes similar in ratio to the wide type; +++ denotes enhanced solubilisation; - indicates no solubilisation activity. Three out of 2208 mutants from *Enterobacter* sp. Wi28 had reduced halo size on the TCap plates. Seven out of 2496 mutants from *Pseudomonas* sp. Ha200 had reduced MPS, whereas two mutants, B31 and B42, demonstrated similar solubilisation ability to the wildtype (Table 3.3.2). Nineteen mutants were obtained from 1584 mutants from *Burkholderia* sp. Ha185. Mutant F86 showed enhanced P solubilisation ability on NBRIP plates, where the ratio of the halo size to the colony size was greater than the wildtype *Burkholderia* sp. Ha185.

Each mutant was patched onto M9 minimal media which had either 0.4% casamino acid or 0.4% glucose as the sole carbon source. Mutants that failed to grow or had weak growth on glucose M9 minimal media were considered auxotrophic mutants, which have an inability to synthesise organic compounds, such as amino acids that are required for growth. Auxotrophic mutants would have resulted from disruption of genes involved in amino acid biosynthesis following insertion of the mini-Tn5Km1 transposon (Shaw et al., 1979). These mutants are indicated as "AUX" in Table 3.3.1. Growth of the auxotrophic mutants was severely limited on both M9 minimal medium supplemented with casamino acid or glucose as the only carbon source (Figure 3.3.1). Four non-auxotrophic mutants able to grow on both casamino and glucose minimal medium, were derived from *Pseudomonas* sp. Ha200: B8, B31, B50, and B42. There was only one non-auxotrophic mutant from *Enterobacter* sp. Wi28, labeled D23, and five mutants derived from *Burkholderia* sp. Ha185, labeled F13, F18, F80, F85, and F86 (Table 3.3.1, Figure 3.3.1).



Figure 3.3.1 Image of mini-Tn5Km1 transposon mutants derived from *Burkholderia* sp. Ha185 patched on casamino (C, left) and glucose (G, right) M9 minimal medium. Blue arrows denote wildtype *Burkholderia* sp. Ha185. Mutants F13 and F18 showed growth on both plates, whereas mutants F55, F57, F59 and F62 failed to grow on either medium.

3.3.2. Identification of mini-Tn5Km1 transposon insertion site

Each mutant was subjected to genome walking by touchdown PCR (Figure 3.1.4). The mutation site of the *Burkholderia* sp. Ha185 F18 and F86 mutants, that were difficult to genome walk using touchdown PCR, were identified by the conventional cloning strategy outlined in method 3.2.7 (Figure 3.2.5). The significant results of the BlastX searches are listed in Table 3.3.1, along with the corresponding accession number, E-value and the % identity to the protein. Biological processes or pathways of each gene were searched against the IntoPro (Protein sequence analysis & classification) and KEGG pathway databases.

Sequencing results identified that the auxotrophic mutants had transposon insertions in genes that could be categorised into three groups, i) nucleic acid synthesis, ii) amino acid biosynthesis, and iii) glutamate synthesis (Table 3.3.1). Genes involved in pyrimidine and purine synthesis (highlighted in purple, Table 3.3.1) are implicated in DNA synthesis and are required for bacterial replication. Another set of auxotrophic mutants had insertions in genes involved in amino acid biosynthesis, specifically the genes involved in the synthesis of aromatic amino acids such as phenylalanine, histidine and tryptophan (highlighted in green, Table 3.3.1). These aromatic compounds are synthesised by the chorismate pathway, a process that imposes a significant metabolic burden on the host. Of interest, transposon mutagenesis of the three bacterial isolates in this study resulted in

transposon insertions in the gene encoding the glutamate synthase enzyme (Table 3.3.1, highlighted in orange). The enzyme glutamate synthase is required for the early stages of ammonia assimilation in bacteria and the resultant product, glutamate, is an important precursor for many amino acids. All of the biological processes and pathways mentioned above are essential for bacterial metabolism. Therefore, mutations in genes involved in these pathways may result in a significantly reduced growth rate. This most likely explains the lack of growth on glucose M9 minimal media where organic nutrients were limited. For these reasons, the auxotrophic mutants were not considered for further study, as their growth rates would have significantly affected experiments in relation to MPS.

3.3.3. Phosphate solubilisation by wildtype and mutants on tricalcium phosphate agar plates

The ability of wildtype isolates and non-auxotrophic mutants to solubilize mineral P was measured using two different agar media to determine the reproducibility of using agar plates for testing P solubilisation. The TCaP medium contains additional nitrate, manganese, iron and trace elements (Appendix A.1.4) whereas the NBRIP medium lacks trace elements but is widely used for isolating and testing P solubilising bacteria (Nautiyal, 1999). Table 3.3.2 shows the solubilisation index (SI) of *Pseudomonas* sp. Ha200, *Enterobacter* sp. Wi28, *Burkholderia* sp. Ha185 and their derivative mutants on NBRIP and TCaP plates. In general, there was no significant difference in terms of P solubilisation for wildtype *Pseudomonas* sp. Ha200 and *Enterobacter* sp. Wi28 on both TCaP and NBRIP plates, but the solubilisation by *Burkholderia* sp. Ha185 was reduced on TCaP plates (Table 3.3.2).

Several non-auxotrophic mutants that exhibited reduced MPS on both TCaP and NBRIP plates (Table 3.3.2) had insertions in genes involved in the direct oxidation pathway of *Pseudomonas* sp. Ha200 (Table 3.3.1). These mutants had the transposon inserted in either the genes encoding quinoprotein glucose dehydrogenase (B8), glucose-6-phosphate-1-dehydrogenase (B31) or 35 bp upstream of pyrroloquinoline quinone PqqA (B50). The *Pseudomonas* sp. Ha200 mutants B8 and B50 showed reduced SI on NBRIP plates with 0.00 ± 0.00 and 0.57 ± 0.14 respectively compared to wildtype control (1.26 ± 0.14 ; $p < 0.05$). In contrast, mutant B31, where the mutation occurred in glucose-6-phosphate-1-dehydrogenase, demonstrated no significant difference in ability to solubilise P on NBRIP plates but had a significantly reduced SI on TCaP plates (1.56 ± 0.10 ; $p < 0.05$), in comparison with the wildtype *Pseudomonas* sp. Ha200 (1.63 ± 0.10) (Table 3.3.2).

Table 3.3.1 Mutant library of *Pseudomonas* sp. Ha200 (B), *Enterobacter* sp. Wi28 (D) and *Burkholderia* sp. Ha185 (F).

Isolate	Mutant	MPS Phenotype ^a	Accession Number ^b	Organism ^b	BlastX closest match to mutated ORF ^c	Biological process or pathway	E-Value	Identity
<i>Pseudomonas</i> sp. Ha200	B8	-	YP_350305.1	<i>Pseudomonas fluorescens</i> Pf0-1	Quinoprotein glucose dehydrogenase	Direct oxidation pathway	3.00E-94	91%
	B31	++	ZP_10650857.1	<i>Pseudomonas</i> sp. GM50	Glucose-6-phosphate 1-dehydrogenase	Pentose phosphate pathway	5.00E-88	100%
	B50	+	YP_002875094.1	<i>Pseudomonas fluorescens</i> SBW25	Pyrrroquinoline quinone PqqA	Direct oxidation pathway	8.00E-91	94%
	B42	++	ZP_10594719.1	<i>Pseudomonas</i> sp. GM102	Flagellar motor switch protein G	Chemotaxis	4.00E-148	100%
	B34 ^{AUX}	-	ZP_10663122.1	<i>Pseudomonas</i> sp. GM48	Histidinol dehydrogenase	Histidine biosynthesis	0.00E+00	97%
	B45 ^{AUX}	+	YP_350846.1	<i>P. fluorescens</i> Pf0-1	Phosphoribosylformimino-5-aminoimidazole Carboxamideribotideisomerase	Histidine biosynthesis	1.00E-160	99%
	B35 ^{AUX}	-	ZP_10682030.1	<i>Pseudomonas</i> sp. GM30	Anthranilate synthase component I	Tryptophan biosynthesis	5.00E-79	86%
	B46 ^{AUX}	+	ZP_10682026.1	<i>Pseudomonas</i> sp. GM30	Anthranilatephosphoribosyltransferase	Tryptophan biosynthesis	7.00E-159	97%
	B37 ^{AUX}	+	ZP_10620673.1	<i>Pseudomonas</i> sp. GM78	Glutamate synthase small subunit	Glutamate synthesis	1.00E-57	100%
<i>Enterobacter</i> sp. Wi28	D22 ^{AUX}	-	YP_001175330.1	<i>Enterobacter</i> sp. 638	Carbamoyl phosphate synthase large subunit	Pyrimidine synthesis	2.00E-143	94%
	D5 ^{AUX}	-	YP_003614144.1	<i>Enterobacter cloacae</i> ATCC 13047	Amidophosphoribosyltransferase	Purine synthesis	8.00E-133	93%
	D23	+	YP_003940046.1	<i>Enterobacter cloacae</i> SCF1	Glutamate synthase, small subunit	Glutamate synthesis	6.00E-39	75%
<i>Burkholderia</i> sp. Ha185	F65 ^{AUX}	+	ZP_06465278.1	<i>Burkholderia</i> sp. CCGE1003	2-dehydro-3-deoxyphosphogluconate aldolase	Phosphorylative pathway	6.00E-30	74%
	F59 ^{AUX}	-	YP_560625.1	<i>Burkholderia xenovorans</i> LB400	3-dehydroquinate synthase	Chorismate biosynthesis	3.00E-161	95%
	F55 ^{AUX}	-	YP_004229710.1	<i>Burkholderia</i> sp. CCGE1001	Shikimate kinase	Chorismate biosynthesis	1.00E-26	81%
	F68 ^{AUX}	+	ZP_06297177.1	<i>Burkholderia</i> sp. CCGE1001	Chorismate synthase	Chorismate biosynthesis	1.00E-77	98%
	F66 ^{AUX}	-	YP_001897167.1	<i>Burkholderia phytofirmans</i> PsJN	Phosphoribosyl-AMP cyclohydrolase	Histidine biosynthesis	1.00E-93	96%
	F78 ^{AUX}	-	YP_003908394.1	<i>Burkholderia</i> sp. CCGE1003	Imidazole glycerol phosphate synthase (subunit HisF)	Histidine biosynthesis	3.00E-55	98%
	F57 ^{AUX}	-	ZP_02882233.1	<i>Burkholderia graminis</i> C4D1M	Tryptophan synthase, beta subunit	Tryptophan biosynthesis	5.00E-81	95%
	F62 ^{AUX}	-	YP_001896485.1	<i>B. phytofirmans</i> PsJN	Carbamoyl phosphate synthase large subunit	Pyrimidine synthesis	1.00E-154	99%
	F77 ^{AUX}	-	YP_001896485.1	<i>B. phytofirmans</i> PsJN	Carbamoyl phosphate synthase large subunit	Pyrimidine synthesis	1.00E-154	98%
	F69 ^{AUX}	-	YP_003908510.1	<i>Burkholderia</i> sp. CCGE1003	Orotate phosphoribosyltransferase	Pyrimidine biosynthesis	1.00E-110	99%
F76 ^{AUX}	-	YP_001890498.1	<i>B. phytofirmans</i> PsJN	Amido phosphoribosyltransferase	Purine synthesis	5.00E-70	87%	
F70 ^{AUX}	-	ZP_06842396.1	<i>Burkholderia</i> sp. Ch1-1	Glutamate synthase (ferredoxin)	Glutamate synthesis	3.00E-71	92%	

F72 ^{AUX}	-	ZP_06297057.1	<i>Burkholderia</i> sp. CCGE1001	Adenylylsulfatereductase, thioredoxin dependent	Cysteine biosynthetic process	4.00E-71	91%
F81 ^{AUX}	++	YP_001894616.1	<i>B. phytofirmans</i> PsJN	Sulfate adenylyltransferase subunit 2	Hydrogen sulfide biosynthesis	7.00E-82	98%
F13	+	YP_003907489.1	<i>Burkholderia</i> sp. CCGE1003	Hypothetical protein	Unknown	3.00E-38	84%
F18 [†]	+	YP_557627.1	<i>B. xenovorans</i> LB400	Bifunctional uroporphyrinogen-III synthetase/uroporphyrin-III C-methyltransferase	Haem biosynthesis	1.00E-111	93%
F80	+	ZP_02886362.1	<i>Burkholderia graminis</i> C4D1M	Penicillin-binding protein, 1A family	Peptidoglycan biosynthesis	2.00E-105	92%
F85	++	YP_004228782.1	<i>Burkholderia</i> sp. CCGE1001	Multi-sensor signal transduction, histidine kinase	Peptidyl-histidine phosphorylation	9.00E-146	98%
F86 [†]	+++	YP_559465.1	<i>B. xenovorans</i> LB400	Dihydrolipoamide acetyltransferase	Glucose metabolism	0.00E+00	99%

a; Phenotype of the mutant on tricalcium phosphate agar plate (TCaP); + indicates reduced solubilisation, ++ denotes similar ratio to the wide type, +++ denotes enhanced solubilisation; - no solubilisation activity

b; Bacteria species and GenBank accession number searched using BlastX against the reference proteins database at NCBI in November 2012

c; DNA sequence flanking the transposon insertion site obtained by touchdown PCR

d; Colours represent similar biological pathways identified by IntoPro and KEGG pathway database where highlighted; dark blue, pentose phosphate pathway and direct oxidation pathway; green, aromatic amino acid synthesis; orange, glutamate synthesis; purple, pyrimidine and purine synthesis; light blue, others.

†; Transposon insertion site identified by cloning strategy with pUC19 vector

AUX; Auxotrophic mutant - unable to synthesise an organic compound required for its own growth

The *Enterobacter* sp. Wi28 D23 mutant, where the transposon had inserted into the *gltD* gene encoding the small subunit of glutamate synthase, had significantly reduced ability to solubilise TCaP with a SI of 0.33 ± 0.24 (D23) compared to the wildtype 1.31 ± 0.24 on NBRIP plate, but there was no significant difference between the mutant or wildtype strain on the TCaP plates (1.53 ± 0.17).

The non-auxotrophic *Burkholderia* sp. Ha185 mutant F13, had an insertion in a gene encoding an hypothetical protein (Table 3.3.1). The SI of this strain showed no significant difference compared to the wildtype control on both NBRIP and TCaP plates (Table 3.3.2). The mutation in the bifunctional Uroporphyrinogen III synthase gene (*hemX*) in *Burkholderia* sp. Ha185 (F18) resulted in a significantly reduced SI on NBRIP plates (2.23 ± 0.32 , $p < 0.05$) when compared with the wildtype but there was no significant difference in SI when F18 and the wildtype were compared on TCaP plates (2.11 ± 0.26 and 1.83 ± 0.26 respectively).

Table 3.3.2 Solubilisation Index of wildtype *Pseudomonas* sp. Ha200, *Enterobacter* sp. Wi28, *Burkholderia* sp. Ha185 and their derivative mutants on TCaP and NBRIP plates.

	Average SI \pm SEM TCaP Plate	Average SI \pm SEM NBRIP
<i>Pseudomonas</i> sp. Ha200	1.63 ± 0.10	1.26 ± 0.14
B8	0.00 ± 0.00 *	0.00 ± 0.00 *
B31	1.56 ± 0.10 *	1.22 ± 0.14
B50	1.46 ± 0.10 *	0.57 ± 0.14 *
B42	1.39 ± 0.10 *	1.29 ± 0.14
<i>Enterobacter</i> sp. Wi28	1.34 ± 0.17	1.31 ± 0.24
D23	1.53 ± 0.17	0.33 ± 0.24 *
<i>Burkholderia</i> sp. Ha185	2.11 ± 0.26	3.30 ± 0.32
F13	1.49 ± 0.26	3.11 ± 0.32
F18	1.83 ± 0.26	2.23 ± 0.32 *
F80	1.28 ± 0.26 *	2.18 ± 0.32 *
F85	1.83 ± 0.26	3.27 ± 0.32
F86	2.03 ± 0.26	3.50 ± 0.32

* indicates a statistically significant difference between means at a 5% level compared to the appropriate wildtype strain

The *Burkholderia* sp. Ha185 mutant F80, containing a mutation in the gene encoding the penicillin-binding protein (1A family) involved in cell wall formation, exhibited a significant reduction in SI on both NBRIP and TCaP plates relative to the wildtype *Burkholderia* sp. Ha185 (2.18 ± 0.32 and 1.28 ± 0.26 respectively; $p < 0.05$). Independent *Burkholderia* sp. Ha185 mutants in the gene encoding for histidine kinase (F85) or dihydrolipoamide cetyltransferase (F86), showed no significant differences on either the NBRIP or the TCaP plate compared to the wildtype strain.

Overall, the results show there are discrepancies in the SI when measured on either TCaP or NBRIP plates, although TCaP was the only source of insoluble P in both media (**Figure 3.3.2**). The inconsistencies of the SI between these two different media and for the comparison of the wildtype strain and its mutant derivatives on the same media indicated using an agar plate based assay for P solubilisation was an unreliable method. This is in an agreement with Bash et al. (2013) who suggested liquid culture testing should replace the traditional plate assays in determining P solubilisation. Therefore, a liquid culture assay was used that enabled the determination of MPS in a homogenous solution. Liquid culture also allows the surface contact of bacterial cells to TCaP. Only a couple of non-auxotrophic mutants from *Pseudomonas* sp. Ha200, *Enterobacter* sp. Wi28 and *Burkholderia* sp. Ha185 were selected for the liquid culture assay due to a limited amount of incubator space available at the time of this study. The non-auxotrophic mutant B8 that had a mutation on the membrane bound quinoprotein glucose dehydrogenase of *Pseudomonas* sp. Ha200, was an ideal mutant for confirming the direct oxidation pathway involved in P solubilisation as outlined in Chapter 1.3.3. The only non-auxotrophic mutant from *Enterobacter* sp. Wi28 (D23) was also selected for liquid culture assay. Although there were discrepancies in the SI on TCaP and NBRIP plates, the DNA sequence analysis of the genes involved in non-auxotrophic mutant F13 and F18 revealed that they encoded a hypothetical protein and a bifunctional uroporphyrinogen III synthase protein respectively. As these genes have not previously been implicated in P solubilisation, these mutants were also chosen for further analysis.

3.3.4. Phosphate solubilisation by wildtype and mutants in tricalcium phosphate liquid culture medium

The use of the liquid culture assay allowed quantification of the amount of free P in the culture filtrate which provided an indirect measurement of TCaP solubilised or released by the wildtype bacterium and its mini-Tn5Km1 transposon derived mutants. This assay measures the amount of soluble P in the culture filtrate, and excludes the amount of P in the bacterial cells. Of the three wildtype strains, *Burkholderia* sp. Ha185 had the highest rate of soluble P released with an average of 16.91 ± 0.24 mM of soluble P detected at 72 h (**Figure 3.3.2**). *Pseudomonas* sp. Ha200 released an average of 12.42 ± 0.57 mM and for *Enterobacter* sp. Wi28, 8.21 ± 0.58 mM soluble P was detected from the filtrate at 72 h. The *Burkholderia* sp. Ha185 non-auxotrophic mutants F13 and F18 had similar growth rates to the wildtype, with initial cell densities of approximately $4.00 \log_{10}$ cfu mL⁻¹ increasing to around $6.00 \log_{10}$ cfu mL⁻¹ by 72 h (Table 3.3.3). However, the ability of *Burkholderia* sp. Ha185 F13 and F18 mutants to solubilise hydroxyapatite was significantly reduced (0.55 ± 0.09 and

0.31 ± 0.16 mM of P detected in the final filtrate, respectively, **Figure 3.3.2**). The auxotrophic *Burkholderia* sp. Ha185 mutant F65, containing a mutation in the 2-dehydro-3-deoxyphosphogluconate aldolase gene, was unable to solubilise mineral P. Accordingly, the growth of this mutant decreased from 4.33 log₁₀ cfu mL⁻¹ down to 3.13 log₁₀ cfu mL⁻¹ over 72 hours.

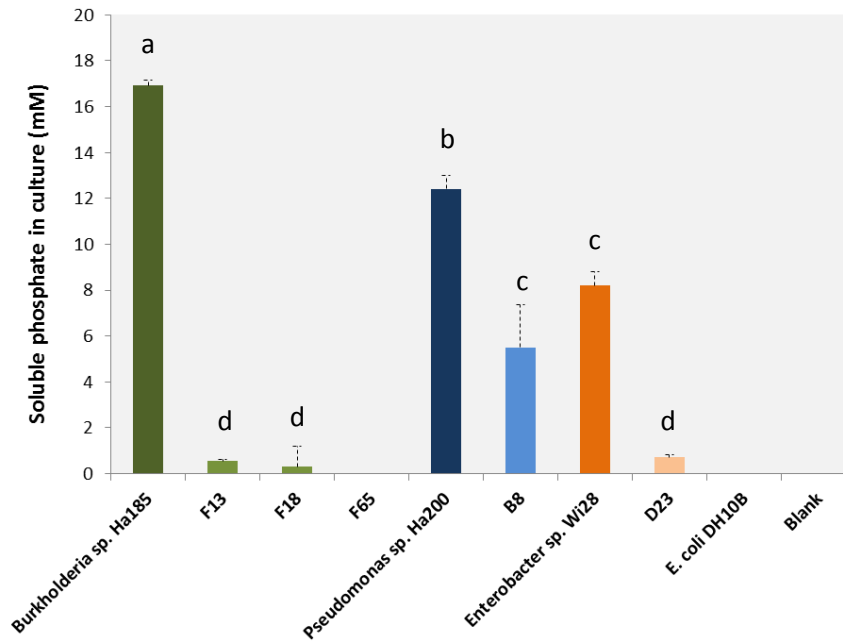


Figure 3.3.2 Soluble phosphate measured by molybdenum blue reagent after incubating wildtype strains and their derivative non-auxotrophic mutants in TCaP liquid culture assay. All treatments were incubated at 25°C except for *E. coli* DH10B which was incubated at 37°C. Error bars represent the SEM of three independent experiments. Tukey's test was used to compare treatment pairs and treatments which do not have a letter in common are significantly different at the 5% level.

The *Pseudomonas* sp. B8 mutant, where the transposon was inserted on the quinoprotein glucose dehydrogenase (*gcd*) gene implicated in the direct oxidation pathway, solubilised approximately 50% of the P solubilised by the wildtype, with an average of 5.51 ± 1.87 mM and 12.41 ± 0.57 mM soluble P respectively ($p < 0.001$). *Enterobacter* sp. Wi28 D23, with a mutation in the glutamate synthase gene, exhibited a 10-fold reduction in the ability to solubilise P with 0.70 ± 0.12 mM soluble P, compared to the wildtype where 8.21 ± 0.58 mM of soluble P was detected in the filtrate (**Figure 3.3.2**). However, the growth of mutant D23 in the liquid culture assay did not increase over 72 h, with a starting 4.14 log₁₀ cfu mL⁻¹ and a final concentration of 3.88 log₁₀ cfu mL⁻¹ at 72 h (Table 3.3.3). In contrast, the wildtype *Enterobacter* sp. Wi28 had a starting average cell density of 4.86 log₁₀ cfu mL⁻¹, increasing to 7.94 log₁₀ cfu mL⁻¹ after 72 h (Table 3.3.3). Under limited soluble P, the *E. coli* DH10B bacteria culture did not grow over the 72 h duration at 37°C. The growth of *E. coli* DH10B declined

from 4.32 log₁₀ cfu mL⁻¹ to 2.03 log₁₀ cfu mL⁻¹ and, as expected, there was no free P detected in the culture filtrate (Table 3.3.3).

Table 3.3.3 Colony forming units of wildtype *Burkholderia* sp. Ha185, *Pseudomonas* sp. Ha200, *Enterobacter* sp. Wi28, and their derivative mutants in TCaP liquid culture assay before incubation and at 72 h.

	Initial cell number (0 h) (Log ₁₀ cfu mL ⁻¹)	Final cell number (72 h) (Log ₁₀ cfu mL ⁻¹)
<i>Burkholderia</i> sp. Ha185	4.53	6.72
F13	4.44	6.60
F18	3.95	6.26
F65	4.33	3.13
<i>Pseudomonas</i> sp. Ha200	4.39	5.58
B8	4.72	7.40
<i>Enterobacter</i> sp. Wi28	4.86	7.94
D23	4.14	3.88
<i>E. coli</i> DH10B[†]	4.32	2.03
Blank	0.00	0.00

[†] *E. coli* DH10B was incubated at 37°C

3.3.5. Genes involved in phosphate solubilisation in *Pseudomonas* sp. Ha200

Mini-transposon random mutagenesis was used to create a mutant library of strains with mutations in genes such that the ability of *Pseudomonas* sp. Ha200, *Burkholderia* sp. Ha185 and *Enterobacter* sp. to solubilise insoluble mineral P was impaired (Table 3.3.1). Several non-auxotrophic mutants were tested for the ability to solubilise TCaP on plates and the solubilisation indices were determined (Table 3.3.2). The mini-Tn5*Km1* transposon derived mutants that had significantly reduced ability to solubilise TCaP were identified (Figure 3.3.2). This was performed using a liquid culture assay where cultures were incubated in an orbital shaker so the insoluble TCaP would be homogeneously distributed within the liquid medium. The transposon mutants tested were F13 and F18 derived from *Burkholderia* sp. Ha185, B8 mutant from *Pseudomonas* sp. Ha200 and D23 from *Enterobacter* sp. Wi28. This section focuses on genes of *Pseudomonas* sp. Ha200 involved in P solubilisation that have been identified by mutagenesis, gene sequencing and annotation, and P solubilisation assays.

In *Pseudomonas* sp. Ha200 mutant B8, the mini-Tn5*Km1* transposon had inserted at 1818 bp from the initiation codon of the *gcd* gene (Table 3.2.1), and is thereafter called *gcd*::Tn5(B8). The *Pseudomonas* sp. Ha200 *gcd* gene sequence was aligned with similar DNA regions from five closely related *Pseudomonas* species, *P. brassicacearum*, *P. fluorescens* SBW25, *P. syringae* pv. *tomato*, *P. fluorescens* Pf-5 and *P. fluorescens* Pf0-1. The most conserved regions of DNA identity from the resultant consensus sequence were used to design a series of degenerate primers. Degenerate primers were designed from both the 5' (B8B11-Gcd-LR and B8B11-Gcd-L2) and the 3' (B8B11-Gcd-RF and B8B11-Gcd-R1) ends of the transposon insertion site of mutant B8 (Table 3.2.1). The degenerate

primers were then used to perform PCR on *Pseudomonas* sp. Ha200 gDNA, giving a ~550-bp PCR product from the 5' end and a ~1200-bp from the 3' end of the *gcd*::Tn5(B8) mutation site. Because the degenerate primers were used, the resultant PCR products were cloned into the vector pGEM[®]-T Easy vector allowing their sequencing using M13F and M13R primers (Section 3.2.6). From this sequence, template specific primers (**Table 3.2.1**) were then designed to enable primer walking using the primers listed in **Table 3.2.1**, targeting the *gcd* region. Using this strategy, a region totaling 3468 bp was sequenced. The resultant consensus sequence was then annotated and compared against protein databases (BlastX) via NCBI genome browser (**Table 3.3.4**). The results showed the entire sequence was comprised of a partial sequence coding for the carbohydrate-selective porin (*oprB* gene) located upstream 5' to the *gcd* gene (Figure 3.3.3). This enzyme acts as a carbohydrate transporter and has been found to diffuse glucose across the outer membrane of *P. aeruginosa* (Wylie and Worobec, 1995). Located 3' to the *gcd* gene is the 5' region of the *lon* gene which encodes an ATP-dependent protease La and has a major role in eliminating misfolded proteins (Lee et al., 2006). A BlastX comparison of the complete *gcd* gene revealed its closest orthologs of its gene product to be the *gcd* genes products of *Pseudomonas* sp. GM24 (ZP_10694921.1, **Table 3.3.4**). The bacterium *Pseudomonas* sp. GM24 was isolated from the rhizosphere of the eastern cottonwood, *Populus deltoids* (Pelletier et al., 2012).

To determine if the gene order of *Pseudomonas* sp. Ha200 was conserved across closely related species, gene orthologue neighbourhood analysis of the *gcd* gene across several *Pseudomonas* spp. where full genome sequences are available was performed using the Integrated Microbial Genomes (IMG) (<http://img.jgi.doe.gov/>). There was little homology with neighbouring genes such as the *oprB* and *lon* gene (Figure 3.3.4). The exception was *P. putida* UW4, which had the same gene order as *Pseudomonas* sp. Ha200 at this region. Neighbourhood connection was also not found using STRING (<http://string.embl.de/>) to look for interactions between these genes. This indicates the *gcd* gene regulation is unlikely to be related to neighbouring gene sequences.

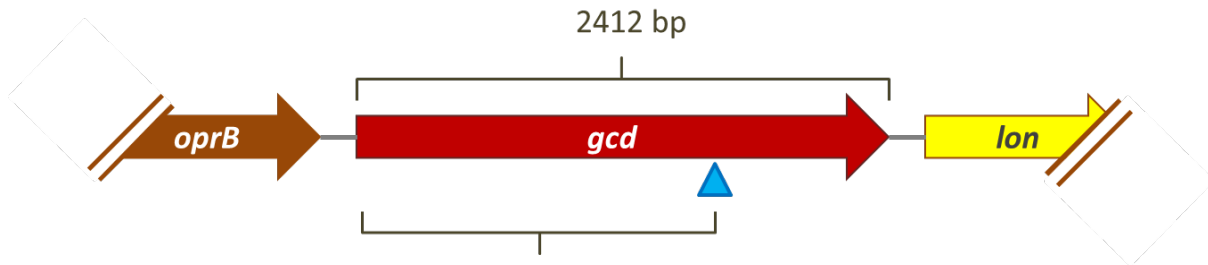


Figure 3.3.3 Schematic of the *Pseudomonas* sp. Ha200 glucose dehydrogenase (*gcd*) encoding region. Membrane bound quinoprotein glucose dehydrogenase (*gcd*) of *Pseudomonas* sp. Ha200 with partial sequence of an *oprB* gene upstream (brown arrow) of the *gcd* and a partial *lon* sequence (yellow arrow) located downstream. Blue arrow denotes mini-transposon Tn5km1 insertion site at 1818 bp 3' of the *gcd* open reading frame (Mutant B8). (Sequence accession No. JX282600).

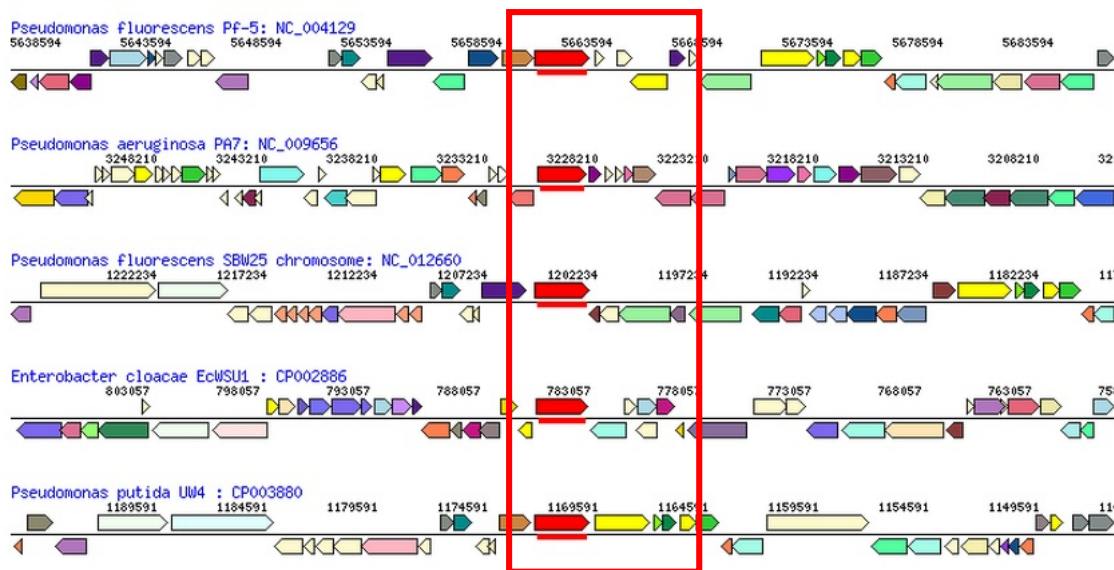


Figure 3.3.4 Schematic representation of the membrane bound quinoprotein glucose dehydrogenase (*gcd*) arrangement in different gram-negative *Pseudomonas* spp. bacteria species and an *Enterobacter* sp. isolate. Gene ortholog neighbourhood analysis of *gcd* genes undertaken using the Integrated Microbial Genomes (IMG) system with *P. fluorescens* Pf-5, *P. aeruginosa* PA7, *P. fluorescens* SBW25, *P. putida* UM4, and *Enterobacter cloacae* EcWSU1. The open reading frame for *gcd* is highlighted in red (), *oprB* in brown () and *lon* gene in yellow () in the red highlighted box.

Table 3.3.4 Predicted homology for *Pseudomonas* sp. Ha200 ORFs identified from DNA sequencing.

ORF	Amino Acid	Nucleotides ^a	G+C %	Degree of similarity ^{b,c}	Gene, species ^c	Accession No. ^c
<i>gcd</i> Operon						
<i>oprB</i> (Partial)	51	1 – 153	59.9	100/100//460 (410 – 460) 98/100//460 (410 – 460)	Carbohydrate-selective porin <i>oprB</i> [<i>Pseudomonas mandelii</i> JR-1] Carbohydrate-selective porin [<i>Pseudomonas</i> sp. GM21]	ZP_11110104.1 ZP_10697552.1
<i>gcd</i>	806	211 – 2729	63.0	91/94//803 (74 – 803)	Membrane-bound PQQ-dependent dehydrogenase, glucose/quininate/shikimate family [<i>Pseudomonas</i> sp. GM24]	ZP_10694921.1
<i>lon</i> (Partial)	117	3117 – 3468	62.4	91/95//803 (74 – 803) 98/99//805 (58 – 174) 98/99//805 (58 – 174)	Quinoprotein glucose dehydrogenase [<i>Pseudomonas</i> sp. UW4] ATP-dependent protease La [<i>Pseudomonas</i> sp. GM67] PIM1 peptidase [<i>P. mandelii</i> JR-1]	YP_007028001.1 ZP_10634656.1 ZP_11110108.1
<i>pqq</i> Operon						
<i>pqqA</i>	25	123 – 197	50.7	96/100//38 (15 – 38) 96/100//24 (1 – 24)	Coenzyme PQQ precursor peptide <i>pqqA</i> [<i>Pseudomonas</i> sp. GM41(2012)] Coenzyme PQQ synthesis protein <i>pqqA</i> [<i>Pseudomonas fluorescens</i> Pf0-1]	ZP_10667191.1 YP_350885.1
<i>pqqB</i>	354	284 – 1346	62.9	96/97//303 (1 – 160) 96/98//303 (161 – 303) 93/96//303 (1 – 160) 97/97//303 (161 – 303)	Coenzyme PQQ biosynthesis protein B [<i>Pseudomonas</i> sp. GM18] Pyrroloquinoline quinone biosynthesis protein <i>pqqB</i> [<i>P. mandelii</i> JR-1]	ZP_10703244.1 ZP_11114780.1
<i>pqqC</i> (Partial)	93	1343 – 1623	64.1	98/98//102 (1 – 92) 98/98//250 (1 – 93)	Pyrroloquinoline quinone (coenzyme PQQ) biosynthesis protein C [<i>Pseudomonas</i> sp. GM16] Coenzyme PQQ biosynthesis protein C [<i>Pseudomonas</i> sp. GM24]	ZP_10714250.1 ZP_10689940.1

^a Nucleotide sequence is a continuum from the published sequence GenBank Accession No. JX282600

^b Amino acid similarity (% identity/% similarity//over amino acid residues) in relation to sequence generated in this study

^c BlastX results based on NCBI search in March 2013

The other *Pseudomonas* sp. Ha200 non-auxotrophic mutant B50 demonstrated a partial reduction in MPS. The partial sequence of the transposon insertion site was determined by genome walking followed by primer walking from known sequences (Section 3.2.6). Primer walking PCR was performed using degenerate primers B50B54-PQQA-RF and B50B54-PQQA-R1 (Table 3.2.2) designed from the 3' end of where the transposon was inserted. These primers were designed from DNA sequence alignments, using Vector NTI® (Life Technologies, California, USA), of four related species including *P. brassicacearum*, *P. stutzeri* DSM 4166, *P. fluorescens* Pf0-1, *P. fluorescens* SBW25, and *P. syringae*. The PCR products from primer walking using *Pseudomonas* sp. Ha200 genomic DNA as a template gave a ~1300-bp PCR product from the 3' end of the B50 mutation site. The ~1300-bp amplicon was cloned into the vector pGEM®-T Easy enabling the sequencing of the cloned region using M13F and M13R primers (Section 3.2.6). From the resultant DNA sequence assembly, the ~1300-bp consensus sequence was searched against NCBI protein database using BlastX. The resultant best match gene alignments are listed in Table 3.3.4 where the *Pseudomonas* sp. Ha200 *pqqA* gene was found to share highest identity to the closely related to *Pseudomonas* sp. GM41(2012) and *P. fluorescens* Pf0-1.

Because the genome of *P. fluorescens* Pf0-1 has been sequenced and annotated, the strain was used as the model system in this study. In addition to this, *P. fluorescens* Pf0-1 is a soil bacterium also known to solubilise P (Miller et al., 2010). Gene ortholog neighbourhood analysis of *pqqF* from *P. fluorescens* Pf0-1 revealed evidence that some of the *pqq* genes are present in other bacterial families, such as the Enterobacteriaceae (Figure 3.3.5). Bacteria from this family (for example *Klebsiella* spp., *Cronobacter* spp., and *Erwinia* spp.) have been found to encode of *pqqB - E* and *pqqF*, but lack *pqqA* (Figure 3.3.5). Neighbourhood analysis shows the order of the *pqq* operon—*pqqF* followed by *pqqA-E*, which is unique to many *Pseudomonas* species, for example, *P. putida*, *P. fluorescens*, and *P. syringae* (Figure 3.3.5).

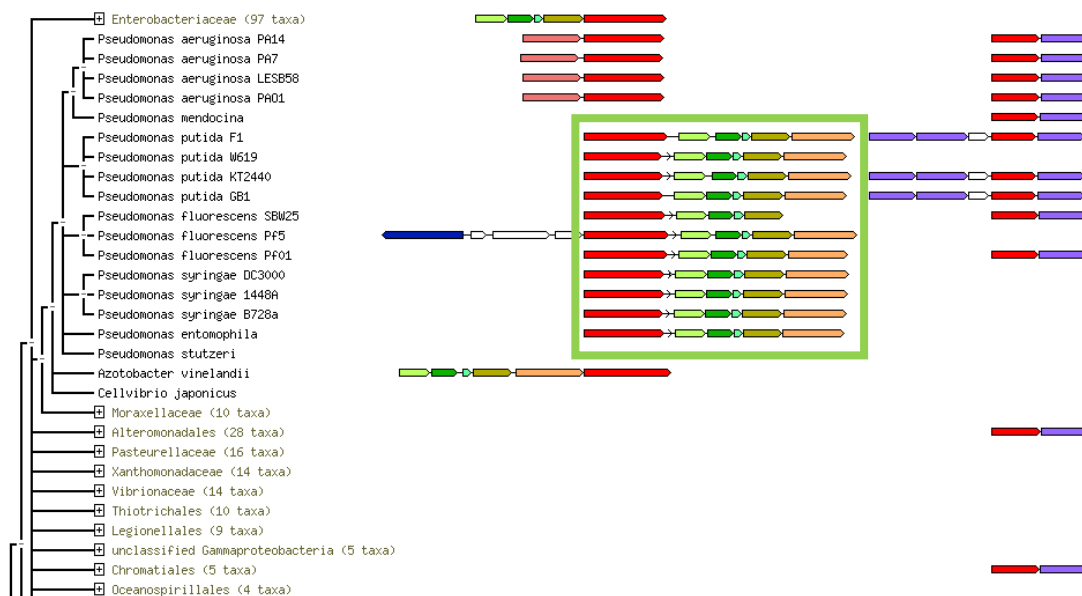


Figure 3.3.5 Schematic diagram of *pqq* gene ortholog neighbourhood analysis across several bacteria families by STRING 9.05. Green highlighted box indicates *pqq* operon with seven open reading frames from 5' to 3' which consist of *pqqF* (red), *pqqA* (black), *pqqB* (light green), *pqqC* (dark green), *pqqD* (light blue), *pqqE* (brown), and peptidase S9 (orange). Immediate neighbourhood genes are connected by black lines, and genes with same colours indicate orthologous proteins.

From the gene ortholog neighbourhood analysis of *pqqF* from *P. fluorescens* Pf0-1, the DNA sequence of the entire *pqq* operon from this strain was aligned with sequence from the *Pseudomonas* sp. Ha200 genes *pqqA* to *pqqC*. A schematic of the *P. fluorescens* Pf0-1 *pqq* operon is shown in Figure 3.3.6 and represents the gene sequence of *Pseudomonas* sp. Ha200. The mini-Tn5*Km1* transposon in B50 is inserted 35 bp upstream from the *pqqA* initiation codon and from the sequence alignment, it is predicted to be inserted 2552 bp downstream from the start codon of the *pqqF* gene (Figure 3.3.6). The translated product of *pqqA* is predicted to encode a peptide precursor of coenzyme PQQ which is required for P solubilisation via the membrane bound quinoprotein glucose dehydrogenase (Gcd) (Goosen et al., 1992). Although the location of the transposon is not in an open reading frame encoding for a complete gene, this isolate (mutant B50) has significantly reduced ability to solubilise P on both TCaP and NBRIP plates (Table 3.3.2). The transposon insertion within 35 bp of the initiation codon, which is a non-coding region upstream of *pqqA*, may interact with the putative promoter region and is likely to interfere the transcription process of this entire gene sequence (from *pqqF*-E, Figure 3.3.6). It is also plausible that the non-polar mini-Tn5*Km1* transposon insertion can allow read through from a 5' located promoter.

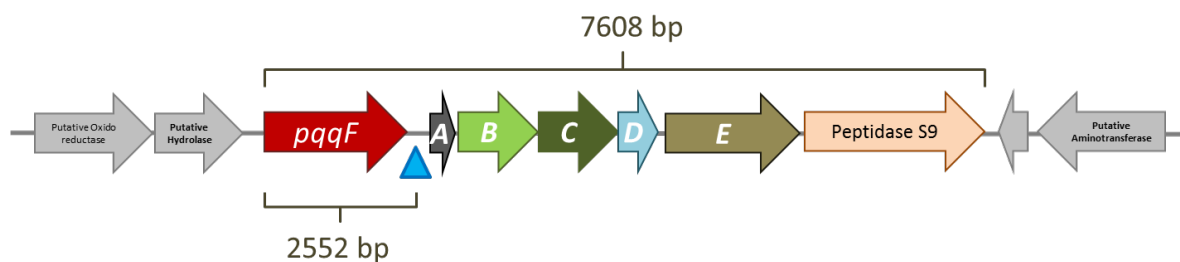


Figure 3.3.6 Schematic diagram of the *Pqq* open reading frame of *Pseudomonas fluorescens* Pf0-1 which consists of *pqqF*, *pqqA – E*, followed by a putative Peptidase S9. The blue arrow indicates the location of mini-transposon Tn5km1 in mutant B50 which is predicted from the alignment of this region in *Pseudomonas* sp. Ha200 with *P. fluorescens* Pf0-1 to be inserted at 2552 bp from the *pqqF* initiation codon.

3.3.6. Phosphate solubilisation of *Pseudomonas* sp. Ha200 and mutant strain B8 involved in organic acid production

The liquid culture assay allowed quantification of the amount of P released by *Pseudomonas* sp. Ha200 and its derivative mini-Tn5Km1 transposon mutant *gcd*::Tn5(B8). This liquid culture medium facilitated the use of HPLC enabling the quantification of organic acids released by the isolates (Chapter 2). *Pseudomonas* sp. Ha200 and *gcd*::Tn5(B8) that contained a mutation in the *gcd* gene encoding for membrane bound quinoprotein glucose dehydrogenase were cultured in the HSU HydroxP liquid culture assay (Appendix A.2.4). Culture filtrates were collected at 24, 36, 48 and 72 h of incubation and soluble P released was determined by colourimetry. Wildtype *Pseudomonas* sp. Ha200 increasingly released organic acid throughout the incubation period. The amount of organic acid released also correlated with the amount of P released into the liquid culture. Wildtype *Pseudomonas* sp. Ha200 released a high amount of 2-keto-D-gluconic acid (2-KGA) with the highest concentration of 23.50 ± 2.83 mM at 48 h (Table 3.3.5). The wildtype strain also released D-Gluconic Acid (GA) and pyruvic acid (PyrA) at basal levels with 5.90 ± 0.54 mM and 9.85 ± 1.24 mM respectively (48h). It is interesting to note that the amount of each organic acid in the culture was reduced at 72 h; in particular GA was not detected at this time point. This suggests carbon recycling after cell density had reached a certain level. For the mutant strain *gcd*::Tn5(B8), both GA and 2-KGA were not detected at any time point, but PyrA levels were not significantly different from the wildtype at 72 h (4.81 ± 1.24 and 4.99 ± 0.50 mM respectively, $p > 0.05$). The amount of P released into the culture was also significantly reduced compared to the wildtype at each of the time points assessed ($p < 0.001$; Table 3.3.5).

HPLC analysis revealed the presence of a yet to be defined organic acid named “Unknown2”, which had a retention time of 10.98 min using a Rezex ROA-Organic Acid HPLC ion-exclusion column (Table 3.3.5). The amount of the Unknown2 presented here is an arbitrary number taken from the HPLC because the molecular mass of this organic acid is unknown. Therefore, direct comparison between Unknown2 and other organic acids such as 2-KGA cannot be made. However, the result shows *gcd::Tn5(B8)* also had significantly reduced production of Unknown2 compared to the wildtype at 72 h (17.85 ± 2.27 and 3.91 ± 0.19 respectively, $p < 0.001$). This suggests that “Unknown2” also plays a role in P solubilisation.

Table 3.3.5 Soluble phosphate and organic acids released from HSU HydroxP liquid culture assay by wildtype *Pseudomonas* sp. Ha200 and *gcd::Tn5(B8)* over 72 h.

Isolates		P Conc (mM) [†]		Organic acid concentration (mM) ⁺		
Time post inoculation (h)		Unknown2 [§]		2-Keto-D-Gluconic Acid	D-Gluconic Acid	Pyruvic Acid
<i>Pseudomonas</i> sp. Ha200	24	4.34 ± 0.09	1.80 ± 0.24	5.37 ± 0.33	1.40 ± 0.12	0.16 ± 0.25
	36	11.23 ± 0.11	13.27 ± 2.52	8.96 ± 1.50	2.01 ± 0.57	7.51 ± 1.22
	48	19.00 ± 0.09	24.87 ± 2.97	23.50 ± 2.83	5.90 ± 0.54	9.85 ± 1.24
	72	20.95 ± 0.38	17.85 ± 2.27	20.60 ± 2.38	nd	4.99 ± 0.50
<i>gcd::Tn5(B8)</i>	24	0.14 ± 0.00***	nd	nd	nd	nd
	36	1.24 ± 0.01***	nd	nd	nd	0.03 ± 0.01***
	48	2.12 ± 0.07***	1.63 ± 0.19***	nd	nd	2.02 ± 0.25***
	72	5.31 ± 0.04***	3.91 ± 0.19***	nd	nd	4.81 ± 1.24

⁺ Value represents mean ± standard error of the mean ($n=3$); nd, none detected

[†] Phosphate concentration determined by Murphy and Riley’s colorimetric method

[§] Unknown organic acid presented in arbitrary units (AU)

*** Significantly different from the control *Pseudomonas* sp. Ha200 at corresponding time point ($p < 0.001$).

In an attempt to identify “Unknown2”, a mixture of 2-KGA (peak A, 200 ppm) and 5-keto-D-gluconic acid (5-KGA, peak B2, 200 ppm) was made and analysed by HPLC (Figure 3.1.12). The chromatogram was compared with the supernatant of wildtype *Pseudomonas* sp. Ha200 incubated for 24 h in HSU HydroxP medium. The resultant chromatograph revealed that Unknown2 (peak B1) was different from 5-KGA (peak B2) with a retention time slightly earlier than 5-KGA (10.98 min and 11.02 min, respectively). Therefore “Unknown2” is not likely to be 5-KGA. However, mutant strain *gcd::Tn5(B8)* with its mutation in *gcd* also produced less “Unknown2”. Furthermore, the retention time of Unknown 2 is between 2-KGA (peak A), 5-KGA (peak B2) and GA (peak C), indicating the organic acid

exhibited similar charges and the structure of this molecule may be similar. One possible organic acid might be the 2, 5-diketo-gluconic acid (2, 5-KGA) which is produced by a different pathway.

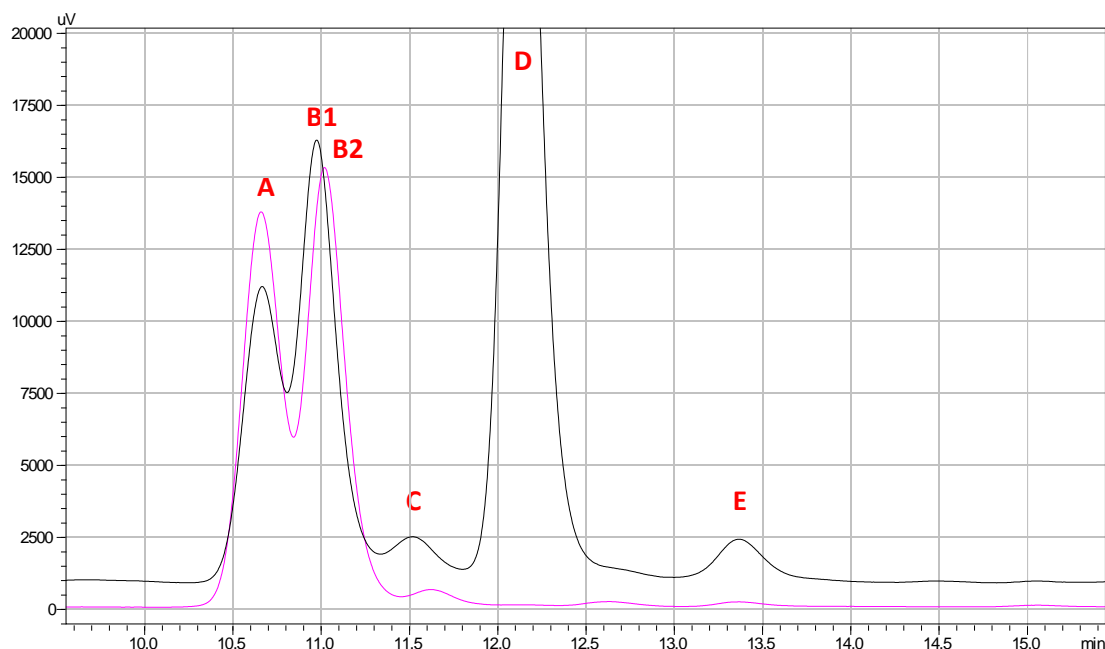


Figure 3.3.7 Chromatogram of organic acids released by wildtype *Pseudomonas* sp. Ha200 in HSU HydroxP liquid culture medium at 24 h (black) and standard solution of 2-keto-D-gluconic acid (200 ppm) and 5-keto-D-gluconic acid (200 ppm) resuspend in HSU medium control (pink). Supernatants were analysed for organic acid by high performance liquid chromatography (HPLC) (n = 3). Peak A denotes 2-Keto-D-Gluconic acid (2-KGA, 10.64 min), B1 denotes peak unknown2 (Un2, 10.98 min), B2 denotes 5-Keto-D-Gluconic acid (5-KGA, 11.02 min), C denotes D-Gluconic acid (GA, 11.55 min), D denotes pyruvic acid (PyrA, 12.11 min) and E is an unknown peak.

3.4 Discussion

Three strains—*Enterobacter* sp. Wi28, *Pseudomonas* sp. Ha200, and *Burkholderia* sp. Ha185—were selected for this study (discussion in Chapter 2). Two non-auxotrophic mutants with mutations affecting their ability to solubilise P were identified. These mutants were found to contain transposon insertions in genes involved in the well characterised direct oxidation pathway of glucose metabolism. In the *Pseudomonas* sp. Ha200 strain *gcd*::Tn5(B8), the insertion occurred in the *gcd* gene, encoding enzyme quinoprotein glucose dehydrogenase (Gcd), while the insertion in the mutant B50 was located upstream of *pqqA* encoding pyrroloquinoline quinone PqqA. Mutations in these genes have been well characterised in *Pseudomonas* spp. for their role in P solubilisation where they are involved in the production of GA by Gcd facilitated by the co-factor PQQ (de Werra et al., 2009) (Figure 3.1.13).

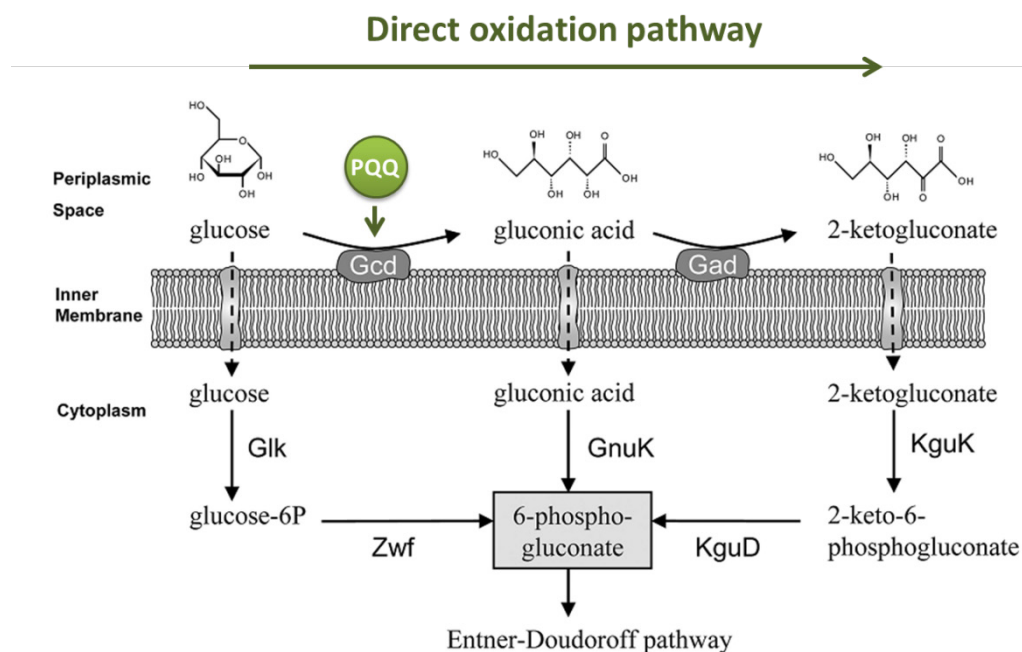


Figure 3.4.1 Glucose dehydrogenase (Gcd) and gluconate dehydrogenase (Gad) involved in periplasmic glucose metabolism via direct oxidation pathway involved with pyrroloquinoline quinone (PQQ) in *Pseudomonas* spp.. Glk, glucokinase; Zwf, glucose-6-phosphate 1-dehydrogenase; GnuK, gluconokinase; KguK, 2-ketogluconate kinase; and KguD, 2-ketogluconate 6-phosphate reductase. (Modified from de Werra et al., 2009) (detailed mechanism outlined in Chapter 1).

Current literature has implicated gluconic acid (GA) released by PSB as the key organic acid responsible for P solubilisation. This was validated through this study where the production of 2-KGA was identified as the major organic acid released by *Pseudomonas* sp. Ha200, and the amount of P solubilised is correlated with the amount of 2-KGA released. Previous research has failed to identify the key organic acid produced by bacteria, possibly due to the similar structure of GA and 2-KGA making them difficult to separate them in a column using HPLC. This study has shown that GA and 2-KGA co-eluted when analysed using the Prevail™ organic acid column for HPLC, but can be separated using the Rezex ROA-Organic Acid H+ (8%) column (See discussion from Chapter 2). Moreover, many researchers have not included 2-KGA analysis in their study. For example, Farhat et al., (2013) determined the amount of GA produced by a recombinant *E. coli* strain that carries both *gcd* and *pqqABCDE* genes from *Serratia marcescens* CTM 50650. Castagno et al. (2011) determined the amount of GA produced by plant growth promoting P solubilising bacteria reside in different

genera (*Pantoea*, *Erwinia*, *Pseudomonas*, *Rhizobium* and *Enterobacter*). However, the production of 2-KGA was not investigated in either study.

Results from this study show production of 2-KGA by *Pseudomonas* sp. Ha200 is the key organic acid responsible for HydroxP solubilisation in liquid culture, whereas GA was produced at basal levels from 24 h to 48 h, and was below the detection limit at 72 h. Interestingly, mutation in the *gcd* gene (*gcd::Tn5(B8)*), abolished the production of GA, and 2-KGA was not detected. This also correlated with the reduced soluble P found in the culture filtrate. This result indicates production of 2-KGA by *Pseudomonas* sp. Ha200 is dependent on the production of GA, which corresponds to the direct oxidation pathway as described by de Werra et al. (2009). This also further indicates glucose was first converted to GA by the membrane bound PQQ-dependent Gcd, then oxidised to 2-KGA possibly by gluconate dehydrogenase (Gad) in the periplasmic space of *Pseudomonas* sp. Ha200 cell, followed by transportation of 2-KGA out of the cell.

One of the important plant growth promoting traits is phytase production by rhizobacteria (Chapter 1). It was found that organic acids such as citric acid improved phytate solubilisation before phytase hydrolysis takes place, this organic acid-driven solubilisation is theorised to be the preliminary step in the hydrolysis of the phytate salt (Tang et al., 2006). Giles et al. (2013) found that organic acid producing *Pseudomonas* sp. CCAR59 in the rhizosphere of tobacco plants improved calcium phytate solubilisation and subsequently increased the availability of P to plants increasing plant growth. The *Pseudomonas* sp. Ha200 strain and its mutant derivative *gcd::Tn5(B8)* that is unable to produce GA and subsequently 2-KGA from this study were provided to Dr. Courtney Giles (University of Vermont, Burlington, USA). The strains were used to enable comparison between the wildtype and its *gcd* mutant derivative that is unable to produce GA and subsequently 2-KGA for their role in phytate solubilisation (Giles et al., 2014).

Furthermore, *gcd::Tn5(B8)* mutant was shown to only have a partial reduction in MPS in the HSU liquid culture assay. This indicates apart from P solubilisation by 2-KGA derived from GA, another organic acid also contributed significantly to the MPS phenotype, the “Unknown 2” organic acid (Un2). It was also found Un2 was released during HydroxP solubilisation by all the effective P solubilising *Pseudomonas* strains previously described in Chapter 2, EN101, EE131, EE132, EE127, and Wh15. This may indicate the release of Un2 is common within the genus *Pseudomonas* and is related to MPS. It was shown that the amount of Un2 decreased to a near basal level in the *gcd::Tn5(B8)* mutant. Therefore, the production of Un2 is dependent, but not limited to, the direct oxidative pathway (GA and 2-KGA production), and is possibly involved in the tricarboxylic acid cycle (TCA). The chemical composition of this organic acid molecule is uncertain, but is postulated to be 2, 5-KGA that

possesses similar chemical composition to 2-KGA and 5-KGA. To find out the composition of this molecule, Liquid chromatography–mass spectrometry (Tandem MS, LC-MS/MS) could be employed in the future to determine the mass-to-charge ratio by multiple steps mass spectrometry analysis.

Biosynthesis of cofactor PQQ is pre-requisite for P solubilisation by Gcd, as shown by Kim et al. (2003). The authors cloned *pqqA-F* from *Enterobacter intermedium* (60-2G) in different fragments and expressed them in *E. coli* DH5 α that has Gcd without the *pqq* gene cluster, confirming the importance of *pqqA-E* for P solubilisation via the direct oxidative pathway. However, it has also been shown that biosynthesis of PQQ does not require *pqqA* in *Methylobacterium extorquens* AM1 (Toyama & Lidstrom, 1998), and the significance of the *pqqA* gene within the cluster for PQQ production remains debatable (Ge et al., 2013). In this study, the results show the *Pseudomonas* sp. Ha200 B50 mutant, with the transposon insertion 35 bp upstream of the *pqqA* initiation codon, had partial reduction in MPS on both TCaP and NBRIP plates. Therefore, it was postulated the mutation occurred within the promoter region of the *pqq* gene cluster. This result highlights the importance of *pqqA* transcription regulation and correlates with the result from Gómez et al., (2010) who found mutation of *pqqA* in *Enterobacter intermedium* 60-2G reduced MPS on NBRIP, while in the complemented strain the MPS phenotype was restored. It is known that there might be multiple copies of *pqqA* within a bacterial genome. For example, there are five copies of *pqqA* in the *Methylovorus* sp. MP688 genome, each of which possess different promoter activity and are transcribed independently from the *pqqBCDE* operon (Ge et al., 2013). Furthermore, it was also found there is a second copy of a *pqqA*-like gene present in both *Pseudomonas fluorescens* F113 and *P. fluorescens* Pf-5 (Miller et al., 2010), which is likely to increase PQQ production and consequently Gcd activity. Therefore, it is also likely that multiple *pqqA* exist in *Pseudomonas* sp. Ha200. Transcription of the second *pqqA* likely complements the B50 mutation, resulting in only partial reduction in MPS. However, further investigation of the presence of multiple *pqqA* genes present in *Pseudomonas* sp. Ha200 is required. Together, transcription of *pqqA* is pre-requisite to the production of PQQ and the PqqA peptide is a precursor of the PQQ cofactor.

Random mutagenesis of *Enterobacter* sp. Wi28 using the mini-Tn5*Km1* generated 2208 mutants, but most retained the ability to solubilise P. It was found that this isolate produced Un2, PyrA, and DL-lactic acid during HydroxP solubilisation, but no GA and 2-KGA was detected (Chapter 2). Furthermore, it was found that this isolate is able to utilise variable sugar substrates for P solubilisation such as fructose, inositol and mannitol (Dr. Carolyn Mander, personal communication). This suggests *Enterobacter* sp. Wi28 solubilises P by secondary metabolites (organic acids) produced via the TCA cycle because it is postulated that carbon substrates other than glucose are converted to

fructose-6-P within the cytosol via the Embden-Meyerhof-Parnas pathway and then subjected to fructolysis before entering the TCA cycle (Wisselink et al., 2002). The results suggest that P solubilisation by *Enterobacter* sp. Wi28 does not occur by the direct oxidation pathway at the cellular membrane, and the bacteria possibly lacks the *pqq* gene cluster similar to *E. coli* MC1061 (Rodríguez et al., 2000). This would account for the inability to obtain non-auxotrophic mutants from *Enterobacter* sp. Wi28 with impaired MPS but able to maintain cellular growth. The only *Enterobacter* sp. Wi28 non-auxotrophic mutant with impaired MPS ability that was obtained in this study was D23, which contained an insert in the *gltD* gene encoding a glutamate synthase. However, this mutant derivative was significantly impaired in growth and was therefore not a suitable candidate for further investigation.

The relationship between *Gcd*, the *pqqA-E* operon and P solubilisation of *Pseudomonas* spp. is well understood (Intorne et al., 2009, Farhat et al., 2013), and no novel genes implicated in MPS from the *Enterobacter* sp. Wi28 isolate were identified. Therefore, study of these isolates was not pursued. Instead, the bacterium *Burkholderia* sp. Ha185 was chosen for further study of novel genetic determinants of P solubilisation. Sequencing of the transposon insertion points generated from random mutagenesis, revealed two non-auxotrophic mutants in genes that had not previously been implicated in P solubilisation, F13 and F18. Mutant F13 had a mutation in a gene encoding for a hypothetical protein that is closely related to *Burkholderia* sp. CCGE1003 (YP_003907489.1) and F18 had a mutation in a gene encoding bifunctional uroporphyrinogen-III synthetase/uroporphyrin-III C-methyltransferase which is closely related to *Burkholderia xenovorans* LB400 (YP_557627.1) (**Table 3.3.1**). Mutation in these novel genes independently resulted in reduced P solubilisation compared to the wildtype *Burkholderia* sp. Ha185. Detail of these two novel genes and the relationship to P solubilisation are investigated and discussed in Chapter 4.

Chapter 4

Genes Involved in Phosphate Solubilisation by *Burkholderia* sp. Ha185

4.1 Introduction

Two mutants derived from *Burkholderia* sp. Ha185, previously identified by mini-Tn5Km1 transposon mutagenesis in Chapter 3, had mutations in novel genes. One gene encoded a hypothetical protein, while the other encoded a bifunctional uroporphyrinogen III synthase/uroporphyrin-III C-methyltransferase. Neither of these novel genes have previously been implicated in phosphate (P) solubilisation. Therefore, these genes were chosen for further study to understand their role in P solubilisation in *Burkholderia*.

The genus *Burkholderia* was first described in 1950 when Walter Burkholder reported a “sour skin” disease in an onion bulb and named the isolate *Pseudomonas cepacia* (Burkholder, 1950). The genus *Burkholderia* was classified as *Pseudomonas* for many decades. It was not until the 1990s when Yabuuchi et al. (1992) recategorised seven *Pseudomonas* species as *Burkholderia* spp. using 16S rRNA gene sequencing and DNA-DNA homology. To date, more than 40 different *Burkholderia* species have been sequenced and characterised. *Burkholderia* spp. belong to the Burkholderiaceae family, within the class Betaproteobacteria, and have a genome with an average size of 7.5 Mb comprising two large chromosomes. This multireplicon genome and the presence of multiple insertion sequences contribute to the high genome plasticity and diversity of the *Burkholderia* genus (Mathenthiralingam and Drevinek, 2007). The adaptability of the genome explains how *Burkholderia* spp. can inhabit a wide range of ecological niches, including soil, waste environments, plants, fungi and animals (including humans), can exist as endosymbionts and are used as biocontrol agents (Salles et al., 2004; Inglis et al., 200; Tong et al., 1996; Partida-Martinez and Hertweck, 2005; Galyov et al., 2010; Compant et al., 2008; Cuong et al., 2011).

4.1.1. Genome sequencing of *Burkholderia* sp. Ha185

To study *Burkholderia* sp. Ha185, genomic DNA was subjected to low coverage draft genome sequencing by the Macrogen sequencing service (Macrogen Inc., Korea) (Section 4.2). The resulting genome data revealed that 11% of the sequenced DNA was unique, with no significant similarity to DNA sequences in the current National Centre for Biotechnology Information (NCBI) GenBank nucleotide database, while the remaining 89% of the genome had the highest identity to bacteria of the genus *Burkholderia* (Supplemental folder 1) and could be aligned to DNA sequences from the NCBI nucleotide database. The majority of DNA sequences showed similarity to both *Burkholderia xenovorans* LB400 (Accession No. PRJNA57823, Chain et al., 2006) and *Burkholderia phytofirmans* PsJN (Accession No. PRJNA58729, Weilharter et al., 2011) (Supplemental folder 1). Further details on these two species are outlined in the following section.

4.1.1.1 Introduction to *Burkholderia xenovorans* LB400

The bacterium *B. xenovorans* LB400 was initially isolated from polycyclic aromatic hydrocarbon-contaminated soil from a landfill in Moreau, NY, USA and was originally classified as *Pseudomonas* strain LB400 (Bopp et al. 1986). This isolate was later classified as *B. xenovorans* LB400 as it can be differentiated phenotypically from other *Burkholderia* species by its inability to assimilate L-arabinose (Goris et al. 2004). *B. xenovorans* LB400 contains two chromosomes and a megaplasmid (1.47 Mb), with a total genome size of 9.73 Mb and a GC content of 62.6% (Table 4.1.1). This species was later grouped within the *Burkholderia* plant-associated beneficial and environmental group (PBE) by Suárez-Moreno et al. (2012), and is phylogenetically distant to the “pseudomallei” group and the *Burkholderia cepacia* complex (BCC) (Figure 4.1.1). Isolates found in the BCC are opportunistic human pathogens that can infect and colonise the lungs of compromised cystic fibrosis patients through direct patient-to-patient contact (Whiteford et al., 1995). Furthermore, pulmonary colonisation by BCC isolates causes chronic infection, often leading to an accelerated decline in pulmonary function and increased risk of death from “cepacia syndrome” (Jones et al., 2004, Alexander et al., 2008, De Soyza et al., 2010). In contrast, isolates from the PBE group are typically plant beneficial bacteria and can survive in nutrient-limited environments by degrading recalcitrant compounds (Suárez-Moreno et al., 2012). They have also been used in phytoremediation (Hong et al., 2007), bioremediation (Caballero-Mellado et al., 2007) and as biocontrol agents (Warmink et al., 2011). *B. xenovorans* LB400 is best known for its ability to degrade the environmental organic toxicant polychlorinated biphenyl, and for its use as a model organism for studying aromatic degradation pathways (Denef et al., 2006, Méndez et al., 2011). *B. xenovorans* LB400 has potential applications in bioremediation of highly-contaminated industrial waste soils because of its ability to degrade xenobiotic aromatic toxicants

including toluene, benzene, benzoate, phenol, pentachlorophenol and many other environmental pollutants (Pérez-Pantoja et al., 2011, Haller et al., 2012).

4.1.1.2 Introduction to *Burkholderia phytofirmans* PsJN

Basic Local Alignment Search Tool nucleotide (BLASTn) data provided by Macrogen revealed significant DNA similarity between *Burkholderia* sp. Ha185 and *B. phytofirmans* strain PsJN. A strain that was originally identified as *Pseudomonas* sp. PsJN was isolated from surface-sterilised onion root rhizosphere (Frommel et al., 1991), and was later shown to be a plant-beneficial endophytic bacterium (Nowak and Shulaev, 2003; Compant et al., 2008). *B. phytofirmans* PsJN contains two chromosomes and one plasmid (Table 4.1.1) and colonises a variety of plants, including potato, tomato, chickpea and grape. Most importantly, *B. phytofirmans* PsJN can stimulate plant growth (Nowak et al., 1995; Pillay and Nowak, 1997; Sessitsch et al., 2005; Compant et al., 2005; Barka et al., 2006). *B. phytofirmans* PsJN inoculation enhanced the development of secondary roots and root hairs in potato plants, resulting in larger root systems (Nowak, 1998). This strain was also found to reduce susceptibility to vascular wilt diseases caused by the potato pathogen *Verticillium albo-atrum* and the tomato pathogen *Verticillium dahliae* (Nowak, 1998; Sharma and Nowak, 1998). *B. phytofirmans* PsJN also reduced grey mould infection of grapevines (Barka et al., 2000), and enhanced cold-tolerance of grapevine plantlets (Barka et al., 2006, Fernandez et al., 2012). Furthermore, *B. phytofirmans* PsJN exhibited other plant-beneficial properties, such as production of 1-aminocyclopropane-1-carboxylate (ACC) deaminase and auxin (Sun et al., 2009), as well as producing the quorum-sensing signal compound, 3-hydroxy-C8-homoserine lactone, enabling population-dependent coordinated gene expression (Sessitsch et al., 2005). A recent study showed that *B. phytofirmans* PsJN not only significantly improved overall biomass production of ryegrass, but also degraded hydrocarbons, reducing their toxicity in soil (Afzal et al., 2013). Based on these capabilities, *B. phytofirmans* strain PsJN is considered to be a plant growth-promoting rhizobacteria (PGPR) (Compant et al., 2008) of the PBE group (Figure 4.1.1).

A genome-based BLASTn comparison of *Burkholderia* sp. Ha185 revealed similarity to both *B. phytofirmans* strain PsJN and *B. xenovorans* LB400. A BLASTn analysis of the *Burkholderia* sp. Ha185 16S rRNA gene sequence retrieved from Contig001233 (total size 1679 bp) revealed 98% identity to the *B. xenovorans* LB400 16S rRNA gene sequence available from the GenBank database (Chapter 2).

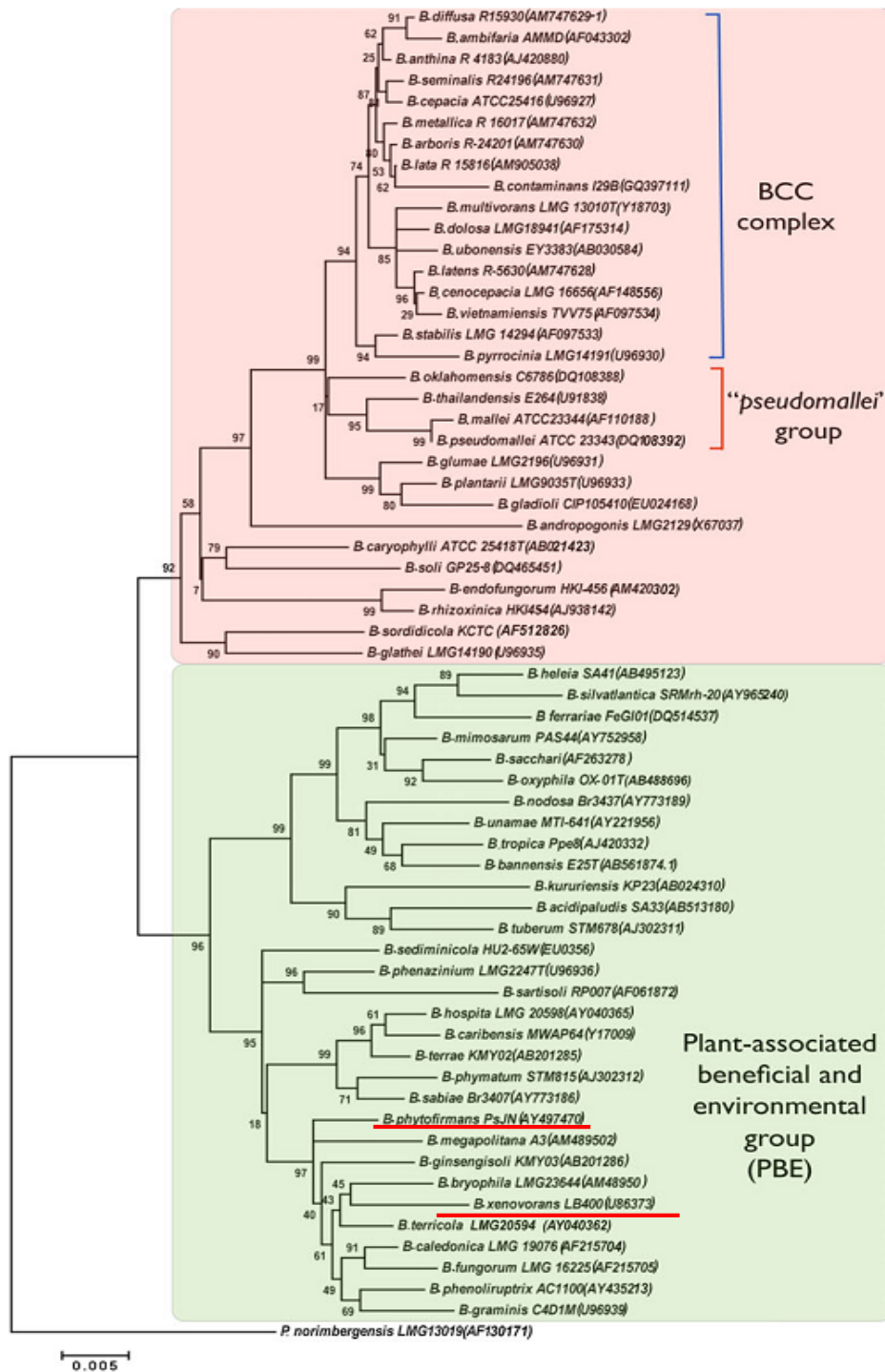


Figure 4.1.1 Phylogenetic tree based on 16S rRNA nucleotide sequences from *Burkholderia* species. *Pandoraea norimbergensis* LMG 13019 was used as an outgroup (scale bar = 0.005 nucleotide substitutions per nucleotide position). Pathogenic *Burkholderia* spp. are highlighted by the pink box, while the green box indicates the plant-associated beneficial and environmental (PBE) group. *B. phytofirmans* PsJN and *B. xenovorans* LB400, which are closely related to *Burkholderia* sp. Ha185, are underlined in red (figure adapted from Suárez-Moreno et al. (2012). Permission granted: order License ID 3187961127968).

Table 4.1.1 Description of *B. xenovorans* LB400, *B. phytofirmans* PsJN and *Burkholderia* sp. Ha185.

Organism	<i>B. xenovorans</i> LB400	<i>B. phytofirmans</i> PsJN	<i>Burkholderia</i> sp. Ha185
Chromosomes	2	2	Possibly 2 [‡]
Plasmids	1 (a megaplasmid)	1	Unknown
Size	9.73 Mb	8.21 Mb	~8.55 Mb
%GC	62.6%	62.3%	~62.7%
Genes	9,043	7,484	-
Proteins	8,702	7,241	-
BioProject (NCBI)	PRJNA57823	PRJNA58729	-
Descriptions	Degrades the environmental pollutant polychlorinated biphenyl, and aromatic toxicants such as toluene, benzene, benzoate, phenol, and pentachlorophenol. Model bioremediator for xenobiotic aromatic toxicants degradation.	Plant-beneficial bacterium that colonises potato, tomato, chickpea and grapevine. Exhibits epiphytic and endophytic colonisation of grapevine roots and enhances cold tolerance of grapevine plantlets. Protects against plant pathogens, produces ACC deaminase, auxin and quorum-sensing signal compound.	Production of phytase, ACC deaminase, auxin, and siderophore (Chapter 2). Insoluble P solubilisation, including dicalcium phosphate anhydrate, tricalcium phosphate and hydroxyapatite (Chapter 2, 3 and 4). Produces 2-KGA organic acid, which is involved in P solubilisation (Chapter 2 and 4). Endophytic and colonises rhizoplane and rhizosphere of ryegrass root (Chapter 5).
References	Jones et al. (2004); Deneff et al. (2006); Alexander et al. (2008); De Soyza et al. (2010); Méndez et al. (2011); Pérez-Pantoja et al. (2011); Suárez-Moreno et al. (2012); Haller et al. (2012).	Frommel et al. (1991); Nowak et al. (1995); Pillay and Nowak, 1997; Sharma and Nowak, 1998; Nowak and Shulaev, 2003; Sessitsch et al. (2005); Compant et al. (2005); Barka et al. (2006); Compant et al. (2008).	This study

Note: [‡] *Burkholderia* contains a minimum of two large chromosomal replicons (Mahenthiralingam and Drevinek, 2007).

4.2 Methods

4.2.1. Genome sequencing of *Burkholderia* sp. Ha185

Genomic DNA from *Burkholderia* sp. Ha185 was prepared (as described in Appendix C.2.1 with a DNA A260/280 ratio of 1.89) and was subjected to low-coverage draft genome sequencing by Macrogen (Seoul, South Korea) using a GS-FLX Titanium next generation sequencing platform (454 Life Sciences, Branford, CT, USA). Sequencing generated 199,790 reads (8,549,297 bp) that were *de novo* assembled into 1,718 contigs with an average size of 4,976 bp by Macrogen (Supplemental folder 1). The draft genome facilitated the rapid retrieval of partial or full DNA sequences of genes implicated in mineral phosphate solubilisation (MPS). This enabled the design of primers and annotation of genes. On completion of the draft genome project, Macrogen provided a BLASTn service via the NCBI nucleotide database (Supplemental folder 1).

4.2.2. Identify proteins of interest within the *Burkholderia* sp. Ha185 genome

To identify proteins of interest within the *Burkholderia* sp. Ha185 genome, a BLAST database containing the contig files (Supplemental folder 1) of the low-coverage genome sequences of *Burkholderia* sp. Ha185 was constructed using the makeblastdb tool of the blast+ program (Version 2.2.28) (Altschul et al., 1990). The nucleotide database was then translated into all six possible reading frames using tBLASTn software (blast+ version 2.2.28). The query protein sequences were then downloaded from UniProt (Apweiler et al., 2013) (<http://www.uniprot.org>). The tBLASTn program was used to search the *Burkholderia* sp. Ha185 genome protein database using a protein query in either the predicted ORFs or the nucleotide sequence database. The nucleotide sequence at the region of a hit was extracted from the database using the extractseq suite from EMBOSS (version 6.5.0) (Rice et al., 2000).

4.2.3. Inorganic phosphate solubilisation

4.2.3.1 Hydroxyapatite solubilisation by *Burkholderia* sp. Ha185 and the derivative mutants in HSU liquid culture assay

Burkholderia sp. Ha185 and its corresponding mutants were grown in Luria Broth (LB) broth for 48 h at 25°C with appropriate antibiotics (shaking at 250 rpm) until the OD₆₀₀ reached approximately 4.0. Each isolate was then pelleted by centrifugation for 3 min at 5900 × *g* at room temperature. Starter cultures were prepared by discarding the supernatant and resuspending each cell pellet to an OD₆₀₀ of 2.0 in filter-sterilised HSU liquid culture medium minus hydroxyapatite (HydroxP) (Appendix A.2.4). Aliquots of resuspended starter cultures (100 µL) were then pipetted into the HSU HydroxP medium, resulting in an approximate final bacterial suspension concentration of 6.00 log₁₀ cfu mL⁻¹, as validated by serial dilution plating (Appendix B.2). The HSU liquid culture medium was then incubated at 25°C with shaking at 250 rpm in a Raytek orbital incubator. At 24, 48 and 72 h post-inoculation, 1 mL of culture was pelleted by centrifugation at 15,700 × *g* for 10 min. The supernatant was filtered using a 0.22-µm PVDF syringe filter (13 mm diameter, Thermo Fisher Scientific, MA, USA). Filtrates from HSU liquid cultures were harvested at different time points and the concentration of organic acid in the filtrates was determined using high-performance liquid chromatography (HPLC) (Method described in Chapter 2.2.3.4). Quantification of free P released by *Burkholderia* sp. Ha185 and its mutants *bxpC*::Tn5(F13) and *hemX*::Tn5(F18), as well as the complementation strains 1311CMPB2, CD3ME12 and DXDME6, was then determined using the method of Murphy and Riley (as described in Chapter 2.2.1.1). Each isolate was cultured in 50 mL HSU liquid medium containing hydroxyapatite (Ca₅(PO₄)₃(OH); HydroxP) as the only source of P in 250 mL Erlenmeyer flasks (Appendix A.2.4). The medium was adjusted to pH 6.5 prior to autoclaving for 15 min at 1.1 kg cm⁻², 121°C. A HSU buffer-only negative control was included in all assays. Colony forming units were also determined for each culture at 24, 48 and 72 h post-inoculation by serial dilution plating. This experiment was performed three times.

After 72 h of incubation, the pH of the wildtype *Burkholderia* sp. Ha185 bacterial filtrate was determined as follows. A 45-mL aliquot of the remaining culture was pelleted by centrifugation for 10 min at 5900 × *g* (room temperature) in a 50-mL conical centrifuge tube (Fisher Scientific, NH, USA). The supernatant was transferred into a new 50-mL conical centrifuge tube and the pH of the filtrate was determined using a Handylab pH meter (SCHOTT® Instruments, NY, USA) at room temperature.

To determine the amount of soluble P in bacterial cells, 1 mL of each bacterial culture was collected at the end of the 72-h incubation described above. Cells were centrifuged for 1 min at 15,700 × *g*, the

supernatant was discarded, and the pellet was resuspended in 1 mL of HSU buffer without HydroxP and glucose. This washing procedure was then repeated twice further. One millilitre of washed cell suspension was then sonicated by high frequency ultrasound to disrupt cell membranes and release the cellular components. Each sample was sonicated three times for 30 s using a Soniprep 150 Ultrasonic Disintegrator (Sanyo Gallenkamp PLC, Leicester, UK) with 30 s intervals between pulses, during which time the sample was stored on ice. The intensity was gradually increased during each 30 s pulse to a final intensity of 13 μ A. Sonicated samples were centrifuged at 15,700 $\times g$ for 10 min to pellet the cell lysate, and the supernatants were filtered using a 0.22- μ m PVDF syringe filter then stored at -20°C . The concentration of soluble P in samples was determined using the method of Murphy and Riley (Chapter 2.2.1.1), and the organic acid profiles were determined by HPLC (Chapter 2.2.4).

Two other variations of the HSU liquid culture assay were also performed in this study. In one assay, 55.5 mM glucose in the HSU HydroxP medium was replaced with 54.9 mM mannitol as the sole carbon source, indicated by “+M” or “+Mannitol” in graphs or HydroxP-M in the main text. Soluble P (0.64 g Na_2HPO_4 and 0.15 g KH_2PO_4 in 50 mL) was also used instead of HydroxP as the only P source, referred to as “+P” or “+Soluble P” in graphs and tables or HSU-P in the main text.

4.2.3.2 *Hydroxyapatite solubilisation by organic acids*

To determine the potential roles of selected organic acids in the solubilisation of HydroxP, an experiment was performed using defined organic acid concentrations. Filter-sterilised stock solutions (500 mM) of DL-lactic acid (LA, pH 2.06), D-gluconic acid (GA, pH 2.31), pyruvic acid (PyrA, pH 1.70), 2-keto-D-gluconic acid (2-KGA, pH 5.04) and D-malic acid (MA, pH 2.10) in HSU buffer (without glucose) were prepared as described in Appendix A.2.4 and Section 4. Microcentrifuge tubes containing 900 μ L of HSU HydroxP medium and final concentrations of 1, 5, 10, 25 and 50 mM of each organic acid in a total volume of 1 mL were prepared. A tube with no added organic acid was used as the negative control. Each of the samples was incubated in an Eppendorf Thermomixer[®] comfort (Hamburg, Germany) with shaking at 1000 rpm at 25°C for 24 h. Following incubation, the samples were centrifuged at 15,700 $\times g$ for 10 min to pellet the excess HydroxP and the supernatants were collected. The amount of soluble P released was determined by colourimetry (Chapter 2.2.1.1). Each result was subtracted from the negative control, giving the difference in soluble P that was solubilised by organic acid. Three independent replicates of this experiment were performed.

4.2.4. Optimisation of PCR for amplification of the GC-rich *hem* operon

To enable complementation of the *bxpC::Tn5(F13)* mutant, standard PCR was performed to amplify *hemC* using *hemC*-specific primers (Table 4.2.2). PCR was performed using Platinum® *Taq* DNA Polymerase High Fidelity (Life Technologies, Carlsbad, CA, USA) according to manufacturer's instructions, and the PCR parameters are described in Appendix C.2.9. However, because of the GC-rich content of the region to be amplified (GC% 65.3% for *hemC*, 67.5% for *hemX* and 63.9% for *hemY*), DNA could not be successfully amplified from the *hem* operon. To overcome this, the PCR was optimised using temperature gradient PCR and by the addition of dimethyl sulfoxide (DMSO) to the reaction (final concentration 5% (v/v)). The addition of DMSO facilitates DNA separation by disrupting base pairing from secondary structure formations in GC-rich regions, and lowers the melting temperature of double stranded DNA (Sun et al., 1993; Turner et al., 1995; Baskaran et al., 1996).

PCR amplification was performed in 0.2-mL Thermo-Tubes using a C1000 Touch™ Thermo Cycler (Bio-Rad, Hercules, CA, USA). Each reaction contained approximately 10 ng of *Burkholderia* sp. Ha185 genomic DNA (gDNA) template extracted with a *SolG* Genomic DNA Prep kit (SolGent, Daejeon, Korea) according to the manufacturer's instructions. Each PCR reaction contained final concentrations of 1× High Fidelity PCR buffer, 0.2 mM dNTPs, 2 mM MgCl₂, 0.2 μM each forward and reverse primer, 1 U *Taq* polymerase, approximately 10 ng of gDNA and 5% (v/v) DMSO. The *hemX* region was amplified as follows: 94°C for 5 min, followed by 35 cycles of 94°C for 30 s, temperature gradient of 58–67°C for 30 s, 68°C for 3 min for amplifying *hemX* or 4 min for amplifying both *hemC* + *hemX*, and a final extension step of 68°C for 8 min. PCR products were purified using a High Pure PCR Product Purification kit (Roche, Basel, Switzerland) according to manufacturer's instructions. The size of PCR products was confirmed by gel electrophoresis as outlined in Appendix C.2.10.

4.2.5. Quantifying gene expression using Reverse Transcriptase-qPCR

4.2.5.1 Isolation of RNA from *Burkholderia* sp. Ha185 and synthesis of complementary DNA

To enable quantification of selected genes throughout the growth cycle of *Burkholderia* sp. Ha185 in HSU HydroxP medium, wildtype *Burkholderia* sp. Ha185 was incubated in liquid broth with glucose as described in Section 4.2.1. Wildtype *Burkholderia* sp. Ha185 was also grown in HSU HydroxP with mannitol as the sole carbon source (HydroxP-M), and HSU buffer with glucose and soluble P instead

of HydroxP (HSU-P). Total cellular RNA was isolated using RNeasy Protect Bacteria Reagent and RNeasy Mini Kit (Qiagen, Hilden, Germany) at five time points: 24, 36, 40, 48 and 72 h post-inoculation. Samples from each cell culture (200 μ L) were independently aliquoted into 1.5 mL tubes containing 400 μ L of RNeasy Protect Bacteria Reagent. The samples were then processed following the protocol supplied by the manufacturer. Pellets were stored at -80°C or processed immediately following the RNeasy Mini Kit protocol for enzymatic lysis and proteinase K (Roche) digestion of bacteria, followed by high-quality RNA purification using silica-membrane RNeasy spin columns. On-column DNase digestion was performed using 3 μ L of recombinant RNase-free DNase I (Roche) with 77 μ L of $10\times$ incubation buffer per column, and incubation at room temperature for 15 min. RNA was then eluted by RNase-free water using the RNeasy Mini Kit protocol. The concentration of the resultant RNA was measured using a Nanodrop ND-1000 spectrophotometer (Eppendorf, Hamburg, Germany) and the purity and integrity were confirmed by 1% agarose gel electrophoresis. Purified RNA was again treated with RNase-free DNase and used as a template for cDNA synthesis using reverse transcriptase. RNase-free DNase (Roche, 0.5 μ L) was added to 0.8 μ L DNase buffer and 6.7 μ L of RNA. Samples were gently mixed using a pipette and incubated at 37°C for 15 min. Samples were centrifuged briefly before adding RNase-free EDTA to a final concentration of 8 mM (pH 8.0) (Life Technologies), followed by incubation at 75°C for 10 min in a Mastercycler EP thermal cycler (Eppendorf, Hamburg, Germany). Following incubation, samples were centrifuged briefly and then placed on ice before cDNA synthesis. The concentration of DNase-treated RNA was measured again by Nanodrop spectrophotometer and the purity and integrity were confirmed by 1% agarose gel electrophoresis.

Reverse transcription PCR reactions were performed using a Transcriptor High Fidelity cDNA Synthesis Kit (Roche) according to the manufacturer's instructions. A final volume of 11.4 μ L, containing 60 μ M random hexamer primers, ~ 100 ng of DNase treated RNA and 7.4 μ L of PCR-grade water, was incubated at 65°C for 10 min in a Mastercycler EP thermal cycler and was centrifuged briefly prior to cDNA synthesis. The following were then added to each reaction to the final concentration of: $1\times$ Transcriptor High Fidelity Reverse Transcriptase Reaction Buffer, 5 mM DTT, 20 U of Protector RNase Inhibitor and 10 U of Transcriptor High Fidelity Reverse Transcriptase, in a final volume of 20 μ L. Reactions were gently mixed by pipetting and then incubated at 53°C for 30 min in a Mastercycler EP thermal cycler, followed by 85°C for 5 min to inactivate the reverse transcriptase. The reaction was stopped by placing the tube on ice, and then cDNA was stored at -80°C .

4.2.5.2 PCR using cDNA template

To ascertain whether the *bxp* and *hem* genes were contained within an operon, primer sets (Table 4.2.2) were constructed to bridge the intergenic space or the overlap between each open reading frame (ORF) (Figure 4.3.3). RNA was extracted from *Burkholderia* sp. Ha185 that had been cultured in HSU HydroxP liquid medium for 36 h, as described in Section 4, using the RNA extraction method outlined in Section 4.2.5. UltraPure™ diethyl pyrocarbonate (DEPC)-treated water (Life Technologies) was used as a negative control. cDNA was synthesised by reverse transcription PCR (Section 4.2.5). PCR reactions were performed in a C1000 Touch™ Thermo Cycler (Bio-Rad) in a final volume of 20 µL containing 1× High Fidelity PCR buffer, 0.2 mM dNTPs, 2 mM MgCl₂, 200 nM each forward and reverse primer, 1 U of Platinum® *Taq* DNA Polymerase High Fidelity (Life Technologies) and ~1 ng DNA template. Standard PCR was then performed using the following thermal cycler parameters: 94°C for 5 min, followed by five cycles of 94°C for 30 s, 55°C for 30 s, 68°C for 1 min per kb, and 30 cycles of 94°C for 30 s, 50°C for 30 s, 68°C for 1 min per kb, and a final extension step of 68°C for 5 min.

Because of the high GC content of the *hem* genes, the PCR reaction had to be optimised for each primer set as described in Section 4.2.4. Genomic DNA (gDNA) from *Burkholderia* sp. Ha185 was extracted as described in Appendix C.2.1, and was used as the positive control. DNase-treated RNA (diluted 1:100 with UltraPure™ DEPC-treated water) was used as a negative control in each experiment. PCR products were confirmed by gel electrophoresis on 1% agarose gels in TBE buffer and visualised on a UV transilluminator.

4.2.5.3 Reverse Transcriptase-qPCR from cDNA template

Primers for qRT-PCR were designed using the web-based Primer-BLAST tool (Ye et al., 2012). Primers used in this study are listed in Table 4.2.2. A dilution series of *Burkholderia* sp. Ha185 gDNA was used to determine the lowest concentration of template that would produce a product and keep background amplification to a minimum. qRT-PCR reactions were performed using a Corbett Rotor-Gene™ 6000 (Qiagen). All reactions contained 1× SensiMix™ SYBR No-ROX mix (BioLine, London, UK), approximately 50 ng of template DNA (equivalent RNA concentration as measured by Nanodrop ND-1000 spectrophotometer), 250 nM of the appropriate forward and reverse primers and DNase/RNase-free water in a final volume of 10 µL. Cycling for qRT-PCR was as follows: initial step of 50°C for 2 min, a polymerase activation step of 95°C for 10 min, followed by 35 cycles of 95°C for 15 s and 60°C for 15 s, and a final step of 72°C for 15 s. Data were acquired at the end of each cycle. A high resolution melting (HRM) curve was generated post-amplification to identify amplified products

and distinguish PCR amplicons from primer dimers or background artefacts. The HRM analysis was performed as follows: 1 cycle of 95°C for 1 min and 50°C for 1 min, followed by a temperature gradient of 50–95°C increasing 0.5°C per cycle, and a pause of 2 s after each step.

Reverse transcriptase-qPCR is the relative quantification of mRNA expressed by a gene or multiple target genes relative to the levels of internal control mRNA expressed by reference genes. Unlike absolute quantification, relative quantification does not require RNA of standard concentrations. Raw qRT-PCR data were imported directly from the Corbett Rotor-Gene™ 6000 and the R-value and PCR efficiency for each primer set were determined using LinRegPCR (Ramakers et al., 2003). Raw data were also analysed using the REST-MCS © version 2 software (Pfaffl, 2001), allowing comparison of four target genes, *hemC*, *hemX*, *bxpC* and *ppc*, against three reference genes, *gltB*, *recA* and *gyrB*. The analysis is based on a mathematical model determining the relative quantitation of a target gene, which is normalised by a non-regulated reference gene:

$$\text{Ratio} = \frac{(E_{\text{target}})^{\Delta\text{CP}_{\text{target}}(\text{MEAN control} - \text{MEAN sample})}}{(E_{\text{ref}})^{\Delta\text{CP}_{\text{ref}}(\text{MEAN control} - \text{MEAN sample})}}$$

Where E_{target} is the RT-qPCR efficiency of target gene transcript; E_{ref} is the RT-qPCR efficiency of a reference gene transcript; $\Delta\text{CP}_{\text{target}}$ is the crossing point (CP) difference between the control and sample of the target gene transcript; $\Delta\text{CP}_{\text{ref}}$ is the CP difference between the control and sample of the reference gene transcript. The CP is defined as the point at which the fluorescence rises appreciably above the background fluorescence (Pfaffl, 2004).

High resolution melting analysis (HRM) provides fast and reliable post-PCR analysis of PCR integrity, and is also able to distinguish PCR amplicons from primer dimers or background artefacts as well as any contamination during qRT-PCR preparation. The analysis was performed using inbuilt Corbett Rotor-Gene™ 6000 software following the acquisition of HRM data. Data is plotted as the derivative of fluorescence versus temperature (dF/dT vs. T) (Figure 4.3.27).

4.2.6. Protein expression

4.2.6.1 pARA- and pGEX-based expression of *bxpC*

To enable expression of BxpC in its native form, the plasmid pARAC3, encoding *bxpC* (bases 55–357 of the complete 357 bp gene sequence) minus the predicted BxpC signal sequence, was induced by the addition of L-arabinose. *Escherichia coli* DH10B containing pARAC3 was inoculated into 50 mL of LB broth containing 50 µL ampicillin (100 g/mL). The culture was incubated at 37°C with shaking at 250 rpm to OD₆₀₀ = 1.0, after which the culture was centrifuged at 1600 × *g* for 10 min. The cell pellet was re-suspended in 50 mL of 40% LB broth containing 0.2% arabinose and the respective antibiotics. The culture was incubated at room temperature (50 rpm) overnight. Following incubation, the culture was centrifuged for 10 min at 1600 × *g* and the cell pellet was resuspended in 800 µL of 1× HSU buffer (Appendix A.2.5). The pARA vector without the insert was used as a negative control and was prepared as described for pARAC3.

Because of difficulties in obtaining high yields of BxpC, *bxpC* lacking the predicted signal sequences (described above) was fused to a GST tag coding sequence, generating the vector pGEXL3. A starter culture of *E. coli* DH10B containing pGEXL3 was prepared as described above for pARAC3. When the cells reached OD₆₀₀ = 1.0, 300 µL of freshly prepared isopropylthio-β-galactoside (IPTG) (100 mM stock solution) were added to the flask, and the culture was incubated at room temperature (approximately 20°C, 50 rpm) or at 37°C (250 rpm) overnight. The cells were then pelleted by centrifugation at 1600 × *g* (10 min) and cell pellets were resuspended in 800 µL of 1× HSU buffer (Appendix A.2.5). The HSU buffer does not contain soluble P so it can be used in further experiments where soluble P is to be quantified. The vector pGEX without the insert was used as a negative control.

Each sample was then transferred to a 1.5 mL microcentrifuge tube and sonicated three times for 30 s each (Section 4). Following sonication, 1 µL (10 U) of DNase (Roche) was added to degrade and remove single-stranded and double-stranded DNA. DNA digestion was performed at room temperature for 10 min (slow rotation) prior to centrifugation for 10 min at 5900 × *g*. Supernatants were removed and sterilised through a 0.22-µm syringe PVDF filter (13 mm, LabService). Cell pellets were resuspended in 200 µL of 1× HSU buffer. All samples were stored at 4°C.

4.2.6.2 Protein purification using a GST tag

To purify BxpC from the sonicated pGEXL3 filtrate, GST-BxpC tag fusion protein was bound to Glutathione Sepharose™ 4B resin (GE Healthcare, Little Chalfont, UK) according to the manufacturer's protocol. An 800- μ L aliquot of the sonicated pGEXL3 filtrate (Section 4.2.6) was incubated at 4°C (slow rotation) with 1 mL of pre-activated glutathione sepharose resin overnight. The resin was then washed with 5 mL of 1 \times HSU buffer (Appendix A.2.5), followed by centrifugation for 5 min at 500 \times *g*. The supernatant was then analysed by sodium dodecyl sulphate-polyacrylamide gel electrophoresis (SDS-PAGE) (Section 4.2.6.3). The washing step was repeated three times to ensure removal of unbound proteins. The 220-amino acid (26 kDa) GST tag from pGEX-6P-1 was removed during protein purification using PreScission™ protease (GE Healthcare) according to the manufacturer's protocol. The PreScission protease cleaves the specific amino acid sequence Leu-Glu-Val-Leu-Phe-Gln-Gly-Pro, which is fused to the GST tag, between the glutamine (Gln) and glycine (Gly) residues. To cleave the GST-BxpC fusion protein, the resin was incubated with 24 μ L of PreScission protease and 276 μ L of cleavage buffer (50 mM Tris-HCl, 150 mM NaCl, 1 mM EDTA, 1 mM dithiothreitol, pH 7.0) for 4 h at 4°C with slow rotation, followed by three washes with 500 μ L of cleavage buffer. Each eluate was collected in a 1.5 mL microcentrifuge tube and concentrated using a 10-kDa centrifugal filter (Amicon® Ultra, Merck Millipore, Darmstadt, Germany) to a final volume of 20 μ L.

4.2.6.3 Acrylamide gel electrophoresis

Sodium dodecyl sulphate-polyacrylamide gel electrophoresis (SDS-PAGE) was performed as described by Laemmli (1970) on one-dimensional 15% polyacrylamide slab gels containing 0.1% SDS. The SDS-PAGE gel composition is detailed in Appendix A.2.7. Protein samples were heated to 95°C for 10 min with Tris(2-carboxyethyl)phosphine (TCEP) loading buffer. The TCEP buffer helps to reduce disulphide bonds and facilitates protein separation on SDS-PAGE. Samples (25 μ L) were then loaded into gel wells and SDS-PAGE was performed on a miniature vertical slab gel unit (Hoefer Scientific Instruments, Holliston, MA, USA) at constant voltage (200 mV for 1 h 15 min). The SDS-PAGE gel was silver-stained using the method of Blum et al. (1987). The molecular weights of apparent protein bands were determined by comparison with the Precision Plus Protein™ molecular weight ladder (Bio-Rad).

4.2.7. Statistical analysis

All numerical data are expressed as the mean of three replicates \pm the standard error of the mean (mean \pm SEM). One-way analysis of variance (ANOVA) was used to calculate significant differences between treatments (* $p < 0.05$, ** $p < 0.01$, *** $p < 0.001$). Generalised Linear Modelling was used to generate pair-wise correlations between soluble P realised over time, culture filtrate pH, and soluble P and 2-KGA concentration in the cytosol. Differences between treatment groups were tested using the Tukey Method at the 5% level. Analyses were performed using Minitab version 15 (Minitab, Inc., www.minitab.com).

Table 4.2.1 Bacterial strains and plasmid used in this study.

Strains and plasmids	Description	References
Strains		
<i>E. coli</i> DH10B	F- <i>mcrA</i> Δ <i>mrr-hsdRMS-mcrBCΔ80d <i>lacZ</i>ΔM15 Δ<i>lacX74</i>endA1 <i>recA1</i>deoRΔara, <i>leu7697</i> <i>araD139</i> <i>galU</i> <i>galk</i> <i>nupG</i> <i>rpsL</i> λ-</i>	Lorow and Jessee, (1990)
EC100D <i>pir</i> +	F' <i>mcrA</i> Δ (<i>mrr-hsdRMS-mcrBC</i>) ϕ 80d <i>lacZ</i> Δ M15 Δ <i>lacX74</i> <i>recA1</i> <i>endA1</i> <i>araD139</i> Δ (<i>ara, leu</i>)7697 <i>galU</i> <i>galk</i> λ - <i>rpsL</i> <i>nupG</i> <i>pir</i> ⁺ (DHFR)	Metcalfe et al. (1994)
S17-1 λ <i>pir</i>	<i>hsdR</i> Pro Δ <i>recA</i> - RP4-2 Tc::Mu Kan::Tn7 integrated in the chromosome: <i>pir</i> gene	Miller and Mekalanos, (1988)
<i>Burkholderia</i> sp. Ha185	Gm ^R ; Field isolate from Haast, New Zealand, <i>Burkholderia</i> sp. parent strain containing pBBR1MCS-5 broad host range vector	This study
<i>bxpC</i> ::Tn5(F13)	Gm ^R , Kn ^R ; <i>bxpC</i> ::Tn5(F13) insertion at 44 bp 5' of the initiation codon; derivative of <i>Burkholderia</i> sp. Ha185(pBBR1MCS-5)	This study
<i>hemX</i> ::Tn5(F18)	Gm ^R , Kn ^R ; <i>hemX</i> ::Tn5(F18) insertion at 50 bp 5' of the initiation codon; derivative of <i>Burkholderia</i> sp. Ha185(pBBR1MCS-5)	This study
1311CMPB2	Gm ^R , Kn ^R , Tc ^R ; containing p1311CMPB bearing <i>bxpC</i> from <i>Burkholderia</i> sp. Ha185; derivative of <i>bxpC</i> ::Tn5(F13)	This study
CD3ME12	Gm ^R , Kn ^R , Tc ^R ; containing pCD3ME bearing <i>hemC</i> and <i>hemX</i> from <i>Burkholderia</i> sp. Ha185; derivative of <i>hemX</i> ::Tn5(F18)	This study
DXDME6	Gm ^R , Kn ^R , Tc ^R ; containing pCD3ME bearing <i>hemX</i> from <i>Burkholderia</i> sp. Ha185; derivative of <i>hemX</i> ::Tn5(F18)	This study
Plasmids		
pBBR1MCS-5	Gm ^R ; broad host range vector	Kovach et al. (1995)
pME6010	Tc ^R ; 8270 bp; broad-host range shuttle vector replicable in Gram-negative bacteria	Heeb et al. (2000)
p1311CMPB	Tc ^R ; pME6010 containing the 1136 bp <i>Bgl</i> II PCR product bearing <i>bxpC</i> from <i>Burkholderia</i> sp. Ha185	This study
pCD3ME	Tc ^R ; pME6010 containing the 3876 bp <i>Bam</i> HI PCR product bearing <i>hemC</i> and <i>hemX</i> from <i>Burkholderia</i> sp. Ha185	This study
pDXDME	Tc ^R ; pME6010 containing the 2854 bp <i>Bam</i> HI PCR product bearing <i>hemX</i> from <i>Burkholderia</i> sp. Ha185	This study
pGEM [®] -T Easy	Am ^R ; <i>lacZ</i> multi-cloning site	Promega
pAY2-4	Am ^R ; arabinose expression vector	Shaw et al. (2003)
pGEX-6P-1	Am ^R ; IPTG inducible expression vector for protein expression with the GST tag	GE Healthcare
pARAC3	Am ^R ; arabinose expression vector pAY2-4 bearing <i>bxpC</i> (55–357 bp) from <i>Burkholderia</i> sp. Ha185 ligated into a 5' <i>Nde</i> I and a 3' <i>Eco</i> RI restriction site of pAY2-4	This study
pGEXL3	Am ^R ; IPTG inducible expression vector pGEX-6P-1 bearing <i>bxpC</i> (55–357 bp) from <i>Burkholderia</i> sp. Ha185 ligated into a 5' <i>Bam</i> HI and a 3' <i>Sal</i> I restriction site	This study

Table 4.2.2 Oligonucleotide primers used in this study.

Purpose	Oligonucleotides	Sequence (5' → 3') ^a
Gene complementation	cBxpCF	AAAAAAGATCTTAATGCTCCGAGACCAAGCGC
	cBxpCR	AAAAAAGATCTATAACGTCCCGGCTCTACCG
	cHemCF	AAAGGATCCGACTGCAA TGTGAACAGCAC
	cHemXR	AAAGGATCCTATTCTG GCATGCGATGCGC
	cHemXF	AAAGGATCCGCTGCA TCACGAACACAC
	cHemXR2	AAAGGATCCTACAGCAGGATGAACAGCACCACC
<i>bxp</i> operon	F13HypoF	ACGTTGCCAGCGCGTGCTTGG
	F13AR	TCACGTACATTGGCAGGAGCC
	F13AF	ATCGACATCCAGGCGCTCAGCG
	F13BR	ACTTGTGGCGAATCAGCACG
	F13BF2	CGAGTTGCATTGAGCTTGG
	F13CR2	ACGCCTTCTGTGATTGCTCA
	F13CF	AAGACGTGCGCCGACGGTGG
	F13DR	AATGACAGCCACATGTCGCG
	F13DF	ATCATGTATCGTGCCCGAAGC
	F13ER	TGTCCGCGAGTTCACCGACG
	F13EF	ACATTGACCGCTATCGTTGCTG
	F13HypoR	ACTCCTAACGCGCATCATGC
	<i>hem</i> operon	PPCF
HemCR		ATCGCCACGTGTCGTCATTCCGAGG
HemCF		ATGGCTCGCGCCGCTGCATCACG
HemDXR		TCGAGTGCCGCGAACAGGCCTTCG
HemDXF2		GACAACGCGATCGACCAGAT
HemYR2		CCCGCATAACAGATTGCCGAT
HemYF2		GCGTCTGTTGCGTCGTTATC
MfspR		ATGGCCGCGCTCACGCTCGC
MetfF		TACCGCGCCGACGAATGGGT
PPCR2		TCTGCGCGGATTCCGTGGG
MfspF		ATGTAGCCCGACACCGGACC
SDRR		TACGCCGGCCAATCGTCAGC
Primer walking		PAAR153F
	PAAR755R	ATGACAGCCACATGTCGCGAGATGGC
	342F	ATCGACGAAGCCGACTGGCTCGATGC
	042R	TCTCGCGATAATGCTGGCTCGCC
qRT-PCR primer sets	qGyrBF	GGATGAGCGGTATTTGAAGG
	qGyrBR	ATATGCACGAGCCAACCTCAC
	qRecAF	CGTATCGGTTTCGATCAAGAAG
	qRecAR	CGAAATACCTTCGCCATACAG
	qGltBF	GATCTTCGCGATGTCCTTG
	qGltBR	GGACACGAACAACATCAACC
	qHemXF	CACGCATGACTGAAACGAC
	qHemXR	ATCACGACGACAAACCACAG
	qBxpCF	GACGGTGGGAATGTATATGATG
	qBxpCR	ACGCCTTCTGTGATTGCTC
	qPpcF	CATTACGAAGCGGTGATCG
	qPpcR	GGAATACTCGGCATACGGCA
	qHemCF	ATCCTCGGAATGACGACACG
	qHemCR	ACGTCTTTGAGCGAATGCAC

<i>bxpC</i> expression	ParaNF ParaER GexBF GexSR	AAACATATGAAGACGTGCGCCGACGGTGGGAATGT AAAGAATTCTATTTCTCGAGAAGAGTCTTCAA AAAGGATCCAAGACGTGCGCCGACGGTGGGAATGT AAAGTCGACTATTTCTCGAGAAGAGTCTTCAA
Gene sequencing	M13F [†] M13R [†] pGEX5 [†] pGEX3 [†]	GTA AACGACGGCCAGT GCGGATAACAATTTACACAGG GGCAAGCCACGTTTGGTG GGAGCTGCATGTGTCAGAGG

Oligonucleotide primers designed and used in this study

^a Underscore denotes designed restriction site

[†] Oligonucleotide from Macrogen universal primer list

4.3 Results

4.3.1. Physiology of *Burkholderia* sp. Ha185

Cell morphology of *Burkholderia* sp. Ha185 may provide insight into how the bacterium interacts with HydroxP particles or with plants. Transmission electron microscopy (performed previously by Dr Daria Rybakova, AgResearch, Lincoln, and reproduced here with permission) of *Burkholderia* sp. Ha185 revealed that the bacterium is a single cell of ~1500–2200 nm in length and 800 nm in diameter. The bacterium has a single flagellum (Figure 4.3.1 - red arrow), which may be involved in locomotion.

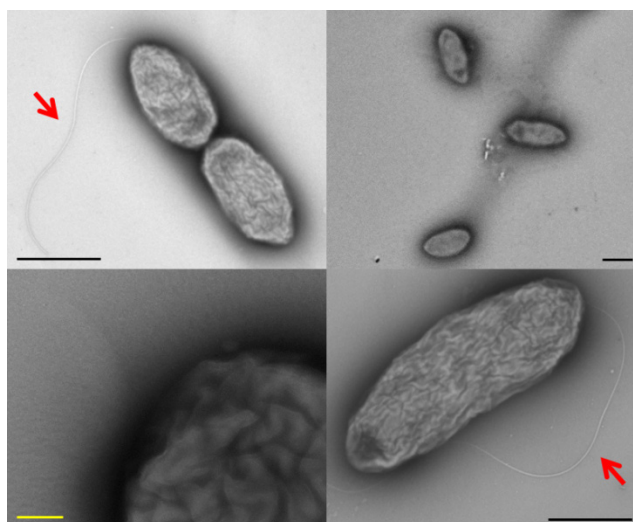


Figure 4.3.1 Electron microscope images of *Burkholderia* sp. Ha185. Red arrow indicates a single flagellum. Image taken by Dr Daria Rybakova, AgResearch, Lincoln. Black scale bar = 1000 nm, yellow scale bar = 100 nm.

4.3.2. The *bxp* operon

4.3.2.1 *bxp* genes arrangement, annotation and transcription

The non-auxotrophic *Burkholderia* sp. Ha185 mini-Tn5Km1 transposon mutant, F13, constructed in Chapter 3, was tested for its ability to solubilise tricalcium P (TCaP) in a liquid medium. The mutant had a reduced ability to solubilise TCaP, although its cell growth relative to the wildtype *Burkholderia* sp. Ha185 was unaffected at 72 h (Chapter 3.3.4). Results from genome walking using touchdown PCR (Chapter 3.2.6) and DNA sequencing revealed that the F13 mutant contained a single transposon insertion in a gene encoding a hypothetical protein. The hypothetical protein showed 92% identity to a protein of unknown function from *Burkholderia* sp. CCGE1003 (InterPro, IPR009739) that contained a duf1311 protein domain (Table 4.3.3 and Table 4.3.2). To retrieve the peripheral DNA sequence of areas located 3' and 5' of the F13 transposon insertion point, the low-coverage draft *Burkholderia* sp. Ha185 genome sequence was subjected to BLASTn analysis using the DNA sequence derived from touchdown PCR as the query in NCBI nucleotide database. The sequence aligned to both Contig00153 (total size 12,162 bp) and Contig00755 (total size 2283 bp), with a 120-bp space between the two regions. To close this gap, two specific primers (PAAR153F and PAAR755R) were designed from the 3' end of Contig00153 (total size 12,162 bp) and 5' end of Contig00755 (total size 4000 bp), respectively (Table 4.2.2), to yield an 862-bp amplicon (Appendix C.2.9). The PCR product was ligated into the pGEM-T Easy vector (Appendix C.2.11) and the insertion was confirmed by *Eco*RI restriction profile (Appendix C.2.3). A clone with the correct insertion was then sequenced using the M13F and M13R primers (Appendix C.2.12). The resultant sequence was aligned to Contig00153 and Contig00755 using Geneious version 6.1.5 (Biomatters, Auckland, New Zealand; <http://www.geneious.com>) to obtain sequence corresponding to the 120-bp gap, giving a full sequence of approximately 15 kb. Analysis of the resultant consensus sequence using Vector NTI (Life Technologies) predicted 12 ORFs (Figure 4.3.2). Four ORFs were also present in the same direction (5' to 3'), with the two outer ORFs (opposite strand) named *orfA* and *orfB* (Figure 4.3.3). The reference protein database of the NCBI was searched by BLASTx using the protein sequence of each ORF. The protein orthologs with the greatest similarity are listed in Table 4.3.1. BLASTx revealed a cluster of five ORFs with unknown functions, oriented on the same strand. Because there were no functional orthologs, these genes were assigned the names "*bxpA–E*", corresponding to each of the five genes in order (Figure 4.3.3), where *bxp* stands for *Burkholderia xenovorans* phosphate-related gene. Sequence alignment of the F13 insertion point region revealed that the mini-Tn5Km1 transposon had inserted 44-bp from the 5' end of the predicted ORF *bxpC* (Figure 4.3.3). Therefore, the F13 mutant described in Chapter 3 is hereafter designated "*bxpC*::Tn5(F13)".

Protein sequence analysis showed that BxpA consists of 845 amino acids and is 86% similar to the Rhs element VgrG protein (valine-glycine repeat protein G, IPR006533) of *Burkholderia* sp. CCGE1003 (YP_003907491.1) (Table 4.3.2 and Figure 3.1.16). A domain search using BLASTp revealed that there are four discrete domains (Figure 3.1.16) within BxpA: a phage late control gene D protein domain (Phage_GPD); a phage-related baseplate assembly protein (Phage_base_V); a putative type VI secretion system Rhs element, Vgr (T6SS_Vgr); and an uncharacterised protein domain (duf2345). Together, these domains are related to a Rhs element VgrG protein involved in type VI secretion systems (T6SS) that plays a role in protein transport (Filloux et al., 2008). The VgrG domain is usually located near a set of T6SS loci (containing 12–25 genes) and has been proposed to bind or puncture target cells, delivering effector domains encoded within the C-terminal regions into the target cell cytosol. The N-terminal of VgrG, known as “evolved VgrGs”, may serve in assembly of the T6SS machinery (Pukatzki et al., 2007). However, Barret et al. (2011) aligned 34 *Pseudomonas* spp. genomes and identified three conserved regions containing lone *vgrG* genes outside of the T6SS locus, and named these regions “orphan VgrGs”. The role of orphan VgrGs remains unknown but it is hypothesised that genes within VgrG islands are involved in secretion (Barret et al., 2011).

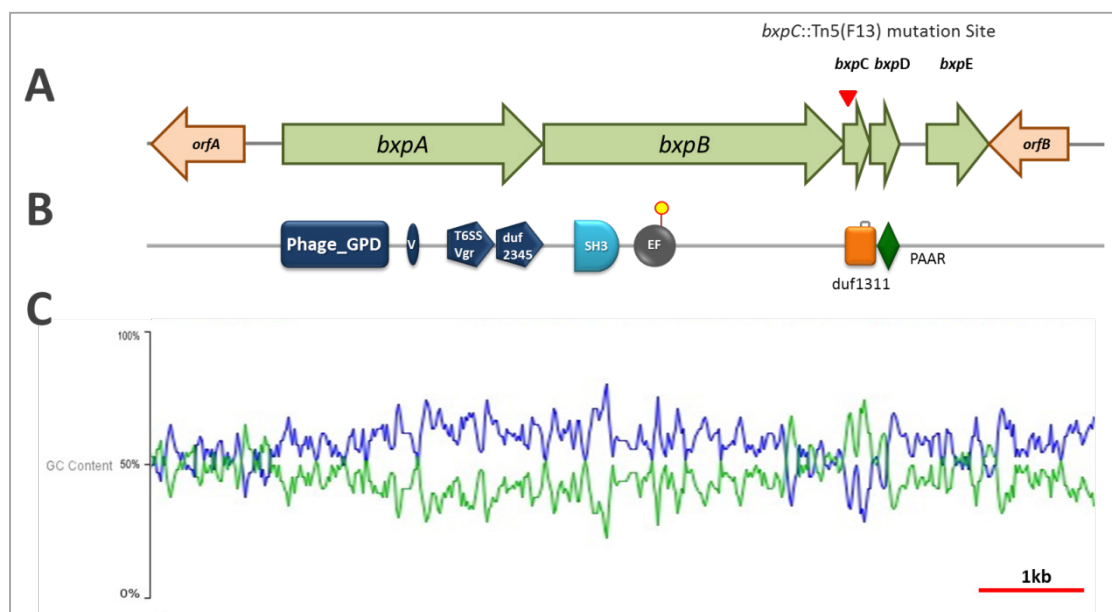


Figure 4.3.2 Schematic representation of the *Burkholderia* sp. Ha185 *bxp* gene arrangement (A), domain annotations at the relative location of each open reading frame (B) and GC content of the *bxp* operon (C). Green arrows denote the five ORFs, *bxpA*, *bxpB*, *bxpC*, *bxpD*, and *bxpE*, thought to compose the *bxp* operon (refer to Table 3.1.11 and Table 3.1.12 for gene annotation). The *bxpC*::Tn5(F13) mutation site located 44 bp from the 5' end of *bxpC* is indicated by a red arrow. Open reading frames in the 3' to 5' direction in orange arrow are hypothetical proteins with unknown functions. Results of domain annotation by BLASTp, MyHit MotifScan and ScanProsite are shown in B, where VgrG-related proteins found in BxpA are in blue. The bacterial SH3 domain found in BxpB is shown in light blue box, followed by the EF-hand calcium-binding domain in grey circle. The yellow circle indicates the calcium binding site (amino acids 708–720, DTNHDGKITAQEL). A protein of unknown function (duf1311) domain is shown in orange, and the disulphide bond formed by two cysteine residues (linking amino acid residues 59 and 82 of the BxpC protein) is indicated by grey line. The PAAR domain is indicated by a green diamond. The GC content (%) is indicated by the blue line, and the AT content (%) is indicated by the green line in (C). Sliding window size: 70. Diagram drawn to scale relative to the DNA sequence. Scale bar indicates 1 kb.

Table 4.3.1 Predicted *bxp* operon homology for *Burkholderia* sp. Ha185 ORFs identified from DNA sequencing and protein sequence analysis

ORFs	Amino acid	Nucleotides ^a	G+C (%)	Degree of similarity ^{b,c}	Protein, species ^c	Accession no.
<i>orfA</i> [‡]	274	1–882	51.8	67/78//307 (13–302) 49/65//299 (1–296)	Hypothetical protein Bphy_4812 (<i>Burkholderia phymatum</i> STM815) Conserved protein of unknown function (<i>Ralstonia solanacearum</i> CMR15)	YP_001860966.1 CBJ36248.1
<i>orfB</i> [‡]	293	8280–9104	58.5	27/45//193 25/43//241	Hypothetical protein (<i>Cellvibrio</i> sp. BR) Hypothetical protein CTU_17330 (<i>Cronobacter turicensis</i> z3032)	WP_007638193.1 YP_003210096.1
<i>bxp</i> operon						
<i>bxpA</i>	845	1339–3873	59.6	86/92//836 (1–836) 69/80//835 (1–835)	Rhs element VgrG protein (<i>Burkholderia</i> sp. CCGE1003) Rhs element VgrG protein (<i>Burkholderia ubonensis</i> Bu)	YP_003907491.1 ZP_02380915.1
<i>bxpB</i>	962	3930–6815	57.2	76/85//976 (193–976) 66/79//911 (160–911)	Hypothetical protein (<i>Burkholderia</i> sp. CCGE1003) Hypothetical protein Bpse38_16427 (<i>Burkholderia thailandensis</i> MSMB43)	YP_003907490.1 ZP_02464959.1
<i>bxpC</i>	118	6834–7187	39.8	81/92//357 (1–118) 76/85//147 (1–146)	Hypothetical protein (<i>Burkholderia</i> sp. CCGE1003) Hypothetical protein B1M_34534 (<i>Burkholderia</i> sp. TJI49)	YP_003907489.1 ZP_11937170.1
<i>bxpD</i>	83	7200–7451	59.1	86/92//83 (1–83) 84/91//83 (1–83)	PAAR repeat-containing protein (<i>Burkholderia ambifaria</i> MC40-6) PAAR repeat-containing protein (<i>Burkholderia cepacia</i> GG4)	YP_001816415.1 YP_006617974.1
<i>bxpE</i> [‡]	159	7756–8232	53.2	52/71//118 (5–116) 53/71//118 (5–118)	Hypothetical protein (<i>Acinetobacter</i> sp. NIPH 284) Hypothetical protein predicted by Glimmer/Critica (<i>Stenotrophomonas maltophilia</i>)	WP_005160908.1 WP_006375896.1

^a Nucleotide sequence is a continuum from the published sequence, GenBank accession no. KJ415239

^b Amino acid similarity (% identity/% similarity//over amino acid residues) in relation to sequence generated in this study

^c BLASTx results based on NCBI protein database search performed in March 2013

[‡]BLASTx results based on NCBI protein database search performed in May 2013

Table 4.3.2 Predicted domains and ligand-binding motifs for the *Burkholderia* sp. Ha185 *bxp* operon

ORFs	Amino acid	Protein annotation ^a	Domains ^b , ligand-binding motif ^c	Amino acid range
<i>orfA</i>	274	Hypothetical protein	No domain found	
<i>orfB</i>	293	Hypothetical protein	No domain found	
<i>bxp</i> operon				
<i>bxpA</i>	845	Rhs element VgrG protein	<ul style="list-style-type: none"> - Phage late control gene D protein (Phage_GPD)^b, phage late control gene D proteins and related bacterial sequences. - Phage-related baseplate assembly protein (Phage_base_V)^b, a family of phage baseplate assembly proteins responsible for forming the small spike at the end of the tail. - Putative type VI secretion system Rhs element Vgr (T6SS_Vgr, duf586, IPR006533)^b, a family of putative type VI secretion system Rhs element Vgr proteins from Proteobacteria. - Uncharacterised protein conserved in bacteria (duf2345, IPR018769)^b, a family found in various bacterial hypothetical proteins, as well as Rhs element Vgr proteins. 	55–378 435–468 548–661 696–855
<i>bxpB</i>	962	Hypothetical protein	Bacterial SH3 domain ^e (IPR003646) ^d EF-hand calcium-binding domain (EF_HAND_2, IPR018247) ^{cd} †D-{W}-[DNS]-{ILVIFYW}-[DENSTG]-[DNQGHRK]-{GP}-[LIVMC]-[DENQSTAGC]-x(2)-[DE]-[LIVMFYW] ^c	300–370 695–730 708–720
<i>bxpC</i>	118	Hypothetical protein	Protein of unknown function (duf1311, IPR009739) ^{bd} , the family consists of several bacterial proteins of around 120 residues in length. Members of this family contain four highly conserved cysteine residues. The function of this family is unknown.	20–112
<i>bxpD</i>	83	PAAR repeat-containing protein	PAAR motif (PAAR, IPR008727) ^{bd} , a motif that is usually found in pairs in a family of bacterial membrane proteins.	5–81
<i>bxpE</i>	159	Hypothetical protein	No domain found but is predicted to be a transmembrane protein ^f	

^a Protein annotation based on Table 4.3.1

^b Domain search based on BLASTp analysis

^c Domain and ligand search based on MyHit MotifScan and ScanProsite

^d InterPro accession number is presented as IPR followed by six digit numbers

^e Family and domain search through Pfam carried out in Oct 2013

^f Transmembrane protein predicted by SOSUI: classification and secondary structure prediction system for membrane proteins (Mitaku et al., 2002)

† The PA (PAttern) indicates unique signature of consensus pattern of ligand-binding motif

The 962 amino acid translated product of *bxpB* shows 85% similarity to a hypothetical protein from *Burkholderia* sp. CCGE1003 (YP_003907490.1). A protein domain search of the BxpB sequence using ScanProsite (de Castro et al., 2006) and MyHit (Pagni et al., 2007) predicted an EF-hand calcium-binding domain (IPR018247), with the calcium-binding motif located at amino acids 708–720 (Figure 3.1.16). A Pfam search predicted that BxpB contains a bacterial SH3 domain (IPR003646) from amino acids 300–370. Proteins with this domain are known to be membrane-associated but their function is not clear.

The BLASTp analysis showed that the BxpC sequence is 92% similar to a hypothetical protein from *Burkholderia* sp. CCGE1003 (YP_003907489.1). BxpC contains a putative duf1311 domain (IPR009739), which is found in a family of proteins of unknown function. Proteins in this family are typically 120 amino acid residues in length and contain four highly conserved cysteine residues (Figure 3.1.16). The GC plot of the *bxp* operon (Figure 3.1.16 (C)) generated by Geneious (version 6.1.5) showed that the *bxpA–E* operon has an overall GC content of 56.9%, while the predicted overall GC content of the *Burkholderia* sp. Ha185 genome is 62.7%. Interestingly, the *bxpC* ORF is significantly less GC rich, with a GC content of 39.8%.

BxpD (83 amino acid) showed 92% similarity to a PAAR repeat-containing protein from *Burkholderia ambifaria* MC40-6 (YP_001816415.1). The associated PAAR motif (IPR008727) is a conserved bacterial membrane protein. The translated product of *bxpE* comprises 159 amino acid residues and shows 71% similarity to a hypothetical protein from *Acinetobacter* sp. NIPH 284 (WP_005160908.1). Neither ScanProsite nor MyHits was able to identify any motifs in BxpE.

Both *orfA* and *orfB* are in the opposite orientation to the *bxp* operon. Their translated products are homologous to the hypothetical proteins YP_001860966.1 and WP_007638193.1, respectively (Table 4.3.1). Functional domains for *orfA*- and *orfB*-homologous proteins have not been identified (Table 4.3.2).

4.3.2.2 Confirming the *bxp* operon by PCR

To ascertain whether the *bxp* genes are components of an operon, primer sets were designed to amplify between each of the ORFs (Figure 4.3.3). Forward and reverse primers are listed in Table 4.2.2. All primer sets produced PCR amplicons of predicted sizes when *Burkholderia* sp. Ha185 gDNA was used as a template (Figure 4.3.3 (B)). When cDNA was used as the template, primer sets 2 (F13AF/F13BR), 3 (F13BF/F13CR), 4 (F13CF/F13DR) and 5 (F13DF/F13ER) amplified products of the

predicted size, indicating that *bxpA–E* are transcribed as one single transcript. However, no product was obtained between *orfA* and *bxpA* (primer set F13HypoF/F13AR) or *bxpE* and *orfB* (primer set F13EF/F13HypoR) when cDNA was used as a template. These results confirmed that *Burkholderia* sp. Ha185 *bxpA–E* are transcribed as a single operon, and that *orfA* and *orfB* are transcribed independently of this operon.

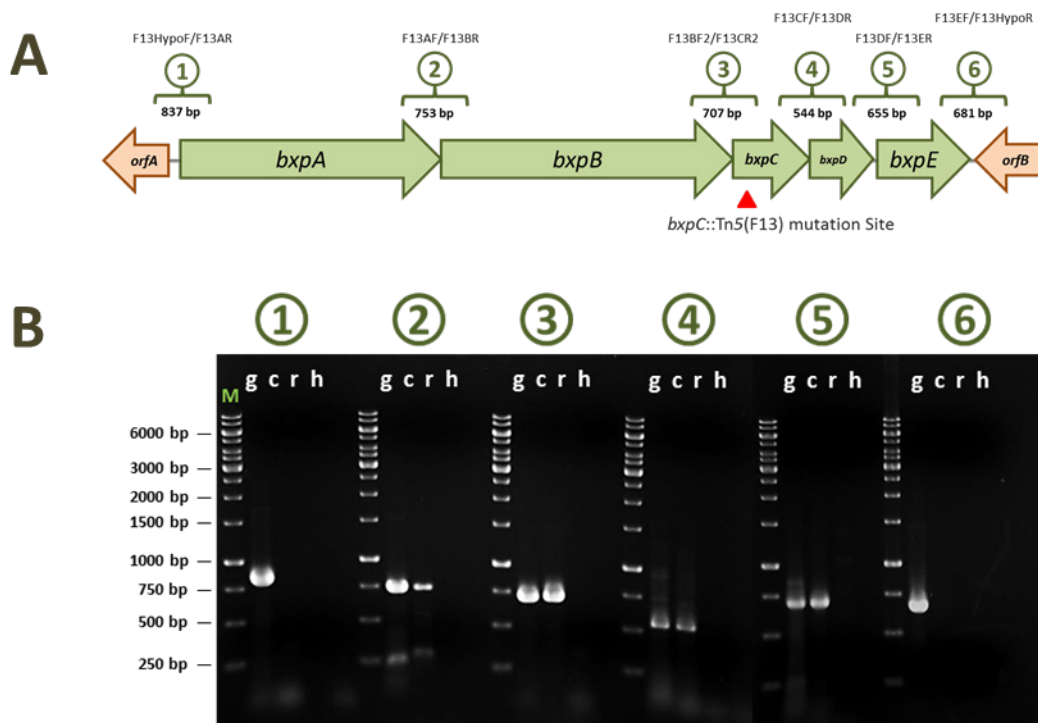


Figure 4.3.3 Schematic representation of the *Burkholderia* sp. Ha185 *bxp* gene arrangement and the location of the Tn5 transposon insertion (A), and agarose gel showing the corresponding amplification products (B). (A) Green arrows denote the five ORFs, *bxpA*, *bxpB*, *bxpC*, *bxpD* and *bxpE*, predicted to compose the *bxp* operon (refer to Table 4.3.3 for gene annotation). The *bxpC::Tn5(F13)* mutation site, located 44-bp from the 5' end of *bxpC*, is indicated by a red arrow. ORFs in the reverse direction, shown in orange, are hypothetical proteins with unknown functions. Numbers in green circles indicate independent primer sets, with primer names stated above, and predicted PCR product sizes stated below (bp). Gel electrophoresis (B) of PCR products using primers sets corresponding to each number from the circles in (A). gDNA (indicated as “g”) was used as a positive control, and RNA (r) and UltraPure™ DEPC-treated water were used as negative controls, and cDNA (c) is the tested sample. M denotes GeneRuler™ 1 kb molecular marker.

4.3.2.3 Trans-complementation of the *bxpC::Tn5(F13)* mutant

To enable complementation of the mutated gene in *bxpC::Tn5(F13)*, the entire *bxpC* region from the gDNA of wildtype *Burkholderia* sp. Ha185 was PCR-amplified and cloned into the broad host range pACYC177-pVS1 shuttle vector pME6010 (Tc^R, Table 4.2.1) (Heeb et al., 2000). The resulting complementation plasmid was named p1311CMPB (Figure 4.3.5), and was transformed into *Burkholderia* sp. Ha185 *bxpC::Tn5(F13)* cells, generating the complementation strain 1311CMPB2. To construct p1311CMPB, the primer pair cBxpCF/cBxpCR (Table 4.2.2, Figure 3.1.18) was used to amplify a region encompassing all of *bxpC* as well as the 399 bp 5' of the initiation codon of *bxpC*, from wildtype *Burkholderia* sp. Ha185 gDNA. The resultant 1136-bp *bxpC* amplicon, containing peripheral *Bgl*II restriction enzyme sites was cloned into the pGEM-T Easy vector (Appendix C.2.11) to generate p1311CMPB, which was end sequenced using M13F and M13R primers. A *Bgl*II restriction digest released the fragment from p1311CMPB, which was then ligated into the analogous site of pME6010. A 2- μ L aliquot of the ligation was then transformed into *E. coli* DH10B (Table 4.2.1) and the transformants were plated on LB agar containing tetracycline (30 μ g/mL), to select for the pME6010 vector. The resulting colonies were then patched onto LB agar containing either tetracycline (30 μ g/mL) or ampicillin (100 μ g/mL) to confirm the insertion of the fragment into pME6010 and the loss of the ampicillin resistant pGEM-T Easy vector. Plasmid DNA from several ampicillin-sensitive colonies was then extracted and digested with *Kpn*I, releasing a \sim 920 bp fragment, and with *Bgl*II and *Apa*LI, releasing two fragments of \sim 270 bp and \sim 870 bp. The confirmed construct was designated p1311CMPB.

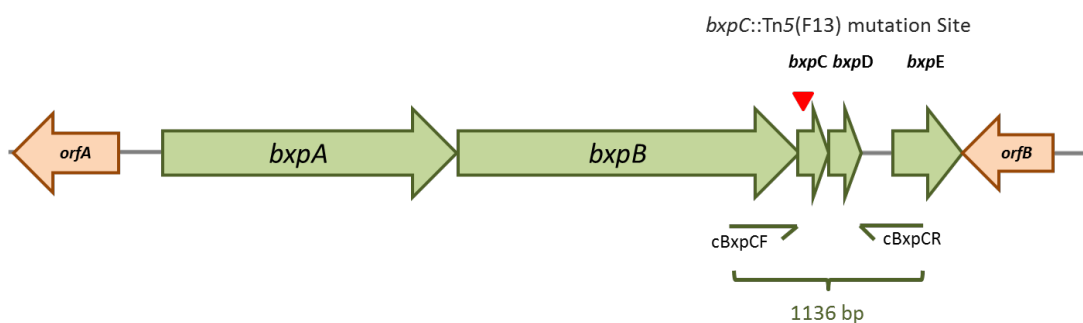


Figure 4.3.4 Schematic diagram of the *bxp* operon. Green arrows denote the five ORFs, *bxpA*, *bxpB*, *bxpC*, *bxpD* and *bxpE*, predicted to compose the *bxp* operon. The *bxpC::Tn5(F13)* mutation site, located 44 bp from the 5' end of *bxpC*, is indicated by a red arrow. Primers cBxpCF and cBxpCR amplified a 1136-bp fragment containing the *bxpC* and *bxpD* ORFs. Open reading frames *orfA* and *orfB*, in the reverse orientation and indicated in orange, are hypothetical proteins with unknown functions (refer to Table 3.1.12 for gene annotation).

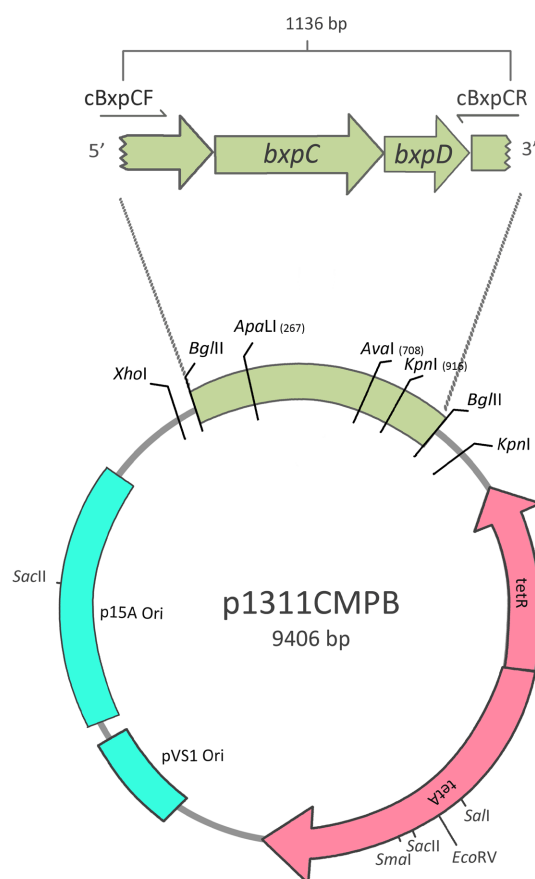


Figure 4.3.5 Diagram of the p1311CMPB plasmid construct. The *bxpC* complementation plasmid was constructed by ligating the PCR amplicon (as shown in Figure 3.1.18) into the *Bgl*II site of the pME6010 plasmid. Plasmid p1311CMPB confers tetracycline resistance to the host cell. Diagram not to scale.

To enable complementation of the *bxpC* mutant, p1311CMPB was electroporated into *Burkholderia* sp. Ha185 *bxpC*::Tn5(F13) electrocompetent cells, and cells were plated onto LB agar plates containing tetracycline (30 µg/mL) to select for p1311CMPB and kanamycin to select for the mini-Tn5*Km1* transposon. The plates were then incubated for 3 days at 25°C. Plasmid DNA from several transformants was extracted and validated by *Kpn*I and *Bgl*II restriction profiles, and the confirmed transformant was designated 1311CMPB2.

Strain 1311CMPB2 was then assessed for restoration of the P-solubilising phenotype. A 1311CMPB2 culture was grown in LB broth overnight, and then 1 µL of culture, containing approximately 10⁵ cfu, was dropped on a HydroxP agar plate (Appendix A.2.2). The same amount of wildtype *Burkholderia* sp. Ha185 and its mutated derivatives *bxpC*::Tn5(F13) and *hemX*::Tn5(F18), cultured under the same conditions, were used as positive and negative controls respectively. The plates were then incubated

for two weeks at 25°C to allow the development of the zones of clearance. As shown in Figure 3.1.20, growth assays showed that the wildtype *Burkholderia* sp. Ha185 strain can solubilise HydroxP, as shown by a visible halo around the circular colony. The *bxpC*::Tn5(F13) mutant showed a reduced zone of clearance, with an irregular colony shape and an undulate margin. The complementation strain, 1311CMPB2, solubilised HydroxP to a level comparable to the wildtype. It was also noted that colonies of 1311CMPB2 also exhibited an irregular shape, similar to the mutated strain *bxpC*::Tn5(F13).

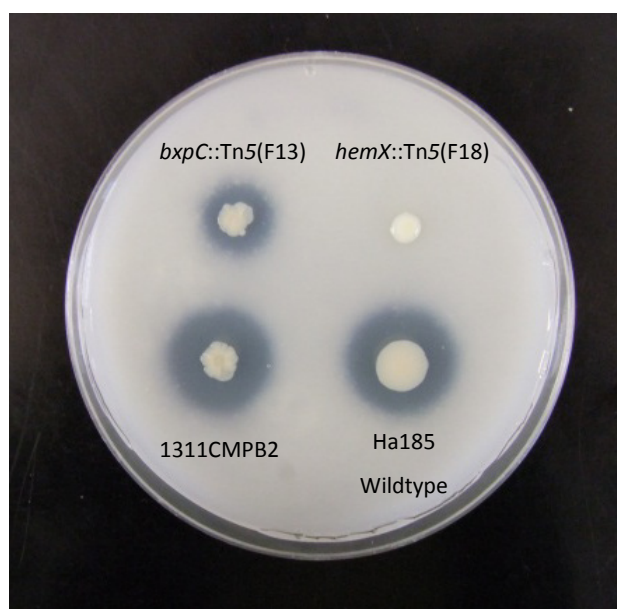


Figure 4.3.6 Phosphate solubilisation assay. Bacterial strains *Burkholderia* sp. Ha185 wildtype, *hemX*::Tn5(F18), *bxpC*::Tn5(F13) and complementation strain 1311CMPB2 were incubated for 2 weeks at 25°C on a hydroxyapatite agar plate. Note the lobate edges of *bxpC*::Tn5(F13) and 1311CMPB2 relative to wildtype.

4.3.3. The *hem* operon

4.3.3.1 *hem* gene arrangement, annotation and transcription

A non-auxotrophic mini-Tn5Km1 transposon mutant, *Burkholderia* sp. Ha185 F18, was previously shown to have a reduced ability to solubilise TCaP in liquid medium, but maintained a similar growth rate to the wildtype strain at 72 h (Chapter 3.3.4). Results from genome walking and DNA sequencing revealed that the F18 mutant had a transposon inserted into the gene coding for a bifunctional

uroporphyrinogen-III synthetase/uroporphyrin-III C-methyltransferase (HemX). HemX showed 89% identity to the HemX sequence of *B. xenovorans* LB400 (YP_557627.1) (Table 4.3.3). To retrieve the *hemX*-encoding contig from the *Burkholderia* sp. Ha185 draft genome, the DNA sequence generated from genome walking in the F18 mutant was used as template for BLASTn analysis of the low coverage *Burkholderia* sp. Ha185 genome sequences. The sequence aligned to the 3' end of Contig00342 (~800 bp were aligned), and contained a partial *hemY* ORF corresponding to the 5' end of the gene. To determine the complete *hemY* DNA sequence along with its unidentified neighbouring contig, the partial *hemY* DNA sequence was aligned with the *hemY* region from its closest relative, *B. xenovorans* LB400 (NC_007951.1), using Geneious version 6.1.5. The consensus DNA sequence corresponding to the region ~2 kb downstream of the *B. xenovorans* LB400 *hemY* gene was then aligned against the *Burkholderia* sp. Ha185 draft genome sequence, where the 8414-bp Contig00042 was found to be the most significant match. Sequence alignment of both Contig00342 (total size 7981 bp) and Contig00042 (total size 20,066 bp) with *B. xenovorans* LB400 revealed there was a 16-bp gap between these two contigs. Two primer pairs were then designed to amplify the region between the 3' end of Contig00342 and the 5' end of Contig00042 (Table 4.2.2).

The high GC content of this region meant that PCR amplification was difficult, and the PCR parameters were modified to achieve optimal amplification. A final concentration of 5% (v/v) DMSO was added to each sample and a temperature gradient was used to optimise PCR conditions (details are outlined in Section 4.2.4 and Section 4.3.3.3). The resulting ~750 bp amplicon generated using primer pair 342F/042R was cloned into pGEM-T Easy (Appendix C.2.11), and sequenced using M13F and M13R primers (Appendix C.2.12). The resultant DNA sequence was aligned to both Contig00342 and Contig00042, resulting in a final contig, designated Contig00342+Contig00042, of ~28 kb. The region flanking the F18 mini-Tn5Km1 transposon insertion site within Contig00342 was annotated using Geneious version 6.1.5. Genes located 5' or 3' of the F18 insertion point were then annotated and characterised until regions that were not related to the *hem* were identified. The region encompassing the *hem* genes was annotated and searched against the reference protein database from GenBank using BLASTx. Proteins that showed the highest similarity are listed in Table 4.3.3. BLASTx also confirmed that the *hem* ORFs are oriented in the same direction and correspond to three *hem*-related genes, termed *hemC*, *hemX* and *hemY* (Figure 4.3.7). Through DNA sequence analysis, the termination codon of *hemC* overlaps with the initiation codon of *hemX* and there is a two codon intergenic space between *hemX* and *hemY*. The opposing ORFs such as *ppc*, *mfs* and *sdr* are divergently transcribed. Therefore, a *hem* operon is defined in this study as comprise of *hemC*, *hemX* and *hemY* in *Burkholderia* sp. Ha185. Genome walking in the F18 mutant indicated that the mini-

Tn5Km1 transposon is inserted 50 bp from the *hemX* initiation codon (Figure 4.3.7). Therefore, mutant F18 described in Chapter 3 is hereafter referred to as “*hemX*::Tn5(F18)”.

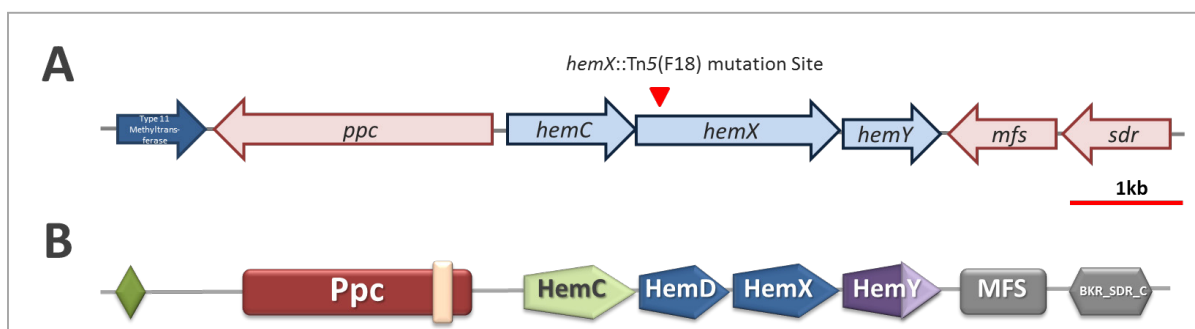


Figure 4.3.7 Schematic representation of *Burkholderia* sp. Ha185 *hem* gene arrangement (A) and domain annotations at the relative location of each open reading frame (B). (A) Blue arrows denote the three open reading frames, *hemC*, *hemX* and *hemY*, predicted to compose the *hem* operon. The *hemX*::Tn5(F18) mutation site, located 50 bp from the 5' end of *hemX*, is indicated by a red arrow. Open reading frames in the reverse orientation, presented in pink, are *ppc*, *mfs* and *sdr* (refer to Table 3.1.13 and Table 3.1.14 for gene annotation). (B) Results of domain annotation by BLASTp, MyHit MotifScan and ScanProsite, where the green diamond indicates a methyltransferase domain; the red rectangle represents a phosphoenolpyruvate carboxylase domain, with an active site at amino acids 288–299, in the reverse orientation (light orange box); the HemC domain is indicated by the green pentagon; the translated product of the *hemX* ORF consists of both the HemD and HemX domains, denoted by blue pentagons; the HemY domain is indicated by a purple pentagon, with a tetratricopeptide repeat domain indicated by a light purple triangle at amino acids 304–396; the grey rectangle represents a major facilitator superfamily domain; and the grey hexagon represents a putative beta-ketoacyl acyl carrier protein reductase (BKR_SDR_C). Red scale bar indicates 1 kb.

Having established that the *hem* operon is composed of *hemC*, *hemX* and *hemY* (Figure 4.3.7), an amino acid sequence search was conducted to further characterise the predicted protein products of the operon. Results revealed that the HemC sequence of *Burkholderia* sp. Ha185 is 90% similar to that of the HemC protein of *B. phytofirmans* PsJN (YP_001894712.1), which codes for a porphobilinogen deaminase. Porphobilinogen deaminase catalyses the initial reaction in porphyrin biosynthesis by polymerising four porphobilinogen molecules into hydroxymethylbilane, followed by uroporphyrinogen-III synthetase (encoded by *hemD*), to produce a tetrapyrrole compound, uroporphyrinogen-III (IPR022417) (Figure 3.1.22). *Burkholderia* sp. Ha185 HemX shows 89% similarity to HemX of *B. xenovorans* LB400 (YP_557627.1). Interestingly, *Burkholderia* sp. Ha185 HemX is divided into two domains, consisting of both the HemD and HemX domains, in a single polypeptide (Figure 4.3.7, Table 4.3.5). This protein codes for the bifunctional uroporphyrinogen-III synthetase enzyme, which also functions as a uroporphyrin-III C-methyltransferase. This suggests that during haem biosynthesis, it is possible that hydroxymethylbilane is transformed into precorrin-1 via

uroporphyrinogen III as an intermediate in a single step by HemX (Figure 3.1.22) via a yet to be determined mechanism. *hemY* is located 3' of *hemX*, and its translated protein product shows 96% similarity to HemY of *Burkholderia* sp. Ch1-1 (ZP_10030324.1) (Table 4.3.3). HemY is an uncharacterised protein of unknown function, but contains a tetratricopeptide repeat domain at amino acids 304–396 that is involved in protein-protein interactions (IPR013026) and is known to be a membrane protein.

ppc is located on the opposing strain of the *hem* ORFs, and its translated product shows 89% identity to the phosphoenolpyruvate carboxylase (PEPC) protein (IPR022805) of *B. phytofirmans* PsJN (YP_001894711.1). PEPC is involved in the tricarboxylic acid cycle (TCA) cycle (Table 4.3.3) where it catalyses the irreversible carboxylation of phosphoenolpyruvate to form oxaloacetate and phosphate, which supplies 4C oxaloacetate directly from pyruvate and facilitates carbon flow through the TCA cycle. Motif scanning of the PEPC protein showed that the active site is located between amino acid residues 288 and 299 of the PEPC protein (Figure 4.3.7).

The gene located upstream of *ppc* is predicted to encode a type 11 methyltransferase and showed 87% amino acid sequence identity to *B. phytofirmans* PsJN (YP_001894710.1). The type 11 methyltransferase is responsible for transferring a methyl group from the ubiquitous S-adenosyl-L-methionine (SAM) to a variety of atoms, such as nitrogen, oxygen or carbon, and is often involved in modifying DNA, RNA and proteins (IPR013216). The translated product of the *mfs* gene encodes a predicted major facilitator superfamily protein (MFS) and is 94% orthologous to the MFS protein from *B. phytofirmans* PsJN (YP_001894734.1) (Table 4.3.3). MFS proteins are membrane transporters that can transport small solutes across the cell membrane in response to chemiosmotic ion gradients, and can function as uniporters, symporters or antiporters (IPR011701, IPR020846). The gene of the next ORF that is divergently transcribed, designated *sdr*, encodes a protein with 97% identity to the short-chain dehydrogenase/reductase (SDR) protein of *Burkholderia* sp. CCGE1003 (YP_003906199.1). Members of this enzyme family have oxidoreductase activity and are capable of transferring electrons from one molecule to another using the cofactor NAD⁺ or NADP (IPR002198). *Burkholderia* sp. Ha185 SDR also contains a putative beta-ketoacyl acyl carrier protein reductase (BKR_SDR_c) domain (Table 4.3.4).

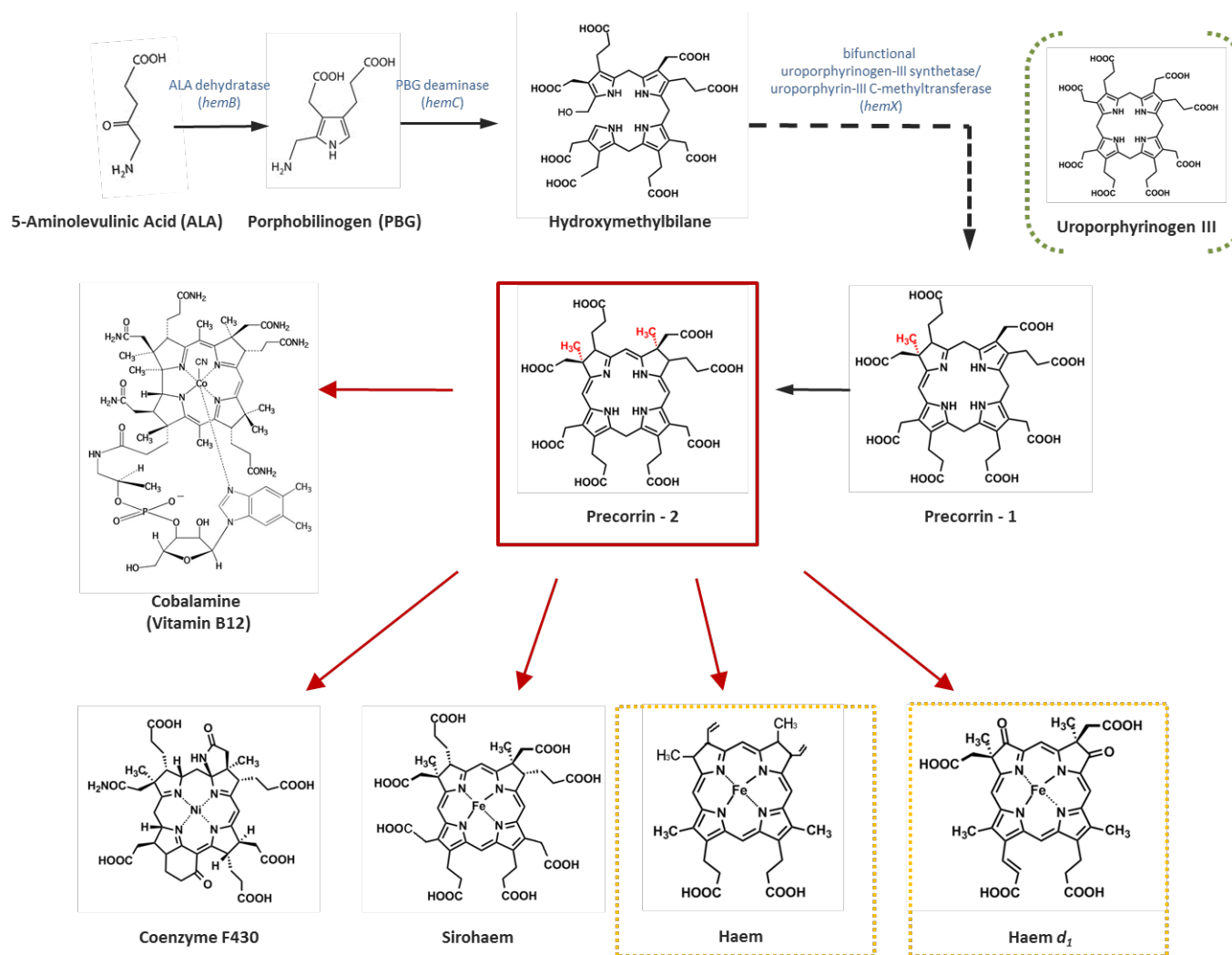


Figure 4.3.8 Schematic diagram of precorrin-2 biosynthesis. *hemX* codes for a bifunctional uroporphyrinogen-III synthetase/uroporphyrin-III C-methyltransferase, which is hypothesised to synthesise precorrin-1 (dash arrow) via the intermediate uroporphyrinogen III (green dashed bracket). Precorrin-2 (highlighted in red box) is an important branch point leading to biosynthesis of different tetrapyrrole compounds, cobalamin (vitamin B12), coenzyme F430, sirohaem, haem and haem d_1 .

4.3.3.2 Defining functional protein association networks of HemX through STRING analysis

To understand the functional interactions of HemX with other proteins, or protein networks, *Burkholderia multivorans* 17616 was used as a model for analysis using the Search Tool for the Retrieval of Interacting Genes (STRING) database, version 9.05 (Szklarczyk et al., 2011). STRING uses experimental data and predicted protein interactions to predict significant functional connections and the relationship between two proteins. STRING also provides a benchmark confidence score relating to the functional classification scheme of the Kyoto Encyclopedia of Genes and Genomes (KEGG) database, where low confidence scores are defined as <0.4, medium scores are 0.4–0.7 and high scores are >0.7 (Von Mering et al., 2005). Two closely-linked proteins with associated described functions will have a high confidence score.

STRING analysis predicted strong relationships between HemX and HemC (0.989), HemE (0.912) and HemY (0.909) (Figure 4.3.9). A relationship was also predicted between HemX and CobI (precorrin-2 C(20)-methyltransferase), though with a lower confidence score (0.899), suggesting that HemX might be involved in converting precorrin-1 to precorrin-2. Together, HemC, HemX and HemY were implicated in porphyrin synthesis via the intermediate uroporphyrinogen-III, which forms precorrin-2. This is an important branch point leading to biosynthesis of different tetrapyrrole compounds, such as the corrinoid cobalamine (vitamin B12), coenzyme F430, sirohaem, haem and haem d_1 (Warren et al., 1990, Parmar-Bhundia, 2010 and Bali et al., 2011). An outline of the haem biosynthesis pathway is shown in Figure 4.3.7. A strong relationship was predicted between HemX and HemE (0.912), where *hemE* encodes uroporphyrinogen decarboxylase. This suggested that the next step in the haem biosynthesis pathway is the decarboxylation of precorrin-2 to either haem or haem d_1 , as highlighted in the yellow box in Figure 4.3.8. The function of HemY remains unknown, although there was a predicted linkage between HemX and HemY (0.909). A weak association (0.670) was also observed between HemX and PEPC, despite the gene sequence being located upstream of *hemC* (Figure 4.3.7).

To determine whether cobalamine is directly involved in P solubilisation, cobalamine sourced from Sigma (CAS 68-19-9) was exogenously supplied to a HSU liquid culture of the *hemX::Tn5*(F18) mutant or wildtype *Burkholderia* sp. Ha185 at a final concentration of 1.4 nM. Result showed there were no differences in the concentration of P released by the two isolates were observed (data not shown).

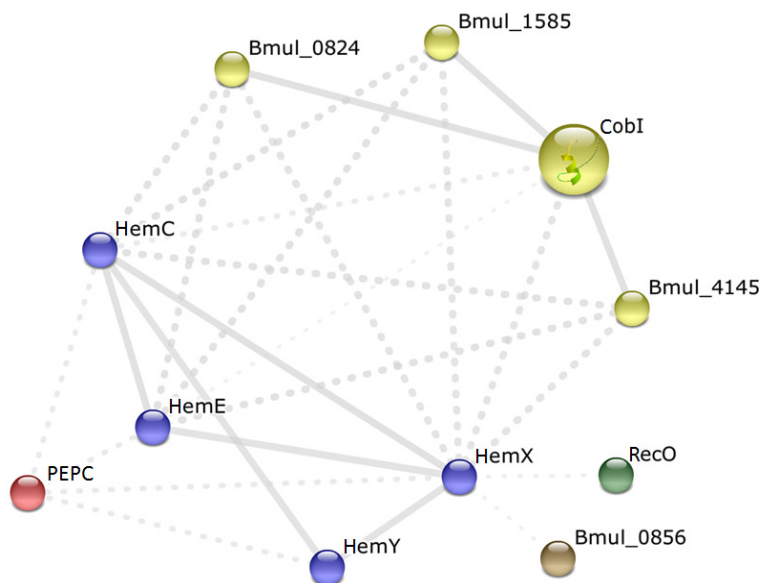


Figure 4.3.9 Protein networks of HemX as determined by STRING analysis using *Burkholderia multivorans* 17616 as a model organism. The following proteins were included in the analysis: HemX, bifunctional uroporphyrinogen-III synthetase/uroporphyrin-III C-methyltransferase; HemY, putative enzyme of haem biosynthesis; HemE, uroporphyrinogen decarboxylase; HemC, porphobilinogen deaminase; PEPC, phosphoenolpyruvate carboxylase; RecO, DNA repair protein RecO; CobI, precorrin-2 C(20)-methyltransferase; Bmul_0856, hypothetical protein; Bmul_0824, Bmul_1585 and Bmul_4145, uroporphyrin-III C-methyltransferase; Bmul_0856, hypothetical protein. Nodes are clustered in colours, where the same colour indicates strong protein-protein associations with a solid grey line linking each protein, and weaker protein associations are indicated by dashed lines (grey).

Table 4.3.3 Predicted *hem* operon homology of *Burkholderia* sp. Ha185 ORFs identified from DNA sequencing and protein sequence analysis.

ORF	Amino acid	Nucleotides ^a	G+C (%)	Degree of similarity ^{b,c}	Protein, species ^c	Accession no.
<i>hem</i> operon						
<i>mts</i> (partial)	250	1–420	63.1	87/93//250 (111–250)	Type 11 methyltransferase (<i>Burkholderia phytofirmans</i> PsJN)	YP_001894710.1
				87/93//250 (111–249)	Methylase involved in ubiquinone/menaquinone biosynthesis (<i>Burkholderia</i> sp. Ch1-1)	ZP_10030329.1
<i>ppc</i>	1141	580–3822	65.6	93/95//1075 (90–1075)	Phosphoenolpyruvate carboxylase (<i>B. phytofirmans</i> PsJN)	YP_001894711.1
				93/95//2985 (20–994)	Phosphoenolpyruvate carboxylase (<i>Burkholderia xenovorans</i> LB400)	YP_557625.1
<i>hemC</i>	375	4174–5301	65.3	95/97//342 (1–317)	Porphobilinogen deaminase (<i>B. phytofirmans</i> PsJN)	YP_001894712.1
				95/97//349 (1–318)	Porphobilinogen deaminase (<i>Burkholderia</i> sp. CCGE1001)	YP_004227335.1
<i>hemX</i>	673	5301–7322	67.5	89/93//672 (1–672)	Bifunctional uroporphyrinogen-III synthetase/uroporphyrin-III C-methyltransferase (<i>B. xenovorans</i> LB400)	YP_557627.1
				89/92//672 (1–672)	Putative enzyme of haem biosynthesis (<i>Burkholderia</i> sp. Ch1-1)	ZP_10030325.1
<i>hemY</i>	396	7325–8515	63.9	96/97//396 (1–396)	Putative enzyme of haem biosynthesis (<i>Burkholderia</i> sp. Ch1-1)	ZP_10030324.1
				95/97//396 (1–396)	Hypothetical protein Bxe_A3409 (<i>B. xenovorans</i> LB400)	YP_557628.1
<i>mfs</i>	439	8747–10066	63.8	94/97//439 (1–439)	Major facilitator superfamily protein (<i>B. phytofirmans</i> PsJN)	YP_001894734.1
				92/96//439 (1–439)	Major facilitator superfamily metabolite/H(+) symporter (<i>B. xenovorans</i> LB400)	YP_557634.1
<i>sdr</i>	252	10186–11001	64.3	97/99//252 (1–252)	Short-chain dehydrogenase/reductase (<i>Burkholderia</i> sp. CCGE1003)	YP_003906199.1
				98/98//252 (1–252)	Short-chain dehydrogenase/reductase (<i>Burkholderia</i> sp. CCGE1001)	YP_004227370.1

^a Nucleotide sequence is a continuum from the published sequence, GenBank accession no. KJ470766

^b Amino acid similarity (% identity/% similarity//over amino acid residues) in relation to sequence generated in this study

^c BLASTx results based on NCBI protein database carried out in March 2013

Table 4.3.4 Predicted domains and ligand-binding motifs for the *Burkholderia* sp. Ha185 *hem* operon.

ORFs	Amino Acid	Protein annotation ^a	Domains ^b , ligand-binding motif ^c	Amino acid range
<i>hem</i> operon				
<i>mts</i>	250	Type 11 methyltransferase	Methyltransferase domain (Methyltransferase_11, IPR013216) ^{bd} , members of this family are SAM dependent methyltransferases.	1–32
<i>ppc</i>	1141	Phosphoenolpyruvate carboxylase	Phosphoenolpyruvate carboxylase (PEPC, IPR022805) ^{bd} † [VTI]-x-T-A-H-P-T-[EQ]-x(2)-R-[KRHAQ] (active site) ^c	149–1110 288–299
<i>hemC</i>	375	Porphobilinogen deaminase	Porphobil_deam (hemC; N-terminal, IPR022417; C-terminal, IPR022418) ^{bd} Porphobilinogen deaminase, dipyromethane cofactor binding domain	30–252
<i>hemX</i>	673	Bifunctional uroporphyrinogen-III synthetase/uroporphyrin-III C-methyltransferase	HemD (IPR003754) ^{bd} , a protein that catalyses the asymmetrical cyclization of tetrapyrrole (linear) to uroporphyrinogen-III, the fourth step in the biosynthesis of haem. HemX (IPR007470) ^{bd} , uroporphyrin-III C-methyltransferase, a membrane protein involved in coenzyme metabolism	21–286 299–673
<i>hemY</i>	396	Putative enzyme of haem biosynthesis	HemY (IPR010817) ^{bd} , a predicted protohaem IX synthesis protein, trans-membrane protein involved in coenzyme metabolism. Tetratricopeptide repeat domain (TPR, IPR013026) ^{bd} , involved in a variety of functions including protein-protein interactions, but common features in the interaction partners have not been defined. † [WLF]-X(2)-[LIM]-[GAS]-X(2)-[YLF]-X(8)-[ASE]-X(3)-[FYL]-X(2)-[ASL]-X(4)-[PKE] ^c	7–396 304–396
<i>mfs</i>	439	Major facilitator superfamily protein	Major Facilitator Superfamily (MFS, IPR020846) ^{bd} , MFS proteins transport a variety of substrates across cytoplasmic or internal membranes.	36–439
<i>sdr</i>	252	Short-chain dehydrogenase/reductase SDR	putative beta-ketoacyl acyl carrier protein reductase, subgroup 3, classical (c) SDR (BKR_SDR_c) ^b , a member of the SDR family, catalyses the NADPH-dependent reduction of acyl carrier protein in the first reductive step of <i>de novo</i> fatty acid synthesis.	22–252

^a Protein annotation based on Table 4.3.3^b Domain search based on BLASTp^c Domain and ligand search based on MyHit MotifScan and ScanProsite^d InterPro accession number is presented as IPR followed by six digit numbers

† The PA (PAttern) indicates unique signature of consensus pattern of ligand-binding motif

4.3.3.3 *Trans-complementation of the hemX::Tn5(F18) mutant*

Vectors harbouring *hemX* were constructed to validate that the mutated *hemX* gene could be complemented *in trans*. The entire *hemC* + *hemX* and *hemX* gene regions were amplified and the resultant amplicons were independently cloned into the broad host range shuttle vector pME6010 (Tc^R, **Table 4.2.1**) (Heeb et al., 2000). To PCR amplify *hemC* and *hemX*, the primer pair cHemCF/cHemXR was designed to amplify a region beginning 299 bp upstream of the 5' end of *hemC*, encompassing the putative promoter region, and ending 409 bp downstream of the 3' end of *hemX* (Figure 3.1.24). This region was amplified from wildtype *Burkholderia* sp. Ha185 gDNA, generating a 3876-bp amplicon with a GC content of 66.4%. To amplify *hemX* only, cHemXF was used instead of cHemCF (located 400 bp upstream of *hemX*), resulting in a 2854-bp amplicon with a GC content of 67.5% (**Figure 4.3.11**). The resulting complementation vectors were designated pCD3ME and pDXDME respectively.

Initial attempts to amplify the *hem* region produced multiple non-specific PCR products (**Figure 4.3.11** (A)). Because of the high GC content of the *hem* gene fragments, a gradient PCR approach was performed to define the optimal annealing temperature (Section 4.2.4). The annealing temperature of each primer set was tested from 58–67°C for the *hemX* PCR, and to 66°C for the *hemC* + *hemX* amplification. Because *Taq* polymerase starts amplification at temperatures equal to or greater than 68°C, annealing temperatures above 67°C were not tested. The optimal primer annealing temperatures were 67°C for *hemX* and 66°C for *hemC* + *hemX* (**Figure 4.3.11** (B)) to produce amplicons of the expected sizes (~2800 bp and ~3800 bp, respectively) and fewer nonspecific bands. DMSO was also added to the reaction (final concentration 5% (v/v)) to disrupt hydrogen bond formation in the GC-rich region. The PCR fragments were cloned into pGEM-T Easy and the end sequence was confirmed using the M13F and M13R primers. Using a strategy similar to that used to construct p1311MPB described in section 4.3 (**Figure 4.3.5**), each of the inserts were cleaved from pGEM-T Easy using *Bam*HI, and ligated into the compatible *Bg*II site of the pME6010 vector to generate the respective constructs, pCD3ME and pDXDME. Plasmids pCD3ME and pDXDME were independently transformed into *E. coli* DH10B and selected on LB agar containing tetracycline. Resulting colonies were patched onto LB agar containing tetracycline or ampicillin to confirm the insertion of the fragment into pME6010 and the loss of the pGEM-T Easy vector. Plasmid DNA from several transformants was prepared and digested with the restriction enzymes *Nco*I, *Sac*I, *Cl*aI and *Bg*II in independent reactions. The resulting profiles were compared with the DNA sequence to confirm the correct insertion.

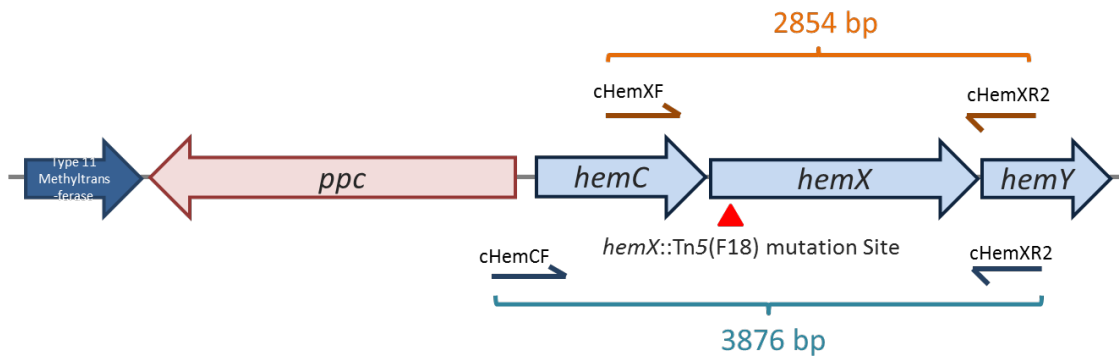


Figure 4.3.10 Schematic diagram of the *hem* operon, consisting of three ORFs: *hemC*, *hemX* and *hemY*. The *hemX*::Tn5(F18) mutation site, located 50 bp of the 5' end of the *hemX* gene, is denoted by a red triangle. Primer pair cHemXF/cHemXR2 was used to amplify a 2854-bp product containing *hemX*, flanked with *Bam*HI restriction sites. Primer pair cHemCF/cHemXR2 amplified the entire *hemC* + *hemX* gene region to give a PCR product of 3876 bp, flanked with *Bam*HI restriction sites. Diagram not to scale.

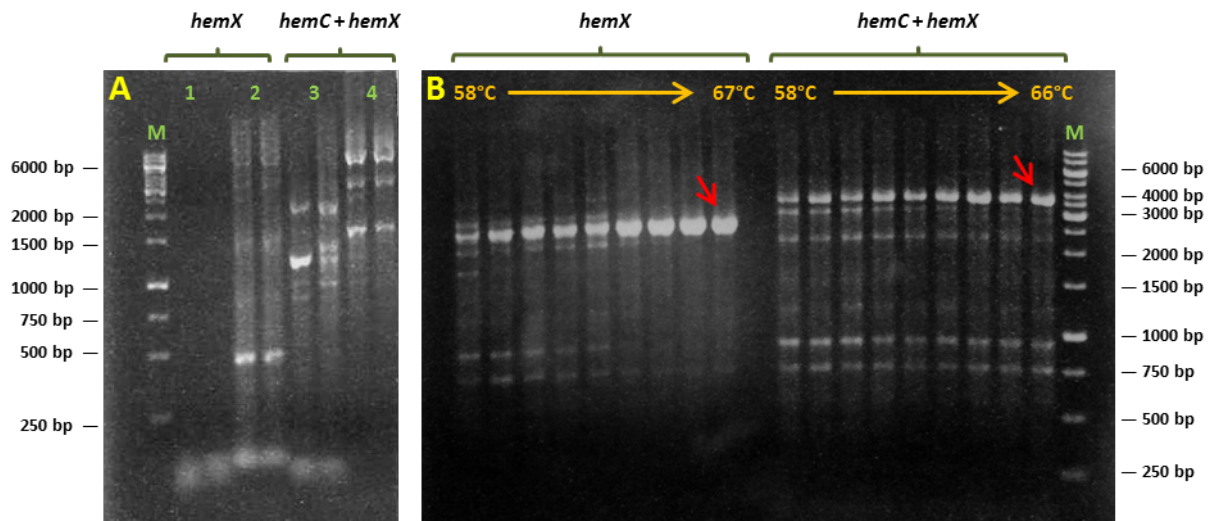


Figure 4.3.11 DNA gel electrophoresis of PCR optimisation for the *hemC* + *hemX* and *hemX* DNA amplifications. PCR reactions were performed using an annealing temperature of 55°C for 5 cycles, followed by 50°C for 30 cycles (A), resulting in nonspecific amplicons. Primer pairs 1 (cHemXF/cHemXR) and 2 (cHemXF/cHemXR2) amplified amplified *hemX*, and primer pairs 3 (cHemCF/cHemXR) and 4 (cHemCF/cHemXR2) amplify the entire *hemC* and *hemX* gene regions. Primers and nucleotide sequences are listed in Table 4.2.2. PCR was optimised by adding 5% (v/v) DMSO to each reaction and an annealing temperature gradient from 58–67°C for *hemX*, and up to 66°C for *hemC* + *hemX*, using primer pairs 2 (cHemCF/cHemXR2) and 4 (cHemXF/cHemXR2), respectively. Red arrows denote expected amplicon sizes of 2854 bp for *hemX* and 3876 bp for *hemC* + *hemX*.

The plasmids pCD3ME and pDXDME were independently electroporated into *hemX*::Tn5(F18) electrocompetent cells. Following electroporation, cells were plated on LB agar plates containing tetracycline and kanamycin and incubated for 3 days at 25°C (Appendix B.2). Plasmid DNA was extracted from several transformants and validated using the restriction enzymes *Bgl*III, *Nru*I, *Sal*I and *Nar*I.

Restoration of the P-solubilising phenotype for each successful transformant was confirmed by placing 1 µL of bacterial culture (containing approximately 10⁵ cfu) onto a HydroxP agar plate (Appendix A.2.2) and incubating the plates for 2 weeks at 25°C to allow the development of zones of clearance (Figure 3.1.26). Wildtype *Burkholderia* sp. Ha185 and the *hemX*::Tn5(F18) mutant were also transferred from liquid culture onto the agar plates as positive and negative controls, respectively. *Burkholderia* sp. Ha185 solubilised HydroxP, as shown by a large halo around the circular colony. The *hemX*::Tn5(F18) mutant produced no halo and the colony remained circular, indicative of impaired P solubilisation (Figure 3.1.26). In contrast, the *hemX*::Tn5(F18) complemented clones containing the *hemC* + *hemX* complementation plasmid pCD3ME (CD3ME2, CD3ME3, CD3ME4, CD3ME8, CD3ME11 and CD3ME12) produced halos, indicating P solubilisation activity. Isolate CD3ME12, which produced the largest halo, was used for subsequent experiments. Complementation clones that contained the *hemX* complementation plasmid pDXDME (DXDME1, DXDME3, DXDME5 and DXDME6) also had restored MPS, as indicated by halo formation around the colonies. The DXDME6 clone was chosen for further experiments because of its ability to solubilise P and its circular colony form on HydroxP plates.

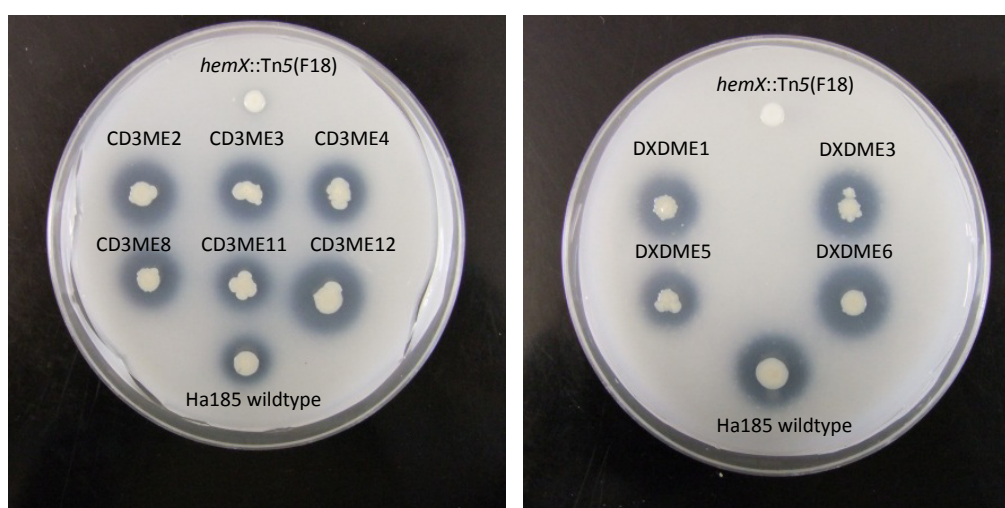


Figure 4.3.12 Phosphate solubilisation by *Burkholderia* sp. Ha185 wildtype, mutant *hemX*::Tn5(F18) and its complementation strains. All isolates were inoculated on hydroxyapatite agar plates and incubated for 2 weeks at 25°C. The *hemX* complementation strains CD3ME12 and DXDME6 contain *hemC* + *hemX* and *hemX* alone on the respective plasmids pCD3ME and pDXDME. Note the lobate edges of the complemented strains.

4.3.4. Defining the mechanism of phosphate solubilisation by *Burkholderia* sp. Ha185 and the *bxpC*::Tn5(F13) and *hemX*::Tn5(F18) mutants

4.3.4.1 Mannitol utilisation by *Burkholderia* sp. Ha185

During the course of the study, it was observed that *Burkholderia* sp. Ha185 did not solubilise HydroxP when mannitol was used in place of glucose as the carbon source (Figure 3.1.27). This suggested that *Burkholderia* sp. Ha185 is not able to utilise mannitol for P solubilisation. Furthermore, on HydroxP-M media, *Burkholderia* sp. Ha185 appears yellow when P is limited, possibly as a consequence of not being able to solubilise P on mannitol (Figure 3.1.27). When grown on the HydroxP-G medium, containing glucose as the sole carbon source, *Burkholderia* sp. Ha185 appears white. Interestingly, the *hemX*::Tn5(F18) mutant with impaired HydroxP solubilisation also appeared yellow when grown in HSU HydroxP liquid culture medium (result not shown). The cause of the yellow pigmentation is unknown but appears to be linked to the process of P solubilisation. To investigate mannitol metabolism of *Burkholderia* sp. Ha185 in relation to HydroxP solubilisation, mannitol was used as the sole carbon source in experiments to quantify the amount of P released in liquid culture assay using HydroxP as the only P source. The effects on culture pH and the organic acid profile during growth using mannitol as the only carbon source were determined as described in Section 4.3.3.3.

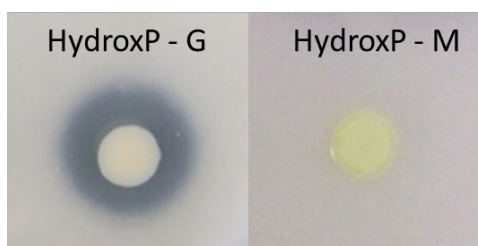


Figure 4.3.13 *Burkholderia* sp. Ha185 ($\sim 10^5$ cfu) inoculated onto HydroxP agar containing either glucose (HydroxP - G) or mannitol (HydroxP - M). Zone of clearance on the HydroxP - G plate indicates hydroxyapatite solubilisation by *Burkholderia* sp. Ha185 after plates were incubated for 14 days at 25°C. Note the *Burkholderia* sp. Ha185 does not solubilise HydroxP when mannitol was supplied as the sole carbon source indicated by lack of zone of clearance as well as appears yellow in colour.

4.3.4.2 Phosphate released by *Burkholderia* sp. Ha185 wildtype and the derivative mutant strains

Wildtype *Burkholderia* sp. Ha185 and its mini-Tn5km1 transposon mutants, *bxpC*::Tn5(F13) and *hemX*::Tn5(F18), and their complemented mutants, 1311CMPB2, CD3ME12 and DXDME6, were cultured in HSU HydroxP liquid broth to quantify their ability to solubilise P. Cell numbers of the wildtype strain increased from 6.34 ± 0.12 to $8.53 \pm 0.39 \log_{10}$ cfu mL⁻¹ over the 72 h incubation period. The *Burkholderia* sp. Ha185 mini-Tn5Km1 transposon mutants *bxpC*::Tn5(F13) and *hemX*::Tn5(F18) reached a final cell density of 7.76 ± 0.26 and $7.68 \pm 0.25 \log_{10}$ cfu mL⁻¹, respectively (Figure 3.1.28), although the *bxpC*::Tn5(F13) mutant showed a lower cell density ($0.61 \log_{10}$ cfu mL⁻¹) compared with the other strains over the first 24 h (Figure 3.1.28). The complemented mutants 1311CMPB2 and DXDME6 exhibited similar growth rates to the wildtype over the 72-h growth period, but CD3ME12 demonstrated a lower growth rate than the wildtype from 48–72 h post-inoculation. Although the growth rate of wildtype *Burkholderia* sp. Ha185 in mannitol appeared to be lower initially compared with wildtype control in glucose (Figure 3.1.28), the final cell density was $9.28 \pm 0.02 \log_{10}$ cfu mL⁻¹, which was not significantly different from the wildtype *Burkholderia* sp. Ha185 control in HSU HydroxP glucose medium ($8.53 \pm 0.39 \log_{10}$ cfu mL⁻¹, $p > 0.05$). There was no change in the cell density of the wildtype *Burkholderia* sp. Ha185 in HSU-P over the first 24 h, but by 72 h it had increased to $8.40 \pm 0.01 \log_{10}$ cfu mL⁻¹, which was not significantly different from the wildtype control in HSU HydroxP medium ($p > 0.05$).

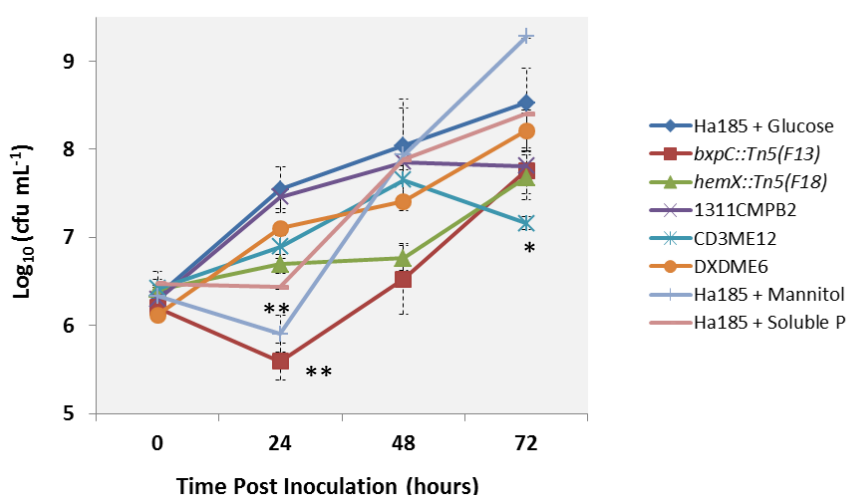


Figure 4.3.14 Growth of *Burkholderia* sp. Ha185 and its derivatives in HSU hydroxyapatite liquid culture medium. Cell were counted at 24, 48 and 72 h post-inoculation. Colony counts were obtained by serial dilution plating on LB agar and calculated as \log_{10} cfu mL⁻¹. Isolates were grown in HSU HydroxP liquid culture supplied with glucose. Ha185 was also cultured in broth containing mannitol as the sole carbon source (labelled “Ha185 + Mannitol”). The culture labelled “Ha185 + Soluble P” contained soluble P instead of HydroxP. Wildtype *Burkholderia* sp. Ha185 in HSU HydroxP medium supplied with glucose was used as the control in this experiment (Ha185 + Glucose). Error bars denote SEM of three independent experiments ($n=3$). * Significantly different from the wildtype *Burkholderia* sp. Ha185 in glucose at $p < 0.05$. ** Significantly different from the wildtype at $p < 0.01$.

The colourimetric assay showed that there was an increase in soluble P concentration in culture filtrate of the wildtype *Burkholderia* sp. Ha185 strain between the 24 and 48 h time points (from 0.21 ± 0.03 to 16.29 ± 1.35 mM; **Figure 4.3.15**). The amount of soluble P only increased slightly between 48 h and 72 h, indicating limited solubilisation activity was occurring between those time points (**Table 4.3.5**). For both mutant derivatives *bxpC::Tn5*(F13) and *hemX::Tn5*(F18), low P concentrations were detected at 72 h (3.09 ± 1.07 mM and 1.87 ± 0.57 mM respectively). Similarly low P concentrations were detected for wildtype *Burkholderia* sp. Ha185 when grown in the presence of mannitol (HydroxP-M), with only 1.82 ± 0.72 mM soluble P recovered from the culture filtrate at 72 h. This suggests mannitol metabolism is not involved in P solubilisation in *Burkholderia* sp. Ha185.

The *bxpC::Tn5*(F13) complemented mutant strain, 1311CMPB2, showed restoration of the MPS phenotype on HydroxP agar (**Figure 4.3.6**), and also solubilised P in the liquid culture assay at a similar level to that of the wildtype (**Figure 4.3.15**). Statistical analysis revealed no significant difference in P concentration in the 1311CMPB2 culture filtrate at 48 h and 72 h when compared with the wildtype control ($p > 0.05$, **Table 4.3.5**). The *hemX::Tn5*(F18) mutant complementation strains, CD3ME12 and DXDME6, had significantly lower amounts of P in the culture filtrates compared with the control at 48 h (5.55 ± 0.12 , 9.82 ± 0.23 and 16.29 ± 1.35 mM respectively, $P < 0.001$), while at 72 h there was no significant difference in P concentration relative to the wildtype control ($p > 0.05$, **Table 4.3.5**). Both isolates demonstrated MPS phenotype restoration on HydroxP agar (**Figure 4.3.12**) as well as in the HSU HydroxP liquid culture medium (**Figure 4.3.15**).

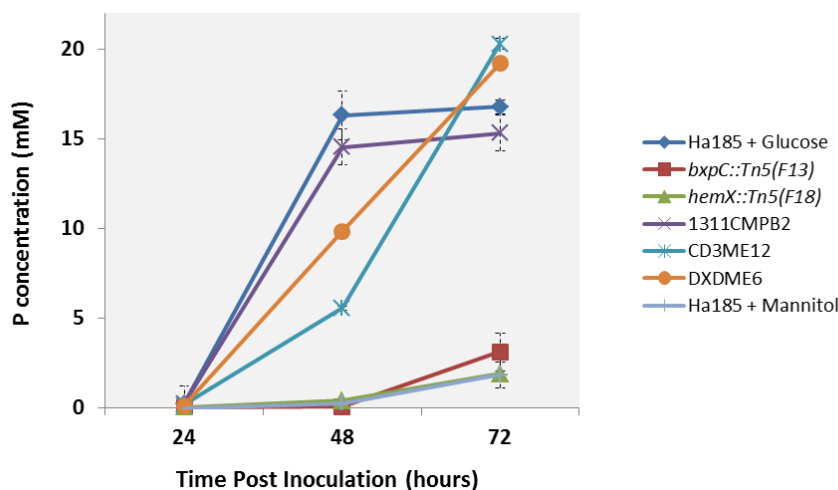


Figure 4.3.15 Phosphate released by *Burkholderia* sp. Ha185 and its derivatives in HSU hydroxyapatite liquid culture medium with glucose. Each flask was incubated at 25°C with shaking at 250 rpm. All isolates were grown in HSU HydroxP liquid medium supplemented with glucose, except one culture where Ha185 was grown with mannitol as the sole carbon source (“Ha185 + Mannitol”). One millilitre of each culture was sampled at 24, 48 and 72 h post-inoculation to quantify soluble phosphate concentration using the Murphy and Riley colourimetric method (Chapter 3.3.8) at a wavelength of 850 nm. Error bars denote SEM of three independent experiments ($n=3$).

Table 4.3.5 Soluble phosphate released by *Burkholderia* sp. Ha185 and its derivatives grown in HSU hydroxyapatite liquid culture medium with either glucose or mannitol.

Isolates	P concentration in the culture (mM) ^{+ §}		
	24 h	48 h	72 h
Time Post-Inoculation			
<i>Burkholderia</i> sp. Ha185	0.21 ± 0.03 ^f	16.29 ± 1.35 ^{abc}	16.77 ± 0.38 ^{abc}
<i>bxpC::Tn5(F13)</i>	nd	0.06 ± 0.03 ^f	3.09 ± 1.07 ^{ef}
1311CMPB2	0.22 ± 0.16 ^f	14.52 ± 1.71 ^c	15.29 ± 3.60 ^{bc}
<i>hemX::Tn5(F18)</i>	0.02 ± 0.02 ^f	0.37 ± 0.17 ^f	1.87 ± 0.57 ^{ef}
CD3ME12	0.17 ± 0.02 ^f	5.55 ± 0.12 ^{de}	20.28 ± 0.3 ^a
DXDME6	0.11 ± 0.01 ^f	9.82 ± 0.23 ^d	19.19 ± 0.16 ^{ab}
[†] <i>Burkholderia</i> sp. Ha185 + Mannitol	nd	0.25 ± 0.12 ^f	1.82 ± 0.72 ^{ef}

⁺ Value represents mean ± standard error of mean ($n=3$); nd, not detected.

[†] Wildtype *Burkholderia* sp. Ha185 grown in HSU HydroxP medium with 54.9 mM mannitol as carbon source

[§] Statistical analysis carried out using the Tukey Method. Groups that do not have a letter in common differ significantly at the 5% level.

4.3.4.3 Culture acidification, phosphate solubilisation and organic acid production

The pH of the HSU HydroxP medium prior to inoculation was 6.5. When the wildtype *Burkholderia* sp. Ha185 was incubated in this medium with the addition of 54.9 mM mannitol, the pH decreased to 4.98 ± 0.02 after 72 h, and there was no significant difference compared with cultures containing glucose (pH 5.07 ± 0.02 , $p > 0.05$, **Figure 4.3.16** (A)). Interestingly, the P concentration was significantly higher when the wildtype strain was cultured in glucose medium (16.77 ± 0.38 mM) compared with medium supplemented with mannitol (1.82 ± 0.72 mM) as the sole carbon source (**Figure 4.3.16** (B)). There were no significant differences in the final culture pH ($p > 0.05$) between the two *Burkholderia* sp. Ha185 mini-Tn5Km1 transposon mutants, *bxpC*::Tn5(F13) (pH 4.96 ± 0.15) and *hemX*::Tn5(F18) (pH 4.96 ± 0.15), and the control (pH 5.07 ± 0.02). The amount of P released by these two transposon mutants was significantly lower than that released by the wildtype grown in HSU HydroxP with glucose, but did not significantly differ from the wildtype grown in HSU HydroxP with mannitol (**Figure 4.3.16** (B)). The *bxpC*::Tn5(F13) mutant solubilised P on hydroxP plates, but a longer incubation period was required than with the wildtype (**Figure 3.1.20**). This is reflected in the significantly lower amount of P released in the liquid culture assay by *bxpC*::Tn5(F13) at 72 h in comparison with the wildtype (**Figure 4.3.16**). Therefore, further investigation is needed to determine the time point at which mutant *bxpC*::Tn5(F13) begins P solubilisation. While the pH reduction caused by the three complemented mutants (1311CMPB2, CD3ME12 and DXDME6) was significantly lower than that of the wildtype grown in glucose ($p < 0.001$), the concentration of P in the filtrates from the mutant strain cultures did not significantly differ from the wildtype glucose control at 72 h. Interestingly, the pH of the growth medium increased to 7.23 ± 0.01 at 72 h ($p < 0.001$) when the *Burkholderia* sp. Ha185 strain was incubated with soluble P (HSU-P) instead of HydroxP. Because all the P in HSU-P medium is in a soluble form, P solubilisation cannot be measured in that medium.

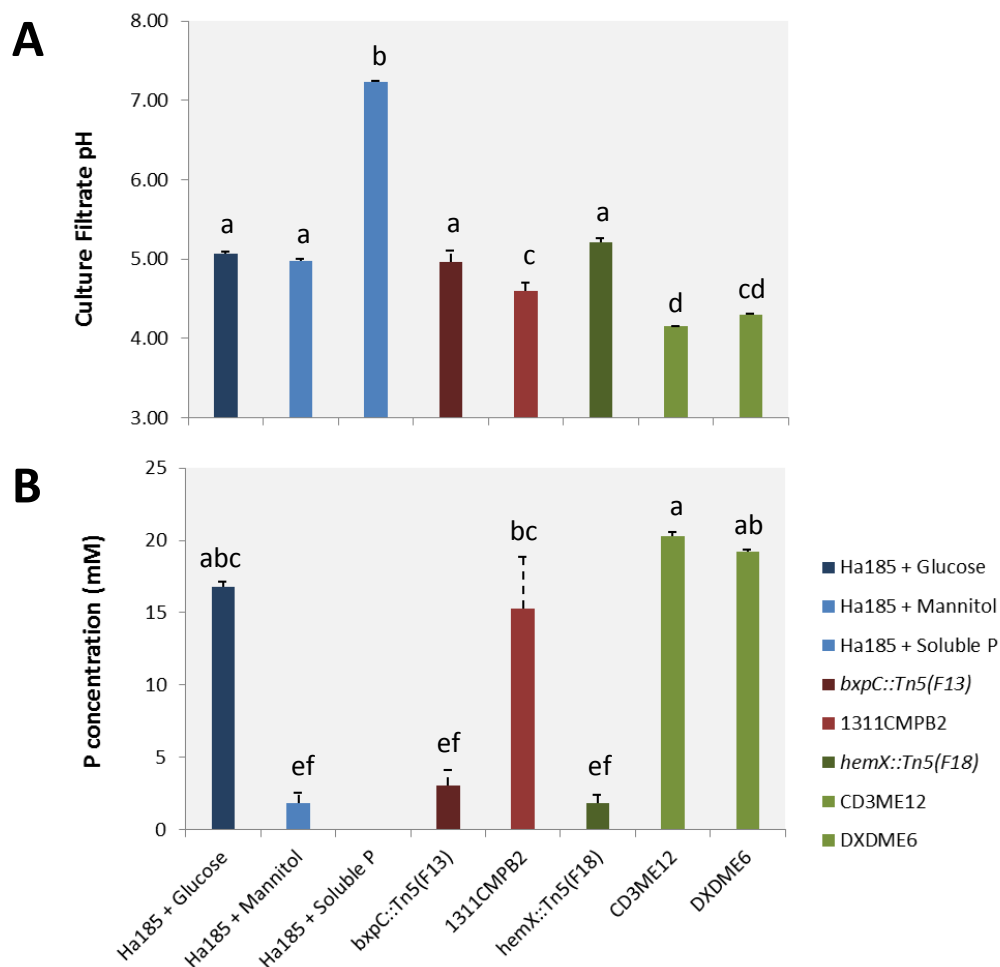


Figure 4.3.16 The pH of the medium (A) and amount of phosphate released (B) in the bacterial culture filtrates following 72 h incubation in HSU hydroxyapatite medium. Error bars denote SEM of three independent experiments ($n=3$). Statistical analysis was carried out using the Tukey method and groups with different letters differ significantly at the 5% level.

To ascertain which organic acids were involved in HydroxP solubilisation, culture filtrates were collected from the HSU HydroxP medium at 24, 48, and 72 h. This allowed changes in organic acid profiles to be monitored over time. HPLC analysis identified 2-KGA as the most abundant organic acid in the *Burkholderia* sp. Ha185 culture filtrate at 48 and 72 h post-inoculation in HSU HydroxP liquid culture medium (Table 4.3.6). A trace amount of GA (0.43 ± 0.07 mM) was initially present in the 24-h culture, which increased to 2.24 ± 0.36 mM at 48 h but was not detected at 72 h post-inoculation. Figure 4.3.17 shows two chromatograms generated from HPLC analysis of wildtype *Burkholderia* sp. Ha185 cultures at 48 h (A) and 72 h (B) post-inoculation in HSU HydroxP medium (performed in triplicate). High levels of 2-KGA (41.74 ± 0.73 mM) were detected at 48 h, and lower concentrations of other organic acids were also detected. These included GA (2.24 ± 0.36 mM), PyrA (2.70 ± 0.29

mM) and LA (2.04 ± 0.81 mM) (Figure 4.3.17 (A)). Low concentrations of LA were also detected at 72 h (not significantly different from concentration at 48 h; $p > 0.05$). In contrast, the concentration of 2-KGA decreased significantly to 32.18 ± 4.05 mM at 72 h compared with the concentration at 48 h ($p < 0.001$), and neither GA nor PyrA were detected at 72 h (Figure 4.3.17(B), Table 4.3.6). This data links with an absence of released P at the 48 and 72 h time points (Table 4.3.5). When wildtype *Burkholderia* sp. Ha185 was cultured in HSU-P medium (without HydroxP), basal levels of both 2-KGA and GA were detected at 24, 48 and 72 h, with a gradual increase over time (Table 4.3.6), but there was no statistical difference in the concentration of GA between the 48 and 72 h time points (2.96 ± 0.07 mM and 2.71 ± 0.43 mM, respectively).

HPLC assessment of the *bxpC*::Tn5(F13) mutant under the same conditions did not identify any significant differences in 2-KGA, GA or PyrA production at 24 h compared with the wildtype grown in HSU HydroxP medium. However, the concentrations of these organic acids were significantly lower at 48 and 72 h (Figure 4.3.17 (C)) compared with the wildtype control, except for PyrA, which was not detected in the control but was identified in the *bxpC*::Tn5(F13) mutant at 72 h post-inoculation (0.67 ± 0.04 mM) (Table 4.3.6). A similar profile was also observed for the *hemX*::Tn5(F18) mutant, which produced low levels of organic acids at all time points assessed (Table 4.3.6). Two unknown peaks, Unknown 3 (Un3, 12.78 min) and Unknown 4 (Un4, 13.36 min), were detected by HPLC at 72 h post-inoculation in culture supernatants derived from the *hemX*::Tn5(F18) mutant (Figure 4.3.17 (D)). These peaks were not observed in the wildtype *Burkholderia* sp. Ha185 supernatant at any of the time points examined. However, it should be noted that samples were diluted in HSU medium prior to HPLC analysis, therefore the concentrations of each organic acid found in the samples are within the concentration range used in the standard curve. Culture supernatants from the wildtype strain were diluted 20.2-fold prior to HPLC analysis, whereas samples derived from mutant strains were undiluted (Figure 4.3.17). The amount of LA at 72 h was also lower in both mutants compared with the wildtype control in HSU HydroxP medium ($p < 0.001$). Assessment of the *bxpC*::Tn5(F13) complemented mutant, 1311CMPB2, where BxpC is provided *in trans*, revealed an organic acid profile that was similar to the control at each time point, however a lower LA concentration was detected at 72 h (0.70 ± 0.24 mM, $p < 0.01$) compared with the wildtype control.

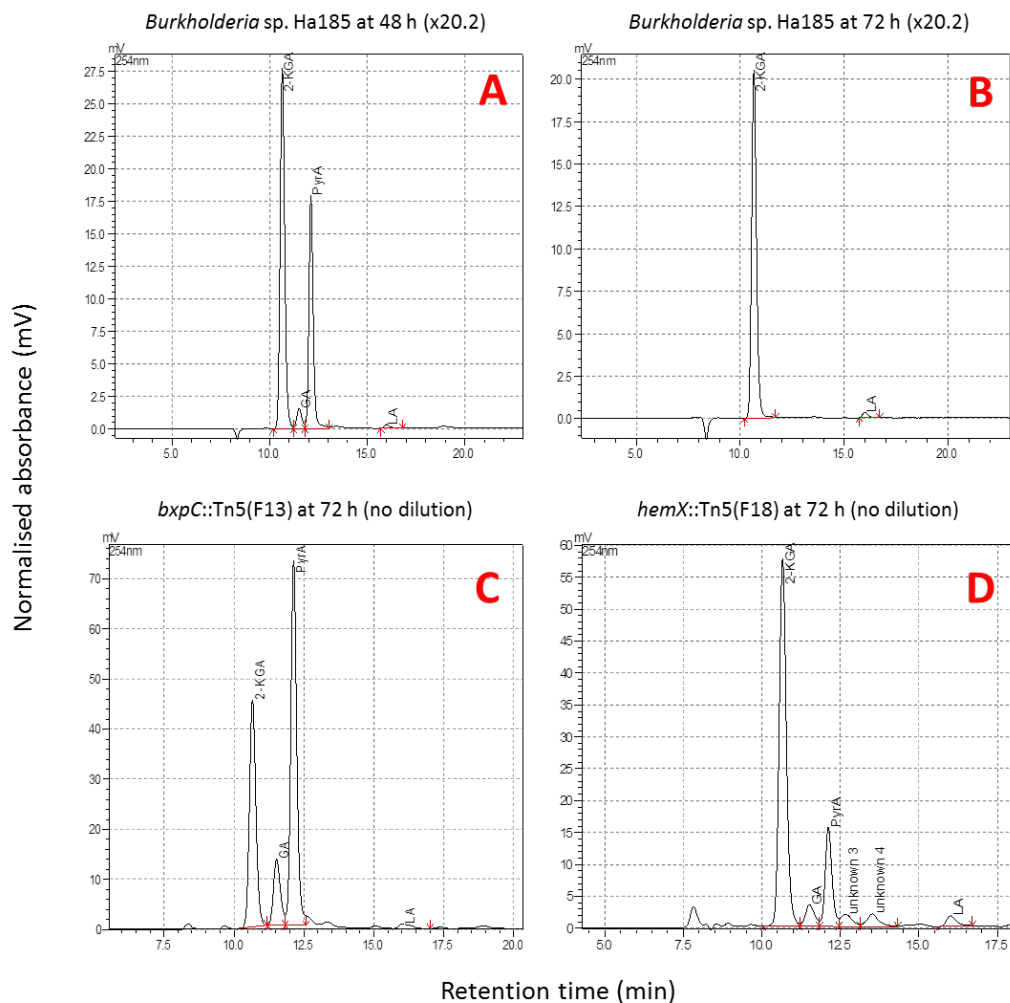


Figure 4.3.17 Chromatograms of organic acids released by wildtype *Burkholderia* sp. Ha185 and derivative mutants. Wildtype *Burkholderia* sp. Ha185 at 48 h (A) and 72 h (B) post-inoculation in HSU HydroxP liquid culture medium (dilution factor = 20.2). Derivative mutants *bxpC::Tn5(F13)* (C) and *hemX::Tn5(F18)* (D) at 72 h post-inoculation in HSU HydroxP medium (undiluted). Peak 2-KGA, GA, PyrA and LA eluted at 10.64, 11.55, 12.11 and 15.99 min, respectively. Unknown 3 and Unknown 4 correspond to the peaks at 12.78 and 13.36 min, respectively. Culture supernatants were analysed for organic acid using high performance liquid chromatography (refer to Table 4.3.6 for numerical values). Note that vertical axis of A, B, C and D differ.

In general, the organic acid profile produced by CD3ME12 (*hemX::Tn5(F18)* with *hemC* and *hemX* complemented *in trans*) did not differ significantly from the wildtype control in HSU HydroxP medium at 24 and 48 h post-inoculation. The exception was 2-KGA, for which concentrations in the complemented strain were significantly higher (55.52 ± 0.27 mM) at 72 h in comparison with the wildtype control in HSU HydroxP medium ($p < 0.001$) (Figure 4.3.18). In contrast, the *hemX::Tn5(F18)* mutant complemented with *hemX*, DXDME6, produced significantly lower levels of 2-KGA at 48 h (22.91 ± 0.65 mM, $p < 0.001$) compared with the wildtype control in HSU HydroxP medium (Figure 4.3.18). The concentrations of PyrA and LA of DXDME6 were also significantly lower at 24 h

compared with the wildtype control in HSU HydroxP medium (Table 4.3.6). However, the amounts of GA produced by DXDME6 did not significantly differ from the wildtype control in HSU HydroxP medium ($p > 0.05$) (Table 4.3.6). Furthermore, the DXDME6 complemented strain produced significantly more 2-KGA than the control at 72 h, with 2-KGA concentrations of 48.53 ± 0.57 and 32.18 ± 4.05 mM respectively ($p < 0.01$).

Table 4.3.6 Organic acid concentrations in culture supernatants of wildtype *Burkholderia* sp. Ha185 and its derivatives at 24, 48 and 72 h post-inoculation in HSU HydroxP culture with glucose or mannitol.

Time Post-Inoculation (h)		Organic acid concentration (mM) [†]			
		2-Keto-D-Gluconic Acid (2-KGA)	D-Gluconic Acid (GA)	Pyruvic Acid (PyrA)	DL-Lactic Acid (LA)
24 h	<i>Burkholderia</i> sp. Ha185	0.14 ± 0.04	0.43 ± 0.07	0.02 ± 0.01	nd
	<i>bxpC</i> ::Tn5(F13)	nd	0.04 ± 0.00	0.01 ± 0.00	nd
	1311CMPB2	0.21 ± 0.15	0.39 ± 0.15	0.04 ± 0.03	nd
	<i>hemX</i> ::Tn5(F18)	nd	nd	nd	nd
	CD3ME12	0.09 ± 0.01	0.36 ± 0.02	0.01 ± 0.00	nd
	DXDME6	nd	0.27 ± 0.01	0.01 ± 0.00	nd
	[‡] <i>Burkholderia</i> sp. Ha185 + Mannitol	nd	nd	nd	nd
	[§] <i>Burkholderia</i> sp. Ha185 + Soluble P	0.28 ± 0.00	1.19 ± 0.01	nd	nd
48 h	<i>Burkholderia</i> sp. Ha185	41.74 ± 0.73	2.24 ± 0.36	2.70 ± 0.29	2.04 ± 0.81
	<i>bxpC</i> ::Tn5(F13)	nd	0.19 ± 0.04***	0.01 ± 0.00***	nd
	1311CMPB2	35.23 ± 3.82	2.74 ± 0.27	2.65 ± 0.32	1.16 ± 0.04
	<i>hemX</i> ::Tn5(F18)	nd	0.05 ± 0.01***	0.01 ± 0.00***	nd
	CD3ME12	34.46 ± 6.84	3.04 ± 0.44	2.68 ± 0.38	1.27 ± 0.19
	DXDME6	22.91 ± 0.65***	2.20 ± 0.08	0.74 ± 0.01***	0.79 ± 0.01*
	[‡] <i>Burkholderia</i> sp. Ha185 + Mannitol	nd	nd	0.30 ± 0.00***	nd
	[§] <i>Burkholderia</i> sp. Ha185 + Soluble P	1.63 ± 0.07***	2.96 ± 0.07	Nd	nd
72 h	<i>Burkholderia</i> sp. Ha185	32.18 ± 4.05	nd	Nd	2.26 ± 0.45
	<i>bxpC</i> ::Tn5(F13)	5.00 ± 1.55***	1.12 ± 0.13**	0.67 ± 0.04	0.23 ± 0.02***
	1311CMPB2	41.10 ± 8.26	nd	Nd	0.70 ± 0.24**
	<i>hemX</i> ::Tn5(F18)	0.55 ± 0.28***	0.21 ± 0.03	0.14 ± 0.08	0.19 ± 0.10***
	CD3ME12	55.52 ± 0.27***	0.92 ± 0.03***	nd	1.12 ± 0.01*
	DXDME6	48.53 ± 0.57**	nd	nd	1.21 ± 0.03
	[‡] <i>Burkholderia</i> sp. Ha185 + Mannitol	nd	nd	0.68 ± 0.16	3.33 ± 0.11
	[§] <i>Burkholderia</i> sp. Ha185 + Soluble P	2.46 ± 0.30***	2.71 ± 0.43***	nd	nd

[†] Value represents mean ± standard error of mean ($n=3$); nd, none detected

[‡] Wildtype *Burkholderia* sp. Ha185 grown in HSU HydroxP medium with 54.9 mM mannitol as carbon source

[§] Wildtype *Burkholderia* sp. Ha185 grown in HSU HydroxP medium where HydroxP was replaced with Soluble P

Control wildtype *Burkholderia* sp. Ha185 is highlighted green at each time point.

* Significantly different from the control within each column at $p < 0.05$.

** Significantly different from the control within each column at $p < 0.01$.

*** Significantly different from the control within each column at $p < 0.001$.

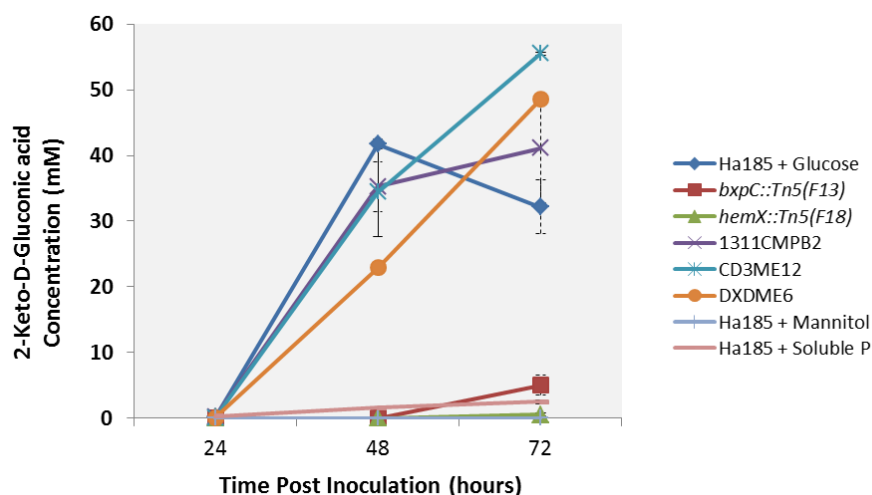


Figure 4.3.18 Quantification of 2-keto-D-gluconic acid from HSU hydroxyapatite culture filtrate by HPLC analysis. One millilitre of culture was collected at 24, 48 and 72 h post-inoculation from cultures grown in HSU HydroxP medium. Glucose was used as the sole carbon source in all except one treatment where Ha185 was grown in HydroxP-M (Ha185 + Mannitol). Ha185 + Soluble P indicates Ha185 cultured in HSU medium with soluble P substituted for HydroxP. Error bars denote SEM of three independent experiments ($n=3$).

When the wildtype *Burkholderia* sp. Ha185 was grown in HydroxP-M medium, a different organic acid profile was observed compared with growth in medium containing glucose as the sole carbon source. **Figure 4.3.19** shows the chromatogram of *Burkholderia* sp. Ha185 in HSU HydroxP medium 72 h post-inoculation (**Figure 4.3.19 (A)**), where 2-KGA was produced at a concentration of 32.18 ± 4.05 mM. The peak with a retention time of 12.11 min indicates PyrA was produced at 72 h post-inoculation (**Figure 4.3.19 (B)**), but at a lower concentration (0.68 ± 0.16 mM, **Table 4.3.6**) than during culture with glucose as the carbon source. Although the amount of PyrA is low, it is possibly one of the organic acids involved in P release following 72 h cultivation in mannitol, with 1.82 ± 0.72 mM of soluble P detected in the filtrate at this time point. DL-lactic acid was also detected at low concentrations (3.33 ± 0.11 mM, 15.99 min), but there was no significant difference compared with the HSU HydroxP glucose medium control (2.26 ± 0.45 mM, $p > 0.05$). Two unknown peaks, Un3 and Un4, were observed in the filtrate of wildtype *Burkholderia* sp. Ha185 cultures grown in HydroxP-M medium following 72 h incubation (**Figure 4.3.19 (B)**). The relative concentrations of these unknown organic acids could not be determined here. Interestingly, the *hemX::Tn5(F18)* mutant also released Un3 and Un4 at low absorbance when incubated in HSU HydroxP medium (**Figure 4.3.17 (D)**). It should be noted that samples derived from the wildtype strain were diluted 20.2-fold prior to being analysed by HPLC. Furthermore, the *hemX::Tn5(F18)* mutant turned yellowish following incubation in HSU HydroxP liquid medium for 72 h (data not shown), as well as on HydroxP agar plates. It was

suspected that this was caused by secretion of a yellow pigment, similar to wildtype *Burkholderia* sp. Ha185 on a HydroxP-M agar plate (Figure 3.1.27). This further indicated that carbon metabolism of *hemX::Tn5(F18)* in glucose may be similar to that of the wildtype *Burkholderia* sp. Ha185 grown in mannitol.

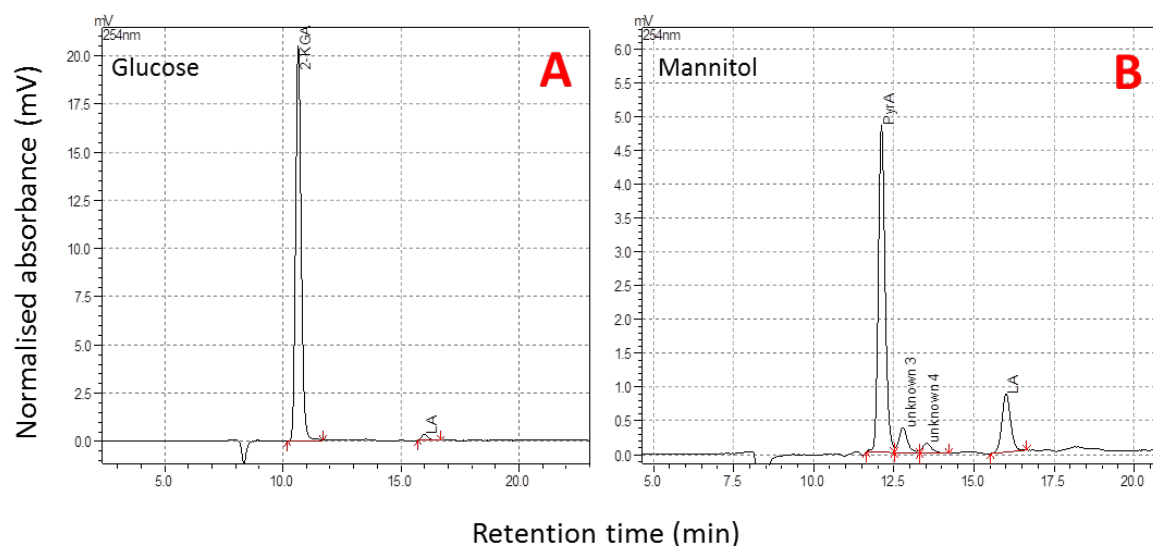


Figure 4.3.19 Chromatograms showing organic acids released by wildtype *Burkholderia* sp. Ha185 in HSU HydroxP liquid culture medium at 72 h with glucose (A) and in mannitol medium (HydroxP-M) (B). 2-KGA, PyrA and LA eluted at 10.64, 12.11 and 15.99 min, respectively. Unknown 3 and Unknown 4 were present at 12.78 min and 13.36 min, respectively. Supernatants were analysed for organic acid content using high performance liquid chromatography (dilution factor = 20.2). Vertical axis of A and B differ.

4.3.4.4 Soluble phosphate and 2-keto-D-gluconic acid in the bacterial cytosol

The *bxpC::Tn5(F13)* mutant, harbouring a mini-Tn5Km1 transposon inserted into *bxpC*, had an inability to solubilise P (Table 4.3.5) and produced significantly less 2-KGA than the wildtype when incubated in HSU HydroxP liquid medium (Figure 4.3.18). To ascertain whether hypothetical proteins encoded by genes in the *bxpC* operon are involved in transport of elements, such as P or organic compounds like 2-KGA, from the cell into the culture supernatant, the cells were sonicated. This enabled differences in key components between the culture filtrate and lysed cells to be determined. Cultures of each isolate were pelleted following 72 h of incubation in HSU HydroxP glucose medium and the cell pellets were sonicated. The wildtype strain grown in HydroxP-M or in HSU-P medium was also investigated. Significantly more P was detected within cells that had been grown with glucose, as opposed to mannitol, as the carbon source (517.77 ± 61.69 nM and 217.06 ± 113.22 nM, respectively; $p < 0.001$, Figure 3.1.34 (A)). No P was detected within cells grown in the HSU-P culture medium. It is possible that amount of P in 1 mL of HSU-P culture medium is below the detection limit (< 100 nM).

In future studies a more sensitive assay such as the malachite green colourimetric assay, as described by D'Angelo et al. (2001), could be used to estimate lower quantities of soluble P (1 nM to 100 nM). The amount of soluble P did not differ significantly between *bxpC::Tn5*(F13), *hemX::Tn5*(F18), CD3ME12, DXDME6 and the wildtype *Burkholderia* sp. Ha185 when cells were grown in HydroxP-M medium ($p > 0.5$, Figure 4.3.20 (A)). A slightly higher level of soluble P was identified in 1311CMPB2 (333.32 ± 101.71 nM), but it did not differ significantly from the wildtype *Burkholderia* sp. Ha185 grown in HSU HydroxP medium (Figure 4.3.20 (A)).

To determine the organic acid profile of *Burkholderia* sp. Ha185, its mutants and complemented derivatives, sonicated filtrates derived from 1 mL of culture of each strain incubated in HSU HydroxP medium were assessed by HPLC analysis. The analysis showed there was 969.00 ± 147.50 μ M of 2-KGA in wildtype *Burkholderia* sp. Ha185 cells grown in glucose, which did not significantly differ from the complemented strain 1311CMPB2 (934.00 ± 148.00 μ M, $p > 0.05$) (Table 4.3.7), validating complementation and the ability of *bxpC* to work *in trans*. Assessment of the *bxpC::Tn5*(F13) sonicated cell pellet revealed significantly lower levels of 2-KGA relative to the wildtype control (419.00 ± 87.86 μ M, $p < 0.01$, Figure 4.3.20 (B)). No 2-KGA was detected in the *hemX::Tn5*(F18) cell pellet (Table 4.3.7). The sonicated filtrates of cell pellet from the two complemented isolates CD3ME12 and DXDME6 also had significantly lower 2-KGA levels (302.58 ± 122.25 μ M, $p < 0.01$, and 99.00 ± 4.00 μ M, $p < 0.001$, respectively) compared with the wildtype control cells grown in HSU HydroxP medium. However, the ability to release P from HydroxP was restored in these strains (Table 4.3.5), and the production of 2-KGA in the culture was also elevated (Table 4.3.6), suggesting that each of the mutations had been complemented to restore the wildtype phenotype.

There was no 2-KGA detected in the sonicated filtrate of cells grown in medium supplemented with mannitol instead of glucose, and wildtype *Burkholderia* sp. Ha185 also did not produce 2-KGA in medium supplemented with soluble P (HSU-P). Interestingly, a low level of LA was found in wildtype *Burkholderia* sp. Ha185 cultures grown in the presence of mannitol (147.00 ± 4.45 μ M), and was significantly higher than the amount detected in cultures grown in HSU HydroxP supplemented with glucose (52.00 ± 5.26 μ M, $p < 0.001$). No GA was detected in any of the isolates grown under the conditions tested (Table 4.3.7).

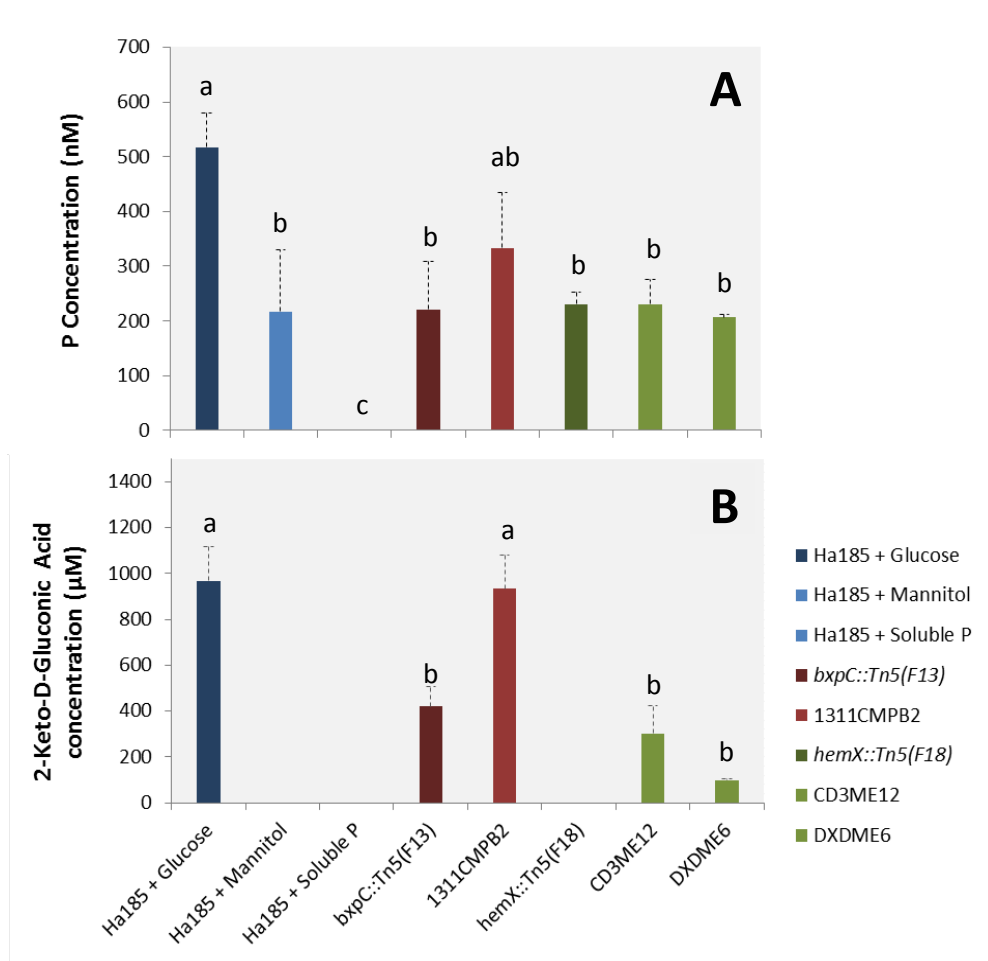


Figure 4.3.20 Soluble phosphate and 2-keto-D-gluconic acid quantification from 1 mL of sonicated filtrate from cell pellet of bacteria grown in HSU hydroxyapatite liquid culture medium. (A) One millilitre of bacterial cells were pelleted and sonicated following 72 h incubation at 25°C. Sonicated cell pellets were filter sterilised, and soluble phosphate was measured by Murphy and Riley's colourimetric method at 850 nm without any dilution. (B) 2-KGA was quantified by HPLC. All isolates were grown in HSU HydroxP medium with glucose. Ha185 was also grown in medium containing mannitol as the carbon source. Ha185 + Soluble P was grown in HSU medium supplemented with soluble P. Error bars denote SEM of three independent experiments ($n=3$). Statistical analysis was carried out using Tukey's Method; groups with different letters differ significantly at the 5% level.

Table 4.3.7 Organic acids present in sonicated cultures of wildtype *Burkholderia* sp. Ha185 and derivative mutant cells collected 72 h post-inoculation in HSU HydroxP medium with glucose or mannitol.

	Organic acid concentration (μM) [†]			
	2-keto-D-gluconic acid	D-gluconic acid	Pyruvic acid	DL-lactic acid
<i>Burkholderia</i> sp. Ha185	969.00 \pm 147.50	nd	nd	52.00 \pm 5.26
<i>bxpC</i> ::Tn5(F13)	419.00 \pm 87.86**	nd	26.38 \pm 14.48*	25.00 \pm 10.98*
1311CMPB2	934.00 \pm 148.00	nd	nd	nd
<i>hemX</i> ::Tn5(F18)	nd	nd	nd	nd
CD3ME12	302.58 \pm 122.25**	nd	nd	nd
DXDME6	99.00 \pm 4.00***	nd	nd	nd
[†] Ha185 + Mannitol	nd	nd	3.00 \pm 0.36*	147.00 \pm 4.45***
[§] Ha185 + Soluble P	nd	nd	nd	nd

[†] Value represents mean \pm SEM ($n=3$); nd, not detected

[‡] Wildtype *Burkholderia* sp. Ha185 grown in HSU HydroxP medium with 54.9 mM mannitol as the carbon source

[§] Wildtype *Burkholderia* sp. Ha185 grown in HSU HydroxP medium supplemented with soluble phosphate

* Significantly different from the control within each column at $p < 0.05$.

** Significantly different from the control within each column at $p < 0.01$.

*** Significantly different from the control within each column at $p < 0.001$.

4.3.4.5 Concentration of soluble phosphate and 2-keto-D-gluconic acid released over time

To determine the amount of P released over time by *Burkholderia* sp. Ha185 in culture, and the relationship between soluble P and 2-KGA released in the culture supernatant, samples were taken at 24, 48 and 72 h post-inoculation from wildtype cultures grown in HSU HydroxP medium. To reduce the total number of samples taken from a single culture and minimise the potential fluctuation in total bacterial cells relative to culture volume, a duplicate flask was prepared and sampled at 36, 40 and 44 h post-inoculation. These experiments showed there was a rapid increase in P released between the 36 and 40 h time points which correlated with increased 2-KGA production at 40 h during the stationary phase (**Figure 4.3.21 (A & B)**). Although GA increased over time, concentrations were relatively low compared with the amount of 2-KGA released (**Figure 4.3.21 (A)**). Low levels of PyrA and LA were present at all time points tested. There was a small decrease in soluble P concentration between 48 and 72 h (17.61 ± 0.40 and 16.94 ± 0.48 mM, respectively), and the concentration of 2-KGA also decreased slightly over this period (**Table 4.3.8, Figure 4.3.21**). GA and PyrA were not detected at 72 h, while the level of LA was slightly higher at 72 h than at 48 h.

Table 4.3.8 Organic acids produced by wildtype *Burkholderia* sp. Ha185 collected at various time points following incubation in HSU HydroxP medium containing glucose.

<i>Burkholderia</i> sp. Ha185 [‡]		Organic acid concentration (mM) ⁺			
Time Post-Inoculation (h)	P concentration (mM)	2-keto-D-gluconic acid	D-gluconic acid	Pyruvic acid	DL-lactic acid
24 h	0.17 ± 0.01	0.14 ± 0.04	0.43 ± 0.07	0.02 ± 0.01	nd
36 h	3.40 ± 0.01	4.15 ± 0.71	0.88 ± 0.17	1.20 ± 0.19	nd
40 h	13.55 ± 0.11	22.60 ± 0.57	1.14 ± 0.01	3.76 ± 0.08	2.52 ± 0.04
44 h	15.44 ± 0.19	29.29 ± 0.43	1.68 ± 0.06	2.48 ± 0.03	2.85 ± 0.11
48 h	17.61 ± 0.40	41.74 ± 0.73	2.24 ± 0.36	2.70 ± 0.29	2.04 ± 0.81
72 h	16.94 ± 0.48	32.18 ± 4.05	nd	nd	2.26 ± 0.45

⁺ Value represents mean ± SEM ($n=3$); nd, not detected

[‡] Wildtype *Burkholderia* sp. Ha185 grown in HSU HydroxP medium with 55.5 mM glucose as the carbon source

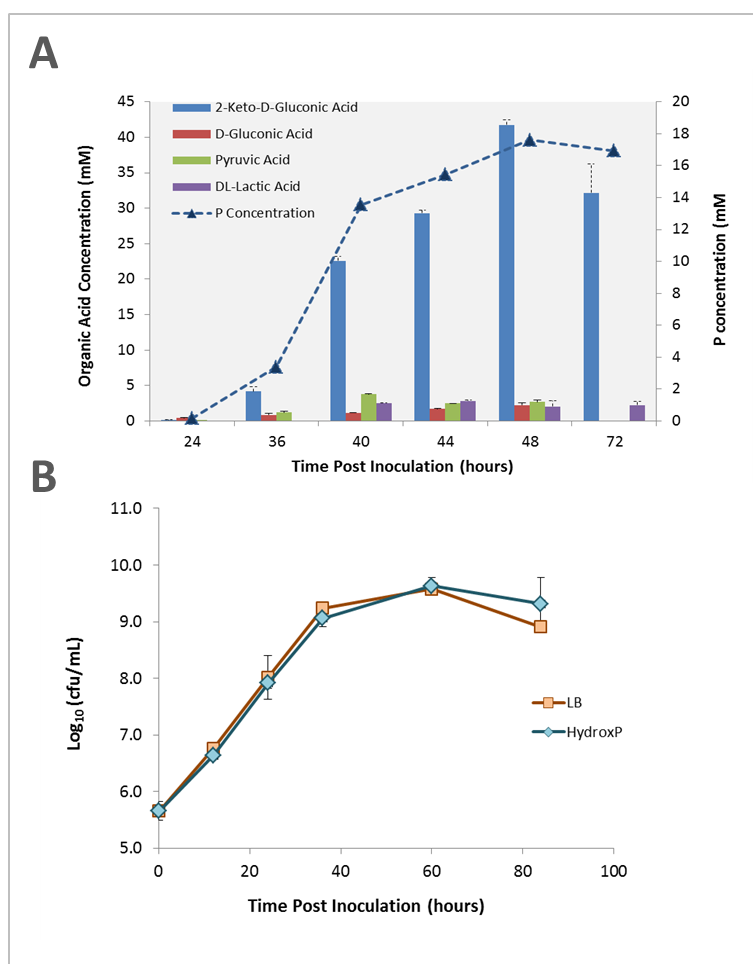


Figure 4.3.21 Liquid culture assay of *Burkholderia* sp. Ha185. Amounts of organic acids and soluble phosphate released by wildtype *Burkholderia* sp. Ha185 at 24, 36, 40, 44, 48 and 72 h post-inoculation (A). Bars indicate concentrations of organic acids in mM measured using HPLC. Blue dashed line indicates P released by the wildtype strain over the 72 h culture period in HSU HydroxP liquid medium (mM) determined using Murphy and Riley's colourimetric method. Growth curve of *Burkholderia* sp. Ha185 in LB broth and HydroxP liquid culture over 84 h (B). Error bars are SEMs of three independent experiments ($n=3$).

There was a clear correlation between the amount of 2-KGA produced by bacterial cells and the amount of P released from HydroxP (**Figure 4.3.21** (A & B)). The graph could be used to calculate the amount of P solubilised by *Burkholderia* sp. Ha185 given the amount of 2-KGA produced in liquid culture. To understand the chemical process of HydroxP dissolution using 2-KGA, a formula was derived to describe the process whereby the carboxyl groups of two 2-KGA molecules are readily deprotonated by a single calcium ion from HydroxP, forming a stable calcium 2-ketogluconate compound (**Figure 4.3.22**). This reaction occurs under acidic conditions and releases hydrogen phosphate as soluble P. The reaction scheme is outlined below as a two-step linear formula:

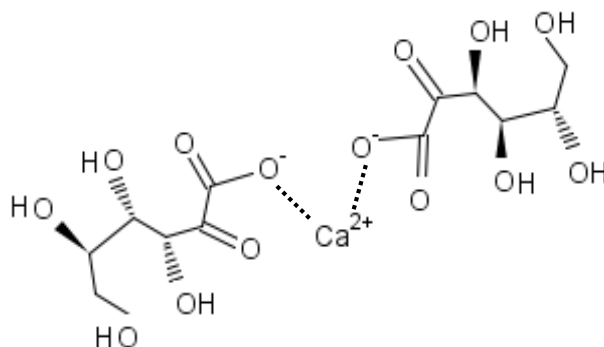
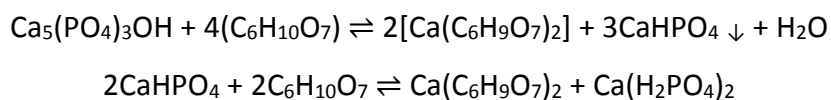


Figure 4.3.22 Structure of calcium 2-keto-gluconate

The formula above shows the two-step process. The first step involves dissolution of the calcium from HydroxP to form calcium 2-ketogluconate, where the calcium ion is chelated by two 2-KGA molecules. This releases dicalcium phosphate anhydrous (CaHPO_4), which is readily precipitated into an insoluble form (pH dependent). The second step of the process involves further breaking down the CaHPO_4 compound by additional 2-KGA molecules, which chelates the calcium ion and releases free P ions. Figure 3.1.37 shows a graph of expected values (open triangle, dashed line), using the derived formula, as well as the observed values from wildtype *Burkholderia* sp. Ha185 (**Table 4.3.8**) releasing soluble P from the HSU HydroxP liquid culture medium (solid triangle, blue line). The observed value of 22.60 ± 0.57 mM 2-KGA released 13.55 ± 0.11 mM soluble P by *Burkholderia* sp. Ha185 at 40 h (**Table 4.3.8**), whereas it was expected that 45.20 mM of 2-KGA would be required to

release same amount of soluble P (Figure 3.1.37). This showed that the observed 2-KGA values were almost two-fold less than the expected values calculated using the reaction scheme outlined above. This suggested that an additional mechanism, other than 2-KGA production alone, may be involved in HydroxP solubilisation by *Burkholderia* sp. Ha185.

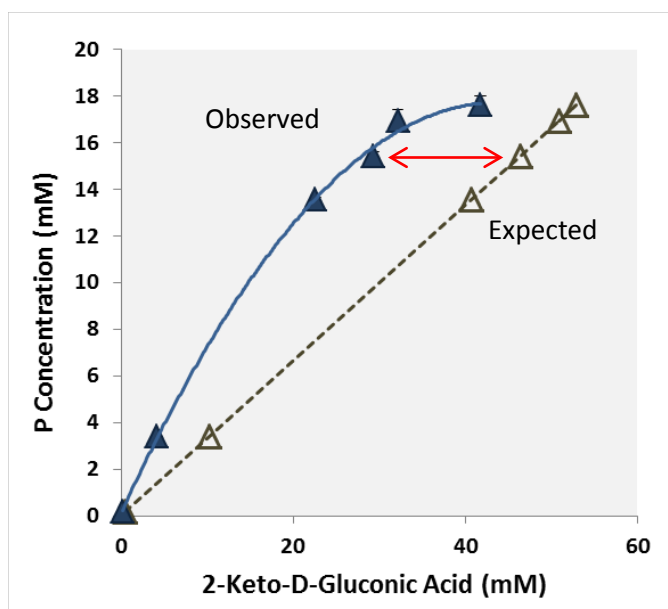


Figure 4.3.23 Observed relationship between soluble phosphate concentration and 2-keto-D-gluconic acid released by wildtype *Burkholderia* sp. Ha185 in HSU HydroxP liquid culture medium based on a second order polynomial regression (blue solid line, solid triangle) ($R^2= 0.999$, $p < 0.001$). Dashed line represents expected response of P release versus 2-KGA production, where two 2-KGA molecules chelate a single calcium ion (open triangle). Error bars are SEMs of three independent experiments ($n=3$).

4.3.4.6 Hydroxyapatite solubilisation by organic acids *in vitro*

Previous results identified a clear correlation between organic acid production and P solubilisation (Section 4.3.4.5). To define and clarify the role of organic acid production in MPS and differentiate it from other factors, such as enzyme production, the ability of organic acids that were released by *Burkholderia* sp. Ha185 in HSU HydroxP liquid culture medium were investigated. Organic acids include LA, GA, PyrA and 2-KGA (Table 4.3.6), along with MA were assessed *in vitro* over a range of concentrations for their direct ability to release soluble P. Malic acid was included because it contains carboxyl groups at the C₁ and C₄ positions (Figure 3.1.38). The concentrations of tested organic acids were within the range of production by *Burkholderia* sp. Ha185 (1, 5, 10, 25 and 50 mM). The concentration of soluble P in the culture filtrate correlated with the concentration of the organic acid added to the HSU HydroxP medium. With the exception of 2-KGA, more inorganic P was solubilised as the concentration of organic acid increased. No soluble P was released by 2-KGA at any of the

concentrations tested (Figure 4.3.25). This suggested that 2-KGA used in this experiment (CAS Number 1040352-40-6; obtained from Sigma-Aldrich, Saint Louis, MO, USA) in the form of “2-keto-D-gluconic acid hemicalcium salt hydrate” was not capable of solubilising HydroxP. This could be because the C₁ hydroxyl group was saturated and stabilised by a calcium ion, and therefore no further dissociation of calcium ions from HydroxP could occur.

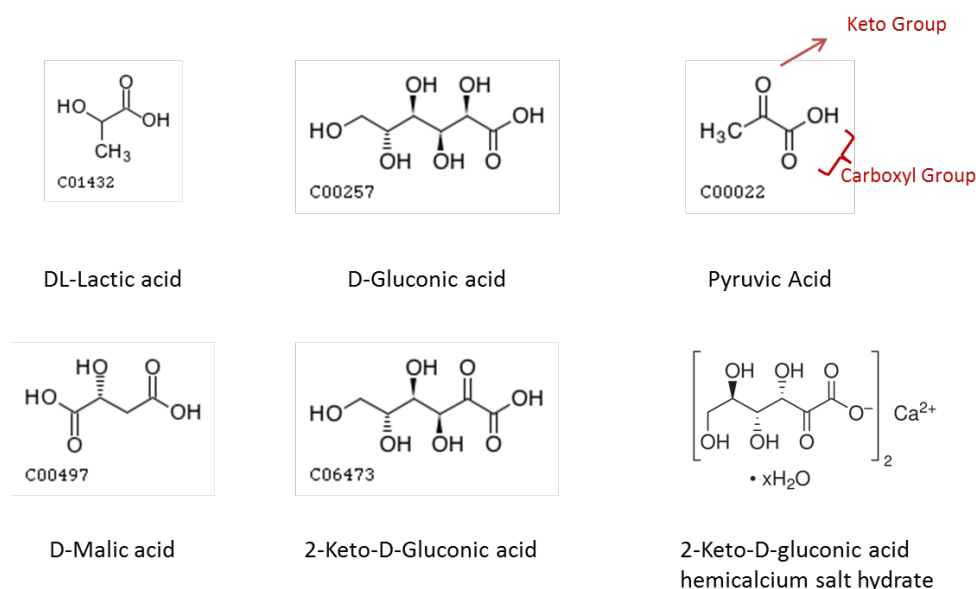


Figure 4.3.24 Chemical structure of organic acids produced by *Burkholderia* sp. Ha185. Diagrams were obtained from the KEGG database, apart from 2-keto-D-gluconic acid (hemicalcium salt hydrate), which was obtained from Sigma-Aldrich. The molecule entry number is also included.

HydroxP solubilisation was more pronounced when organic acids were used at concentrations above 25 mM. There was a significant difference in the amount of P released by MA compared with the other organic acids tested at 25 mM ($p < 0.001$) (Figure 4.3.25). There was also a significant difference between PyrA and LA at 25 mM, with 11.47 ± 0.55 mM and 8.55 ± 0.65 mM of P being solubilised, respectively ($p < 0.001$). The amount of P solubilised by GA (9.97 ± 0.45 mM) at 25 mM did not differ from that released by PyrA or LA ($p > 0.05$). At higher organic acid concentrations (50 mM), the differences between each organic acid were greater and more significant ($p < 0.001$). MA released 27.35 ± 0.58 mM of P, PyrA solubilised 21.64 ± 0.83 mM, GA solubilised 18.34 ± 0.42 mM and LA released 15.62 ± 0.49 mM of P from HydroxP. The pH of medium supplemented with GA (pH 2.31) was slightly higher than that containing LA (pH 2.06) initially, but GA solubilised more P than LA. Although the pH of MA medium (pH 2.10) was also initially higher than LA and PyrA (pH 1.70), MA

solubilised the greatest amount of HydroxP at concentrations of 5 mM and above, compared with the other organic acids tested (Figure 4.3.25). MA contains carboxyl groups at the C₁ and C₄ positions (Figure 3.1.38). This could account for its increased ability to solubilise HydroxP in comparison with other organic acids, as both carboxyl groups can participate in the reaction. This experiment showed that organic acids can solubilise HydroxP in the order MA > PyrA > GA > LA.

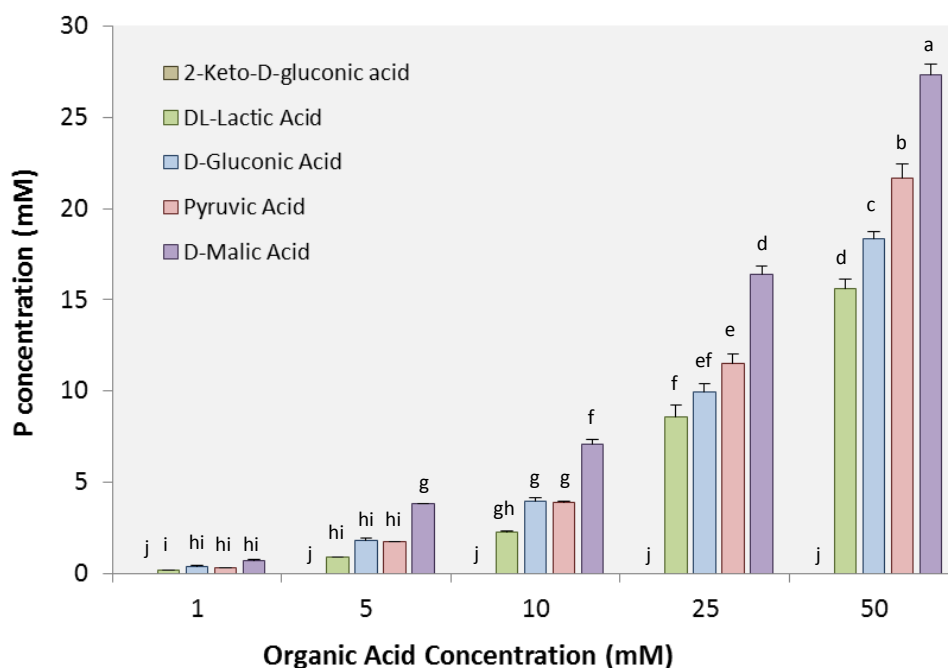


Figure 4.3.25 Hydroxyapatite solubilised by 2-keto-D-gluconic acid, DL-lactic acid, D-gluconic acid, pyruvic acid and D-malic acid in 1 mL of HSU HydroxP medium without glucose. Each organic acid was tested at 1, 5, 10, 25 and 50 mM. A sample with no organic acid was used as a negative control. Samples were incubated at 25°C for 24 h, and phosphate concentration in the culture filtrate was measured by the Murphy and Riley method (Chapter 3.3.8). Error bars are SEMs of three independent experiments (n=3). Statistical analysis was carried out using the Tukey Method, and groups with different letters differ significantly at the 5% level.

4.3.4.7 Relative expression levels of *hemC*, *hemX*, *bxpC* and *ppc* as determined by qRT-PCR

Burkholderia sp. Ha185 mutants *bxpC*::Tn5(F13) and *hemX*::Tn5(F18) have transposons inserted into the previously uncharacterised gene *bxpC* and *hemX*, respectively. From results determined so far, both of these genes appear to be involved in the ability to solubilise HydroxP (Section 4.3.4.2 and Section 4.3.4.3). To define the relative RNA levels of *bxpC* and *hemX*, along with neighbouring genes such as *ppc* and *hemC*, in *Burkholderia* sp. Ha185, qRT-PCR was undertaken. At various time points, expression of these genes in cells grown in HSU HydroxP liquid culture medium was compared with

expression in HSU-P culture medium. Comparison to HydroxP-M, which contains mannitol as the carbon source, was not undertaken because the central catabolism involving the TCA cycle is expected to alter in response to different carbon sources. Wildtype *Burkholderia* sp. Ha185 had lower 2-KGA production when incubated in HSU-P compared with HSU HydroxP medium. The overall pH also increased, but the final cfu counts were not significantly different when grown in HSU-P compared with HSU HydroxP (Section 4.3.4). Therefore, it was determined that HSU-P, which contains soluble P instead of HydroxP, was a suitable control. An uninoculated culture was included as a negative control.

Multiple pairs of qRT-PCR primers, designed to amplify *hemC*, *hemX*, *bxpC* and *ppc*, as well as the reference genes *gltB*, *recA* and *gyrB*, were designed using the web-based program Primer-BLAST (Ye et al., 2012) as outlined in Section 4.2.5.3. Protein networks obtained by STRING analysis suggested that there was a strong relationship between HemX and HemC (0.989) (Figure 4.3.9), and a weaker association to the PEPC protein (0.670). Therefore, both *hemC* and *ppc* were included in this study to determine the regulation of genes in the *hem* operon. The PCR efficiency and R^2 value for each primer pair were determined by qRT-PCR analysis of a dilution series of cDNA, and further analysed using linear regression PCR (LinRegPCR) (Ruijter et al., 2013). The most efficient primer pairs with RT-qPCR efficiency (E) between 1.60 and 2.10 and a R^2 value of >0.980 were chosen for the following experiments, and are listed in **Table 4.2.2** and **Table 4.3.9**. The primer efficiency was taken into account in calculations of RNA expression ratios. Therefore, primer ratios were maintained at a constant concentration (250 nM) for both forward and reverse primers. Levels of transcript from each *Burkholderia* sp. Ha185 gene expressed during culture in HSU HydroxP liquid culture medium at different time points were compared with levels present in HSU-P liquid medium cultures. RNA concentrations were standardised at each step of the analysis using a Nanodrop spectrophotometer (Section 4.2.5.1) to account for variations between cultures and sampling times.

Table 4.3.9 PCR efficiencies and R² values for primer pairs used in this study

Gene	Primer Pair	PCR Efficiency [†]	R ² Value*
<i>hemC</i>	qHemCF/R	1.80	0.99996
<i>hemX</i>	qHemXF/R	1.83	0.99998
<i>bxpC</i>	qBxpCF/R	1.91	0.99996
<i>ppc</i>	qPpcF/R	1.91	0.99997
<i>gltB</i>	qGltBF/R	1.90	0.99988
<i>recA</i>	qRecAF/R	1.85	0.99995
<i>gyrB</i>	qGyrBF/R	1.80	0.99998

* R² corresponds to the slope of the linear section of the amplification curve when presented in a log scale. Optimal R² values are >0.980.

† PCR efficiency corresponds to the number of copies of each template generated after one PCR cycle. An optimised PCR has an efficiency of 1.6–2.10.

The mRNA levels were examined individually for *hemC*, *hemX*, *bxpC* and *ppc* using REST–MCS© version 2 software (Pfaffl, 2001) (Section 4.2.5.3), and expression levels were normalised against the reference genes *gltB*, *recA* and *gyrB*. The analysis showed a significant increase ($p < 0.05$) in *hemC* expression ($\log_2 2.62 \pm 0.99$) compared with the reference genes at 24 h post-inoculation (Figure 3.1.40), but no difference in expression compared with the controls at 36 h, 40 h and 72 h. As 2-KGA production increased, expression of *ppc* decreased significantly at 36 and 40 h ($p < 0.05$) (Figure 3.1.40). Expression of *hemC* was lowest at 48 h post-inoculation ($\log_2 -3.78 \pm 0.64$), and was significantly lower than reference genes ($p < 0.05$). At 48 h, 2-KGA produced by *Burkholderia* sp. Ha185 in HSU HydroxP medium was at its highest concentration (41.74 ± 0.73 mM, **Table 4.3.6**). The relative expression of *bxpC* was also at its highest at 48 h post-inoculation ($\log_2 2.81 \pm 0.81$), and was significantly higher than the reference genes ($p < 0.05$). At 72 h post-inoculation, the expression level of *bxpC* dropped to $\log_2 1.38 \pm 0.47$ ($p < 0.05$), correlating with a significant reduction in the concentration of 2-KGA (32.18 ± 4.05 mM). With the exception of *hemX*, which was significantly suppressed ($\log_2 -1.38 \pm 0.48$, $p < 0.05$), there were no significant differences between the target and the reference genes by 72 h post-inoculation ($p > 0.05$) (Figure 3.1.40).

High resolution melting analysis showed that the ~150-bp PCR amplicons of all target and reference genes, except *bxpC*, required high temperatures to denature dsDNA. This may be explained by the high average GC content of the *Burkholderia* sp. Ha185 genome. The HRM analysis provides fast and reliable post-PCR analysis of PCR integrity, and is also able to distinguish PCR amplicons from primer dimers or background artefacts as well as any contamination during qRT-PCR preparation

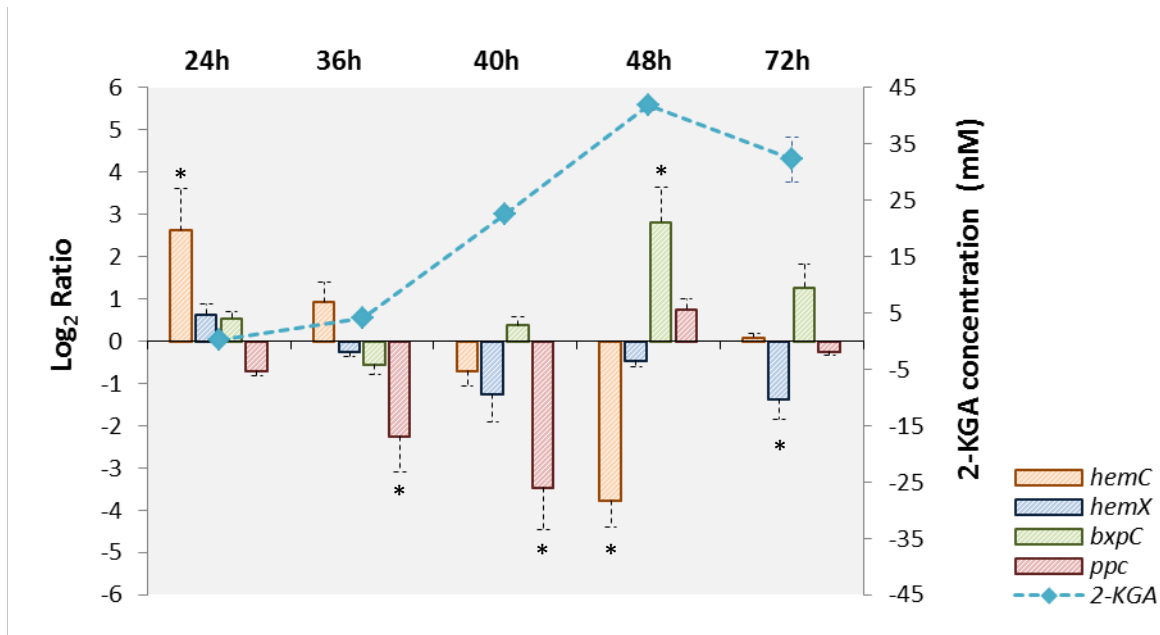


Figure 4.3.26 Expression ratios of the *Burkholderia* sp. Ha185 *hemC*, *hemX*, *bxpC* and *ppc* genes at 24, 36, 40, 48 and 72 h post-induction. Expression ratios were calculated using REST-MCS[®] version 2 software and were normalised against reference genes *gltB*, *recA* and *gyrB*. Expression ratios are the difference in gene expression of wildtype *Burkholderia* sp. Ha185 cultured in HSU HydroxP medium at each time point relative to the RNA expression in cultures incubated in HSU-P medium. The amount of 2-KGA released, as determined by HPLC analysis from the same experiment, is plotted on the second Y-axis (blue dashed line). Error bars are the SEM for all sample replicates (n = 3). *Significantly different from the wildtype control *Burkholderia* sp. Ha185 in glucose at $p < 0.05$.

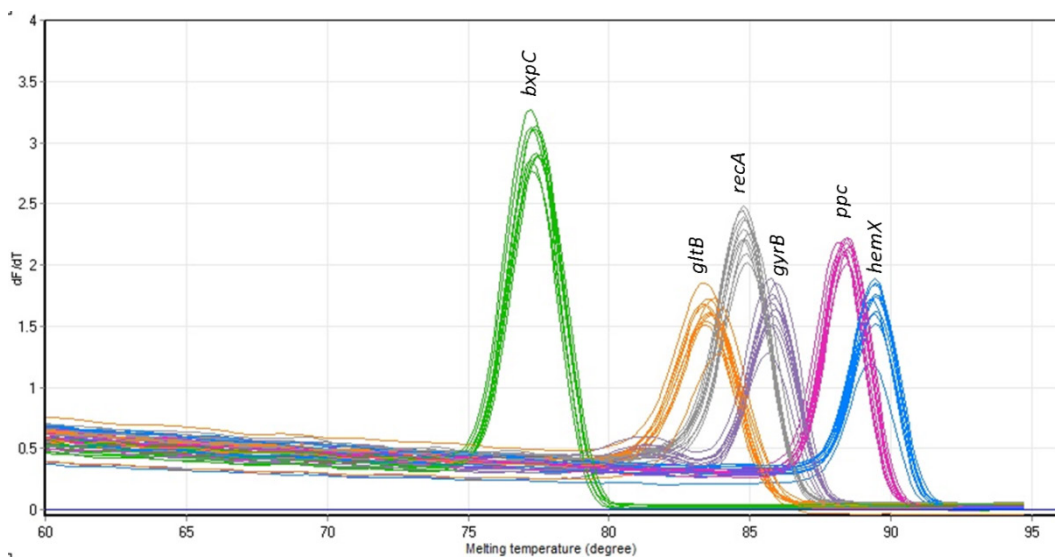
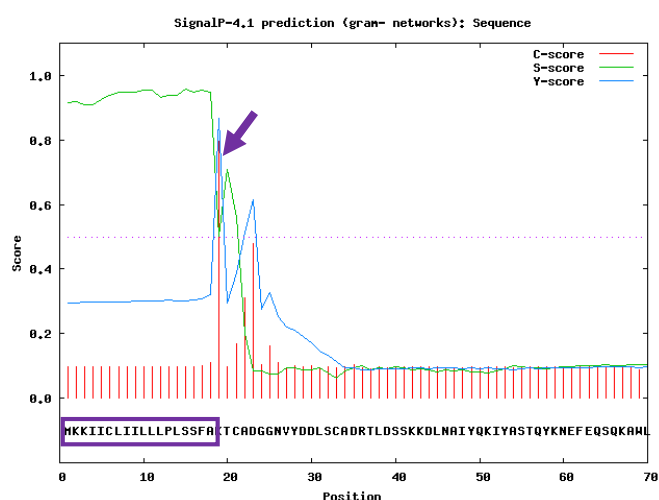


Figure 4.3.27 Analysis of the High resolution melting analysis (HRM) plot from *Burkholderia* sp. Ha185 (-dF/dT vs T). Individual genes are highlighted in different colours; *bxpC*, green; *gltB*, orange; *recA*, grey; *gyrB*, dark purple; *ppc*, pink; *hemX*, blue.

4.3.5. Defining the role and expression of BxpC

4.3.5.1 Cloning *bxpC* into the *pAY2-4* and *pGEX* expression vectors

To understand how BxpC is involved in P solubilisation, the BxpC-encoding region was cloned into the arabinose inducible vector pAY2-4 (Shaw et al., 2003), allowing expression of the protein in its native state. To assist with downstream purification of the truncated BxpC protein, the *bxpC* region was also ligated into the IPTG-inducible vector pGEX-6P-1 (Am^R, Table 4.2.19), enabling the N-terminus fusion of BxpC to the 26-kDa glutathione S-transferase (GST) tag. The commercially-available vector pGEX-6P-1, which contains a GST sequence at the multiple cloning site was used (Figure 4.3.29). The translated product of the 357-bp *bxpC* gene was predicted to be a 118 amino acid peptide. Bioinformatic analysis of the BxpC amino acid sequence using the SignalP 4.1 Server (Petersen et al., 2011) revealed the presence of a type I protein signal peptide sequence, which is predicted to cleave between amino acids at positions 18 and 19 (between the alanine and the lysine) (Figure 4.3.28). Using the Compute pI/Mw tool (Gasteiger et al., 2005), the active BxpC protein was predicted to be 101 amino acid residue in length and 11.2 kDa.



# Measure	Position	Value	Cutoff	signal peptide?
max. C	19	0.795		
max. Y	19	0.868		
max. S	15	0.957		
mean S	1-18	0.938		
D	1-18	0.901	0.570	YES

Figure 4.3.28 Output from the SignalP 4.1 web-server for BxpC sequence analysis. The predicted cleavage site is displayed as the “C-score”, with 0.795 at position 19 (indicated by purple arrow). The predicted signal peptide is recorded as the “S-score”, with 0.938 from positions 1–18 (indicated by purple highlighted box). The ‘Y-score’ is a combination of C- and S-scores, with a 0.868 at position 19. The predicted cleavage site is located between positions 18 and 19, with the local sequence context “SFA-KT”. The D-score, 0.901, is the associated cutoff value and describes which networks were used to make the prediction: D-cutoff is 0.570 and the network is SignalP-noTM.

The 55–357 bp region of *bxpC* was amplified and cloned into the pAY2-4 expression vector, allowing expression of a 101 amino acid residue region of the BxpC protein, lacking its signal sequence. Primer set ParaNF/ParaER, containing a 3' *NdeI* site and a 5' *EcoRI* site, respectively, was designed and standard PCR was performed (Appendix C.2.9) using wildtype *Burkholderia* sp. Ha185 gDNA as the template. The resultant 303-bp amplicon was digested with *NdeI* and *EcoRI* and ligated in-frame into the analogous sites of pAY2-4, where the unique *NdeI* site contained the initiation codon (CATATG) (Appendix C.2.3). Following overnight ligation (Appendix C.2.11), the reaction was ethanol precipitated and digested with *Ascl*, cutting internal to the multiple cloning site of pAY2-4 and enriching for transformants with cloned inserts. The digested ligation was transformed into *E. coli* DH10B (Appendix C.2.7, **Table 4.2.1**) and plated on LB agar containing ampicillin. The resulting construct was validated by restriction digest and DNA sequencing using the araF and araR primers (Appendix C.2.12). The validated construct was designated pARAC3.

To clone *bxpC* into the pGEX-6P-1 expression vector, the 55–357 bp region of *bxpC* was amplified using wildtype *Burkholderia* sp. Ha185 gDNA as the template. The primers GexBF and GexSR were designed to enable in-frame ligation with pGEX-6P-1 (Table 4.2.2) and to remove the predicted signal sequence from the BxpC protein. These primers were designed with a *BamHI* restriction site at the 5' end of the GexBF primer and a *Sall* site at the 3' end of the GexSR primer. Standard PCR was performed as described in Appendix C.2.9. The resultant 303-bp amplicon was digested with restriction enzymes *BamHI* and *Sall* and ligated in-frame into the analogous sites of the pGEX-6P-1 expression vector (Appendix C.2.11, **Figure 4.3.29**), and in-frame with the 3' end of the gene encoding for the GST protein. This resulted in an N-terminal GST-BxpC protein fusion. The ligation was then enriched for cloned inserts by digestion with *EcoRI*. The *EcoRI* site was located internal to the region of vector DNA where the amplicon with no *EcoRI* site was cloned. The resultant digest (2 μ L) was then transformed into *E. coli* DH10B and plated on LB agar containing ampicillin. A *BamHI* and *Sall* restriction digest profile of plasmid DNA from several transformants was then assessed and a clone with the expected restriction pattern was further validated by DNA sequencing using pGEX5 and pGEX3 primers performed by the Macrogen sequencing service (Appendix C.2.12).

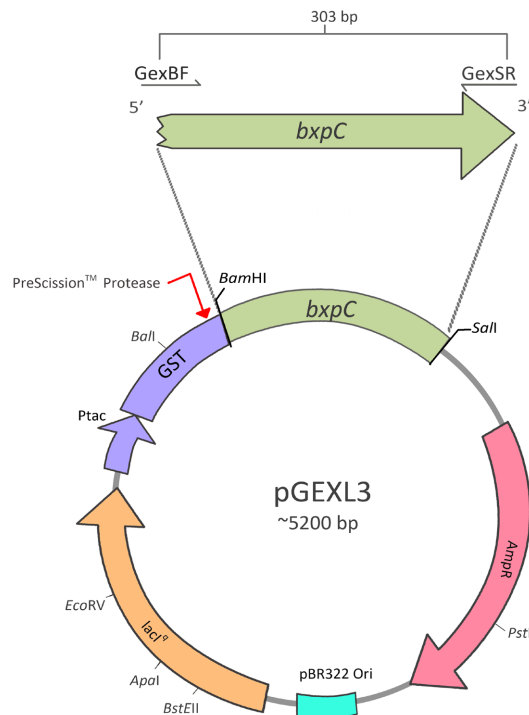


Figure 4.3.29 Diagram of the pGEXL3 plasmid construct. pGEXL3 was constructed by ligating the *bxpC* amplicon between the *Bam*HI and *Sal*I restriction sites in the pGEX-6P-1 expression vector. Plasmid pGEXL3 confers ampicillin resistance to the host cell. Red arrow denotes the PreScission™ Protease protein cutting site between the glutamine and glycine residues (Leu-Glu-Val-Leu-Phe-Gln-Gly-Pro).

4.3.5.2 Expression of *BxpC* using expression vectors pAY2-4 and pGEX

BxpC was expressed as outlined in Section 4.2.6 using construct pARAC3 in *E. coli* DH10B. Vector pAY2-4 without the insert was used as a negative control. Following a 22-h induction by 0.2% (w/v) arabinose at 37°C and at room temperature, bacterial cells were harvested by centrifugation and the resuspended cell pellet was sonicated (Section 4.2.6). Aliquots of the cell pellet and sonicated filtrate were independently separated on 15% polyacrylamide gels (as described in Section 4.2.6.3). The gels were then silver-stained as described by Blum et al. (1987). Visual assessment of the SDS-PAGE results revealed a prominent band (denoted by a red arrow in Figure 3.1.44) of approximately 14 kDa in the lane corresponding to the induced pARAC3 culture, which was not present in the negative control, pAY2-4. This band was also not visible in either the sonicated cell pellet or the sonicated filtrate (L4 and L6, respectively), or in the negative control, pAY2-4 (cell, L3, and sonicated filtrate, L5) (Figure 3.1.44). This indicated that *BxpC* was not produced at a high level. A protein of the predicted

mass was detected in the cell pellet when induced at 37°C (L2), but not in the cell pellet or in the sonicated filtrate when induced at 20°C.

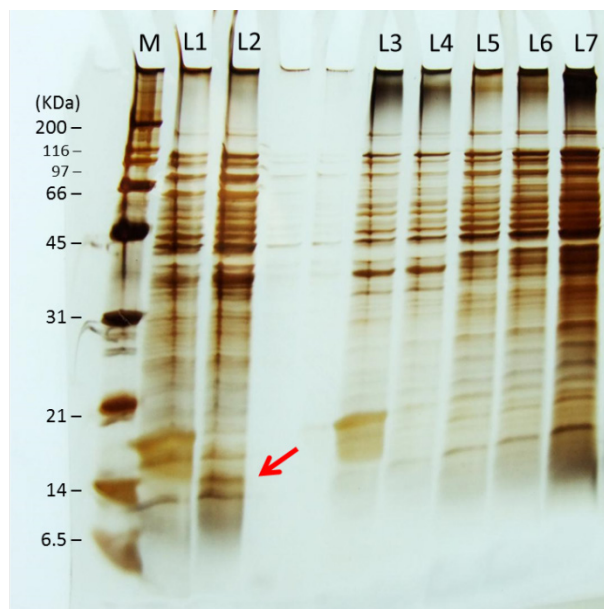


Figure 4.3.30 Silver-stained polyacrylamide gel (15%) showing proteins expressed by pAY2-4 and pARAC3. L1, negative control pAY2-4; L2, pARAC3 cell pellet. Both cultures were induced at 37°C for 22 h. Red arrow denotes the location of the predicted BxpC protein (14 kDa). L3 and L4, sonicated *E. coli* pAY2-4 and pARAC3 cell pellets, respectively, induced at 20°C for 22 h. L5, sonicated filtrate of *E. coli* pAY2-4. L6, sonicated filtrate of pARAC3 induced with 0.2% (w/v) arabinose at 20°C for 22 h; L7 shows two-fold higher gel loading of sample shown in L6. M denotes Precision Plus Protein molecular weight ladder.

To mitigate solubility issues and facilitate purification of BxpC, the *bxpC* fragment was placed in-frame with the GST tag of the pGEX-6P-1 expression vector. The *bxpC* fragment, lacking the region encoding the predicted signal sequence, was cloned into the pGEX-6P-1 expression vector. The resultant vector, pGEXL3, encodes a GST-BxpC fusion protein, enabling purification of the protein through binding of the GST tag to glutathione Sepharose™ 4B resin, where glutathione is a (Glu-Cys-Gly) specific substrate for the GST protein. Analysis of the resultant SDS-PAGE of the induced constructs revealed the presence of the GST-BxpC fusion protein in both the cell pellet and sonicated filtrate fractions. The protein was observed at ~38 KDa (Figure 3.1.45, green arrow), consistent with the expected size of the soluble GST-BxpC fused protein in the filtrate. As expected, the GST-BxpC protein was not present in the filtrate after binding to the glutathione resin (L4-L7). SDS-PAGE analysis of the bound protein resin showed a dominant band at ~38 KDa (Figure 3.1.45). Following

cleavage by PreScission™ protease, a faint band was observed at the predicted size (Figure 3.1.45, L11, red arrow). To concentrate the protein, 1.5 mL of total protease-cleaved protein solution was centrifuged through a 10-kDa centrifugal filter (Section 4.2.6.2), and the final 30 μ L retentate in the filter was pipetted to resuspend the protein. A 20 μ L aliquot of this resuspension was separated by SDS-PAGE (L12, Figure 3.1.45). The SDS-PAGE revealed a band of the predicted size (14 kDa, denoted by red arrow), indicating that BxpC is cleaved by the protease. The remaining resin contained a band at \sim 26 kDa and another at \sim 44 kDa, corresponding to the predicted sizes of the GST tag and PreScission™ protease, respectively.

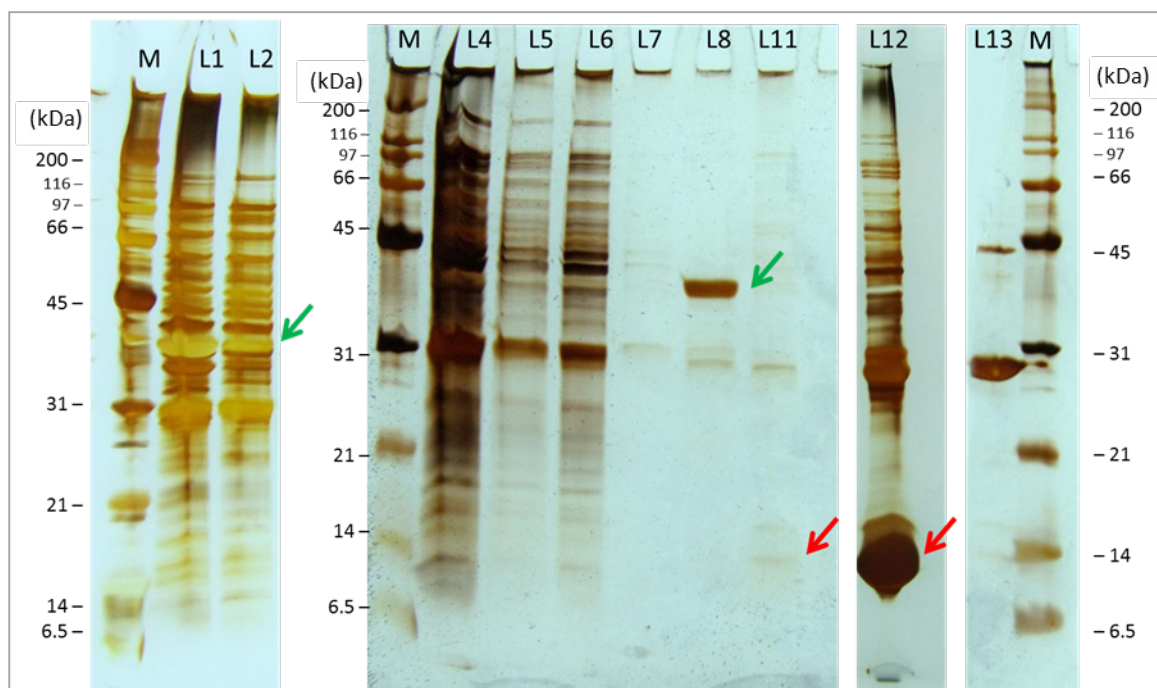


Figure 4.3.31 SDS-polyacrylamide slab gel (15%) showing expressed GST-BxpC. Sonicated cell pellet of *E. coli* DH10B pGEXL3 (L1) induced by IPTG at 20°C for 22 h, and its sonicated filtrate (L2). Green arrow indicates GST-BxpC protein fusion at \sim 38 kDa. Lanes 4–7, (L4-7) indicates bead eluents following each washing step. Lane 8, (L8) present GST-BxpC fusion protein purified using the Glutathione Sepharose™ 4B resin. Eluent from the resin is shown in L11. Concentrated BxpC is indicated by a red arrow (\sim 14 kDa, L12). Lane 13, Glutathione Sepharose™ 4B resin following protein cleavage by PreScission™ Protease. M denotes Precision Plus Protein™ molecular weight ladder. The polyacrylamide slab gel was stained using silver stain.

4.3.5.3 *In silico* analysis of BxpC

Protein annotation, including secondary and tertiary structure prediction, was used to predict the function of BxpC. This was performed using the Phyre² and I-TASSER servers (Kelley et al., 2009; Zhang, 2008). The Phyre² server uses known protein structures from the Structural Classification of Proteins (SCOP) database and is augmented with the Protein Data Bank (PDB) and the Pfam databases. In contrast, the I-TASSER server builds three-dimensional (3D) protein models by assembling Local Meta-Threading-Server (LOMETS) alignments (Wu and Zhang, 2007), and the functions are derived by aligning the predicted protein with 3D models from the BioLiP protein function database (Yang et al., 2013). Insights into the function of BxpC, such as the ligand-binding site, were also predicted by the COFACTOR server using the 3D structure model provided by the Phyre² or the LOMETS server. The BxpC structure was aligned using the COFACTOR server structure with global functional libraries from the PDB, and the 3D protein model was constructed by TM-align from the homologous functional templates (Roy et al., 2012). 3D protein structure used in this study was computed and simulated using Jmol (<http://www.jmol.org/>).

The Phyre² server was used to model BxpC by aligning the amino acid sequence of a secreted protein of unknown function containing a duf1311 domain (PDB3gi7A, crystal structure of a duf1311 family protein (pp0307, NP_742474.1) from *Pseudomonas putida* kt2440 at 1.85 Å resolution) with the BxpC sequence. Analysis showed that although the amino acid sequence was not conserved between BxpC and the duf1311 protein domain from *P. putida* kt2440 (19% amino acid identity), 93% of the secondary structure was within the 99.9% confidence limits when the proteins were aligned (Figure 3.1.46). The predicted secondary structure of BxpC consists of three major α -helices that make up 82% of the total amino acid sequence.

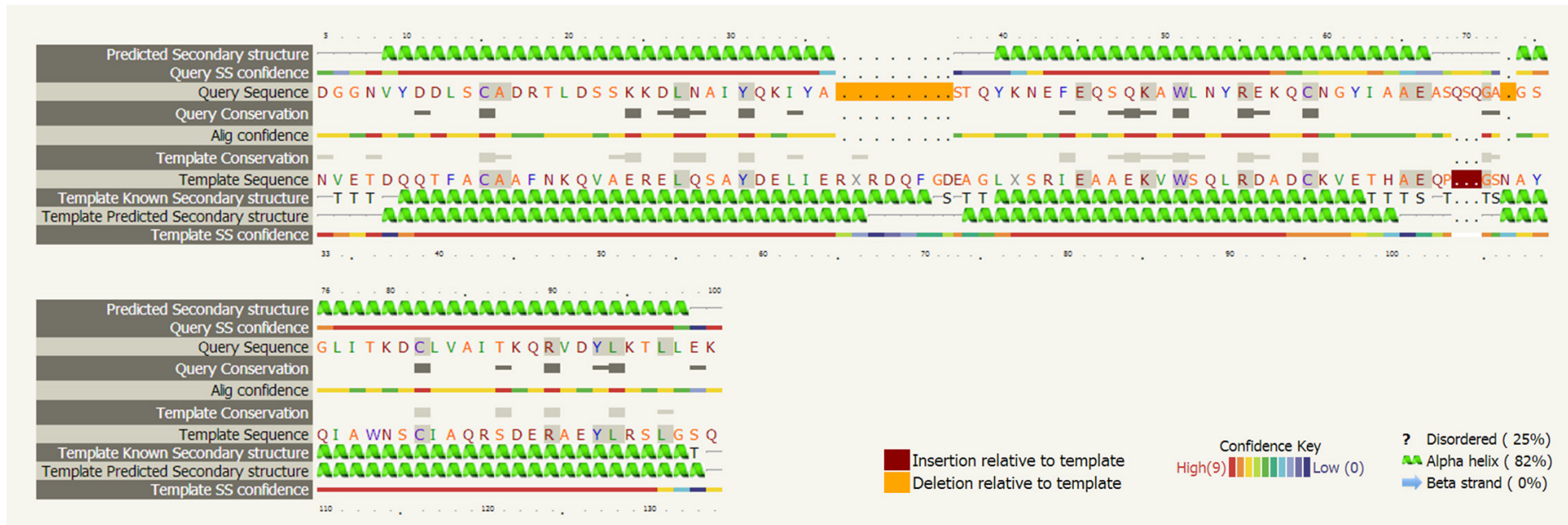


Figure 4.3.32 Secondary structure and disorder prediction using the Phyre² web-based server for BxpC aligned with the sequence of a protein of unknown function, **duf1311 (PDB3gi7A)**. The predicted secondary structure of BxpC is shown in the top row. The secondary structure confidence (SS confidence) is indicated by colour from red to purple, where red is high confidence (9) and purple is low confidence (0). Sequence highlighted in orange indicates deletion relative to the template protein sequence, while dark red highlighting indicates sequence insertion relative to the template. Query conservation shows residue conservation across the detected sequence homologues, where no symbol indicates no conservation, a thin grey bar indicates moderate conservation and a large grey block indicates a high degree of conservation.

To predict the tertiary structure of BxpC, the BxpC amino acid sequence from residues 19–101 (without the signal sequence) was submitted to the I-TASSER server, and the ligand-binding site was confirmed using the COFACTOR server. The 3D model predicted by I-TASSER was retrieved and its tertiary structure and any modifications were visualised with Jmol. The predicted tertiary structure retrieved from the I-TASSER server was generated using the PDB3gi7A protein structure (1.85 Å resolution crystal structure of pp0307) from *P. putida* kt2440 which also contains a duf1311 domain as a template. The predicted tertiary structure of BxpC, shown in Figure 3.1.47, is consistent with the secondary structure shown in Figure 3.1.46. BxpC is composed of three major α -helices constrained by a disulphide bridge formed by two internal cysteine residues (residues 59 and 82), denoted by yellow arrows in Figure 3.1.47. There are two predicted outer cysteine residues that both reside on the first α -helix at positions 3 and 15 (Figure 3.1.47). The cofactor binding site was predicted by both I-TASSER and COFACTOR, where the use of the calcium binding site of cytochrome *c* nitrite reductase from *Sulfurospirillum deleyianum* as a template (PDB1qdb, 1.9 Å resolution) provided the highest score (Einsle et al., 1999). Calcium is predicted to bind at the Tyr49, Lys67 and Asn71 residues of BxpC in a cavity (depicted by pink sphere in Figure 3.1.47).

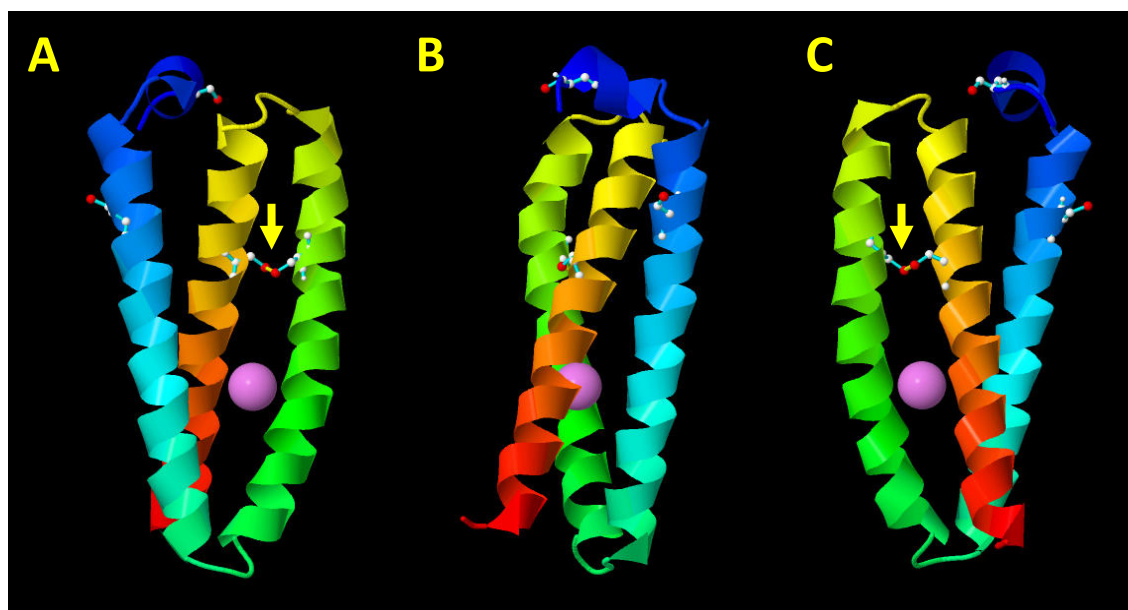


Figure 4.3.33 Tertiary structure of BxpC predicted by I-TASSER using the crystal structures of a duf1311 family protein (PDB3gi7A) and cytochrome *c* nitrite reductase (PDB1qdbA) as templates. The predicted 3D structure of BxpC shown in B is rotated 90° clockwise from Y-axis of A, and the structure shown in C is rotated 90° clockwise from Y-axis of B. Four cysteine residues are indicated by the side chain molecule, where carbon is indicated in white, red represents sulphide atoms, and the disulphide bridge is depicted by a yellow bond, indicated by the yellow arrow. The pink sphere denotes the predicted calcium binding site.

The secondary and tertiary structures of BxpC predicted by Phyre² and I-TASSER are shown as a monomer. However, the biological form of the duf1311 family protein is predicted to be tetrameric (PDB3gi7, unpublished data from the Joint Center for Structural Genomics). Visualisation of the duf1311 family protein (PDB3gi7) using Jmol revealed that it consists of four subunits, in which two subunits form a dimer domain (α and β domain, **Figure 4.3.34**). The protein structure is predicted to be stabilised by six disulphide bridges, with one internal disulphide bridge in each monomer, and one link from the $\alpha 1$ subunit to the $\beta 1$ subunit, and another from the $\alpha 2$ subunit to the $\beta 2$ subunit (**Figure 4.3.34** (B)). This resulted in a pseudo C2 symmetrical protein structure, as shown in **Figure 4.3.34** (A). The duf1311 family protein contains four highly conserved cysteine residues and is predicted to be insoluble. Using the web-based tool Recombinant Protein Solubility Prediction (Harrison, 2000), the secreted BxpC protein was predicted to be 65.2% probability of being insoluble, and had a CV-CV' value of 0.63 if over-expressed in *E. coli*. The function of this protein family remains unknown.

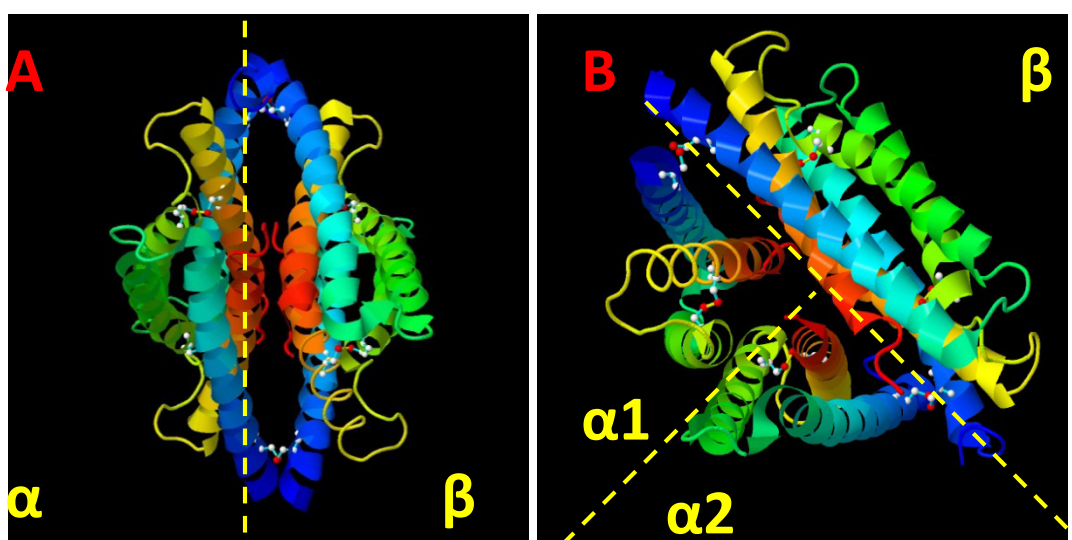


Figure 4.3.34 Quaternary protein structure of the tetrameric duf1311 family protein (PDB3gi7). Each of the α and β domains, separated by yellow dashed lines (A), consists of two subunits ($\alpha 1/\alpha 2$ and $\beta 1/\beta 2$ (B)).

4.3.5.4 *BxpC* sequence alignment

Protein sequence alignment was performed using ClustalW to determine amino acid residue conservation between proteins with a duf1311 domain (Figure 3.1.49). The protein database was searched by BLASTp, using the BxpC sequence from *Burkholderia* sp. CCGE1003 as a query and the sequences with the highest protein homology were retrieved (protein sequence rows 2–7). BxpC orthologues were identified in *Burkholderia* sp. CCGE1003, *B. multivorans* and *Burkholderia gladioli* strain BSR3, as well as in several more distant *Acinetobacter* spp. The *P. putida* kt2440 protein

(NP_742474.1, Figure 3.1.49, highlighted yellow, row 8) used to compute the secondary (Figure 3.1.46) and tertiary (Figure 3.1.47) structures was included in the alignment. This protein was also subjected to BLASTp, and several proteins from *Pseudomonas* spp. with similarity to duf133 from *P. putida* kt2440 were identified. These protein sequences are also included in the ClustalW alignment (Figure 3.1.49, rows 9–14). The sequence alignment showed that the amino acid associated with the calcium binding site of BxpC, Tyr49, is highly conserved within the duf1311 protein family (highlighted pink in Figure 3.1.49), while the Lys67 residue is less conserved. However, the amino acid of the third binding site varies within the duf1311 protein family (indicated by red arrow). The possible active site cavity for metal binding of the duf1311 proteins is denoted by orange parentheses in Figure 3.1.49, and is located in the second α -helix. Interestingly, the *P. putida* kt2440 *Pseudomonas* orthologues appear to be more divergent in the second α -helix region (Figure 3.1.49).

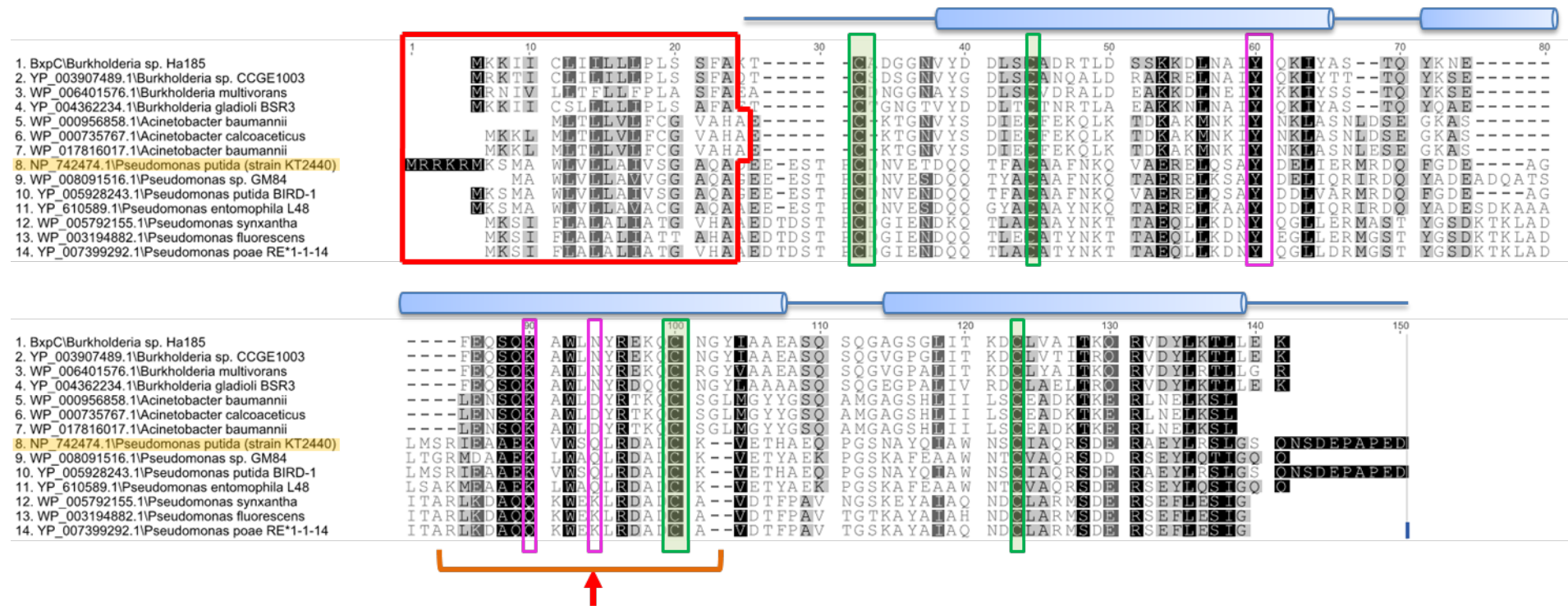


Figure 4.3.35 *Burkholderia* sp. Ha185 BxpC and homologous protein sequences obtained by BLASTp (rows 1–7) were aligned to a hypothetical protein with a duf1311 domain (highlighted in yellow) from *P. putida* kt2440 (row 8, NP_742474.1). Protein sequences shown in rows 9–14 were identified from BLASTp analysis using the hypothetical protein with a duf1311 domain from *P. putida* kt2440 as the query sequence. Sequences were aligned using ClustalW in Geneious. The red box indicates a type I signal peptide sequence as predicted by SignalP 4.1. BxpC secondary structure as annotated by Phyre², indicated by blue tubes, shows three α -helices. Pink highlights denote the predicted calcium binding site of BxpC as annotated by I-TASSER and COFACTOR using cytochrome c nitrite reductase from *Sulfurospirillum deleyianum* as a template (PDB1qdbA). The calcium is predicted to bind at Tyr49, Lys67 and Asn71 of BxpC from *Burkholderia* sp. Ha185. Red arrow indicates a non-conserved calcium binding site at Asn71, and the orange parentheses indicate a possible active site cavity for metal binding of the duf1311 protein family. Protein tertiary structure is constrained by four cysteine residues, highlighted in a green box. GenBank accession numbers of the amino acid sequences are indicated, followed by the species.

4.3.6. *hemX* encodes a bifunctional uroporphyrinogen-III synthetase/uroporphyrin-III C-methyltransferase

The *hemX*::Tn5(F18) mutant had an impaired ability to solubilise HydroxP on both HydroxP agar plates and in liquid culture medium (Figure 3.1.20, Figure 4.3.15). In addition, HPLC analysis revealed that the *hemX*::Tn5(F18) mutant produced lower levels of 2-KGA than the wildtype strain (Table 4.3.6). The wildtype phenotype could be restored through complementation, with the complemented mutants CD3ME12 and DXDME6 exhibiting HydroxP solubilisation and 2-KGA production. A BLASTx search of the protein database predicted that *hemX* of *Burkholderia* sp. Ha185 encodes a bifunctional uroporphyrinogen-III synthetase/uroporphyrin-III C-methyltransferase, which is most closely related to HemX of *B. xenovorans* LB400 (Table 4.3.3).

Gene annotation and protein alignment using tools associated with the GenBank database were carried out to provide insights into the function of HemX in relation to P solubilisation. STRING analysis of HemX amino acid sequence with corresponding regions in different Gram-positive and Gram-negative bacterial species revealed that HemX from *Burkholderia* spp. showed low protein similarity to HemX from other bacterial genera (Figure 4.3.36). HemX amino acid sequences from *Burkholderia* spp. showed less than 50% homology to the HemX regions of the closely related bacteria *Cupriavidus taiwanensis* and *Ralstonia solanacearum*, and were less than 10% similar to other bacterial families within the Proteobacteria. *Burkholderia* spp. HemY amino acid sequence was also dissimilar to HemY identified in other bacterial species. Interestingly, protein sequences of both PPC and HemC were highly conserved within the Proteobacteria (>60% homology), and these regions showed 40% similarity across all Gram-positive species examined (Figure 4.3.36).

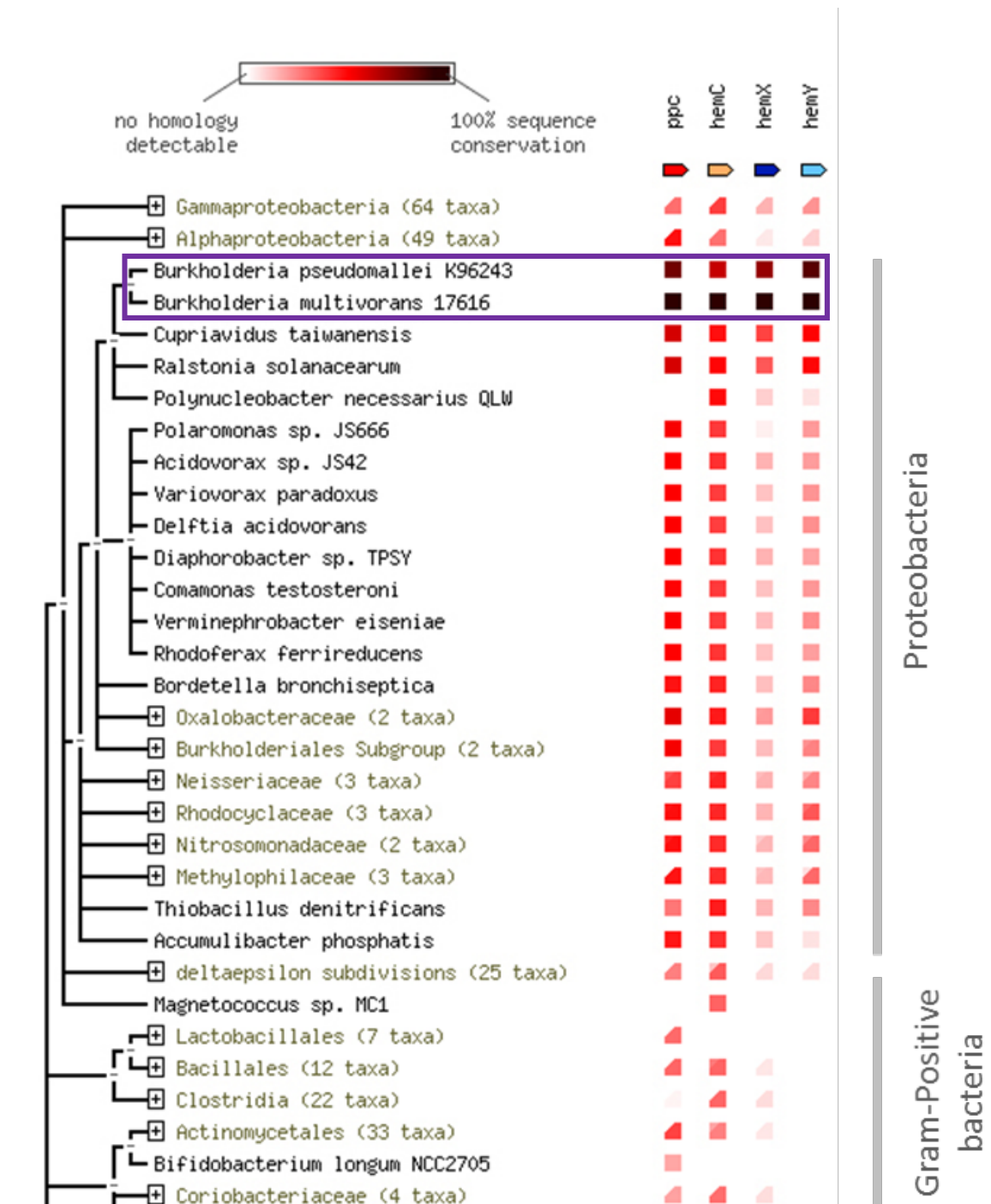


Figure 4.3.36 Co-occurrence analysis of *Burkholderia* spp. PPC, HemC, HemX and HemY regions across different bacterial families using STRING 9.05. *B. pseudomallei* K96243 and *B. multivorans* 17616 (highlighted in purple box) were used as the consensus amino acid sequence. The occurrence pattern is coloured from white to black, where no homology is indicated by white squares and 100% homology is indicated by black squares.

4.3.6.1 Relationship between HemX and haem-dependent gluconate 2-dehydrogenase (acceptor)

Previous experiments (Section 4.3.4.5) showed a strong correlation between release of soluble P from HydroxP in liquid culture medium and the production of 2-KGA over time (**Figure 4.3.21**) by *Burkholderia* sp. Ha185. The impaired ability of the mini-Tn5Km1 transposon mutant *hemX::Tn5(F18)* to produce 2-KGA (**Table 4.3.6**) indicated the importance of *hemX* during the biosynthesis of 2-KGA. To determine the relationship between proteins encoded by the *Burkholderia* sp. Ha185 *hem* operon, production of 2-KGA and observed P solubilisation, the potential presence of a protein capable of producing 2-KGA in *Burkholderia* sp. Ha185 was investigated. The enzyme gluconate 2-dehydrogenase (GADH) mediates the conversion of GA to 2-KGA at the bacterial cytoplasmic membrane and is associated with an electron transport chain system (Matsushita et al., 1982). Membrane-bound GADH in *Erwinia cyripedii* ATCC 29267, encoded by the *gadH* operon, is made up of three subunits: a FAD-dependent dehydrogenase (subunit I, *gadH(I)*), a cytochrome *c* (subunit II, *gadH(II)*) and a protein with GADH activity (subunit III, *gadH(III)*). Genes coding for these protein subunits have been cloned into *E. coli* JM109 (Yum et al., 1997). The authors found that GADH was constitutively formed when expressed in *E. coli*, and its activity increased two-fold with the addition of GA to the liquid culture medium. A *B. phytofirmans* PsJN protein annotated as gluconate 2-dehydrogenase (acceptor) (GADH acceptor), which is predicted to be capable of producing 2-KGA was investigated. Sixteen GADH protein sequences from *B. phytofirmans* PsJN from the UniProt database were retrieved for further analysis. These proteins were then aligned using ClustalW (BLOSUM matrix) in Geneious version 6.1.5. From the resultant amino acid alignment, three contigs were identified as sharing sequence conservation with the FAD-dependent dehydrogenase (subunit I) from *E. cyripedii* ATCC 29267, and were identified as belonging to the oxidoreductase superfamily of the GADH peripheral membrane-bound proteins. To determine if a homologous protein exists in wildtype *Burkholderia* sp. Ha185, the draft genome sequence (Supplemental folder 1) was first translated in all six reading frames using the gene prediction software Prodigal (Prokaryotic Dynamic Programming Genefinding Algorithm; Hyatt et al. (2010)), followed by ClustalW sequence alignment (Geneious version 6.1.5) against the FAD-dependent dehydrogenase proteins of *E. cyripedii* ATCC 29267 and *B. phytofirmans* PsJN (**Figure 4.3.37**). Sequence alignment showed a FAD-binding site (GO:0050660) (purple box) with consensus amino acid residues ([VD]-X-[V]-X(2)-[G]-X-[GW]-X-[G]-X-[I]-X(3)-[EL]-X(3)-[GL]-X-[VV]-X-[LERG]-X(2)), two glucose-methanol-choline oxidoreductase domains, a N-terminal domain (GMC_OxRdtase_N, red box) and a C-terminal domain (GMC_OxRdtase_C, green box) (**Figure 4.3.37**).

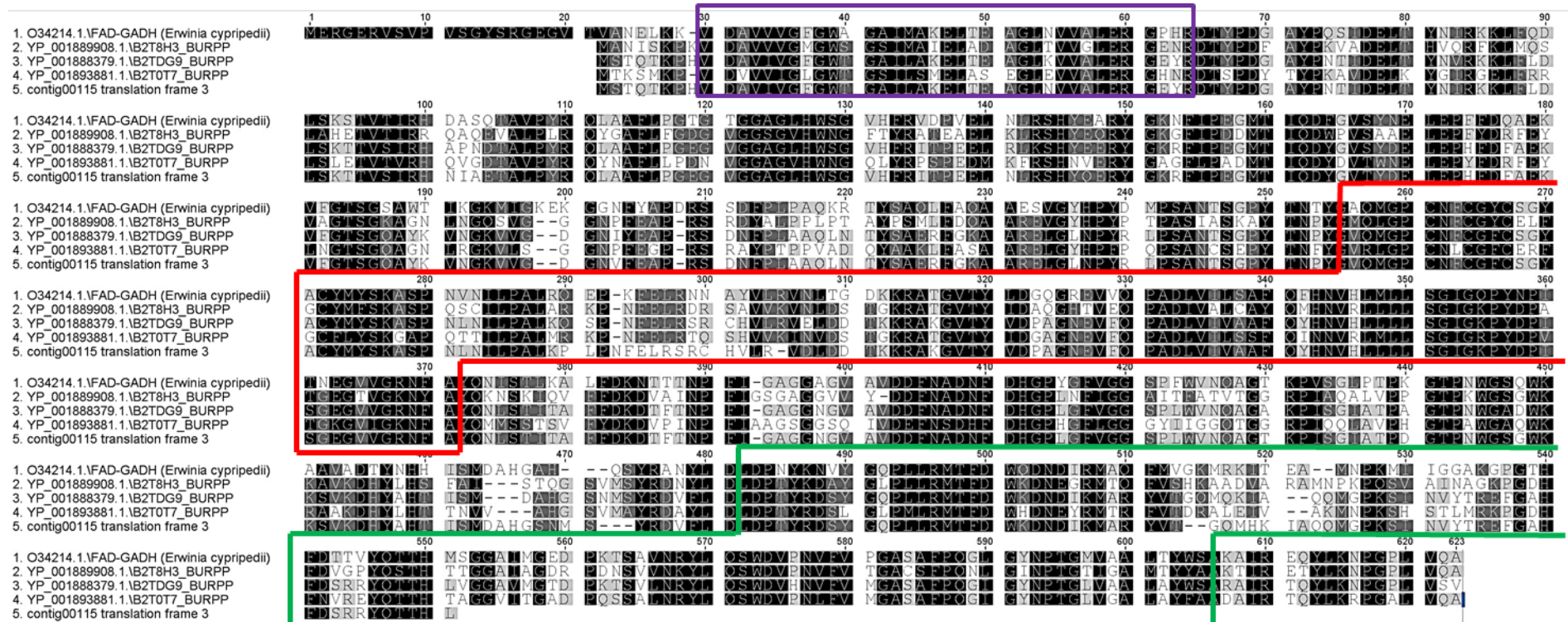


Figure 4.3.37 ClustalW alignment of FAD-dependent gluconate 2-dehydrogenase (subunit I) from *E. cyripedii* ATCC 29267, *B. phytofirmans* PsJN and protein sequences from *Burkholderia* sp. Ha185 (Contig00115). The FAD binding site is highlighted in a purple box (consensus amino acid residues 9–42, [VD]-X-[V]-X(2)-[G]-X-[GW]-X-[G]-X-[I]-X(3)-[EL]-X(3)-[GL]-X-[VV]-X-[LARG]-X(2)). The red box indicates glucose-methanol-choline oxidoreductase domain, N-terminal (GMC_OxRdtase_N) domain, and the glucose-methanol-choline oxidoreductase. The C-terminal (GMC_OxRdtase_C) domain is highlighted in the green box. Sequences from *B. phytofirmans* PsJN (rows 2–4) are identified by the protein accession number (GenBank database), followed by the protein entry name (UniProt database). Sequences derived from the *Burkholderia* sp. Ha185 draft genome (row 5) are identified by the contig number.



Figure 4.3.38 ClustalW alignment of haem-dependent gluconate 2-dehydrogenase (acceptor) (subunit II) from *B. phytofirmans* strain PsJN and protein sequences from *Burkholderia* sp. Ha185. The predicted haem-binding motif is highlighted in a purple box (consensus amino acid residues 96–100, 266–270 and 415–419), where the CXXCH amino acid motif is highly conserved in the centre of a cytochrome *c* domain. Three cytochrome *c* units are found in gluconate 2-dehydrogenase (acceptor) (HEM-GADH), and are highlighted in red boxes. Sequences from *B. phytofirmans* PsJN (rows 1–10) are identified by the protein accession number (GenBank database), followed by the protein entry name (UniProt database). Sequences derived from the *Burkholderia* sp. Ha185 draft genome (rows 11–17) are identified by the contig numbers.



Figure 4.3.39 ClustalW alignment of gluconate 2-dehydrogenase (acceptor) (subunit III) from *B. phytofirmans* strain PsJN, *E. cyripedii* and protein sequences from *Burkholderia* sp. Ha185. The twin arginine translocation (Tat) signal profile (Prosite PS51318) is located at residues 1–50 in the consensus sequence. The signal peptide binding site is highlighted in a green box, with the consensus sequence [ST]-R-R-X-F-L-X and a short AXA motif of each protein sequence underlined in red. Sequence from *E. cyripedii* (row 1) is identified by the protein accession number (GenBank database). Sequences from *B. phytofirmans* PsJN (rows 2–4) are identified by the protein accession number (GenBank database), followed by the protein entry name (UniProt database). The sequence derived from the *Burkholderia* sp. Ha185 draft genome (row 5) is identified by the contig number.

A pattern search for a consensus sequence for the haem-binding motif (Prosite pattern PDOC00169, Cys-X-X-Cys-His (CXXCH)) of ten GADH acceptor sequences from *B. phytofirmans* PsJN was performed using the FUZZPRO program from the EMBOSS suite (Rice et al., 2000). The histidine residue of this consensus sequence is one of the axial ligands of the haem iron, and X represents any amino acid. Using this method, five protein sequences (Contig00045_7, Contig00515_5, Contig00971_1, Contig00004_16 and Contig00223_5), each with three haem-binding motifs, were identified in the *Burkholderia* sp. Ha185 draft genome. However, contig00447 contains two separate proteins, Contig00447_2 has two haem-binding motifs and Contig00447_3 possesses only one haem-binding motif. This may be a result of sequencing error, resulting in a frame shift of translated amino acid sequence. Protein sequence alignment of haem-dependent GADH from *B. phytofirmans* PsJN and proteins retrieved from *Burkholderia* sp. Ha185 by ClustalW revealed three highly conserved regions of the haem-binding motif, as shown in Figure 4.3.40 (outlined by a purple box containing the consensus sequence, CXXCH).

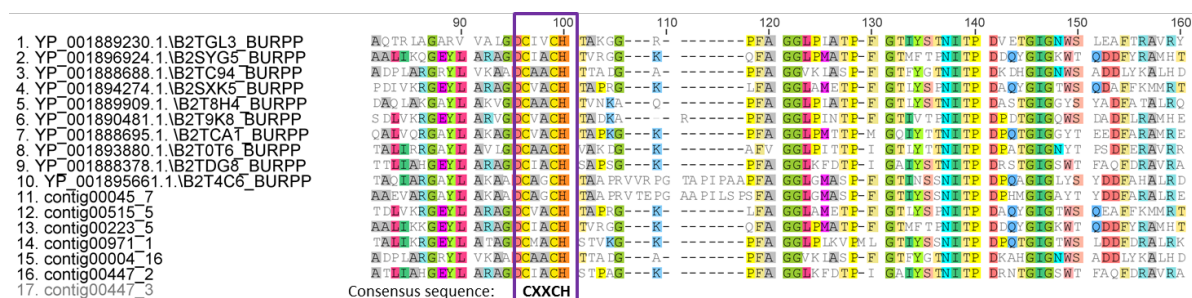


Figure 4.3.40 ClustalW alignment of partial haem-dependent gluconate 2-dehydrogenase (acceptor) sequences from *B. phytofirmans* strain PsJN and *Burkholderia* sp. Ha185 (81–160 amino acid residues). The predicted haem-binding motif CXXCH is highlighted in a purple box (consensus amino acid residues 96–100), and shows the motif is highly conserved. Sequences (rows 1–10) from *B. phytofirmans* PsJN are identified by the protein accession number (GenBank database), followed by the protein entry name (UniProt database). Translated sequences derived from the *Burkholderia* sp. Ha185 draft genome are identified by the contig numbers (rows 11–17).

Amino acid alignment and protein annotation suggested the presence of three cytochrome *c* domains (highlighted by red boxes in Figure 4.3.38). Within the ClustalW alignment, three haem-binding motifs were identified, which are located between residues 96–100, 266–270 and 415–419 of the consensus sequence (Figure 4.3.38). The haem-binding motif is located near the N-terminus of the first cytochrome class I subunit (InterPro: IPR003088), and the other two haem-binding motifs are located near the centre of the cytochrome *c* domain (IPR009056) (Figure 4.3.38). These proteins contain a cytochrome *c* subunit (IPR014353), a signature of membrane-bound alcohol

dehydrogenases, which resides in proteins that catalyse the conversion of GA to 2-KGA in the presence of haem cofactor(s).

The third component of the GADH enzyme, subunit III, which was described as an uncharacterised protein, is reportedly required for the GADH activity (Yum et al., 1997). It was shown that the three complete ORFs coding for the FAD-dependent GADH, the haem-dependent GADH and subunit III are essential for converting GA to 2-KGA (Yum et al., 1997). The gene coding for subunit III was identified upstream of the FAD-dependent *gadh(I)* in Contig00115, and aligned with three *gadh(III)* (acceptor) sequences from *B. phytofirmans* PsJN, and with one sequence from *E. cyripedii* ATCC 29267 encoding a GADH Subunit III (Figure 3.1.53). The amino acid sequence alignment revealed the consensus sequence from 1–50 consists of a twin arginine translocation signal profile (Tat) (Prosite PS51318), with a consensus short AXA motif and a consensus sequence ([ST]-R-R-X-F-L-X) for signal peptide binding (Figure 3.1.53).

4.4 Discussion

4.4.1. Direct oxidation pathway in *Burkholderia* spp.

Low coverage sequencing of the *Burkholderia* sp. Ha185 strain genome in this study provided a genome database that helped to identify genes of interest and facilitate further molecular manipulation. The enzyme PQQ-dependent quinoprotein glucose dehydrogenase (PQQ-GCD) converts glucose to GA at the periplasmic membrane, mediated by the cofactor PQQ (Goldstein and Liu, 1987; De Werra et al., 2009). Genes that encode Gcd have been identified in the genomes of *B. xenovorans* LB400 (YP_559501.1 and YP_555448.1) and *B. phytofirmans* PsJN (YP_001895316.1). The presence of a PQQ binding motif within these Gcd protein sequences was confirmed by the presence of the bacterial quinoprotein dehydrogenases signature 2 Prosite pattern (PS00364, W-x(4)-[YF]-D-x(3)-[DN]-[LIVMFYT]-[LIVMFY](3)-x(2)-G-x(2)-[STAG]-[PVT]). Interestingly, *B. xenovorans* LB400 contains the *pqqBCDE* operon, coding for pyrroloquinoline quinone, whereas *B. phytofirmans* PsJN does not contain any of the *pqq* genes. A search of the *Burkholderia* sp. Ha185 genome revealed that neither *gcd* nor the *pqqABCDEF* operon were present. This suggests that the direct oxidation pathway, via PQQ-dependent Gcd, does not occur in *Burkholderia* sp. Ha185. However, a basal level of GA was detected by HPLC from HSU HydroxP liquid culture assay, with the highest concentration (2.24 ± 0.36 mM) measured at 48 h post-inoculation. This indicated that GA is synthesised by

Burkholderia sp. Ha185 using an alternate pathway. This could be accomplished via one of two possible proteins:

- i) An unknown protein that has similar properties to the membrane bound PQQ-Gcd. This would possibly also involve a redox cofactor for an oxidation-reduction process to take place in the periplasmic space, where it acts on the CH-OH group of glucose.
- ii) Gluconic acid might be synthesised by a putative Gcd inside the cytoplasm (Figure 3.1.55).

In agreement with the second scenario, a predicted ORF (245 amino acid residues, Contig00150 + Contig00211) was identified in the *Burkholderia* sp. H185 genome. This protein shows 96% identity to a putative Gcd of *B. xenovorans* LB400 (YP_554209.1), which has a short-chain dehydrogenases/reductases family signature (Prosite pattern PS00061) and is a NAD(P)-dependent oxidoreductase. It is possible that GA is synthesised in *Burkholderia* sp. Ha185 by this putative NAD(P)-dependent Gcd inside the cytoplasm before converting it to 2-KGA in the periplasmic space. However, a low level of GA was detected at every time point tested during HydroxP solubilisation. This indicates either the conversion of GA to 2-KGA is too rapid to allow detection of GA in the culture filtrate, and/or GA remained inside the bacterial cytosol and was not transported outside of the cell. However, no GA was detected in the HSU HydroxP liquid culture filtrate or the *Burkholderia* sp. Ha185 sonicated cell pellet at 72 h post-inoculation, possibly indicating that all of the GA was converted to 2-KGA.

4.4.2. 2-ketogluconic acid is the predominant organic acid released by *Burkholderia* sp. Ha185

It was identified that 2-KGA was the predominant organic acid released by *Pseudomonas* spp. strains and *Burkholderia* sp. Ha185, a finding that as discussed in Chapter 2, contradicts other previous findings. There are two possible reasons for why 2-KGA is the predominant organic acid released by *Burkholderia* sp. Ha185 and the other EPS strains identified in Chapter 2:

(i) 2-keto gluconic acid is more effective at MPS than GA.

First, 2-KGA has a lower pK_a dissociation constant than GA, indicating that it is a stronger acid and would theoretically be more effective at dissolution of HydroxP (as discussed in Chapter 2.4.2). However, the form of 2-KGA used in this study (hemicalcium salt hydrate) could not solubilise HydroxP, possibly due to excess calcium bound to 2-KGA at pH 5.04 (500 mM) (Section 4.3.4.6). This

suggested that MPS is pH dependent. Furthermore, using the two-step linear formula derived from HydroxP solubilisation by 2-KGA (Section 4.3.4.5), the observed amount of 2-KGA released by *Burkholderia* sp. Ha185 in the culture filtrate was two-fold lower than the predicted value.

These observations suggest that although 2-KGA was the key organic acid responsible for HydroxP solubilisation by chelating calcium and thus releasing soluble P, decreasing the pH, possibly by protonation at the peripheral plasma membrane of the bacterial cell wall, may also facilitate P solubilisation. It has been reported that 2-KGA is the predominant organic acid produced by microorganisms found in the rhizosphere of agriculture soil (Webley and Duff, 1965). Furthermore, the authors proposed that calcium chelation by 2-KGA-producing P solubilising bacteria is the primary mechanism for P solubilisation in soil, and that 2-KGA is an effective chelating agent. However, this concept was opposed by Moghimi and Tate (1978), who suggested that chelation alone is insufficient for P solubilisation, and that alternatively, a rapid decrease in the pH of the surrounding environment is required for the reaction to occur. This theory is consistent with findings from the current study in that although 2-KGA can theoretically chelate calcium ions, HydroxP solubilisation is also a result of increased solubility of calcium salt at low pH.

(ii) Metabolic energy could be wasted by releasing GA.

Second, it is likely that secretion of GA outside of bacterial cell is a metabolically inefficient pathway. The uptake of GA by the cell leads to its conversion by gluconokinase (encoded by *gunk*, also known as *gntK* in *Burkholderia* spp.) to 6-phospho-D-gluconate (6P-GA) using ATP (de Werra et al., 2009) (Figure 3.1.55). tBLASTn identified a *gntK* orthologue in Contig00630 of the *Burkholderia* sp. Ha185 draft genome, the translated product of which shows 95% amino acid sequence identity to GntK of *B. phytofirmans* PsJN (YP_001896982.1) (Section 4.2.2). Furthermore, HPLC analysis of *Burkholderia* sp. Ha185 HSU HydroxP culture filtrate revealed that 2-KGA concentration was significantly lower at day 7 than at day 3 (Chapter 2.4.3.1). Based on these findings, it is postulated that re-uptake of GA increases carbon flux to the Entner-Doudoroff pathway (ED pathway), replenishing the TCA cycle when glucose is depleted (Figure 3.1.55). Therefore, it is possible that re-uptake of 2-KGA by the cell plays a role in replenishing the TCA cycle under carbon-limiting conditions.

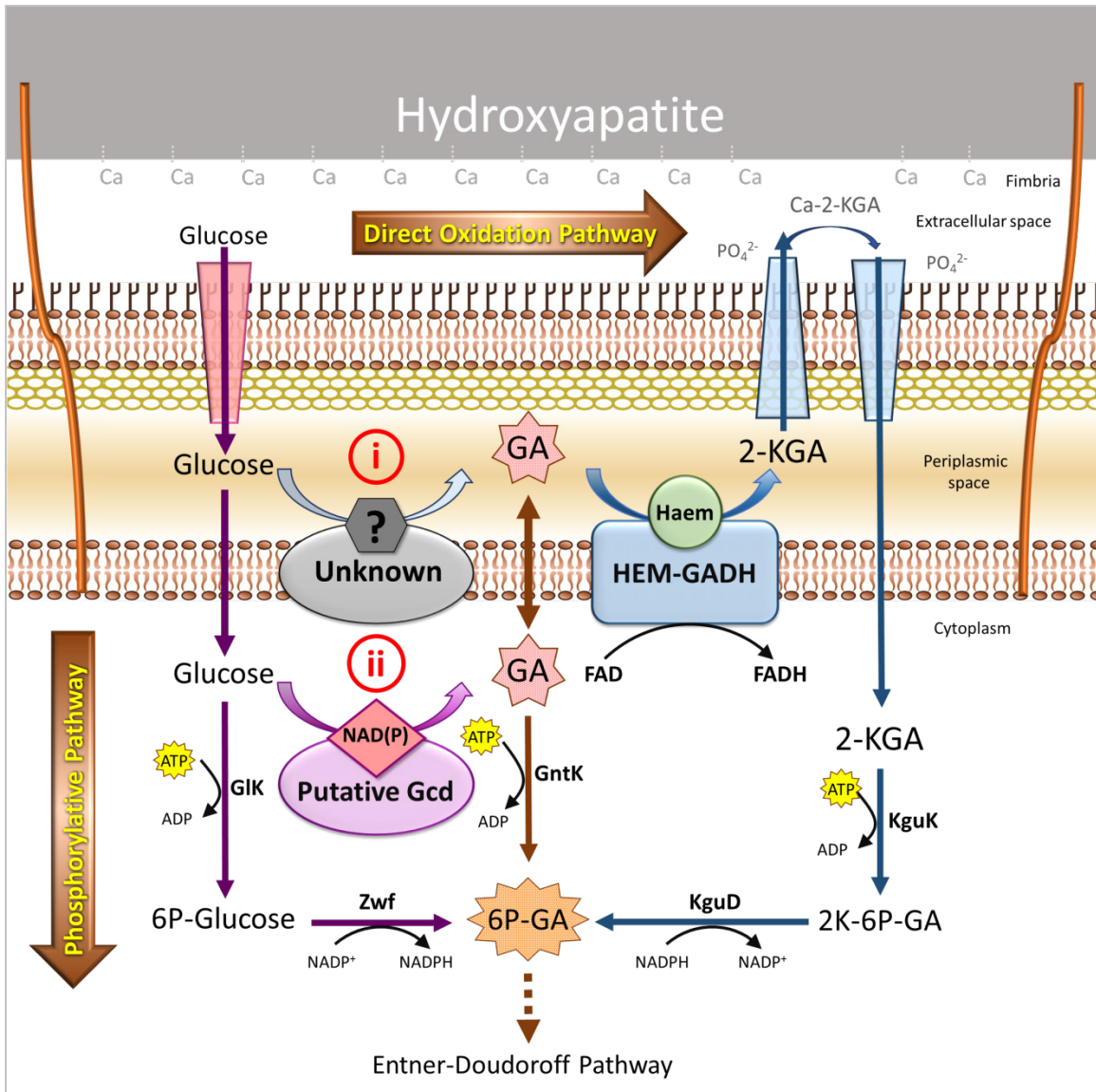


Figure 4.4.1 Direct oxidation pathway model for *Burkholderia* sp. Ha185. Hydroxyapatite solubilisation by 2-KGA derived from membrane-bound haem-dependent gluconate 2-dehydrogenase (HEM-GADH) using GA as a substrate and a haem molecule as the cofactor. Two possible pathways might be involved in oxidising glucose to GA in *Burkholderia* sp. Ha185: (i) an unknown membrane-bound enzyme also possesses a redox cofactor for the oxidation-reduction process or, (ii) NAD(P)-dependent putative glucose dehydrogenase (Gcd) is involved in converting glucose to GA in the cytoplasm. The phosphorylative pathway involves glucokinase (GIK, Contig00197), gluconokinase (GntK, Contig00630), 2-ketogluconate kinase (KguK, Contig00700), glucose-6-phosphate 1-dehydrogenase (Zwf, Contig00007), 2-ketogluconate-6-phosphate reductase (KguD, Contig00314), glucose 6-phosphate (6P-Glucose), 6-phosphogluconate (6P-GA) and 2-keto-6-phosphogluconate (2K-6P-GA).

The re-uptake of 2-KGA by the cell would enable its conversion to 2-keto-6-phosphogluconate (2K-6P-GA) by 2-ketogluconate kinase (KguK). A *kguK* gene coding for this enzyme was found in Contig00700 of the *Burkholderia* sp. Ha185 genome, the translated product of which showed 96%

amino acid identity to KguK of *B. phytofirmans* PsJN (YP_001895901.1). Although 2-KGA can also be reduced to 6P-GA by the phosphorylative pathways, an additional step of reducing the 2K-6P-GA to 6P-GA by 2-ketogluconate-6-phosphate reductase (KguD, Contig00314, 96% identity to KguD of *B. xenovorans* LB400, YP_559944.1) is required. Therefore, it is postulated that retaining GA within the bacterial cell is metabolically more efficient than transporting it outside of the cell for P solubilisation. Consequently, it is possible that 2-KGA is a preferred secondary metabolite for *Burkholderia* sp. Ha185 over GA, as it is more efficient in HydroxP solubilisation, whereas the retention of GA in the cell regulates the central metabolism of both the ED pathway and the TCA cycle. It is possible that GA is only secreted to the periplasmic space when required. To investigate these proposed theories, microarray-based expression comparison of mutations in *glk*, *gntK* and/or *kguK* in response to transcriptional control during HydroxP solubilisation by *Burkholderia* sp. Ha185 should be undertaken.

Interestingly, MA had a greater ability than PyrA and GA to solubilise HydroxP. MA also has a lower dissolution constant ($pK_{a1} = 3.40$, $pK_{a2} = 5.20$) than GA ($pK_a = 3.86$) (Sillén et al., 1958). Furthermore, MA contains carboxyl groups at the C₁ and C₄ positions, and oxygen molecules at these two positions can theoretically chelate calcium from HydroxP, and thus solubilise P. However, it was found that *Burkholderia* sp. Ha185 did not release MA during HydroxP solubilisation. This suggests that even though MA was more efficient at solubilising HydroxP than GA, PyrA and LA, secreting MA is not an effective pathway for *Burkholderia* sp. Ha185. MA is generated by fumarase and/or malate dehydrogenase (MDH), where fumarase hydrates fumaric acid to MA, and MDH can catalyse the interconversion between oxaloacetate and malate (Garrett and Grisham, 1995). Lü et al. (2012) identified a highly efficient TCaP-solubilising fungus, *Penicillium oxalicum* C2, from Mexican stonecrop rhizospheric soil. The authors amplified the gene coding for the mMDH protein and cloned it into pET32a, generating pET32a-mMDH. The construct expressed in *E. coli* BL21(DE3) exhibited higher MDH activity and TCaP solubilisation than the negative control construct in a plate assay. Organic acid profiling of the culture filtrates from *E. coli* BL21(DE3) pET32a-mMDH revealed increased secretion of MA, acetic acid, citric acid, oxaloacetic acid and LA, all of which are secondary metabolites of the TCA cycle (Xiaorong et al., 2012). However, the inability to detect these organic acids (except from the breakdown product LA from PyrA) during HydroxP solubilisation by *Burkholderia* sp. Ha185 suggests that this may not be the preferred P solubilisation pathway for *Burkholderia* sp. Ha185.

4.4.3. Mannitol metabolism of *Burkholderia* sp. Ha185

It was observed that *Burkholderia* sp. Ha185 was unable to utilise mannitol for HydroxP solubilisation. Interestingly, in the HSU HydroxP liquid culture assay, the *hemX::Tn5(F18)* mutant either secreted or released additional, yet to be characterised, organic acids Un3 and Un4. A similar organic acid profile was observed for *Burkholderia* sp. Ha185 grown in medium with mannitol as the sole carbon source. This suggests that the central glucose metabolism of *hemX::Tn5(F18)* has possibly shifted to a pathway similar to that of mannitol metabolism. Mannitol metabolism has been studied using lactic acid- and acetic acid-producing bacteria as model systems (Wisselink et al., 2002; Richhardt et al., 2012). Although mannitol metabolism has not been well investigated in *Burkholderia* spp., *Burkholderia* spp. can utilise mannitol as a carbon source for cellular growth (Andreolli et al., 2011, Chen et al., 2012, Weber et al., 2012). In particular, isolates DNB16 (closely related to *Burkholderia oxiphila* OX-01) and PP52-1 (related to *Burkholderia mimosarum* PAS44 (Figure 4.1.1) were found to assimilate mannitol (25 mM) as a main carbon source and maintain high cell growth, whereas both isolates failed to grow in 25 mM of sucrose over a 24 h period (Weber et al., 2012). Mannitol catabolism has been investigated by Richhardt et al. (2012) using the Gram-negative α -proteobacterium *Gluconobacter oxydans* as a model. In this system, mannitol is first transported into the cell by a mannitol-specific transporter, where it is converted to fructose then fructose-6-phosphate (fructose-6-P), before entering the fructolysis pathway or the ED pathway. It then moves through the TCA cycle inside the cytosol (Figure 4.4.2). In contrast, in lactic acid bacteria, mannitol is typically oxidised by mannitol 1-phosphate dehydrogenase to the intermediate fructose-6-P directly (Wisselink et al., 2002). There were no matches to the mannitol dehydrogenase domain from either *B. phytofirmans* PsJN (YP_001888457.1) or *Burkholderia phymatum* STM815 (YP_001856736.1) in the *Burkholderia* sp. Ha185 genome using tBLASTn (Section 4.2.2).

Another enzyme involved in the fructolysis pathway is the *pgi* gene-product glucose-6-phosphate isomerase, which isomerises fructose-6-P to glucose-6-P (Figure 4.4.2). DNA comparison of the *B. xenovorans* LB400 (YP_558734.1) *pgi* sequence to the draft *Burkholderia* sp. Ha185 sequence revealed a *pgi* orthologue in Contig00924 (637–2259 bp). Hence, *Burkholderia* sp. Ha185 should also be able to isomerise fructose-6-P to glucose-6-P, which would then enter the TCA cycle via the ED pathway. This pathway would bypass the formation of GA, which would correlate with the inability to detect GA in the HSU HydroxP-M *Burkholderia* sp. Ha185 liquid culture supernatant. The inability of *Burkholderia* sp. Ha185 to solubilise HydroxP in the presence of mannitol as the sole carbon source was confirmed by the lack of halo formation in the HydroxP-M plate assay (Section 4.3.4). Interestingly, a basal level of HydroxP solubilisation by *Burkholderia* sp. Ha185 did occur using mannitol as the carbon source (1.82 ± 0.72 mM, 72 h), possibly due to released PyrA and LA. This

suggests that fructolysis and the ED pathway are not likely pathways for HydroxP solubilisation, and that PyrA involved in the TCA cycle is implicated in MPS.

4.4.4. pH-dependent hydroxyapatite solubilisation

Using glucose as the sole carbon source, the pH of the *Burkholderia* sp. Ha185 culture filtrate at 72 h was 5.07 ± 0.02 (Section 4.3.4.3). However, when mannitol was used in place of glucose, a low level of HydroxP was solubilised, decreasing the pH to 4.98 ± 0.02 . Analysis of the pH level over time during HydroxP solubilisation by *Burkholderia* sp. Ha185 revealed that the initial culture pH was 6.5, which decreased to 5.36 ± 0.02 at 24 h, and to 4.24 ± 0.05 at 48 h, followed by a subsequent increase to 5.10 ± 0.04 at 72 h. This suggests that HydroxP solubilisation requires a decrease in pH to occur. The decrease in pH during P solubilisation is widely reported, although some researchers have suggested that decreased pH is an important factor, but is not the only mechanism involved in P solubilisation (Asea et al., 1988; Kim et al., 1997). Identification and quantification of organic acids released during HydroxP solubilisation by *Burkholderia* sp. Ha185 showed that high concentrations of 2-KGA were present in the culture medium (Table 4.3.6), and that 2-KGA is the predominant organic acid found in the liquid culture filtrate at 48 and 72 h. Even though the pH of the HydroxP-M *Burkholderia* sp. Ha185 culture dropped to 4.98 ± 0.02 at 72 h, HydroxP could not be solubilised without the presence of 2-KGA. This highlighted the importance of the carboxyl group of 2-KGA for chelating calcium from HydroxP, and subsequently releasing soluble P into the liquid culture medium. Although high 2-KGA concentrations were identified in the 72 h culture, it is suspected that this 2-KGA is calcium-bound, meaning that no additional HydroxP solubilisation could take place. The final pH was ~ 5.10 , which correlates with a reduction in 2-KGA concentrations in the culture filtrate at 72 h. HPLC analysis was unable to identify the difference between calcium-bound and oxidised forms of 2-KGA. This is because sulphuric acid was employed as the mobile phase for the HPLC Rezex ROA-Organic Acid H+ (8%) column to allow the separation of organic anions. Therefore, any solute passing through the HPLC column is in its oxidised form (2-KGA).

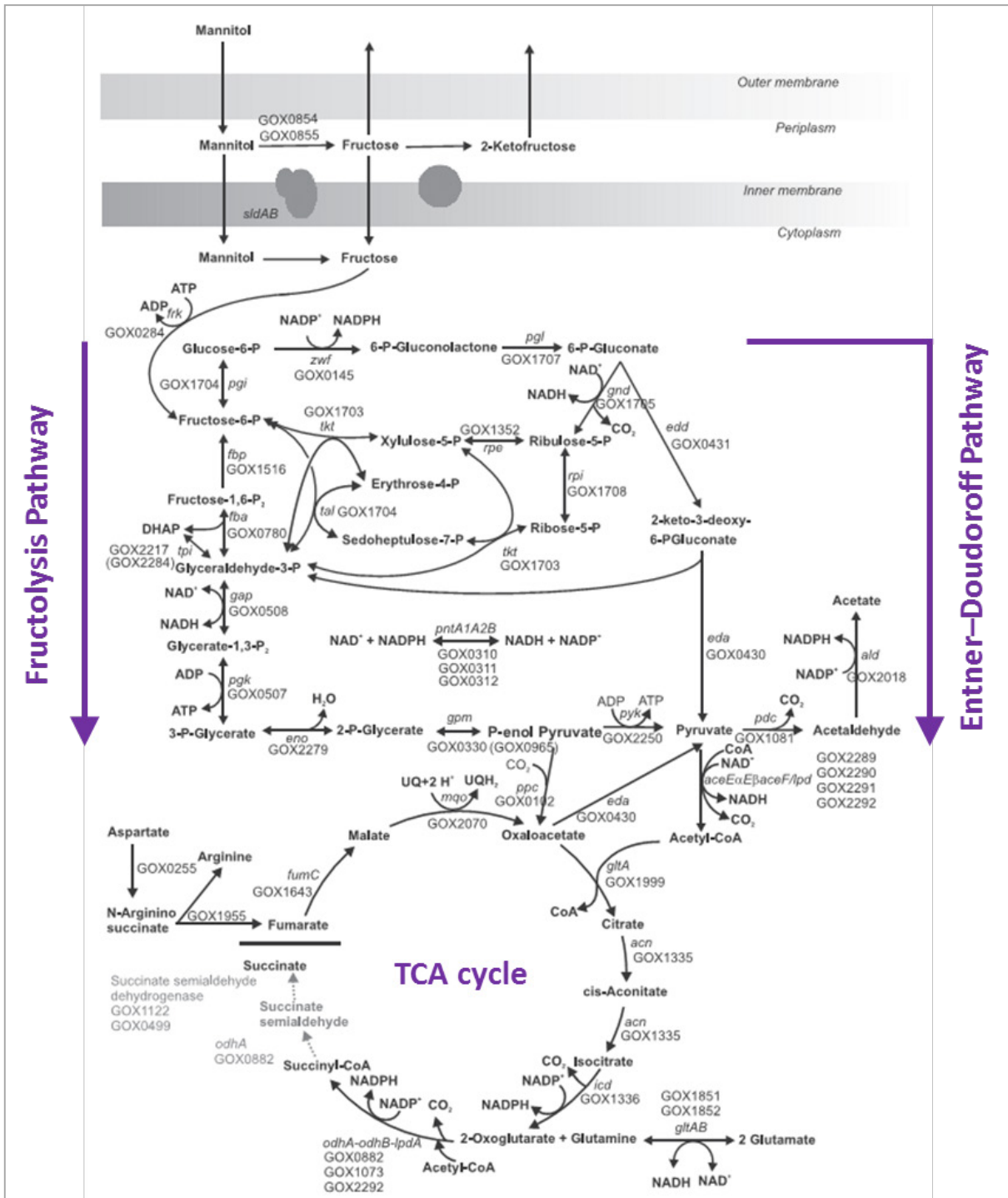


Figure 4.4.2 Schematic of the central carbon metabolism of acetic acid bacterium *Gluconobacter oxydans* using mannitol as a substrate. Diagram modified from Richardt et al. (2012).

Interestingly, the complemented *hemX*::Tn5(F18) strain CD3ME12, containing *hemC* + *hemX* on the *trans* complementation plasmid pCD3ME, released significantly more 2-KGA than wildtype

Burkholderia sp. Ha185 in the HSU HydroxP medium at 72 h. The pH of the final CD3ME12 culture filtrate was also significantly lower than the wildtype control. The complemented *hemX::Tn5(F18)* strain DXDME6, expressing *hemX* alone on the pDXDME vector, also had a significantly lower culture pH and elevated 2-KGA production compared with the wildtype at 72 h. These differences may be due to elevated synthesis of the precursor of haem cofactor, resulting from overexpression of *hemC* + *hemX* or *hemX* by the high copy number shuttle vector pME6010. Although the end product of haem biosynthesis involving genes from the *hem* operon is not known, it is thought to be either haem or haem d_1 porphyrin (Section 4.3.3.1). These porphyrin molecules are structurally similar but have slight differences in functional groups, however both contain a ferrous ion (Fe^{2+}) centre that acts as an electron sink. Cobalamine (vitamin B12), which shares a similar ring structure with the porphyrin molecule, was also exogenously added to a *hemX::Tn5(F18)* mutant HSU HydroxP liquid culture assay (Section 4.3.3.2). The inability of cobalamine to restore loss of P solubilisation by *hemX::Tn5(F18)* indicated that one of the end products of the haem biosynthesis pathway, cobalamine, is not involved in P solubilisation by *Burkholderia* sp. Ha185.

Furthermore, the final pH increased from 6.5 to 7.23 ± 0.01 at 72 h post-inoculation when *Burkholderia* sp. Ha185 was incubated in HSU-P culture medium (soluble P was supplied instead of HydroxP). This suggests that acidification by *Burkholderia* sp. Ha185 is not necessary under P-rich conditions, and that the maintenance of a near neutral pH is preferable.

4.4.5. Genes of the *hem* operon

Random mutagenesis undertaken in Chapter 3 identified a *Burkholderia* sp. Ha185 mutant, later designated *hemX::Tn5(F18)*, with a transposon insertion in *hemX* resulting in impaired HydroxP solubilisation, as visualised on a HydroxP plate. The HSU HydroxP liquid culture medium assay showed that 2-KGA is the predominant organic acid released by *Burkholderia* sp. Ha185, and is likely responsible for the HydroxP solubilisation as 2-KGA was not detected at 48 h in the *hemX::Tn5(F18)* mutant culture where a basal level of HydroxP was solubilised, possibly by the PyrA. Co-occurrence analysis (Section 4.3.3.2) of *hemX* revealed a multi-domain (*hemD* and *hemX*) ORF that synthesises bifunctional uroporphyrinogen III synthase/uroporphyrin-III C-methyltransferase, and is conserved within the *Burkholderia* spp.

The *mfs* gene codes for the MFS protein, which transports various molecules such as sugars, oligosaccharides, phosphate, sodium ions, aromatic compounds and small metabolites (Pao et al.,

1998). Interestingly, proteins in this major facilitator superfamily of transmembrane transporters, such as the feline leukaemia virus subgroup C receptor 1 (FLVCR1), were reported to export haem molecules, and FLVSCR2 was found to import haem in mammalian cells (Quigley et al., 2004; Duffy et al., 2010). Furthermore, the haem carrier protein 1 (HCP1) of the Caco-2 cell line (human epithelial colorectal adenocarcinoma cells), which also belongs to the major facilitator superfamily, acts as a haem-Fe transporter (Le Blanc et al., 2012). This evidence suggests that the protein encoded by *mfs* downstream of the *hem* operon might also involve in haem transportation.

qRT-PCR analysis of *hemC*, *hemX* and *ppc* revealed that *hemC* is significantly over-expressed at 24 h post-inoculation in HSU HydroxP liquid culture medium relative to the expression of reference genes (*gltB*, *recA*, and *gyrB*) from cultures grown in HSU HydroxP or HSU-P liquid medium. However, the expression of *hemC* and *hemX* was comparable to that of reference genes at 36 and 40 h when HydroxP was being solubilised. This suggested that *Burkholderia* sp. Ha185 haem biosynthesis only occurs in the early stages of cell growth. The non-proteinaceous haem may be recycled by the bacteria, negating the need for it to be constitutively synthesised. Interestingly, *hemC* was significantly under-expressed compared with the reference genes at 48 h when nutrients are depleted, and 2-KGA was found at highest concentration in the culture filtrate. Furthermore, *ppc* was significantly under-expressed during HydroxP solubilisation at 36 and 40 h. *ppc* encodes the enzyme PEPC, which catalyses the formation of oxaloacetate from phosphoenolpyruvate (PEP) and a hydrocarbonate ion, which replenishes carbon flow through the TCA cycle (Eikmanns et al., 1989; Peters-Wendisch et al., 1993). Buch et al. (2010) studied glucose catabolism of *P. fluorescens* ATCC 13525 over-expressing *ppc* from *Synechococcus elongates* PPC 6301. The authors reported that carbon flow through the direct oxidation pathway was increased under P limiting conditions. Over-expression of *S. elongates ppc* enhanced the intracellular phosphorylative pathway and resulted in increased P solubilisation by increasing concentrations of organic acid from the TCA cycle, such as PyrA and acetic acid. Interestingly, extracellular GA levels were significantly reduced when *ppc* was over-expressed in *P. fluorescens* ATCC 13525. In the current study, genes from the *hem* operon were not over-expressed compared with reference genes during HydroxP solubilisation, but *ppc*, located 5' of the *hem* gene cluster, was comparatively under-expressed. This indicates that in HSU HydroxP liquid culture, genes involved in the direct oxidation pathway (i.e. *hem*) and genes involved in the ED pathway (i.e. *ppc*) are inversely expressed (Figure 3.1.40).

4.4.6. Haem-dependent gluconate 2-dehydrogenase

Complementation of *hemX::Tn5(F18)* using the vectors pCD3ME or pDXDME, bearing *hemC* + *hemX* and *hemX*, respectively, not only increased HydroxP solubilisation, but also resulted in greater amounts of 2-KGA in the culture supernatant relative to the wildtype *Burkholderia* sp. Ha185 at 72 h. This indicates that *hemX* is directly involved in the production of 2-KGA, and is the first report of *hemX* playing a role in HydroxP solubilisation.

Mutation of *hemX* (*hemX::Tn5(F18)*) reduced the amount of 2-KGA produced and impaired HydroxP solubilisation. This indicated that the haem redox cofactor is the key molecule for function of the GADH enzyme complex (Section 4.3.6). Peripheral membrane-bound GADH is composed of three subunits belonging to the oxidoreductase superfamily. These proteins use the CH-OH group from GA as an electron donor and the ferrous ion (Fe^{2+}) from the haem cofactor as an electron acceptor (Matsushita et al., 1982). Therefore, because of the haem-dependency of *Burkholderia* sp. Ha185 GADH, it is hereafter named “HEM-GADH”. It is suspected that HEM-GADH also consists of three protein subunits: a FAD-dependent GADH (subunit I, gene located in Contig00115), subunit III (gene located upstream of Contig00115), and a haem-dependent GADH (encoded by *gadh(II)*) (Figure 3.1.57). Within the *Burkholderia* sp. Ha185 genome, six ORFs were identified that align to *gadh(II)* of *B. phytofirmans* PsJN. However, it is unknown which ORF contributes to the overall HEM-GADH complex. The sequence of the *Burkholderia* sp. Ha185 *gadh(II)* homologue located in Contig00447 shows 87% DNA sequence identity to *gadh(II)* of *B. phytofirmans* PsJN (241745–246148 bp), which is located downstream of the *gadh(III)* and *gadh(I)* ORFs (Figure 3.1.57). To confirm the function of the HEM-GADH complex in *Burkholderia* sp. Ha185, the presence of these three subunits in a single operon needs to be confirmed. The three ORFs could then be expressed in a bacterial host that does not possess the HEM-GADH complex, but does contain the *hem* cluster, such as the *E. coli* strain BL21(DE3) (*hemC*, YP_003001366.1; *hemD*, YP_003001365.1; *hemX*, YP_003056242.1; and *hemY*, YP_003056241.1). However, because *E. coli* strain BL21(D3) does not contain a PQQ operon, and is unable to synthesis PQQ, the direct oxidation pathway converting glucose to GA is not likely to occur by Gcd (*gcd*, YP_003052795.1) in the periplasmic space. For this reason, to synthesise GA, which is the substrate for the HEM-GADH complex, exogenous PQQ would be required for the oxidation to take place.

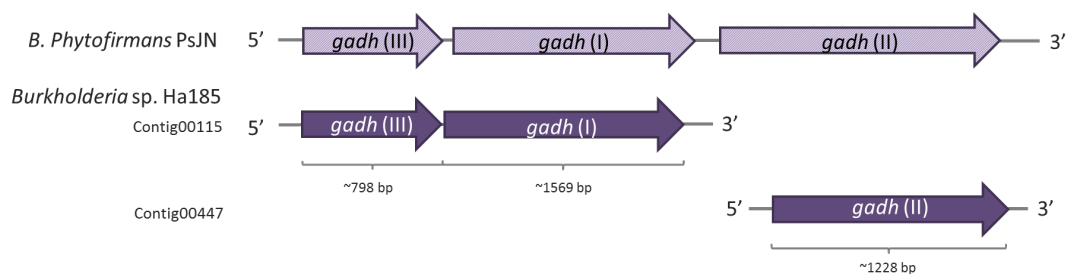


Figure 4.4.3 *Burkholderia* sp. Ha185 Contig00447 and Contig00115 (dark purple) are homologous to the *B. phytofirmans* PsJN *gadh* operon (chromosome 1; 241,745–246,148 bp, light purple). *gadh*(I), *gadh*(II) and *gadh*(III) code for FAD-dependent GADH, haem-dependent GADH and GADH protein, respectively.

Furthermore, given the high level of genome plasticity and gene redundancy in *Burkholderia*, it is possible that all six independent ORFs (**Figure 4.3.38**) coding for the haem-dependent GADH(II) are involved in the HEM-GADH complex, which oxidises GA to 2-KGA. To investigate the function of each haem-dependent GADH within the HEM-GADH complex, each *gadh*(III) homologue from *Burkholderia* sp. Ha185 needs to be independently cloned into an expression vector along with the *gadh*(I) and *gadh*(III) ORFs (Contig00115) and expressed in *E. coli* BL21(D3) to confirm the production of 2-KGA, and subsequent solubilisation of HydroxP.

The haem-dependent GADH (subunit II) of *E. cyripedii* ATCC 29267, located within the *gadh* operon, also consists of three haem-binding motifs (CXXCH) that are identical to those in HEM-GADH, as described earlier. Yum et al. (1997) determined that the optimal pH for GADH activity is pH 5.0, which was within previously reported range of pH 4.0–5.0 (Matsushita et al., 1982). These findings are in agreement with findings of the current study, where during the HydroxP solubilisation, the pH dropped from 6.5 (0 hours) to 4.24 ± 0.05 (48 h), a pH postulated to be optimal for HEM-GADH activity. Yum et al. (1997) also found that when exogenous PQQ was added to a culture of *E. coli* JM109 pGA313 (containing the *gadh* operon), all glucose present in the medium was converted into 2-KGA, with a basal level of GA present in the medium. A similar approach was undertaken by Kumar et al. (2013), who successfully cloned the *P. putida* KT 2440 *gadh* operon into the plasmid pCNK14 and expressed it in *Enterobacter asburiae* PSI3. The authors found that the pCNK14 transformant exhibited P rock (PR) solubilisation, with the production of both GA and 2-KGA in a Tris-rock P-buffered medium. The *E. asburiae* PSI3 negative control (without the *gadh* operon) did not solubilise PR, but did produce high concentrations of GA, and no 2-KGA was detected. The authors concluded that PR solubilisation was as a result of releasing 2-KGA along with GA. This also confirmed the

phenomenon discussed earlier (Chapter 2.4.2) whereby GA alone is probably insufficient for PR solubilisation, thus production of 2-KGA is necessary for HydroxP solubilisation.

The third subunit of GADH is a protein involved in converting GA to 2-KGA. The N-terminus of the protein contains a conserved domain with a Tat signal profile (Prosite PS51318). Proteins that contain a Tat signal profile are exported by the Tat system located in the cytoplasmic membrane of the bacterial cell. One of the features of this transportation pathway is that Tat translocates fully folded proteins from the cytoplasm across the inner cytoplasmic membrane using a transmembrane proton electrochemical gradient (Wickner and Schekman, 2005). This is unlike the Sec protein pathway, which transports unfolded proteins (Mori and Ito, 2001). The N-terminal signal peptide of proteins containing a consensus double arginine motif ([ST]-R-R-X-F-L-X) target the Tat apparatus for protein translocation to the cytoplasmic membrane (Lee et al., 2006). Based on this information, it is likely the GADH-encoding ORF (subunit III, *gadh(III)*) located in Contig00115, whose translated product contains the Tat signal profile, is transported via the Tat pathway (Figure 3.1.53).

Interestingly, the *Gluconobacter oxydans* mutant strain MF1, containing a mutation in *gadh(I)*, was still able to convert 84% of available glucose into 5-KGA, with no 2-KGA by-product (Elfari et al., 2005). Similarly, a mutation in *gadh(I)* of *Gluconobacter* strains THE42, THE55 and THG42 increased the production of 5-KGA by converting almost 90% of glucose into 5-KGA (Saichana et al., 2009). Hence, the inability to detect 5-KGA organic acid from either the *hemX::Tn5(F18)* mutant or the wildtype *Burkholderia* sp. Ha185 strain, combined with bioinformatic analysis results, indicates that a PQQ-dependent gluconate-5-dehydrogenase may not be present in this bacterial strain.

4.4.7. Gene redundancy in *Burkholderia* sp. Ha185

The production of 2-KGA was not completely abolished in the *hemX::Tn5(F18)* mutant, suggesting that another protein with similar function to HEM-GADH may also be produced. *Burkholderia* species are well known for having large multireplicon genomes, with many strains having at least two individual chromosomes (Mahenthiralingam and Drevinek, 2007). The draft genome sequence of *Burkholderia* sp. Ha185 revealed a genome size of approximately 8.55 Mb, which is relatively large compared with the 4.6-Mb of *E. coli* genome. A large amount of gene redundancy is found in *Burkholderia* species genomes. Many *Burkholderia* strains contain multiple paralogous genes, which are involved in processes such as benzoate degradation and formaldehyde oxidation in *B. xenovorans* LB400, and salicylate transport in *Burkholderia cenocepacia* (Denef et al., 2006; Marx et al., 2004;

Drevinek et al., 2008;). Gene duplication and redundancy are thought to reflect the ability of *Burkholderia* to occupy a wide range of ecologically diverse habitats, as outlined in Section 4.1.1.1. The high level of genome plasticity and gene redundancy in *Burkholderia* increases the likelihood of the presence of another protein that, when produced inside the cytosol, has a similar function to HEM-GADH. A candidate for this would be a NADPH-dependent gluconic acid-2-dehydrogenase that converts GA to 2-KGA inside the cytoplasm (Elfari et al., 2005). An extended time period was required for the *hemX::Tn5(F18)* mutant to convert GA to 2-KGA (Section 4.3.4). To confirm the existence of another protein that might have similar function to HEM-GADH, the HSU HydroxP liquid culture assay should be continued beyond 72 h to determine the presence of a haem-independent pathway for synthesising 2-KGA. A genomic search for proteins with similar properties may also be helpful.

Furthermore, it is also possible that in the absence of haem, another cofactor with a similar structure to haem or haem d_1 could bind to HEM-GADH and act as a pseudo-cofactor to activate the protein. The 5' location of *hemC* means that it is likely to be translated in a *hemX::Tn5(F18)* background, enabling the constitutive biosynthesis of hydroxymethylbilane. The affinity of haem to HEM-GADH is unknown, therefore the possibility of another cofactor with a similar molecular structure acting on HEM-GADH with low binding affinity cannot be ruled out.

4.4.8. Genes of the *bxp* operon and their resultant protein function

Random transposon mutagenesis performed in Chapter 3 generated a mutant library for *Burkholderia* sp. Ha185. A transposon insertion in *bxpC* generated a strain (*bxpC::Tn5(F13)*) with decreased ability to solubilise HydroxP compared with the wildtype. However, unlike *hemX::Tn5(F18)*, HydroxP solubilisation was not completely abolished. This indicates *bxpC* is not directly linked to *Burkholderia* sp. Ha185 HydroxP solubilisation, but is dependent on the presence of this gene. Reverse transcription PCR revealed that the *bxp* genes were transcribed as a single transcript during HydroxP solubilisation, hence a complete *bxp* operon was defined. The *bxp* operon consists of five ORFs, *bxpA–E*, with no clear functions. Suggested functions for each ORF were extrapolated from experimental data and bioinformatic analysis, as outlined below.

4.4.8.1 *bxpA* is related to *vgrG* from T6SS loci

Amino acid sequence analysis of BxpA revealed similarity to Rhs element VgrG protein from *Burkholderia* sp. CCGE1003 (YP_003907491.1), which contains several conserved domains related to the T6SS (Table 4.3.2). T6SSs are a newly defined mechanism for protein transportation in bacteria that were first described in human pathogens *Pseudomonas aeruginosa* and *Vibrio cholerae* by

Mougous et al. (2006) and Pukatzki et al. (2006). Genes involved in T6SSs are widespread throughout Gram-negative bacterial genomes, including *Burkholderia* spp., *Pseudomonas* spp., *Yersinia* spp., *Klebsiella* spp. and *Salmonella* spp. (Miyata et al., 2013; Zhang et al., 2011; Gueguen et al., 2013; Sarris et al., 2011; Mulder et al., 2012). T6SSs have not only been implicated in the virulence of human, animal and plant pathogens (Sana et al., 2012, Hasan et al., 2013; Liu et al., 2013; Marchi et al., 2013), but also in bacterial interactions and competition (Russell et al., 2011; Kapitein and Mogk, 2013). T6SS proteins are usually encoded within a conserved locus composed of 12–25 core proteins. The T6SS apparatus is a long tubular structure composed of an inner tube of Hcp and a VipA/VipB contractile sheath (Boyer et al., 2009; Records, 2011, **Figure 4.4.4**). In appearance, the T6SS apparatus is structurally similar to the cell-puncturing device of T4 bacteriophages, with an inverted phage tail appearance on the surface of the bacterial cell known as VgrG (Leiman et al., 2009; Cascales and Cambillau, 2012, **Figure 4.4.4**). A tertiary tetrameric VgrG needle complex protein structure (PDB 2p5z) with C3 symmetry structurally resembles the T4 bacteriophage tail spike (gp27 - gp5, PDB 1k28) (Cascales and Cambillau, 2012) (**Figure 4.4.4**). VgrG is an effector delivery mechanism that injects proteins or toxins directly into target cell membranes (Hood et al., 2010; Russell et al., 2011, Records, 2011).

The translated product of *bxpA* shows 86% sequence identity to the Rhs element VgrG protein of *Burkholderia* sp. CCGE1003, and is postulated to have a similar structure and function to the Rhs element and VgrG protein. A typical Rhs element protein consists of repeated β -strands forming a single long β -sheet shell-like structure, as recently identified for the Tc-BC protein subcomplex of the ABC toxin complex of *Yersinia entomophaga* (Busby et al., 2013). VgrG also contains a β -helix formed by nine short β -strands, resulting in a tube-like structure (Shneider et al., 2013, **Figure 4.4.4**). Therefore, it is postulated that *bxpA* codes for a protein that forms a β -barrel-like cavity, similar to both the C protein of the ABC toxin complex and VgrG. Interestingly, *bxpA* encodes a conserved hypothetical protein that contains a C-terminal extension of a duf2345 domain (IPR018769), which indicates that BxpA could be one of the “evolved” VgrG proteins. Typically, VgrG proteins have a C-terminal extension(s) that carries functional effector domains involved in peptidoglycan binding, mannose binding and adhesion activity (Records, 2011; Pukatzki et al. 2007). It is therefore possible that the C-terminal extension of BxpA has a function in plant-microbe or bacterial interactions.

Within the T6SS locus, *vgrG* is commonly found in proximity to *hcp*, the translated product of which interacts with VgrG to form the T6SS (Boyer et al., 2009). However, recent studies showed that “orphan” *vgrG* genes are often found scattered within bacterial genomes as single genes instead of being part of the T6SS locus (Barret et al., 2011). The role of orphan VgrG proteins is not known, but

it was suggested that they may also interact with effector proteins via a different secretion apparatus (Bröms et al., 2012).

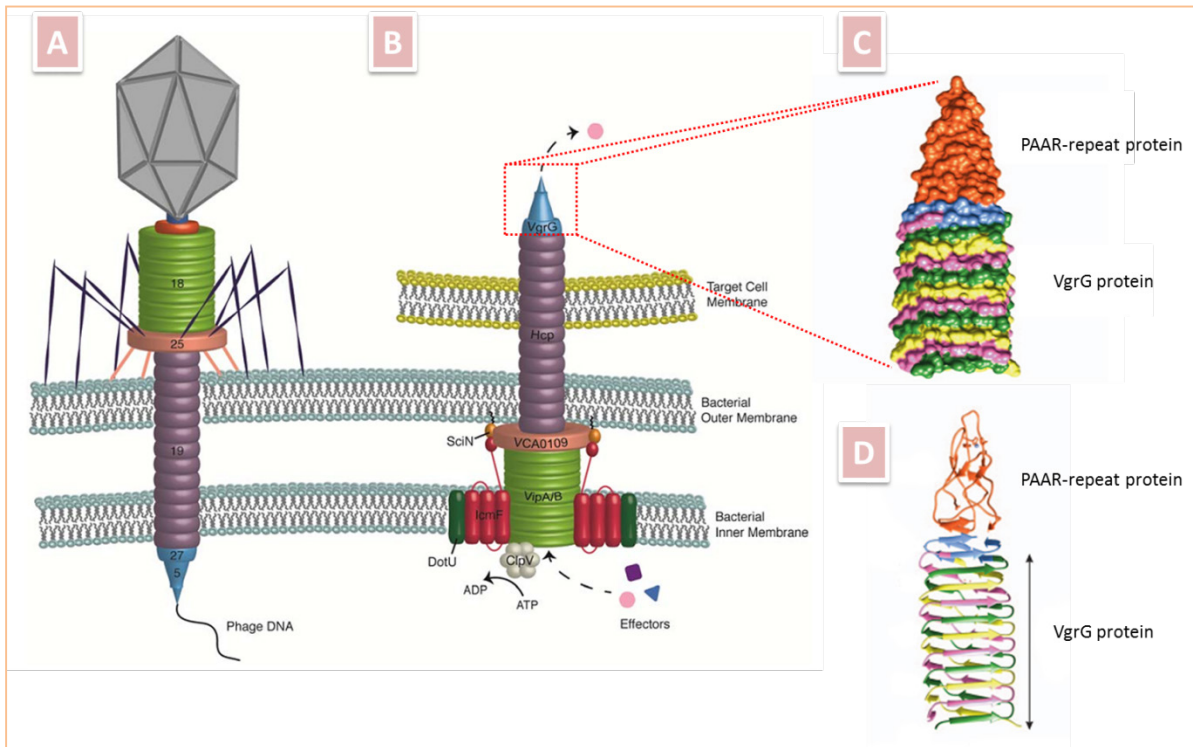


Figure 4.4.4 Schematic representations showing bacteriophage T4 structure (A), T6SS assembly (B), the solid surface of the VgrG-PAAR complex crystal structure (C) and secondary protein structure of the VgrG-PAAR complex, represented in a ribbon diagram (D). The T6SS model was predicted by protein sequence homology between T6SS and bacteriophage proteins, and the same colour indicates protein homologues (A and B). The valine-glycine repeats G (VgrG) trimer is located at the tip of the pseudo C6 symmetry of the internal tubes haemolysin co-regulated protein (Hcp). The VipA/VipB tubule is similar in structure to the T4 tail-sheath protein, and VCA0109 is part of the phage tail baseplate. Membrane proteins IcmF and DotU, and outer membrane lipoprotein SciN, possibly provide structural stability. Cytosolic protein AAA⁺ chaperone (ClpV) is hypothesised to be involved in depolymerizing the VipA/VipB sheath-like structure tubule, and the C-terminal ATP-binding domain is postulated to provide energy required for the contraction (diagram modified from review articles, Records (2011) and Shneider et al. (2013)).

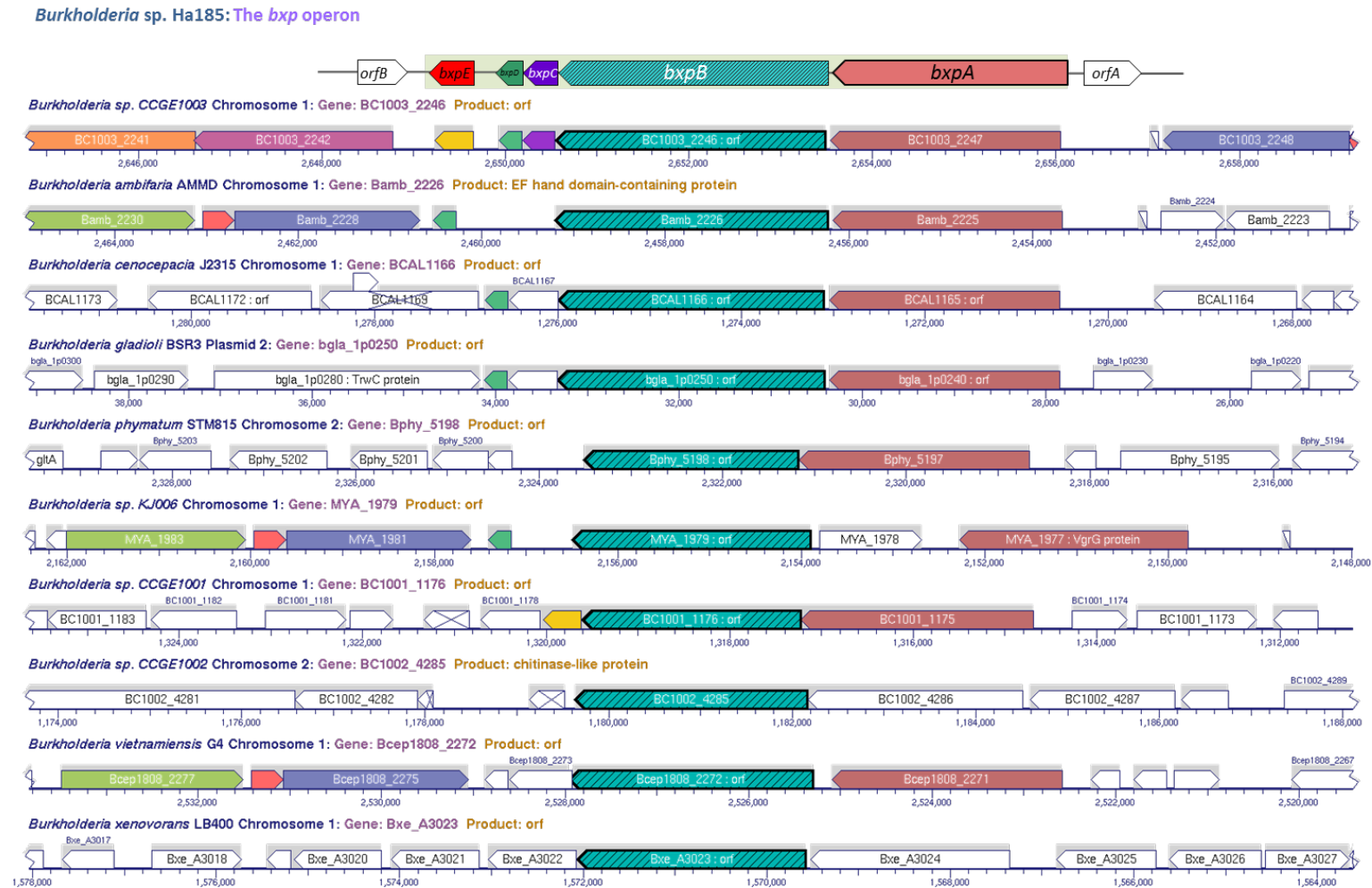


Figure 4.4.5 Rhs element Vgr protein alignment of *Burkholderia* sp. Ha185 and *Burkholderia* spp. using the BioCyc database collection. Gene colour indicates orthologous groups. *Burkholderia* sp. Ha185 *bxpA* is indicated by a brown arrow; opaque green arrow (dash), *bxpB*; purple arrow, *bxpC*; green arrow, *bxpD*; bright red arrow, *bxpE*. Grey shaded area indicates predicted open reading frame. Green shaded area of the *bxp* operon of *Burkholderia* sp. Ha185 was confirmed as one single transcript by PCR amplification from cDNA (Section 4.3.2.2).

4.4.8.2 *BxpB* contains a classical EF-hand calcium binding domain

Assessment of genes orthologous to the Rhs element VgrG gene from *Burkholderia* sp. CCGE1003 (BC1003_2246, P_003907491.1), performed using the BioCyc Database collection, identified a gene coding for a hypothetical protein (BC1003_2247, P_003907490.1) predicted to be similar to BxpB, which is located downstream of the gene coding for the Rhs element VgrG protein (**Figure 4.4.4**). Furthermore, several other *Burkholderia* spp. also contain the same gene arrangement, in which genes orthologous to *bxpA* accompany genes orthologous to *bxpB* of *Burkholderia* sp. Ha185 (**Figure 4.4.4**). Interestingly, a classic orphan *vgrG* is typically found in close proximity to an *hcp* gene (Barret et al., 2011). However, no *hcp* was identified within the the *bxp* operon of *Burkholderia* sp. Ha185, or in the adjoining regions (**Figure 4.4.4**). Through phylogenetic analysis of *P. aeruginosa*, Barret et al. (2011) reported that orphan *vgrG* loci are found in close proximity to cargo genes. This indicates that a gene such as *bxpB*, located 3' of *bxpA*, may be a cargo gene, as characterised by Barret et al. (2011).

A Pfam search with BxpB predicted the presence of a bacterial SH3 domain and a mononuclear EF-hand calcium-binding domain. This indicates that BxpB is likely to be a membrane-associated protein containing a calcium-binding site (Ca^{2+}), and has a possible a role in transporting small molecules, including ions, sugars or small peptides. A motif search of *bxpB* predicted an EF-hand calcium-binding domain located at residues 695–730 of the BxpB sequence of *Burkholderia* sp. Ha185 (helix-loop-helix structure as predicted by Phyre², which represents a canonical EF-hand structure). A classical EF-hand calcium-binding domain, such as those found in calmodulin and the S100 protein family, consists of two or more EF-hand motifs that undergo dramatic protein conformational change when bound to a calcium ion. This exposes a hydrophobic binding site for other downstream effector proteins during enzymatic reactions, such as grancaicin (Ikura, 1996; Schäfer and Heizmann, 1996). This reaction is regulated by the surrounding calcium concentration. There are two classes of EF-hand motif. One acts as an enzyme modulator for signalling proteins (calmodulin), while the other facilitates calcium buffering and protein transportation (calbindin D_{9k}) (Ikura, 1996). An EF-hand calcium-binding domain is also found in proteins from Gram-negative bacteria, and proteins with a single EF-hand motif have been implicated in a wide range of cellular processes, such as efflux transport, stress response, redox reactions and cell wall modification (Zhou et al., 2006). The interaction of Ca^{2+} with the mononuclear EF-hand BxpB protein from *Burkholderia* sp. Ha185 is unclear, and the Ca^{2+} binding affinity to BxpB has yet to be determined. However, BxpB is also predicted to have a role in maintaining the structural stability of protein complexes.

4.4.8.3 *BxpC* contains a conserved *duf1311* domain with unknown function

The *bxpC* transposon insertion mutant (*bxpC*::Tn5(F13)) showed decreased HydroxP solubilisation compared with the wildtype, however solubilisation was not completely abolished. Instead, over an extended time period, HydroxP solubilisation was observed on a HydroxP plate. In the HSU liquid culture assay, the ability to release soluble P from HydroxP was significantly impaired, and levels of 2-KGA were also decreased. Wildtype levels of HydroxP solubilisation and released 2-KGA were restored by *trans*-complementation of the mutant with a functional copy of *bxpC*. The restored phenotype of the complemented *bxpC* mutant, 1311CMPB2, suggested that it could uptake released 2-KGA from the culture medium. *bxpC* was found to be significantly overexpressed at 48 h, a time point where released 2-KGA was at its highest and *hemC* was significantly under-expressed. This suggested that expression of *bxpC* was inversely proportional to that of *hemC* at 48 h when 2-KGA was present in high concentrations. Furthermore, although extracellular calcium ion concentrations were not determined in this study, it is hypothesised that calcium ion concentration would also peak at 48 h as break down products of solubilised HydroxP. It is possible that calcium exists as both a 2-KGA-chelated complex and as individual calcium ions, and that the expression of *bxpC* may be influenced by calcium.

Protein sequence searches with BLASTx and BLASTp predicted that *bxpC* encodes a unique hypothetical protein. The predicted protein sequence is orthologous to a *Burkholderia* sp. CCGE1003MEo (YP_003907490.1) protein with a conserved *duf1311* domain that includes four highly conserved cysteine residues. Through the IPTG-driven expression of *bxpC* in pGEX-6P-1, a protein with the expected 11-kDa mass was observed post cleavage of the purification tag. While the protein could also be expressed from the pAY2-4 expression vector with no tag, it was highly insoluble and was unable to be visualised by SDS-PAGE. Protein sequence analysis using the Phyre² server showed that BxpC consists of three α -helices, and a calcium binding site at the centre of the protein was revealed by I-TASSER. Two of the BxpC α -helices were predicted to be anchored together by a disulphide bridge. The overall predicted protein structure was highly similar to a hypothetical protein (NP_742474.1) from *P. putida* kt2440, which belongs to the *duf1311* protein family (PDB3gi7). Based on *in silico* analysis by I-TASSER, BxpC is predicted to exist as a stable tetramer in biological systems, with the tetrameric protein held together by two cysteine residues on the α -helix (I) of each subunit.

The crystal structure of *duf1311* proteins from *P. putida* kt2440 indicates that this protein family contains a SO_4^{2-} binding site instead of a calcium binding site. Therefore, the *duf1311* protein family may have specific subfunctions, highlighting the uniqueness of BxpC. Amino acid sequence alignment of BxpC of *Burkholderia* sp. Ha185 with homologous proteins revealed a highly conserved calcium

binding residue at Tyr49, and a partially conserved residue at Lys67 (Figure 4.3.35). However, the third binding site (Asn71) varied among duf1311 family proteins. This suggests that the amino acid at the nonconserved position (Figure 4.3.35, red arrow) may determine the ligand-binding specificity of this site for different metal ions in this protein family, especially on the α -helix (II) of BxpC. Based on the protein tertiary structure prediction by I-TASSER, it is likely that α -helix (I) and (II) form an active site cavity, allowing metal ion binding. The duf1311 protein of *P. putida* kt2440 contains a sulphate ion ligand-binding site, consisting of Arg79, Ser88, Pro91 and Lys96, within the region encompassing part of the α -helix (II). However, the amino acid sequences of the α -helix (II) region of *P. putida* kt2440 and its *Pseudomonas* orthologues were highly divergent (Figure 4.3.35), indicative of an alternate function. This indicates that amino acid residues within the active site cavity (indicated by the orange parenthesis in Figure 4.3.35) may determine the differences in ligand binding. The calcium binding site within the protein complex suggests that BxpC may interact with calcium ions, and is likely to be involved in chelating calcium-bound 2-KGA.

With the exception of *Burkholderia* sp. CCGE1003, no gene orthologues of *Burkholderia* sp. Ha185 *bxpC* were found in other available *Burkholderia* spp. genomes (Figure 4.4.5). The GC content plot of the *bxp* cluster shows that *bxpC* has a significantly lower GC content (39.8%) than the rest of the *bxp* operon (average 56.9%). This could indicate that *bxpC* has been recently acquired from another organism, possibly by horizontal gene transfer. Several proteins with duf1311 domains have been identified within T6SS loci. The gene EPIR_3054, encoding a protein that shows 91% identity to the duf1311 protein, is located downstream of *vgrG* in *E. tasmaniensis* Et1/99 (De Maayer et al., 2011; Smits et al., 2013). Buijuy (2011) also reported a conserved duf1311 domain within the T6SS gene clusters of *Salmonella enterica* subspecies enterica (I) serotypes Enteritidis and Gallinarum (ORF SEN0998 and ORF SG1025, respectively) that are in close proximity to a gene encoding a Hcp-like protein. This indicates that proteins containing a conserved duf1311 domain are often associated with T6SSs. Although the precise function of the duf1311 domain in BxpC is unclear, the protein contains a type I protein signal peptide sequence, meaning that this protein is secreted like an effector protein. Proteins secreted by T6SSs are mostly found without N-terminal signal peptides, such as the VgrG and Hcp proteins (Filloux et al., 2008). However, an effector protein, ribose binding protein (RbsB), from *Rhizobium leguminosarum* also contains a signal peptide sequence, prompting Pukatzki et al. (2009) to propose that this protein is secreted by the T6SS. RbsB contains a conserved domain involved in sugar transportation, and RbsB homologues have been implicated in the uptake of ribose (Bladergroen et al., 2003; Pukatzki et al., 2009). BxpC also contains a signal peptide, but unlike the gene that encodes RbsB (which is located downstream of the T6SS cluster in *R.*

leguminosarum (Bladergroen et al., 2003)), *bxpC* was not found in the T6SS locus in *Burkholderia* sp. Ha185 (Contig 0007). Therefore, it is unlikely BxpC is secreted via the T6SS, but is possibly transported independently of the *bxp* operon by the Sec pathway, followed by secretion of BxpC outside of the cell through the Type II, Type IV or Type V bacterial protein secretion pathway (Henderson et al., 2004). This is also an event that can occur independently of the T6SS. In addition to the divergent GC content of *bxpC*, the presence of a signal sequence provides further evidence that *bxpC* has been acquired from another part of the genome, or from another organism. The latter hypothesis is supported by the significant difference in GC skew. Furthermore, combined with the existence of a predicted calcium binding site in BxpC, we propose that BxpC may play a role in capturing calcium-bound 2-KGA, and forms a BxpC-Ca-2-KGA compound, which is then transported back into the bacterial cell via the Bxp complex.

4.4.8.4 *BxpD* contains a newly-described PAAR-repeat protein interacts with VgrG

Several orthologues of *Burkholderia* sp. Ha185 *bxpD*, coding for a PAAR-repeat-containing protein, were identified downstream of *bxpA* and *bxpB* in the genomes of other *Burkholderia* spp. (Figure 4.4.5). Genes coding for the PAAR-repeat protein are also commonly located downstream of *vgrG* (Pukatzki et al., 2007; Suarez et al., 2008; Leiman et al., 2009; Shneider et al., 2013). This pattern also occurs within the *bxp* operon of *Burkholderia* sp. Ha185. The structure of the PAAR-repeat protein was recently resolved by Shneider et al. (2013), who expressed *V. cholerae* VCA0105 and *E. coli* c1882 PAAR proteins and found that both bound to the C-terminal end of VgrG, as well as to the C-terminal end of the gp5 β -helix of *V. cholerae* O1 biovar El Tor N16961. The crystal structure of the PAAR-repeat protein revealed a spike appearance, suggesting it acts like a piercing tip to puncture or open the target cell envelope during the initial secretion event (Shneider et al., 2013). Typical PAAR domains conserved within the CL15808 superfamily consist of 95–130 amino acid residues, such as the PF05488, COG4104 and PF13665 families that carry either N- or C-terminal extension domains. However, the BxpD PAAR-repeat protein from *Burkholderia* sp. Ha185 consists of 84 amino acid residues that do not possess either N- or C-terminal extensions. This indicates that protein encoded by the upstream ORF, BxpC, may be an independent effector protein that is secreted or translocated out of the cell. BxpD from *Burkholderia* sp. Ha185 belongs to Class I of the seven types of domain architecture of PAAR-repeat proteins as characterised by Shneider et al. (2013).

4.4.8.5 Unknown function of BxpE

Because of the lack of existing knowledge on protein orthologues of BxpE from *Burkholderia* sp. Ha185, BxpE is not discussed in great detail here. BLASTp analysis revealed that BxpE is orthologous to a hypothetical protein found in *Acinetobacter* sp. NIPH 284 and *Stenotrophomonas maltophilia* (WP_005160908.1 and WP_006375896.1, respectively). Both of these bacteria belong to the phylum Proteobacteria, but are Gammaproteobacteria rather than Betaproteobacteria like *Burkholderia* sp. Ha185. However, it was found that *bxpE* is transcribed as part of the *bxp* operon. Furthermore, transmembrane protein prediction by TMpred (Prediction of Transmembrane Regions and Orientation, Hofmann et al., 1993) revealed three strong transmembrane helices that are speculated to be formed at the inner membrane of the *Burkholderia* sp. Ha185 cell. The possible transmembrane helices are located at residues 15–34, 76–99 and 102–137 of BxpE. Therefore, it is predicted that BxpE is part of the Bxp complex. Though the exact function of this protein remains unknown, it may be involved in structural stabilisation.

4.4.9. Putative transport model of the Bxp complex

Combining experimental evidence with bioinformatic analysis, a model of the Bxp complex is proposed here (Figure 4.4.6). Bxp likely forms a small protein machinery complex that functions in transporting small molecules across the cellular membrane of *Burkholderia* sp. Ha185. This machinery is postulated to have a similar structure to the tip of the T6SS spike complex, and act like a miniature partial T6SS apparatus. BxpD, the PAAR-repeat protein, is proposed to form a cone-shaped spike, similar to a sharp tip, which connects to the β -barrel tube-like cavity made by β -strands of the BxpA Rhs element VgrG protein. This structure is possibly analogous to the VgrG spike of the T6SS (Figure 4.4.6). Calcium-induced protein conformational change of BxpB by an EF-hand motif may be required to activate protein translocation. Translocation of BxpC out of the bacterial cell as an effector protein or a regulatory protein may be performed by the Sec transportation system. While soluble P concentrations peaked, and high levels of calcium ions were also hypothesised to be present in the culture at 72 h, *bxpC* was found to be significantly upregulated. This suggests the Bxp complex is regulated by differences in membrane potential, possibly caused by high calcium concentrations in the surrounding environment. It has yet to be validated whether the Bxp complex is directly involved in organic anion transport, specifically 2-KGA. However, the increase in intracellular 2-KGA levels in the *bxpC::Tn5(F13)* complemented strain, 1311CMPB2, suggests a possible role in import. Therefore, it is likely BxpC is secreted and acts as a cargo protein, capturing 2-

KGA. The BxpC-Ca-2-KGA compound is then imported into the cell via the Bxp complex. This scenario would tie in with the decrease in detectable 2-KGA in the culture supernatant from 48 h onwards, which coincides with the increase in expression of *bxpC*. In this scenario, capture of 2-KGA by BxpC would prevent its detection in the culture supernatant.

The hypothesis that the Bxp complex has the ability to import 2-KGA has yet to be validated, but this is the first report of genes related to a bacterial T6SS being involved in P solubilisation. If correct, this would greatly enhance our understanding of P metabolism in *Burkholderia* spp. and other bacteria. Furthermore, this would be the first description of a possible role for a duf1311 domain, where the domain is associated with proteins involved in the transport of carbon molecules, such as in the case of the BxpC-Ca-2KGA compound. In addition to this key finding, it is also the first report of an orphan VgrG protein that harbours a protein related to T6SS, BxpD (PAAR repeat-containing protein), within a *Burkholderia* genome.

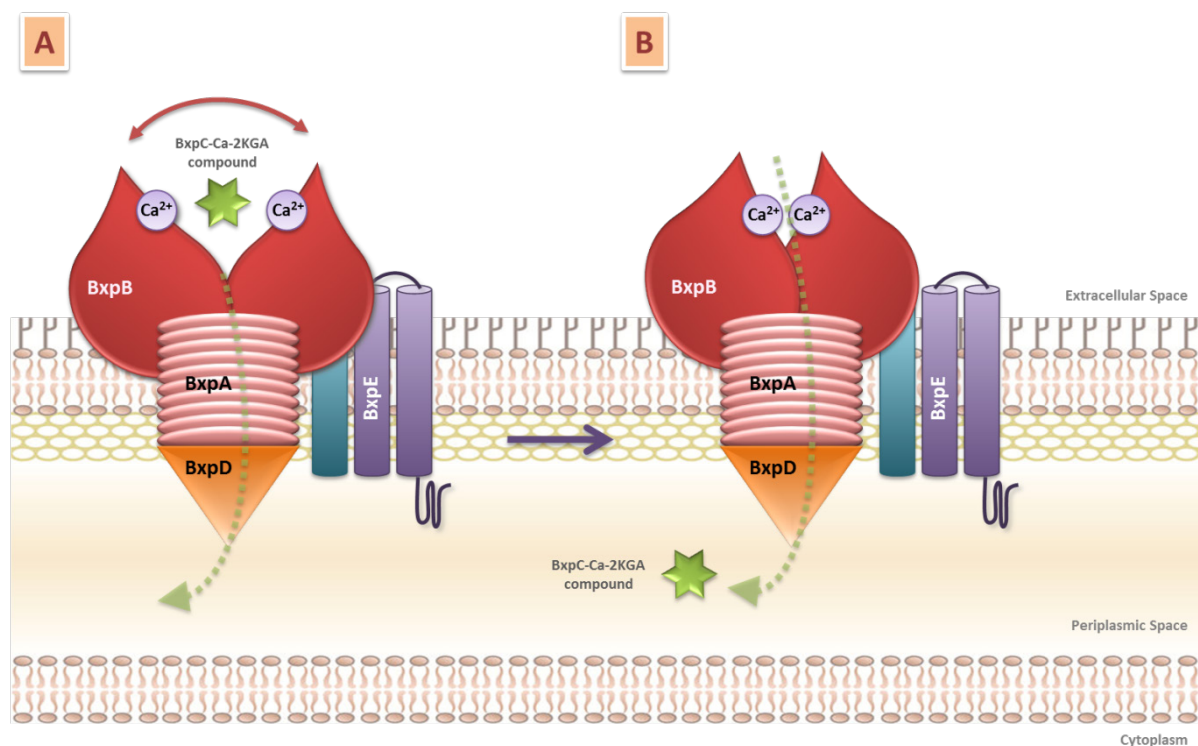


Figure 4.4.6 Proposed model for Bxp complex-mediated transportation of 2-KGA from the extracellular space into the periplasmic space of *Burkholderia* sp. Ha185. BxpA protein forms a β -barrel-like cavity tube and attaches to the BxpD protein, which has a cone-shaped spike-like structure. Membrane-bound BxpB contains an EF-calcium-binding domain that may undergo conformational changes from structure A to structure B during the transportation of calcium-bound 2-KGA by the tetrameric BxpC protein complex (BxpC-Ca-2KGA compound, as indicated by green star). The BxpE transmembrane helices may play a role in complex stabilisation.

4.4.10. Alternative model of the Bxp complex

Studies of T6SS have demonstrated their role in injecting toxins directly into target bacterial cells, as occurs with the effector protein Tse2 found in *P. aeruginosa* (Hood et al., 2010). Overexpression of Tse2 inhibited the growth of *P. aeruginosa*, confirming the hypothesis that T6SS plays a role in interbacterial interaction pathways. Interestingly, *tsi2*, an ORF located adjacent to the Tse2-encoding gene, *tse2*, encodes a cytoplasmic cognate immunity protein that inhibits the activity of Tse2 through a direct interaction (Hood et al., 2010). This finding helped to elucidate the toxin-immunity system, where immunity genes are mostly found directly downstream of the corresponding effector gene and *verG* in T6SS gene clusters (Hood et al., 2010; English et al., 2012; Unterweger et al., 2014). In the current study, mutation of *bxpC* reduced bacterial growth in the first 24 h during HydroxP solubilisation (Figure 4.3.14), and caused irregular cell morphology on HydroxP agar plates (Figure 4.3.6). This indicated that *bxpC*::Tn5(F13) cells may be unable to protect themselves from fratricide from adjacent cells in the culture. If this is the case, BxpC may be one of the cognate immunity proteins of *Burkholderia* sp. Ha815. Although the exact role of proteins encoded by the *bxp* operon is not known, the possibility that *bxpB* and *bxpC* are the effector-immunity pair cannot be ruled out. Therefore, genes from the *bxp* operon may be co-regulated with the T6SS loci in *Burkholderia* sp. Ha185, as effector protein secretion is T6SS-dependent. To determine whether the *bxp* operon does contain the effector-immunity pair, mutation of each of the *bxp* genes, followed by a bacterial killing assay as described by MacIntyre et al., (2010) should be carried out.

A more recent study has identified several MIX effector protein clusters, which mediate antibacterial activity, in *Vibrio parahaemolyticus* (Salomon et al., 2014). However, the MIX proteins are not required for the structural component of the T6SS machinery, and are predominately located at the N-terminal ends of proteins. Surprisingly, the majority of the MIX protein is predicted to contain transmembrane helices (Salomon et al., 2014) that are similar to the VasX protein of *Vibrio cholerae*. VasX functions as pore-forming toxin and contains three transmembrane domains in its C-terminus. VasX is important for T6SS-dependent killing, damaging the inner membrane of target cells (Miyata et al., 2011; Miyata et al., 2013). BxpE identified from *Burkholderia* sp. Ha185 is also predicted to have three transmembrane helices. However, the toxicity of BxpE remains to be elucidated.

Chapter 5

In situ Localisation of *Burkholderia* sp. Ha185 in the Rhizosphere of Ryegrass

5.1 Root colonisation by *Burkholderia phytofirmans* strain PsJN

Many species of *Burkholderia* are classed as plant growth-promoting rhizobacteria, and belong to the plant-associated beneficial and environmental group, as defined by Suárez-Moreno et al. (2012) (Chapter 4.1). *Burkholderia phytofirmans* strain PsJN, which is closely related to the *Burkholderia* sp. Ha185 strain used in this study, colonises a range of plant crops, including potato, tomato, chickpea, grapevine, onion roots, maize, barley and sugarcane (Chapter 4.1; Luvizotto et al., 2010; Mitter et al., 2013). In particular, *B. phytofirmans* was found to colonise Red Pontiac potato plantlets, leading to increased plant shoot height and weight, and production of larger roots (Da et al., 2012). Under greenhouse conditions, inoculation with *B. phytofirmans* PsJN increased dry weight of switchgrass cv. Alamo by 54.1% relative to the uninoculated control. The bacterium was also found to promote and enhance tiller production (Kim et al., 2012). Green fluorescent protein (GFP) tagged *B. phytofirmans* PsJN has been visualised on the leaves and sheaths of switchgrass (Kim et al., 2012), and on the root surface, specifically at the root tip, of *Arabidopsis thaliana* (Poupin et al., 2013). *B. phytofirmans* PsJN increased root length and the number of root hairs, accelerating growth rate and flowering time, and shortening the vegetative period of the *A. thaliana* plant (Poupin et al., 2013). *B. phytofirmans* PsJN is endophytic in *Vitis vinifera* L. cv. Chardonnay grapevine plantlets, where it protects plants from common grey mould disease caused by *Botrytis cinerea* (Compant et al., 2005). It has also been reported to increase root growth, enhance carbon dioxide fixation and improve cold tolerance of grapevine plantlets by increasing production of trehalose and trehalose 6-phosphate (Barkar et al., 2006; Theocharis et al., 2012; Fernandez et al., 2012).

There is increasing evidence that *Burkholderia* spp. are capable of plant root colonisation (Luvizotto et al., 2010; Mattos et al., 2008). To determine if *Burkholderia* sp. Ha185 is also capable of colonising plant roots, plasmid pWM1007, which encodes the constitutively-expressed green fluorescent protein (GFP) gene (*gfp*) from *Aequorea victoria* that has been codon optimised for expression in various species of bacteria (Miller et al., 2000), was cloned into *Burkholderia* sp. Ha185. The GFP fluoresces in the absence of any co-factor or substrate other than oxygen, and is stable and resistant

to photobleaching (Bukholm et al., 1987; Miller et al., 2000). For these reasons, GFP was an ideal marker candidate to visualise *Burkholderia* sp. Ha185 in the environment.

Burkholderia sp. Ha185(pBBR1MCS-5) strains were transformed with pWM1007 to investigate colonisation of the rhizosphere of ryegrass using fluorescence microscopy. Using a gnotobiotic *in vivo* plant assay developed in this study, GFP-tagged *Burkholderia* sp. Ha185 was inoculated onto sterilised germinated ryegrass. In independent experiments, two in-frame *gfp* fusions to BxpC and HemX (Chapter 3 and 4) were constructed to determine the *in situ* location of their expression in the rhizosphere in the presence of insoluble hydroxyapatite (HydroxP) as the sole P source.

5.2 Methods

5.2.1. Construction of GFP-tagged *Burkholderia* sp. Ha185

To construct the constitutive *Burkholderia* sp. Ha185 GFP-tagged variants Ha185(pWM1007), pWM1007 plasmid DNA was prepared as described in Appendix C.2.2, and electroporated into electrocompetent *Burkholderia* sp. Ha185 cells (Appendix C.2.5 and C.2.8). The transformants were then plated on LB agar plates containing 50 µg/mL kanamycin to select for the pWM1007 plasmid, and were incubated for 72 h at 25°C. The plates were then placed on a UV-Transilluminator (UVP, CA, USA) and colonies that fluoresced green were selected. Plasmid DNA from a fluorescent colony was extracted (Appendix C.2.2) and validated by restriction enzyme analysis and sequencing for the presence of pWM1007 (Appendix C.2.12). This fluorescent transformant was designated *Burkholderia* sp. Ha185(pWM1007) (Figure 5.2.1; Table 5.2.1). The intensity of fluorescence was measured to determine its potential for use in a plant assay. Strain Ha185(pWM1007) was assessed by fluorescent microscopy using an Olympus BX50 microscope equipped with an Olympus DP12 digital camera and Olysia BioReport 5.0 Image software. The sample was excited using a U-MWIB filter with excitation bandwidth of 460–490 nm.

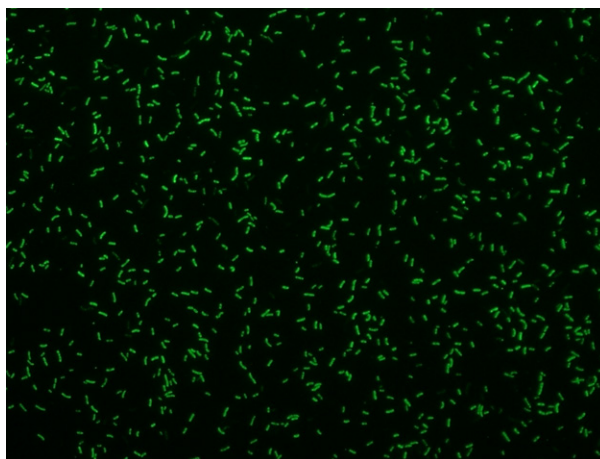


Figure 5.2.1 GFP-tagged *Burkholderia* sp. Ha185(pWM1007) expressing GFP constitutively under fluorescent microscope (x60 magnification).

5.2.2. Construction of in-frame *bxpC::gfp* and *hemX::gfp* fusions

5.2.2.1 Construction of *bxpC::gfp*(Ha185)

To determine the location of *Burkholderia* sp. Ha185 when expressing *bxpC* during P solubilisation in a plant system, an in-frame *bxpC-gfp* translation fusion was constructed to enable visualisation of fluorescence under conditions where *bxpC* is induced. To construct the *bxpC-gfp* gene fusion, the primers gBxpFK and gBxpRH (**Table 5.2.2**) were used to amplify partial *bxpB* and the first 36 nucleotides of *bxpC* from wildtype *Burkholderia* sp. Ha185 (Appendix C.2.9). The first round of PCR generated a 920-bp amplicon encompassing a partial *bxpB* ORF (863 bp) and 36 bp of the 5' end of the *bxpC* ORF. The amplicon was flanked by a *KpnI* restriction site at the 5' end and a *HindIII* site at the 3' end (Figure 5.2.2). In a separate reaction, the pWM1007-encoded *gfp* region was amplified using primers gfpFH and gfpRKH, producing a 717-bp amplicon flanked by a 5' *HindIII* site and 3' *KpnI/HindIII* sites. Both PCR amplicons were then digested independently using *HindIII* (Appendix C.2.3), and the DNA was ethanol precipitated (Appendix C.2.4). The precipitated products were then ligated (Appendix C.2.11). To eliminate an additional cloning step, the resultant ligation was used as a template for a subsequent PCR using the primer pair gBxpFK/gfpRKH (Appendix C.2.9). This allowed the amplification of 1637-bp amplicon containing the associated region 5' of *bxpC* and *gfp* with an in-frame gene fusion coding for an additional lysine-leucine dipeptide (AAGCTT, the *HindIII* restriction enzyme site) between the two fragments (a schematic diagram of the fusion point is given in Figure 5.2.3). The resultant amplicon, *bxpC::gfp*, was digested with restriction enzyme *KpnI* and ligated into the analogous site of the suicide plasmid pJP5608 (Figure 5.2.2). A 1- μ L aliquot of the ligation mixture was electroporated into *Escherichia coli* strain EC100D pir+ (**Table 5.2.1**), and the transformants were

plated onto LB agar plates containing tetracycline (30 µg/mL) to select for pJP5608. Plasmid DNA was then extracted from several independent colonies and validated by restriction enzyme digest profile. The correct construct was expected to release a ~1640-bp product when digested with *KpnI*, and DNA fragments of ~780 bp, ~2300 bp and ~5300 bp when digested with *HindIII*. The *bxp* and *gfp* sequences were validated by DNA sequencing using the M13F and M13R primers (Appendix C.2.12), and the junction points were validated by sequencing using specific primers (Unknown_F and Prob_R) located upstream of the junction point (**Table 5.2.2**). The correct plasmid, designated pBxpCGFP, was then electroporated into *E. coli* S17-1 λpir (**Table 5.2.1**). The correct transconjugant was used to conjugate pBxpCGFP to wildtype *Burkholderia* sp. Ha185 (pBBR1MCS-5), as outlined in Chapter 3.2.2 for construction of the mini-Tn5*Km1* transposon mutant library. Several of the putative recombinants were then patched onto LB agar plates containing both gentamicin (15 µg/mL) and tetracycline (30 µg/mL), and the plates were incubated at 25°C for 72 h.

Through the process of homologous recombination, the suicide vector can insert in one of two possible orientations. Recombinants were selected in which the DNA had integrated in the correct orientation, allowing the correct expression of the translational fusion. Transconjugants were independently assessed by colony PCR using a primer designed upstream and external to the recombined *bxpC::gfp* region, and a reverse primer located within the *gfp* fragment (PARP_F and Probe_R) (**Table 5.2.2**). PCR of a recombinant with the insertion in the correct orientation generated a 1921-bp PCR amplicon (Figure 5.2.3). The primer PARP_R, designed internal to the *bxpB* ORF, was also used in combination with primer PARP_F to give a 840-bp amplicon (Figure 5.2.3). The *Burkholderia* sp. Ha185 *bxpC::gfp* translational reporter fusion recombinant was designated *bxpC::gfp*(Ha185).

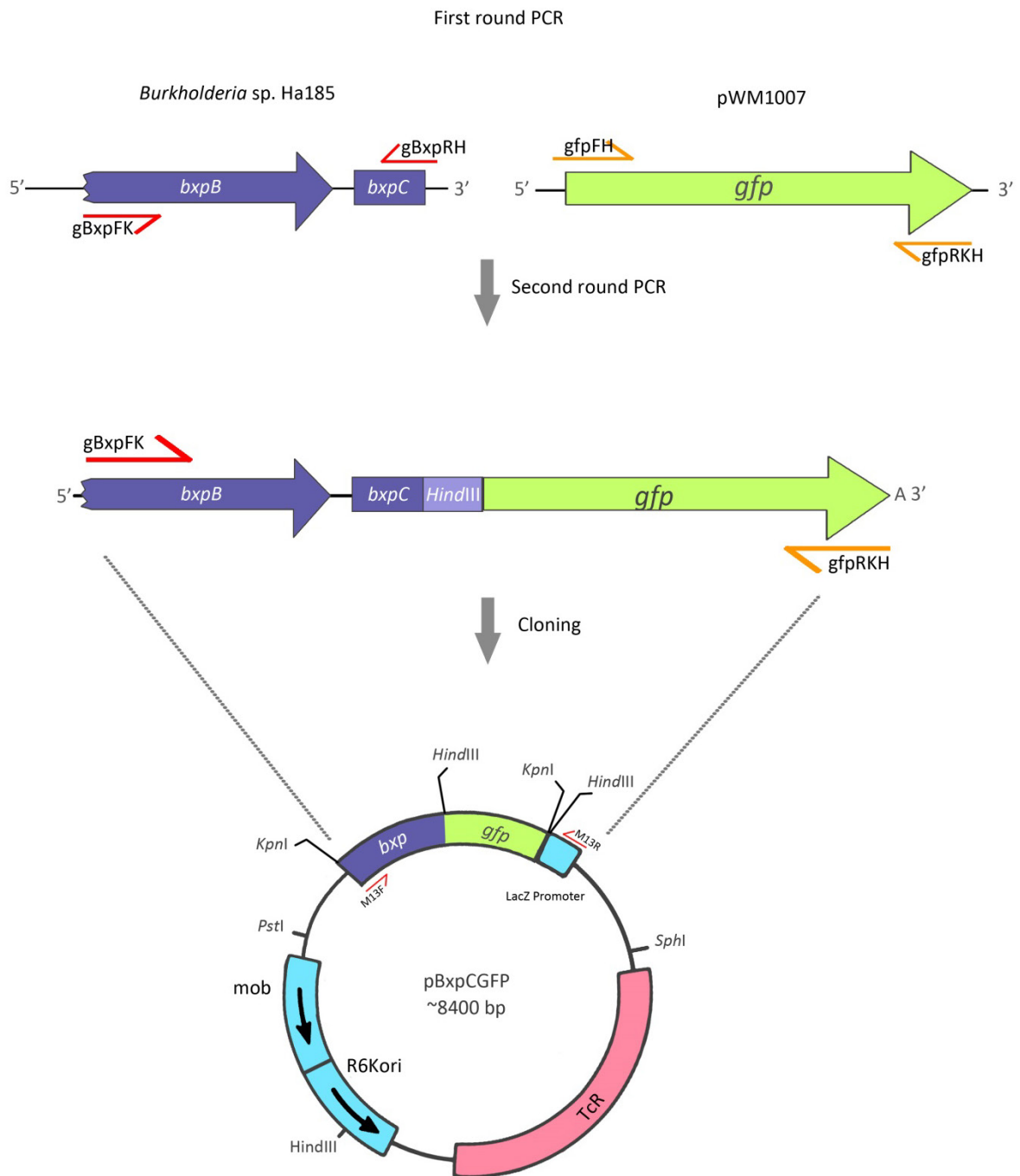


Figure 5.2.2 Cloning strategy for in-frame *gfp* gene fusion for *bxpC::gfp* where *bxpC::gfp* was cloned into *KpnI* site of the pJP5608 vector resulting pBxpCGFP. Integration of the vector into the Ha185(pBBR1MCS-5) genome confers tetracycline resistance to the host cell.

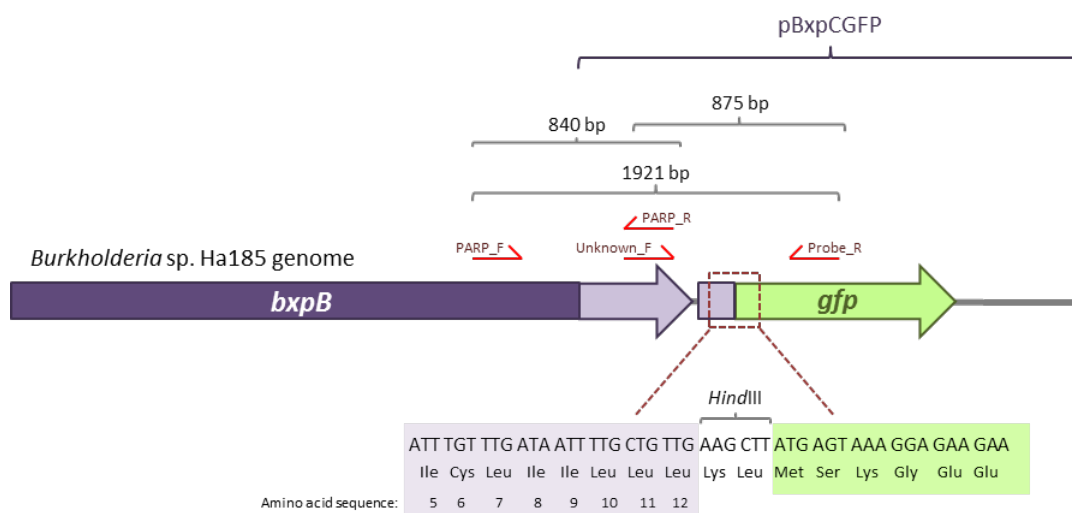


Figure 5.2.3 Schematic of in-frame gene fusion of the *bxpC::gfp* gene recombinant from pBxpCGFP transconjugated into *Burkholderia* sp. Ha185 genome. Primers listed were used in colony PCR to confirm the integrity of successful transconjugant. Dash box indicates the fusion point of *bxpC::gfp* with a *HindIII* restriction site creating an in-frame gene fusion.

5.2.2.2 Construction of *hemX::gfp*(Ha185)

The *hemX* in-frame *gfp* gene fusion was constructed in a similar manner to the *bxpC::gfp* fusion. Primer pair gHemFK/gHemRH (Table 5.2.2) was used to amplify the partial *hemC* and *hemX* ORFs from wildtype *Burkholderia* sp. Ha185 gDNA (Figure 5.2.4). Because of the high GC content of the *hem* operon, temperature gradient PCR (55–67°C) was performed with addition of dimethyl sulfoxide to optimise amplification, as described in Chapter 4.2.2. An annealing temperature of 67°C was determined to be optimal and was used to amplify genes from the *hem* operon. The first round PCR produced a 772-bp amplicon encompassing a 725-bp partial *hemC* fragment, a 5' *KpnI* restriction site and 51 bp of sequence upstream of the *hemX* initiation codon and a distal 3' *HindIII* restriction site. The *gfp* amplicon was generated as described in Section 5, and both *hemX* and *gfp* PCR amplicons were digested with *HindIII* and then ligated overnight. A 1- μ L aliquot of the resultant ligation was subjected to a second round of PCR using primer pair gHemFK/gfpRKH, which amplified both partial *hem* genes and the *gfp* ORF (Appendix C.2.9). Temperature gradient PCR was also carried out to define the optimal annealing temperature of the *hem* primer set (gHemFK and gfpRKH), and was determined to be 65°C. The PCR generated a 1515-bp amplicon encompassing an in-frame gene fusion with an additional lysine-leucine dipeptide (AAGCTT, the *HindIII* restriction enzyme site) between the two fragments (Figure 5.2.4), similar to the *bxpC::gfp* gene fusion construct (Section 5). The amplicon was digested with *KpnI* and then ligated into the analogous site in pJP5608 (similar rationale as shown in Figure 5.2.2). The resultant construct, designated pHemXGFP, contained an in-frame *hemX::gfp* gene fusion fragment and was electroporated into *E. coli* EC100D pir⁺ (Table 5.2.1),

then plated on LB agar containing tetracycline (30 µg/mL). The restriction enzyme profiles of several of the resultant transformants were assessed by *Kpn*I digestion, releasing fragments of ~1560 bp and ~6700 bp, *Hind*III digestion, releasing ~2180 bp, ~780 bp and ~4300 bp fragments, and *Sac*I digestion, releasing fragments of ~1000 bp and ~7000 bp. Restriction digestion indicated the presence of the correct clone. The *hemX::gfp* fusion point was then validated by sequencing using the primers M13F and M13R (Appendix C.2.12). The correct construct, designated pHemXGFP, was then electroporated into *E. coli* S17-1 λpir and conjugated to Ha185(pBBR1MCS-5) on LB agar plates for 7 h at 25°C. The transconjugants were resuspended in LB broth, and aliquots were plated on LB agar plates containing tetracycline (30 µg/mL) and gentamicin (15 µg/mL) and then incubated at 25°C for 72 h. To validate the *hemX::gfp* recombinant, several transconjugants were assessed by colony PCR. With reference to Figure 5.2.4, the HemP_F primer, located upstream of the *hemX::gfp* insertion, and the Probe_R primer, designed from the internal *gfp* fragment, were used for PCR amplification (Appendix C.2.9), where a 2047-bp product indicated that the fragment had integrated in the desired orientation (Table 5.2.2, Figure 5.2.4). To validate that the pJP5608 suicide vector had not recombined upstream of the *hemX::gfp* fusion, the primer HemP_R, inside the *hemC* fragment, was used in combination with the primer HemP_F for PCR analysis (Appendix C.2.9). The correct transconjugant was expected to generate a 858-bp amplicon (Figure 5.2.4). The *Burkholderia* sp. Ha185 *hemX::gfp* transcriptional reporter fusion recombinant was designated *hemX::gfp*(Ha185).

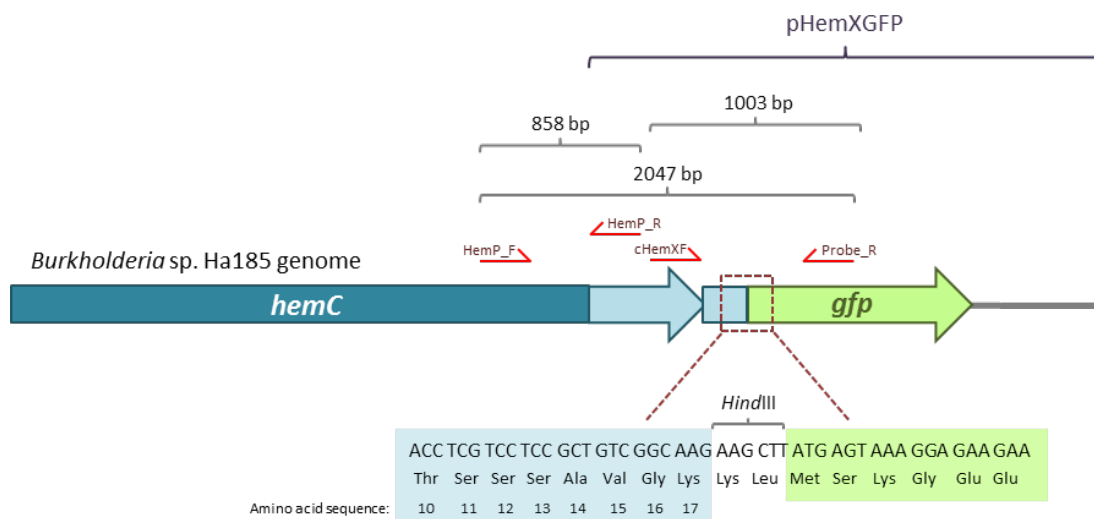


Figure 5.2.4 Schematic of the in-frame gene fusion of the *hemX::gfp* gene recombinant from pHemXGFP transconjugated into *Burkholderia* sp. Ha185 genome. Relative locations of the primers used to validate the correct orientation of the *hemX::gfp*(Ha185) fusion. Dash box indicates the fusion point of *hemX::gfp* with a *Hind*III restriction site creating an in-frame fusion that was validated by DNA sequence analysis.

Table 5.2.1 Bacteria strains and plasmids used in this study

Bacterial strains and plasmids	Description	References
Strains		
<i>E. coli</i> DH10B	F- <i>mcrA</i> Δ <i>mrr-hsdRMS-mcrBC</i> Δ 80d <i>lacZ</i> Δ M15 Δ <i>lacX74</i> endA1 <i>recA1</i> deoR Δ ara, <i>leu7697</i> ara Δ 139 <i>galU galK nupG rpsL</i> Δ -	Lorow and Jessee, (1990)
<i>E. coli</i> EC100D pir+	F' <i>mcrA</i> Δ (<i>mrr-hsdRMS-mcrBC</i>) ϕ 80d <i>lacZ</i> Δ M15 Δ <i>lacX74</i> <i>recA1</i> <i>endA1</i> <i>araD139</i> Δ (<i>ara, leu</i>)7697 <i>galU galK</i> λ^- <i>rpsL nupG pir</i> ⁺ (DHFR)	Metcalf et al. (1994)
<i>E. coli</i> S17-1 λ pir	<i>hsdR</i> Pro Δ <i>recA</i> - RP4-2 Tc::Mu Kn::Tn7 integrated in the chromosome: <i>pir</i> gene	
<i>Burkholderia</i> sp. Ha185	Field isolate from Haast, New Zealand, <i>Burkholderia</i> sp. parent strain	This study
<i>Burkholderia</i> sp. Ha185(pBBR1MCS-5)	Gm ^R ; <i>Burkholderia</i> sp. Ha185 containing pBBR1MCS-5 broad host range vector	This study
<i>Burkholderia</i> sp. Ha185(pWM1007)	Gm ^R , Kn ^R ; GFP-tagged stain, derivative of <i>Burkholderia</i> sp. Ha185(pBBR1MCS-5)	
<i>bxpC::gfp</i> (Ha185)	Tc ^R , Gm ^R ; containing pPARP7A bearing the <i>bxpC::gfp</i> in-frame fusion gene, derivative of <i>Burkholderia</i> sp. Ha185(pBBR1MCS-5)	This study
<i>hemX::gfp</i> (Ha185)	Tc ^R , Gm ^R ; containing pHemP6A bearing the <i>hemX::gfp</i> in-frame fusion gene, derivative of <i>Burkholderia</i> sp. Ha185(pBBR1MCS-5)	This study
Plasmids		
pBBR1MCS-5	Gm ^R ; broad host range vector	Kovach et al. (1995)
pWM1007	Kn ^R ; pMW10 Δ <i>lacZ</i> Ω [(T1) ₄ -P _c - <i>gfp</i> -T1]	Miller et al. (2000)
pJP5608	Tc ^R ; broad host range vector	Kovach et al. (1995)
pBxpCGFP	Tc ^R ; pJP5608 containing 1649 bp <i>bxpC::gfp</i> PCR product, bearing partial <i>bxpB</i> gene (863 bp) and 36 bp from the start codon of <i>bxpC</i> gene from <i>Burkholderia</i> sp. Ha185. In-frame fusion with 717 bp <i>gfp</i> sequence from pWM1007	This study
pHemXGFP	Tc ^R ; pJP5608 containing 1515 bp <i>hemX::gfp</i> PCR product, bearing partial <i>hemC</i> gene (725 bp) and 51 bp from the start codon of <i>hemX</i> gene from <i>Burkholderia</i> sp. Ha185. In-frame fusion with 717 bp <i>gfp</i> sequence from pWM1007	This study
pGEM [®] -T Easy	Am ^R ; <i>lacZ</i> multi-cloning site	Promega

Table 5.2.2 A list of oligonucleotide primers used in this study

Purpose	Oligonucleotides	Sequences (5'→3') ^a
<i>gfp</i> fusion	gBxpFK	AAGGTACCATCACGACGGCAAGATAACGGC
	gBxpRH	AAAAAGCTTCAACAGCAAAATTATCAAACAAATG
	gHemFK	AAGGTACCAATACGAGTCGCTGGCCGCG
	gHemRH	AAAAAGCTTCTTGCCGACAGCGGAGGACGAGG
	gfpFH	AAAAAGCTTATGAGTAAAGGAGAAGAACTTTTCACTGG
	gfpRKH	AAAAAGCTTGGTACCTTATTTGTAGAGCTCATCCATGC
<i>gfp</i> validation	Unknown_F	AGTGAGGTCGCTGGTTGTCGC
	Probe_R	AATGGTCTGCTAGTTGAACGC
	PARP_F	CCGTTATGGGTTGATGCGAG
	PARP_R	AACCTCGGTCGCTGTAACCT
	F13B_F	TAATGCTCCGAGACCAAGCGC
	F13C_R	ACCTTGAGATTGCGAGGCCTCG
	HemP_F	GCTACTGCGGAAGTGCCTA
	HemP_R	AGCCGCGTATCCAGATTGCC
	cHemXF	AAAGGATCCGCTGCATCACGAACACAC

^a Underscore denotes designed restriction site

5.2.3. In vivo ryegrass plant bioassay

5.2.3.1 Perlite tube preparation

To prepare near gnotobiotic conditions before ryegrass samples were inoculated with the bacteria to be assessed, lightweight perlite (Egmont Commercial Ltd, Christchurch, New Zealand) was used to simulate soil conditions (Figure 5.2.5(C)). Perlite ore (74% silica) is an inert volcanic rock that can expand 25-fold in size after heating at high temperature (850–900°C), whereby it becomes highly porous. Perlite has many advantages as a growth medium, in particular, it does not contain P making it an ideal substrate for assays where P is to be added into the system. The lightweight and porous structure of perlite is conducive to plant root growth, enabling the root to extend without obstruction. The large pore size also allows the bacteria to readily access and colonise roots, and perlite can absorb and retain water. Various bacteria can survive in perlite for longer than 180 days, and perlite supports growth of soy bean (*Glycine max* (L.) Merr.) as effectively as peat (Daza et al., 2000). Daza et al. (2000) used perlite as a bacterial carrier for introducing plant growth-promoting bacteria into the field. In the current study, perlite was used as a growth medium for both bacteria and ryegrass roots. Perlite can be sterilised by autoclaving without altering any of the properties mentioned above. The ability to separate the perlite from the SpecM liquid medium (Appendix A.1.2)

enabled the rapid enumeration of rhizobacteria around roots, on root surfaces and between the perlite particles. For these reasons, perlite was chosen as the growth matrix for ryegrass and *Burkholderia* sp. Ha185 for assessment of the effect of P on plant growth. Test tubes (16 × 150 mm) containing perlite to a height of 3 cm from the base were prepared and autoclaved for 15 min (1.1 kg/cm², 121°C). Tubes were then dried upright for 72 h at 80°C under sterile conditions (capped with foil).

5.2.3.2 Ryegrass seed preparation and germination

Non-endophyte perennial ryegrass seeds were surface-sterilised by soaking in 70% ethanol (1 min) followed by washing with 0.5% sodium hypochlorite for 20 min with slow rotation in a sterilised 50 mL conical centrifuge tube. Seeds were rinsed six times with distilled water and then dried in a laminar flow cabinet for 1 h. The sterilised ryegrass seeds were inoculated onto inverted tryptic soy agar plates (2% (w/v) tryptic soy broth and 6% (w/v) agar) and allowed to germinate at 25°C for 72 h (Figure 5.2.5 (D)). This step enabled the detection of any seedlings with microbial contamination, and seedlings with observable bacterial or fungal growth were discarded.

5.2.3.3 Plant inoculation with GFP-tagged *Burkholderia* sp. Ha185

The GFP-tagged strain Ha185(pWM1007) and the two in-frame *gfp* fusion derivatives, *bxpC::gfp*(Ha185) and *hemX::gfp*(Ha185), were prepared by inoculating a single colony into a McCartney bottle containing 3 mL of Luria Bertani (LB) broth with appropriate antibiotic when required (Figure 5.2.5 (A)). The cultures were incubated at 20°C (250 rpm) for 48 h prior to inoculation into perlite tubes. One millilitre of each culture was pelleted by centrifugation at 8000 × *g* for 1 min, and the pellet was resuspended in Hoagland's solution without soluble phosphate (Hog-P) (Appendix A.1.7) to OD₆₀₀ ~0.8. A stock solution was then prepared for each bacterial sample, containing 8.9 mL of Hog-P solution, 0.1 mL of bacterial culture (OD₆₀₀ = 0.8) and 1 mL of hydroxyapatite (HydroxP, Ca₅(PO₄)₃(OH)) insoluble mixture (Figure 5.2.5 (B)). The insoluble HydroxP mixture was prepared by mixing 1.0 g of HydroxP with 10 mL of sterile Hog-P solution. One millilitre of stock solution containing 1.86 mg of P and approximately 10⁶ bacterial cells was pipetted directly into the perlite in the test tube. Three millilitres of Hog-P solution was then added to the test tube to give a final volume of 4 mL. One millilitre of Hog-P solution was substituted for the bacterial suspension in an uninoculated control (Figure 5.2.5 (C)). Dilution plating (Appendix B.2) and bacterial enumeration was carried out for each stock solution to determine the number of bacterial cells and

whether there was any contamination. Two germinated sterile ryegrass seeds were placed on top of the perlite in each tube using sterile forceps (Figure 5.2.5 (E)). Tubes were covered with gas-permeable adhesive seal (Thermo Scientific, Waltham, MA, USA) to allow gas exchange and minimise the potential for contamination (Figure 5.2.5 (F)). Perlite tubes were then incubated at 20°C with 16 h light followed by 8 h of dark using a CAT610/620 phytotron climate simulator (Contherm Scientific Co., Upper Hutt, New Zealand) (Figure 5.2.5 (G)). One millilitre of sterilised Hog-P solution was added to each perlite tube (samples and negative control without bacterial inoculation) at days 7 and 14 to replenish the moisture content. The plant assay was carried out in triplicate for each treatment, and the experiment was repeated three independent times.

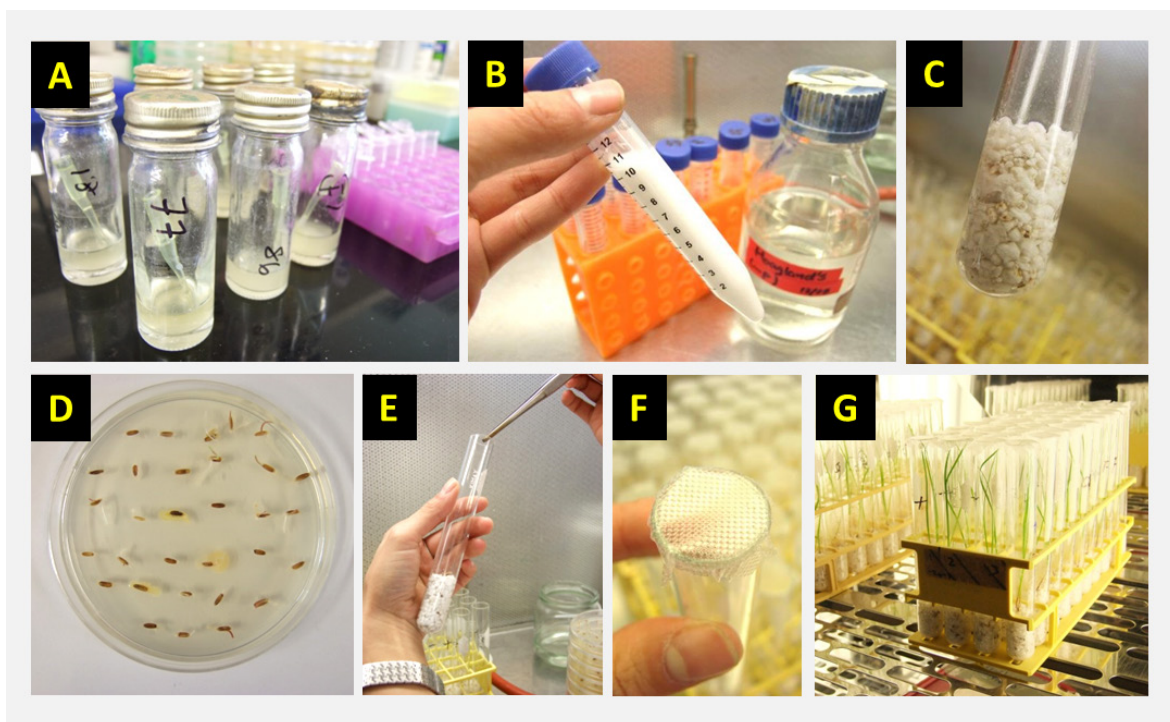


Figure 5.2.5 A work-flow photograph of plant assay preparation. Overnight cultures of wildtype *Burkholderia* sp. Ha185, PARP7A and HemP6A (A); bacterial stock solution (B); 1 mL of the bacterial stock solution was pipetted into each perlite tube that contained 3 cm of perlite at its base (C); Pre-sterilised ryegrass seed grown on inverted tryptic soy agar at 25°C for 72 h (D); Placement of sterile ryegrass seed onto the top of the perlite (E); Gas permeable adhesive seal placed over the mouth of the tube to prevent contamination (F); ryegrass were grown in perlite tube inside the Contherm CAT610/620 phytotron incubator for 14 days at 20°C (G).

5.2.3.4 Ryegrass and bacterial cell harvesting

To investigate the *in situ* colonisation of Ha185(pWM1007) and the two derivative *gfp* fusion isolates, inoculated ryegrass seedlings were harvested at 7, 14 and 21 days. Perlite around the root surface was gently removed using forceps, and the root was immersed in SpecM solution (Appendix A.1.2) to remove excess perlite particles. To visualise bacterial colonisation on the rhizoplane and in the rhizosphere, roots were examined by bright-field and fluorescence microscopy using an Olympus BX50 microscope equipped with an Olympus DP12 digital microscope camera and Olysia BioReport 5.0 Image software. A U-MWIB filter with an excitation band width of 330–385 nm was used to visualise isolates expressing *gfp*. The same preparation was used for visualising bacteria on the ryegrass root using an inverted Leica TCS SP5 confocal microscope equipped with lasers with emission band widths of 501–551 nm for green fluorescence and 601–754 nm for red fluorescence. Images were assessed using Leica Application Suite Advanced Fluorescence imaging software from Leica Microsystems. Plants were harvested in triplicate for each treatment at each time point. The Ha185(pWM1007)-inoculated plant assay was performed in triplicate at each time point, and a pattern of colonisation was derived from overall observations of three independent experiments.

5.2.3.5 Hydroxyapatite solubilisation by *Burkholderia* sp. Ha185 in a plant-based plate assay

A plate-based assay was used to determine whether wildtype *Burkholderia* sp. Ha185 can colonise the rhizosphere of ryegrass roots growing on Hyp-G plates (plate preparation described in Chapter 2.2.1.4). Germinated ryegrass seeds were prepared as described in Section 5.2.2.4, and 1 μ L of broth culture of the wildtype *Burkholderia* sp. Ha185 or the mini-Tn5Km1 transposon mutants (*hemX::Tn5(F18)* or *bxpC::Tn5(F13)*) (prepared as described in Section 5.2.2.5) was pipetted onto the germinated seeds placed on Hyp-G plates. The plates were then incubated in the dark at 25°C for 72 h, after which they were incubated at ambient temperature for 7–14 days.

5.3 Results

5.3.1. Phosphate solubilisation by *Burkholderia* sp. Ha185 in the rhizosphere

As shown in Figure 5.3.1 (A), wildtype *Burkholderia* sp. Ha185 colonised the root surface of ryegrass seedlings grown on Hyp-G plates. Similar growth was observed for the *hemX::Tn5(F18)* mutant, which has a reduced ability to solubilise P (Chapter 4.3.2), and was also found to colonise the

ryegrass root (Figure 5.3.1 (B)). In the absence of bacteria, ryegrass roots grown on the Hyp-G medium produced no zone of hydroxyapatite solubilisation (Figure 5.3.1 (A) control). The uninoculated ryegrass displayed a long, thin root phenotype with an array of dense, fine root hairs, while in the presence of *Burkholderia* sp. Ha185, the main root was shorter, with fewer and shorter root hairs (Figure 5.3.1 (A)). The *hemX::Tn5(F18)* mutant-inoculated plants exhibited reduced zones of solubilisation, and the ryegrass root was longer, thinner and had more fine root hairs than the ryegrass root treated with *Burkholderia* sp. Ha185 (Figure 5.3.1 (B)). This indicated that although *hemX::Tn5(F18)* was able to colonise the rhizosphere, the reduced P solubilisation exhibited by the strain resulted in different root morphology compared with *Burkholderia* sp. Ha185-treated ryegrass (Figure 5.3.1 (A & B)). Ryegrass inoculated with *bxpC::Tn5(F13)* at day 7 produced smaller zones of solubilisation around the primary root compared with the *Burkholderia* sp. Ha185-treated ryegrass (Figure 5.3.1 (D)). The reduced P solubilisation was consistent with the HSU HydroxP liquid culture assay described in Chapters 3 and 4. Of interest, the *bxpC::Tn5(F13)*-inoculated ryegrass (Figure 5.3.1 (D)) not only exhibited elongated roots, but the meristems appeared clustered, and the numbers of secondary lateral roots were increased relative to the uninoculated control. Elevated numbers of fine, dense root hairs were also observed, which were comparable with the uninoculated control at day 7 (Figure 5.3.1 (C, D)).

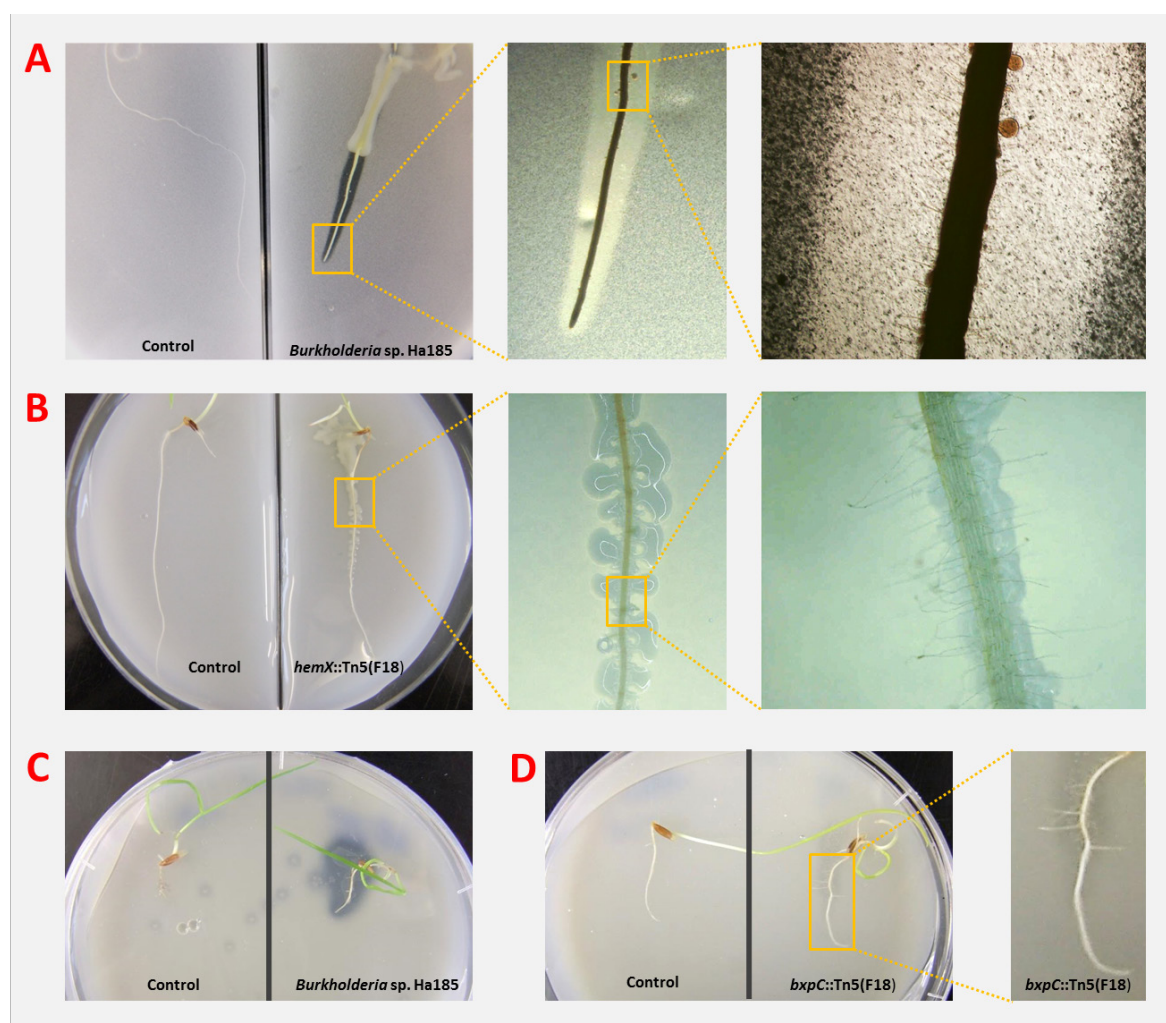


Figure 5.3.1 Gyegrass growing on Hyp-G plate inoculated with (A) wildtype *Burkholderia* sp. Ha185 and *hemX::Tn5(F18)* (B) for 14 days. Uninoculated ryegrass is included as a negative control. Images taken using a stereo zoom microscope Olympus SZX12 equipped with an Olympus DP12 digital microscope camera. Images of wildtype *Burkholderia* sp. Ha185 colonising around the ryegrass root using the stereo zoom microscope (A) were taken by adjusting the slit aperture illuminator which enables a shadow effect of ryegrass root allowing greater contrast of the transparent zone of clearing of the HydroxP agar around the root. Ryegrass growing on Hyp-G plate inoculated with wildtype *Burkholderia* sp. Ha185 (C) and *bxpC::Tn5(F18)* (D) for 7 days and a close up photograph of *bxpC::Tn5(F18)* inoculated ryegrass root at day 7.

5.3.2. In situ colonisation of GFP-tagged Ha185(pWM1007) on ryegrass roots

The plant-root based plate assay described above demonstrated root colonisation by both wildtype *Burkholderia* sp. Ha185 and *hemX::Tn5(F18)*. It also showed that *Burkholderia* sp. Ha185 can solubilise the HydroxP surrounding the ryegrass root, leading to the formation of a shorter and thicker root compared with the uninoculated control. To visualise the location of Ha185(pWM1007) in the rhizosphere, the plant assay outlined in Section 5.2.3 was used. At 7, 14 and 21 days of growth,

root samples were assessed using both fluorescence and confocal microscopy. Regions where Ha185(pWM1007) was observed are depicted in a schematic of the ryegrass root (Figure 5.3.2). Visualisation of the GFP-tagged Ha185 strain using fluorescence microscopy revealed that Ha185(pWM1007) was primarily located on the root hairs at the maturation zone at 7-days post-inoculation (Figure 5.3.2, Figure 5.3.3, B, C). The maturation zone is composed of a mass of dense root hairs and is a complex region where cellular differentiation occurs (Figure 5.3.3, A; Figure 5.3.5, B). The large surface area combined with release of root exudates make this region conducive to bacterial colonisation (Figure 5.3.3, B). The Ha185(pWM1007) strain was also observed adhering to the rhizoplane of primary roots, and was located between rhizodermis cells ((Figure 5.3.3, D; Figure 5.3.5, C, D).

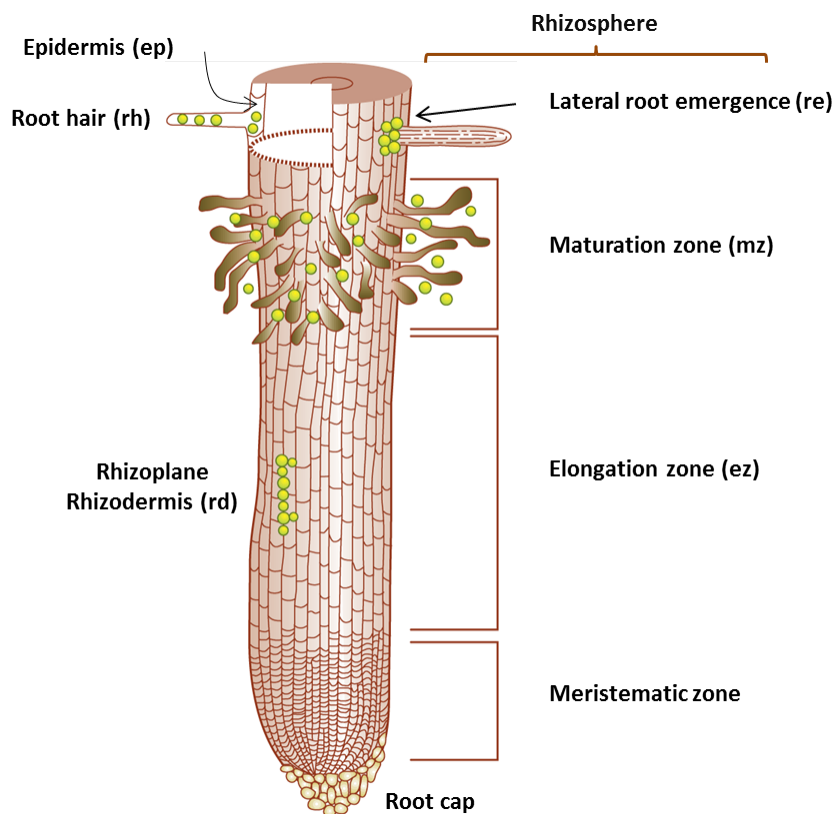


Figure 5.3.2 Schematic of colonisation pattern of Ha185(pWM1007) on ryegrass root during plant growth. Isolate Ha185(pWM1007) indicated by green circles are found to colonise at the maturation zone (mz), around lateral root emergence (re), on rhizoplane along and in between rhizodermis cells (rd), and inside root hair (rh) as well as inside epidermis cells (ep).

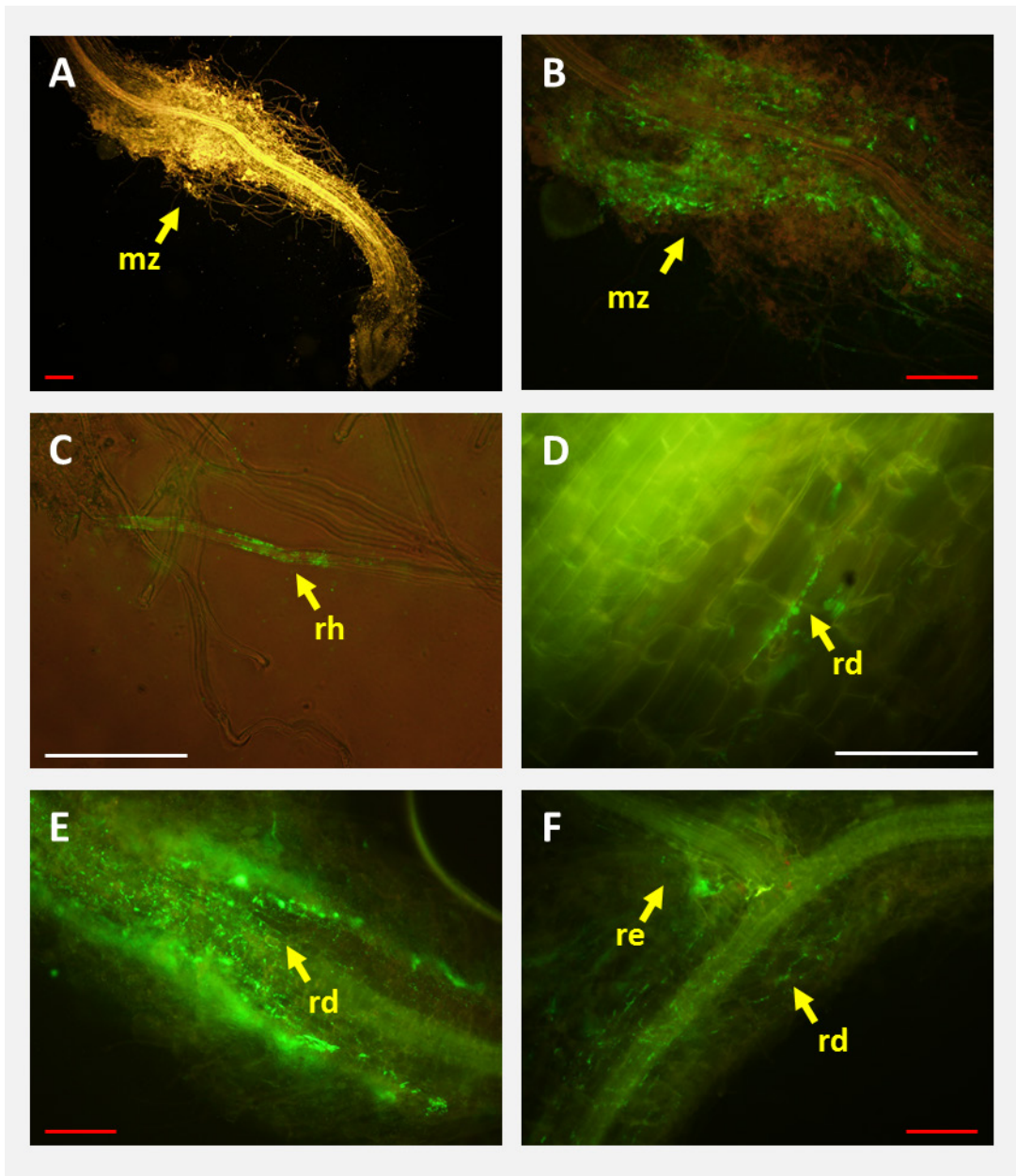


Figure 5.3.3 Brightfield and fluorescent microscope images of GFP-tagged Ha185(pWM1007) colonising at various locations on ryegrass root; at the maturation zone (mz) (A (bright field), B) on root hairs (rh) (C) during first week of inoculation; on the rhizoplane in between rhizodermis cells (rd) (D, E, F); and around lateral root emergence (re) (F) at 14 days after inoculation. Yellow arrows denote the location of Ha185(pWM1007). Red scale bar = 200 μ m, white scale bar = 100 μ m.

At 14-days post-inoculation, GFP-tagged Ha185(pMW1007) was observed near the centre of the primary root (Figure 5.3.3, D, E, F), and was predominantly on the rhizoplane, specifically between the rhizodermis cells (Figure 5.3.3, E, F). During this time at 14-days post-inoculation, fewer bacteria were visualised around the root hairs at the maturation zone. This is possibly the result of the growth of lateral root primordia, which occurred at the maturation zone, and the appearance of a lateral root apical meristem, which provided the opportunity for Ha185(pWM1007) to colonise at the root of emergence (Figure 5.3.3, F; Figure 5.3.4, A, B). Of interest, the Ha185(pWM1007) strain was not observed colonising either the primary or secondary root cap, and fewer cells were observed on the rhizoplane of the meristematic zone where plant cellular division takes place (Figure 5.3.2).

At 14-days post-inoculation Ha185(pWM1007)-inoculation, bacterial cells had colonised the inside of outer epidermal cells as well as inside the root hair (Figure 5.3.4, C, D). Based on these observations, it is possible that Ha185(pWM1007) gained entry to the epidermis via the root hair to colonise the inside of individual epidermal cells (Figure 5.3.5, E, F). However, it is not known whether Ha185(pWM1007) can bypass the epidermal cell plasma membrane and travel to adjacent cells. Ha185(pWM1007) was also observed inside the root, with the bacteria appearing as disconnected chains (Figure 5.3.4, E, F). It is interesting to note that Ha185(pWM1007) was predominantly found along the primary root, with few cells observed around or inside the secondary roots. The precise sites of Ha185(pWM1007) colonisation inside the root have yet to be determined. At 21-days post-inoculation, Ha185(pWM1007) was observed inside and along the primary root, possibly in the area of the root stele (Figure 5.3.4, E), and was also observed inside of the meristematic zone of the ryegrass root.

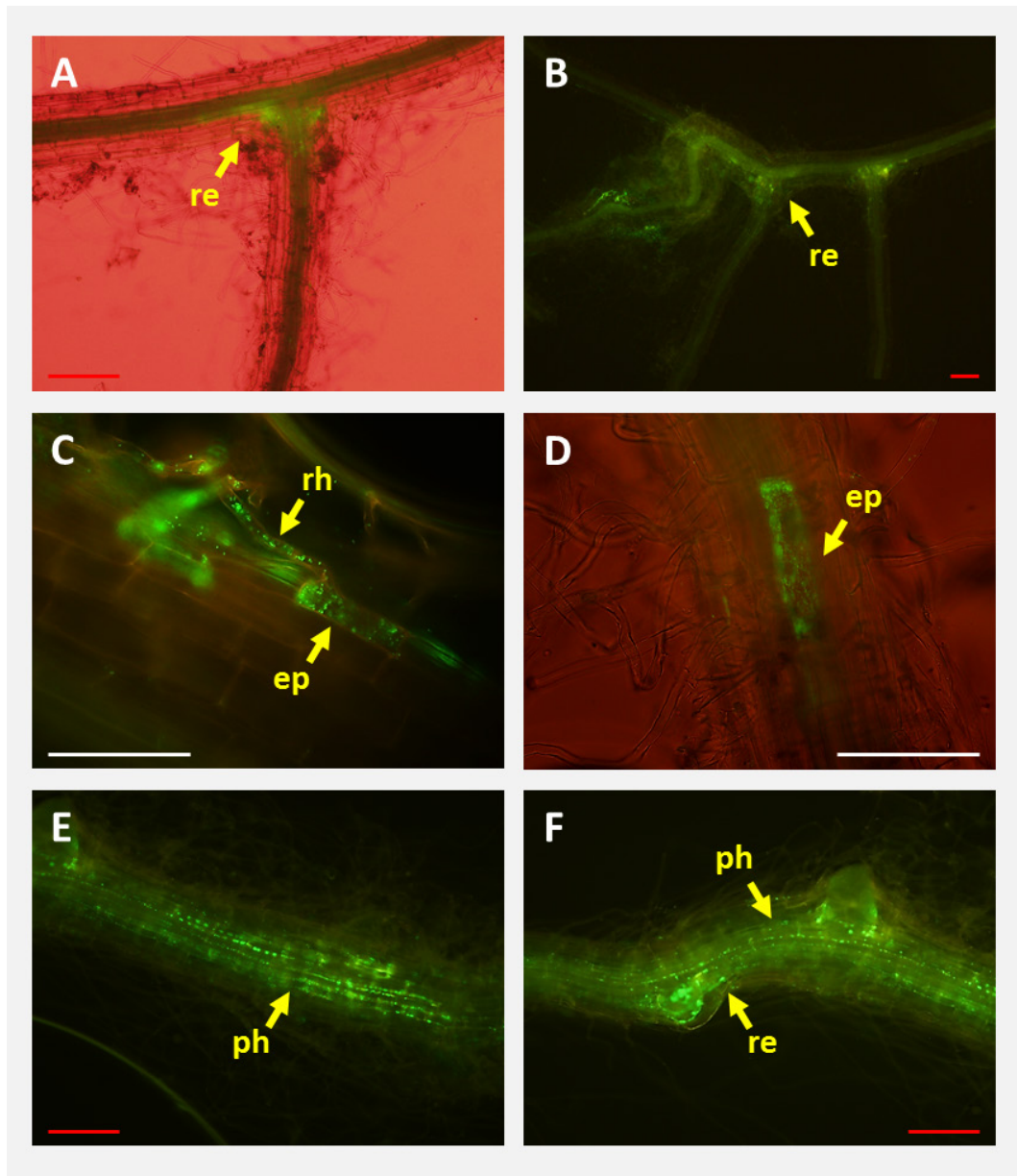


Figure 5.3.4 Brightfield and fluorescent microscope images of GFP-tagged Ha185(pWM1007) colonising both rhizodermis and epidermis of ryegrass root; at the lateral root emergence (re) (A, B, F) after 14 days of inoculation; inside root hair (rh) (C), epidermis (ep) (C, D) and inside root stele of the primary root along root phloem (ph) (E,F) after 21 days of inoculation. Yellow arrows indicates localisation of Ha185(pWM1007). Red scale bar = 200 µm, white scale bar = 100 µm.

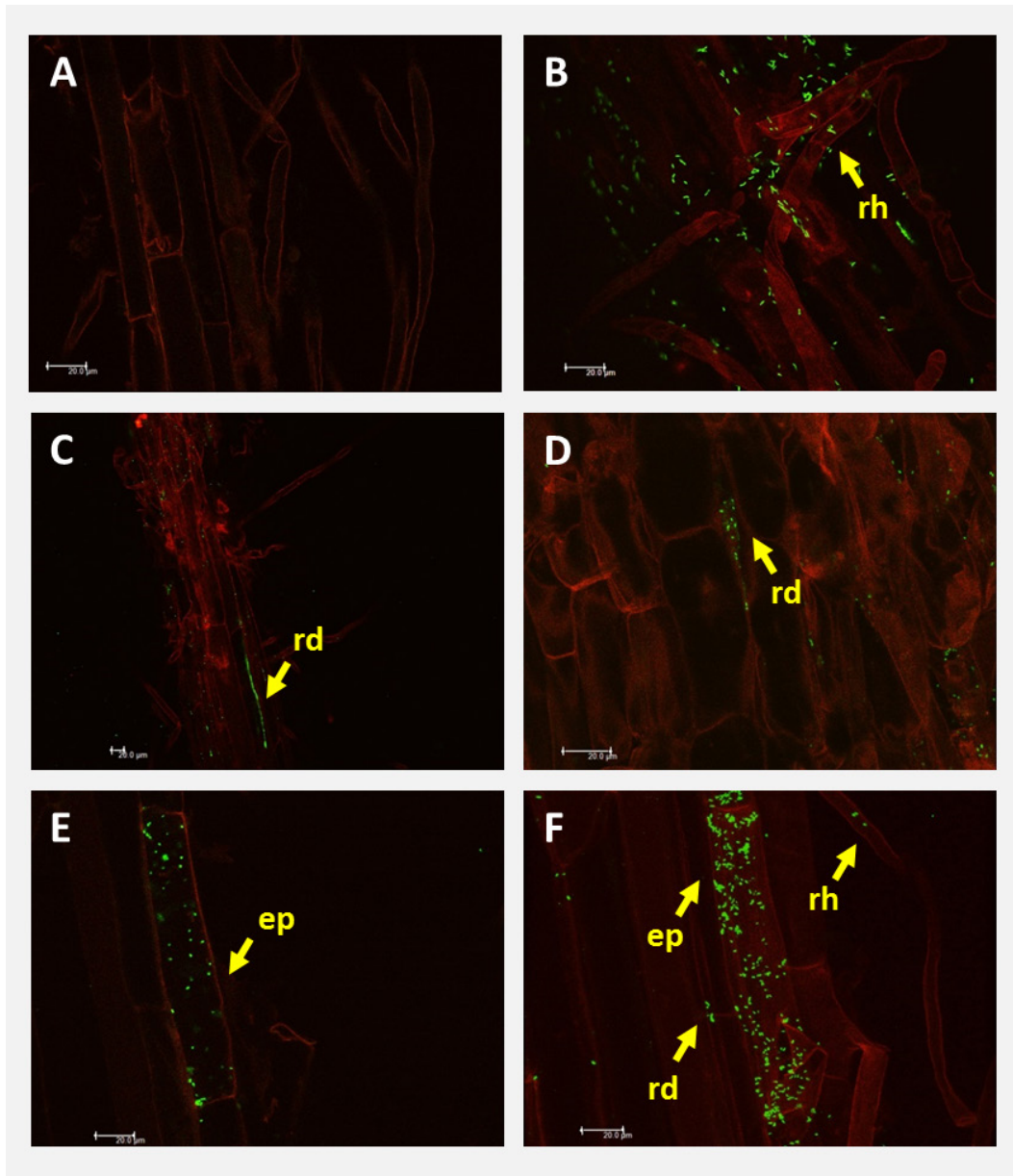


Figure 5.3.5 Confocal microscope images of Ha185(pWM1007) colonisation. Uninoculated ryegrass root (A); Ha185(pWM1007) adhering to root hairs (rh) (B, F) and colonising the rhizoplane and between rhizodermis root cells (rd) (C, D) at day 7; and inside epidermis cells (ep) (E, F) at day 14. Emission bandwidth for green fluorescence is 501nm - 551nm, and for red fluorescents is 601nm - 754nm. Scale bar = 20 μm.

5.3.3. Visualisation of *bxpC::gfp*(Ha185) and *hemX::gfp*(Ha185) fusion strains using fluorescence and confocal microscopy

To confirm that the *hemX::gfp*(Ha185) and *bxpC::gfp*(Ha185) translational reporter gene fusions had integrated into the *Burkholderia* sp. Ha185 genome and fluoresced during HydroxP solubilisation, *hemX::gfp*(Ha185) and *bxpC::gfp*(Ha185) were patched onto Hyp-G plates (Appendix A.2.2). The plates were then incubated for 72 h, allowing growth of the bacterium. A single colony was transferred onto a glass slide with 50 μ L of SpecM solution (Appendix A.1.2), and visualised with a fluorescence microscope, using the U-MWU filter as outlined in Section 5. Fluorescence microscopy revealed that both *hemX::gfp*(Ha185) and *bxpC::gfp*(Ha185) were expressing *gfp* (Figure 5.3.6 A & B, and C & D respectively). However, low fluorescence intensity was observed, and not all bacterial cells fluoresced green, with various fluorescence intensities observed within the bacterial population for both gene fusion constructs.

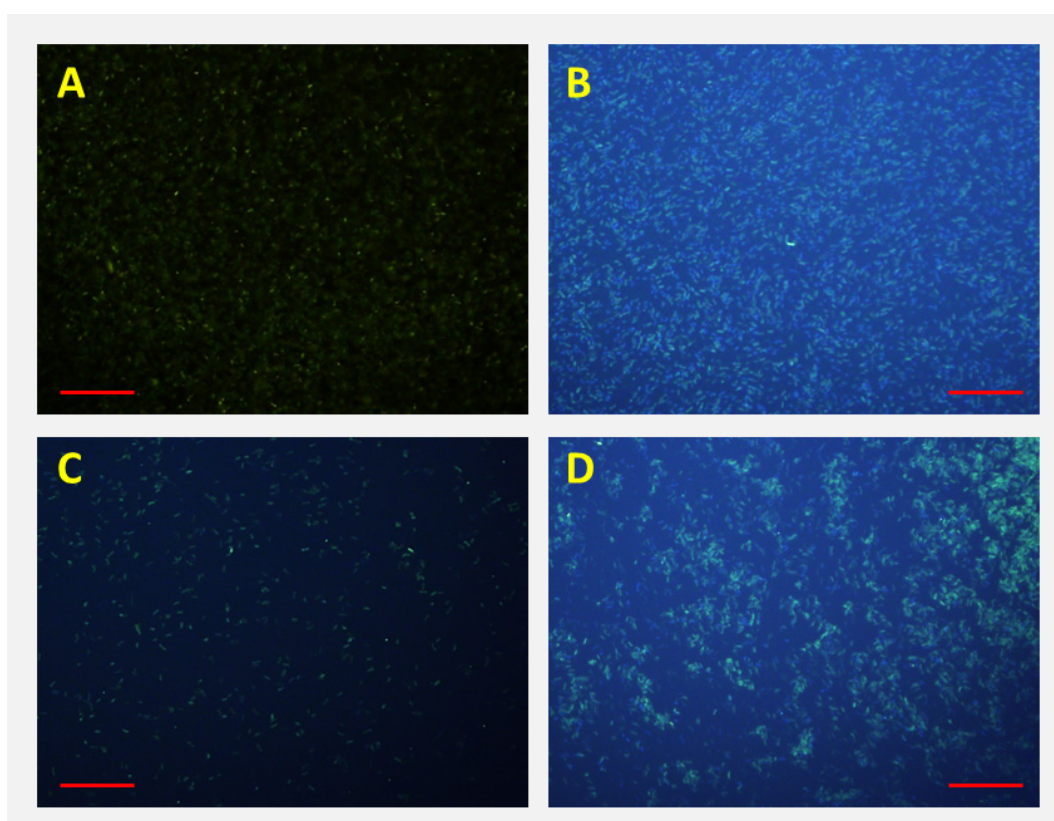


Figure 5.3.6 Fluorescent microscope images of *hemX::gfp*(Ha185) (A & B) and *bxpC::gfp*(Ha185) (C & D). (A) Filter U-MWIB ; (B-D) U-MWU filter. Red scale bar = 50 μ m.

To define the locations where BxpC and HemX are expressed *in situ*, plants inoculated with with the two *gfp*-fusion strains, *hemX::gfp*(Ha185) and *bxpC::gfp*(Ha185), were examined by confocal and fluorescence microscopy. No GFP florescence was observed at day 7 in plants inoculated with *bxpC::gfp*(Ha185), but several fluorescent particles were observed in plants inoculated with *hemX::gfp*(Ha185). Confocal microscopy revealed that these particles displayed various shapes and lengths (ranging from 1.5–3.0 μm) (Figure 5.3.7 (B)). The fluorescent particles moved vigorously in random motion but distinct from Brownian motion. It was uncertain whether these particles were *hemX::gfp*(Ha185) bacterial cells, but due to the irregular shape, it was postulated that the fluorescent particles were composed of both HydroxP particles and *hemX::gfp*(Ha185). Mobile particles were not observed in the uninoculated control (Figure 5.3.7 (A)). It is possible that the HemX-GFP fusion protein was expressed at the periplasmic membrane of the bacterial cell when in contact with HydroxP particles. Further investigation is required to confirm this hypothesis by visualising *hemX::gfp*(Ha185) when HydroxP particles are being solubilised in the HSU liquid culture assay. Interestingly, no GFP-expressing *bxpC::gfp*(Ha185) cells were observed at 7-days post-inoculation, but several fluorescent cells were observed at day 14 (Figure 5.3.7, C, D). These cells were found adhering to the root hairs of the primary root, and were only found to express BxpC-GFP on the root hair.

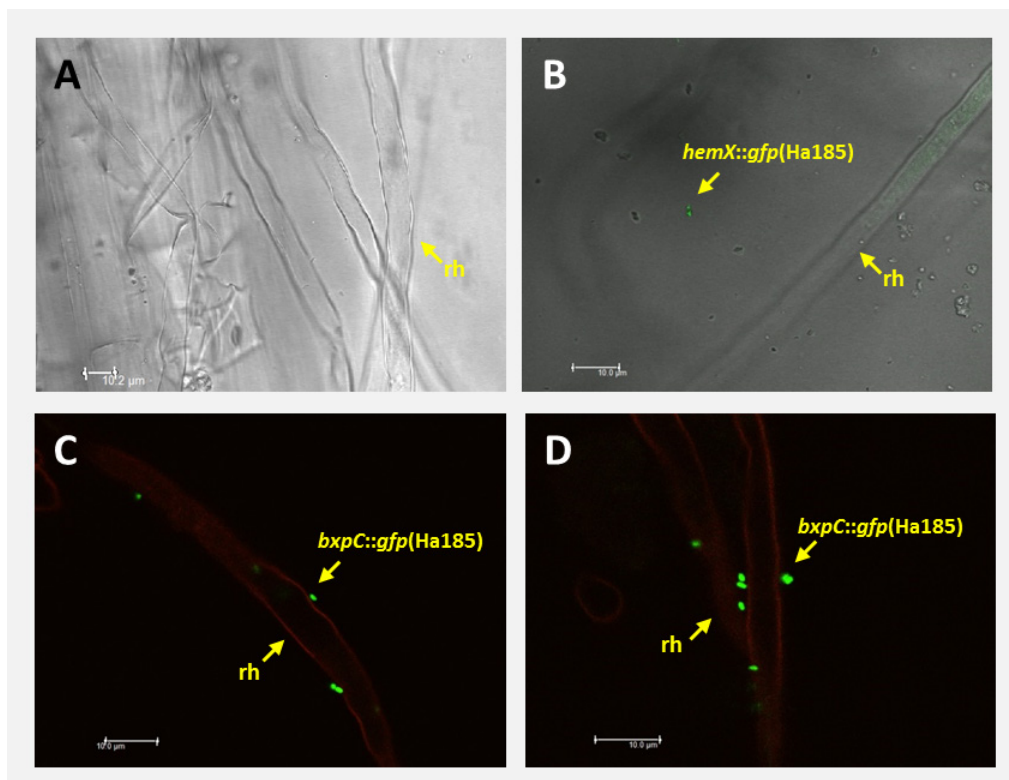


Figure 5.3.7 Confocal microscope images of *hemX::gfp*(Ha185) and *bxpC::gfp*(Ha185) colonisation. Ryegrass root hair without bacterial inoculation as negative control (A), and *hemX::gfp*(Ha185) expressing GFP around root hair at day 7 (B). *bxpC::gfp*(Ha185) adhering to root hairs (C, D) at day 14. Emission bandwidth for green fluorescence is 501nm - 551nm, and for red fluorescence is 601nm - 754nm. Scale bar = 10 μm .

5.4 Discussion

5.4.1. Root colonisation by *Burkholderia* sp. Ha185

Uninoculated ryegrass grown on Hyp-G plates did not produce zones of clearance, indicating the inability of the plant root to solubilise P in the absence of rhizobacteria. Root exudates contain several low molecular weight organic acids that are involved in P solubilisation and mineralisation (Mimmo et al., 2011; Khorassani et al., 2011; Oburger et al., 2011), and have been implicated in defining the structure of rhizosphere microbial communities (Dennis et al., 2010; Shi et al., 2011). Moreover, enhanced efflux of root exudates and organic acid excretion for P solubilisation in soil are thought to increase the efficiency of P use and may therefore be useful in soil P management (Richardson et al., 2011; Wang et al., 2013). The concentration of organic acids in ryegrass root exudates is relatively low, although lactic, fumaric, oxalic and glycolic acids are released under low P conditions (Zyśko et al., 2012). Results of the current study showed that in the absence of *Burkholderia* sp. Ha185, the ryegrass root alone is unable to solubilise HydroxP (Figure 5.3.1; uninoculated control). *hemX::Tn5(F18)* and *bxpC::Tn5(F13)* released less than basal levels of 2-KGA, GA, PyrA and LA in liquid culture compared to wildtype (Chapter 4.3.3.3), and showed little HydroxP solubilisation around the root. In contrast, HydroxP was readily solubilised by *Burkholderia* sp. Ha185, indicating a potential role for phosphate-solubilising bacteria in improving P management, and the important role of P solubilisation by *hemX* or *bxpC*.

Significant findings of the current study were that the uninoculated plant roots did not exhibit zones of clearance, and the roots were longer than those grown in the presence of wildtype *Burkholderia* sp. Ha185. This suggests that in the absence of P, the ryegrass root is required to extend further in search of nutrients. Furthermore, the primary root was also extended in ryegrass plants inoculated with *hemX::Tn5(F18)*, and had longer and more densely packed root hairs. This phenotype is similar to that of uninoculated ryegrass in a P-limiting environment, validating the role of *hemX* in P solubilisation, where it mediates the release of P from HydroxP. Li et al. (2012) found that the primary root length of maize (*Zea mays*) was increased under conditions of P-starvation, and under P-limiting conditions, root hairs of barley (*Hordeum vulgare*) increased in both density and length (Brown et al., 2012). Both of these studies concluded that the production of root hairs is an important factor for P accumulation, and for tolerance of a P-deficient environment, which is consistent with the findings of this study. Both uninoculated ryegrass and *hem::Tn5(F18)*-treated plants had elongated roots and increased amounts of root hair growth (Figure 5.3.1 (A & B)). Increased root length and root hair density would increase the root surface area, maximising contact

with the surrounding environment, and allowing more nutrients to be absorbed. In agreement with this scenario, the phenotype of the *hemX::Tn5(F18)*-treated plant was similar to the uninoculated control, where P levels were insufficient for plant growth.

Interestingly, ryegrass inoculated with *bxpC::Tn5(F13)* not only had increased root length and fine root hairs, but the number of secondary lateral roots was also increased. Johnson et al. (1996) reported that under P-limiting conditions, white lupin (*Lupinus albus* L.) meristems were clustered and meristem emergence was more pronounced at the proteoid root zones, relative to P treated lupin. This resulted in a greater number of secondary lateral roots. However, elevated meristem emergence and enhanced lateral root formation was not observed in the uninoculated ryegrass control under the same P-limited conditions. Although some studies have correlated enhanced lateral root formation with P-starvation, auxin regulation and effects of sucrose on various plants (Pérez-Torres et al., 2008; Jain et al., 2007), the mechanism of *bxpC::Tn5(F13)*-induced ryegrass lateral root formation is yet to be determined. Furthermore, root physiology and P responses of perennial ryegrass are poorly understood.

Results of the plant root-based assay (Section 5.3.1) demonstrated that ryegrass roots inoculated with wildtype *Burkholderia* sp. Ha185 produce shorter primary roots and fewer root hairs. Although in these experiments the root diameter was not measured, the ryegrass root appeared to be thicker and more robust. In future studies, precise measurement of root length and root diameter should be carried out to investigate the effect of *Burkholderia* sp. Ha185 on the root system and structure of ryegrass. *B. phytofirmans* strain PsJN, which is closely related to *Burkholderia* sp. Ha185 (Chapter 4.1.2), has been shown to increase potato fresh root weight by 108% over the uninoculated control (Da et al., 2012). The potato plants also produced a larger root system, with enhanced secondary roots and more root hairs, and tolerance of potato plantlets to abiotic and biotic stresses was also improved (Nowak, 1998).

5.4.2. Colonisation pattern of *Burkholderia* sp. Ha185 on ryegrass roots

Burkholderia sp. strain Ha185(pWM1007) initially colonised at the maturation zone (at day 7), where dense root hairs were formed during epidermal cell differentiation. The maturation zone consists of “root hair cells”, the pattern of cell division of which differs from that of non-hair cells (elongation zone), and is highly regulated by plant hormones auxin and ethylene (Bruex et al., 2012). *Burkholderia* sp. Ha185 is capable of producing auxin (Chapter 2.3.4), and therefore the presence of

this isolate at the maturation zone may enhance auxin regulation and benefit the ryegrass root. At 21-days post-inoculation, Ha185(pWM1007) predominantly colonised the primary root, with fewer colonies observed on lateral roots. This may suggest that the strain remains on the primary root where there is a rich supply of sugars and nutrients. This pattern of colonisation varies from that described by Sessitsch et al. (2005), who found that GFP-expressing *B. phytofirmans* PsJN cells colonised lateral roots more heavily than primary roots of chickpea (*Cicer arietinum* L.), a dicot. Perennial ryegrass (Poaceae) is a monocot, hence there are fundamental differences in root structure and in how the supply of nutrients is regulated in the root system (Hall et al., 1996). This may alter the colonisation pattern of bacteria such as *Burkholderia* spp.

Of interest, *B. phytofirmans* PsJN was also observed inside the epidermal cells of chickpea roots (Sessitsch et al., 2005), similar to the identification of GFP-tagged *Burkholderia* sp. Ha185 inside the outer epidermal cells in the current study. This observation confirms the endophytic properties of this bacterium. A similar colonisation pattern was also noted by Compant et al. (2005), who reported that GFP-tagged *B. phytofirmans* PsJN (PsJN::gfp2x) were found inside grape root epidermal cells. However, Ha185(pWM1007) was observed inside individual root hairs at the maturation zone, which connect to a single epidermal cell (Figure 5.3.4 (C)). Therefore, it is postulated that *Burkholderia* sp. Ha185 colonised epidermal cells via the root hair. It is possible that cell wall-degrading enzymes such as endoglucanase or endopolygalacturonase are produced by *Burkholderia* sp. Ha185, which could degrade the thin layer of the root hair instead of the thicker outer cells. To determine if *Burkholderia* sp. Ha185 produce endoglucanase and endopolygalacturonase enzymes, further bioinformatic analysis and Kim and Wimpenny medium plate-based assays (Kim and Wimpenny, 1981; Reinhold-Hurek et al., 1993) need to be undertaken.

Both the maturation zone (where dense root hairs are formed) and the area of lateral root emergence (where there are “cracks” in the ryegrass root) were identified as hotspots for *Burkholderia* sp. Ha185 colonisation. *Burkholderia* sp. Ha185(pWM1007) colonisation was observed at cracks of lateral root emergence, a location where root exudate leakage is postulated to play a role in attracting microbes (Bais et al., 2004). Similar colonisation at the junction of lateral root emergence of the primary root of Chardonnay plantlets was also observed by *Burkholderia* strain PsJN::gfp2x (Compant et al., 2005). Furthermore, *Burkholderia vietnamiensis* MGK3 also intensively colonises this area (Govindarajan et al., 2008). Colonisation by *Burkholderia* sp. Ha185 at the lateral root emergence would provide opportunities for the bacterium to enter (“crack entry”) internal tissues, where endophytic bacteria could possibly gain access to the inner cortical cells (instead of

through cells) and finally reach the central cylinder of the root stele (Figure 5.3.8). However, confocal microscopy did not show direct invasion of cortical cells by *Burkholderia* sp. Ha185.

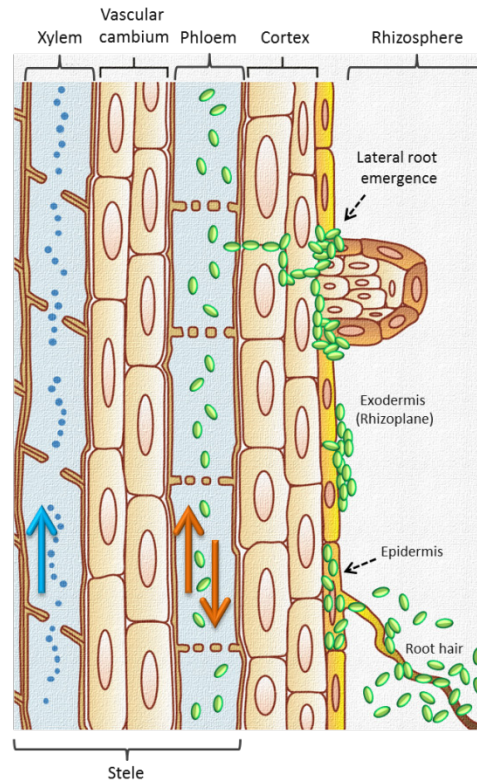


Figure 5.3.8 Model of *Burkholderia* sp. Ha185(pWM 1007) ryegrass root colonisation. Green ovals depict GFP-tagged Ha185 bacteria that were observed on the rhizoplane of ryegrass root (rhizodermis), in between rhizodermis cells, around root hairs, inside root epidermis cells, at the lateral root emergence, in between cortex, and in the phloem of ryegrass root. Blue arrow denotes the direction of water travel up the xylem. Brown arrow indicates the flow of nutrients in the phloem.

With reference to Figure 5.3.8, the root stele is typically composed of several transportation systems and several different cell types. The xylem transports water molecules upward against gravity by osmosis, whereas the phloem is involved in transporting carbohydrates synthesised during photosynthesis (such as sucrose and glucose) in both directions (Lalonde et al., 2003). The root phloem is composed of sieve tube elements, with sieve pores located in between to allow the transportation of sugars derived from photosynthesis, which are actively pumped from leaves to roots in both directions, crossing sieve pores (Figure 5.3.8). It is hypothesised that Ha185(pWM1007) gains entry to the root stele by “crack entry” during the development of lateral roots, and the bacteria then move between the cortex cells and eventually reach the root stele. The identification of the GFP-tagged isolate inside and along the root suggests that it may be able to travel within the primary root via the phloem, which carries materials in both directions (Figure 5.3.8). Sugar provided

by the ryegrass root would represent a rich carbon source for Ha185(pWM1007) growth and colonisation. However, inoculation of chickpea plants and Chardonnay plantlets with GFP-expressing *B. phytofirmans* PsJN showed that bacteria were found in the xylem vessels of the root instead of in the phloem inside the stele. This strain also colonised the root tip of both of these plant species (Sessitsch et al., 2005; Compant et al., 2005). However, using the monocot, ryegrass, and *Burkholderia* sp. Ha185(pWM1007) as a model, bacteria were not observed to colonise at the rhizodermis of the meristematic zone, nor at the end of root tip (Figure 5.3.2). Therefore, it is unlikely that bacteria gain entry through the root tip and enter the xylem vessel by travelling up the ryegrass root. To confirm the precise *in situ* localisation of *Burkholderia* sp. Ha185 inside the root system, glutaraldehyde or formaldehyde root fixation followed by staining of cross-sections of ryegrass root with Safranin-O or Fast Green, as described in Rennie et al. (2013), should be undertaken.

5.4.3. Expression of in-frame *hemX::gfp*(Ha185) and *bxpC::gfp*(Ha185) gene fusions

Quantitative measurements of both bacteria and HydroxP particles from the HSU liquid culture assay were made using qNano, the iZon sensing nanopore (Appendix E). HydroxP-insoluble particles were similar in size to *Burkholderia* sp. Ha185, making it difficult to differentiate between the two. However, the results suggested aggregation of particles, possibly representing a direct interaction between the bacteria and HydroxP. Such a scenario would explain the appearance of irregular green fluorescent shapes observed 7-days post-inoculation of ryegrass with HydroxP and the translational gene fusion strain *hemX::gfp*(Ha185). It is possible that the irregular particles were a composite of both *hemX::gfp*(Ha185) and HydroxP, where P solubilisation occurred around the root hair but not on the rhizoplane of ryegrass roots. Interestingly, genes located downstream of *hemX*, *hemY* (encodes a membrane protein), and on the opposing strain *mfs* (coding for a major facilitator superfamily protein), the translated products of which are membrane transporters (Chapter 4.3.2). It is therefore possible that *gfp* was expressed during *hemX* expression, and that the haem cofactor complex was transported to the periplasmic membrane. This also supports results from qNano analysis (Appendix E), which suggested that P solubilisation by *Burkholderia* sp. Ha185 occurs when the HydroxP particles are in close proximity to the bacterial cell wall. Assessment using *in vitro* HSU HydroxP liquid culture assay of *hemX::gfp*(Ha185) in conjunction with fluorescence microscopy could confirm this theory. Furthermore, gene expression results from qRT-PCR (Chapter 4.3.3.7) showed that genes from the *hem* operon were over-expressed at 24 h in the HSU HydroxP liquid culture assay.

Therefore, an earlier sampling time (i.e. 24–72 h post-inoculation) of *hemX::gfp*(Ha185)-inoculated ryegrass may be ideal for determining *gfp* expression.

Confocal microscopy of ryegrass seedlings inoculated with the translational gene fusion *bxpC::gfp*(Ha185) revealed several *bxpC::gfp*(Ha185) cells fluorescing green on root hairs. This differed from *hemX::gfp*(Ha185)-inoculated seedlings where the bacteria were observed around the rhizosphere but not adhering to the plant root. The translated product of *bxpC* is a hypothetical protein suspected to be involved in P solubilisation, possibly associated with 2-KGA transportation via the Bxp complex. 2-KGA is produced by both plants and microorganisms and is widely abundant in soil, with the highest concentrations occurring in agricultural soil where it typically resides as calcium-bound 2-KGA (Webley and Duff, 1965). In addition, Moghimi et al. (1978) found that 2-KGA accounted for 20% of the rhizospheric-derived products of wheat seedlings. In a P-limiting environment, the root hair is considered to be the key site of P accumulation (Brown et al., 2012). It is therefore possible that the visualisation of *bxpC::gfp*(Ha185) at the root hair is linked to 2-KGA transportation after HydroxP has been solubilised. This differed from *hemX::gfp*(Ha185), which could be visualised in proximity, but not attached to, root hairs of ryegrass.

Chapter 6

General Discussion

6.1 Effective phosphate solubilisers

A promising strategy for improving the utilisation of P in soil-plant systems is the use of effective phosphate-solubilising microorganisms. The objective of this study was to identify novel genes implicated in P solubilisation. Three bacteria from different genera, (*Enterobacter*, *Pseudomonas* and *Burkholderia*) isolated from distinct geographic locations that were amenable to molecular manipulation were subjected to transposon mutagenesis (Chapter 3). The genes identified in *Pseudomonas* sp. Ha200 are involved in the known and well characterised PQQ pathway. Therefore these genes identified were not studied further but the information was integrated into a publication by Giles et al. (2014). In addition, through the assessment of culture supernatants of several *Pseudomonas* spp. strains using HPLC, an unknown organic acid was detected (Un2) which may also be involved in P solubilisation.

6.2 Hydroxyapatite solubilisation by 2-ketogluconate released by *Burkholderia* sp. Ha185

The key aim of this study was to identify unique genes involved in P solubilisation. The strain *Burkholderia* sp. Ha185 was isolated from native forest at Haast, New Zealand, and exhibited significant ability to solubilise calcium P in the presence of glucose. Genome sequencing revealed that *Burkholderia* sp. Ha185 is a member of the plant-associated beneficial and environmental group of the *Burkholderia* genus, which is closely related to *B. phytofirmans* PsJN and *B. xenovorans* LB400 (Suárez-Moreno et al., 2012).

Burkholderia sp. Ha185 was found to have several plant growth promoting traits such as production of phytohormone-auxin (IAA), ACC deaminase, phytase, siderophores and exhibited the ability to solubilise various forms of insoluble calcium P (Chapter 2, **Figure 6.4.1**). In this study an *in vitro* HSU hydroxyapatite liquid culture assay was developed allowing the determination of the amount of P released together with determination of organic acids released by *Burkholderia* sp. Ha185 during hydroxyapatite (HydroxP) solubilisation. 2-Ketogluconic acid (2-KGA) is the predominant organic acid released by *Burkholderia* sp. Ha185 (Chapter 2.3.4.1 & 4.3.3) while gluconic acid (GA) was detected only at basal level in culture supernatants. This result contrasts with the widely accepted view that

GA plays a key role in P solubilisation (de Werra et al., 2009). The differing results likely reflect analytical difficulties in HPLC and/or the natural chemical properties of 2-KGA which is more efficient at chelating calcium from the less soluble HydroxP as opposed to GA at solubilising more soluble TCaP. The rapid decrease in pH during the production of 2-KGA may reflect its low dissociation constant (pK_a) facilitating dissolution. It is possible that protonation at the peripheral bacterial cell wall plasma membrane enhances the solubility of calcium salt at low pH. Therefore, low pH (to ~ 4.24) of the culture supernatant as well as released of strong carboxylic acid, 2-KGA, are required for solubilising the less soluble form of calcium P, HydroxP.

6.3 Novel genes associated with phosphate solubilisation

Historically genes thought to be involved in P solubilisation are involved in the direct oxidation pathway by PQQ dependent membrane bound glucose dehydrogenase (Gcd). In this process glucose is oxidised to GA at the periplasmic space of the bacterial cell. The redox cofactor PQQ is thought essential for this reaction to occur. However, no genes involved in the PQQ pathway were found through random mutagenesis of *Burkholderia* sp. Ha185 (Chapter 3.3). Furthermore, assessment of the draft *Burkholderia* sp. Ha185 genome sequence did not identify any PQQ-dependent *gcd* or components of the *pqq* operon. This indicated *Burkholderia* sp. Ha185 may solubilise P by an alternate and potentially novel route. Two unique mechanisms not previously implicated in P solubilisation were identified through this study. Thus, to our knowledge this is the first time that the genes *bxpC* and *hemX* have been implicated in P solubilisation. Both *bxpC*::Tn5(F13) and *hemX*::Tn5(F18) mutants had impaired P solubilisation that was directly correlated to reduced 2-KGA production. Furthermore, gene complementation of these mutants restored the mineral P solubilisation (MPS) phenotype validating the role of these genes in HydroxP solubilisation.

6.3.1. *hemX* involved in 2-keto-gluconic acid production

The *hemX*::Tn5(F18) mutant was unable to solubilise HydroxP in plate and HSU HydroxP liquid culture assays (Chapter 4.3.2). Organic acid analysis revealed that not only was production of 2-KGA minimal at 72 h, but the organic acid profile was analogous to *Burkholderia* sp. Ha185 when utilising mannitol as the sole carbon with the secretion or released of Un3 and Un4 organic acids (as discussed in Chapter 4.4.3). By disrupting the *hemX*, glucose metabolism had possibly shifted to a pathway similar to that of mannitol metabolism. Complementation of the *hemX* in *hemX*::Tn5(F18) mutant restored the MPS phenotype, and 2-KGA was detected in the culture supernatant (Chapter 4.3.3.3). This

validated the significance of the role of *hemX* in *Burkholderia* sp. Ha185 P solubilisation. Bioinformatic analysis of genes within the *hemX* operon revealed the pathway could be implicated in haem or haem d_1 biosynthesis and the role of the final haem molecule could be a redox cofactor for the haem-dependent gluconate 2-dehydrogenase (GADH) which is involved in the overall HEM-GADH complex (**Figure 6.4.1**). The HEM-GADH complex was found to be responsible for oxidising GA to 2-KGA (Yum et al., 1997). Furthermore, sequence alignment of the *Burkholderia* sp. Ha185 gene involved in the HEM-GADH revealed the presence of haem-binding motifs and suggested that haem cofactor(s) are involved in P solubilisation (Chapter 4.3.5.1).

Results from qRT-PCR revealed that *hemC* located upstream of *hemX* was upregulated within the initial 24 hours of cell growth. At 40 h during HydroxP solubilisation there was no significant *hemC* or *hemX* expression, and at 48 h *hemC* was significantly suppressed at a time with the maximum concentration of P and 2-KGA (Chapter 4.3.3.7). This indicated that the haem biosynthesis of *Burkholderia* sp. Ha185 occurs at cell growth stage (mid-log phase, Appendix B.2). The chemical structure of haem molecule may be stable throughout growth and it is possibly reused by the bacteria, and so constitutive synthesis of the haem molecule is unnecessary. Further evidence of this was provided by the increased halo size relative to the wildtype in the CD3ME12 and DXDME6 complemented strains.

The mutant *hemX::Tn5(F18)* has been shown to cause enhanced root elongation and increased numbers of fine dense root hairs, as seen in the uninoculated control, possibly as a result of P-starvation. Confocal microscopy of the *hemX::gfp(Ha185)* in-frame gene fusion mutant revealed that the *hemX* was expressed at 7-days post-inoculation of ryegrass in close proximity to root hair. The irregular shape of the fluorescent particles from the *hemX::gfp(Ha185)* treated ryegrass may represent a HydroxP bound *hemX::gfp(Ha185)* that was fluorescing through the process of HydroxP solubilisation at the cell wall surface (Chapter 5.3.5). This scenario would be in agreement with oxidising GA to 2-KGA by HEM-GADH complex which comprised three components of membrane proteins and the reaction is known to occur at the periplasmic space of bacteria (Yum et al., 1997). Furthermore, the quantitative size measurement of particles using qNano (Appendix E), where HydroxP formed larger particles in the presence of *Burkholderia* sp. Ha815, indicated that the bacterium and HydroxP had combined during the HydroxP solubilisation.

6.3.2. Putative 2-keto-gluconate transporter model of the Bxp complex

Results from plate and HSU HydroxP liquid culture assays showed that the *bxpC::Tn5(F13)* mutant impaired HydroxP dissolution (Chapter 4.3.1.3) and significantly reduced 2-KGA released in comparison with the wildtype *Burkholderia* sp. Ha185. The complemented strain 1311CMPB2 recovered the MPS phenotype and the production of 2-KGA was restored (Chapter 4.3.3). This validated the importance of *bxpC* in HydroxP solubilisation of *Burkholderia* sp. Ha185 and is the first account of *bxpC* involvement in P solubilisation. Of particular note, the BxpC protein contains a duf1311 domain that is shared by a large group of small hypothetical proteins across a wide range of bacteria including *Burkholderia* spp., *Pseudomonas* spp. and *Acinetobacter* spp. (Chapter 4.3.5.4). It is proposed that other members of this family may have a significant role in the transport of small elemental based compounds that may differ in composition to BxpC-Ca-2KGA. In contrast to *hem*, the *bxpC* was up-regulated at 48 h when 2-KGA was found at the highest concentration in the culture filtrate. Decreased expression of the *bxpC* at 72 h linked to decreased 2-KGA concentration in the culture filtrate. Furthermore, the *bxpC* complemented mutant 1311CMPB2 increased cellular uptake of 2-KGA as measured by the HPLC assessment of the sonicated filtrate, suggesting that it is possible the BxpC is involved in the transportation of 2-KGA. *In silico* analysis and protein tertiary structure prediction revealed the BxpC is a tetrameric protein with a calcium binding site within each monomer. This indicates that BxpC may interact with calcium ions and could potentially chelate calcium bound 2-KGA compound. Based on results of qRT-PCR and bioinformatics analysis of *bxpC* and its associated ORFs presented in Chapter 4, we propose that genes from the *bxp* operon translate to several proteins that may form a Bxp protein complex.

The GabY protein from *Burkholderia cepacia* which shares similarities with transmembrane amino acid ABC transporters was found to be associated with P solubilisation (Chapter 1.3.5, Zhao et al., 2013). Interestingly, the *gabY* also possesses signal peptide residues and Zhao et al. (2013) concluded that GabY protein is a membrane bound protein and could be linked to organic acid secretion. Similarly, it is postulated that the Bxp complex from *Burkholderia* sp. Ha185 possesses a function for its own organic anion transportation by undergoing a conformational change which facilitates the translocation of the chelated BxpC-Ca-2KGA compound.

In the presence of the plant, the *bxpC::Tn5(F13)* mutant not only enhanced root elongation but the meristems appeared clustered and the number of secondary lateral roots were also increased. However, the precise reason for these changes remains unclear. Using confocal microscopy of the *Burkholderia bxpC::gfp*(Ha185), the bacterium was found to fluoresce at 14-days post-inoculation on the root hair of the primary root of ryegrass. It is hypothesised that the *bxpC::gfp*(Ha185) fluoresced

during BxpC-Ca-2KGA transportation via the Bxp complex (Chapter 4.4.8). The discovery of the *bxpC* and its associated *bxp* operon provided a unique insight of P solubilisation that, based on the results of this study, appears to be linked to organic anion transportation. This challenges the conventional view of P solubilisation by the direct oxidation pathway via the PQQ-dependent glucose dehydrogenase and subsequent release of GA. Furthermore in an analogy to siderophores, evolutionary adaptation may lead to competition between the plant root and bacteria as well as competition between different bacterial species. Therefore, systems such as the Bxp complex identified through the course of this study may prevent other organisms (that do not contain the relevant BxpC importation machinery) from acquiring 2-KGA which is involved in central carbon metabolism.

6.4 Plant root associated *Burkholderia* sp. Ha185

Observations using GFP-tagged *Burkholderia* sp. Ha185 by fluorescent microscopy revealed that Ha185(pWM1007) primarily colonised at the root maturation zone where dense fine root hairs are found during cellular differentiation. Dense root hairs at the maturation zone provided a stable habitat for bacterial interactions. Moreover, the bacterium was also found to colonise the zone of lateral root emergence during the growth of lateral root primordia where “cracks” were located, possibly allowing entry into the stele. Cracks at root emergence may provide the opportunity for Ha185(pWM1007) to source nutrients from close to, or from inside of the plant root. *Burkholderia* sp. Ha185 was not only able to colonise the rhizoplane of the ryegrass root, but is also endophytic (Chapter 5.3.4). Although the exact location of Ha185(pWM1007) colonising inside the ryegrass stele has yet to be determined, it is possible that *Burkholderia* sp. Ha185 is able to move within the phloem of the primary root where the main supply of carbon sugar is transported. Understanding the colonisation pattern of plant associated PSB such as *Burkholderia* sp. Ha185 on plant root will improve our utilisation of biofertilisers. This will lead to a targeted selection of the most suitable biofertiliser bacteria for application through a variety of methods including seed inoculation or post-emerging application.

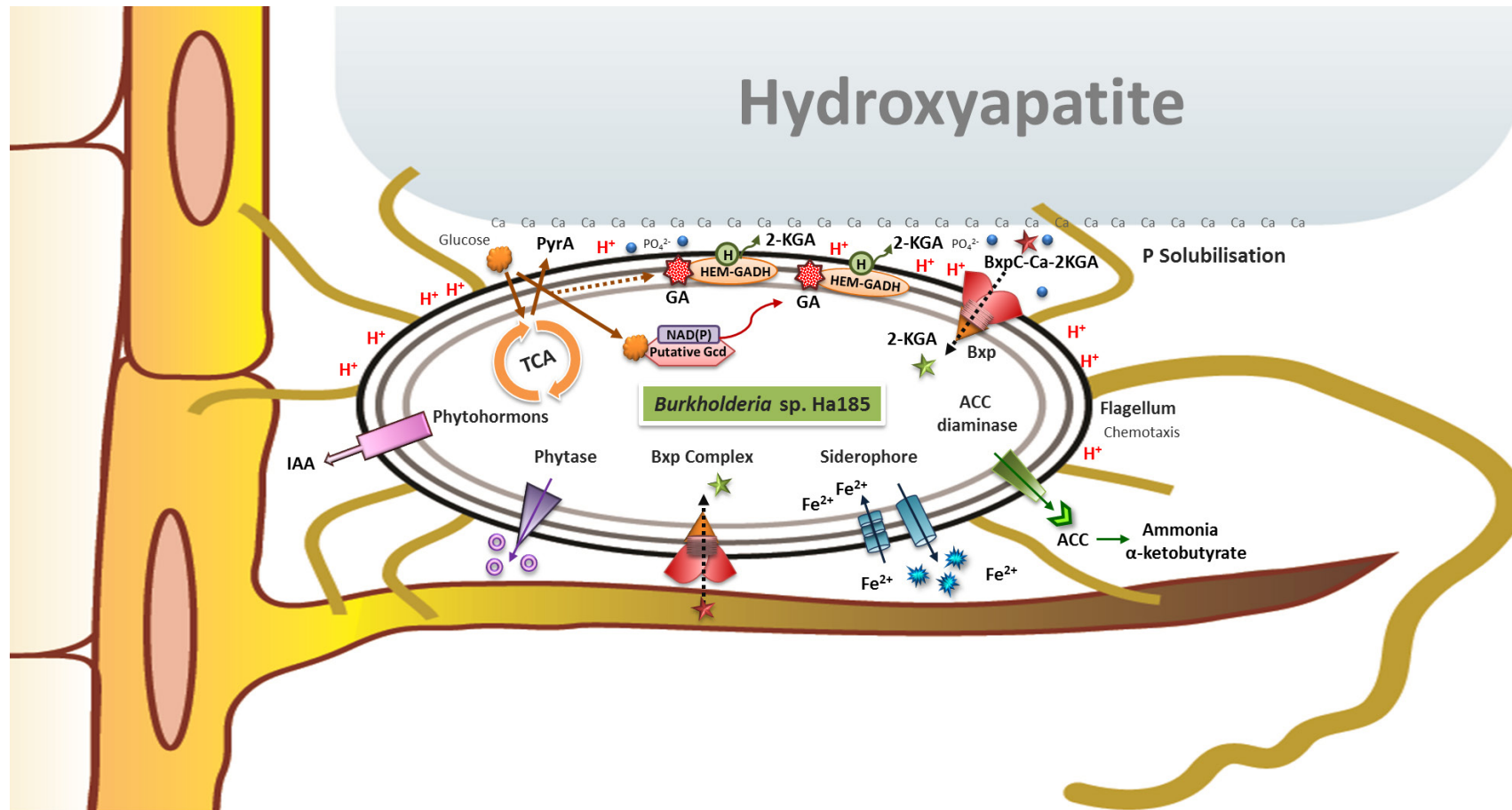


Figure 6.4.1 Schematic diagram of *Burkholderia* sp. Ha185 in close proximity to a hydroxyapatite compound, plant root and root hair. *Burkholderia* sp. Ha185 releases plant growth promoting traits; phytohormones IAA, phytase, siderophore, and ACC deaminase. Synthesis of 2-KGA by *Burkholderia* sp. Ha185 HEM-GADH is facilitated by haem cofactor (green circle). It is hypothesized that 2-KGA is released for chelating calcium at close proximity to hydroxyapatite which forms BxpC-Ca-2KGA compound (red star) and release phosphate ions. This reaction is facilitated by decreasing surrounding pH. It is postulated that calcium bound 2-KGA (BxpC-Ca-2-KGA) is transported back into *Burkholderia* sp. Ha185 cell via the Bxp complex. (Diagram not to scale)

6.5 Future research

6.5.1. Identify the unknown organic acid

An unknown organic acid (Un2) was either secreted or released during HydroxP solubilisation by several EPS *Pseudomonas* spp. strains (Chapter 2.3.4.1). In particular, isolate EE132 (identified to be *Pseudomonas jessenii* with 98 % 16S rRNA similarity) was shown to release Un2 in an unknown concentration and a basal level of GA and PyrA. However, this isolate is capable of releasing high concentration of P from HydroxP indicating Un2 might potentially have a role in solubilising HydroxP. Interestingly, it was shown *gcd::Tn5(B8)* mutant of *Pseudomonas* sp. Ha200 that had a mutation in the PQQ-dependent *gcd* decreased the amount of Un2 to a near basal level with no 2-KGA and GA detected (Chapter 3.3.6). This indicated the production of Un2 is dependent but not limited to the direct oxidative pathway. It is postulated that Un2 is 2, 5-KGA that possesses similar chemical composition to 2-KGA and 5-KGA. To define and confirm the chemical composition of this molecule, Liquid chromatography–mass spectrometry (Tandem MS, LC-MS/MS) could be employed to determine the mass-to-charge ratio by multiple steps mass spectrometry analysis.

6.5.2. Identify the full complement of components involved in the HEM-GADH complex

Six independent ORFs were identified, the translated products of which contained haem-binding motifs that aligned to amino acid sequence of haem-dependent gluconate 2-dehydrogenase (Acceptor) (Subunit II) of *B. phytofirmans* PsJN. To confirm the function of the HEM-GADH complex of *Burkholderia* sp. Ha185 (which is comprised of three subunits), the genes encoding for the complex could be expressed *in trans* in *E. coli* BL21(D3) which possesses the *hem* operon in the genome. This would be expected to result in solubilisation of HydroxP by *E. coli* BL21(D3) through release of 2-KGA in the HSU HydroxP liquid culture assay (as discussed in Chapter 4.4.6). Organic acid profiling at key time points should be confirmed by HPLC analysis as described in Chapter 2.2.4.

Moreover, qRT-PCR could be employed to determine the gene expression of genes involved in the HEM-GADH complex of wildtype *Burkholderia* sp. Ha185 and define the relationship between gene expression and HydroxP solubilisation. We hypothesise that *gadh(II)* of *Burkholderia* sp. Ha185 will be up-regulated during HydroxP solubilisation at 36 and 48 h from the HSU HydroxP liquid culture assay, and down-regulated at 72 h when solubilisation is no longer occurring.

6.5.3. Identify the key function of BxpC protein

The translated product of the *Burkholderia* sp. Ha185 *bxpC* encodes a predicted tetrameric BxpC protein bearing a duf1311 domain of unknown function. Based on results of this study, it is proposed that the protein forms a complex and functions as a cargo protein which binds to calcium bound 2-KGA allowing its transport back into *Burkholderia* sp. Ha185 via the Bxp complex (as discussed in Chapter 4.4.8.3). To determine the role of BxpC protein and confirm that BxpC and its orthologs are cargo proteins, the protein needs to be purified and the calcium binding site of the active site cavity of BxpC protein needs to be validated.

The pH of culture supernatant ranged from 4.24 - 5.36 during HydroxP solubilisation by *Burkholderia* sp. Ha185. Furthermore, Matsushita et al. (1982) found the optimal pH for the HEM-GADH activity (synthesising 2-KGA) was between pH 4.0 - 5.0. Therefore, the BxpC protein may be stable within this pH range. From here, size exclusion chromatography could be used to separate BxpC protein after the binding with Ca-2-KGA compound (can be purchased from Sigma CAS No. 1040352-40-6) and the BxpC-Ca-2KGA compound may release additional 2-KGA via denaturing the protein complex by increasing or decreasing the optimal pH or subject to proteinase K for 10 mins at high temperature (ie. 75°C). Additional 2-KGA derived from the denatured BxpC can be detected using HPLC analysis as described in Chapter 2.2.3.4. This will strengthen the knowledge and the understanding of the role of BxpC protein in *Burkholderia* sp. Ha185 and conserved uncharacterised proteins with the duf1311 domain.

6.5.4. Defining the interrelationship between the expression of *hemX::Tn5(F18)* and *bxpC::Tn5(F13)*

To strengthen understanding of the role of BxpC protein as a cargo protein for Ca-2KGA transportation, the *bxpC* expression of the *hemX::Tn5(F18)* mutant could be determined using qRT-PCR. It was demonstrated the *hemX::Tn5(F18)* mutant has impaired HydroxP solubilisation ability (Chapter 4.3.3.2) and a low level of 2-KGA was released. Based on the assumption that BxpC is produced in response to elevated levels of 2-KGA in the culture supernatant, we hypothesises that in the *hemX::Tn5(F18)* strain there will be no relative expression of the *bxpC* at 48 h and 72 h post-inoculation in the HSU HydroxP liquid culture medium due to lack of 2-KGA production. Furthermore, the *bxpC* expression would expected to be recovered by applying calcium bound 2-KGA (sourced from Sigma-Aldrich) exogenously to the HSU HydroxP liquid culture of *hemX::Tn5(F18)* strain at 72 h. This would further validate the role of Bxp complex in the transportation of calcium bound 2-KGA compound.

References

- Afzal, M., Khan, S., Iqbal, S., Mirza, M.S. and Khan, Q.M. (2013) Inoculation method affects colonization and activity of *Burkholderia phytofirmans* PsJN during phytoremediation of diesel-contaminated soil. *International Biodeterioration & Biodegradation* 85, 331-336.
- Ahemad, M. and Khan, M.S. (2011) Effects of insecticides on plant-growth-promoting activities of phosphate solubilizing rhizobacterium *Klebsiella* sp. strain PS19. *Pesticide Biochemistry and Physiology* 100, 51-56.
- Ahmad, F., Ahmad, I. and Khan, M. (2008) Screening of free-living rhizospheric bacteria for their multiple plant growth promoting activities. *Microbiological Research* 163, 173-181.
- Alexander, B., Petzold, E., Reller, L., Palmer, S., Davis, R., Woods, C. and Lipuma, J. (2008) Survival after lung transplantation of cystic fibrosis patients infected with *Burkholderia cepacia* complex. *American Journal of Transplantation* 8, 1025-1030.
- Altschul, S.F., Gish, W., Miller, W., Myers, E.W. and Lipman, D.J. (1990) Basic local alignment search tool. *Journal of Molecular Biology* 215, 403-410.
- Ambrosini, A., Beneduzi, A., Stefanski, T., Pinheiro, F.G., Vargas, L.K. and Passaglia, L.M. (2012) Screening of plant growth promoting Rhizobacteria isolated from sunflower (*Helianthus annuus* L.). *Plant and Soil* 356, 245-264.
- Anderson, G. (1980) Assessing organic phosphorus in soils, Khasawneh, F.E. (Ed), *The role of phosphorus in agriculture*, 411-431. ASA, Madison WI.
- Andreolli, M., Lampis, S., Zenaro, E., Salkinoja-Salonen, M. and Vallini, G. (2011) *Burkholderia fungorum* DBT1: a promising bacterial strain for bioremediation of PAHs-contaminated soils. *FEMS Microbiology Letters* 319, 11-18.
- Andrews, S.C., Robinson, A.K. and Rodríguez-Quñones, F. (2003) Bacterial iron homeostasis. *FEMS Microbiology Reviews* 27, 215-237.
- Angus, A.A., Lee, A., Lum, M.R., Shehayeb, M., Hessabi, R., Fujishige, N.A., Yerrapragada, S., Kano, S., Song, N. and Yang, P. (2013) Nodulation and effective nitrogen fixation of *Macropodium atropurpureum* (siratro) by *Burkholderia tuberum*, a nodulating and plant growth promoting beta-proteobacterium, are influenced by environmental factors. *Plant and Soil*, 1-20.
- Apweiler, R., Martin, M.J., O'Donovan, C., Magrane, M., Alam-Faruque, Y., Alpi, E., Antunes, R., Arganiska, J., Casanova, E.B. and Bely, B. (2013) Update on activities at the Universal Protein Resource (UniProt) in 2013. *Nucleic Acids Research* 41, D43-D47.
- Asea, P.E.A., Kucey, R.M.N. and Stewart, J.W.B. (1988) Inorganic phosphate solubilization by two *Penicillium* species in solution culture and soil. *Soil Biology and Biochemistry* 20, 459-464.
- Awasthi, R., Tewari, R. and Nayyar, H. (2011) Synergy between plants and P-solubilizing microbes in soils: effects on growth and physiology of crops. *International Research Journal of Microbiology* 2, 484-503.

- Babu-Khan, S., Yeo, T., Martin, W., Duron, M., Rogers, R. and Goldstein, A. (1995) Cloning of a mineral phosphate-solubilizing gene from *Pseudomonas cepacia*. *Apply Environmental Microbiology* 61, 972-978.
- Bache, B. (1964) Aluminium and iron phosphate studies relating to soils. *Journal of Soil Science* 15, 110-116.
- Bais, H.P., Park, S.-W., Weir, T.L., Callaway, R.M. and Vivanco, J.M. (2004) How plants communicate using the underground information superhighway. *Trends in Plant Science* 9, 26-32.
- Bali, S., Lawrence, A.D., Lobo, S.A., Saraiva, L.M., Golding, B.T., Palmer, D.J., Howard, M.J., Ferguson, S.J. and Warren, M.J. (2011) Molecular hijacking of siroheme for the synthesis of heme and d^1 heme. *Proceedings of the National Academy of Sciences* 108, 18260-18265.
- Barea, J.M., Navarro, E. and Montoya, E. (1976) Production of plant growth regulators by rhizosphere phosphate-solubilizing bacteria. *Journal of Applied Microbiology* 40, 129-134.
- Barka, E.A., Belarbi, A., Hachet, C., Nowak, J. and Audran, J.C. (2000) Enhancement of *in vitro* growth and resistance to gray mould of *Vitis vinifera* co-cultured with plant growth-promoting rhizobacteria. *FEMS Microbiology Letters* 186, 91-95.
- Barka, E.A., Nowak, J. and Clément, C. (2006) Enhancement of chilling resistance of inoculated grapevine plantlets with a plant growth-promoting rhizobacterium, *Burkholderia phytofirmans* strain PsJN. *Applied and Environmental Microbiology* 72, 7246-7252.
- Barret, M., Egan, F., Fargier, E., Morrissey, J.P. and O’Gara, F. (2011) Genomic analysis of the type VI secretion systems in *Pseudomonas* spp.: novel clusters and putative effectors uncovered. *Microbiology* 157, 1726-1739.
- Bartel, B. (1997) Auxin biosynthesis. *Annual Review of Plant Biology* 48, 51-66.
- Bashan, Y., Kamnev, A.A. and de-Bashan, L.E. (2013) A proposal for isolating and testing phosphate-solubilizing bacteria that enhance plant growth. *Biology and Fertility of Soils*, 1-2.
- Bashan, Y., Kamnev, A.A. and de-Bashan, L.E. (2013) Tricalcium phosphate is inappropriate as a universal selection factor for isolating and testing phosphate-solubilizing bacteria that enhance plant growth: a proposal for an alternative procedure. *Biology and Fertility of Soils*, 1-15.
- Baskaran, N., Kandpal, R.P., Bhargava, A.K., Glynn, M.W., Bale, A. and Weissman, S.M. (1996) Uniform amplification of a mixture of deoxyribonucleic acids with varying GC content. *Genome Research* 6, 633-638.
- Bayer, T.K., Schallenberg, M. and Martin, C.E. (2008) Investigation of nutrient limitation status and nutrient pathways in Lake Hayes, Otago, New Zealand: A case study for integrated lake assessment. *New Zealand Journal of Marine and Freshwater Research* 42, 285 - 295.
- Beauchemin, D. (2008) Inductively coupled plasma mass spectrometry. *Analytical Chemistry* 80, 4455-4486.

- Beauchemin, D. (2010) Inductively coupled plasma mass spectrometry. *Analytical Chemistry* 82, 4786-4810.
- Belimov, A., Hontzeas, N., Safronova, V., Demchinskaya, S., Piluzza, G., Bullitta, S. and Glick, B. (2005) Cadmium-tolerant plant growth-promoting bacteria associated with the roots of Indian mustard (*Brassica juncea* L. Czern.). *Soil Biology and Biochemistry* 37, 241-250.
- Beneduzi, A., Ambrosini, A. and Passaglia, L.M. (2012) Plant growth-promoting rhizobacteria (PGPR): Their potential as antagonists and biocontrol agents. *Genetics and Molecular Biology* 35, 1044-1051.
- Berendsen, R.L., Pieterse, C.M. and Bakker, P.A. (2012) The rhizosphere microbiome and plant health. *Trends in Plant Science* 17, 478-486.
- Bhattacharyya, P. and Jha, D. (2012) Plant growth-promoting rhizobacteria (PGPR): emergence in agriculture. *World Journal of Microbiology and Biotechnology* 28, 1327-1350.
- Bladergroen, M., Badelt, K. and Spaink, H. (2003) Infection-blocking genes of a symbiotic *Rhizobium leguminosarum* strain that are involved in temperature-dependent protein secretion. *Molecular Plant-Microbe Interactions* 16, 53-64.
- Bolan, N., White, R. and Hedley, M. (1990) A review of the use of phosphate rocks as fertilizers for direct application in Australia and New Zealand. *Australian Journal of Experimental Agriculture* 30, 297-313.
- Bolan, N.S., Naidu, R., Mahimairaja, S. and Baskaran, S. (1994) Influence of low-molecular-weight organic acids on the solubilization of phosphates. *Biology and Fertility of Soils* 18, 311-319.
- Bopp, L.H. (1986) Degradation of highly chlorinated PCBs by *Pseudomonas* strain LB400. *Journal of Industrial Microbiology* 1, 23-29.
- Bray, J.R. and Curtis, J.T. (1957) An ordination of the upland forest communities of southern Wisconsin. *Ecological Monographs* 27, 325-349.
- Braz, R.R. and Nahas, E. (2012) Synergistic action of both *Aspergillus niger* and *Burkholderia cepacea* in co-culture increases phosphate solubilization in growth medium. *FEMS Microbiology Letters* 332, 84-90.
- Brindley, A.A., Zajicek, R., Warren, M.J., Ferguson, S.J. and Rigby, S.E. (2010) NirJ, a radical SAM family member of the d^1 heme biogenesis cluster. *FEBS Letters* 584, 2461-2466.
- Bröms, J.E., Meyer, L., Sun, K., Lavander, M. and Sjöstedt, A. (2012) Unique substrates secreted by the Type VI Secretion System of *Francisella tularensis* during intramacrophage infection. *PLoS One* 7, e50473.
- Brown, L., George, T., Thompson, J., Wright, G., Lyon, J., Dupuy, L., Hubbard, S. and White, P. (2012) What are the implications of variation in root hair length on tolerance to phosphorus deficiency in combination with water stress in barley (*Hordeum vulgare*). *Annals of Botany* 110, 319-328.

- Brown, S.D., Utturkar, S.M., Klingeman, D.M., Johnson, C.M., Martin, S.L., Land, M.L., Lu, T.-Y.S., Schadt, C.W., Doktycz, M.J. and Pelletier, D.A. (2012) Twenty-one genome sequences from *Pseudomonas* species and 19 genome sequences from diverse bacteria isolated from the rhizosphere and endosphere of *Populus deltoides*. *Journal of Bacteriology* 194, 5991-5993.
- Bruex, A., Kainkaryam, R.M., Wieckowski, Y., Kang, Y.H., Bernhardt, C., Xia, Y., Zheng, X., Wang, J.Y., Lee, M.M. and Benfey, P. (2012) A gene regulatory network for root epidermis cell differentiation in *Arabidopsis*. *PLoS Genetics* 8, e1002446.
- Buch, A., Archana, G. and Naresh Kumar, G. (2008) Metabolic channeling of glucose towards gluconate in phosphate-solubilizing *Pseudomonas aeruginosa* P4 under phosphorus deficiency. *Research in Microbiology* 159, 635-642.
- Buch, A., Archana, G. and Naresh Kumar, G. (2010) Heterologous expression of phosphoenolpyruvate carboxylase enhances the phosphate solubilizing ability of fluorescent pseudomonads by altering the glucose catabolism to improve biomass yield. *Bioresource Technology* 101, 679-687.
- Buell, C.R., Joardar, V., Lindeberg, M., Selengut, J., Paulsen, I.T., Gwinn, M.L., Dodson, R.J., Deboy, R.T., Durkin, A.S. and Kolonay, J.F. (2003) The complete genome sequence of the *Arabidopsis* and tomato pathogen *Pseudomonas syringae* pv. *tomato* DC3000. *Proceedings of the National Academy of Sciences* 100, 10181-10186.
- Buijuy, C.J.B. (2011) Characterization of the type VI protein secretion system encoded in the *Salmonella* pathogenicity island 19 and its role in the pathogenicity of serotypes Gallinarum and Enteritidis: PhD Thesis, Universidad de Chile.
- Bukholm, G. and Kapperud, G. (1987) Expression of *Campylobacter jejuni* invasiveness in cell cultures coinfecting with other bacteria. *Infection and immunity* 55, 2816-2821.
- Bull, C., De Boer, S., Denny, T., Firrao, G., Fischer-Le Saux, M., Saddler, G., Scortichini, M., Stead, D. and Takikawa, Y. (2010) Comprehensive list of names of plant pathogenic bacteria, 1980-2007. *Journal of Plant Pathology* 92, 551-592.
- Bull, C., De Boer, S., Denny, T., Firrao, G., Fischer-Le Saux, M., Saddler, G., Scortichini, M., Stead, D. and Takikawa, Y. (2012) List of new names of plant pathogenic bacteria (2008-2010). *Journal of Plant Pathology* 94, 21-27.
- Burd, G.I., Dixon, D.G. and Glick, B.R. (2000) Plant growth-promoting bacteria that decrease heavy metal toxicity in plants. *Canadian Journal of Microbiology* 46, 237-245.
- Burkholder, W.H. (1950) Sour skin, a bacterial rot of onion bulbs. *Phytopathology* 40, 115 - 117.
- Busby, J.N., Panjikar, S., Landsberg, M.J., Hurst, M.R. and Lott, J.S. (2013) The BC component of ABC toxins is an RHS-repeat-containing protein encapsulation device. *Nature* 501, 547-550.
- Bustin, S. (2000) Absolute quantification of mRNA using real-time reverse transcription polymerase chain reaction assays. *Journal of Molecular Endocrinology* 25, 169-193.

- Byrne, S.L., Foito, A., Hedley, P.E., Morris, J.A., Stewart, D. and Barth, S. (2011) Early response mechanisms of perennial ryegrass (*Lolium perenne*) to phosphorus deficiency. *Annals of Botany* 107, 243-254.
- Caballero-Mellado, J., Onofre-Lemus, J., Estrada-de los Santos, P. and Martínez-Aguilar, L. (2007) The tomato rhizosphere, an environment rich in nitrogen-fixing *Burkholderia* species with capabilities of interest for agriculture and bioremediation. *Applied and Environmental Microbiology* 73, 5308-5319.
- Caruso, B.S. (2000) Integrated assessment of phosphorus in the Lake Hayes catchment, South Island, New Zealand. *Journal of Hydrology* 229, 168-189.
- Cascales, E. and Cambillau, C. (2012) Structural biology of type VI secretion systems. *Philosophical Transactions of the Royal Society B: Biological Sciences* 367, 1102-1111.
- Castagno, L., Estrella, M., Sannazzaro, A., Grassano, A. and Ruiz, O. (2011) Phosphate-solubilization mechanism and *in vitro* plant growth promotion activity mediated by *Pantoea eucalypti* isolated from *Lotus tenuis* rhizosphere in the Salado River Basin (Argentina). *Journal of Applied Microbiology* 110, 1151-1165.
- Chain, P.S., Deneff, V.J., Konstantinidis, K.T., Vergez, L.M., Agulló, L., Reyes, V.L., Hauser, L., Córdova, M., Gómez, L. and González, M. (2006) *Burkholderia xenovorans* LB400 harbors a multi-replicon, 9.73-Mbp genome shaped for versatility. *Proceedings of the National Academy of Sciences* 103, 15280-15287.
- Chakrabarti, R. and Schutt, C.E. (2002) Novel sulfoxides facilitate GC-rich template amplification. *Biotechniques* 32, 866-875.
- Chen, W.-M., De Faria, S.M., James, E.K., Elliott, G.N., Lin, K.-Y., Chou, J.-H., Sheu, S.-Y., Cnockaert, M., Sprent, J.I. and Vandamme, P. (2007) *Burkholderia nodosa* sp. nov., isolated from root nodules of the woody Brazilian legumes *Mimosa bimucronata* and *Mimosa scabrella*. *International Journal of Systematic and Evolutionary Microbiology* 57, 1055-1059.
- Chen, W.-M., James, E.K., Coenye, T., Chou, J.-H., Barrios, E., De Faria, S.M., Elliott, G.N., Sheu, S.-Y., Sprent, J.I. and Vandamme, P. (2006) *Burkholderia mimosarum* sp. nov., isolated from root nodules of *Mimosa* spp. from Taiwan and South America. *International Journal of Systematic and Evolutionary Microbiology* 56, 1847-1851.
- Chen, W.-M., Prell, J., James, E.K., Sheu, D.-S. and Sheu, S.-Y. (2012) Effect of phosphoglycerate mutase and fructose 1, 6-bisphosphatase deficiency on symbiotic *Burkholderia phymatum*. *Microbiology* 158, 1127-1136.
- Chen, Y.P., Rekha, P.D., Arun, A.B., Shen, F.T., Lai, W.A. and Young, C.C. (2006) Phosphate solubilizing bacteria from subtropical soil and their tricalcium phosphate solubilizing abilities. *Applied Soil Ecology* 34, 33-41.
- Chu, H.-M., Guo, R.-T., Lin, T.-W., Chou, C.-C., Shr, H.-L., Lai, H.-L., Tang, T.-Y., Cheng, K.-J., Selinger, B.L. and Wang, A.H.-J. (2004) Structures of *Selenomonas ruminantium* phytase in complex with

persulfated phytate: DSP phytase fold and mechanism for sequential substrate hydrolysis. *Structure* 12, 2015-2024.

Clarke, K.R., Somerfield, P.J. and Chapman, M.G. (2006) On resemblance measures for ecological studies, including taxonomic dissimilarities and a zero-adjusted Bray–Curtis coefficient for denuded assemblages. *Journal of Experimental Marine Biology and Ecology* 330, 55-80.

Clarke, K.R., Somerfield, P.J. and Gorley, R.N. (2008) Testing of null hypotheses in exploratory community analyses: similarity profiles and biota-environment linkage. *Journal of Experimental Marine Biology and Ecology* 366, 56-69.

Collavino, M.M., Sansberro, P.A., Mroginski, L.A. and Aguilar, O.M. (2010) Comparison of *in vitro* solubilization activity of diverse phosphate-solubilizing bacteria native to acid soil and their ability to promote *Phaseolus vulgaris* growth. *Biology and Fertility of Soils* 46, 727-738.

Compant, S., Kaplan, H., Sessitsch, A., Nowak, J., Ait Barka, E. and Clément, C. (2008) Endophytic colonization of *Vitis vinifera* L. by *Burkholderia phytofirmans* strain PsJN: from the rhizosphere to inflorescence tissues. *FEMS Microbiology Ecology* 63, 84-93.

Compant, S., Reiter, B., Sessitsch, A., Nowak, J., Clément, C. and Barka, E.A. (2005) Endophytic colonization of *Vitis vinifera* L. by plant growth-promoting bacterium *Burkholderia* sp. strain PsJN. *Applied and Environmental Microbiology* 71, 1685-1693.

Condrón, L., Di, H., Goh, K., Campbell, A. and Harrison, R. (1995) Agronomic effectiveness of partially acidulated phosphate rock fertilisers in selected New Zealand soils. *Australian Journal of Experimental Agriculture* 35(3), 387 – 393.

Condrón, L. and Goh, K. (1989) Effects of long-term phosphatic fertilizer applications on amounts and forms of phosphorus in soils under irrigated pasture in New Zealand. *Journal of Soil Science* 40, 383-395.

Condrón, L.M., Turner, B.L., Cade-Menun, B.J., Sims, J. and Sharpley, A. (2005) Chemistry and dynamics of soil organic phosphorus. *Phosphorus: Agriculture and the Environment*, 87-121.

Cordell, D., Drangert, J.-O. and White, S. (2009) The story of phosphorus: Global food security and food for thought. *Global Environmental Change* 19, 292-305.

Cordero, P., Cavigliasso, A., Príncipe, A., Godino, A., Jofré, E., Mori, G. and Fischer, S. (2012) Genetic diversity and antifungal activity of native *Pseudomonas* isolated from maize plants grown in a central region of Argentina. *Systematic and Applied Microbiology* 35(5), 342-51.

Cronin, S.J., Manoharan, V., Hedley, M.J. and Loganathan, P. (2000) Fluoride: A review of its fate, bioavailability, and risks of fluorosis in grazed-pasture systems in New Zealand. *New Zealand Journal of Agricultural Research* 43, 295 - 321.

Crosa, J.H. and Walsh, C.T. (2002) Genetics and assembly line enzymology of siderophore biosynthesis in bacteria. *Microbiology and Molecular Biology Reviews* 66, 223-249.

- Cuong, N.D., Nicolaisen, M.H., Sørensen, J. and Olsson, S. (2011) Hyphae-colonizing *Burkholderia* sp.—a new source of biological control agents against sheath blight disease (*Rhizoctonia solani* AG1-IA) in rice. *Microbial Ecology* 62, 425-434.
- Curl, E.A. and Truelove, B. (1986) *The rhizosphere*: Springer-Verlag.
- Da, K., Nowak, J. and Flinn, B. (2012) Potato cytosine methylation and gene expression changes induced by a beneficial bacterial endophyte, *Burkholderia phytofirmans* strain PsJN. *Plant Physiology and Biochemistry* 50, 24-34.
- Dalal, R. (1977) Soil organic phosphorus. *Advance in Agronomy* 29, 83-117. Academic Press Inc, New York.
- D'Angelo, E., Crutchfield, J. and Vandiviere, M. (2001) Rapid, sensitive, microscale determination of phosphate in water and soil. *Journal of Environmental Quality* 30, 2206-2209.
- Dary, M., Chamber-Pérez, M., Palomares, A. and Pajuelo, E. (2010) "In situ" phytostabilisation of heavy metal polluted soils using *Lupinus luteus* inoculated with metal resistant plant-growth promoting rhizobacteria. *Journal of Hazardous Materials* 177, 323-330.
- Daza, A., Santamaria, C., Rodriguez-Navarro, D., Camacho, M., Orive, R. and Temprano, F. (2000) Perlite as a carrier for bacterial inoculants. *Soil Biology and Biochemistry* 32, 567-572.
- de Castro, E., Sigrist, C.J., Gattiker, A., Bulliard, V., Langendijk-Genevaux, P.S., Gasteiger, E., Bairoch, A. and Hulo, N. (2006) ScanProsite: detection of PROSITE signature matches and ProRule-associated functional and structural residues in proteins. *Nucleic Acids Research* 34, W362-W365.
- de Freitas, J.R., Banerjee, M.R. and Germida, J.J. (1997) Phosphate-solubilizing rhizobacteria enhance the growth and yield but not phosphorus uptake of canola (*Brassica napus* L.). *Biology and Fertility of Soils* 24, 358-364.
- de Lorenzo, V., Herrero, M., Jakubzik, U. and Timmis, K.N. (1990) Mini-Tn5 transposon derivatives for insertion mutagenesis, promoter probing, and chromosomal insertion of cloned DNA in gram-negative eubacteria. *Journal of Bacteriology* 172, 6568-6572.
- de Soyza, A., Meachery, G., Hester, K.L., Nicholson, A., Parry, G., Tocewicz, K., Pillay, T., Clark, S., Lordan, J.L. and Schueler, S. (2010) Lung transplantation for patients with cystic fibrosis and *Burkholderia cepacia* complex infection: A single-center experience. *The Journal of Heart and Lung Transplantation* 29, 1395-1404.
- de Werra, P., Pechy-Tarr, M., Keel, C. and Maurhofer, M. (2009) Role of Gluconic Acid Production in the Regulation of Biocontrol Traits of *Pseudomonas fluorescens* CHA0. *Applied Environmental Microbiology* 75, 4162-4174.
- Denef, V., Klappenbach, J., Patrauchan, M., Florizone, C., Rodrigues, J., Tsoi, T., Verstraete, W., Eltis, L. and Tiedje, J. (2006) Genetic and genomic insights into the role of benzoate-catabolic pathway redundancy in *Burkholderia xenovorans* LB400. *Applied and Environmental Microbiology* 72, 585-595.

Dennis, P.G., Miller, A.J. and Hirsch, P.R. (2010) Are root exudates more important than other sources of rhizodeposits in structuring rhizosphere bacterial communities? *FEMS Microbiology Ecology* 72, 313-327.

Deutscher, J., Francke, C. and Postma, P.W. (2006) How phosphotransferase system-related protein phosphorylation regulates carbohydrate metabolism in bacteria. *Microbiology and Molecular Biology Reviews* 70, 939-1031.

Di Simine, C., Sayer, J. and Gadd, G. (1998) Solubilization of zinc phosphate by a strain of *Pseudomonas fluorescens* isolated from a forest soil. *Biology and Fertility of Soils* 28, 87-94.

Díaz, K., Valiente, C., Martínez, M., Castillo, M. and Sanfuentes, E. (2009) Root-promoting rhizobacteria in *Eucalyptus globulus* cuttings. *World Journal of Microbiology and Biotechnology* 25, 867-873.

Dodds, P.N. and Rathjen, J.P. (2010) Plant immunity: towards an integrated view of plant–pathogen interactions. *Nature Reviews Genetics* 11, 539-548.

Donald, C. and Williams, C. (1954) Fertility and productivity of a podzolic soil as influenced by subterranean clover (*Trifolium subterraneum* L.) and superphosphate. *Crop and Pasture Science* 5, 664-687.

Dorozhkin, S.V. and Epple, M. (2002) Biological and medical significance of calcium phosphates. *Angewandte Chemie International Edition* 41, 3130-3146.

Dörr, J., Hurek, T. and Reinhold-Hurek, B. (1998) Type IV pili are involved in plant–microbe and fungus–microbe interactions. *Molecular Microbiology* 30, 7-17.

Drancourt, M., Bollet, C., Carlioz, A., Martelin, R., Gayral, J.-P. and Raoult, D. (2000) 16S ribosomal DNA sequence analysis of a large collection of environmental and clinical unidentifiable bacterial isolates. *Journal of Clinical Microbiology* 38, 3623-3630.

Drevinek, P., Holden, M.T., Ge, Z., Jones, A.M., Ketchell, I., Gill, R.T. and Mahenthiralingam, E. (2008) Gene expression changes linked to antimicrobial resistance, oxidative stress, iron depletion and retained motility are observed when *Burkholderia cenocepacia* grows in cystic fibrosis sputum. *BMC Infectious Diseases* 8, 121.

Duff, R. and Webley, D. (1959) 2-Ketogluconic acid as a natural chelator produced by soil bacteria. *Chemistry and Industry*, 1376-1377.

Duffy, S.P., Shing, J., Saraon, P., Berger, L.C., Eiden, M.V., Wilde, A. and Taylor, C.S. (2010) The Fowler syndrome-associated protein FLVCR2 is an importer of heme. *Molecular and Cellular Biology* 30, 5318-5324.

Duine, J.A. (1991) Quinoproteins: enzymes containing the quinonoid cofactor pyrroloquinoline quinone, topaquinone or tryptophan-tryptophan quinone. *European Journal of Biochemistry* 200, 271-284.

- Eikmanns, B.J., Follettie, M.T., Griot, M.U. and Sinskey, A.J. (1989) The phosphoenolpyruvate carboxylase gene of *Corynebacterium glutamicum*: molecular cloning, nucleotide sequence, and expression. *Molecular and General Genetics MGG* 218, 330-339.
- Einsle, O., Messerschmidt, A., Stach, P., Bourenkov, G.P., Bartunik, H.D., Huber, R. and Kroneck, P.M. (1999) Structure of cytochrome c nitrite reductase. *Nature* 400, 476-480.
- Elfari, M., Ha, S.-W., Bremus, C., Merfort, M., Khodaverdi, V., Herrmann, U., Sahm, H. and Görisch, H. (2005) A *Gluconobacter oxydans* mutant converting glucose almost quantitatively to 5-keto-D-gluconic acid. *Applied Microbiology and Biotechnology* 66, 668-674.
- Elkoca, E., Kantar, F. and Sahin, F. (2008) Influence of nitrogen fixing and phosphorus solubilizing bacteria on the nodulation, plant growth, and yield of chickpea. *Journal of Plant Nutrition* 31, 157 - 171.
- English, G., Trunk, K., Rao, V.A., Srikannathasan, V., Hunter, W.N. and Coulthurst, S.J. (2012) New secreted toxins and immunity proteins encoded within the Type VI secretion system gene cluster of *Serratia marcescens*. *Molecular Microbiology* 86, 921-936.
- Epstein, E. and Arnold, J.B. (1972) *Mineral Nutrition of Plants: Principles and Perspectives*. Sinauer Associates, Inc. Sunderland, Massachusetts.
- Esitken, A., Yildiz, H.E., Ercisli, S., Figen Donmez, M., Turan, M. and Gunes, A. (2010) Effects of plant growth promoting bacteria (PGPB) on yield, growth and nutrient contents of organically grown strawberry. *Scientia Horticulturae* 124, 62-66.
- Fankem, H., Ngo Nkot, L., Deubel, A., Quinn, J., Merbach, W., Etoa, F.-X. and Nwaga, D. (2008) Solubilization of inorganic phosphates and plant growth promotion by strains of *Pseudomonas fluorescens* isolated from acidic soils of Cameroon. *African Journal of Microbiology Research* 2, 171-178.
- Farhat, M.B., Fourati, A. and Chouayekh, H. (2013) Coexpression of the pyrroloquinoline quinone and glucose dehydrogenase genes from *Serratia marcescens* CTM 50650 conferred high mineral phosphate-solubilizing ability to *Escherichia coli*. *Applied Biochemistry and Biotechnology*, 1-13.
- Fellay, R., Frey, J. and Krisch, H. (1987) Interposon mutagenesis of soil and water bacteria: a family of DNA fragments designed for *in vitro* insertional mutagenesis of gram-negative bacteria. *Gene* 52, 147-154.
- Fernandez, O., Vandesteene, L., Feil, R., Baillieul, F., Lunn, J.E. and Clément, C. (2012) Trehalose metabolism is activated upon chilling in grapevine and might participate in *Burkholderia phytofirmans* induced chilling tolerance. *Planta* 236, 355-369.
- Fibach-Paldi, S., Burdman, S. and Okon, Y. (2012) Key physiological properties contributing to rhizosphere adaptation and plant growth promotion abilities of *Azospirillum brasilense*. *FEMS Microbiology Letters* 326, 99-108.
- Filloux, A. (2013) Microbiology: A weapon for bacterial warfare. *Nature* doi:10.1038/nature12545.

Filloux, A., Hachani, A. and Bleves, S. (2008) The bacterial type VI secretion machine: yet another player for protein transport across membranes. *Microbiology* 154, 1570-1583.

Franceschini, A., Szklarczyk, D., Frankild, S., Kuhn, M., Simonovic, M., Roth, A., Lin, J., Minguez, P., Bork, P. and von Mering, C. (2013) STRING v9. 1: protein-protein interaction networks, with increased coverage and integration. *Nucleic Acids Research* 41, D808-D815.

Galyov, E.E., Brett, P.J. and DeShazer, D. (2010) Molecular insights into *Burkholderia pseudomallei* and *Burkholderia mallei* pathogenesis. *Annual Review of Microbiology* 64, 495-517.

Gamalero, E., Berta, G., Massa, N., Glick, B.R. and Lingua, G. (2008) Synergistic interactions between the ACC deaminase-producing bacterium *Pseudomonas putida* UW4 and the AM fungus *Gigaspora rosea* positively affect cucumber plant growth. *FEMS Microbiology Ecology* 64, 459-467.

Garrett, R.H. and Grisham, C.M. (1995) *Molecular Aspects of Cell Biology*: Saunders College Pub.

Gasteiger, E., Hoogland, C., Gattiker, A., Wilkins, M.R., Appel, R.D. and Bairoch, A. (2005) Protein Identification and Analysis Tools on the ExPASy Server. *The Proteomics Protocols Handbook*, 571-607.

Ge, X., Wang, W., Du, B., Wang, J., Xiong, X. and Zhang, W. (2013) Multiple pqqA genes respond differently to environment and one contributes dominantly to pyrroloquinoline quinone synthesis. *Journal of Basic Microbiology* DOI: 10.1002/jobm.201300037.

Giles, C.D., Hsu, P.-C., Richardson, A.E., Hurst, M.R.H. and Hill, J.E. (2014) Plant assimilation of phosphorus from an insoluble organic form is improved by addition of an organic anion producing *Pseudomonas* sp. *Soil Biology and Biochemistry* 68, 263-269.

Giles, C.D., Richardson, A.E., Druschel, G.K. and Hill, J.E. (2012) Organic anion-driven solubilization of precipitated and sorbed phytate improves hydrolysis by phytases and bioavailability to *nicotiana tabacum*. *Soil Science* 177, 591-598.

Glick, B.R. (2012) Plant growth-promoting bacteria: Mechanisms and applications. *Scientifica* 2012, <http://dx.doi.org/10.6064/2012/963401>.

Glick, B.R., Cheng, Z., Czarny, J. and Duan, J. (2007) Promotion of plant growth by ACC deaminase-producing soil bacteria. *New Perspectives and Approaches in Plant Growth-Promoting Rhizobacteria Research* 119, 329-339.

Glick, B.R., Penrose, D.M. and Li, J. (1998) A model for the lowering of plant ethylene concentrations by plant growth-promoting bacteria. *Journal of Theoretical Biology* 190, 63-68.

Glick, B.R., Todorovic, B., Czarny, J., Cheng, Z., Duan, J. and McConkey, B. (2007) Promotion of plant growth by bacterial ACC deaminase. *Critical Reviews in Plant Sciences* 26, 227-242.

Goldstein, A.H., Braverman, K. and Osorio, N. (1999) Evidence for mutualism between a plant growing in a phosphate-limited desert environment and a mineral phosphate solubilizing (MPS) rhizobacterium. *FEMS Microbiology Ecology* 30, 295-300.

- Goldstein, A.H. and Liu, S.T. (1987) Molecular cloning and regulation of a mineral phosphate solubilizing gene from *Erwinia Herbicola*. *Nature Biotech* 5, 72-74.
- Gómez, W., Buena, L., Castro, L.T., Chaparro, V., Ball, M.M. and Yarzabal, L.A. (2010) Evidence for gluconic acid production by *Enterobacter intermedium* as an efficient strategy to avoid protozoan grazing. *Soil Biology and Biochemistry* 42, 822-830.
- Goosen, N., Huinen, R. and Van de Putte, P. (1992) A 24-amino-acid polypeptide is essential for the biosynthesis of the coenzyme pyrrolo-quinoline-quinone. *Journal of Bacteriology* 174, 1426-1427.
- Goris, J., De Vos, P., Caballero-Mellado, J., Park, J., Falsen, E., Quensen, J.F., Tiedje, J.M. and Vandamme, P. (2004) Classification of the biphenyl- and polychlorinated biphenyl-degrading strain LB400T and relatives as *Burkholderia xenovorans* sp. nov. *International Journal of Systematic and Evolutionary Microbiology* 54, 1677-1681.
- Govindarajan, M., Balandreau, J., Kwon, S.-W., Weon, H.-Y. and Lakshminarasimhan, C. (2008) Effects of the inoculation of *Burkholderia vietnamensis* and related endophytic diazotrophic bacteria on grain yield of rice. *Microbial Ecology* 55, 21-37.
- Gueguen, E., Durand, E., Zhang, X.Y., d'Amalric, Q., Journet, L. and Cascales, E. (2013) Expression of a *Yersinia pseudotuberculosis* Type VI secretion system is responsive to envelope stresses through the OmpR transcriptional activator. *PLoS one* 8, e66615.
- Gujar, P.D., Bhavsar, K.P. and Khire, J.M. (2013) Effect of phytase from *Aspergillus niger* on plant growth and mineral assimilation in wheat (*Triticum aestivum* Linn.) and its potential for use as a soil amendment. *Journal of the Science of Food and Agriculture* 93(9), 2242-2247.
- Guo, H. and Xiong, J. (2006) A specific and versatile genome walking technique. *Gene* 381, 18-23.
- Gupta, M., Bisht, S., Singh, B., Gulati, A. and Tewari, R. (2011) Enhanced biomass and steviol glycosides in *Stevia rebaudiana* treated with phosphate-solubilizing bacteria and rock phosphate. *Plant Growth Regulation* 65, 449-457.
- Guttman, D.S., Vinatzer, B.A., Sarkar, S.F., Ranall, M.V., Kettler, G. and Greenberg, J.T. (2002) A functional screen for the type III (Hrp) secretome of the plant pathogen *Pseudomonas syringae*. *Science* 295, 1722-1726.
- Gyaneshwar, P., Kumar, G.N. and Parekh, L. (1998) Effect of buffering on the phosphate-solubilizing ability of microorganisms. *World Journal of Microbiology and Biotechnology* 14, 669-673.
- Gyaneshwar, P., Naresh Kumar, G., Parekh, L.J. and Poole, P.S. (2002) Role of soil microorganisms in improving phosphate nutrition of plants. *Plant and Soil* 245, 83-93.
- Gyaneshwar, P., Parekh, L., Archana, G., Poole, P., Collins, M., Hutson, R. and Kumar, G.N. (1999) Involvement of a phosphate starvation inducible glucose dehydrogenase in soil phosphate solubilization by *Enterobacter asburiae*. *FEMS Microbiology Letters* 171, 223-229.

- Hall, J.A., Peirson, D., Ghosh, S. and Glick, B.R. (1996) Root elongation in various agronomic crops by the plant growth promoting rhizobacterium *Pseudomonas putida* GR12–2. *Israel Journal of Plant Sciences* 44, 37-42.
- Hallenbeck, W.H. (1984) Human health effects of exposure to cadmium. *Experientia* 40, 136-142.
- Haller, H., Jonsson, A. and Fröling, M. (2012) Turning waste into a resource for remediation of contaminated soil in tropical developing countries. *Proceedings Linnaeus Eco-Tech 2012*, 468-480.
- Hameeda, B., Harini, G., Rupela, O.P., Wani, S.P. and Reddy, G. (2008) Growth promotion of maize by phosphate-solubilizing bacteria isolated from composts and macrofauna. *Microbiological Research* 163, 234-242.
- Hammond-Kosack, K.E. and Parker, J.E. (2003) Deciphering plant–pathogen communication: fresh perspectives for molecular resistance breeding. *Current Opinion in Biotechnology* 14, 177-193.
- Hardoim, P.R., Nazir, R., Sessitsch, A., Elhottová, D., Korenblum, E., van Overbeek, L.S. and van Elsas, J.D. (2013) The new species *Enterobacter oryziphilus* sp. nov. and *Enterobacter oryzendophyticus* sp. nov. are key inhabitants of the endosphere of rice. *BMC Microbiology* 13, 164.
- Hardoim, P.R., Nazir, R., Sessitsch, A., van Overbeek, L.S. and van Elsas, J.D. (2011) *Enterobacter oryziphilus* sp. nov. and *Enterobacter oryzendophyticus* sp. nov., isolated from the endosphere of rice roots. *Bacterial Endophytes of Rice—Their Diversity, Characteristics and Perspectives*, 101.
- Hariprasad, P. and Niranjana, S. (2009) Isolation and characterization of phosphate solubilizing rhizobacteria to improve plant health of tomato. *Plant and Soil* 316, 13-24.
- Harris, J.N., New, P.B. and Martin, P.M. (2006) Laboratory tests can predict beneficial effects of phosphate-solubilising bacteria on plants. *Soil Biology and Biochemistry* 38, 1521-1526.
- Harrison, M.J. (1996) A sugar transporter from *Medicago truncatula*: altered expression pattern in roots during vesicular-arbuscular (VA) mycorrhizal associations. *The Plant Journal* 9, 491-503.
- Harrison, R.G. (2000) Expression of soluble heterologous proteins via fusion with NusA protein. *Innovations* 11, 4-7.
- Hasan, N.A., Ceccarelli, D., Grim, C.J., Taviani, E., Choi, J., Sadique, A., Alam, M., Siddique, A.K., Sack, R.B. and Huq, A. (2013) Distribution of virulence genes in clinical and environmental *Vibrio cholerae* strains in Bangladesh. *Applied and Environmental Microbiology* 79, 5782-5785.
- Hayat, R., Ali, S., Amara, U., Khalid, R. and Ahmed, I. (2010) Soil beneficial bacteria and their role in plant growth promotion: a review. *Annals of Microbiology* 60, 579-598.
- Haygarth, P.M., Bardgett, R.D. and Condon, L.M. (2013) Phosphorus and nitrogen cycles and their management. Wiley-Blackwell; 1st edition (March 4, 2013).
- Haynes, R. and Williams, P. (1992) Long-term effect of superphosphate on accumulation of soil phosphorus and exchangeable cations on a grazed, irrigated pasture site. *Plant and Soil* 142, 123-133.

- Heeb, S., Itoh, Y., Nishijyo, T., Schnider, U., Keel, C., Wade, J., Walsh, U., O'Gara, F. and Haas, D. (2000) Small, stable shuttle vectors based on the minimal pVS1 replicon for use in gram-negative, plant-associated bacteria. *Molecular Plant-Microbe Interactions* 13, 232-237.
- Henderson, I.R., Navarro-Garcia, F., Desvaux, M., Fernandez, R.C. and Ala'Aldeen, D. (2004) Type V protein secretion pathway: the autotransporter story. *Microbiology and Molecular Biology Reviews* 68, 692-744.
- Herrmann, A.M., Clode, P.L., Fletcher, I.R., Nunan, N., Stockdale, E.A., O'Donnell, A.G. and Murphy, D.V. (2007) A novel method for the study of the biophysical interface in soils using nano-scale secondary ion mass spectrometry. *Rapid Communications in Mass Spectrometry* 21, 29-34.
- Herrmann, A.M., Ritz, K., Nunan, N., Clode, P.L., Pett-Ridge, J., Kilburn, M.R., Murphy, D.V., O'Donnell, A.G. and Stockdale, E.A. (2007) Nano-scale secondary ion mass spectrometry—a new analytical tool in biogeochemistry and soil ecology: a review article. *Soil Biology and Biochemistry* 39, 1835-1850.
- Hider, R.C. (1984) Siderophore mediated absorption of iron. *Structure and Bonding* 58:25-87.
- Hider, R.C. and Kong, X. (2010) Chemistry and biology of siderophores. *Natural Product Reports* 27, 637-657.
- Hoagland, D.R. and Arnon, D.I. (1950) The water-culture method for growing plants without soil. *Circular California Agricultural Experiment Station* 347.
- Hofmann, K. (1993) TMbase-A database of membrane spanning protein segments. *Biol Chem Hoppe-Seyler* 374, 166.
- Hong, S. and Cho, K. (2007) Effects of plants, rhizobacteria and physicochemical factors on the phytoremediation of contaminated soil. *Korean Journal of Microbiology and Biotechnology* 35, 261.
- Honma, M. and Shimomura, T. (1978) Metabolism of 1-aminocyclopropane-1-carboxylic acid. *Agricultural and Biological Chemistry* 42, 1825-1831.
- Hsu, P.H. (1964) Adsorption of phosphate by aluminum and iron in soils. *Soil Science Society of America Journal* 28, 474-478.
- Hussain, M.I., Asghar, H.N., Akhtar, M.J. and Arshad, M. (2013) Impact of phosphate solubilizing bacteria on growth and yield of maize.
- Hwangbo, H., Park, R.D., Kim, Y.W., Rim, Y.S., Park, K.H., Kim, T.H., Suh, J.S. and Kim, K.Y. (2003) 2-ketogluconic acid production and phosphate solubilization by *Enterobacter intermedius*. *Current Microbiology* 47, 0087-0092.
- Hyatt, D., Chen, G.-L., LoCascio, P., Land, M., Larimer, F. and Hauser, L. (2010) Prodigal: prokaryotic gene recognition and translation initiation site identification. *BMC Bioinformatics* 11, 119.

- Iacobellis, N., Lavermicocca, P., Grgurina, I., Simmaco, M. and Ballio, A. (1992) Phytotoxic properties of *Pseudomonas syringae* pv. *syringae* toxins. *Physiological and Molecular Plant Pathology* 40, 107-116.
- Idris, E.E., Iglesias, D.J., Talon, M. and Borriss, R. (2007) Tryptophan-dependent production of indole-3-acetic acid (IAA) affects level of plant growth promotion by *Bacillus amyloliquefaciens* FZB42. *Molecular Plant-Microbe Interactions* 20, 619-626.
- Ikura, M. (1996) Calcium binding and conformational response in EF-hand proteins. *Trends in Biochemical Sciences* 21, 14-17.
- Illmer, P. and Schinner, F. (1992) Solubilization of inorganic phosphates by microorganisms isolated from forest soils. *Soil Biology and Biochemistry* 24, 389-395.
- Inglis, T., Garrow, S., Henderson, M., Clair, A., Sampson, J., O'Reilly, L. and Cameron, B. (2000) *Burkholderia pseudomallei* traced to water treatment plant in Australia. *Emerging Infectious Diseases* 6, 56.
- Intorne, A., de Oliveira, M., Lima, M., da Silva, J., Olivares, F. and de Souza Filho, G. (2009) Identification and characterization of *Gluconacetobacter diazotrophicus*; mutants defective in the solubilization of phosphorus and zinc. *Archives of Microbiology* 191, 477-483.
- Isogai, A., Fukuchi, N., Yamashita, S., Suyama, K. and Suzuki, A. (1990) Structures of syringostatins A and B, novel phytotoxins produced by *Pseudomonas syringae* pv. *syringae* isolated from lilac blights. *Tetrahedron Letters* 31, 695-698.
- Jackson, R.W., Athanassopoulos, E., Tsiamis, G., Mansfield, J.W., Sesma, A., Arnold, D.L., Gibbon, M.J., Murillo, J., Taylor, J.D. and Vivian, A. (1999) Identification of a pathogenicity island, which contains genes for virulence and avirulence, on a large native plasmid in the bean pathogen *Pseudomonas syringae* pathovar phaseolicola. *Proceedings of the National Academy of Sciences USA* 96, 10875-10880.
- Jacobsen, K.R., Fisher, D., Maretzki, A. and Moore, P. (1992) Developmental changes in the anatomy of the sugarcane stem in relation to phloem unloading and sucrose storage. *Botanica Acta* 105, 70-80.
- Jaeger, C., Lindow, S., Miller, W., Clark, E. and Firestone, M. (1999) Mapping of sugar and amino acid availability in soil around roots with bacterial sensors of sucrose and tryptophan. *Applied and Environmental Microbiology* 65, 2685-2690.
- Jain, A., Poling, M.D., Karthikeyan, A.S., Blakeslee, J.J., Peer, W.A., Titapiwatanakun, B., Murphy, A.S. and Raghothama, K.G. (2007) Differential effects of sucrose and auxin on localized phosphate deficiency-induced modulation of different traits of root system architecture in *Arabidopsis*. *Plant Physiology* 144, 232-247.
- Jangid, K., Whitman, W.B., Condon, L.M., Turner, B.L. and Williams, M.A. (2013) Progressive and retrogressive ecosystem development coincide with soil bacterial community change in a dune system under lowland temperate rainforest in New Zealand. *Plant and Soil* 367, 235-247.

- Järup, L. and Åkesson, A. (2009) Current status of cadmium as an environmental health problem. *Toxicology and Applied Pharmacology* 238, 201-208.
- Jha, B.K., Pragash, M.G., Cletus, J., Raman, G. and Sakthivel, N. (2009) Simultaneous phosphate solubilization potential and antifungal activity of new fluorescent pseudomonad strains, *Pseudomonas aeruginosa*, *P. plecoglossicida* and *P. mosselii*. *World Journal of Microbiology and Biotechnology* 25, 573-581.
- Johnson, J.F., Vance, C.P. and Allan, D.L. (1996) Phosphorus deficiency in *Lupinus albus* (altered lateral root development and enhanced expression of phosphoenolpyruvate carboxylase). *Plant Physiology* 112, 31-41.
- Jones, A., Dodd, M., Govan, J., Barcus, V., Doherty, C., Morris, J. and Webb, A. (2004) *Burkholderia cenocepacia* and *Burkholderia multivorans*: influence on survival in cystic fibrosis. *Thorax* 59, 948-951.
- Jones, D.L. (1998) Organic acids in the rhizosphere—a critical review. *Plant and Soil* 205, 25-44.
- Kapitein, N. and Mogk, A. (2013) Deadly syringes: type VI secretion system activities in pathogenicity and interbacterial competition. *Current Opinion in Microbiology* 16, 52–58.
- Karagöz, K., Ateş, F., Karagöz, H., Kotan, R. and Çakmakçı, R. (2012) Characterization of plant growth-promoting traits of bacteria isolated from the rhizosphere of grapevine grown in alkaline and acidic soils. *European Journal of Soil Biology* 50, 144-150.
- Kelley, L.A. and Sternberg, M.J. (2009) Protein structure prediction on the Web: a case study using the Phyre server. *Nature Protocols* 4, 363-371.
- Khalid, A., Arshad, M. and Zahir, Z. (2004) Screening plant growth-promoting rhizobacteria for improving growth and yield of wheat. *Journal of Applied Microbiology* 96, 473-480.
- Khan, F. and Ansari, A. (2005) Eutrophication: An ecological vision. *The Botanical Review* 71, 449-482.
- Khan, M.S., Zaidi, A., Wani, P.A. and Oves, M. (2009) Role of plant growth promoting rhizobacteria in the remediation of metal contaminated soils. *Environmental Chemistry Letters* 7, 1-19.
- Khasawneh, F.E. and Doll, E.C. (1979) The Use of Phosphate Rock for Direct Application to Soils. *Advances in Agronomy* ed. Brady, N.C. Academic Press, 159-206.
- Khorassani, R., Hettwer, U., Ratzinger, A., Steingrobe, B., Karlovsky, P. and Claassen, N. (2011) Citramalic acid and salicylic acid in sugar beet root exudates solubilize soil phosphorus. *BMC Plant Biology* 11, 121.
- Kim, B. and Wimpenny, J. (1981) Growth and cellulolytic activity of *Cellulomonas flavigena*. *Canadian Journal of Microbiology* 27, 1260-1266.
- Kim, C.H., Han, S.H., Kim, K.Y., Cho, B.H., Kim, Y.H., Koo, B.S. and Kim, Y.C. (2003) Cloning and Expression of Pyrroloquinoline Quinone (PQQ) Genes from a phosphate-solubilizing bacterium *Enterobacter intermedium*. *Current Microbiology* 47, 457-461.

- Kim, K.Y., Jordan, D. and Krishnan, H.B. (1998) Expression of genes from *Rahnella aquatilis* that are necessary for mineral phosphate solubilization in *Escherichia coli*. FEMS Microbiology Letters 159, 121-127.
- Kim, K.Y., McDonald, G.A. and Jordan, D. (1997) Solubilization of hydroxyapatite by *Enterobacter agglomerans* and cloned *Escherichia coli* in culture medium. Biology and Fertility of Soils 24, 347-352.
- Kim, N. (2005) Cadmium accumulation in Waikato soils. Environment Waikato Technical Report 2005/51.
- Kim, S., Lowman, S., Hou, G., Nowak, J., Flinn, B. and Mei, C. (2012) Growth promotion and colonization of switchgrass (*Panicum virgatum*) cv. Alamo by bacterial endophyte *Burkholderia phytofirmans* strain PsJN. Biotechnol Biofuels 5, 37.
- Korbie, D.J. and Mattick, J.S. (2008) Touchdown PCR for increased specificity and sensitivity in PCR amplification. Nature Protocols 3, 1452-1456.
- Kovach, M.E., Elzer, P.H., Steven Hill, D., Robertson, G.T., Farris, M.A., Roop II, R.M. and Peterson, K.M. (1995) Four new derivatives of the broad-host-range cloning vector pBBR1MCS, carrying different antibiotic-resistance cassettes. Gene 166, 175-176.
- Kubista, M., Andrade, J.M., Bengtsson, M., Forootan, A., Jonák, J., Lind, K., Sindelka, R., Sjöback, R., Sjögreen, B., Strömbom, L., Ståhlberg, A. and Zoric, N. (2006) The real-time polymerase chain reaction. Molecular Aspects of Medicine 27, 95-125.
- Kumar, A., Bhargava, P. and Rai, L.C. (2010) Isolation and molecular characterization of phosphate solubilizing *Enterobacter* and *Exiguobacterium* species from paddy fields of Eastern Uttar Pradesh, India. African Journal of Microbiology Research 4, 820-829.
- Kumar, C., Yadav, K., Archana, G. and Kumar, G.N. (2013) 2-ketogluconic acid secretion by incorporation of *Pseudomonas putida* KT 2440 gluconate dehydrogenase (*gad*) operon in *Enterobacter asburiae* PSI3 improves mineral phosphate solubilization. Current Microbiology 67, 388-394.
- Kumar, V., Singh, P., Jorquera, M.A., Sangwan, P., Kumar, P., Verma, A. and Agrawal, S. (2013) Isolation of phytase-producing bacteria from Himalayan soils and their effect on growth and phosphorus uptake of Indian mustard (*Brassica juncea*). World Journal of Microbiology and Biotechnology, 1-9.
- Laemmli, U.K. (1970) Cleavage of structural proteins during the assembly of the head of bacteriophage T4. Nature 227, 680-685.
- Lalonde, S., Tegeder, M., Throne-Holst, M., Frommer, W. and Patrick, J. (2003) Phloem loading and unloading of sugars and amino acids. Plant, Cell & Environment 26, 37-56.
- Le Blanc, S., Garrick, M.D. and Arredondo, M. (2012) Heme carrier protein 1 transports heme and is involved in heme-Fe metabolism. American Journal of Physiology-Cell Physiology 302, C1780-C1785.

- Lee, I., Berdis, A.J. and Suzuki, C.K. (2006) Recent developments in the mechanistic enzymology of the ATP-dependent Lon protease from *Escherichia coli*: highlights from kinetic studies. *Molecular BioSystems* 2, 477-483.
- Lee, Y.-K., Senthilkumar, M., Jeong, I.Y., Annapurna, K. and Swarnalakshmi, K. (2011) Gamma-radiation induced modifications in substrate specificity of glucose dehydrogenase and carbon source utilization pattern of phosphate-solubilizing *Pantoea* strains. *Biotechnology Letters* 33, 2391-2396.
- Lei, X.G., Porres, J.M., Mullaney, E.J. and Brinch-Pedersen, H. (2007) Phytase: source, structure and application. *Industrial Enzymes*. 505-529.
- Leiman, P.G., Basler, M., Ramagopal, U.A., Bonanno, J.B., Sauder, J.M., Pukatzki, S., Burley, S.K., Almo, S.C. and Mekalanos, J.J. (2009) Type VI secretion apparatus and phage tail-associated protein complexes share a common evolutionary origin. *Proceedings of the National Academy of Sciences USA* 106, 4154-4159.
- Levano-Garcia, Julio, Sergio Verjovski-Almeida, and A. C. da Silva. (2005) Mapping transposon insertion sites by touchdown PCR and hybrid degenerate primers. *Biotechniques* 38, 225-229.
- Li, J., Ovakim, D.H., Charles, T.C. and Glick, B.R. (2000) An ACC deaminase minus mutant of *Enterobacter cloacae* UW4No longer promotes root elongation. *Current Microbiology* 41, 101-105.
- Li, Z., Xu, C., Li, K., Yan, S., Qu, X. and Zhang, J. (2012) Phosphate starvation of maize inhibits lateral root formation and alters gene expression in the lateral root primordium zone. *BMC Plant Biology* 12:89, doi:10.1186/1471-2229-12-89.
- Lindeberg, M., Biehl, B.S., Glasner, J.D., Perna, N.T., Collmer, A. and Collmer, C.W. (2009) Gene Ontology annotation highlights shared and divergent pathogenic strategies of type III effector proteins deployed by the plant pathogen *Pseudomonas syringae* pv tomato DC3000 and animal pathogenic *Escherichia coli* strains. *BMC Microbiology* 9, S4.
- Liu, J., Guo, J.T., Li, Y.G., Johnston, R.N., Liu, G.R. and Liu, S.L. (2012) The type VI secretion system gene cluster of *Salmonella typhimurium*: required for full virulence in mice. *Journal of Basic Microbiology* 53, 600–607.
- Liu, S.T., Lee, L.Y., Tai, C.Y., Hung, C.H., Chang, Y.S., Wolfram, J.H., Rogers, R. and Goldstein, A.H. (1992) Cloning of an *Erwinia herbicola* gene necessary for gluconic acid production and enhanced mineral phosphate solubilization in *Escherichia coli* HB101: nucleotide sequence and probable involvement in biosynthesis of the coenzyme pyrroloquinoline quinone. *Journal of Bacteriology* 174, 5814-5819.
- Loganathan, P., Hedley, M.J., Grace, N.D., Lee, J., Cronin, S.J., Bolan, N.S. and Zanders, J.M. (2003) Fertiliser contaminants in New Zealand grazed pasture with special reference to cadmium and fluorine; a review. *Australian Journal of Soil Research* 41, 501-532.
- Loganathan, P., Hedley, M.J., Wallace, G.C. and Roberts, A.H.C. (2001) Fluoride accumulation in pasture forages and soils following long-term applications of phosphorus fertilisers. *Environmental Pollution* 115, 275-282.

- López-Bucio, J., Cruz-Ramírez, A. and Herrera-Estrella, L. (2003) The role of nutrient availability in regulating root architecture. *Current Opinion in Plant Biology* 6, 280-287.
- Lorow, D. and Jessee, J. (1990) Max efficiency DH10B: a host for cloning methylated DNA. *Focus* 12, 19.
- Lü, J., Gao, X., Dong, Z. and An, L. (2012) Expression of mitochondrial malate dehydrogenase in *Escherichia coli* improves phosphate solubilization. *Annals of Microbiology* 62, 607-614.
- Lu, J., He, X., Huang, L., Kang, L. and Xu, D. (2012) Two *Burkholderia* strains from nodules of *Dalbergia odorifera* T. Chen in Hainan Island, southern China. *New Forests* 43, 397-409.
- Lucy, M., Reed, E. and Glick, B.R. (2004) Applications of free living plant growth-promoting rhizobacteria. *Antonie van Leeuwenhoek* 86, 1-25.
- Lugtenberg, B. and Kamilova, F. (2009) Plant-growth-promoting rhizobacteria. *Annual Review of Microbiology* 63, 541-556.
- Luvizotto, D.M., Marcon, J., Andreote, F.D., Dini-Andreote, F., Neves, A.A., Araújo, W.L. and Pizzirani-Kleiner, A.A. (2010) Genetic diversity and plant-growth related features of *Burkholderia* spp. from sugarcane roots. *World Journal of Microbiology and Biotechnology* 26, 1829-1836.
- MacIntyre, D.L., Miyata, S.T., Kitaoka, M. and Pukatzki, S. (2010) The *Vibrio cholerae* type VI secretion system displays antimicrobial properties. *Proceedings of the National Academy of Sciences* 107, 19520-19524.
- Madhaiyan, M., Poonguzhali, S. and Sa, T. (2007) Metal tolerating methylotrophic bacteria reduces nickel and cadmium toxicity and promotes plant growth of tomato (*Lycopersicon esculentum* L.). *Chemosphere* 69, 220-228.
- Magnan, C.N., Randall, A. and Baldi, P. (2009) SOLpro: accurate sequence-based prediction of protein solubility. *Bioinformatics* 25, 2200-2207.
- Mahenthalingam, E. and Drevinek, P. (2007) Comparative genomics of *Burkholderia* species. In *Burkholderia - Molecular Microbiology and Genomics* eds. Coenye, T. and Vandamme, P. U.K: Horizon Bioscience, Taylor & Francis. 53 - 79.
- Mander, C., Wakelin, S., Young, S., Condron, L. and O'Callaghan, M. (2012) Incidence and diversity of phosphate-solubilising bacteria are linked to phosphorus status in grassland soils. *Soil Biology and Biochemistry* 44, 93-101.
- Marchi, M., Boutin, M., Gazengel, K., Rispe, C., Gauthier, J.P., Guillerm-Erckelboudt, A.Y., Lebreton, L., Barret, M., Daval, S. and Sarniguet, A. (2013) Genomic analysis of the biocontrol strain *Pseudomonas fluorescens* Pf29Arp with evidence of T3SS and T6SS gene expression on plant roots. *Environmental Microbiology Reports* 5(3), 393-403.
- Marra, L.M., Oliveira, S.M.d., Soares, C.R.F.S. and Moreira, F.M.d.S. (2011) Solubilisation of inorganic phosphates by inoculant strains from tropical legumes. *Scientia Agricola* 68, 603-609.

- Marx, C.J., Miller, J.A., Chistoserdova, L. and Lidstrom, M.E. (2004) Multiple formaldehyde oxidation/detoxification pathways in *Burkholderia fungorum* LB400. *Journal of Bacteriology* 186, 2173-2178.
- Mathesius, U., Mulders, S., Gao, M., Teplitski, M., Caetano-Anollés, G., Rolfe, B.G. and Bauer, W.D. (2003) Extensive and specific responses of a eukaryote to bacterial quorum-sensing signals. *Proceedings of the National Academy of Sciences USA* 100, 1444-1449.
- Matsushita, K., Shinagawa, E. and Ameyama, M. (1982) [31] d-Gluconate dehydrogenase from bacteria, 2-keto-d-gluconate-yielding, membrane-bound. *Methods in Enzymology* 89, 187-193.
- Mattos, K.A., Pádua, V.L., Romeiro, A., Hallack, L.F., Neves, B.C., Ulisses, T.M., Barros, C.F., Todeschini, A.R., Previato, J.O. and Mendonça-Previato, L. (2008) Endophytic colonization of rice (*Oryza sativa* L.) by the diazotrophic bacterium *Burkholderia kururiensis* and its ability to enhance plant growth. *Anais da Academia Brasileira de Ciências* 80, 477-493.
- Mayer, B.J. (2001) SH3 domains: complexity in moderation. *Journal of Cell Science* 114, 1253-1263.
- Méndez, V., Agulló, L., González, M. and Seeger, M. (2011) The homogentisate and homoprotocatechuate central pathways are involved in 3- and 4-hydroxyphenylacetate degradation by *Burkholderia xenovorans* LB400. *PLoS One* 6, e17583.
- Metcalf, W.W., Jiang, W. and Wanner, B.L. (1994) Use of the *rep* technique for allele replacement to construct new *Escherichia coli* hosts for maintenance of R6K λ origin plasmids at different copy numbers. *Gene* 138, 1-7.
- Meyer, J.B., Frapolli, M., Keel, C. and Maurhofer, M. (2011) Pyrroloquinoline quinone biosynthesis gene *pqqC*, a novel molecular marker for studying the phylogeny and diversity of phosphate-solubilizing pseudomonads. *Applied and Environmental Microbiology* 77, 7345-7354.
- Michiels, J., Xi, C., Verhaert, J. and Vanderleyden, J. (2002) The functions of Ca²⁺ in bacteria: a role for EF-hand proteins. *Trends in Microbiology* 10, 87-93.
- Miller, S.H., Browne, P., Prigent-Combaret, C., Combes-Meynet, E., Morrissey, J.P. and O'Gara, F. (2010) Biochemical and genomic comparison of inorganic phosphate solubilization in *Pseudomonas* species. *Environmental Microbiology Reports* 2, 403-411.
- Miller, V.L. and Mekalanos, J.J. (1988) A novel suicide vector and its use in construction of insertion mutations: osmoregulation of outer membrane proteins and virulence determinants in *Vibrio cholerae* requires ToxR. *Journal of Bacteriology* 170, 2575-2583.
- Miller, W.G., Bates, A.H., Horn, S.T., Brandl, M.T., Wachtel, M.R. and Mandrell, R.E. (2000) Detection on surfaces and in Caco-2 cells of *Campylobacter jejuni* cells transformed with new *gfp*, *yfp*, and *cfp* marker plasmids. *Applied and Environmental Microbiology* 66, 5426-5436.
- Mimmo, T., Hann, S., Jaitz, L., Cesco, S., Gessa, C.E. and Puschenreiter, M. (2011) Time and substrate dependent exudation of carboxylates by *Lupinus albus* L. and *Brassica napus* L. *Plant Physiology and Biochemistry* 49, 1272-1278.

- Mitaku, S., Hirokawa, T. and Tsuji, T. (2002) Amphiphilicity index of polar amino acids as an aid in the characterization of amino acid preference at membrane–water interfaces. *Bioinformatics* 18, 608-616.
- Mitter, B., Petric, A., Shin, M.W., Chain, P.S., Hauberg-Lotte, L., Reinhold-Hurek, B., Nowak, J. and Sessitsch, A. (2013) Comparative genome analysis of *Burkholderia phytofirmans* PsJN reveals a wide spectrum of endophytic lifestyles based on interaction strategies with host plants. *Frontiers in Plant Science* 4, 120. doi: 10.3389/fpls.2013.00120.
- Miyata, S.T., Bachmann, V. and Pukatzki, S. (2013) Type VI secretion system regulation as a consequence of evolutionary pressure. *Journal of Medical Microbiology* 62, 663-676.
- Miyata, S.T., Kitaoka, M., Brooks, T.M., McAuley, S.B. and Pukatzki, S. (2011) *Vibrio cholerae* requires the type VI secretion system virulence factor VasX to kill *Dictyostelium discoideum*. *Infection and Immunity* 79, 2941-2949.
- Miyata, S.T., Unterweger, D., Rudko, S.P. and Pukatzki, S. (2013) Dual expression profile of type VI secretion system immunity genes protects pandemic *Vibrio cholerae*. *PLoS pathogens* 9, e1003752.
- Moghimi, A. and Tate, M. (1978) Does 2-ketogluconate chelate calcium in the pH range 2.4 to 6.4? *Soil Biology and Biochemistry* 10, 289-292.
- Moghimi, A., Tate, M. and Oades, J. (1978) Characterization of rhizosphere products especially 2-ketogluconic acid. *Soil Biology and Biochemistry* 10, 283-287.
- Moore, K.L., Schröder, M., Lombi, E., Zhao, F.J., McGrath, S.P., Hawkesford, M.J., Shewry, P.R. and Grovenor, C.R. (2010) NanoSIMS analysis of arsenic and selenium in cereal grain. *New Phytologist* 185, 434-445.
- Moore, K.L., Schröder, M., Wu, Z., Martin, B.G., Hawes, C.R., McGrath, S.P., Hawkesford, M.J., Ma, J.F., Zhao, F.-J. and Grovenor, C.R. (2011) High-resolution secondary ion mass spectrometry reveals the contrasting subcellular distribution of arsenic and silicon in rice roots. *Plant Physiology* 156, 913-924.
- Moriyama, R., Fukuoka, H., Miyata, S., Kudoh, S., Hattori, A., Kozuka, S., Yasuda, Y., Tochikubo, K. and Makino, S. (1999) Expression of a germination-specific amidase, SleB, of *Bacilli* in the forespore compartment of sporulating cells and its localization on the exterior side of the cortex in dormant spores. *Journal of Bacteriology* 181, 2373-2378.
- Mougous, J.D., Cuff, M.E., Raunser, S., Shen, A., Zhou, M., Gifford, C.A., Goodman, A.L., Joachimiak, G., Ordoñez, C.L. and Lory, S. (2006) A virulence locus of *Pseudomonas aeruginosa* encodes a protein secretion apparatus. *Science* 312, 1526-1530.
- Mueller, J.H. and Johnson, E.R. (1941) Acid hydrolysates of casein to replace peptone in the preparation of bacteriological media. *Journal of Immunology* 40, 33-38.

- Mulder, D.T., Cooper, C.A. and Coombes, B.K. (2012) Type VI secretion system-associated gene clusters contribute to pathogenesis of *Salmonella enterica* serovar Typhimurium. *Infection and immunity* 80, 1996-2007.
- Murphy, J. and Riley, J. (1962) A modified single solution method for the determination of phosphate in natural waters. *Analytica Chimica Acta* 27, 31-36.
- Naik, P., Raman, G., Narayanan, K. and Sakthivel, N. (2008) Assessment of genetic and functional diversity of phosphate solubilizing fluorescent *Pseudomonads* isolated from rhizospheric soil. *BMC Microbiology* 8, 230.
- Nautiyal, C.S. (1999) An efficient microbiological growth medium for screening phosphate solubilizing microorganisms. *FEMS Microbiology Letters* 170, 265-270.
- Nowak, J. (1998) Benefits of *in vitro* "biotization" of plant tissue cultures with microbial inoculants. *Vitro Cellular & Developmental Biology-Plant* 34, 122-130.
- Nowak, J. and Shulaev, V. (2003) Priming for transplant stress resistance in *in vitro* propagation. *Vitro Cellular & Developmental Biology-Plant* 39, 107-124.
- Nowak, J., Asiedu, S.K., Lazarovits, G., Pillay, V., Stewart, A., and Smith, C., and Liu, Z. (1995) Enhancement of *in vitro* growth and transplant stress tolerance of potato and vegetable plantlets co-cultured with a plant growth promoting *pseudomonad* bacterium. *Ecophysiology and Photosynthetic in vitro cultures, Aix en Provence (France)*, 1-3.
- Nygren, J., Svanvik, N. and Kubista, M. (1998) The interactions between the fluorescent dye thiazole orange and DNA. *Biopolymers* 46, 39-51.
- Oburger, E., Jones, D.L. and Wenzel, W.W. (2011) Phosphorus saturation and pH differentially regulate the efficiency of organic acid anion-mediated P solubilization mechanisms in soil. *Plant and Soil* 341, 363-382.
- Okamoto, S., Yamanishi, Y., Ehira, S., Kawashima, S., Tonomura, K. and Kanehisa, M. (2007) Prediction of nitrogen metabolism-related genes in *Anabaena* by kernel-based network analysis. *Proteomics* 7, 900-909.
- Oliveira, C.A., Alves, V.M.C., Marriel, I.E., Gomes, E.A., Scotti, M.R., Carneiro, N.P., Guimarães, C.T., Schaffert, R.E. and Sá, N.M.H. (2009) Phosphate solubilizing microorganisms isolated from rhizosphere of maize cultivated in an oxisol of the Brazilian Cerrado Biome. *Soil Biology and Biochemistry* 41, 1782-1787.
- Osamwonyi, U. and Wakil, S. (2012) Isolation of fungal species from fermentating pearl millet gruel and determination of their antagonistic activities against indicator bacterial species. *Nigerian Food Journal* 30(1).
- Østrem, L., Rapacz, M., Jørgensen, M. and Höglind, M. (2011) Effect of developmental stage on carbohydrate accumulation patterns during winter of timothy and perennial ryegrass. *Acta Agriculturae Scandinavica Section B—Soil and Plant Science* 61, 153-163.

O'sullivan, D.J. and O'Gara, F. (1992) Traits of fluorescent *Pseudomonas* spp. involved in suppression of plant root pathogens. *Microbiological Reviews* 56, 662-676.

Otsuka, Y., Muramatsu, Y., Nakagawa, Y., Matsuda, M., Nakamura, M. and Murata, H. (2011) *Burkholderia oxyphila* sp. nov., a bacterium isolated from acidic forest soil that catabolizes (+)-catechin and its putative aromatic derivatives. *International Journal of Systematic and Evolutionary Microbiology* 61, 249-254.

Ozanne, P. and Shaw, T. (1967) Phosphate sorption by soils as a measure of the phosphate requirement for pasture growth. *Crop and Pasture Science* 18, 601-612.

Özkundakci, D., Hamilton, D.P. and Scholes, P. (2010) Effect of intensive catchment and in-lake restoration procedures on phosphorus concentrations in a eutrophic lake. *Ecological Engineering* 36, 396-405.

Pagni, M., Ioannidis, V., Cerutti, L., Zahn-Zabal, M., Jongeneel, C.V., Hau, J., Martin, O., Kuznetsov, D. and Falquet, L. (2007) MyHits: improvements to an interactive resource for analyzing protein sequences. *Nucleic Acids Research* 35, W433-W437.

Pal, S.S. (1998) Interactions of an acid tolerant strain of phosphate solubilizing bacteria with a few acid tolerant crops. *Plant and Soil* 198, 169-177.

Pan, J., Plant, J.A., Voulvoulis, N., Oates, C.J. and Ihlenfeld, C. (2010) Cadmium levels in Europe: implications for human health. *Environmental Geochemistry and Health* 32, 1-12.

Pao, S.S., Paulsen, I.T. and Saier, M.H. (1998) Major facilitator superfamily. *Microbiology and Molecular Biology Reviews* 62, 1-34.

Parani, K. and Saha, B. (2012) Prospects of using phosphate solubilizing *Pseudomonas* as bio fertilizer. *European Journal of Biological Sciences* 4, 40-44.

Parfitt, R., Ross, D., Coomes, D., Richardson, S., Smale, M. and Dahlgren, R. (2005) N and P in New Zealand soil chronosequences and relationships with foliar N and P. *Biogeochemistry* 75, 305-328.

Parfitt, R.L., Baisden, W.T. and Elliott, A.H. (2008) Phosphorus inputs and outputs for New Zealand in 2001 at national and regional scales. *Journal of the Royal Society of New Zealand* 38, 37 - 50.

Park, J.H., Bolan, N., Megharaj, M. and Naidu, R. (2011) Isolation of phosphate solubilizing bacteria and their potential for lead immobilization in soil. *Journal of Hazardous Materials* 185, 829-836.

Park, K.H., Lee, C.Y. and Son, H.J. (2009) Mechanism of insoluble phosphate solubilization by *Pseudomonas fluorescens* RAF15 isolated from ginseng rhizosphere and its plant growth-promoting activities. *Letters in Applied Microbiology* 49, 222-228.

Park, K.-H., Lee, O.-M., Jung, H.-I., Jeong, J.-H., Jeon, Y.-D., Hwang, D.-Y., Lee, C.-Y. and Son, H.-J. (2010) Rapid solubilization of insoluble phosphate by a novel environmental stress-tolerant *Burkholderia vietnamiensis* M6 isolated from ginseng rhizospheric soil. *Applied Microbiology and Biotechnology* 86, 947-955.

- Parmar-Bhundia, V. (2010) Investigating the biosynthesis of heam d1 in *pseudomonas aeruginosa*: a cofactor for dissimilatory nitrite reductase. <https://qmro.qmul.ac.uk/jspui/handle/123456789/509>.
- Partida-Martinez, L.P. and Hertweck, C. (2005) Pathogenic fungus harbours endosymbiotic bacteria for toxin production. *Nature* 437, 884-888.
- Patel, D.K., Archana, G. and Kumar, G.N. (2008) Variation in the nature of organic acid secretion and mineral phosphate solubilization by *Citrobacter* sp. DHRSS in the presence of different sugars. *Current Microbiology* 56, 168-174.
- Paterson, E., Gebbing, T., Abel, C., Sim, A. and Telfer, G. (2007) Rhizodeposition shapes rhizosphere microbial community structure in organic soil. *New Phytologist* 173, 600-610.
- Patten, C.L. and Glick, B.R. (1996) Bacterial biosynthesis of indole-3-acetic acid. *Canadian Journal of Microbiology* 42, 207-220.
- Patten, C.L. and Glick, B.R. (2002) Role of *Pseudomonas putida* indoleacetic acid in development of the host plant root system. *Applied and Environmental Microbiology* 68, 3795-3801.
- Payne, R.W., Murray, D.A., Harding, S.A., Baird, D.B. and Soutar, D.M. (2011) An Introduction to GenStat for Windows (14th Edition). In VSN International. Hemel Hempstead, UK.
- Peer, W.A., Blakeslee, J.J., Yang, H. and Murphy, A.S. (2011) Seven things we think we know about auxin transport. *Molecular Plant* 4, 487-504.
- Peiffer, J.A., Spor, A., Koren, O., Jin, Z., Tringe, S.G., Dangl, J.L., Buckler, E.S. and Ley, R.E. (2013) Diversity and heritability of the maize rhizosphere microbiome under field conditions. *Proceedings of the National Academy of Sciences* 110, 6548-6553.
- Peralta, K.D., Araya, T., Valenzuela, S., Sossa, K., Martínez, M., Peña-Cortés, H. and Sanfuentes, E. (2012) Production of phytohormones, siderophores and population fluctuation of two root-promoting rhizobacteria in *Eucalyptus globulus* cuttings. *World Journal of Microbiology and Biotechnology* 28, 2003-2014.
- Péret, B., Clément, M., Nussaume, L. and Desnos, T. (2011) Root developmental adaptation to phosphate starvation: better safe than sorry. *Trends in Plant Science* 16, 442-450.
- Perez, E., Sulbaran, M., Ball, M.M. and Yarzabal, L.A. (2007) Isolation and characterization of mineral phosphate-solubilizing bacteria naturally colonizing a limonitic crust in the south-eastern Venezuelan region. *Soil Biology and Biochemistry* 39, 2905-2914.
- Pérez-Pantoja, D., Donoso, R., Agulló, L., Córdova, M., Seeger, M., Pieper, D.H. and González, B. (2012) Genomic analysis of the potential for aromatic compounds biodegradation in *Burkholderiales*. *Environmental Microbiology* 14, 1091-1117.
- Pérez-Torres, C.-A., López-Bucio, J., Cruz-Ramírez, A., Ibarra-Laclette, E., Dharmasiri, S., Estelle, M. and Herrera-Estrella, L. (2008) Phosphate availability alters lateral root development in *Arabidopsis* by modulating auxin sensitivity via a mechanism involving the TIR1 auxin receptor. *The Plant Cell Online* 20, 3258-3272.

- Petersen, T.N., Brunak, S., von Heijne, G. and Nielsen, H. (2011) SignalP 4.0: discriminating signal peptides from transmembrane regions. *Nature Methods* 8, 785-786.
- Peters-Wendisch, P.G., Eikmanns, B.J., Thierbach, G., Bachmann, B. and Sahm, H. (1993) Phosphoenolpyruvate carboxylase in *Corynebacterium glutamicum* is dispensable for growth and lysine production. *FEMS Microbiology Letters* 112, 269-274.
- Pfaffl, M.W. (2004) Quantification strategies in real-time PCR. *A-Z of quantitative PCR* 1, 89-113.
- Philippot, L. (2002) Denitrifying genes in bacterial and archaeal genomes. *Biochimica et Biophysica Acta (BBA)-Gene Structure and Expression* 1577, 355-376.
- Pierzynski, G.M. (1991) The chemistry and mineralogy of phosphorus in excessively fertilized soils. *Critical Reviews in Environmental Control* 21, 265 - 295.
- Pikovskaya, R. (1948) Mobilization of phosphorus in soil in connection with vital activity of some microbial species. *Mikrobiologiya* 17, 362-370.
- Pillay, V. and Nowak, J. (1997) Inoculum density, temperature, and genotype effects on *in vitro* growth promotion and epiphytic and endophytic colonization of tomato (*Lycopersicon esculentum* L.) seedlings inoculated with a pseudomonad bacterium. *Canadian Journal of Microbiology* 43, 354-361.
- Pinton, R., Varanini, Z. and Nannipieri, P. (2007) The rhizosphere: biochemistry and organic substances at the soil-plant interface: CRC press. *Annals of Botany* 104(4), ix-x. doi: 10.1093/aob/mcp166
- Poupin, M.J., Timmermann, T., Vega, A., Zuñiga, A. and González, B. (2013) Effects of the Plant Growth-Promoting Bacterium *Burkholderia phytofirmans* PsJN throughout the Life Cycle of *Arabidopsis thaliana*. *PLoS one* 8, e69435.
- Pukatzki, S., Ma, A.T., Revel, A.T., Sturtevant, D. and Mekalanos, J.J. (2007) Type VI secretion system translocates a phage tail spike-like protein into target cells where it cross-links actin. *Proceedings of the National Academy of Sciences* 104, 15508-15513.
- Pukatzki, S., Ma, A.T., Sturtevant, D., Krastins, B., Sarracino, D., Nelson, W.C., Heidelberg, J.F. and Mekalanos, J.J. (2006) Identification of a conserved bacterial protein secretion system in *Vibrio cholerae* using the *Dictyostelium* host model system. *Proceedings of the National Academy of Sciences of the United States of America* 103, 1528-1533.
- Pukatzki, S., McAuley, S.B. and Miyata, S.T. (2009) The type VI secretion system: translocation of effectors and effector-domains. *Current Opinion in Microbiology* 12, 11-17.
- Quigley, J.G., Yang, Z., Worthington, M.T., Phillips, J.D., Sabo, K.M., Sabath, D.E., Berg, C.L., Sassa, S., Wood, B.L. and Abkowitz, J.L. (2004) Identification of a human heme exporter that is essential for erythropoiesis. *Cell* 118, 757-766.
- Rademaker, J. and De Bruijn, F. (1997) Characterization and classification of microbes by rep-PCR genomic fingerprinting and computer assisted pattern analysis. *DNA Markers: Protocols, Applications and Overviews*, 151-171.

- Rajput, M.S., Kumar, G.N. and Rajkumar, S. (2013) Repression of oxalic acid-mediated mineral phosphate solubilization in rhizospheric isolates of *Klebsiella pneumoniae* by succinate. *Archives of Microbiology* 195, 81-88.
- Records, A.R. (2011) The type VI secretion system: a multipurpose delivery system with a phage-like machinery. *Molecular Plant-Microbe Interactions* 24, 751-757.
- Reddy, V.S., Shlykov, M.A., Castillo, R., Sun, E.I. and Saier, M.H. (2012) The major facilitator superfamily (MFS) revisited. *FEBS Journal* 279, 2022-2035.
- Reinhardt, J.A., Baltrus, D.A., Nishimura, M.T., Jeck, W.R., Jones, C.D. and Dangl, J.L. (2009) De novo assembly using low-coverage short read sequence data from the rice pathogen *Pseudomonas syringae* pv. *oryzae*. *Genome Research* 19, 294-305.
- Reinhold-Hurek, B., Hurek, T., Claeysens, M. and Van Montagu, M. (1993) Cloning, expression in *Escherichia coli*, and characterization of cellulolytic enzymes of *Azoarcus* sp., a root-invading diazotroph. *Journal of Bacteriology* 175, 7056-7065.
- Rennie, D.C., Manolii, V.P., Plishka, M. and Strelkov, S.E. (2013) Histological analysis of spindle and spheroid root galls caused by *Plasmiodiophora brassicae*. *European Journal of Plant Pathology*, 1-11.
- Rice, P., Longden, I. and Bleasby, A. (2000) EMBOSS: the European molecular biology open software suite. *Trends in Genetics* 16, 276-277.
- Richardson, A. and Hadobas, P. (1997) Soil isolates of *Pseudomonas* spp. that utilize inositol phosphates. *Canadian Journal of Microbiology* 43, 509-516.
- Richardson, A.E., Hocking, P.J., Simpson, R.J. and George, T.S. (2009) Plant mechanisms to optimise access to soil phosphorus. *Crop and Pasture Science* 60, 124-143.
- Richardson, A.E. (2001) Prospects for using soil microorganisms to improve the acquisition of phosphorus by plants. *Functional Plant Biology* 28, 897-906.
- Richardson, A.E., Hadobas, P.A., Hayes, J.E., O'Hara, C. and Simpson, R. (2001) Utilization of phosphorus by pasture plants supplied with myo-inositol hexaphosphate is enhanced by the presence of soil micro-organisms. *Plant and Soil* 229, 47-56.
- Richardson, A.E., Lynch, J.P., Ryan, P.R., Delhaize, E., Smith, F.A., Smith, S.E., Harvey, P.R., Ryan, M.H., Veneklaas, E.J. and Lambers, H. (2011) Plant and microbial strategies to improve the phosphorus efficiency of agriculture. *Plant and Soil* 349, 121-156.
- Richhardt, J., Bringer, S. and Bott, M. (2012) Mutational analysis of the pentose phosphate and Entner-Doudoroff pathways in *Gluconobacter oxydans* reveals improved growth of a Δ edd Δ eda mutant on mannitol. *Applied and Environmental Microbiology* 78, 6975-6986.
- Roca, A., Pizarro-Tobías, P., Udaondo, Z., Fernández, M., Matilla, M.A., Molina-Henares, M.A., Molina, L., Segura, A., Duque, E. and Ramos, J.L. (2013) Analysis of the plant growth-promoting properties encoded by the genome of the rhizobacterium *Pseudomonas putida* BIRD-1. *Environmental Microbiology* 15(3), 780-794.

- Rodríguez, H. and Fraga, R. (1999) Phosphate solubilizing bacteria and their role in plant growth promotion. *Biotechnology Advances* 17, 319-339.
- Rodríguez, H., Fraga, R., Gonzalez, T. and Bashan, Y. (2006) Genetics of phosphate solubilization and its potential applications for improving plant growth-promoting bacteria. *Plant and Soil* 287, 15-21.
- Rodríguez, H., Gonzalez, T. and Selman, G. (2000) Expression of a mineral phosphate solubilizing gene from *Erwinia herbicola* in two rhizobacterial strains. *Journal of Biotechnology* 84, 155-161.
- Rodríguez-Navarro, D.N., Dardanelli, M.S. and Ruíz-Saíñz, J.E. (2007) Attachment of bacteria to the roots of higher plants. *FEMS Microbiology Letters* 272, 127-136.
- Romantschuk, M. (1992) Attachment of plant pathogenic bacteria to plant surfaces. *Annual Review of Phytopathology* 30, 225-243.
- Roy, A., Yang, J. and Zhang, Y. (2012) COFACTOR: an accurate comparative algorithm for structure-based protein function annotation. *Nucleic Acids Research* 40, W471-W477.
- Rozen, S. and Skaletsky, H. (1999) Primer3 on the WWW for general users and for biologist programmers. *Bioinformatics Methods and Protocols* 365-386.
- Ruijter, J.M., Pfaffl, M.W., Zhao, S., Spiess, A.N., Boggy, G., Blom, J., Rutledge, R.G., Sisti, D., Lievens, A. and Preter, K.D. (2012) Evaluation of qPCR curve analysis methods for reliable biomarker discovery: Bias, resolution, precision, and implications. *Methods* 59(1), 32-46.
- Russell, A.B., Hood, R.D., Bui, N.K., LeRoux, M., Vollmer, W. and Mougous, J.D. (2011) Type VI secretion delivers bacteriolytic effectors to target cells. *Nature* 475, 343-347.
- Ryu, R.J. and Patten, C.L. (2008) Aromatic amino acid-dependent expression of indole-3-pyruvate decarboxylase is regulated by TyrR in *Enterobacter cloacae* UW5. *Journal of Bacteriology* 190, 7200-7208.
- Saharan, B. and Nehra, V. (2011) Plant growth promoting rhizobacteria: a critical review. *Life Science Medicine Research* 21, 1-30.
- Saichana, I., Moonmangmee, D., Adachi, O., Matsushita, K. and Toyama, H. (2009) Screening of thermotolerant *Gluconobacter* strains for production of 5-keto-d-gluconic acid and disruption of flavin adenine dinucleotide-containing d-gluconate dehydrogenase. *Applied and Environmental Microbiology* 75, 4240-4247.
- Saleem, M., Arshad, M., Hussain, S. and Bhatti, A.S. (2007) Perspective of plant growth promoting rhizobacteria (PGPR) containing ACC deaminase in stress agriculture. *Journal of Industrial Microbiology & Biotechnology* 34, 635-648.
- Salles, J.F., Van Veen, J.A. and Van Elsas, J.D. (2004) Multivariate analyses of *Burkholderia* species in soil: effect of crop and land use history. *Applied and Environmental Microbiology* 70, 4012-4020.
- Sana, T.G., Hachani, A., Bucior, I., Soscia, C., Garvis, S., Termine, E., Engel, J., Filloux, A. and Bleves, S. (2012) The second type VI secretion system of *Pseudomonas aeruginosa* strain PAO1 is regulated by

- quorum sensing and Fur and modulates internalization in epithelial cells. *Journal of Biological Chemistry* 287, 27095-27105.
- Salomon, D., Kinch, L.N., Trudgian, D.C., Guo, X., Klimko, J.A., Grishin, N.V., Mirzaei, H. and Orth, K. (2014) Marker for type VI secretion system effectors. *Proceedings of the National Academy of Sciences* 111, 9271-9276.
- Sánchez-Rodríguez, C., Rubio-Somoza, I., Sibout, R. and Persson, S. (2010) Phytohormones and the cell wall in *Arabidopsis* during seedling growth. *Trends in Plant Science* 15, 291-301.
- Sanyal, S. and De Datta, S. (1991) Chemistry of phosphorus transformations in soil. *Advances in Soil Science*, 1-120.
- Sarris, P.F., Zoumadakis, C., Panopoulos, N.J. and Scoulica, E.V. (2011) Distribution of the putative type VI secretion system core genes in *Klebsiella* spp. *Infection, Genetics and Evolution* 11, 157-166.
- Sarwar, M. and Kremer, R. (1995) Determination of bacterially derived auxins using a microplate method. *Letters in Applied Microbiology* 20, 282-285.
- Sashidhar, B. and Podile, A. (2010) Mineral phosphate solubilization by rhizosphere bacteria and scope for manipulation of the direct oxidation pathway involving glucose dehydrogenase. *Journal of Applied Microbiology* 109, 1-12.
- Sashidhar, B. and Podile, A.R. (2009) Transgenic expression of glucose dehydrogenase in *Azotobacter vinelandii* enhances mineral phosphate solubilization and growth of sorghum seedlings. *Microbial Biotechnology* 2, 521-529.
- Schäfer, B.W. and Heizmann, C.W. (1996) The S100 family of EF-hand calcium-binding proteins: functions and pathology. *Trends in Biochemical Sciences* 21, 134-140.
- Schweizer, P., Schlagenhauf, E., Schaffrath, U. and Dudler, R. (1999) Different patterns of host genes are induced in rice by *Pseudomonas syringae*, a biological inducer of resistance, and the chemical inducer benzothiadiazole (BTH). *European Journal of Plant Pathology* 105, 659-665.
- Schwyn, B. and Neilands, J. (1987) Universal chemical assay for the detection and determination of siderophores. *Analytical Biochemistry* 160, 47-56.
- Selvakumar, G., Joshi, P., Nazim, S., Mishra, P.K., Bisht, J.K. and Gupta, H.S. (2009) Phosphate solubilization and growth promotion by *Pseudomonas fragi* CS11RH1 (MTCC 8984), a psychrotolerant bacterium isolated from a high altitude Himalayan rhizosphere. *Biologia* 64, 239-245.
- Sessitsch, A., Coenye, T., Sturz, A., Vandamme, P., Barka, E.A., Salles, J., Van Elsas, J., Faure, D., Reiter, B. and Glick, B. (2005) *Burkholderia phytofirmans* sp. nov., a novel plant-associated bacterium with plant-beneficial properties. *International Journal of Systematic and Evolutionary Microbiology* 55, 1187-1192.
- Shaharoona, B., Arshad, M., Zahir, Z.A. and Khalid, A. (2006) Performance of *Pseudomonas* spp. containing ACC-deaminase for improving growth and yield of maize (*Zea mays* L.) in the presence of nitrogenous fertilizer. *Soil Biology and Biochemistry* 38, 2971-2975.

Shahid, M., Hameed, S., Imran, A., Ali, S. and van Elsas, J.D. (2012) Root colonization and growth promotion of sunflower (*Helianthus annuus* L.) by phosphate solubilizing *Enterobacter* sp. Fs-11. *World Journal of Microbiology and Biotechnology* 28, 2749-2758.

Shapiro, A.L. and Maizel, J.V. (1969) Molecular weight estimation of polypeptides by SDS-polyacrylamide gel electrophoresis: Further data concerning resolving power and general considerations. *Analytical Biochemistry* 29, 505-514.

Sharma, V., Kumar, V., Archana, G. and Kumar, G.N. (2005) Substrate specificity of glucose dehydrogenase (GDH) of *Enterobacter asburiae* PSI3 and rock phosphate solubilization with GDH substrates as C sources. *Canadian Journal of Microbiology* 51, 477-482.

Sharma, V. and Nowak, J. (1998) Enhancement of verticillium wilt resistance in tomato transplants by *in vitro* co-culture of seedlings with a plant growth promoting rhizobacterium (*Pseudomonas* sp. strain PsJN). *Canadian Journal of Microbiology* 44, 528-536.

Shaw, K.J. and Berg, C.M. (1979) *Escherichia coli* K-12 auxotrophs induced by insertion of the transposable element Tn5. *Genetics* 92, 741-747.

Shaw, R.J., McNeill, M.M., Maass, D.R., Hein, W.R., Barber, T.K., Wheeler, M., Morris, C.A. and Shoemaker, C.B. (2003) Identification and characterisation of an aspartyl protease inhibitor homologue as a major allergen of *Trichostrongylus colubriformis*. *International Journal for Parasitology* 33, 1233-1243.

Shi, S., Richardson, A.E., O'Callaghan, M., DeAngelis, K.M., Jones, E.E., Stewart, A., Firestone, M.K. and Condron, L.M. (2011) Effects of selected root exudate components on soil bacterial communities. *FEMS Microbiology Ecology* 77, 600-610.

Shneider, M.M., Buth, S.A., Ho, B.T., Basler, M., Mekalanos, J.J. and Leiman, P.G. (2013) PAAR-repeat proteins sharpen and diversify the type VI secretion system spike. *Nature* 500, 350-353.

Sillén, L.G. and Martell, A. (1958) Stability constants. *Journal of Inorganic and Nuclear Chemistry* 8, 176-195.

Singh, B. and Satyanarayana, T. (2011) Microbial phytases in phosphorus acquisition and plant growth promotion. *Physiology and Molecular Biology of Plants* 17, 93-103.

Singh, J.S. (2013) Plant growth promoting rhizobacteria. *Resonance* 18, 275-281.

Smil, V. (2000) Phosphorous in the environment: Natural Flows and Human Interferences. *Annual Review of Energy and the Environment* 25, 53-88.

Solanki, M.K., Singh, R.K., Srivastava, S., Kumar, S., Kashyap, P.L., Srivastava, A.K. and Arora, D.K. (2013) Isolation and characterization of siderophore producing antagonistic rhizobacteria against *Rhizoctonia solani*. *Journal of Basic Microbiology* doi: 10.1002/jobm.201200564.

Song, O.-R., Lee, S.-J., Lee, Y.-S., Lee, S.-C., Kim, K.-K. and Choi, Y.-L. (2008) Solubilization of insoluble inorganic phosphate by *Burkholderia cepacia* DA23 isolated from cultivated soil. *Brazilian Journal of Microbiology* 39, 151-156.

- Souchie, E.L., Saggin-Júnior, O.J., Silva, E.M.R., Campello, E.F.C., Azcón, R. and Barea, J.M. (2006) Communities of P-solubilizing bacteria, fungi and arbuscular mycorrhizal fungi in grass pasture and secondary forest of Paraty, RJ - Brazil. *Anais da Academia Brasileira de Ciências* 78, 183-193.
- Stackebrandt, E. and Goebel, B. (1994) Taxonomic note: a place for DNA-DNA reassociation and 16S rRNA sequence analysis in the present species definition in bacteriology. *International Journal of Systematic Bacteriology* 44, 846-849.
- Strom, M. and Lory, S. (1993) Structure-function and biogenesis of the type IV pili. *Annual Reviews in Microbiology* 47, 565-596.
- Suarez, G., Sierra, J.C., Sha, J., Wang, S., Erova, T.E., Fadl, A.A., Foltz, S.M., Horneman, A.J. and Chopra, A.K. (2008) Molecular characterization of a functional type VI secretion system from a clinical isolate of *Aeromonas hydrophila*. *Microbial Pathogenesis* 44, 344-361.
- Suárez-Moreno, Z.R., Caballero-Mellado, J., Coutinho, B.G., Mendonça-Previato, L., James, E.K. and Venturi, V. (2012) Common features of environmental and potentially beneficial plant-associated *Burkholderia*. *Microbial Ecology* 63, 249-266.
- Suárez-Moreno, Z.R., Caballero-Mellado, J. and Venturi, V. (2008) The new group of non-pathogenic plant-associated nitrogen-fixing *Burkholderia* spp. shares a conserved quorum-sensing system, which is tightly regulated by the RsaL repressor. *Microbiology* 154, 2048-2059.
- Subramoni, S., Agnoli, K., Eberl, L., Lewenza, S. and Sokol, P.A. (2013) Role of *Burkholderia cenocepacia* *afcE* and *afcF* genes in determining lipid-metabolism-associated phenotypes. *Microbiology* 159, 603-614.
- Sun, Y., Cheng, Z. and Glick, B.R. (2009) The presence of a 1-aminocyclopropane-1-carboxylate (ACC) deaminase deletion mutation alters the physiology of the endophytic plant growth-promoting bacterium *Burkholderia phytofirmans* PsJN. *FEMS Microbiology Letters* 296, 131-136.
- Sun, Y., Hegamyer, G. and Colburn, N. (1993) PCR-direct sequencing of a GC-rich region by inclusion of 10% DMSO: application to mouse c-jun. *Biotechniques* 15, 372.
- Suriyagoda, L.D., Ryan, M.H., Renton, M. and Lambers, H. (2012) Adaptive shoot and root responses collectively enhance growth at optimum temperature and limited phosphorus supply of three herbaceous legume species. *Annals of Botany* 110, 959-968.
- Szklarczyk, D., Franceschini, A., Kuhn, M., Simonovic, M., Roth, A., Minguéz, P., Doerks, T., Stark, M., Müller, J. and Bork, P. (2011) The STRING database in 2011: functional interaction networks of proteins, globally integrated and scored. *Nucleic Acids Research* 39, D561-D568.
- Tang, J., Leung, A., Leung, C. and Lim, B.L. (2006) Hydrolysis of precipitated phytate by three distinct families of phytases. *Soil Biology and Biochemistry* 38, 1316-1324.
- Teng, J.L., Yeung, M.-Y., Yue, G., Au-Yeung, R.K., Yeung, E.Y., Fung, A.M., Tse, H., Yuen, K.-Y., Lau, S.K. and Woo, P.C. (2011) *In silico* analysis of 16S rRNA gene sequencing based methods for identification

of medically important aerobic Gram-negative bacteria. *Journal of Medical Microbiology* 60, 1281-1286.

Theocharis, A., Bordiec, S., Fernandez, O., Paquis, S., Dhondt-Cordelier, S., Baillieul, F., Clément, C. and Barka, E.A. (2012) *Burkholderia phytofirmans* PsJN primes *Vitis vinifera* L. and confers a better tolerance to low nonfreezing temperatures. *Molecular Plant-Microbe Interactions* 25, 241-249.

Tong, S., Yang, S., LU, Z. and He, W. (1996) Laboratory investigation of ecological factors influencing the environmental presence of *Burkholderia pseudomallei*. *Microbiology and Immunology* 40, 451-453.

Toyama, H. and Lidstrom, M.E. (1998) pqqA is not required for biosynthesis of pyrroloquinoline quinone in *Methylobacterium extorquens* AM1. *Microbiology* 144 (1), 183-191.

Trivedi, P. and Sa, T. (2008) *Pseudomonas corrugata* (NRRL B-30409) mutants increased phosphate solubilization, organic acid production, and plant growth at lower temperatures. *Current Microbiology* 56, 140-144.

Trolove, S.N., Hedley, M.J., Kirk, G.J.D., Bolan, N.S. and Loganathan, P. (2003) Progress in selected areas of rhizosphere research on phosphate acquisition. *Australian Journal of Soil Research* 41, 471-499.

Turner, B.L., Papházy, M.J., Haygarth, P.M. and McKelvie, I.D. (2002) Inositol phosphates in the environment. *Philosophical Transactions of the Royal Society of London Series B: Biological Sciences* 357, 449-469.

Turner, B.L., Wells, A., Andersen, K.M. and Condrón, L.M. (2012) Patterns of tree community composition along a coastal dune chronosequence in lowland temperate rain forest in New Zealand. *Plant Ecology* 213, 1525-1541.

Turner, S. and Jenkins, F. (1995) Use of deoxyinosine in PCR to improve amplification of GC-rich DNA. *Biotechniques* 19, 48.

Udvardi, M.K., Czechowski, T. and Scheible, W.-R. (2008) Eleven Golden Rules of Quantitative RT-PCR. *Plant Cell* 20, 1736-1737.

Unterweger, D., Miyata, S.T., Bachmann, V., Brooks, T.M., Mullins, T., Kostiuk, B., Provenzano, D. and Pukatzki, S. (2014) The *Vibrio cholerae* type VI secretion system employs diverse effector modules for intraspecific competition. *Nature communications* 5:3549 | DOI: 10.1038/ncomms4549.

Upadhyay, S., Singh, D. and Saikia, R. (2009) Genetic diversity of plant growth promoting rhizobacteria isolated from rhizospheric soil of wheat under saline condition. *Current Microbiology* 59, 489-496.

Van Loon, L. (2007) Plant responses to plant growth-promoting rhizobacteria. *European Journal of Plant Pathology* 119, 243-254.

- Van Puyvelde, S., Cloots, L., Engelen, K., Das, F., Marchal, K., Vanderleyden, J. and Spaepen, S. (2011) Transcriptome analysis of the rhizosphere bacterium *Azospirillum brasilense* reveals an extensive auxin response. *Microbial Ecology* 61, 723-728.
- Vassileva, M., Serrano, M., Bravo, V., Jurado, E., Nikolaeva, I., Martos, V. and Vassilev, N. (2010) Multifunctional properties of phosphate-solubilizing microorganisms grown on agro-industrial wastes in fermentation and soil conditions. *Applied Microbiology and Biotechnology* 85, 1287-1299.
- Versalovic, J., Koeuth, T. and Lupski, R. (1991) Distribution of repetitive DNA sequences in eubacteria and application to finerprinting of bacterial genomes. *Nucleic Acids Research* 19, 6823-6831.
- Versalovic, J., Schneider, M., De Bruijn, F. and Lupski, J.R. (1994) Genomic fingerprinting of bacteria using repetitive sequence-based polymerase chain reaction. *Methods in Molecular and Cellular Biology* 5, 25-40.
- Vespermann, A., Kai, M. and Piechulla, B. (2007) Rhizobacterial volatiles affect the growth of fungi and *Arabidopsis thaliana*. *Applied and Environmental Microbiology* 73, 5639-5641.
- Vessey, J.K. (2003) Plant growth promoting rhizobacteria as biofertilizers. *Plant and Soil* 255, 571-586.
- Vogel, R., Willmott, G., Kozak, D., Roberts, G.S., Anderson, W., Groenewegen, L., Glossop, B., Barnett, A., Turner, A. and Trau, M. (2011) Quantitative sizing of nano/microparticles with a tunable elastomeric pore sensor. *Analytical Chemistry* 83, 3499-3506.
- Von Mering, C., Jensen, L.J., Snel, B., Hooper, S.D., Krupp, M., Foglierini, M., Jouffre, N., Huynen, M.A. and Bork, P. (2005) STRING: known and predicted protein-protein associations, integrated and transferred across organisms. *Nucleic Acids Research* 33, D433-D437.
- Vyas, P. and Gulati, A. (2009) Organic acid production *in vitro* and plant growth promotion in maize under controlled environment by phosphate-solubilizing fluorescent *Pseudomonas*. *BMC Microbiology* 9, 174.
- Wang, E., Ridoutt, B.G., Luo, Z. and Probert, M.E. (2013) Using systems modelling to explore the potential for root exudates to increase phosphorus use efficiency in cereal crops. *Environmental Modelling & Software* 46, 50-60.
- Wang, G.C. and Wang, Y. (1996) The frequency of chimeric molecules as a consequence of PCR co-amplification of 16S rRNA genes from different bacterial species. *Microbiology* 142, 1107-1114.
- Warmink, J., Nazir, R., Corten, B. and Van Elsas, J. (2011) Hitchhikers on the fungal highway: the helper effect for bacterial migration via fungal hyphae. *Soil Biology and Biochemistry* 43, 760-765.
- Warren, M.J., Stolorich, N.J., Santander, P.J., Roessner, C.A., Sowa, B.A. and Scott, A.I. (1990) Enzymatic synthesis of dihydrosirohydrochlorin (precorrin-2) and of a novel pyrrocorphin by uroporphyrinogen III methylase. *FEBS Letters* 261, 76-80.
- Weber, C.F. and King, G.M. (2012) The phylogenetic distribution and ecological role of carbon monoxide oxidation in the genus *Burkholderia*. *FEMS Microbiology Ecology* 79, 167-175.

- Weber, K. and Osborn, M. (1969) The Reliability of Molecular Weight Determinations by Dodecyl Sulfate-Polyacrylamide Gel Electrophoresis. *Journal of Biological Chemistry* 244, 4406-4412.
- Webley, D. and Duff, R. (1965) The incidence, in soils and other habitats, of micro-organisms producing 2-ketogluconic acid. *Plant and Soil* 22, 307-313.
- Weilharter, A., Mitter, B., Shin, M.V., Chain, P.S., Nowak, J. and Sessitsch, A. (2011) Complete genome sequence of the plant growth-promoting endophyte *Burkholderia phytofirmans* strain PsJN. *Journal of Bacteriology* 193, 3383-3384.
- Whalen, M.C., Innes, R.W., Bent, A.F. and Staskawicz, B.J. (1991) Identification of *Pseudomonas syringae* pathogens of Arabidopsis and a bacterial locus determining avirulence on both Arabidopsis and soybean. *The Plant Cell Online* 3, 49-59.
- Whiteford, M.L., Wilkinson, J.D., McColl, J.H., Conlon, F.M., Michie, J.R., Evans, T.J. and Paton, J.Y. (1995) Outcome of *Burkholderia (Pseudomonas) cepacia* colonisation in children with cystic fibrosis following a hospital outbreak. *Thorax* 50, 1194-1198.
- Wilkinson, D.L. and Harrison, R.G. (1991) Predicting the solubility of recombinant proteins in *Escherichia coli*. *Nature Biotechnology* 9, 443-448.
- Wisselink, H., Weusthuis, R., Eggink, G., Hugenholtz, J. and Grobbee, G. (2002) Mannitol production by lactic acid bacteria: a review. *International Dairy Journal* 12, 151-161.
- Wolk, C.P., Ernst, A. and Elhai, J. (2004) Heterocyst metabolism and development. *Advances in Photosynthesis and Respiration* 1, 769-823.
- Wu, C.H., Mulchandani, A. and Chen, W. (2008) Versatile microbial surface-display for environmental remediation and biofuels production. *Trends in Microbiology* 16, 181-188.
- Wu, S. and Zhang, Y. (2007) LOMETS: a local meta-threading-server for protein structure prediction. *Nucleic Acids Research* 35, 3375-3382.
- Wylie, J.L. and Worobec, E.A. (1995) The OprB porin plays a central role in carbohydrate uptake in *Pseudomonas aeruginosa*. *Journal of Bacteriology* 177, 3021-3026.
- Yabuuchi, E., Kosako, Y., Oyaizu, H., Yano, I., Hotta, H., Hashimoto, Y., Ezaki, T. and Arakawa, M. (1991) Proposal of *Burkholderia* gen. nov. and transfer of seven species of the genus *Pseudomonas* homology group II to the new genus, with the type species *Burkholderia cepacia* (Palleroni and Holmes 1981) comb. nov. *Microbiology and Immunology* 36, 1251-1275.
- Yang, J., Kloepper, J.W. and Ryu, C.-M. (2009) Rhizosphere bacteria help plants tolerate abiotic stress. *Trends in Plant Science* 14, 1-4.
- Yang, J., Roy, A. and Zhang, Y. (2013) BioLiP: a semi-manually curated database for biologically relevant ligand-protein interactions. *Nucleic Acids Research* 41, D1096-D1103.

- Yang, P.-X., Ma, L., Chen, M.-H., Xi, J.-Q., He, F., Duan, C.-Q., Mo, M.-H., Fang, D.-H., Duan, Y.-Q. and Yang, F.-X. (2012) Phosphate solubilizing ability and phylogenetic diversity of bacteria from P-rich soils around Dianchi lake drainage area of China. *Pedosphere* 22, 707-716.
- Yanisch-Perron, C., Vieira, J. and Messing, J. (1985) Improved M13 phage cloning vectors and host strains: nucleotide sequences of the M13mpl8 and pUC19 vectors. *Gene* 33, 103-119.
- Yazdani, M., Bahmanyar, M.A., Pirdashti, H. and Esmaili, M. (2009) Effect of Phosphate solubilization microorganisms (PSM) and plant growth promoting rhizobacteria (PGPR) on yield and yield components of Corn (*Zea mays* L.). *World Academy of Science, Engineering and Technology* 25, 64-66.
- Ye, J., Coulouris, G., Zaretskaya, I., Cutcutache, I., Rozen, S. and Madden, T.L. (2012) Primer-BLAST: A tool to design target-specific primers for polymerase chain reaction. *BMC Bioinformatics* 13, 134.
- Yum, D.-Y., Lee, Y.-P. and Pan, J.-G. (1997) Cloning and expression of a gene cluster encoding three subunits of membrane-bound gluconate dehydrogenase from *Erwinia cyripedii* ATCC 29267 in *Escherichia coli*. *Journal of Bacteriology* 179, 6566-6572.
- Zhang, W., Xu, S., Li, J., Shen, X., Wang, Y. and Yuan, Z. (2011) Modulation of a thermoregulated type VI secretion system by AHL-dependent quorum sensing in *Yersinia pseudotuberculosis*. *Archives of Microbiology* 193, 351-363.
- Zhang, Y. (2008) I-TASSER server for protein 3D structure prediction. *BMC Bioinformatics* 9, 40.
- Zhang, Y.-f., He, L.-y., Chen, Z.-j., Wang, Q.-y., Qian, M. and Sheng, X.-f. (2011) Characterization of ACC deaminase-producing endophytic bacteria isolated from copper-tolerant plants and their potential in promoting the growth and copper accumulation of *Brassica napus*. *Chemosphere* 83, 57-62.
- Zhao, K., Penttinen, P., Zhang, X., Ao, X., Liu, M., Yu, X. and Chen, Q. (2013) Maize rhizosphere in Sichuan, China, hosts plant growth promoting *Burkholderia cepacia* with phosphate solubilizing and antifungal abilities. *Microbiological Research*. 169, 76–82.
- Zhou, Y., Yang, W., Kirberger, M., Lee, H.W., Ayalasomayajula, G. and Yang, J.J. (2006) Prediction of EF-hand calcium-binding proteins and analysis of bacterial EF-hand proteins. *Proteins: Structure, Function, and Bioinformatics* 65, 643-655.
- Zúñiga, A., Poupin, M.J., Donoso, R., Ledger, T., Guiliani, N., Gutiérrez, R.A. and González, B. (2013) Quorum sensing and indole-3-acetic acid degradation play a role in colonization and plant growth promotion of *Arabidopsis thaliana* by *Burkholderia phytofirmans* PsJN. *Molecular Plant-Microbe Interactions* 26, 546-553.
- Zyśko, A., Sanguin, H., Hayes, A., Wardleworth, L., Zeef, L.A., Sim, A., Paterson, E., Singh, B.K. and Kertesz, M.A. (2012) Transcriptional response of *Pseudomonas aeruginosa* to a phosphate-deficient *Lolium perenne* rhizosphere. *Plant and Soil* 359, 25-44.

Appendix A

Chemicals and Reagents

A.1 Buffers and Solutions

A.1.1 Solutions for alkaline lysis plasmid mini-preps

Solution I

9.0 g	Glucose
12.5 mL	1 M Tris-Cl (pH 8.0)
10.0 mL	0.5 M EDTA (pH 8.0)

Dissolve in 400 mL of dsH₂O and adjust the volume to 500 mL. The solution was sterilised by autoclaving for 15 min at 1.1 kg/cm², 121°C and store at 4°C.

Solution II

500 µL	0.2 M NaOH
500 µL	10 % SDS

Add to 4 mL of dsH₂O, (made fresh each time).

Solution III

60.0 mL	3 M potassium acetate
11.5 mL	glacial acetic acid

Add to 28.5 mL of dsH₂O and store at room temperature and the pH was adjusted to 5.2.

A.1.2 SpecM solution

1.0 g	Na ₄ O ₇ P ₂ (Tetrasodium pyrophosphate)
1.0 mL	Tween 80

Add to 1 L of dsH₂O and sterilise by autoclaving for 15 min at 1.1 kg/cm², 121°C, and store at room temperature.

A.1.3 5X M9 salt solution

64.0 g $\text{Na}_2\text{HPO}_4 \cdot 7\text{H}_2\text{O}$

15.0 g KH_2PO_4

2.5 g NaCl

5.0 g NH_4Cl

Dissolve in 800 mL of dsH_2O under low heat. Adjust volume to 1 L and sterilise by autoclaving for 15 min at 1.1 kg/cm², 121°C, and store at room temperature.

A.1.4 10x Trace elements solution

2.8 g H_3BO_3

1.8 g $\text{MnCl}_2 \cdot 4\text{H}_2\text{O}$

0.2 g $\text{ZnSO}_4 \cdot 7\text{H}_2\text{O}$

0.1 g $\text{CuSO}_4 \cdot 5\text{H}_2\text{O}$

0.025 g NaMoO_4

Dissolve in 100 mL of dsH_2O and store at 4°C.

A.1.5 Molybdenum Blue reagent

0.20 g $(\text{NH}_4)_2\text{MoO}_4$

1.44 g $\text{FeSO}_4 \cdot 7\text{H}_2\text{O}$

6.40 mL 10 % H_2SO_4

Dissolve in 10 mL of dsH_2O , and slowly adding 10 % of sulphuric acid drop by drop. Make to a total volume of 20 mL with dsH_2O .

A.1.6 Phosphate buffered saline (PBS)

7.60 g NaCl

1.14 g Na_2HPO_4

0.19 g KCl

0.20 g KH_2PO_4

Dissolve in 800 mL of dsH_2O and adjust the pH to 7.4 followed by adjust volume to 1 L and sterilise by autoclaving for 15 min at 1.1 kg/cm², 121°C. Store at room temperature.

A.1.7 Hoagland's solution

1.65 g	Ca(NO ₃) ₂ ·4H ₂ O
0.50 g	KNO ₃
0.27 g	KH ₂ PO ₄
0.49 g	MgSO ₄ ·7H ₂ O
1 mL	1X Trace elements solution
1 mL	FeEDTA

Dissolve in 800 mL of dsH₂O and adjust the pH to 7.0 followed by adjust volume to 1 L and sterilise by autoclaving for 15 min at 1.1 kg/cm², 121°C. Store at room temperature.

A.1.8 FeEDTA solution

10.4 g	EDTA·2Na
7.80 g	FeSO ₄ ·7H ₂ O
56.1 g	KOH

Dissolve in 800 mL of dsH₂O and adjust the pH to 5.5. Adjust volume to 1 L and sterilise using 0.22 µm PVDF syringe filter. Store at 4°C.

A.2 Media

A.2.1 National Botanical Research Institute's Phosphate (NBRIP) growth media plates

10.0 g	Glucose
0.1 g	(NH ₄) ₂ SO ₄
0.2 g	KCl
5.0 g	MgCl ₂ ·6H ₂ O
0.25 g	MgSO ₄ ·7H ₂ O
5.0 g	Tricalcium phosphate (Ca ₃ (PO ₄) ₂) or Hydroxyapatite (Ca ₅ (PO ₄) ₃ (OH))
15.0 g	Bacto Agar

Dissolve in 800 mL of dsH₂O, and adjust the pH to 7. Make up the volume to 1 L by dsH₂O.

A.2.2 Tricalcium or hydroxyapatite agar plate (TCaP/HydroxP)

10.0 g	Glucose
5.0 g	NH ₄ NO ₃
0.5 g	KCl

0.5 g	MgSO ₄ ·7H ₂ O
100 µL	MnSO ₄ ·H ₂ O (10 mg/mL)
100 µL	FeSO ₄ ·H ₂ O (10 mg/mL)
6.0 g	Tricalcium phosphate (Ca ₃ (PO ₄) ₂) or Hydroxyapatite (Ca ₅ (PO ₄) ₃ (OH))
15.0 g	Agarose agar

Dissolve in 800 mL of dsH₂O and adjust the pH to 6.5 and make up the volume to 1 L by dsH₂O before autoclaving for 15 min at 1.1 kg/cm², 121°C. A 100 µL of 10x trace element solution was added after autoclaving.

A.2.3 Tricalcium Phosphate (TCaP) Liquid culture medium

10 g	Glucose
5g	NH ₄ NO ₃
0.5g	KCl
0.5g	MgSO ₄ ·7H ₂ O
100 µL	MnSO ₄ ·H ₂ O (10 mg/mL)
100 µL	FeSO ₄ ·H ₂ O (10 mg/mL)
6 g	Tricalcium phosphate (Ca ₃ (PO ₄) ₂)

Dissolve in 800 mL of dsH₂O and adjust the pH to 6.5 and make up the volume to 1 L by dsH₂O before autoclaving for 15 min at 1.1 kg/cm², 121°C. A 100 µL of 10x trace element solution was added after autoclaving.

A.2.4 HSU HydroxP Liquid culture medium

10 g	Glucose
100 mL	10x HSU buffer
100 µL	FeSO ₄ ·H ₂ O (10 mg/mL)
6 g	Hydroxyapatite (Ca ₅ (PO ₄) ₃ OH)

Dissolve in 800 mL of dsH₂O, adjust the pH to 6.5 and make up the volume to 1 L by dsH₂O before autoclaving for 15 min at 1.1 kg/cm², 121°C. A 100 µL of 10x trace element solution was added after autoclaving.

A.2.5 10x HSU buffer (pH 5.5)

2.4g	K ₂ SO ₄
2.5g	MgCl ₂
2.5g	NH ₄ Cl
0.3g	CaCl ₂
14.6g	NaCl

Dissolve in 800 mL of dsH₂O, adjust the pH to 5.5 and make up the volume to 1 L by dsH₂O before autoclaving for 15 min at 1.1 kg/cm², 121°C.

A.2.6 M9 minimal medium

200 mL	5 × M9 salts
2 mL	1 M MgSO ₄
1 mL	0.1 M CaCl ₂
12g	Agarose

Dissolve in 700 mL sterile dsH₂O then adjust volume to 1 L. Autoclave to sterilise. Prior to pouring add 20 mL filter-sterilised 0.4 % carbon source of either casamino acids or glucose. Store at room temperature.

A.2.7 SDS-PAGE solution Composition

Separating gel solution

15 % (v/v)	acrylamide
375 mM	Tris/HCl (pH 8.8)
0.1 % (w/v)	SDS
0.05 % (w/v)	ammonium persulphate
0.2 % (v/v)	TEMED

Stacking gel solution

3.6 %	acrylamide
125 mM	Tris/HCl (pH 6.8)
0.1 %	SDS
0.05 %	ammonium persulphate
0.2 %	TEMED

Laemmli loading buffer

62.5 mM	Tris/HCl (pH 6.8)
10 % (v/v)	glycerol
2 % (w/v)	SDS
0.01 % (w/v)	bromophenol blue
5 % (v/v)	2-mercaptoethanol

Laemmli Running Buffer

25 mM	Tris/HCl
200 mM	glycine
0.1 % (w/v)	SDS

Destaining Solution

20 % (v/v)	methanol
7 % (v/v)	acetic acid

Appendix B

Microbiology Techniques

B.1 Optical density reading

The optical density of bacterial cultures was measured using a SmartSpec spectrophotometer (BioRad). A 100 μ L volume of culture was diluted in 900 μ L sterile culture medium and the optical density measured at a wavelength of 600 nm. A 1-mL dsH₂O was used as a blank.

B.2 Growth Curve determination and serial dilution plate counts

A 100 μ L volume of starter culture with an OD₆₀₀ of 4.0 was inoculated into a 250-mL glass flask containing 50 mL sterile LB medium or HSU HydroxP medium (Appendix A.3.4). The flask was incubated with rotation at 250 rpm for 12, 24, 36, 60 and 84 h at 25°C in a Ratek orbital mixer incubator (OM11, Ratek Instruments Pty Ltd, Victoria, Australia). At each time point, 100 μ L of culture were removed for serial dilution analysis. A 1 in10 dilution series was prepared by diluting

100 μL volumes of culture in 900 μL sterile SpecM solution (Appendix A.1.2). Dilutions were carried out in sterile deep-dish 96-well bacterial culture plates, with each dilution mixed thoroughly by pipette. Duplicate 100 μL volumes of the appropriate dilutions were plated on LB agar medium and incubated for 48 h at 25°C. Bacterial colonies were counted and Log_{10} colony forming units (Log_{10} cfu mL^{-1}) was calculated, taking into account the dilution and volume plated. The growth curve experiment was repeated in triplicated at three independent times.

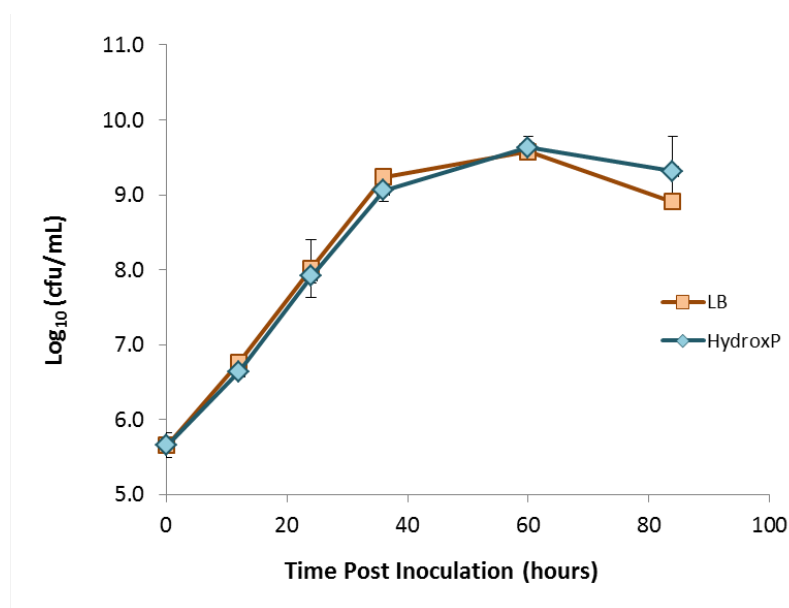


Figure B.2 Growth of *Burkholderia* sp. Ha185 in LB broth medium (orange) and the HSU HydroxP medium (blue). Colony counts were obtained by serial dilution of 100 μL sample aliquots at each time point, and were plated on LB medium. Each data points represent the average of three replicates. Error bars represent standard error of the three replicates.

Appendix C

Molecular Techniques and Manipulation

C.2 DNA techniques and manipulations

C.2.1 Isolation of genomic DNA from bacteria

Genomic DNA (gDNA) was extracted using the Genomic DNA prep kit (SGD41-C100, SolGent, Korea) in accordance with the manufacturer's instructions. A volume of 1.5 mL of overnight bacterial culture was used for each reaction. The DNA concentration of the resultant gDNA was measured using Nanodrop-spectrophotometer (ND-1000 spectrophotometer). Extracted DNA was stored at -20°C for up to 6 months.

C.2.2 Isolation of plasmid DNA from bacteria (mini-preps)

Alkaline lysis extraction of plasmid DNA was performed using a modified method of Birnboim and Doly (Birnboim and Doly, 1979). One millilitre of an overnight bacterial culture was centrifuged for 30 seconds at 15,700 × *g*. The cell pellet was re-suspended in 150 µl of Solution I (A.1.1) followed by addition of 200 µl of Solution II (A.1.1) and the mixture were gently inverted. The cells were incubated at 37 °C for 4 minutes and 150 µl of 3M NaAc was added to the suspension after incubation. The sample was vortexed briefly and incubated on ice for 5 minutes. The resultant white precipitations were centrifuged for 10 minutes at 15,700 × *g* at room temperature. The supernatant was transferred into 1 mL of absolute ethanol (99 %) followed by centrifugation for 5 minutes at 15,700 × *g*. After the removal of the supernatant by aspiration, pellet containing plasmid DNA was dried for 30 minutes at 37 °C, and the dried pellet was resuspended in 30 µl of autoclaved dH₂O.

C.2.3 DNA restriction enzyme digestions

Restriction enzyme digestion of DNA was carried out according to the manufacturer's specifications for buffer, temperature, and enzyme concentration. The reaction comprised a total volume of 10 µL for restriction profile diagnostic containing 10 X NEBuffer 4, 1µl of miniprep DNA, 6 U of restriction enzyme and autoclaved dH₂O. The reaction in a total volume of 100 µL for ligation purpose containing 10 X NEBuffer 4, 3µl of mini-prep DNA or 10 - 20 µL of PCR amplicon, 6 U of restriction enzyme and dsH₂O was used to make up the volume. The digestion incubated for 1.5 hours at 37 °C, or at appropriate temperature. Where required, double digestions were carried out sequentially in

appropriate buffers with ethanol precipitation between the two digestion steps. Ethanol precipitation (Appendix C.2.4) was performed after restriction digest for ligation purpose.

C.2.4 DNA precipitation

DNA precipitation was carried out to concentrate the DNA sample. DNA sample was precipitated with 2 x volume of absolute ethanol and 1/10th the original volume of 3 M sodium acetate. The precipitated DNA was pelleted by centrifugation for 5 minutes at 15,700 × *g*. The aspirated pellet was air dried for 30 minutes at 37°C and then resuspended in 7 µL sterile dsH₂O. The concentration of the DNA to be processed was determined by running 2 µL of the precipitated DNA on a 1 % agarose gel (Appendix C.2.10).

C.2.5 Preparation of chemical-competent cells

One millilitre of an overnight bacterial culture was inoculated in 50 mL of LB broth in a 250 mL conical flask. Cultures were grown at the appropriate temperature with shaking at 250 rpm until an OD₆₀₀ of 0.4 - 0.6 was reached. Bacterial cells were incubated on ice for 20 min prior to centrifugation at 4°C for 10 min (1600 × *g*). The supernatant was discarded and cell pellet was resuspended in 25 mL of ice-cold 0.1 M CaCl₂. The resuspension was centrifuged again at 4°C for 10 min (1600 × *g*) and the cell pellet was resuspended in 1 mL of ice-cold CaCl₂. The final cell resuspension was incubated on ice for 1 h.

C.2.6 Preparation of electrocompetent cells

One millilitre of an overnight bacterial culture was inoculated in 50 mL of LB broth in a 250-mL conical flask. Cultures were grown at the appropriate temperature with shaking at 250 rpm until an OD₆₀₀ of 0.4 - 0.6 was reached. Bacterial cells were incubated on ice for 20 min prior to centrifugation for 10 min at 4°C (2300 × *g*). Supernatants were discarded and bacterial cell pellets were resuspended in 25 mL of ice-cold dsH₂O followed by centrifugation for 10 min at 4°C (2300 × *g*). The above resuspension and centrifugation steps were repeated once followed by resuspending cell pellets in ice-cold sterile 10 % glycerol. The cells were centrifuged for 10 min at 3300 × *g* (4°C) and the washing process was repeated again. Finally, cells were resuspended in 1 mL of ice-cold 10 % glycerol prior incubation on ice for 30 min. Electrocompetent cells were stored at -80°C.

C.2.7 Transformation of chemical-competent cells

DNA was chilled on ice for at least 10 min prior to transformation. For transformation a 2-3 µL volume of plasmid mini-prep DNA or ligation mix was added to a 1.5-mL chilled eppendorftube

containing 100 μL chemical-competent cells and was gently mixed by a small flick on the tube. The sample was incubated on ice for 30 min followed by incubation in a circulating water-bath for 30 sec at 42°C. The sample was then transferred onto ice immediately and 1 mL of LB broth was added in room temperature. Transformed bacterial cells were incubated at the appropriate temperature for 60 min then centrifuged at $5900 \times g$ for 3 min. The supernatant was tipped off and the cell pellet was resuspended in 100 μL of LB broth. Cell suspension was plated on LB agar containing the appropriate antibiotics and incubated overnight at the appropriate temperature.

C.2.8 Transformation of electrocompetent cells

DNA and the electro cuvette were chilled on ice for at least 10 min prior to transformation into electro-chemical cells. A 1 μL volume of chilled plasmid mini-prep or ligation mix was added to 40 μL electrocompetent cells in a 1.5-mL chilled Eppendorf tube and was gently mixed by a small flick on the tube. Samples were transferred to pre-chilled electro-cuvettes and incubated on ice for 30 min. The cuvettes containing electrocompetent cells and DNA were placed into the arm of a BioRad *E. coli* Pulser (BioRad, Hercules, CA) and were subjected to a charge of 2.5 kV, achieving a time constant > 5.2 msec. One millilitre of LB broth at room temperature was added to each sample immediately after the electroporation. Samples were incubated at appropriate temperatures for 60 min before being centrifuged at $5900 \times g$ for 3 min. Supernatant was discarded and cell pellet was resuspended in 100 μL of LB broth. Cell suspensions were plated on LB agar containing appropriate antibiotics and incubated overnight at the appropriate temperatures.

C.2.9 Polymerase chain reaction (PCR)

PCR was carried out in 0.2 mL Thermo-Tube and was performed in C1000 Touch™ Thermo Cycler (Bio-Rad, California, U.S). A non DNA template control was included with all PCR amplification reaction when the primer pair was used for the first time. Each reaction contained approximately 10 ng of gDNA or plasmid DNA template. PCR amplification was carried out using Platinum® Taq DNA Polymerase High Fidelity (Invitrogen, Carlsbad, CA) according to manufacturer's instructions. Each PCR reaction comprised of 10x High Fidelity PCR buffer, 0.2 mM dNTPs, 2 mM of MgCl_2 , 0.2 μM of each forward and reverse primer, 1 U of Taq polymerase, and 0.2 μM for gDNA or 0.4 μM for plasmid DNA as template. Standard PCR cycle was set as follows; 94°C for 5 min, followed by five cycles of 94°C for 30 s, 55°C for 30 s, 68°C for 1 min per kb, and 30 cycles of 94°C for 30 s, 50°C for 30 s, 68°C for 1 min per kb, and a final extension step of 68°C for 5 min then hold at 4°C. PCR products were purified using a High Pure PCR Product Purification kit (Cat. No. 11732676001, Roche, Basel, Switzerland) according to manufacturer's instructions.

C.2.10 Agarose gel electrophoresis

Agarose gels (1 %) were prepared in 1 × TBE buffer (A.2.10), and DNA samples were mixed with 6 × loading dye prior loading into each well. Gels were electrophoresed at 110 V for 50 min followed by staining with ethidium bromide (0.5 µg mL⁻¹) for 15 min and destained in water for 10 min. Gels were visualised using a UVITEC Cambridge, UVIdoc HD2 (UVitec Limited, Cambridge, United Kingdom).

C.2.11 DNA ligation

DNA ligations were carried out according to manufacturer's instruction (Roche Diagnostics GmbH, Mannheim, Germany). A total volume of 10 µL containing 3 µL ligase buffer, digested plasmid and insert at a ratio of 1:3, 2 U of T4 DNA ligase, and sterile dsH₂O. Reactions were incubated overnight at 20°C then stored at -20°C. Ligation of PCR product into commercial pGEM[®]-T Easy Vector System was carried out as detailed in the manufacturer's instructions (Promega #A1360, Madison, USA). Each ligation reaction comprised of 5 µL of 2x Rapid Ligation Buffer (60mM Tris-HCl (pH 7.8), 20mM MgCl₂, 20mM DTT, 2mM ATP and 10 % PEG), 1 µL of pGEM[®]-T Easy Vector (50 ng/µL), 3 U of T4 DNA Ligase, and PCR product. PCR product was quantified using a Nanodrop ND-1000 spectrophotometer prior to ligation to give a 1:3 ratio of vector to insert. Ligations were carried out overnight at 20°C before being stored at -20°C.

C.2.12 DNA sequencing preparation

Plasmid DNA or PCR products were purified according to the manufacturer's instructions using the High Pure Plasmid Isolation Kit or the High Pure PCR Product Purification Kit (Roche Diagnostics GmbH) respectively. Both plasmid and PCR product templates were quantified using a Nanodrop ND-1000 spectrophotometer. Reaction volumes of 20 µL were prepared containing both PCR product and plasmid DNA at a concentration of 50ng µL⁻¹. Sequencing primers were used at 3.2 pM per reaction. Sequencing was performed by the Applied Biosystems 3730xl and 9 ABI 3700 from Macrogen sequencing services (<http://dna.macrogen.com/eng/>).

C.2.13 Colony validation by BOX-PCR genomic fingerprinting

The appearance of *Burkholderia* sp. Ha185 on LB plate is typically circular and raised with an entire margin at the edge of the colony. However, to validate the identity of the strain throughout the course of this study, BOX-repeat-based PCR (BOX-PCR) was undertaken using a single BOX A1R primer as outlined by Versalovic et al., 1994 and Kim et al., 2001 (CTACGGCAAGGCGACGCTGACG). Any suspected contaminants were subjected to BOX-PCR. A single colony sourced from a LB plate on

which the contaminants were observed were suspended in 500 μL of UV-treated distilled water, and vortexed vigorously for at least 2 min and a 2 μL aliquot was then used as a template for BOX-PCR. The BOX-PCR amplification was carried out using Expand Long Template PCR System from Roche (Cat No. 11681834001, Applied Science, Penzberg, Germany). Each PCR reaction comprised 2 μL of resuspended cells as described above, 2 μL of No. 2 template buffer, 1 μL of 500 μM dNTPs, 3.2 μL of (10 μM) primer, 0.4 μL of DNA polymerase and adjusted to 20 μL final volume with distilled water. To minimise degradation of DNA from bacteria-derived DNases present in bacterial cells, the BOX-PCR cycle was modified to reduce the amplification time. BOX-PCR cycle was set as follows; 94°C for 15 min, followed by thirty cycles of 94°C for 15 s, 53°C for 30 s, 68°C for 8 min, and a final extension step of 68°C for 10 min then held at 4°C until DNA fragments were separated by agarose gel electrophoresis (Appendix C.2.9).

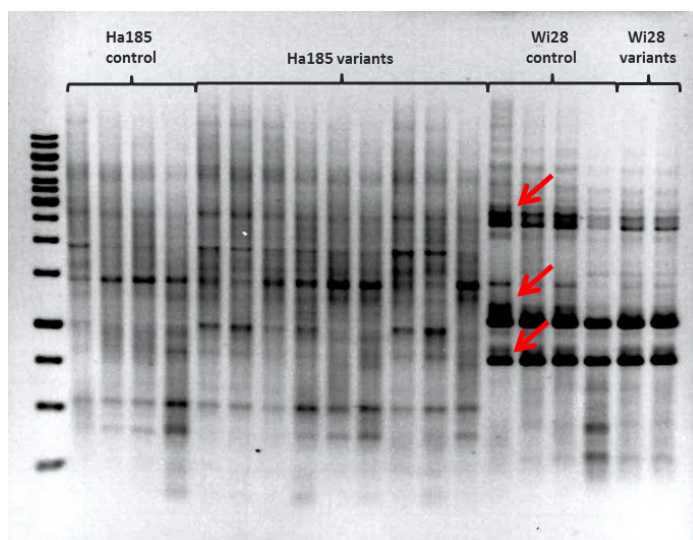


Figure C.2 An example of DNA fingerprinting by BOX-PCR. Isolate Ha185 and its variants displayed similar band patterns. Isolate Wi28 and the variants also display similar band profile. Red arrows indicated band differences between isolates Ha185 and Wi28 which are different bacterial genera (*Burkholderia* sp. Ha185 and *Enterobacter* sp. Wi28 respectively).

C.2.14 Visualising *Burkholderia* sp. Ha185 using a transmission electron microscope

To visualise *Burkholderia* sp. Ha185 bacterial cell, 3 or 5 μ L (1 in 100 dilution using 9 % NaCl) of an LB 48 h culture (20°C) was applied to a freshly glow-discharged plastic-coated 200-mesh grid (Proscitech, Thuringowa, Australia). The grids were glow discharged before applying a sample. The sample was then settled for 30 to 60 s before excess fluid was wicked off using Whatman #1 filter paper. The sample was then stained for 45 seconds with 0.5-1.0% filtered uranyl acetate (pH 5.0). Excess fluid was removed with a filter paper and the grid was left to air dry for 30 mins. Grids were examined using a Morgagni 268D (FEI, USA) transmission electron microscope at a nominal magnification of 8000-70000 operated at 80 KeV. The images were captured using a Megapixel III digital camera (SIS/Olympus, Japan).

Appendix D

High-Throughput Screening of Plant Growth Promoting Traits of Each Phosphate-Solubilising Bacterial Isolates

Table D: Screening for plant growth-promoting traits and identification of phosphate solubilising bacteria.

Location & Soil type		Isolates	Pcon (mM)	ACC	Na-Phy	CaPA	Me-Red	Hyp-G	Hyp-S	FePA
Ballantrae (Pasture soil)	Ba5	0.32	1	1	0	1	0	1	0	
	Ba8	0.49	1	1	0	1	0	1	0	
	Ba6	0.50	1	2	1	1	1	1	0	
	Ba12	0.51	1	1	1	1	1	1	0	
	Ba11	0.58	1	0	0	1	0	1	0	
	Ba31	1.20	0	0	0	0	0	0	0	
	Ba30	1.38	0	0	0	0	0	0	0	
	Ba3	1.61	0	0	0	1	0	0	0	
	Ba29	3.20	1	0	0	1	0	1	1	
	Ba27	3.31	1	2	1	2	1	1	0	
	Ba17	3.64	1	0	0	1	0	0	2	
	Ba40	4.51	1	2	2	2	1	1	1	
	Ba28	4.51	1	2	2	2	1	1	0	
	Ba21	6.24	1	2	2	3	1	1	0	
Whatawhata (Pasture soil)	Wh5	0.59	1	2	2	1	1	1	0	
	Wh23	0.84	0	1	0	0	0	0	0	
	Wh24	1.40	1	1	0	0	0	0	0	
	Wh9	1.67	1	1	0	1	0	0	0	
	Wh7	2.27	1	1	0	0	0	1	0	
	Wh11	2.53	1	3	1	1	1	0	0	

	Wh12	2.57	1	1	1	1	0	0	0
	Wh10	2.78	1	1	1	1	0	0	0
	Wh8	3.16	0	3	2	1	1	1	1
	Wh16	3.21	1	1	0	3	1	0	1
	Wh6	3.57	0	1	0	0	0	0	1
	Wh18	4.39	1	2	1	3	1	0	0
	Wh15	4.86	0	3	1	1	1	0	0
	Wh21	7.03	1	1	1	2	1	1	1
	Wh22	8.55	1	2	3	3	1	0	0
	Wh17	9.08	0	1	0	3	0	0	0
Winchmore (Pasture soil)	Wi21	0.39	1	2	1	1	1	1	0
	Wi30	1.35	1	2	1	1	1	1	0
	Wi6	3.53	0	0	0	0	0	0	0
	Wi16	4.19	0	0	0	0	0	0	0
	Wi17	4.96	1	2	1	3	1	1	0
	Wi11	5.95	1	1	1	2	1	0	1
	Wi18	6.36	1	2	1	3	1	1	0
	Wi3	6.88	0	0	0	1	0	0	0
	Wi14	7.94	1	2	1	2	1	0	2
	Wi28	10.73	1	2	2	3	1	0	2
Haast (Native forest)	Ha190	0.59	1	1	2	1	0	1	0
	Ha187	0.59	1	1	2	1	0	1	0
	Ha194	0.61	1	1	2	1	1	1	0
	Ha188	1.02	0	1	2	1	1	1	1
	Ha184	1.04	0	0	1	1	1	1	0
	Ha197	1.25	1	2	1	0	1	1	1
	Ha180	1.29	0	2	2	1	1	1	0
	Ha179	1.60	1	0	2	0	0	0	1
	Ha178	1.81	1	0	2	1	0	0	0
	Ha196	2.83	1	2	1	1	1	1	0
	Ha192	3.09	1	0	0	1	0	0	0
	Ha193	4.04	1	1	1	1	0	0	0
	Ha182	4.16	1	2	3	0	1	0	0
	Ha189	4.55	1	3	3	0	1	0	0
	Ha185	5.93	1	2	3	1	1	0	0
	Ha183	6.05	1	2	1	1	1	0	0
	Ha186	6.84	1	1	1	1	0	0	0
	Ha181	6.94	1	1	1	1	0	0	0
	Ha200	7.56	0	2	2	3	1	0	2
	Ha198	8.66	0	2	2	3	1	0	2
	Ha191	8.86	0	2	2	3	1	0	1
	Ha195	8.97	0	2	2	3	1	0	2
	Ha203	9.07	0	3	2	3	1	0	2
	Ha201	9.11	0	2	2	2	1	0	1
Ha199	9.77	0	2	2	3	1	0	2	
Ha202	9.98	0	2	2	3	1	0	2	
Ha204	10.07	0	2	2	3	1	0	1	
Eyrewell (Exotic forest)	EE137	0.14	1	1	0	1	0	1	0
	EE138	0.59	1	0	1	0	0	0	0
	EE136	1.47	1	0	0	0	0	0	0
	EE126	2.40	0	1	0	0	0	0	0
	EE128	3.57	1	3	2	1	1	0	1
	EE121	3.92	1	1	1	2	0	1	0
EE130	5.22	1	3	3	3	1	0	0	

	EE131	7.36	1	3	1	3	1	0	1
	EE129	7.51	1	3	1	3	1	0	1
	EE140	7.57	1	0	0	0	0	0	0
	EE132	7.66	1	3	2	3	1	0	0
	EE134	7.84	1	3	1	3	1	0	2
	EE133	8.06	1	3	2	3	1	0	3
	EE122	8.73	1	3	3	2	1	0	0
	EE135	8.77	1	3	1	3	1	0	0
	EE123	8.90	1	3	1	3	1	0	1
	EE124	8.92	1	3	2	3	1	0	1
	EE127	9.05	1	3	2	3	1	0	2
	EE125	9.28	1	3	2	3	1	0	2
Eyrewell (Native forest)	EN113	0.59	1	2	2	2	1	1	0
	EN118	0.88	1	1	1	1	0	1	0
	EN120	1.01	1	1	1	1	1	1	0
	EN106	1.20	1	1	0	1	0	1	0
	EN102	4.83	1	2	2	3	1	0	1
	EN110	5.04	0	1	2	2	1	1	0
	EN116	5.09	0	1	2	2	1	1	0
	EN114	5.13	0	2	1	2	0	1	1
	EN112	5.25	0	2	2	3	1	0	1
	EN111	5.34	1	2	2	3	1	0	2
	EN115	5.38	0	2	2	2	0	1	1
	EN107	5.44	0	2	2	3	0	1	1
	EN103	7.57	1	2	2	3	1	0	2
	EN105	7.73	1	2	2	3	1	0	2
	EN101	8.04	1	2	2	3	1	0	2
	EN117	8.37	1	3	2	3	0	0	2
	EN104	8.53	1	3	2	3	1	1	2
	EN108	9.13	1	3	2	2	1	0	1
EN109	9.37	1	3	2	3	0	0	0	
Internal control	PSB85	10.38	0	2	1	3	0	0	2

Isolates were subjected to 16S rRNA sequencing are highlighted in green.

Appendix E

Quantitative Size Measurement of Hydroxyapatite and *Burkholderia* sp. Ha185 Particles

To gain an understanding of the physical interaction between insoluble P such as HydroxP and *Burkholderia* sp. Ha185 during P solubilisation, qNano (iZon Science Ltd, New Zealand) was used to determine the particle size, concentration and interactions between HydroxP and bacteria measured by iZon's sensing nanopore in real-time. The qNano allows quantitative size measurement of particles that traverse the nanopore which analyses one particle at any given time by detecting a transient change in the ionic current, according to particle sizes (particle volume) and relative surface charges (electrophoretic mobility). This study was performed under the supervision of Dr. Sam Yu (Izon Science Ltd.) using the Scanning Ion Occlusion Sensing (SIOS) technology by qNano (Vogel et al., 2011). Wildtype *Burkholderia* sp. Ha185 was grown in 50 mL HSU HydroxP medium as described in Chapter 4.2.1.1 allowing HydroxP solubilisation over a period of time of 24, 48 and 60 h. Uninoculated HSU HydroxP medium was used as the control. Each sample (100 μ L) was gently diluted with 900 μ L of 1X HSU buffer solution (Appendix A.3.5) before placing 40 μ L onto the iZon's sensing nanopore. Particles with various sizes were then counted using the the iZon sensing nanopore, and information of each individual particle were collected and presented as histograms. The amount of soluble P released was measured by the colourimetric method as described in Chapter 2.2.1.1.

The relative particle size distribution of the HydroxP measured by qNano (Figure E.1) revealed a wide range of HydroxP particle population sizes ranging from 800 - 2800 nm with the majority of the population around 900 nm in size. The *Burkholderia* sp. Ha185 cells were found to range in size from 800 - 1500 nm, and similar to HydroxP, the majority of the population was approximately 900 nm in size. The similar sizes of *Burkholderia* sp. Ha185 and HydroxP particles make them unable to be differentiated by qNano.

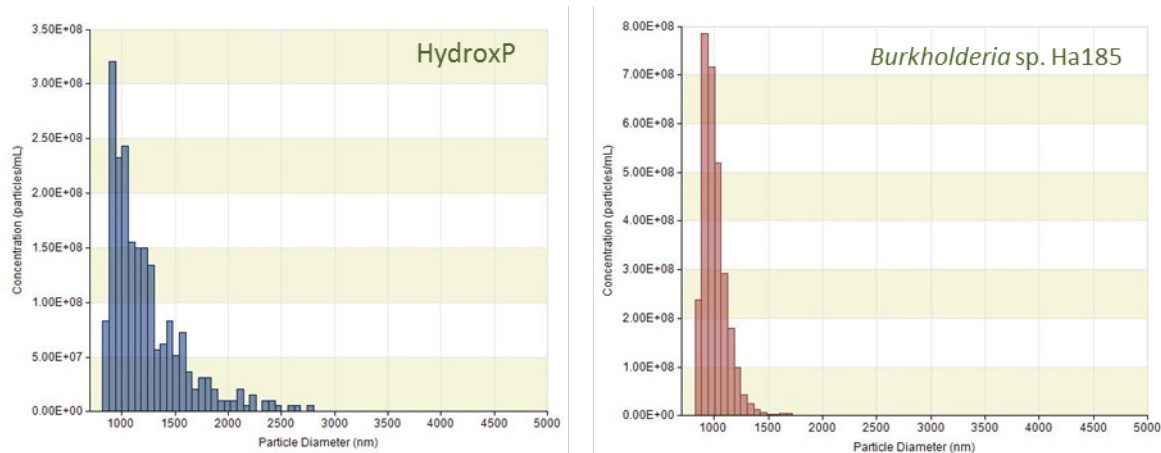


Figure E.1 Size distribution of control HydroxP particles (left) and *Burkholderia* sp. Ha185 bacterial cell particles (right).

When *Burkholderia* sp. Ha185 and HydroxP were in the same solution, particles ranging from 900 - 4800 nm in size were detected at 24 h before P solubilisation by *Burkholderia* sp. Ha185 (Figure E.2) (0.21 ± 0.03 mM P in the culture filtrate). At 24 h, various sized particles (1000 - 4800 nm) were detected, with the majority approximately 1100 nm in size. This suggests that the HydroxP has aggregated in the presence of bacterial cells, or that *Burkholderia* sp. Ha185 was bound to HydroxP enabling P solubilisation to occur in close proximity to the cell. At 48 h where 16.29 ± 1.35 mM soluble P was detected in the solution, there were fewer particles present ranging from 900 - 3300 nm, with the majority of particles about 1000 nm in size. With the increased P concentration and decreased large particle counts at 60 h, it is likely bacterial-HydroxP complexes have broken down to smaller particles and soluble P has been released. At 60 h, most particles were around 900 nm in size, similar to that of the *Burkholderia* sp. Ha185 cells (Figure E.2). The absence of large particles suggests bacterial-HydroxP complexes are no longer present in the medium, and the major population around 900 nm detected may include both dissociated HydroxP particles and *Burkholderia* sp. Ha185 bacterial cells (Figure E.2).

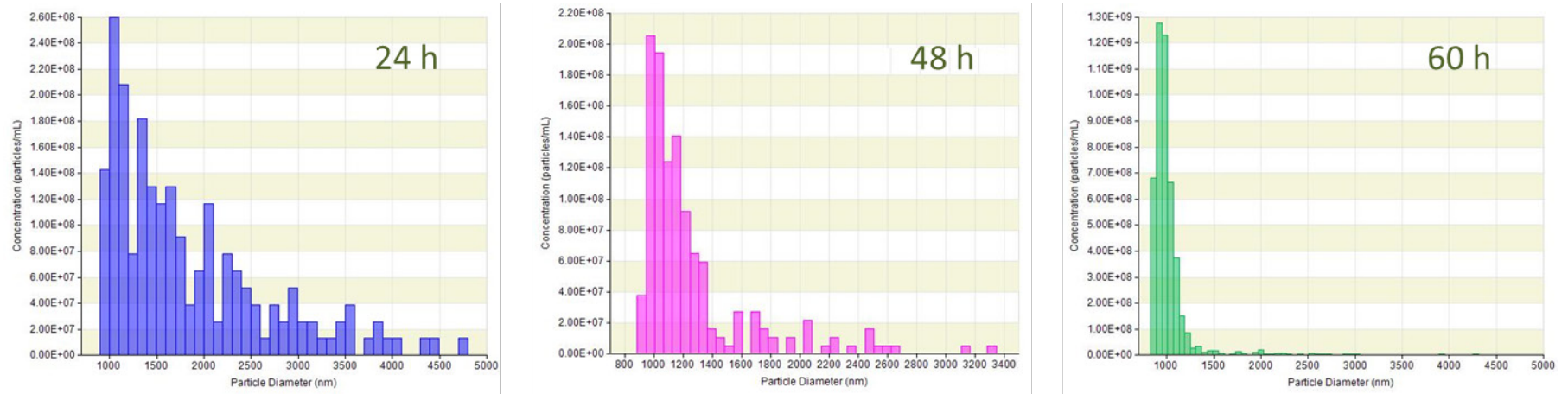


Figure E.2 Size distribution of *Burkholderia* sp. Ha185 in HSU HydroxP medium at 24 h, 48 h and 60 h incubation.